CHAPTER ONE

INTRODUCTION

1.1 Background of the study

Silicon bronze is a copper based alloy containing silicon as the major alloying element usually in the range of 3-5wt% (Mattern *et al.,* 2007). It is a high strength engineering alloy that has excellent resistance to a wide range of corrosive environments (Ketut *et al.,* 2011a). Silicon bronze is among the most widely used copper based alloys because of its combination of corrosion resistance, strength, and formability. Typical rod-shape applications of silicon bronze alloy include electrical conduits, valve stems, tie rods, fasteners, marine and pole-line hardware, nuts, bolts, screws, rivets, nails, and wire (Kulczyk *et al.,* 2012).

The excellent mechanical and functional properties of copper and its alloys have made it attractive to industries for use in various fields of engineering applications. Garcia *et al.* (2010) reported that the increase in demand of copper based alloy for building components of automotive, electrical parts, valves and fittings was because of its combination of excellent properties such as corrosion resistant, ductility, malleability, non-magnetism, wear resistance, machinability; good thermal and electrical conductivities.

Copper is extensively used in chemical, petroleum, automotive and power generating industries. In power generating industry, it is basically used for

production of various equipment such as wire, cables, all parts of electrical and electronics apparatus, locomotive fire boxes, water heating apparatus, water pipes, vessels in brewery, heat transfer equipments and condenser tubes (Shabestari and Moemeni, 2004). These extensive applications of copper in various industries are basically because of its excellent properties such as electrical conductivity, thermal conductivities, excellent corrosion resistance good wear resistance, ease of fabrication and reasonable strength (William, 2010). Because of its high heat conduction, copper is used for soldering iron bits (Shabestari and Moemeni, 2004).

Copper is the oldest industrial element or material widely used in constructions and electronic industries. It has strong affinity with other elements, mostly oxygen and sulphur and therefore does not exist as free element in the earth's crust. Copper is obtained in the earth crust as minerals such as cuprites (Cu_2O), chalcocite (Cu_2S), chalcopyrite ($CuFeS_2$), malachite, azurite and bornite (William, 2010). Research by Shabestari and Moemeni (2003) has shown that copper is a chemical metallic solid with appreciably high melting temperature of 1084^0C. It is reddish orange with FCC crystal structure ($\alpha = 3.6074$Å). Copper has an atomic mass and density more than two and four times higher respectively than silicon. Unlike silicon, copper has a weakly bonded electron in the outer orbital and considerable higher electrical and thermal conductivities. Bosacchi and Franzosi (1976) reported that copper diffuses through the silicon

lattice as a positively charged ion because unlike other elements, it has a weakly bonded single electron in the 4s orbital which allows it to easily give away $4s^1$ electron and significantly reduced its ionic radii. Due to the small effective ionic radius, copper diffuses as interstitial ion rather than substitutional atom.

Silicon is a metalloid and the second most abundant element in the Earth's crust (about 28%), exceeded only by oxygen. The melting point of silicon is 1414°C (2574°F) and the boiling point is 2355°C (4270°F). Its density is 2.33grams per cubic centimeter, and it forms a face-centered cubic structure with a lattice spacing of 5.43Å (Ohkubo *et al.,* 2005). It is relatively inactive and does not combine with oxygen or most other elements at room temperature while at higher temperatures; silicon becomes much more reactive (Božića *et al.,* 2008). Also, water, steam, and most acids have very little effect on silicon. Silicon, carbon and other group IV elements form a face-centered diamond cubic crystal structure with a lattice spacing of 0.5430710nm (Puathawee *et al.,* 2013).

Earlier research by Zhang *et al.* (2003) has shown that commercial copper is soft, ductile and malleable with low tensile strength, containing up to about 0.7% total impurities such as tin, arsenic antimony, lead, bismuth and nickel. The alloying elements help to improve some properties of the alloy depending on their application. Earlier researches by Vilarinho *et al.* (2005); Garcia *et al.* (2010) have shown that the addition of zinc, silicon, iron, lead, aluminium and manganese to copper has significant effects in improving its mechanical

properties. The studies reported decline in electrical and thermal conductivities of copper when it is doped with the elements. This was attributed to the increase in thermal and interfacial resistance. Kumar *et al.* (2007) reported that lead is usually added to copper in the concentration ranging from 1-3wt% to enhance chip fracturing, reduce cutting force and increase the machining rate and ease productivity, reduce tool wear rate and improve surface finish. Lead acts as a microscopic chip breaker and tool lubricant, thereby increasing the brittleness of the alloy.

1.2 Statement of problem

Studies by Mattern *et al.* (2007); Ketut *et al.* (2011a); Kulczyk *et al.* (2012); Puathawee *et al.* (2013) and Božića *et al.* (2008) showed that slowly cooled silicon bronze (Cu-Si) exhibit moderate strength and hardness with very low ductility. The studies attributed this mechanical behaviour to the presence of coarse and segregated primary silicon and copper silicide (Cu_3Si) phases in the alloy structure. This research will develop new silicon bronze of improved strength and hardness without the expense of excellent ductility and electrical conductivity by addition of dopants of various concentrations. This will widens the applications of the alloy in automobile, building and electrical industries.

1.3 Aim of the study

The aim of this research is to study the effect of dopants and heat treatment parameters on the structure, physical and mechanical properties of silicon bronze (Cu-Si).

1.4 Objectives of the study

1. To investigate the effect of dopants on the structure, physical and mechanical properties of silicon bronze.

2. To establish the best alloys compositions of the developed silicon bronze.

3. To examine the effect of solution heat treatment on the structure, physical and mechanical properties of the best alloys compositions.

4. To establish the correlations between the physical and mechanical properties of the studied alloy.

1.5 Scope of the study

1. The alloys studied were Cu-(1-5)wt%Si, Cu-3wt%Si-Zn, Cu-3wt%Si-Sn, Cu-3wt%Si-Mg, Cu-3wt%Si-Mn, Cu-3wt%Si-W, Cu-3wt%Si-Ti, Cu-3wt%Si-Mo and Cu-3wt%Si-Al.

2. Silicon was varied in concentrations of 1, 3 and 5wt%.

3. Dopants used were zinc, tin, magnesium, manganese, tungsten, titanium, molybdenum and aluminium in concentrations of 0.1, 0.2, 0.3, 0.4, 0.5, 0.6, 0.7, 0.8, 1, 1.5, 2, 3 and 5wt% respectively.

4. Heat treatment parameters employed were solutionizing temperature (900^{o}C), soaking time (30mins) and quenching medium (air).

5. The physical and mechanical properties investigated were ultimate tensile strength, percentage elongation, hardness, impact strength, density, electrical resistivity and conductivity.

6. The structural analysis conducted was limited to the use of optical metallurgical microscopy and scanning electron microscopy (SEM) equipped with energy dispersive spectroscopy (EDS).

7. Results generated were analyzed using design expert (DX10) and two-way analysis of variance (ANOVA).

1.6 Justification of the study

This research entitled "the effect of dopants and heat treatment parameters on the structure, physical and mechanical properties of silicon bronze (Cu-3wt%Si) alloy" will help to minimize the cost incurred in industries as a result of failure of silicon bronze. The addition of these dopants will refine and modified the coarse and segregated primary silicon and copper silicide, hence improving the properties of the alloy.

CHAPTER TWO

LITERATURE REVIEW

2.1 Properties of Cu-Si system and copper solubility in silicon

Božića *et al.* (2008) has shown that elements with lower valence usually have a greater solubility than elements with higher valence. In the Cu-Si binary system, copper and silicon have valency of one and four respectively (Mattern *et al.*, 2007). Therefore, each silicon atom has four nearest neighbors in its crystal lattice. Thus, completing all outer electrons shells by forming four sets of paired bonds, silicon forms very stable covalent bonds (Puathawee *et al.*, 2013). Eventual substitution of a silicon atom with copper in the silicon lattice disrupts the covalent sharing of the four electrons from the silicon, because a copper atom can contribute only one electron. Thus, the presence of copper atoms in the silicon lattice causes a situation in which the bonding of its nearest neighboring silicon ions is incomplete, bringing the overall system into a higher energy state (Božića *et al.*, 2008). Increasing the number of substitutional copper atoms replacing silicon atoms in silicon lattice significantly increase the internal energy of the system. Hence, copper will not fill the Si lattice as substitutional atom. Therefore, the solid solubility of copper in silicon is very low.

Figure 2.1 shows the binary phase diagram of Cu-Si alloy. It is evidenced in the phase diagram that the solubility of copper in silicon and vice versa is a function

of temperature. The solubility of copper in silicon changes significantly at different temperatures. The highest solubility of copper in silicon is around 0.003wt% at temperature of 1300°C, while the solubility of Si in fcc-Cu is about 11.25wt% at temperature of 842°C (Kulczyk *et al.*, 2012). The solubility of copper in silicon decreases with decrease in temperature and drops at temperature below 1100°C. The solubility of copper in silicon at room temperature is negligible (2wt%Si). Therefore at low cooling rate, all copper trapped in the silicon will move to the surface of the sample or will precipitate into the Cu_3Si phase (Ketut *et al.*, 2011a).

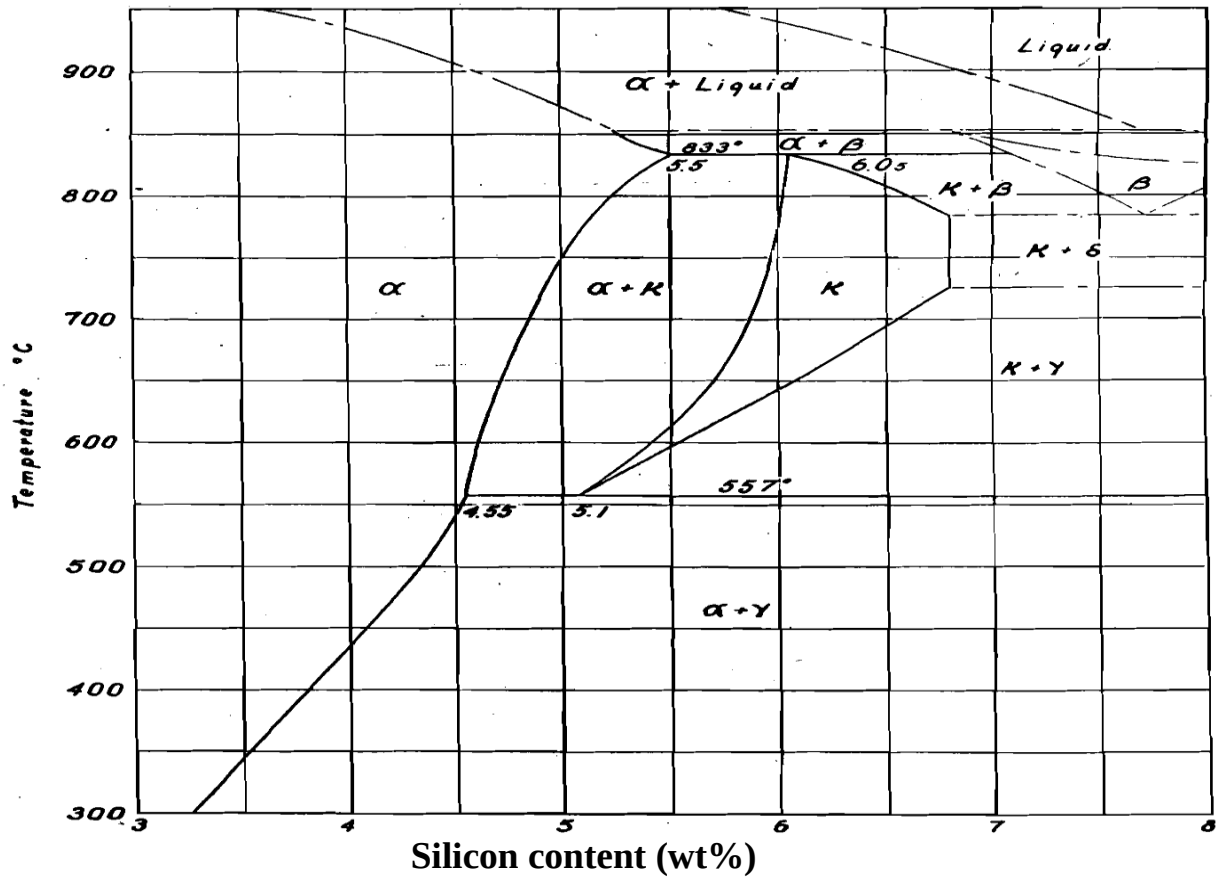

Figure 2.1: Copper-silicon binary phase diagram (Kulczyk *et al.*, 2012).

Ohkubo *et al.* (2005) reported that several inter-metallic phases are formed at the Cu rich side as shown in Figure 2.2. Three inter-metallic phases exist at room temperature: η''- (Cu_3Si), ε-($Cu_{15}Si_4$) and γ-(Cu_5Si). The room temperature Cu_3Si-phase (η'') has two high temperature modifications η' and η (Ohkubo *et al.*, 2005). Furthermore there are three high temperature phases in the system: α, β and κ (Cu_7Si) (Ohkubo *et al.*, 2005).

The possible distribution sites for trapped copper are:

1) Lattice defects such as dislocations or partial dislocations,

2) Grain boundaries,

3) Sample surface, or

4) Precipitation of the copper into Cu-silicides, most likely at the lattice defects or grain boundaries (Ohkubo *et al.*, 2005).

At slow cooling rate, copper will agglomerate at lattice defect sites with lower activation energy and later will move towards grain boundaries (Ohkubo *et al.*, 2005). With enough time, copper will follow grain boundaries to the surface. On the other hand, during rapid cooling, copper atom will not have enough time to diffuse to the nearest grain boundary or surface of the sample. As a result, copper atoms will most likely start to agglomerate around lattice defects and precipitate into Cu-silicide (Ohkubo *et al.*, 2005). Thereafter, copper atoms will move toward the already formed Cu-silicide precipitate inside the silicon grain. The only stable Cu-silicide in hypereutectic Cu-Si alloys at room temperature is Cu_3Si (Ohkubo *et al.*, 2005). Solidifying Cu-Si alloy at the lowest possible

temperature and holding the alloy at the given temperature throughout the solidification process will give the lowest concentration of Cu in the Si dendrites (Ohkubo *et al.*, 2005). Due to the high density difference between Si and Cu, a complex system is formed during solidification. The liquid phase becomes enriched in copper, leading to increasing density and a downward flow tendency at the solidification interface (Ohkubo *et al.*, 2005).

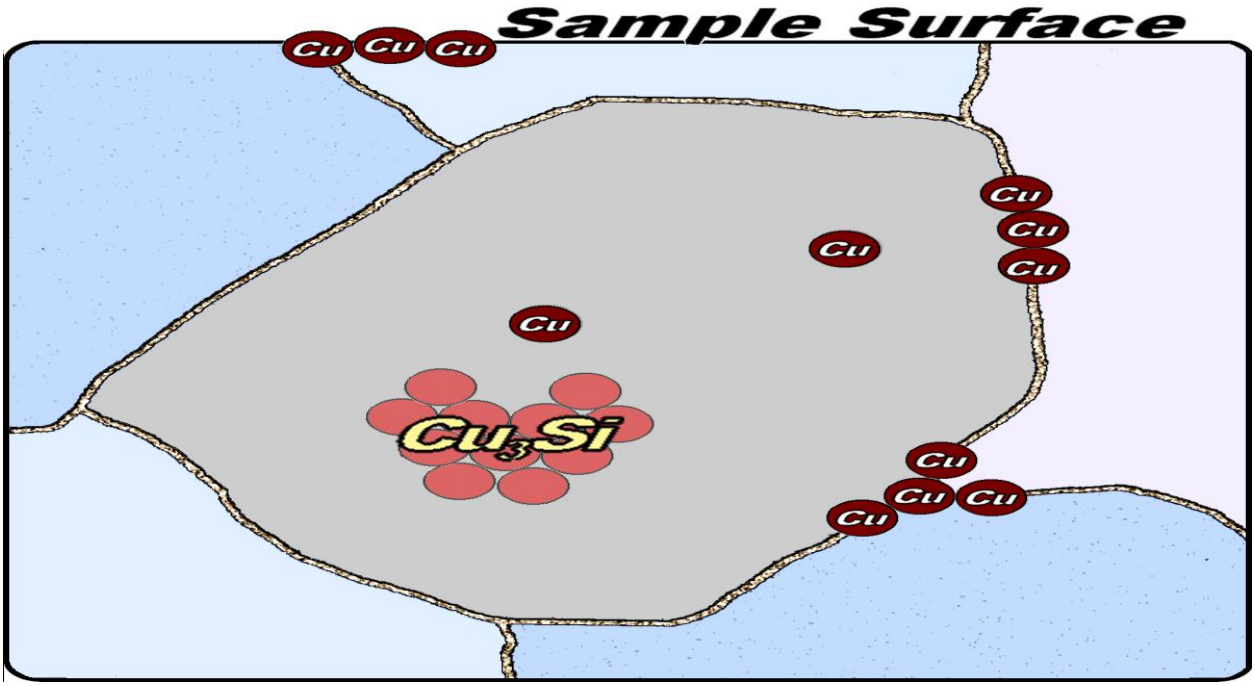

Figure 2.2: Possible copper distribution sites in a silicon sample. (Ohkubo *et al.*, 2005).

The molecular volume of the Cu_3Si is 46 $Å_3$ (Ronay and Schad, 1990). This volume is considerably higher than the molecular volume of silicon that is 20 $Å_3$. This causes a significant increase in internal stresses during Cu_3Si formation and growth (Ronay and Schad, 1990). Furthermore, in the presence of the lattice

defects, copper atoms will rather accumulate on them than form intemetallics (Warta, 2002).

Most elements have low solubility and segregation coefficient in solid silicon. However, copper has a high affinity for a wide range of elements, low activity coefficient, stable intermetallics and low effective ionic radius (Ohkubo *et al.*, 2005). This further reduces the segregation coefficient for most elements in silicon in the presence of Cu (Ohkubo *et al.*, 2005). During solidification of the liquid alloy, pure silicon crystallizes first while the remaining solvent together with the impurity elements solidifies in the gaps between the silicon dendrites. With slow cooling, the impurity elements with low solubility in solid silicon (Au, Co, Cu, Fe, Mn, Ni, Ti, Zr) are retained in the solvent or are deposited at grain boundaries of the alloy (Ohkubo *et al.*, 2005). Homogeneous nucleation requires a higher driving force than heterogeneous nucleation and the most expected site for the silicides heterogeneous-nucleation is at the grain boundaries, lattice defects or the other impurity rich regions (Istratov *et al.*, 1999).

2.2 Review of related literature on the structure and mechanical properties of copper based alloys

2.2.1 Effect of alloying elements on the structure and mechanical properties of copper based alloys

Mattern *et al.* (2007) investigated the influence of silicon content and rapid quenching on the phase formation of Cu–Si alloys. In this experimental study,

the samples were prepared by arc melting of the pure elements on a water-cooled copper mold under a high purity argon atmosphere.

The microstructure was analyzed by scanning electron microscopy (SEM) using a Gemini device (Zeiss) equipped with energy dispersive X-ray fluorescence analysis (EDX). The mass density was determined by the Archimedes principle by weighing samples in air and in dodecan ($C_{12}H_{26}$). The obtained results indicated different meta-stable states on the quenched samples which was dependent on the chemical composition. It was also noted that high temperature phases such as η, σ and κ were preserved at room temperature. The formation of the room temperature phase ε was suppressed by rapid quenching from the melt. The crystal structure of the high temperature phases was analyzed by X-ray powder diffraction. Annealing of the rapidly quenched alloys at T = 500^{o}C caused transformations of the meta-stable phases. The equilibrium states exhibited phase compositions, which were in agreement with the generally accepted phase diagram.

Ketut *et al.* (2011a) investigated the effect of silicon content on the mechanical and acoustical properties of bronze alloys for musical instruments. As-cast Cu-(2.5-7.5) wt. % Si were cut from 250 x 55 x 15 mm of billet and manufactured for tensile, hardness, impact, and damping test specimen. Simply supported beam model was used for measuring damping capacity. Mechanical and damping properties of silicon bronze (Cu-Si) were studied. Investigation of

bronze 20wt. % Sn alloys was conducted as comparison. The results obtained indicated that the mechanical properties and damping capacity of Cu-xSi were higher than Cu-20wt.%Sn bronze alloys. The ductility and impact strength of silicon bronze were also higher than for tin Cu-20 wt.% Sn.

Kulczyk *et al.* (2012) examined the effect of cold working on the structure and mechanical properties of high strength silicon bronze (C65500). The developed alloy (C65500) was subjected to severe plastic deformation by hydrostatic extrusion at room temperature with the goal to increase its strength by grain refinement without modification of the chemical composition. Cumulative hydrostatic extrusion was applied with a total true strain of 4.1. The microstructure of cold worked samples was evaluated by transmission electron microscopy. The size of grains was quantitatively described. The resulting mechanical properties were determined in tensile tests and via microhardness measurements. The results of the study revealed that the applied cumulative hydrostatic extrusion route caused a substantial grain size refinement accompanied by high increase in strength. In comparison to commercial alloy after conventional plastic treatment, ultimate tensile strength and yield strength were higher by 45% and 130% respectively.

Puathawee *et al.* (2013) investigated the effect of silicon and tin addition on the microstructure and microhardness of Cu-Si-Zn alloy. In this study, the

concentration of tin was varied in the range of 0.5, 1.0, 2.0, 3.0 wt%. The silicon brasses were prepared by melting pure elements with a graphite crucible using an induction furnace. The chemical composition of each alloy was determined by X-ray fluorescence spectrometry (XRF). Microstructure of the as-cast alloy was observed by optical microscopy and scanning electron microscopy. The respective chemical analysis of the phases was determined by energy dispersive X-ray spectroscopy (EDS) and the hardness was measured by Vickers hardness test. The results of the study revealed that the hardness of 60Cu-0.5Si-39.5Zn brass was 123.4 HV. It was also indicated that hardness value of the alloy studied increased with increase in silicon content. Moreover, the addition of tin together with silicon increased the amount of beta (β) phase and more uniform dispersive gamma (γ) phase than those of the silicon addition alone. It could be concluded that the tin addition enhanced the hardness of lead-free Cu-Si-Zn brass and tended to be helpful for machining.

Microstructure and microhardness of precipitation hardened Cu-Ti and precipitation/dispersion hardened Cu-Ti-Si alloys were examined by (Božića *et al.*, 2008). Cu-1.2Ti and Cu-1.2Ti-3$TiSi_2$ (wt.%) atomized powders were characterized before and after consolidation by Hot Isostatic Pressing (HIP). Rapidly solidified powders and hot isostatic pressed compacts were subsequently subjected to thermal treatment in hydrogen at temperatures

between 300 and 600°C. The following conclusions were drawn from the results of the study:

1. The rapidly solidified Cu-1.2Ti-3$TiSi_2$ powder microstructure was characterized by the presence of fine, dispersed primary $TiSi_2$ particles and high super saturated solid solution. The microstructure was not completely homogenous but rather exhibited the presence of the homogenous fluctuations in the range of 5–10μm.

2. Cu-1.2Ti-3$TiSi_2$ powder yielded much higher microhardness values compared with the Cu-1.2Ti powder, owing to primary $TiSi_2$ dispersoides formed during atomization.

3. High strengthening of the Cu-Ti-$TiSi_2$ powder was achieved by ageing as a consequence of the simultaneous influence of the following factors: The development of the nodular structure, the precipitation of metastable Cu_4Ti and the presence of primary $TiSi_2$ dispersed phase particles.

4. Obtaining the full density compacts by hot isostatic pressing was possible only at higher temperatures where the maximum strengthening value was achieved.

5. Lower microhardness values of compacts compared to atomized powders achieved by ageing was as a result of stable Cu_4Ti-phase presence in the structure.

Sadayappan *et al.* (2002) investigated the effect of addition of tin (Sn) and other elements on the microstructure of Cu-Zn alloy. Also, the interaction between the grain refiner and minor alloy additions such as Sn, Al, Bi, Se and Pb was evaluated. In the first melt, Cu-Zn alloy was melted and Sn, Al and Pb were added successively. In the second melt, the order was modified as Pb, Sn and Al. The grain size of these castings was evaluated using the scale developed as a part of the investigation. The macro and respective micro structures were also presented. The Cu-36% Zn alloy had a large grain which was rated as 2.5μm. The microstructure of this alloy contained primary α dendrites with some β phase in the interdendritic areas and grain boundaries. It was also observed that every other element added to this alloy modifies the structure both in constituents and size. Tin was completely soluble in copper and forms solid solution with copper. However it did not change the grain size of the alloy. It was also observed that the Cu-36% Zn alloy after an addition of 0.35%Sn still had a coarse and dendritic structure, but the dendrites were longer and well defined.

Rajab and Osama (2014) examined the influence of additions of Al and Ti on performance of leaded brass alloys (CuZn39Pb3). Mechanical properties such as compression strength and hardness of the specimens prepared were determined using compression testing machine and micro-Vickers hardness tester respectively.

The microstructure of the specimens was analyzed using Optical emission spectrometer (OES) and light optical microscope (LOM). The results of the study revealed that addition of Al and Ti modified the microstructure of the alloy and hence increased the compression strength and hardness of the alloy. Maximum compression strength of 103.92KN was obtained at 0.31%wtAl addition while maximum hardness and minimum grain size of 54.10HV and 8.38μm respectively were obtained at 0.54wt% Al addition.

Shufeng *et al.* (2011) investigated the effect of titanium (Ti) addition on microstructures and mechanical properties of Cu40Zn brass using powder metallurgy method. Titanium metal powder was added in concentration of 0.5 and 1wt% and prepared by water atomization process. The alloy powders were solidified at 1053K for 600s by spark plasma sintering (SPS) and extruded subsequently. The results of the study revealed that Cu_2ZnTi intermetallic compound and CuZnTi metastable phase resulted from the reaction between Ti and CuZn showed distinct grain refinement effect of titanium on extruded Cu40Zn brass. The mechanical tests conducted indicated maximum yield strength and ultimate tensile strength of 345MPa and 597MPa respectively, which were about 65.9% and 30.4% higher than that of extruded Cu40Zn brass, respectively.

Haruhiko *et al.* (2010) examined the microstructure and mechanical properties of high strength brass alloy with some elements (Sn, Fe and Cr). This study was

conducted with a view to develop a high strength α-β brass (Cu-40Zn) with additions of elements of small solid solubility in brass. Cu-40Zn with 0.6 wt%Sn, 0.73wt%Cr and 0.51 wt% Fe were prepared by casting. The results of the study indicated an increase in the area ratio of β-phase in the alloy structure. This caused a significant increase in hardness, percentage elongation, yield and ultimate tensile strength of the extruded Cu-40Zn-CrFeSn alloy.

A comparative study of microstructure and mechanical properties between friction stir welded single and double phase brass alloys was examined by (Heidarzadeh and Saeid, 2016). The microstructure of the joints was examined using optical microscope, scanning electron microscope (SEM), scanning transmission electron microscope (STEM), and X-ray diffraction. Furthermore, tensile test and fractography were applied to evaluate the mechanical properties of the joints. The results showed that the grain size of the stir zone in the double phase joint was smaller than that of the single phase alloy. In comparison with base metals, both of the joints contained high density of dislocations with a qualitatively similar texture. However, the dislocation density of the double phase joint was somewhat lower than that of the single phase one. Moreover, the joints had higher tensile strength, lower elongation and less ductile fracture compared to their base metals due to their finer grain size and higher dislocation density. The double phase joint had higher strength and lower elongation than single phase joint due to the effect of the second phase.

Youxiong *et al.* (2014) investigated the effect of iron addition on the microstructure and mechanical properties of Cu–Sn–Zn alloy. The specimens were casted, machined to required dimensions for the mechanical tests and aged at 500^{o}C for 4 hours. Results obtained from the study revealed that the hardness, percentage elongation, yield and ultimate tensile strength increased significantly. The precipitates responsible for the strengthening were identified as bcc Fe with diameters ranging from 20 to 60nm, and the interfacial relationship between the precipitate and copper matrix was $(002)_m/(110)_p$.

Sampath (2006) investigated the grain refining effect of small addition of zirconium (Zr) and titanium (Ti) on the shape-memory effect characteristics and mechanical properties of Cu-Zn-Al alloy with trace amount of aluminium. This study was carried out to produce copper based alloy which will exhibit either high stress recovery or high strain recovery. These properties will widen its use as sensors and actuators in most engineering and medical applications. The results of the study indicated that by very small additions of Zr and Ti to a Cu-Zn-Al shape-memory effect with a low Al content, the shape-recovery strain was increased to as high as 8%. The alloy also exhibited higher hardness and ductility after grain refinement.

The mechanical and corrosion behaviour of iron modified Cu-Zn-Al alloys was investigated by (Kenneth *et al.*, 2013). Cu-Zn-Al alloys containing 20 and 25

wt. % Zn was produced by casting method with and without the addition of 0.1wt% iron. The alloys were subjected to a homogenization at temperature of 800°C for 4 hrs and quenched in water. The quenched specimens were cold-rolled (10%, approximately), annealed at 500^{o}C for two hours and cooled in air. Mechanical properties such as tensile test, fracture toughness and hardness were determined. The samples were also subjected to corrosion test and microstructural analysis. The following conclusions were drawn from the results of the study:

1. Addition of iron modified the structures of the Cu-Zn-Al alloys with near equiaxed grain morphologies developed.
2. The tensile strength, strain to fracture, and fracture toughness of the alloys improved with iron addition.
3. There was no significant difference in the hardness of the iron modified and the unmodified Cu-Zn-Al alloys.
4. The Cu-Zn-Al alloys exhibited good corrosion resistance in 3.5wt%NaCl and 0.3M H_2SO_4 solutions.
5. Cu-20Zn-4Al-xFe was better than Cu-25Zn-4Al-xFe in terms of mechanical properties and corrosion resistance.

The effects of the repeated stress-induced transformation (pseudoelastic fatigue) on the mechanical behaviour and microstructure of Cu–Zn–Al and Cu–Al–Ni

single crystals were studied by (Sade *et al.,* 2007). The following conclusions were drawn from the study:

1. Several microstructural changes occurred during cycling at temperatures above the martensitic transformation temperature M_s in Cu–Zn–Al alloys.

2. Bulk defects consisting of dislocation bands with retained martensite and intrusion–extrusion types of surface defects were observed.

3. The fine characteristics of the defects, such as nucleation and density etc., depended on the working temperature, alloy composition, applied stresses and number of cycles.

4. The presence of defects altered the shape of the stress–strain curves in the pseudoelastic range for Cu–Zn–Al.

5. The diffusive phenomena strongly affect the mechanical behaviour of these alloys both in the parent and martensite phases, slightly above room temperature.

6. The diffusional processes depended on the density of bulk defects.

A study on the stabilization of a Cu-Zn-Al shape memory alloy under stress was carried out by Benchiheub *et al.* (2000). The influence of tensile stresses coupled with temperature cycling was determined on a Cu-Zn-Al shape memory alloy that transformed above room temperature. Results obtained indicated that the application of increasing stresses during thermal cycles caused increased martensite stabilization. The repeated thermal cycling with constant stress as

well as slow temperature rates increased the stabilization. This phenomenon was attributed to a pinning of austenite-martensite interfaces by vacancies. This hypothesis was confirmed by the comparison of experiments with continuous and with stepwise temperature variations.

Ovat *et al.* (2012) examined the influence of addition of aluminium and manganese in different proportions on the mechanical properties of brass. Aluminium and manganese were added individually to the pure red brass in the concentration range of 1-10wt%. Standard specimen preparation methods were employed and the mechanical properties such as tensile strength, impact strength and hardness were determined using Mosanto tensometer and Izod testing machines. Results obtained indicated that the mechanical properties of brass improved when aluminium and manganese concentrations increased to 5%. Further increase in concentration of the elements caused a decrease in all the tested mechanical properties.

2.2.2 Effect of heat treatment parameters on the structure and mechanical properties of copper based alloys

The mechanical properties and shape memory capacity of thin sheets of three Cu-Zn-Al shape memory alloys were studied by Asanović and Delijić (2004).
In quenched specimens, martensitic structure as well as small quantity of α-phase or DO_3-phase was observed. During tensile testing of quenched specimens at room temperature, the stress plateau was observed. The

deformation in the plateau region occurred in the range of 2.6 to 3.6% and disappeared during heating of quenched and deformed specimens above A_f temperature.

Nestorović *et al.* (2003) investigated the effect of cold rolling, annealing time and temperature on the microstructure, mechanical and electrical properties of cast Cu-Zn alloy containing 8wt%Zn. Pure copper and copper alloy (Cu-Zn) were subjected to cold rolling with a different final reduction of 30, 50 and 70%. The cold rolled copper and copper alloy samples were isochronally and isothermally annealed up to recrystallization temperature. Mechanical properties such as hardness and tensile strength were determined. Electrical conductivity and X-ray analysis were also performed. The following conclusions were drawn from the results of the study:

1. Addition of zinc had significant effect on the increase of the recrystallization temperature of the cold rolled copper alloy (Cu-8wt%Zn).

2. The annealing hardening effect of the alloy studied was attained, under recrystallization temperature in the temperature range of 180-300^{o}C, followed with an increase in hardness and electrical conductivity.

3. The amount of strengthening increased with increase in degree of prior cold work.

4. The annealing hardening effect was attained in the time range of 120-240^{o}C.

5. Change of lattice parameter was revealed during annealing when annealing hardening effect was attained.

Harun *et al.* (2012) investigated the microstructure of rapidly and slowly cooled Cu-Zn-Ni alloy subjected under mechanical deformation. The alloy (Cu-12.44wt%Zn-4.75wt%Ni) samples were prepared by vacuum induction melting under an argon atmosphere. The surface morphology of the alloy studied was analyzed using scanning electron microscope (SEM) and X-ray diffractometer (XRD). The thermal energy changes in the alloy were also examined using differential scanning calorimetry (DSC). The scanning electron microscopy analysis revealed annealing twins structures in rapidly and slowly cooled samples. Studies by Harun *et al.* (2012) indicated the disappearance of the existing annealing twins in the rapidly and slowly cooled samples, thereby causing the formation of slip planes lying parallel to each other in between plates in the cold rolled samples. The stress-strain behaviour was associated with applied heat treatment effect on the samples. It was also indicated that the intensities of XRD peaks and density defects decreased and increased respectively with increase in cooling rate of the Cu-Zn-Ni alloy.

The microstructure and mechanical properties of ultra fine grained Cu-Zn and Cu-Al alloys produced by cryorolling and annealing were investigated by Sarma *et al.* (2008). The results of the study revealed that ultrafine grained microstructures with very fine annealing twins were obtained after cryrolling

and annealing at 250°C for 15 min. The study of Young's modulus (*E*) variation with temperature revealed that *E* was lower (about ~15%) in the as-rolled condition and increased to the isotropic value after recrystallization. This variation was attributed to the crystallographic textures that were developed during rolling and recrystallization. The Cu–Al alloy exhibited much higher strength (600 MPa) with similar strain to fracture (0.26) in comparison to Cu–Zn alloy (355MPa). The higher strength of Cu–Al alloy was explained in terms of the higher contribution to solid solution strengthening of Al.

Celik *et al.* (2009) examined the stress-strain behaviour and microstructure of Cu-11.89wt%Zn-7.68wt%Sn alloy subjected under different cooling rate. The prepared samples were homogenized at temperature of 750^{o}C for 30 mins and rapidly cooled in iced-brine and slowly cooled in furnace. The surface morphology of the rapidly and slowly cooled samples was analyzed using scanning electron microscopy (SEM) and X-ray diffractometer (XRD). Mechanical property such as yield strength of the samples was also determined. The following conclusions were drawn from the results of the study:

1. Dendrite structures were revealed in the rapidly cooled sample, while dendrites together with annealing twins were indicated in the slowly cooled sample.

2. The XRD analysis result revealed two different phases such as α-Cu and α-CuSn in both rapidly and slowly cooled samples with more intense peaks on the slowly cooled samples.

3. The amount of α-Cu phase decreases, while that of α-CuSn phase increased with increase in cooling rate.

4. Significant increase in yield strength was indicated as the cooling rate increased after homogenization. This was attributed to the increase in defect density that resulted from rapid cooling.

X-ray diffraction effects given by the austenitic phase during the training process of shape-memory Cu-Zn-Al polycrystals were studied by Jourdan *et al.* (1997). To visualize the grain boundary role on the shape memory property of Cu-Zn-Al alloy, austenitic structure evolution of crystals was subjected to a training treatment by synchrotron X-ray topography in white beam. Single crystals, tri-crystals and polycrystalline samples were also studied. The comparison of results indicated that in polycrystalline samples, large and non recoverable stresses were developed in all grains. These stresses must be taken into account in discussing the origin of the shape memory property.

The effect of solid solutionizing Ti element on microstructure and mechanical properties of extruded Cu-40Zn-Ti ternary alloy was investigated by Haruhiko *et al.* (2011). Cu-40Zn with 0.5wt%Ti alloy ingot was prepared by sand casting

method. The microstructural analysis revealed that cast alloy structure consisted of α - β duplex phase and coarse Cu_2TiZn intermetallic compounds (IMCs) with 10-30μm diameters. The study by Haruhiko *et al.* (2011) indicated that the IMCs dissolved completely in the both α and β phases when solutionized at temperature of 973^{o}K for 15mins. The extruded specimen contained fine precipitates, having a mean particle size of 0.5μm diameter, which was dispersed in both phases. In particular, since the grain growth of α phase was inhibited by the pinning effect of the above fine precipitates at the grain boundaries, α phase consisted of fine grains. The extruded specimen consisted of remarkably fine and uniform α-β phases with an average grain size of 2.14μm. The tensile properties of the extruded specimen indicated an average value of yield strength; 304MPa, ultimate tensile strength; 543MPa, and 44% elongation. The extruded specimen revealed suitable strength and good ductility. The high strengthening mechanism of the wrought brass alloy was mainly due to the grain refinement of α and β phases derived from solid solutionizing Ti elements in the matrix.

Ketut *et al.* (2011b) investigated the effect annealing temperature on the structure of tin bronze (Cu-20%Sn). A simply supported beam model was used for measuring damping capacity. The results obtained showed that the microstructure of the alloy depended on annealing temperature. The logarithmic decrements of the alloys decreased with increase in annealing temperature. The

results of the study also revealed that the internal damping capacity of materials was characterized by the energy dissipation associated with microstructural defects such as grain boundaries, thermo elastic effect, dislocation motion in metals, and non uniform stresses. When the metal was under cyclic loading, phase interface slipping or grain boundary viscous sliding occurred, which resulted in the dissipation of the vibration energy. Since the vibration energy was dissipated, the damping capacity of the alloy increased. On the other hand, it was found that as the annealing temperatures increased; the grain size became larger, leading to reduction of the grain boundary area. The study revealed that the damping capacity increased due to the increase in annealing temperature and grain size. On the other hand, the impact strength and hardness of the materials increased and decreased respectively with increase in the annealing temperature.

Ilangovan and Sellamuthu (2013) studied the effects of tin on hardness, wear rate and coefficient of friction of cast Cu-Ni-Sn alloys. The investigation was carried out to understand the effects of Sn on hardness, wear rate and the coefficient of friction of spinodal Cu-Ni-Sn alloys. Alloys of appropriate compositions were melted in a crucible furnace under argon atmosphere and cast into sand moulds. Solution heat treated and aged specimens were tested for hardness, wear rate and the coefficient of friction. The results of the study revealed that hardness increased when the tin (Sn) content increased from 4% to 8% in the solution heat treated conditions. The peak aging time was

found to decrease with an increase in the Sn content. Further, the coefficient of friction was observed to be independent of hardness whereas the wear rate decreased linearly with hardness irrespective of Sn content.

Song *et al.* (2004) investigated the effects of reactive diffusion on stress evolution in Cu–Sn films. The results of the study showed that during isothermal ageing of Cu and Sn films, Cu_3Sn and Cu_6Sn_5 phases were formed due to the solid state diffusion process. It was also observed from the results of the study that after the complete consumption of the Sn film; only Cu_3Sn was found because Cu was much thicker than Sn. The tensile force was initially induced in the films and then a compressive force developed during the formation of Cu–Sn intermetallic compound. The initial tensile force was due to the inter-diffusion at the interface between Cu and Sn films, which led to the volume shrinkage in the films. On the other hand, the compressive force resulted from the dominant diffusion of Cu into Sn side, which caused the volume expansion in the films.

Eggenschwiler (2001) investigated the effect of addition of antimony (from 0 to 0.58%) on the structure, mechanical properties of a bearing bronze containing 80% copper, 10% tin, and 10%lead. The study revealed that increasing the antimony content from to 0.58% had no effect on the broaching properties and the distribution of the lead particles throughout the copper-tin matrix. There was a slight tendency toward an increased size of the areas of the hard delta

constituent with the higher antimony content. Additions of antimony lowered the impact strength value. The deformation under pounding was markedly lowered with the first addition of antimony, reaching a minimum at 0.2% antimony. Higher antimony additions tended to increase the deformation. The addition of antimony up to about 0.2% slightly increased the Brinell hardness of the alloy, but further addition of antimony, up to 0.58% caused little or no further change in hardness.

Martorano and Capocchi (2000) investigated the dendrite structure control in directionally solidified bronze castings. Tin bronze (Cu-8%Sn) was cast into cylindrical samples using a unidirectional solidification device monitored by thermocouple. Four cylindrical samples were obtained under four different experimental conditions were pouring temperature, heat extraction and addition of inoculants changed. Thermocouple temperature curve did not show any strong effect of inoculants additions, though, at the beginning of solidification, recalescence seemed to decrease with inoculants efficiency. Macrostructures of samples were examined on longitudinal sections and an increase in the columnar zone length was observed when the pouring temperature and heat extraction flux were raised simultaneously. Secondary and primary dendrite plates were seen to form from the coalescence of secondary dendrite arms.

Marcelo and Jose (2000) investigated the effects of processing variables on the micro-segregation of directionally cast samples of Cu-8 wt%Sn alloys. The

samples were previously obtained in four different experimental conditions, which brought about different types of dendritic growth. Each sample had a cylindrical shape and was sectioned into transversal slices whose degree of micro-segregation was measured by microprobe analyses and by quantitative metallography. A decrease in micro-segregation along the longitudinal axis toward the cast sample surface was observed. This behavior was simulated by using a comprehensive micro-segregation mathematical model and detailed thermal history of samples. Columnar and equiaxed regions of cylindrical samples were seen to have different levels of micro-segregation, which might be the result of differences in interdendritic distances (ID). It was also noticed that solute profiles calculated by a mathematical model and those obtained by microprobe analyses showed a better agreement if local dendrite arm spacing was considered in the calculations rather than an average spacing.

Kexing *et al.* (2013) studied crystallization under pressure processing of Cu-10Sn-4Ni-3Pb alloy in a bid to improving the wear resistance, segregation and mechanical properties of the alloy. The wear-resistant tin bronze (Cu-10Sn-4Ni-3Pb) with tin content above 8 wt.% prepared by traditional melting and casting process usually has defects such as low density, poor properties and segregations. The microstructures were observed and analyzed and compared with that by traditional melting and casting process. The results showed that the dendrite has obviously disappeared and the dendritic segregation alleviated by

using the crystallization under 680MPa pressure process, in comparison with the remarkably dendrite microstructure and severe as-cast defects of alloy prepared by traditional melting and casting technology. Based on the experimental study, the properties and microstructures of Cu-10Sn-4Ni-3Pb tin bronze prepared by crystallization under pressure have been improved significantly.

Kumoto *et al.* (2002) investigated the micro-segregation and dendrite arm coarsening in tin bronze. Specimens of the peritectic alloy Cu-10%Sn were subjected to various cooling rates typically observed in industrial casting processes. Some of the specimens were quenched immediately after the end of solidification to avoid further solute homogenization of the dendrite structure during cooling to room temperature. Characterization of specimens was carried out by measuring the distribution of secondary arm spacings and two micro-segregation indices, namely the volume fraction of non-equilibrium phase and the segregation deviation parameter, calculated from a large number of microanalyses at random points.

The following conclusions were made from the result of the study:

1. For Cu-10%Sn alloys, secondary dendrite arm spacing γ_2 decreased with increase in cooling rate or decreasing local solidification time.

2. Greater tin contents in the alloy caused a decrease in secondary dendrite arm spacing in specimens subjected to similar cooling rates.

3. The secondary dendrite arm spacing calculated by Kirkwood's model is eight times as great as the experimental value for some specimens of Cu-10%Sn alloy, whereas that derived from Mortensen's model is only twice as great.

4. Any individual spacing between two secondary arms is usually shorter than ~1.5 times the average spacing in the specimen.

5. The standard deviation of the normalized distribution of secondary arm spacing decreases with an increase in local solidification time.

6. The majority of specimens quenched in water immediately after solidification present micro-segregation indices greater than those measured in non-quenched specimens subjected to the same solidification cooling rate.

7. In non-quenched specimens of Cu-10%Sn alloys there is a tendency of increasing micro-segregation degree with an increase in the solidification cooling rate.

8. In the lower tin region, combined profiles present a negative curvature not observed in results from micro-segregation models based on average secondary arm spacing.

Zhang *et al.* (2003) studied the mechanical properties and tribological behaviour of a cast heat resisting copper base alloy. A block on ring tester and a pin on disk friction tester were used to measure the friction and wear properties at ambient temperature under the condition of lubricated friction and at 500^{o}C under the condition of non lubricated friction, respectively. The block and pin

samples were made of the copper alloys. The ring and disk were made of quenched GCr15 steel with a hardness of HRC 55. The test load was 500N at ambient temperature and 50N at 500°C. The corresponding test pressures were not less than 18MPa and 7.8MPa respectively. The lubricant was commonly used engine oil. The duration in the friction and wear tests was 60 mins in lubricated condition and 10 mins in non lubricated condition. The friction and wear properties of the alloy were equivalent to those of C95500 under the condition of boundary lubrication at ambient temperature, but the wear resistance of the alloy was much better than that of C95500 under the non lubricated condition, both at ambient and elevated temperatures. The wear rate of the alloy at ambient and elevated temperature was about 1/6 and 1/40 of that of C95500, respectively.

The analysis of hard spots in manganese bronzes was the subject to a later research from the University of Illinois by Weins *et al.* (1973). It was reported that the nature of the particle was determined to be dendritic and it was concluded that these particles were precipitated from the liquid itself well before the solidification started. In addition, the particles were found to be rich in manganese, aluminum, iron and silicon. The issue of hard spots was studied more elaborately in Germany as explained in the review by Bohlinger *et al.* (1998). In this review, various hard spots reported in the literature were

catalogued and discussed. Possible steps to be undertaken to reduce hard spot formation were presented.

Uyime *et al.* (2012) studied the effect of heat treatment on the structure and mechanical properties of locally produced aluminium-bronze alloy. Sand casting was used in the production of a dual-phase aluminium bronze alloy with pre-selected composition of 11% Al content. The selected heat treatments were solution heat treatment, normalizing, and ageing. The results showed that normalizing gave the optimum mix of tested mechanical properties with ultimate tensile strength in the range of 325 MPa, elongation of around 60% and Rockwell hardness values of 46.5 - 63.7 HRc, making this alloy suitable as alternatives to steel in low/medium strength structural applications.

Górny *et al.* (2013) investigated the effect of solution heat treatment on the structure and mechanical properties of calcium carbide-modified CuAl10Fe4Ni4 alloy. The result of the study showed that the highest values of Rm were obtained in low-temperature annealing (350°C) but at the cost of plastic properties (A, Z) and at a relatively high hardness. On the other hand, the application of high-temperature annealing (700°C) during toughening leads to the, so-called, bethatision, i.e. obtaining at room temperature a partially transformed β phase at the expense of a brittle γ_2 phase, which enables obtaining much higher plastic properties at lower values of Rm and HBW. Quite notable was the increase of $Rp_{0,2}$ after this heat treatment as compared to as-cast state.

Differences in the properties of alloys unmodified and after variant modification are relatively small with respect to Rm in as-cast state, but with clear improvement in the value of $Rp_{0,2}$ for alloy modified with the additions of Ca + C and CaC_2.

Jinquan *et al.* (2010) studied the effect of heat treatment on microstructure of Cu-Al alloys under 1GPa. The Cu-Al alloy was heat treated at 750°C for 15 minutes under 1GPa. The microstructure of the alloy before and after heat treatment was examined using optical microscope, SEM/EDS and XRD and the micro-hardness of the alloy was also determined. The results showed that heat treatment under 1GPa refined the microstructure; however, it showed little effect on composition of phases and hardness. The microstructure analysis revealed white strip-like area (α phase) and black area (Al_4Cu_9 and $AlCu_3$ phase). The alloy structure consists of α phase, minor Al_4Cu_9 phase and $AlCu_3$ phase. The α-phase is Cu-based solid solution with cubic structure, Al_4Cu_9 phase and $AlCu_3$ phase are cubic and rhombic respectively. XRD results showed that the diffraction peaks of α phase, Al_4Cu_9 phase and $AlCu_3$ phase changed after heat treatment under 1GPa, but no new phase was formed.

Praveen and Prabhash (2013) investigated the effect of solutionizing and ageing temperature on the structure and mechanical properties (ultimate tensile strength, compressive strength and strain) of nickel-aluminium bronze. The solutionizing temperatures employed were 850^{o}C and 900^{o}C for duration of 30

minutes, 60 minutes, 90 minutes and 120 minutes respectively. Similarly, ageing was carried out at 300^{o}C and 500^{o}C for the duration of 120 minutes and 180 minutes respectively. The heat treated samples were subjected to water quenching in order to bring them to ambient temperature. The tensile and compressive strength and ductility of the alloy were determined in different conditions.

The following observations and conclusion were made from the results of the study:

1. The tensile stress increased with strain. The rate of increase in stress was high initially. This was followed by a lower rate of increase in stress with strain, attainment of maximum stress and specimen fracture.

2. The heat treated alloy attained superior tensile strength and elongation as compared to that in the as-cast condition.

3. The aged samples attained higher hardness and tensile strength than those of the solutionized specimens while their elongation tended to follow a reverse trend.

4. During compression loading, higher stress was recorded with increasing strain prior to specimen failure. In this case, the rate of increase in stress was high initially. This was followed by a reduction in the rate of increase in stress and ultimately specimen fracture.

5. The compressive strength of the heat treated alloy samples was somewhat less than that of the as-cast alloy while the aged samples attained higher strength compared to that of the solutionized ones.

6. Maximum reduction in height was obtained on the as-cast alloy specimen.

7. The study showed that it was possible to obtain desired combinations of properties through optimizing the heat treatment type and parameters.

Mechanical characterization of aluminium bronze-iron granules composite was investigated by Sekunowo *et al.* (2013). Cast samples of the composite made from metal mould contain varied amount of iron from 2-10 wt%. The samples were homogenized at 1100^{o}C for 10 minutes in order to relief the as-cast structures. Standard specimens were prepared from these homogenized samples for tensile, charpy impact and micro-hardness tests while the microstructures of the alloy were examined using an optical microscope. The obtained results showed that optimum improved mechanical properties were achieved at 4 wt.% millscale addition with ultimate tensile strength (UTS) of 643.8MPa which represents 10.1% improvement over conventional aluminium bronze. The composite also demonstrated impact resilience of 83.9J and micro-hardness value of 88.7HRB. Millscale presence in the aluminium bronze system induced a stable reinforcing kappa phase by nucleation mechanism which resulted to enhancement of mechanical properties. However, the composite properties were impaired on millscale addition above 4wt% due to grain clustering.

Influence of heat treatment on microstructure and hardness of nickel aluminium bronze (Cu-10Al-5Ni-5Fe) was studied by Prabhash and Praveen (2013). The specimens were solutionized at 850^{o}C and 900^{o}C for 30 minutes, 60 minutes, 90 minutes and 120 minutes. Similarly, the specimens were aged at 300^{o}C and 500^{o}C for 120 minutes and 180 minutes. The heat treated samples were quenched in water. The results showed that the hardness of the alloy increased after the solutionizing and ageing treatments compared to the as cast one. Also, the samples aged at 400^{o}C for 3 hrs attained the highest hardness.

Tribological investigation of aluminium bronze made by centrifugal casting process was studied by Naman (2014). Castings were produced at two different pouring temperatures 1150 °C and 1250 °C and with three different mould rotation speeds 1050 RPM, 1150 RPM and 1250 RPM. Results showed that wear, wear rate and co-efficient of friction increased with increase in amount of the applied load. It was also observed from the results that aluminium bronze produced at pouring temperature 1250 °C and 1250 RPM had minimum wear and wear rate for each applied load and aluminum bronze at 1250 °C pouring temperature and 1250 RPM had better wear resistive property, compared to 1150 °C pouring temperature.

Abdul and Praven (2013) studied the influence of heat treatment on microstructure and mechanical properties of aluminium bronze. The

investigation dealt with the study relating the response of aluminium bronze (Cu-Al-Fe alloy) under the condition of changing heat treatment parameters and type. Solutionizing and ageing heat treatment were employed in this investigation. The solution treatment was carried out at two temperatures (850^{o}C and 900^{o}C) for 0.5, 1, 1.5 and 2 hrs respectively. Similarly, ageing was carried out at 300^{o}C, 400^{o}C and 500^{o}C for 2 and 3 hrs respectively. The heat treated samples were subjected to water quenching in order to bring them to ambient temperature. The results showed that as-cast specimens showed granular structure consisting of primary α, eutectoid $\alpha+\gamma_2$ and Fe rich phase. Solutionizing heat treatment led to the microstructural homogenization by way of the elimination of the dendrite structure and dissolution of the eutectoid phase and other microconstituents to form the single phase structure consisting of β. This was followed by the formation of the β' martensite, retained β and α. Ageing brought about the transformation of the martensite and other microconstituents into the eutectoid phase. The specimens that were solutionized at 850^{o}C for 2 hrs obtained the highest hardness in the category of solutionized specimens while ageing at 300^{o}C for 2 hrs offered maximum hardness amongst the aged specimens. The as-cast specimens obtained the highest compressive strength and strain followed by that of the heat treated specimens while the trend reversed as far as their tensile properties are concerned.

Mustafa (2009) studied the investigation of wear behaviors of C95200 and C95300 Cu-Al-Fe alloys. The study examined dry friction properties of the wear behaviors of the manufactured aluminium bronzes by using pin on disk type wear test device. In his study, alloys were produced by sand casting C95200 and C95300 aluminium bronzes norms. These tests were conducted on two different alloys, in the sliding velocities 1, 1.5 and 2 m/s, with four different loads (25, 37.5, 50 and 62.5 N) and four different sliding distance (500, 1,000, 2,000 and 4,000 m). Wearing specimens tested for hardness and investigated in order to spectral electron microscope photographs. The results obtained showed that grain size and coefficient of friction of C95200 were higher than that of C95300 alloy. Furthermore, C95300 alloys were harder than C95200 because of more aluminium contents. It was also observed from the study that the wear rate increased with load, sliding velocity and distance.

The effects of production methods on the microstructures and mechanical properties of aluminum bronze were studied by Kaplan and Yildiz (2003). The solidification structure, the effects of solution treatment, tempering heat treatment and mold types on the microstructure of the aluminium bronze produced in two different molds were examined. The results showed that the heat treatments have some interesting effects on the mechanical properties, microstructures and phase transformation temperatures of the samples. According to the results of the experiment, the metallographic structure of the

aluminium bronze material was heterogeneous in the preheated die casting specimen before the treatments, but homogenous in the sand casting. It was observed that the structure of the sand mould casting contains fine rounded grains along outermost cross section and lengthwise inclined column grains towards inside and big grains innermost. Considering such grain structure, it was suggested that die mould before casting should be preheated up to 450–500°C to remove the negative effects of heterogeneous solidification structure on the use of the material for technological purposes.

Yuting *et al.* (2015) studied the effect of heat treatment on the microstructure and micro hardness of nickel aluminium bronze. The alloy was prepared using friction stir processing (FSP) technique at a tool rotation of 1200 rpm and a traverse speed of 150 mm/min. A post heat treatment was performed at temperature of 675^{o}C. The results of the study showed that the alloy produced consists of high density dislocations, retained β-phase (β^{1}-phase) and recrystallized grains. When annealed at 675^{o}C, discontinuous static recrystallization took place. The content of β^{1}-phase gradually decreased and fine κ-phase precipitated out. After annealing for 2 hours, both the micro hardness of the FSP samples in the stir zone (SZ) and the difference in hardness between the SZ and the base metal decreased, due to the reduction of the dislocation density and β^{1}-phase accompanying recrystallized grain coarsening.

With further increasing of the annealing time to 4 hours, the aforementioned difference in hardness disappeared.

Peter *et al*. (2014) examined the influence of heat treatment (annealing, quenching and ageing) on the microstructure and mechanical properties of pressed bars made from the CuAl10Ni5Fe4 alloy. The microstructures were observed in light and scanning electron microscopes. The appearance and area fractions of the α and κ-phases and their influence on the mechanical properties were examined. Using DSC and EBSD methods, the presence of the γ_2 phase was monitored, as it is a very hard and brittle phase that impairs the material's corrosion resistance.

The following observations and conclusions were made from the results of the study:

1. The structure of the rapidly cooled specimens was fine consisting of α-phase grains and the α+ κ eutectoid.

2. The structure of the annealed specimens consists of α grains and coarse eutectoid regions with κ_{III}-type precipitates.

3. Maximum hardness was obtained by quenching and ageing at 400°C. This was attributed to the dispersion of fine particles of κ in the martensitic (β') phase.

4. The hardness of the the alloy studied was attributed to the proportion of the very hard γ_2 phase in the β-phase.

5. Upon annealing, with subsequent air cooling, the fraction of γ_2 increased which resulted to the increased hardness of the alloy.

6. The structural analysis revealed light grains of the phase α, grey to light-blue globular particles of the phase κ_{II} and the dark eutectoid α+ κ_{III}.

7. In the as-received state, α grain size was very small: 1 μm to 2 μm.

8. Increasing the annealing temperature led to the increase in the size of α grains and the size of the eutectoid areas between them.

9. Slow cooling in the furnace led to coarsening of the κ precipitates and to the formation of larger amounts of lamellar κ_{III} precipitates in the eutectoid. The phase κ also precipitates along the α grain boundaries.

10. The hardness of the alloy studied decreased with increase in α grain size.

11. Lowest hardness and percentage elongation were obtained in specimens annealed at 850°C with slow cooling rate. This was attributed to κ precipitating more frequently at the α-phase grain boundaries.

12. Rapid cooling leads to a higher proportion of the eutectoid at the expense of the α-phase proportion. In addition, a certain fraction of β- phase was retained in the microstructure (more dark areas in the eutectoid).

Li *et al.* (2009) investigated the microstructure and properties of high-conductivity, super-high-strength Cu-8.0Ni-1.8Si-0.6Sn-0.15Mg alloy. The cast samples were subjected to solution treatment at 970^{o}C for 4 hr, cold rolled to 60% reduction and aged at 500^{o}C for 30 minutes. Results obtained indicated that both the hardness and electrical conductivity increased rapidly with ageing

time up to 30minutes. Maximum hardness, average tensile strength, 0.2% proof strength, elongation and average electrical conductivity of 345Hv, 1180MPa, 795MPa, 2.75%, and 26.5% International Annealed Copper Standard (IACS) respectively were obtained at ageing time of 30mins.

Huang *et al.* (2003) examined the precipitation in Cu-Ni-Si-Zn alloy for lead frame. The samples were solution-treated at 900^{o}C for 2 hrs and quenched in water. Some of the quenched samples were cold rolled prior to ageing treatment while some were not cold rolled. The two-step ageing with and without intermediate cold rolling was carried out at 500 and 450^{o}C for different times (0.5, 1, 8, 10, 16hrs etc.). Results obtained revealed maximum hardness value of 250Hv after cold rolling to 78% and ageing at 450^{o}C for 1 hrs. The conductivity of the specimen increased with ageing time with value of 31%IACS (International Annealed Copper Standard) at 0.5 hrs ageing time. Maximum hardness and electrical conductivity of 240Hv and 24.5%IACS were obtained by the specimen aged at 450^{o}C for 10 hrs and 0.5 hrs respectively without prior cold rolling.

The effect of aluminium on the microstructure and properties of Cu-Ni-Si alloys was investigated by Lei *et al.* (2013). The cast samples were homogenized at 940^{o}C for 4 hrs, hot rolled to 80% at 850^{o}C and solution heat-treated at 970^{o}C for 4 hr. Subsequently, the specimens were cold rolled by 50% and aged at 450^{o}C for 60 minutes. Results obtained indicated that Cu-6wt%Ni-1.4wt%Si-

0.15wt%Mg-0.1wt%Cr alloy obtained maximum hardness, electrical conductivity, tensile strength and percentage elongation of 338 HV, 28.5% IACS, 1040MPa and 3.5% respectively while Cu-6wt%Ni-1wt%Si-0.5wt%Al-0.15wt%Mg-0.1wt%Cr alloy obtained maximum hardness, electrical conductivity, tensile strength and percentage elongation of 343 HV, 28.1% IACS, 1080MPa and 3.1% respectively.

2.3 Summary of reviewed related literature

From the literature reviewed, it was evidenced that limited researches had been carried out on the structure and mechanical properties of silicon bronze. Among all the copper based alloys, silicon bronze has not been explored.

Mattern *et al.* (2007) investigated the influence of silicon content and rapid quenching on the phase formation of Cu–Si alloys. The study indicated different meta-stable phases on the quenched samples which was dependent on the chemical composition. It was also noted that high temperature phases such as η, σ and κ were preserved at room temperature. The formation of the room temperature phase ε was suppressed by rapid quenching from the melt. Ketut *et al.* (2011a) investigated the effect of silicon content on the mechanical and acoustical properties of silicon bronze alloys for musical instruments. The results of the study indicated that the mechanical properties and damping capacity of Cu-xSi were higher than Cu-20wt.%Sn bronze alloys. Puathawee *et al.* (2013) investigated the effect of silicon and tin addition on the

microstructure and microhardness of Cu-Si-Zn alloy. The results obtained indicated that the hardness of 60Cu-0.5Si-39.5Zn brass was 123.4 Hv. It was also noted that the hardness value of the alloy studied increased with increase in silicon content. Moreover, the addition of tin together with silicon increased amount of beta (β) phase and more uniform dispersive gamma (γ) phase than those of the silicon addition alone.

Microstructure and microhardness of precipitation hardened Cu-Ti and precipitation/dispersion hardened Cu-Ti-Si alloys were examined by Božića *et al.* (2008). The obtained results indicated that the rapidly solidified Cu-1.2Ti-3$TiSi_2$ powder microstructure was characterized by the presence of fine, dispersed primary $TiSi_2$ particles and high super saturated solid solution. It was also noted that the microstructure of the studied alloys was not completely homogenous but rather exhibited the presence of the homogenous fluctuations in the range of 5–10μm. Cu-1.2Ti-3$TiSi_2$ powder yielded much higher microhardness values compared with the Cu-1.2Ti powder, owing to primary $TiSi_2$ dispersoides formed during atomization. The study also revealed that high strengthening of the Cu-Ti-$TiSi_2$ powder was achieved by ageing as a consequence of the simultaneous influence of the following factors: The development of the nodular structure, the precipitation of metastable Cu_4Ti and the presence of primary $TiSi_2$ dispersed phase particles. Obtaining the full density compacts by hot isostatic pressing was possible only at higher temperatures where the maximum strengthening value was achieved. It was

concluded that the lower microhardness values of compacts compared to atomized powders achieved by ageing was as a result of stable Cu_4Ti-phase presence in their structure.

2.4 Knowledge gaps

The following knowledge gaps were established from the reviewed literature.

1. Mattern *et al.* (2007) suppressed the room temperature (ε) phase of silicon bronze which is detrimental to the ductility, ultimate tensile strength, hardness and impact strength of the alloy by rapid quenching thereby improving only the ultimate tensile strength and hardness of the alloy. This research was aimed at decreasing, refining and modifying the room temperature (ε) phase of silicon bronze through alloying thereby improving not only the ultimate tensile strength and hardness of the alloy but also the ductility and impact strength

2. Ketut *et al.* (2011a) reported the moderate tensile strength and hardness of silicon bronze of 7wt% silicon concentration with corresponding low ductility and impact strength. This research was aimed at developing silicon bronze of improved tensile strength and hardness without the expense of good ductility and impact strength.

3. Puathawee *et al.* (2013) developed silicon bronze (Cu-0.5wt%Si-39.5wt%Zn) of hardness value of 123.4Mpa which is very low for engineering application. This research was aimed at improving the hardness probably by increasing the silicon content to 3wt% and reducing the zinc content to 3wt%.

4. Božića *et al.* (2008) reported the incomplete homogenization of primary dendritic silicon in Cu-1.2Ti-3TiSi alloy. According to the study, complete homogenization was achieved by ageing heat treatment. Therefore, this research was carried out to achieving complete homogenization of the primary dendritic silicon structure by increasing the titanium content to 2wt% which is more cost effective than ageing heat treatment.

5. Li *et al.* (2009), Huang *et al.* (2003) and Lei *et al.* (2013) employed rolling and subsequent ageing heat treatment to improve only the ultimate tensile strength and hardness of various silicon bronzes with moderate electrical conductivity and very low ductility. This research was carried out to improving both the ultimate tensile strength and hardness of silicon bronze with corresponding excellent electrical conductivity and ductility through the process of alloying and solution heat treatment which is more cost effective than the process adopted by other researchers.

Above all, the effect of other elements such as tin, magnesium, manganese, tungsten, molybdenum and aluminium on the structural modification, physical and mechanical properties of silicon bronze has not been investigated. Hence, this research was carried out to study the effect of dopants and heat treatment parameters on the structure, physical and mechanical properties of silicon bronze (Cu-3wt%Si).

CHAPTER THREE

MATERIALS AND METHOD

3.1 Materials and equipment

The copper and silicon used as the base materials for this research were 99.99 and 99.98% pure respectively. The dopants were added in concentrations of 0.1, 0.2, 0.3, 0.4, 0.5, 0.6, 0.7, 0.8, 0.9, 1, 1.5, 2, 3 and 5% by weight. The choice of these alloying elements and concentrations was informed by earlier researches by Mattern *et al.* (2007); Ketut *et al.* (2011a); Puathawee *et al.* (2013); Božića *et al.* (2008). Other materials used were aluminium oxide powder; for polishing and solution of 10g of iron (III) chloride, $30cm^3$ of HCl and $120cm^3$ of water; for etching. Equipment used for this research were bailout crucible furnace, electronic compact scale (Model: BL20001), hack saw, vice, lathe machine, muffle heat treatment furnace (Model: 5336RB), emery paper of grits sizes, Bosch PHG500-2-1600W hot air gun machine, optical metallurgical microscope (Model: L2003A), digital camera, scanning electron microscopy (SEM) (Model: LEO-430i) equipped with energy dispersive spectroscopy (EDS) (Model: LINK-ISIS-300), pendulum impact testing machine (Model: U1820), portable dynamic hardness testing machine (Model: DHT-6), 100KN JPL tensile strength tester (Model: 130812), voltmeter, ammeter, rheostat and 5V DC motor.

3.2 Materials sourcing

Copper and aluminium used for this research were procured from Cutix Cable Plc Nnewi, Anambra State, Nigeria. Silicon, zinc, tin and magnesium were obtained from Guangznou Jinhuada chemical reagent Co., Ltd., China while manganese, titanium, tungsten and molybdenum powder were supplied by Kermel chemical reagent Co., Ltd. Hebei, Tianjin, China. These materials were manufactured by Guangdong Guangnua Science and Technology Company Ltd., China and supplied by Nwazico laboratory Nigeria Ltd., Onitsha, Anambra State, Nigeria.

3.3 Mould preparation

The mould was prepared by creating a cylindrical hole of dimension 250mm in length and 16mm in diameter as presented in Figure 3.1 in a thick steel plate using a drilling machine according to British standards; BS EN ISO 6892-1:2016, BS EN ISO 6505-1:2014, and BS EN ISO 148-1:2016 for tensile, hardness and impact strength samples respectively. The thick steel plate was split into two parts at the centre. The dome and pin were inserted on the surface of the two split die mould for easy coupling of the mould and removal of the casting.

Figure 3.1: Mould for casting

3.4 Experimental design

The experiment was designed using statistical analysis of variance (design expert- DX10). The actual and coded values of the independent variables and the design layout of the experiment are tabulated in Tables 3.1 and 3.2 respectively.

Table 3.1: Actual and Coded values of the independent variables

Variable	Actual value		Code value	
	Low level	High level	Low level	High level
Dopant concentration (wt%)	0.1	5	- 1	+1

Table 3.2: Design layout (Actual)

Std	Run	Factor 1 A:Dopant wt%	Response 1 %E %	Response 2 UTS MPa	Response 3 Hardness MPa	Response 4 Impact Strength J	Response 5 Electrical resistivity $10^{-3}\Omega m$	Response 6 Electrical conductivity S/m
12	1	0.1	-	-	-	-	-	-
8	2	0.2	-	-	-	-	-	-
13	3	0.3	-	-	-	-	-	-
5	4	0.4	-	-	-	-	-	-
4	5	0.5	-	-	-	-	-	-
9	6	0.6	-	-	-	-	-	-
6	7	0.7	-	-	-	-	-	-
7	8	0.8	-	-	-	-	-	-
1	9	1	-	-	-	-	-	-
11	10	1.5	-	-	-	-	-	-
10	11	2	-	-	-	-	-	-
3	12	3	-	-	-	-	-	-
2	13	5	-	-	-	-	-	-

3.5 Alloy compositions and materials preparation

The alloys studied in this research were Cu-(1-5)wt%Si, Cu-3wt%Si-Zn, Cu-3wt%Si-Sn, Cu-3wt%Si-Mg, Cu-3wt%Si-Mn, Cu-3wt%Si-W, Cu-3wt%Si-Ti, Cu-3wt%Si-Mo and Cu-3wt%Si-Al. The required amounts of the materials for developing these alloys were calculated using weight percent calculation. The weight of each material (in grams) was measured using an electronic compact scale (Model: BL20001) as presented in Figure 3.2a and b.

a **b**

Figure 3.2: (a) Materials and (b) weighing of materials

3.6 Melting and casting of the studied alloys

For the control alloy sample (Cu-3wt%Si), 1000g of copper was charged into the preheated bailout crucible furnace and heated until melting was achieved. Thereafter, 31g of pure silicon powder wrapped in an aluminium foil was introduced into the melt and stirred vigorously to achieve homogeneity. The mixture was left for 10 minutes to achieve a complete dissolution of the silicon metal and stirred again. The prepared permanent mould was preheated at temperature of 200^{o}C. The melt was poured into the preheated permanent mould

and allowed to cool to ambient temperature as presented in Figure 3.3a, b and c. The remaining alloys were developed by repeating the same procedure and doping the alloy with dopants in concentrations of 0.1, 0.2, 0.3, 0.4, 0.5, 0.6, 0.7, 0.8, 1, 1.5, 2, 3 and 5wt%, cast and stored for machining.

a **b** **c**

Figure 3.3: (a) Melting of materials, (b and c) Casting of samples

3.7 Machining of the developed alloys

The developed alloys samples were machined to the required dimension according to the British Standards; BS EN ISO 6892-1:2016, BS EN ISO 6505-1:2014, and BS EN ISO 148-1:2016 for tensile strength, brinell hardness and charpy impact strength tests respectively using lathe machine at Delta State Polytechnic, Ogwashi-uku as presented in Figure 3.4a and b. The tensile test samples were machined to 120mm in length and 10mm in diameter with a gauge diameter and length of 8mm and 50mm respectively. The samples for impact strength test were machined to 55mm x 10mm x 10mm in size with a 2mm deep notch ($\Delta 45^{o}$) inscribed at the centre of the sample using lathe machine while the hardness samples were machined to 20mm in length and

16mm in diameter. The machined samples were stored for structural, mechanical and physical properties investigations.

a **b**

Figure 3.4: (a) Machining of samples and (b) tensile, hardness and impact strength samples

3.8 Heat treatment of the developed alloys

The best alloys compositions in terms of improved mechanical properties were subjected to heat treatment at solutionizing temperature of 900^{o}C for 30 minutes and cooled in air. The choice of these heat treatment parameters was motivated by earlier research conducted by Obi *et al.* (2017). This treatment was carried out at Metallurgical Training Institute (MTI), Onitsha. The samples were charged into a muffle heat treatment furnace (Model: 5336RB), heated up to temperature of 900^{o}C and held for 30 minutes. After been held for 30 minutes at that temperature, the samples were removed from the furnace, cooled in air and stored for structural, mechanical and physical properties investigations.

3.9 Mechanical and physical properties of the developed alloys

3.9.1 Tensile strength test of the developed alloys

An automated 100KN JPL tensile strength tester (Model: 130812) presented in Figure 3.5 was used for determining the tensile strength of the developed alloys at Cutix Cable Plc, Nnewi, Anambra State, Nigeria according to British standard (BS EN ISO 6892-1:2016). The 100KN JPL tensile strength tester used has a control system which consists of reading scale (tensile load in Newton and extension in mm) and buttons (start, off, up and down buttons). The up button was pressed and the movable jaw moved up at a distance of 80mm from the fixed jaw. The test specimen was clamped at the jaws (fixed and movable) of the tensile strength testing machine. The load button (down button) was pressed and a tensile load of 100KN was applied on the specimen as the jaws separate apart until the test specimen fractured. The tensile load and extension at the point of fracture was read directly from the reading scale at the control system and recorded, after which the ultimate tensile strength and percentage elongation were calculated and the values were recorded.

a **b** **c**

Figure 3.5: (a) loading of the sample, (b) pressing of the loading button and (c, d) fractured samples

3.9.2 Hardness test of the developed alloys

The Brinell hardness test was conducted using a portable dynamic hardness testing machine (Model: DHT-6) at Delta State Polytechnic, Ogwashi-uku as presented in Figure 3.6 (a & b) using British standard (BS EN ISO 6505-1:2014). The specimen was placed on an Equotip test block and the machine was operated automatically until the indenter touches the surface of the specimen. The value was read directly from the machine's scale and the result was recorded.

a **b**

Figure 3.6: (a) Brinell hardness test procedures and (b) Tested samples

3.9.3 Impact strength test of the developed alloys

The impact strength of the developed alloys was carried out at the Department of Mechanical Engineering, Delta State Polytechnic, Ogwashi-uku using a pendulum impact testing machine (Model: U1820) presented in Figure 3.7 using British standard (BS EN ISO 148-1:2016). The sample was placed horizontally between the anvils of the machine, separated at a distance of 55mm apart. A striking hammer was lifted to an angle of 270^{o} to the anvils of the machine and

released. The released striking hammer hit the specimen at the face opposite to the notch and breaks it. The reading in joule was taken on the machine's scale and recorded immediately.

Figure 3.7: Fractured impact strength samples

3.10 Calculated density of the developed alloys

The density of the developed alloys was measured using ASTM B777-15 standard. The mass in gram of the samples was measured using an electronic compact scale (Model: BL20001) and recorded. The volume of the sample was calculated using equation 3.1 and recorded. The density of the developed samples was calculated using equation 3.2.

$$\text{Volume} = L \times W \times H \quad (3.1)$$

Where L = length of the sample, W = width of the sample and H = height of the sample

$$\text{Density } (\rho) = \frac{\text{Mass of the sample (g)}}{\text{Volume of the sample } (\text{cm}^3)} \quad (3.2)$$

3.11 Electrical resistivity (ρ) and conductivity (σ) of the developed alloys

Standard Ohm's experiment as presented in Figure 3.8 was adopted in determining the electrical resistivity and conductivity of the developed alloys according to the study by Joseph *et al.* (2014). This was conducted at physics laboratory, St. Raphael secondary school, Awkuzu, Anambra State. The set-up is as presented in the circuit diagram shown in Figure 3.8. A 5 volts (DC) electrical power was supplied through the entire set up. The current and voltage or potential difference (P. d) across the specimens for 1, 2, 3, 4 and 5 minutes were read from the ammeter (A) and voltmeter (V) respectively and recorded. Average values were computed and recorded. The resistance (R) of the specimen to the flow of electricity was calculated from ohm's law as stated in equation 3.2:

$$R = \frac{V}{I} \tag{3.3}$$

where R = resistance (Ω), V = voltage passing through the specimen and I = current (in amperes) passing through the sample.

Resistivity (ρ) is calculated from the expression,

$$\rho = \frac{RA}{L} \tag{3.4}$$

$$A = L \times W \tag{3.5}$$

where ρ = resistivity (Ω-m); R = resistance of the specimen to the flow of electricity; A = cross-sectional area of the specimen in m^2, L = length of the specimen in m and W = width of the specimen in m.

The electrical conductivity (σ) which is the inverse of resistivity is also given as

$$\sigma = \frac{1}{\rho} \tag{3.6}$$

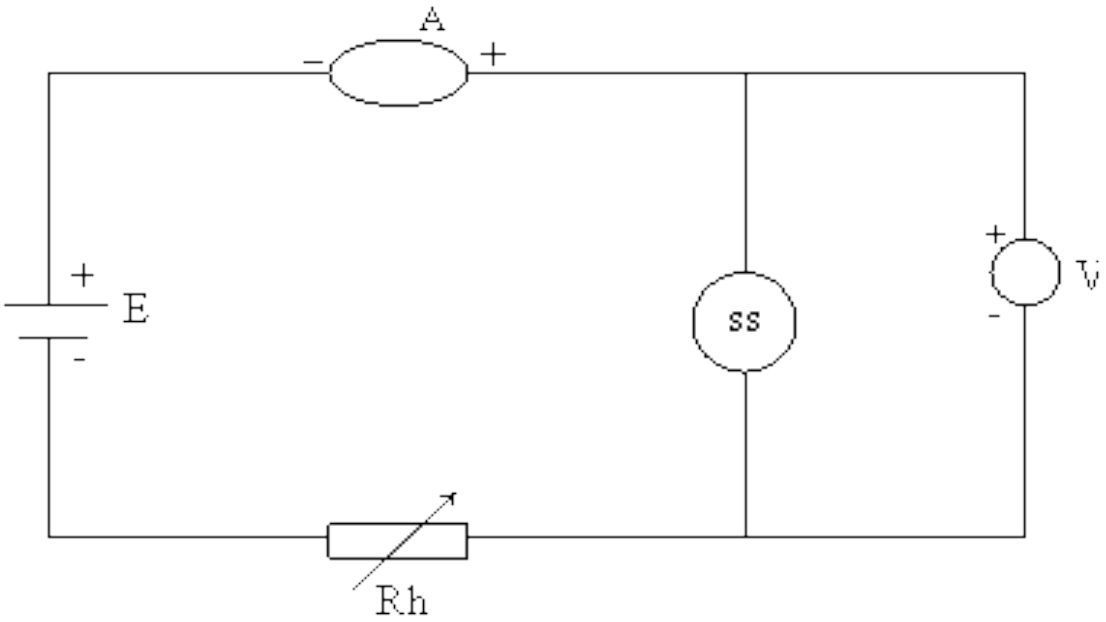

Figure 3.8: Circuit diagram of Ohm's experiment; A = ammeter; Rh = rheostat; ss = specimen, V = voltmeter and E = DC electric power (volt)

3.12 Structural analysis of the developed alloys

The structural analyses of the developed alloys were conducted using an optical metallurgical microscopy (Model: L2003A) and scanning electron microscopy (SEM) (Model: LEO-430i) equipped with energy dispersive spectroscopy (EDS) (Model: LINK-ISIS-300). These were carried out at Metallurgical Development Institute (MTI), Onitsha and Sheda Science and Technology,

Abuja. Prior to these analyses, the specimens were subjected to filing, grinding, polishing and etching as presented in Figure 3.9 a, b, c and d respectively. The filing was done using a rectangular file and an electric grinding machine, after which the specimens were subjected to grinding using an emery paper of grid sizes (400, 600, 800 and 1200μm). The ground specimens were polished to mirror finish using an aluminium oxide powder (gamma alumina, Al_2O_3), rinsed with water and dried using an air-gun drying machine as shown in Figure 3.9e. The specimens were subjected to etching by swabbing them to a mixture of 10g of iron (III) chloride, $30cm^3$ of hydrochloric acid and $120cm^3$ of water) for 60seconds, after which the surface morphology was examined using an optical metallurgical microscope and scanning electron microscopy (SEM) equipped with energy dispersive spectroscopy (EDS) at magnifications of x400 and x1500 respectively.

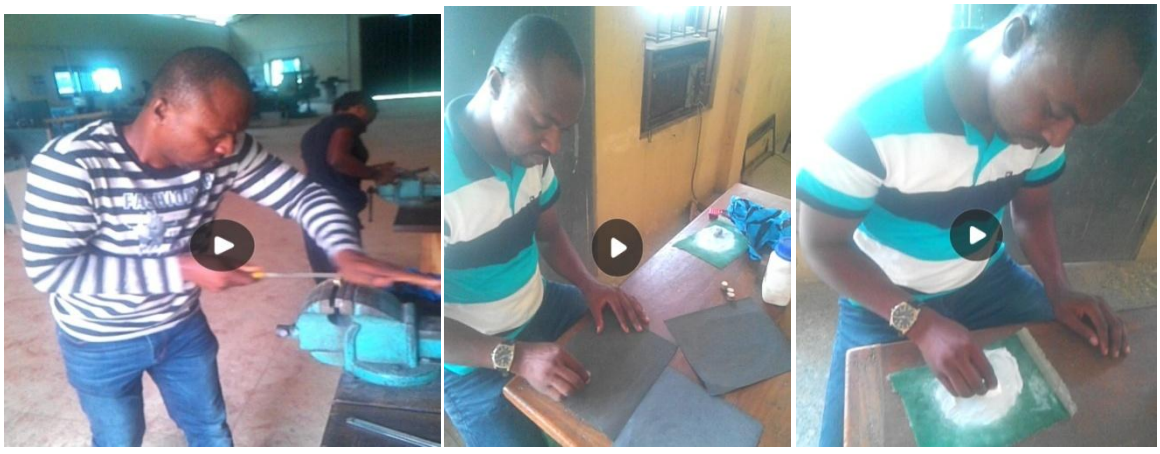

a **b** **c**

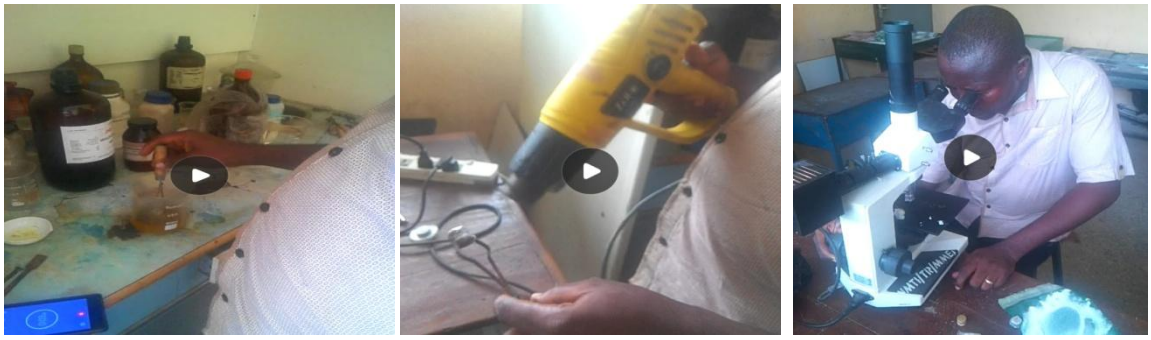

d **e** **f**

Figure 3.9: Sample preparation (a) Filling, (b) grinding, (c) polishing, (d) etching, (e) drying and (f) viewing

CHAPTER FOUR

RESULTS AND DISCUSSION

4.1 Mechanical and physical properties of the studied alloys

The effect of silicon content on the ultimate tensile strength (UTS) and percentage elongation of silicon bronze (Cu-Si) is presented in Table 4.1.

Table 4.1: Effect of silicon content on the ultimate tensile strength (UTS) and percentage elongation of silicon bronze (Cu-Si)

Alloy designation	Alloy composition	UTS (MPa)	%E
BZ_1	Cu -1wt%Si	25	11.0
BZ_2 (Control)	Cu -3wt%Si	34	9.4
BZ_3	Cu -5wt%Si	45	4.2

Figure 4.1 shows the percentage elongation of silicon bronze doped with different concentration of silicon. Figure 4.1 reveals that the percentage elongation of silicon bronze decreased with increase in concentration of silicon. A slight decrease in percentage elongation was noted as the concentration of silicon increased to 3wt%, after which a sharp decrease in percentage elongation was observed as the silicon content increased to 5wt%. This behaviour was as a

result of increase in size and number of the precipitated dendritic primary silicon in the alloy structure (Plate 4.3).

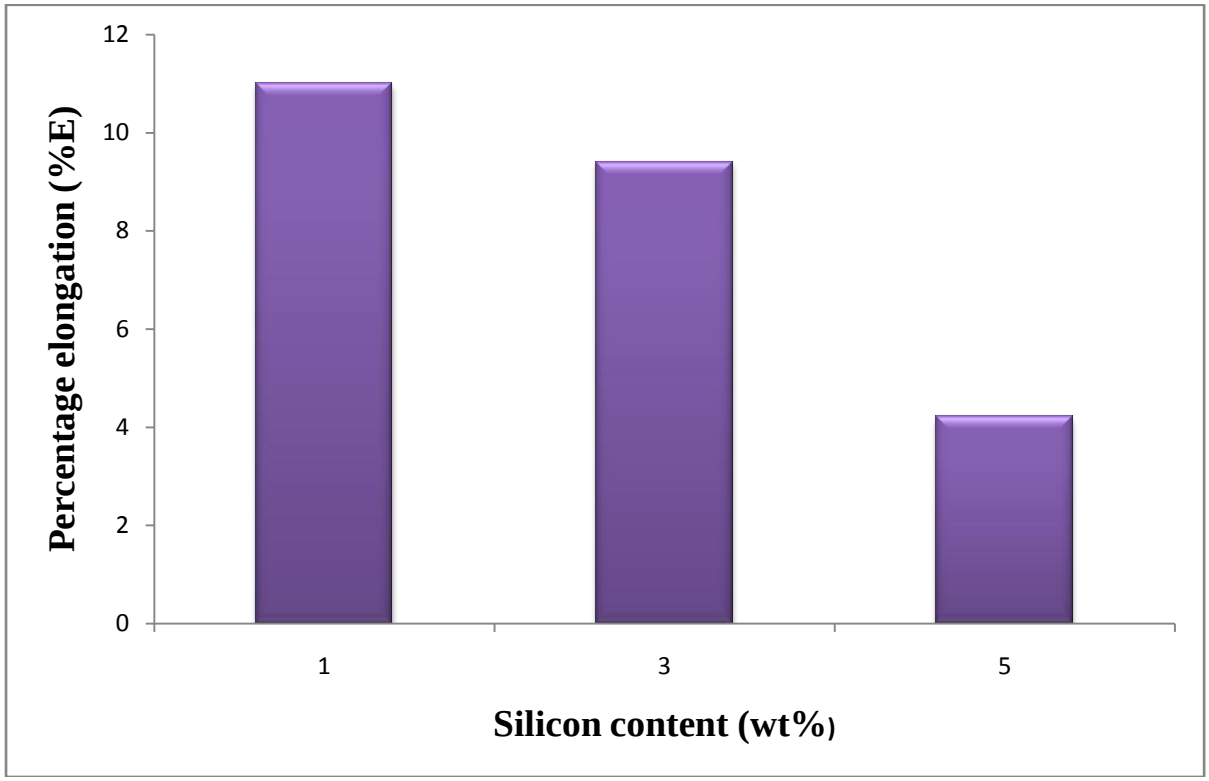

Figure 4.1 Effect of silicon content on the percentage elongation of silicon bronze

Figure 4.2 shows the ultimate tensile strength of silicon bronze doped with different concentration of silicon. Analysis of Figure 4.2 shows that the ultimate tensile strength of silicon bronze increased with increase in concentration of silicon. Maximum ultimate tensile strength was obtained at 5wt% silicon addition. This was achieved as a result of the obstruction of the dislocation motion by the precipitated intermetallic compound of copper silicide (Cu_3Si) in the alloy structure (Plate 4.3).

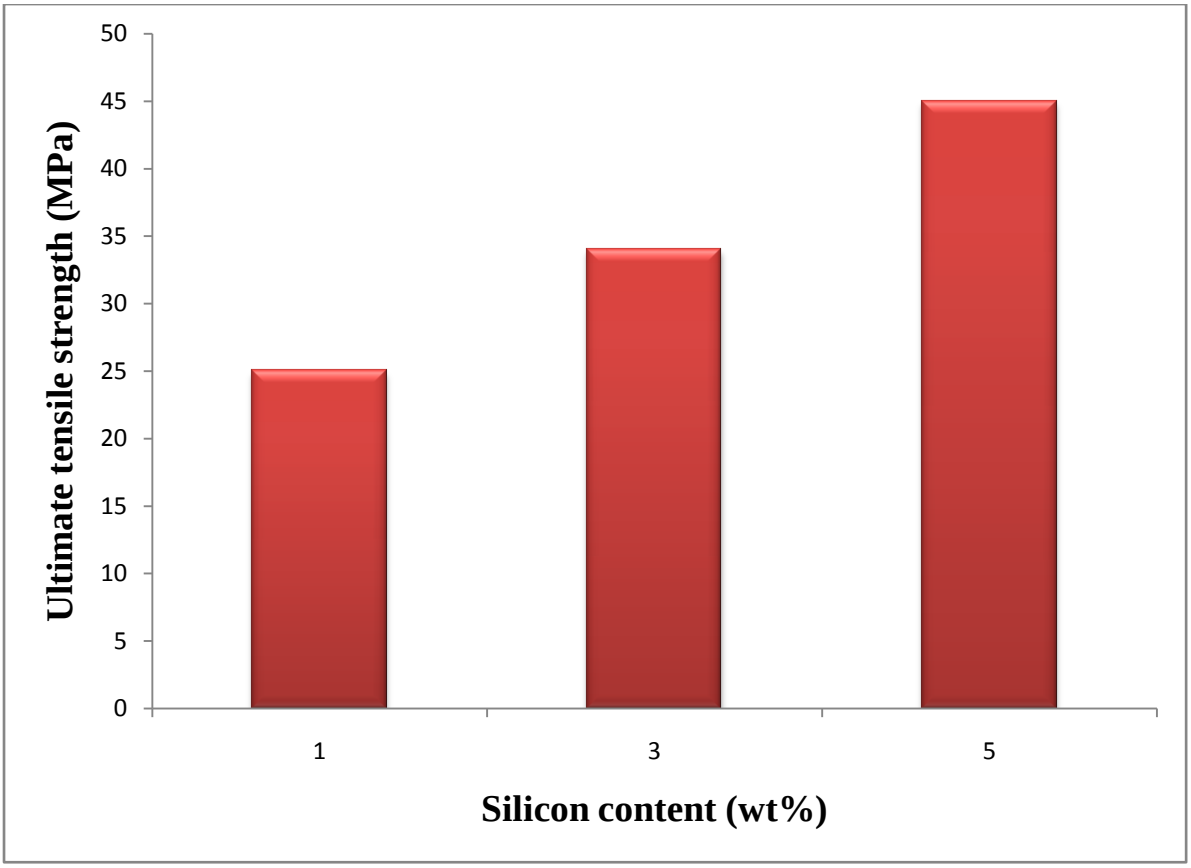

Figure 4.2: Effect of silicon content on the ultimate tensile strength of silicon bronze

The effect of silicon content on the hardness and impact strength of silicon bronze (Cu-Si) is presented in Table 4.2.

Table 4.2: Effect of silicon content on the hardness and impact strength of silicon bronze (Cu-Si)

Alloy designation	Alloy composition	Brinell hardness (MPa)	Impact strength (J)
BZ_1	Cu -1wt%Si	103	15.4
BZ_2	Cu -3wt%Si	180	13.2
BZ_3	Cu -5wt%Si	240	5.9

Figure 4.3 shows the brinell hardness of silicon bronze doped with different concentration of silicon. Figure 4.3 shows that the hardness value of the developed alloy increased as the concentration of silicon increased. Maximum

hardness value was obtained at 5wt% silicon addition (Figure 4.3). This was attributed to the increase in size and number of primary silicon in the alloy structure which impede the dislocation motion (Plate 4.3).

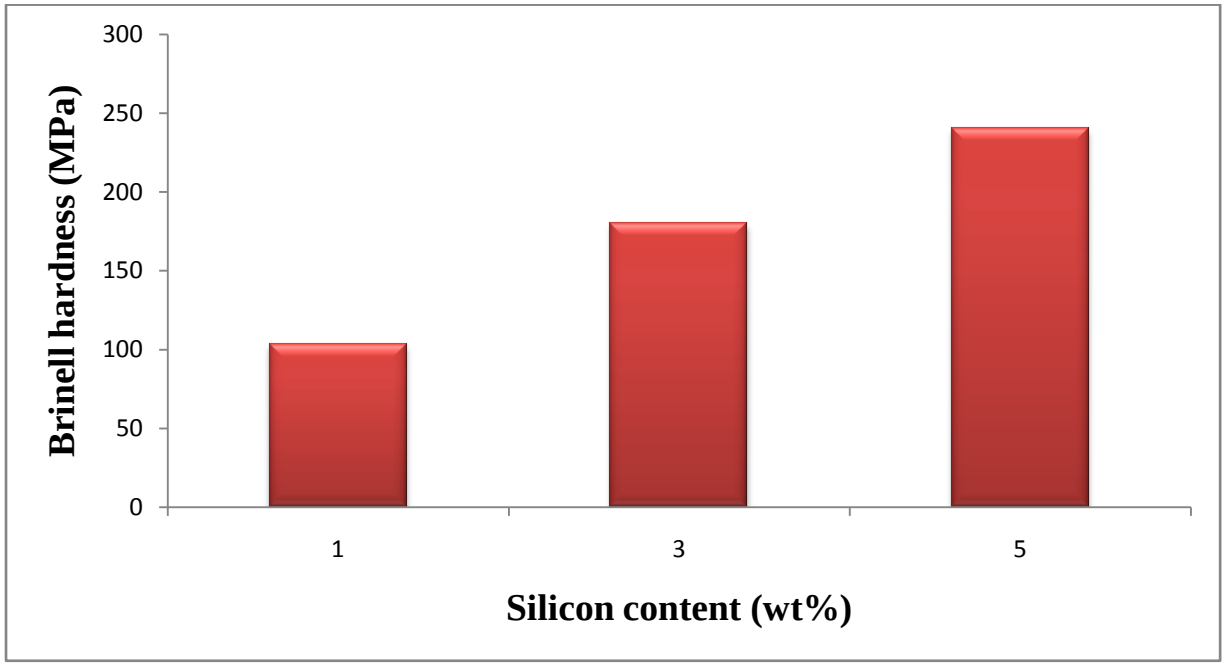

Figure 4.3: Effect of silicon content on the hardness of silicon bronze

The effect of silicon content on the impact strength of silicon bronze is presented in Figure 4.4. Analysis of Figure 4.4 indicates that the impact strength of silicon bronze decreased with increase in silicon concentration. Maximum impact strength value was obtained at 1wt% silicon addition (Figure 4.4). This could be as a result of the presence of primary silicon in the alloy structure (Plate 4.3).

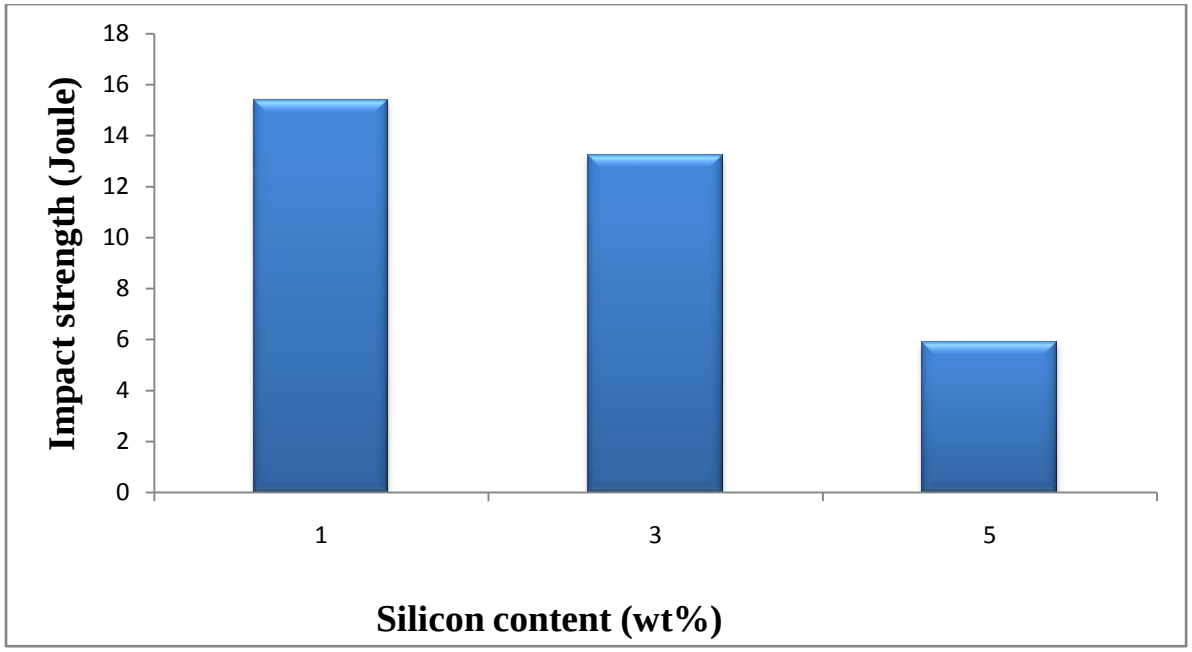

Figure 4.4: Effect of silicon content on the hardness of silicon bronze

Table 4.3 shows the effect of silicon content on the density (ρ), electrical resistivity (ρ) and electrical conductivity (σ) of silicon bronze (Cu-Si).

Table 4.3: Effect of silicon content on the density (ρ), electrical resistivity (ρ) and electrical conductivity (σ) of silicon bronze (Cu-Si)

Alloy designation	Alloy composition	ρ (g/cm^3)	ρ (x10^{-3}Ω-m)	σ(Sm^{-1})
BZ_1	Cu -1wt%Si	8.11	32.01	31.24
BZ_2	Cu -3wt%Si	8.21	37.20	26.88
BZ_3	Cu -5wt%Si	8.34	39.0	25.64

Figure 4.5 depicts the effect of silicon content on the density of silicon bronze. It was noted in Figure 4.5 that the density of silicon bronze increased with increase in silicon content. A sharp increase in density was noted as the silicon content increased to 5wt%.

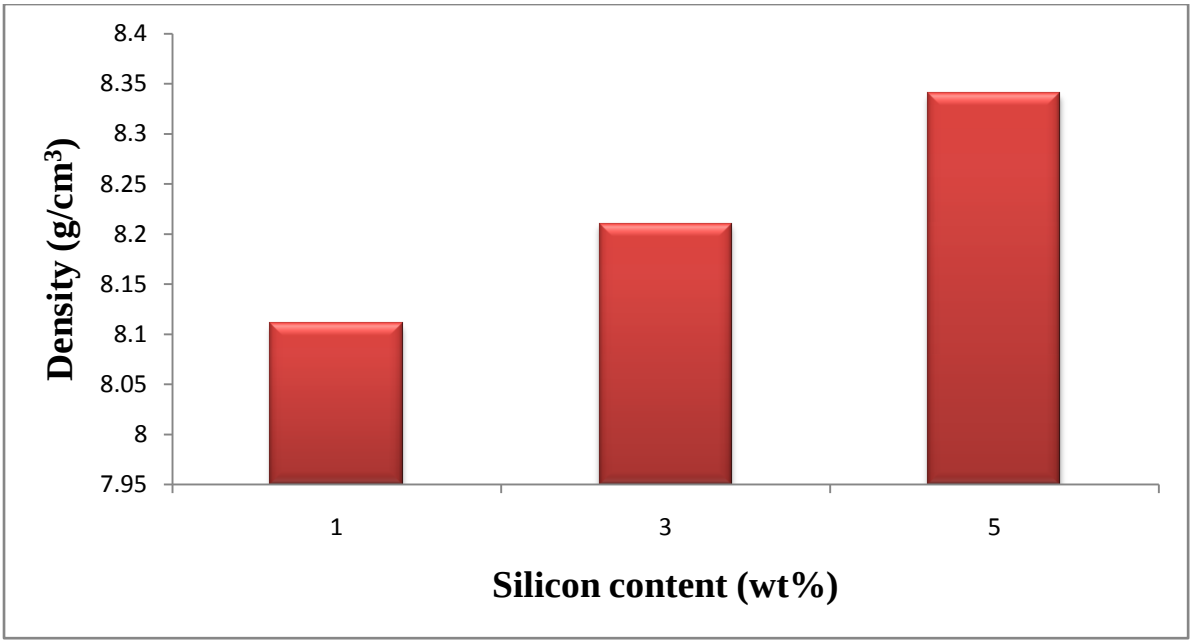

Figure 4.5: Effect of silicon content on the density of silicon bronze

The electrical resistivity (ρ) and conductivity (σ) of silicon bronze doped with different concentration of silicon are presented in Figures 4.6 and 4.7 respectively. A systematic increase in electrical resistivity and decrease in electrical conductivity were observed as the concentration of silicon increased. When silicon was added to copper, the predominant effect on ρ was caused by the scattering of electron on the irregularities of crystal lattice (Nnuka, 1994). Addition of silicon to copper metal increased the impurity level which led to increase in local scattering point (electron scattering) and hence increased the electrical resistivity of the alloy.

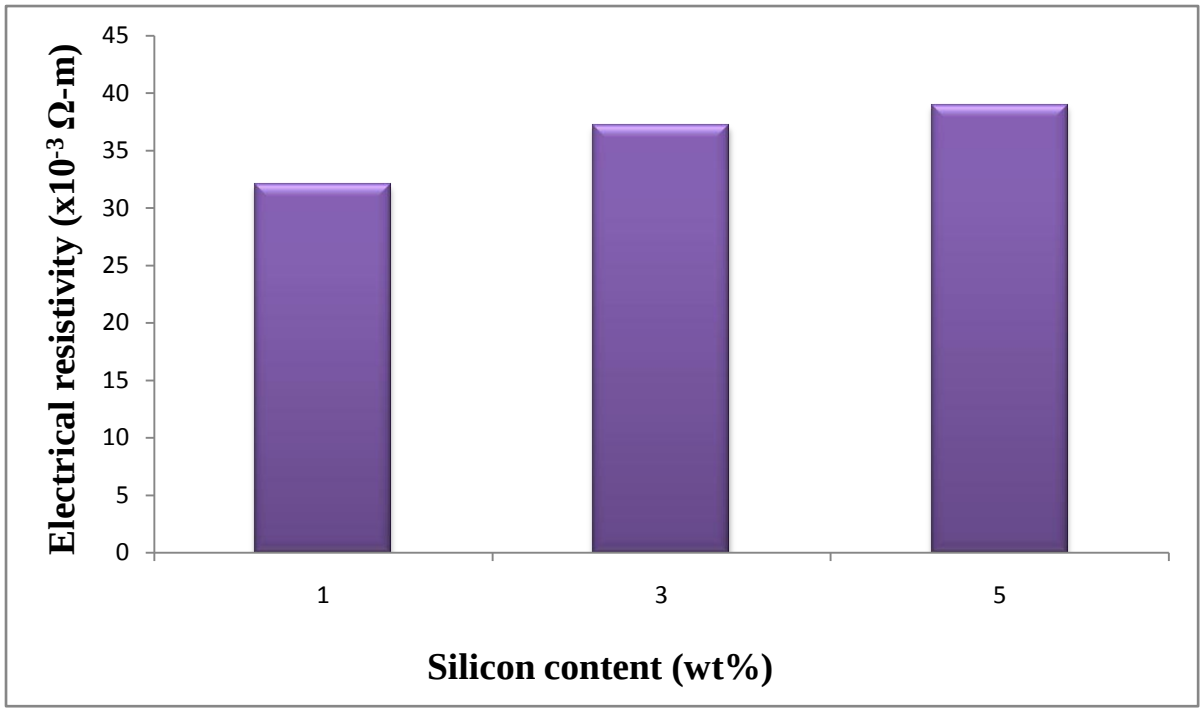

Figure 4.6: Effect of silicon content on the electrical resistivity of silicon bronze

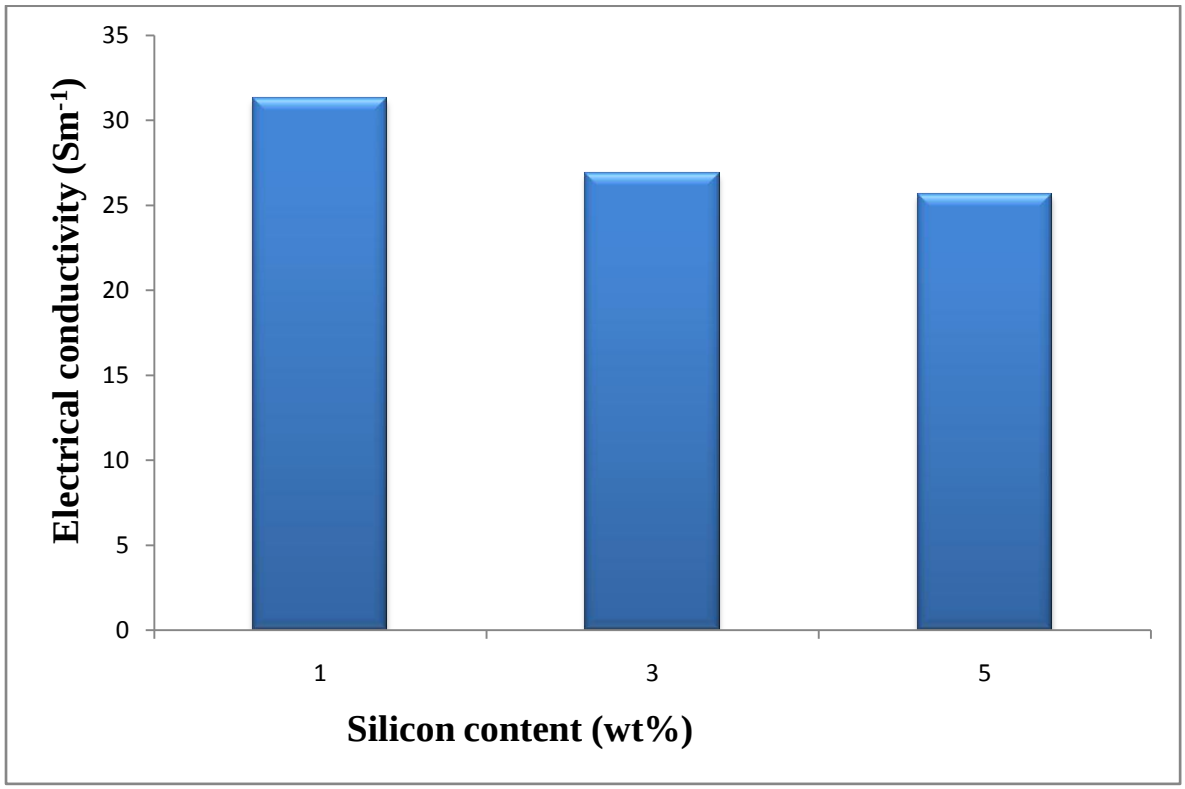

Figure 4.7: Effect of silicon content on the electrical conductivity of silicon bronze

Table 4.4 shows Effect of dopants on the ultimate tensile strength (UTS) and percentage elongation of silicon bronze (Cu-3wt%Si).

Table 4.4: Effect of dopants on the ultimate tensile strength (UTS) and percentage elongation of silicon bronze (Cu-3wt%Si).

Alloy designation	Alloy composition	UTS (MPa)	%E
BZ_4	Cu-3wt%Si-0.1wt%Zn	83	8.4
BZ_5	Cu-3wt%Si-0.2wt%Zn	90	9.8
BZ_6	Cu-3wt%Si-0.3wt%Zn	97	10.5
BZ_7	Cu-3wt%Si-0.4wt%Zn	102	11.4
BZ_8	Cu-3wt%Si-0.5wt%Zn	123	12.9
BZ_9	Cu-3wt%Si-0.6wt%Zn	154	13.5
BZ_{10}	Cu-3wt%Si-0.7wt%Zn	183	15.0
BZ_{11}	Cu-3wt%Si-0.8wt%Zn	200	16.2
BZ_{12}	Cu-3wt%Si-1.0wt%Zn	248	17.6
BZ_{13}	Cu-3wt%Si-1.5wt%Zn	320	15.8
BZ_{14}	Cu-3wt%Si-2wt%Zn	334	13.9
BZ_{15}	Cu-3wt%Si-3wt%Zn	353	11.4
BZ_{16}	Cu-3wt%Si-5wt%Zn	341	9.3
BZ_{17}	Cu-3wt%Si-0.1wt%Sn	104	26.4
BZ_{18}	Cu-3wt%Si-0.2wt%Sn	122	25.9
BZ_{19}	Cu-3wt%Si-0.3wt%Sn	130	25.1
BZ_{20}	Cu-3wt%Si-0.4wt%Sn	142	24.3
BZ_{21}	Cu-3wt%Si-0.5wt%Sn	154	23.4
BZ_{22}	Cu-3wt%Si-0.6wt%Sn	158	22.2
BZ_{23}	Cu-3wt%Si-0.7wt%Sn	164	21.0
BZ_{24}	Cu-3wt%Si-0.8wt%Sn	171	20.3
BZ_{25}	Cu-3wt%Si-1wt%Sn	173	19.5
BZ_{26}	Cu-3wt%Si-1.5wt%Sn	213	14.1
BZ_{27}	Cu-3wt%Si-2wt%Sn	220	12.8
BZ_{28}	Cu-3wt%Si-3wt%Sn	238	11.1
BZ_{29}	Cu-3wt%Si-5wt%Sn	231	9.4
BZ_{30}	Cu-3wt%Si-0.1wt%Mg	201	25.1
BZ_{31}	Cu-3wt%Si-0.2wt%Mg	215	24.0
BZ_{32}	Cu-3wt%Si-0.3wt%Mg	228	23.2
BZ_{33}	Cu-3wt%Si-0.4wt%Mg	231	22.7
BZ_{34}	Cu-3wt%Si-0.5wt%Mg	235	21.8
BZ_{35}	Cu-3wt%Si-0.6wt%Mg	240	21.3
BZ_{36}	Cu-3wt%Si-0.7wt%Mg	264	20.5

Alloy designation	Alloy composition	UTS (MPa)	%E
BZ_{37}	Cu-3wt%Si-0.8wt%Mg	285	19.1
BZ_{38}	Cu-3wt%Si-1wt%Mg	243	18.6
BZ_{39}	Cu-3wt%Si-1.5wt%Mg	238	17.2
BZ_{40}	Cu-3wt%Si-0.1wt%Mn	240	16.8
BZ_{41}	Cu-3wt%Si-0.2wt%Mn	258	14.3
BZ_{42}	Cu-3wt%Si-0.3wt%Mn	264	13.2
BZ_{43}	Cu-3wt%Si-0.4wt%Mn	270	11.8
BZ_{44}	Cu-3wt%Si-0.5wt%Mn	278	10.5
BZ_{45}	Cu-3wt%Si-0.6wt%Mn	312	9.8
BZ_{46}	Cu-3wt%Si-0.7wt%Mn	345	8.7
BZ_{47}	Cu-3wt%Si-0.8wt%Mn	363	7.4
BZ_{48}	Cu-3wt%Si-1wt%Mn	378	6.5
BZ_{49}	Cu-3wt%Si-1.5wt%Mn	367	4.8
BZ_{50}	Cu-3wt%Si-0.1wt%W	238	25.8
BZ_{51}	Cu-3wt%Si-0.2wt%W	242	25.1
BZ_{52}	Cu-3wt%Si-0.3wt%W	264	24.6
BZ_{53}	Cu-3wt%Si-0.4wt%W	268	23.4
BZ_{54}	Cu-3wt%Si-0.5wt%W	272	22.1
BZ_{55}	Cu-3wt%Si-0.6wt%W	278	21.9
BZ_{56}	Cu-3wt%Si-0.7wt%W	281	21.0
BZ_{57}	Cu-3wt%Si-0.8wt%W	286	20.8
BZ_{58}	Cu-3wt%Si-1wt%W	245	20.3
BZ_{59}	Cu-3wt%Si-1.5wt%W	241	19.4
BZ_{60}	Cu-3wt%Si-0.1wt%Ti	109	23.2
BZ_{61}	Cu-3wt%Si-0.2wt%Ti	120	22.4
BZ_{62}	Cu-3wt%Si-0.3wt%Ti	133	21.3
BZ_{63}	Cu-3wt%Si-0.4wt%Ti	159	20.1
BZ_{64}	Cu-3wt%Si-0.5wt%Ti	178	18.8
BZ_{65}	Cu-3wt%Si-0.6wt%Ti	203	14.2
BZ_{66}	Cu-3wt%Si-0.7wt%Ti	228	11.3
BZ_{67}	Cu-3wt%Si-0.8wt%Ti	234	10.4
BZ_{68}	Cu-3wt%Si-1wt%Ti	243	9.1
BZ_{69}	Cu-3wt%Si-1.5wt%Ti	258	8.5
BZ_{70}	Cu-3wt%Si-2wt%Ti	265	7.2
BZ_{71}	Cu-3wt%Si-3wt%Ti	261	6.0
BZ_{72}	Cu-3wt%Si-5wt%Ti	253	5.4
BZ_{73}	Cu-3wt%Si-0.1wt%Mo	43	18.4
BZ_{74}	Cu-3wt%Si-0.2wt%Mo	49	17.8
BZ_{75}	Cu-3wt%Si-0.3wt%Mo	51	17.3
BZ_{76}	Cu-3wt%Si-0.4wt%Mo	53	16.8
BZ_{77}	Cu-3wt%Si-0.5wt%Mo	58	16.4
BZ_{78}	Cu-3wt%Si-0.6wt%Mo	62	15.7

Alloy designation	Alloy composition	UTS (MPa)	%E
BZ_{79}	Cu-3wt%Si-0.7wt%Mo	67	15.3
BZ_{80}	Cu-3wt%Si-0.8wt%Mo	73	14.8
BZ_{81}	Cu-3wt%Si-1wt%Mo	98	14.1
BZ_{82}	Cu-3wt%Si-1.5wt%Mo	130	12.1
BZ_{83}	Cu-3wt%Si-2wt%Mo	125	10.8
BZ_{84}	Cu-3wt%Si-3wt%Mo	118	9.2
BZ_{85}	Cu-3wt%Si-5wt%Mo	107	8.4
BZ_{86}	Cu-3wt%Si-0.1wt%Al	104	28.0
BZ_{87}	Cu-3wt%Si-0.2wt%Al	118	22.2
BZ_{88}	Cu-3wt%Si-0.3wt%Al	138	20.8
BZ_{89}	Cu-3wt%Si-0.4wt%Al	152	15.4
BZ_{90}	Cu-3wt%Si-0.5wt%Al	174	13.7
BZ_{91}	Cu-3wt%Si-0.6wt%Al	187	12.2
BZ_{92}	Cu-3wt%Si-0.7wt%Al	198	11.4
BZ_{93}	Cu-3wt%Si-0.8wt%Al	206	10.2
BZ_{94}	Cu-3wt%Si-1wt%Al	224	9.0
BZ_{95}	Cu-3wt%Si-1.5wt%Al	268	7.8
BZ_{96}	Cu-3wt%Si-2wt%Al	283	6.4
BZ_{97}	Cu-3wt%Si-3wt%Al	314	5.1
BZ_{98}	Cu-3wt%Si-5wt%Al	312	4.3

Figure 4.8 shows the percentage elongation of silicon bronze doped with zinc, tin, magnesium, manganese, tungsten, titanium, molybdenum and aluminium. It was noted in Figure 4.8 that addition of the various alloying elements significantly improved the percentage elongation of silicon bronze. Zinc, manganese and molybdenum showed least effect on the percentage elongation of the studied alloy compared with other dopants (Figure 4.8). This could be attributed to their slight influence on the size of dendritic primary silicon.

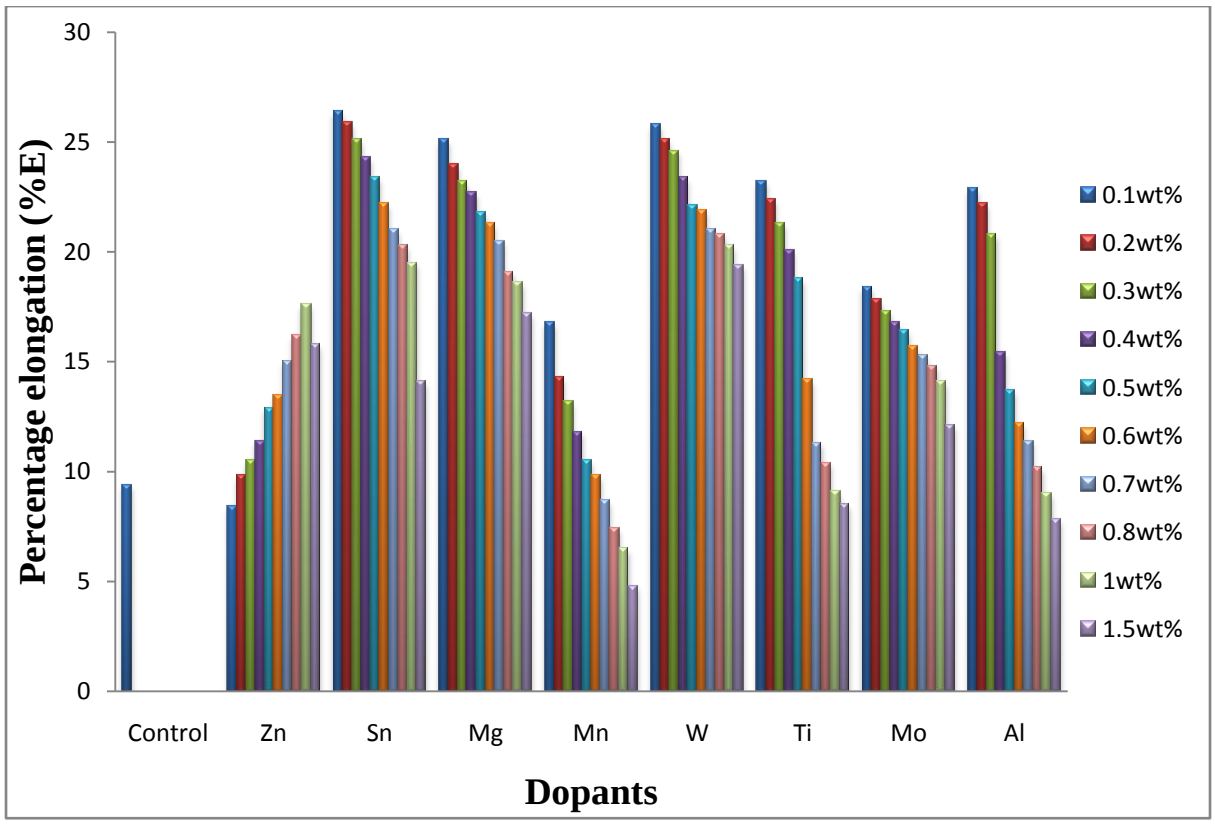

Figure 4.8: Effect of dopants on the percentage elongation of silicon bronze (Cu-3wt%Si)

Figures 4.9-4.16 show the effect of zinc, tin, magnesium, manganese, tungsten, titanium, molybdenum and aluminium contents on the percentage elongation of silicon bronze. Analysis of Figures 4.10-4.16 indicated a systematic decrease in percentage elongation as the concentration of Sn, Mg, Mn, W, Ti, Mo and Al increased. Addition of zinc to silicon bronze showed different effect on the percentage elongation. Analysis of Figure 4.9 shows that the percentage elongation of Cu-3wt%Si-Zn alloy increased as the concentration of zinc increased to 1% by weight. Further increase in zinc concentration resulted to decrease in percentage elongation. This could be attributed to the precipitation of β-phase in the alloy structure (Plate 4.10).

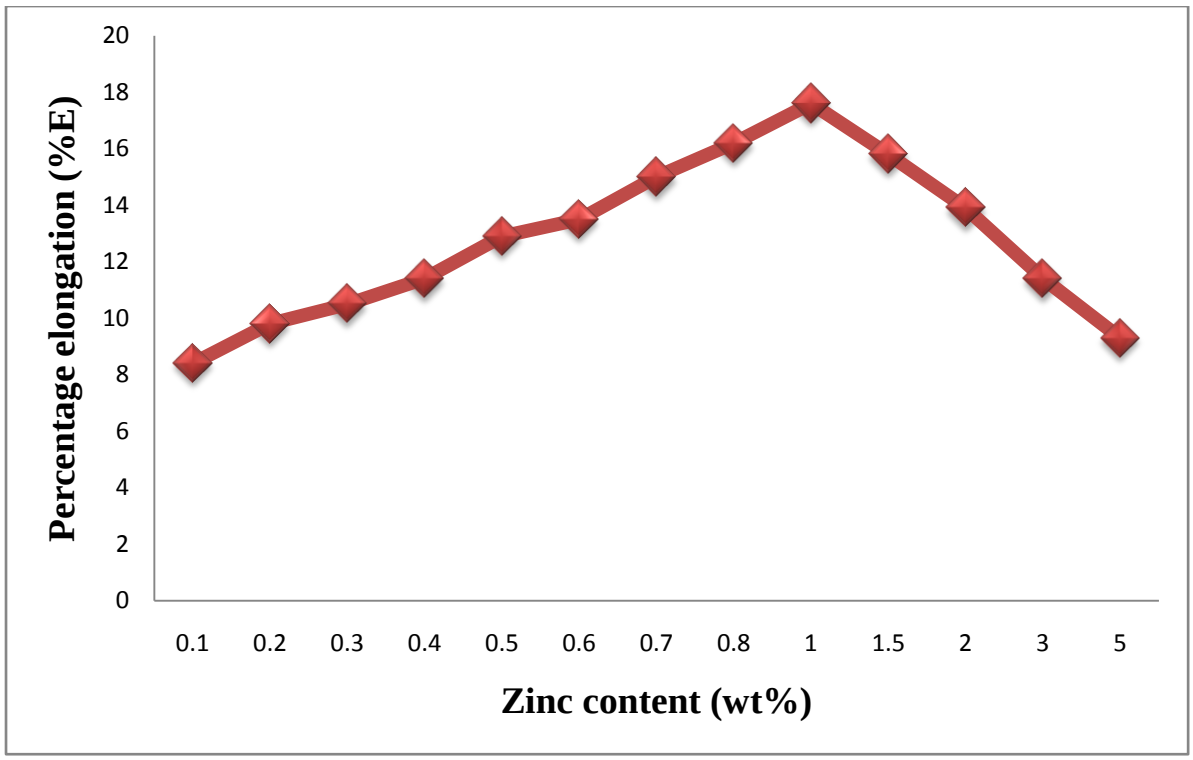

Figure 4.9: Effect of zinc content on the percentage elongation of silicon bronze (Cu-3wt%Si)

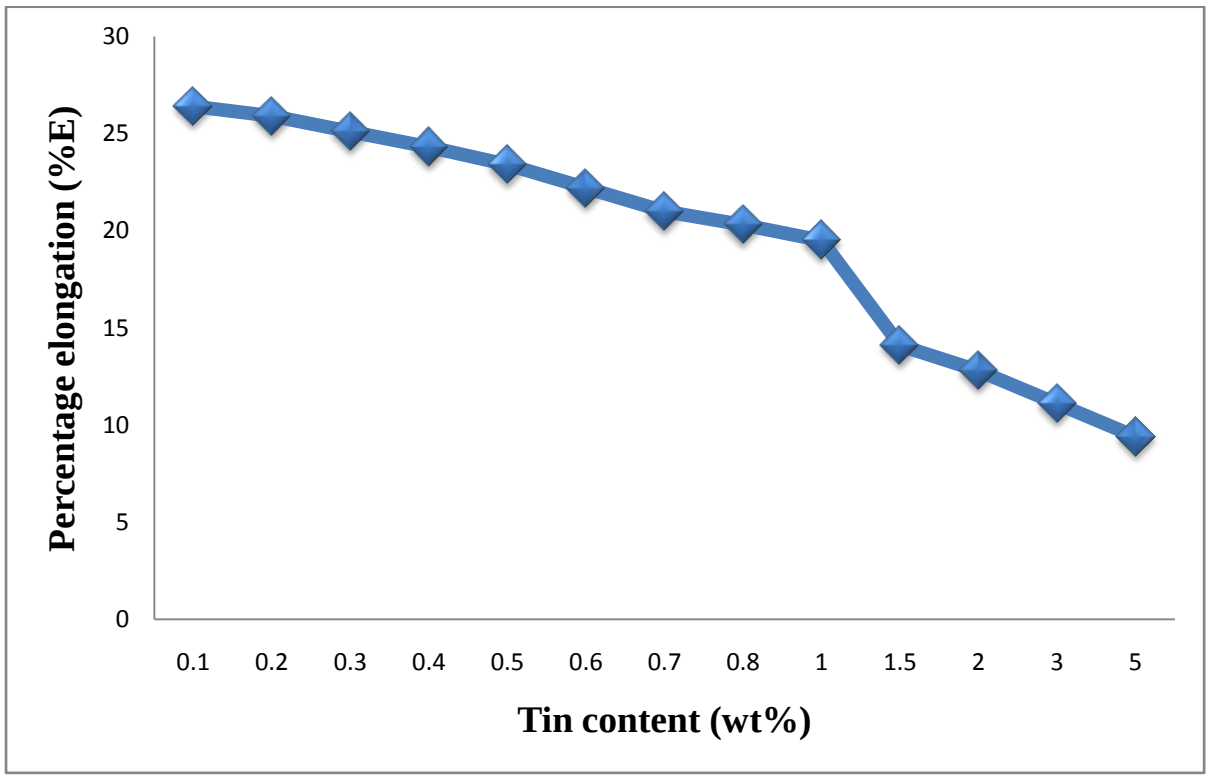

Figure 4.10: Effect of tin content on the percentage elongation of silicon bronze (Cu-3wt%Si)

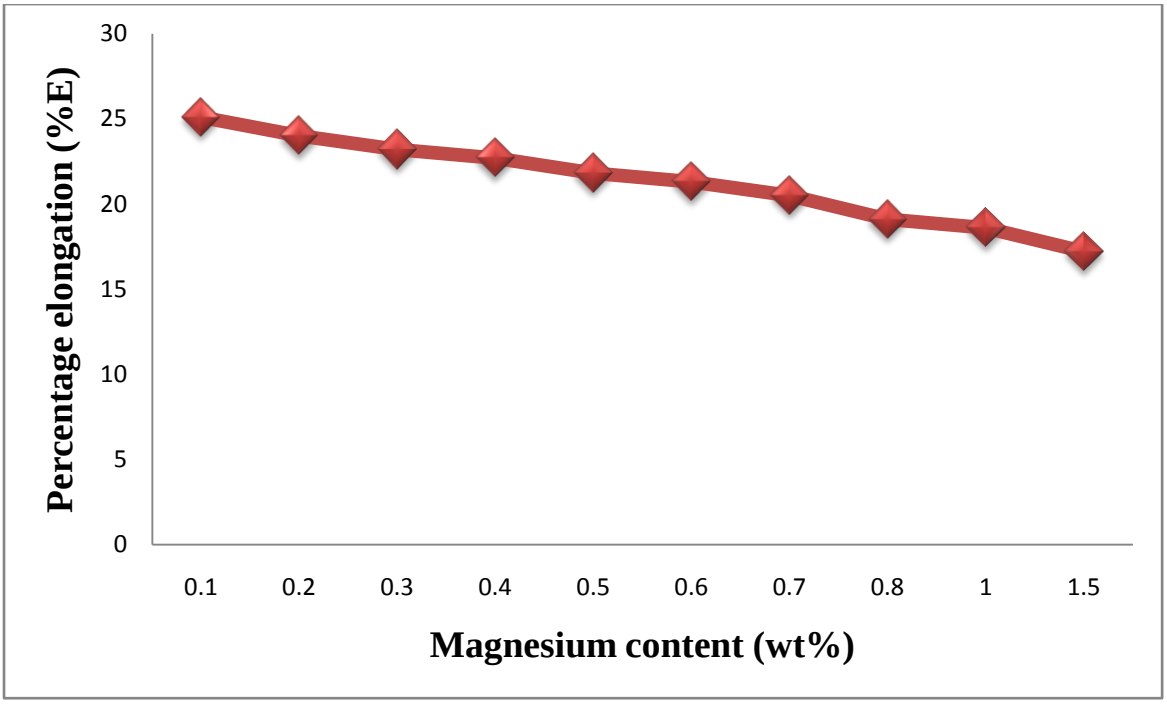

Figure 4.11: Effect of magnesium content on the percentage elongation of silicon bronze (Cu-3wt%Si)

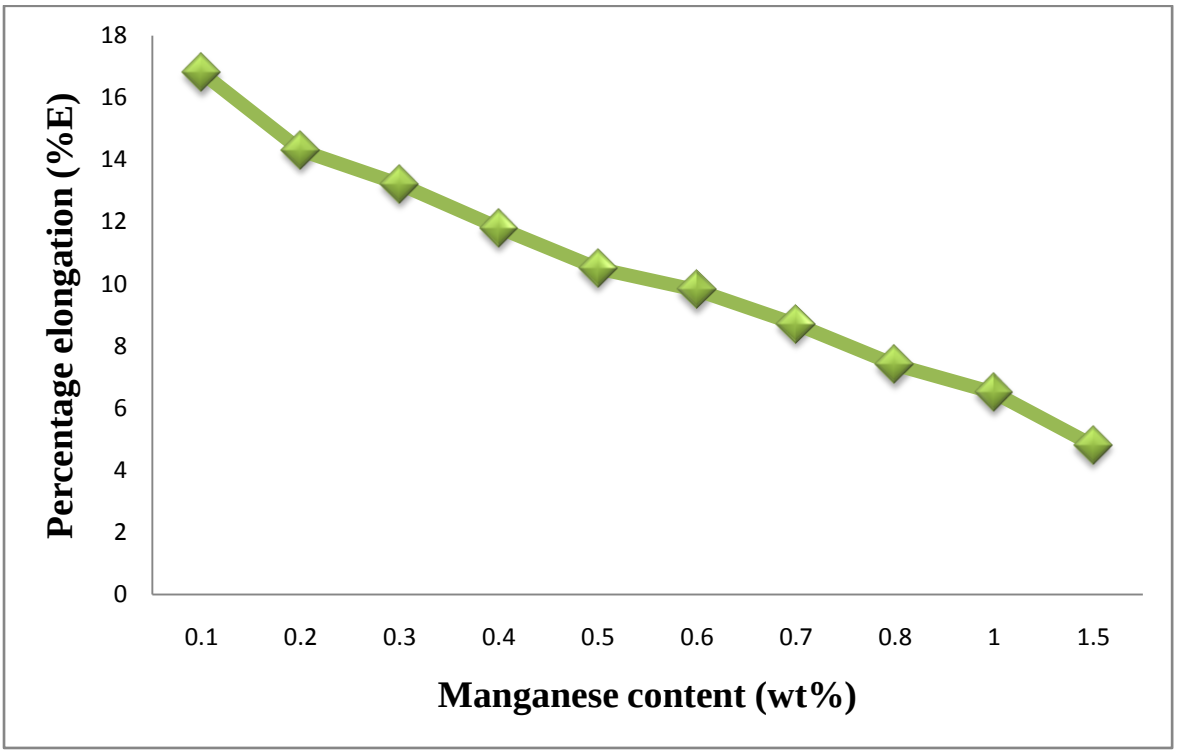

Figure 4.12: Effect of manganese content on the percentage elongation of silicon bronze (Cu-3wt%Si)

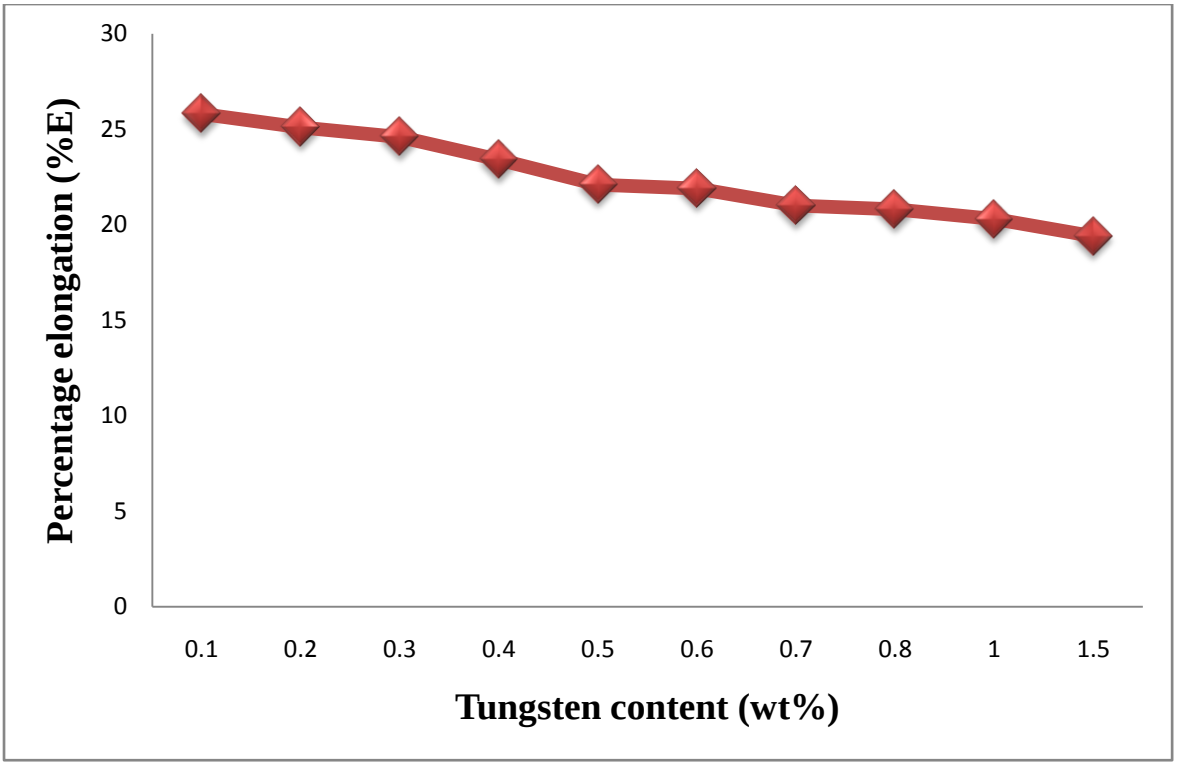

Figure 4.13: Effect of tungsten content on the percentage elongation of silicon bronze (Cu-3wt%Si)

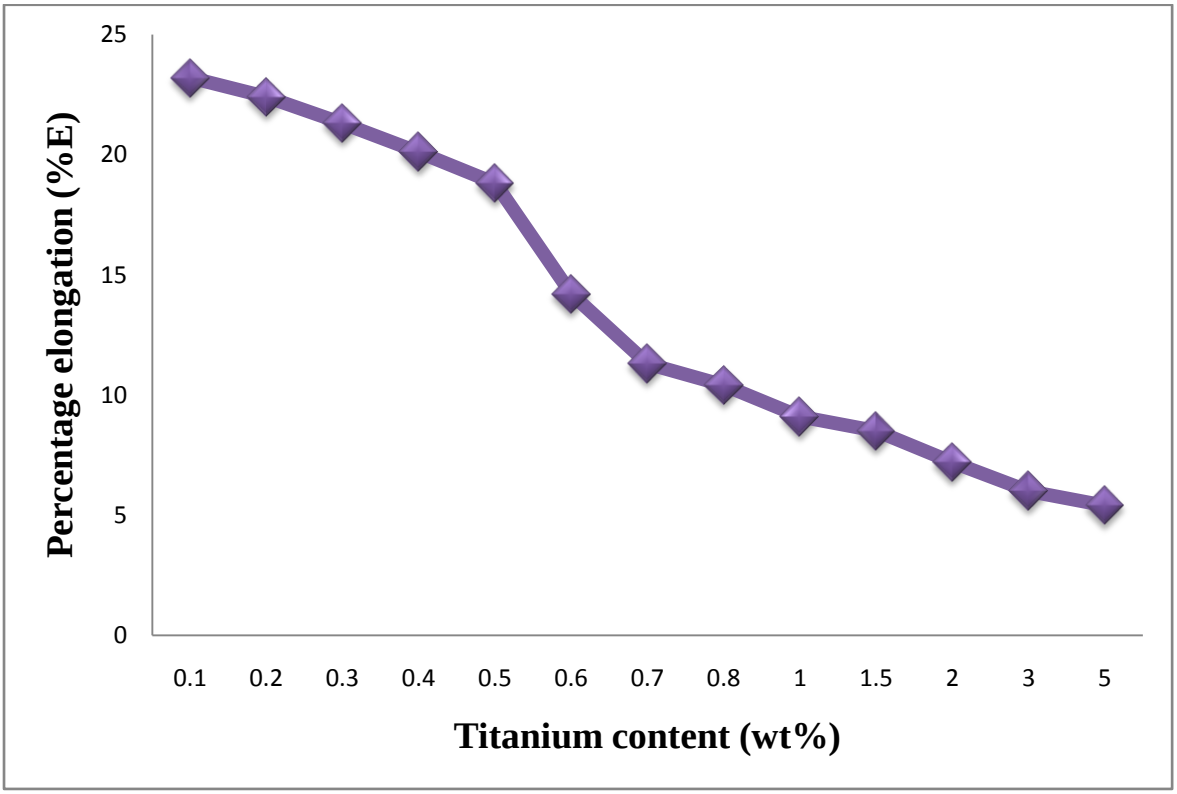

Figure 4.14: Effect of titanium content on the percentage elongation of silicon bronze (Cu-3wt%Si)

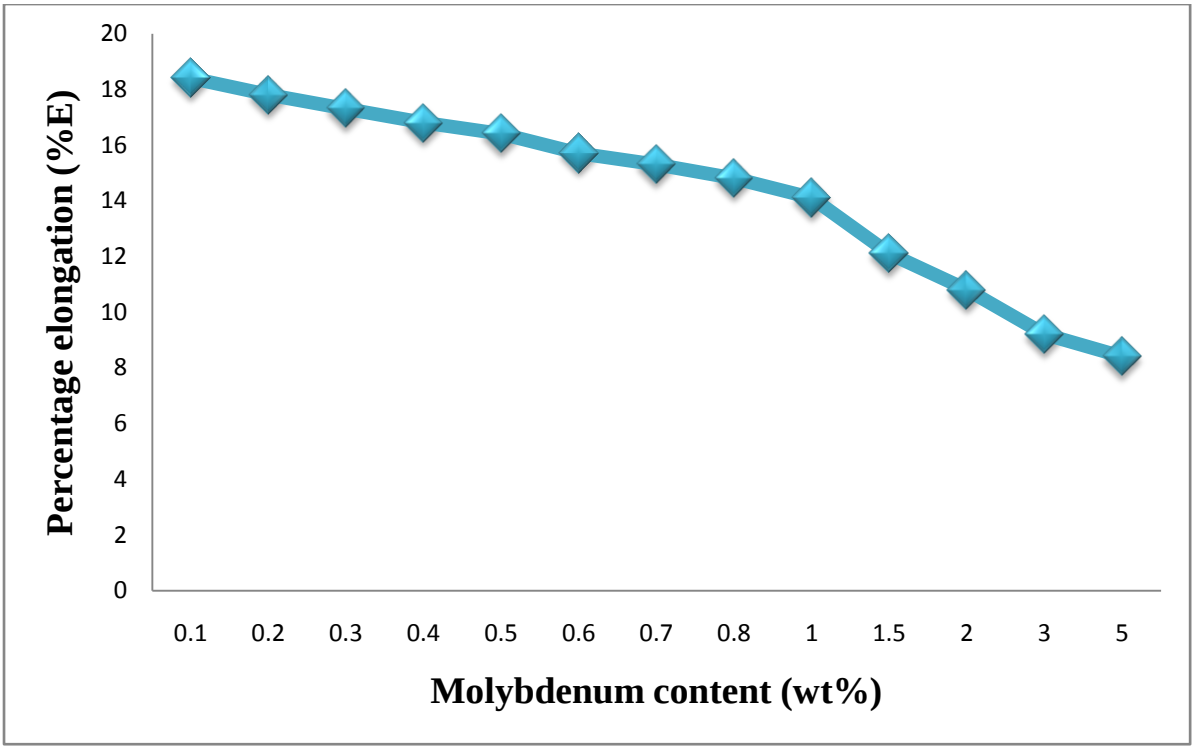

Figure 4.15: Effect of molybdenum content on the percentage elongation of silicon bronze (Cu-3wt%Si)

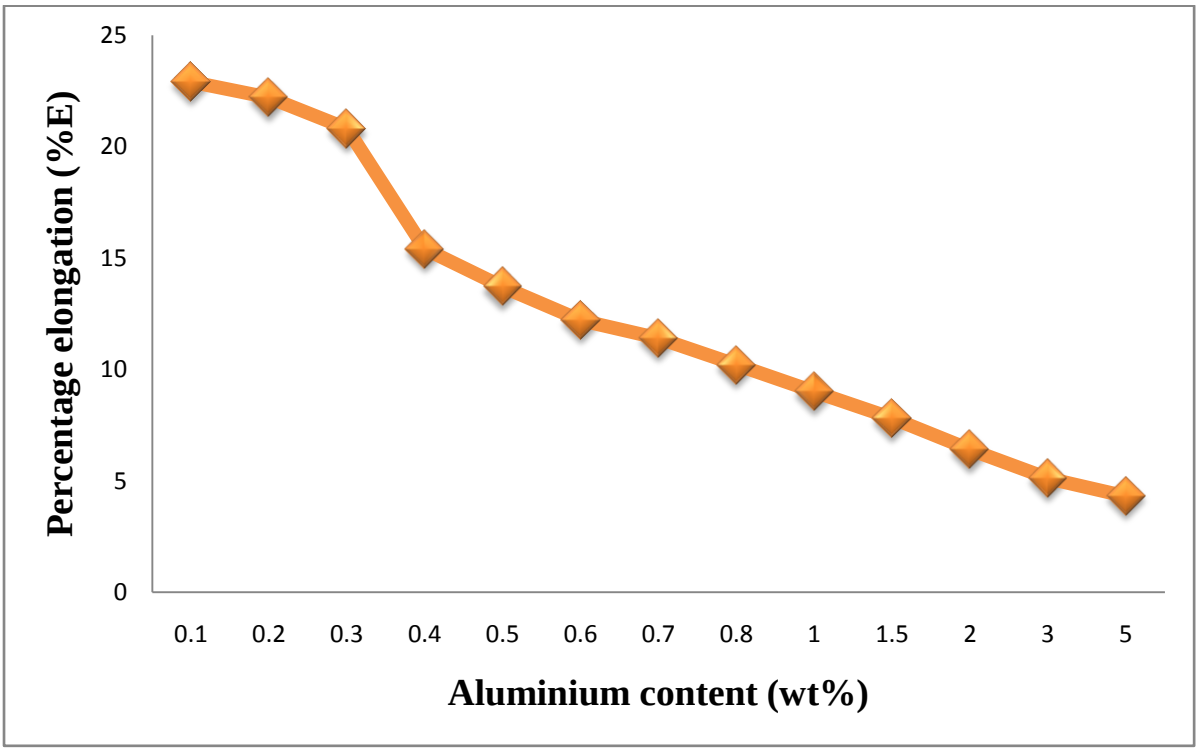

Figure 4.16: Effect of aluminium content on the percentage elongation of silicon bronze (Cu-3wt%Si)

The effect of zinc, tin, magnesium, manganese, tungsten, titanium, molybdenum and aluminium on the ultimate tensile strength of silicon bronze is presented in Figure 4.17. Analysis of Figure 4.17 indicates that all the dopants significantly improved the ultimate tensile strength of silicon bronze. This was as a result of the refining and modifying effect of the dopants on the dendritic primary silicon. It was evidenced in Figure 4.17 that magnesium, manganese, tungsten, titanium, zinc and aluminium showed maximum effect on the ultimate tensile strength of the alloy studied while molybdenum showed least effect.

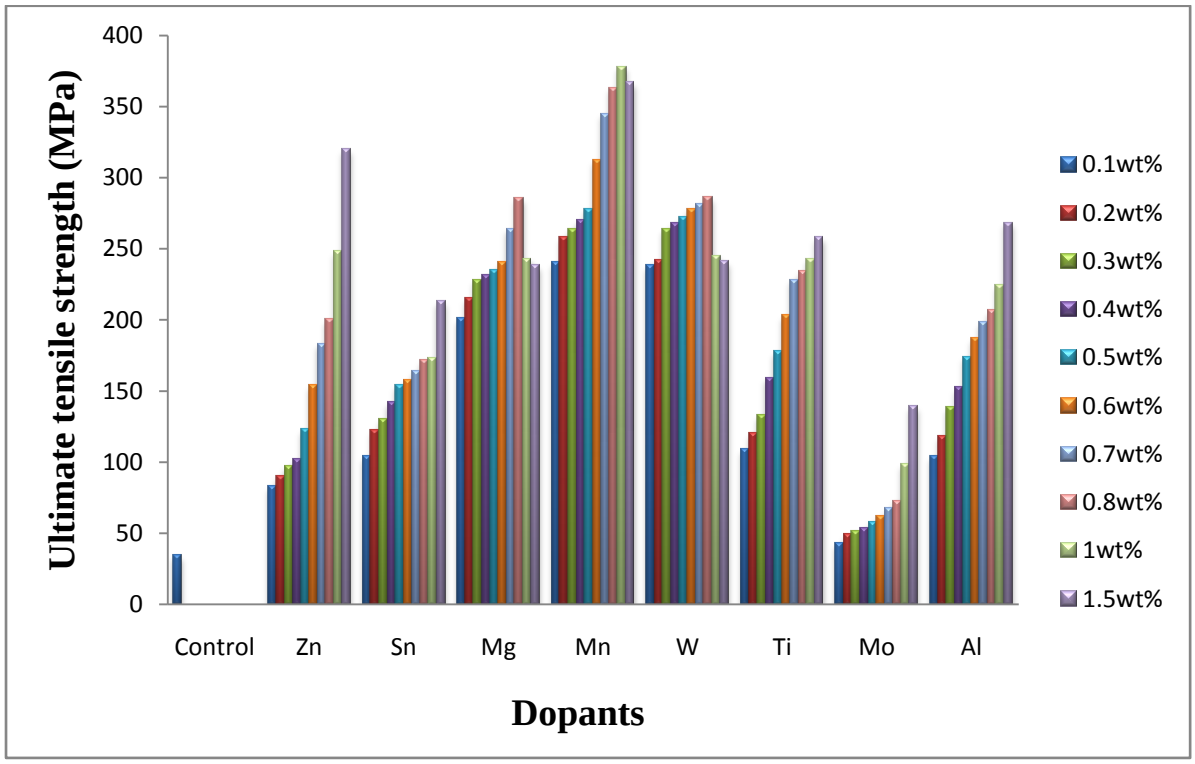

Figure 4.17: Effect of dopants on the ultimate tensile strength of silicon bronze (Cu-3wt%Si)

Figures 4.18-4.25 show the effect of different concentration of alloying elements on the ultimate tensile strength of silicon bronze. Analysis of Figures 4.18-4.25 indicates an increase in ultimate tensile strength as the concentration of the dopants increased. A predominant increase in ultimate tensile strength was observed as the concentration of Zn, Sn, Mg, Mn, W, Ti, Mo and Al increased to 3, 3, 0.8, 1, 0.8, 2, 1.5 band 3% by weight respectively. Addition of these dopants in excess of those concentrations resulted to decrease in ultimate tensile strength of the alloys. This is quantified by the microstructural change.

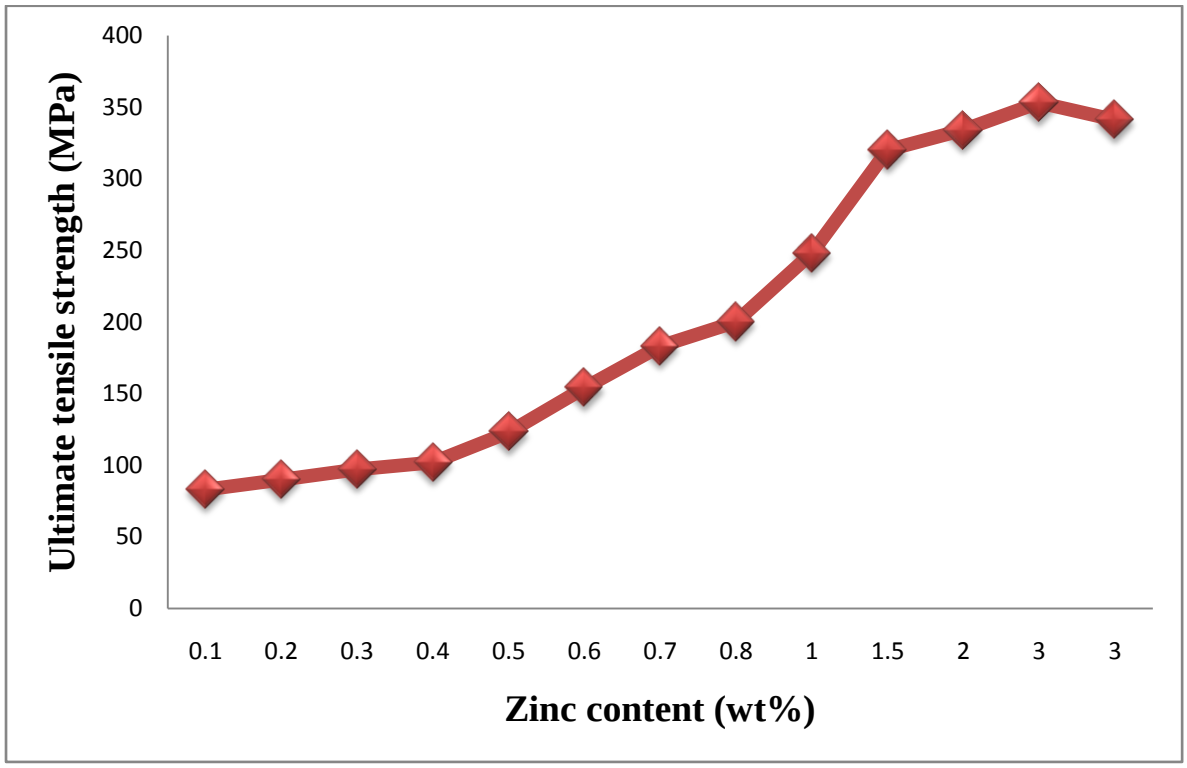

Figure 4.18: Effect of zinc content on the ultimate tensile strength of silicon bronze (Cu-3wt%Si)

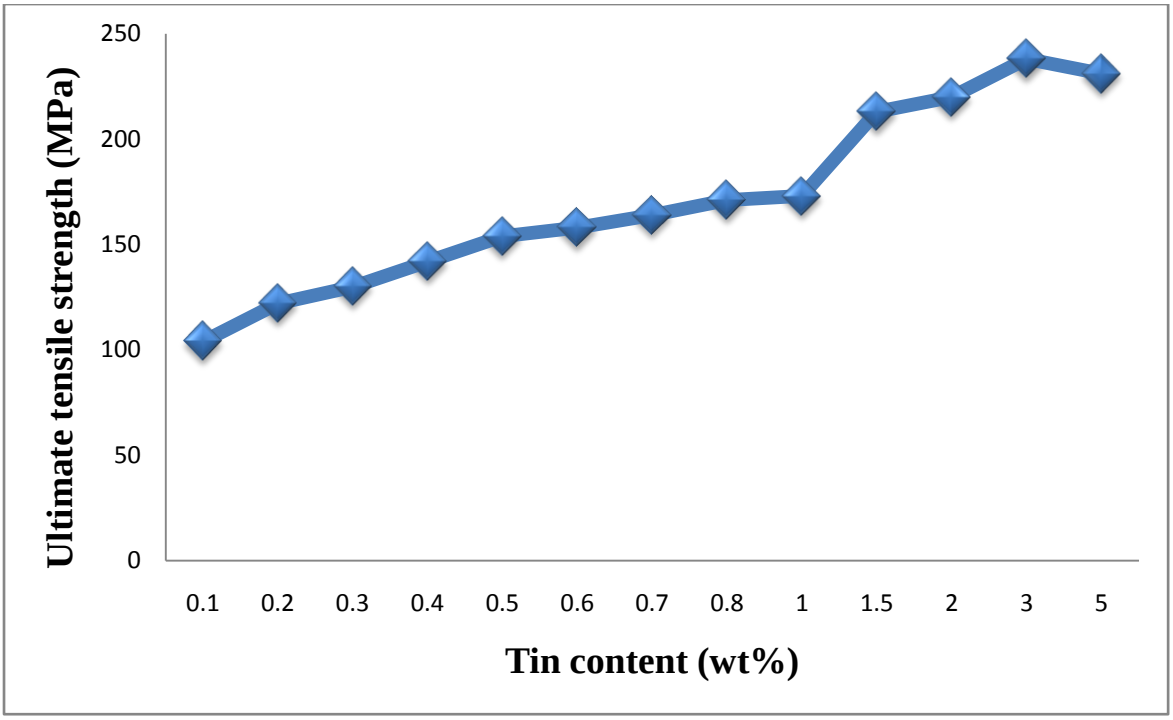

Figure 4.19: Effect of tin content on the ultimate tensile strength of silicon bronze (Cu-3wt%Si)

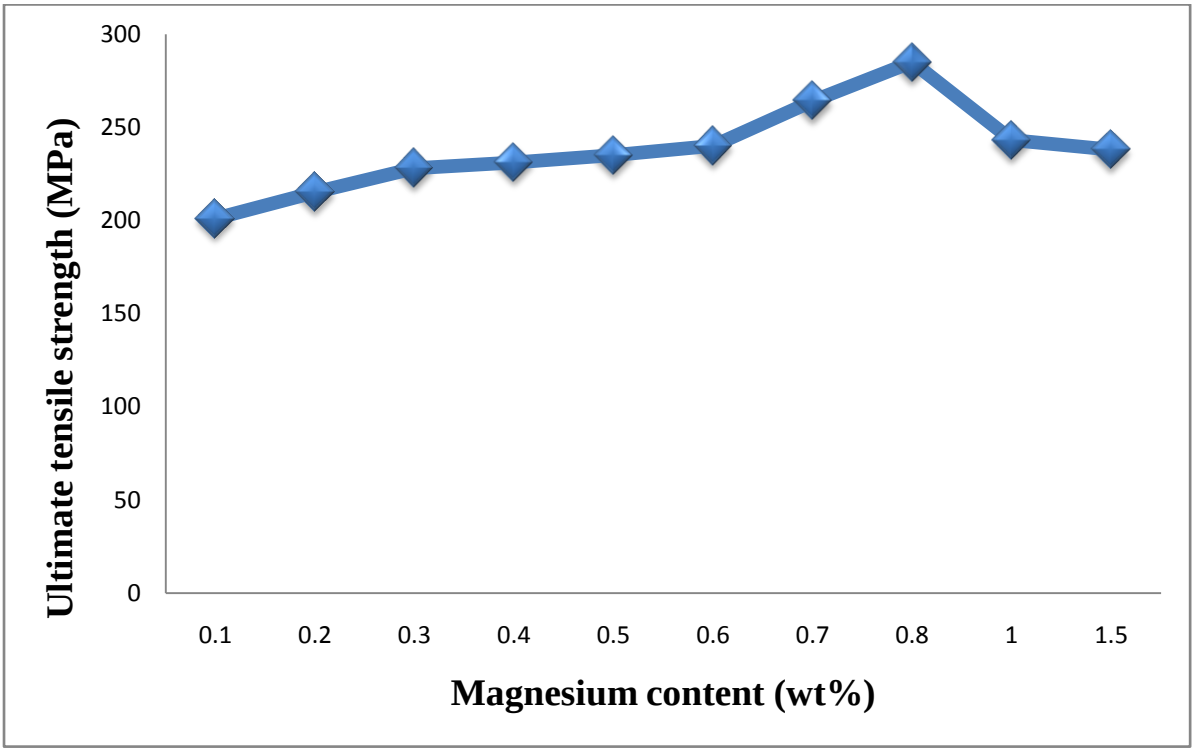

Figure 4.20: Effect of magnesium content on the ultimate tensile strength of silicon bronze (Cu-3wt%Si)

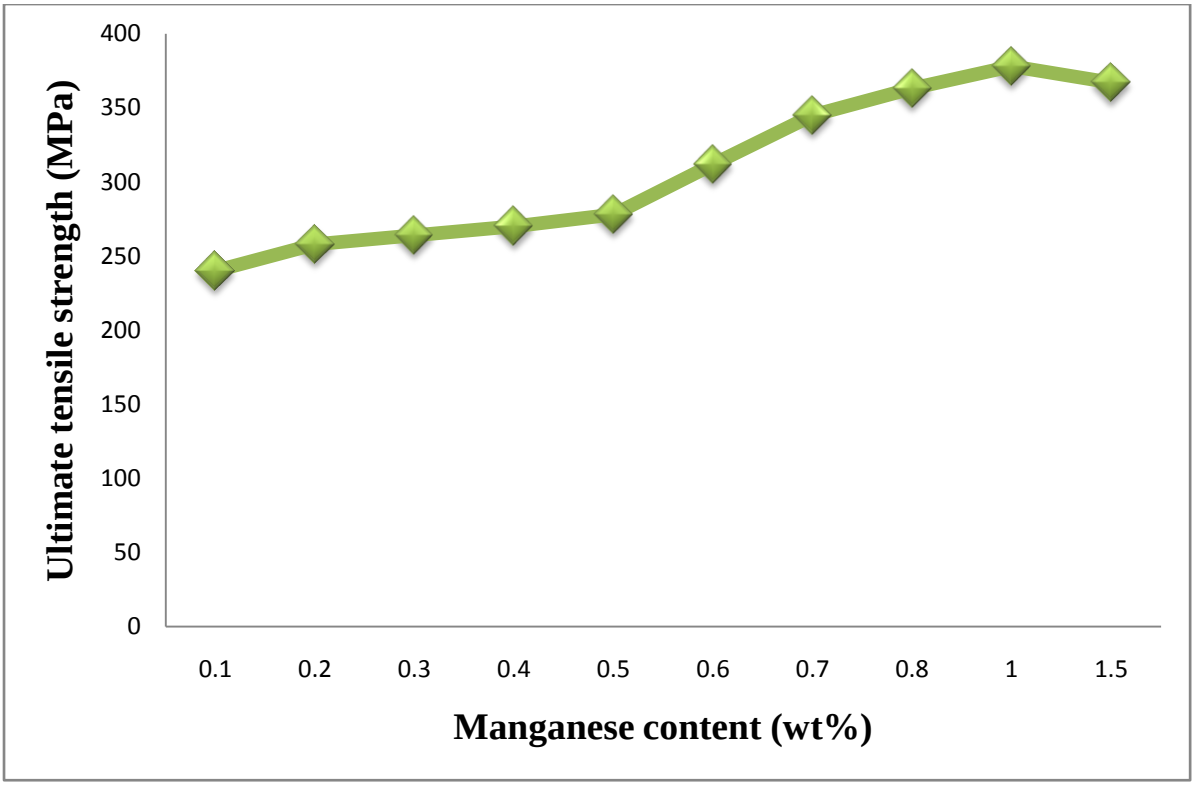

Figure 4.21: Effect of manganese content on the ultimate tensile strength of silicon bronze (Cu-3wt%Si)

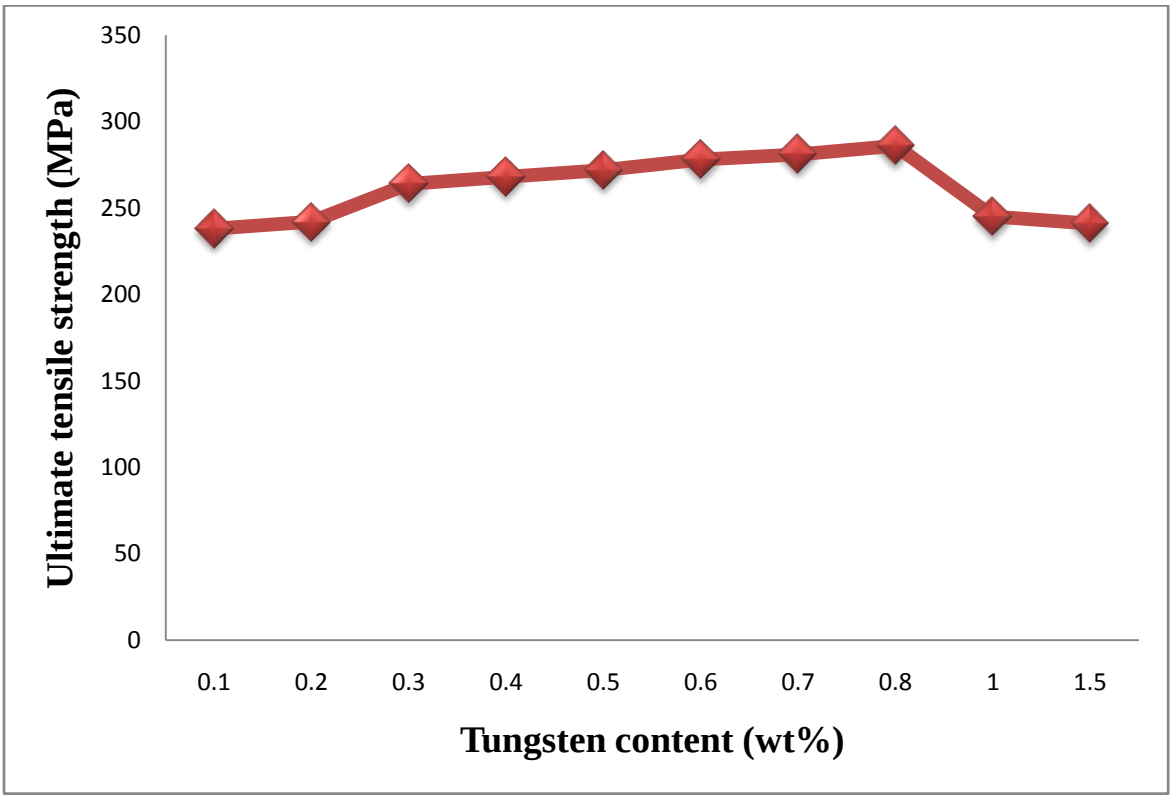

Figure 4.22: Effect of tungsten content on the ultimate tensile strength of silicon bronze (Cu-3wt%Si)

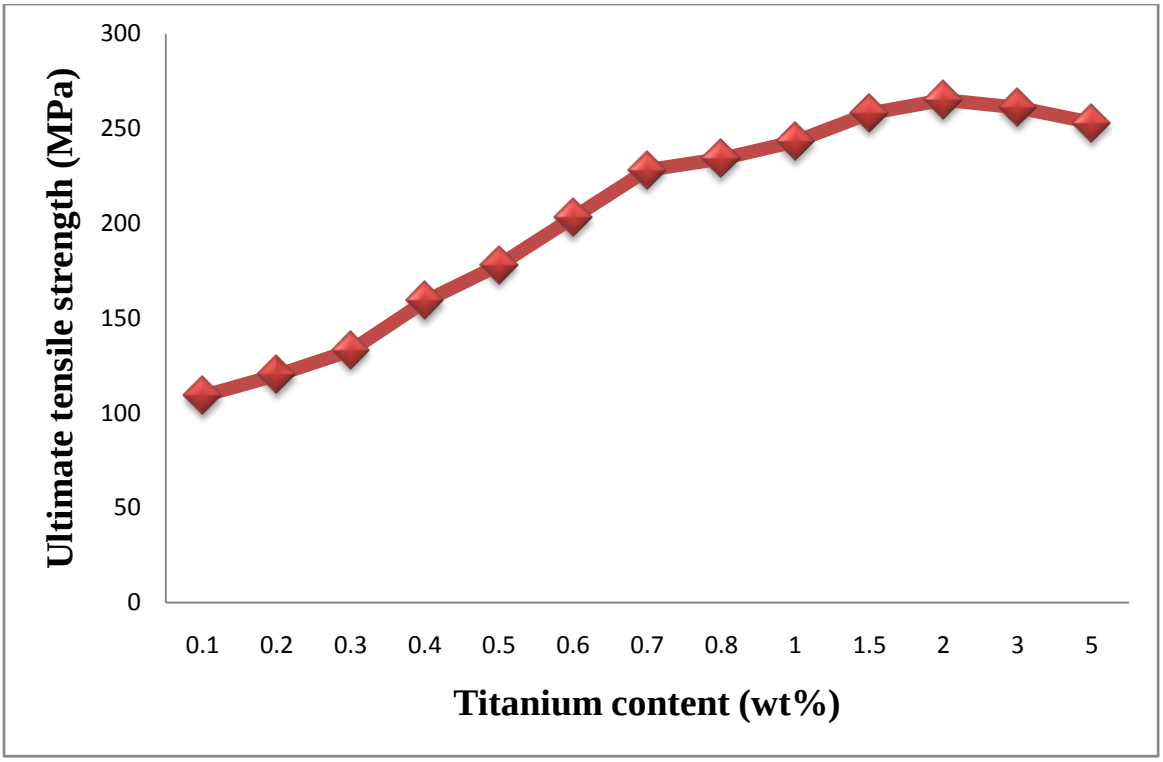

Figure 4.23: Effect of titanium content on the ultimate tensile strength of silicon bronze (Cu-3wt%Si)

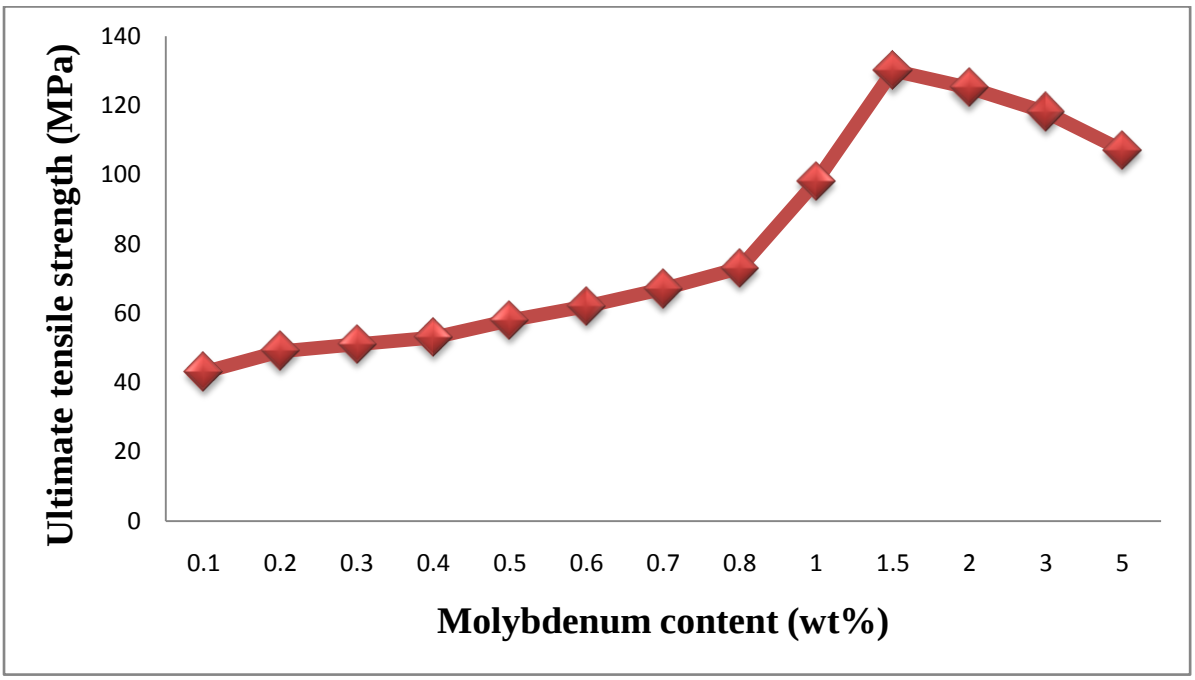

Figure 4.24: Effect of molybdenum content on the ultimate tensile strength of silicon bronze (Cu-3wt%Si)

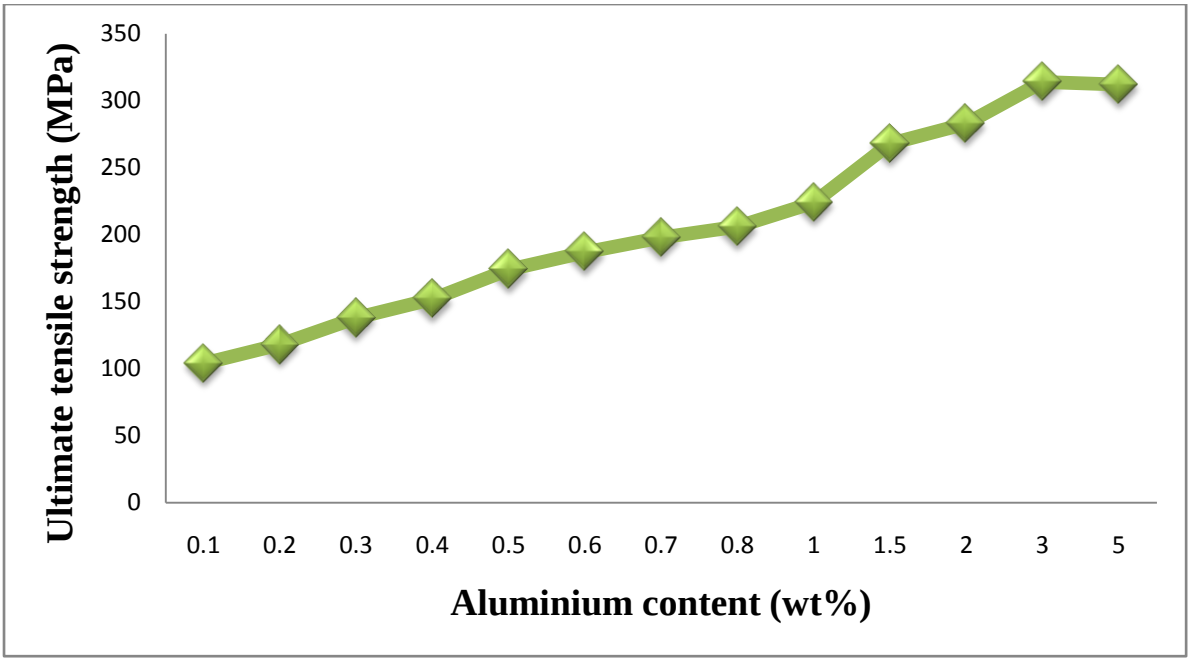

Figure 4.25: Effect of aluminium content on the ultimate tensile strength of silicon bronze (Cu-3wt%Si)

The effect of dopants on the brinell hardness and impact strength of silicon bronze (Cu-3wt%Si) is presented in Table 4.5.

Table 4.5: Effect of dopants on the brinell hardness and impact strength of silicon bronze (Cu-3wt%Si).

Alloy designation	Alloy composition	Brinell hardness (MPa)	Impact strength (J)
BZ_4	Cu-3wt%Si-0.1wt%Zn	243	14.5
BZ_5	Cu-3wt%Si-0.2wt%Zn	238	16.9
BZ_6	Cu-3wt%Si-0.3wt%Zn	231	18.5
BZ_7	Cu-3wt%Si-0.4wt%Zn	224	20.8
BZ_8	Cu-3wt%Si-0.5wt%Zn	216	22.3
BZ_9	Cu-3wt%Si-0.6wt%Zn	213	24.8
BZ_{10}	Cu-3wt%Si-0.7wt%Zn	208	25.6
BZ_{11}	Cu-3wt%Si-0.8wt%Zn	198	27.1
BZ_{12}	Cu-3wt%Si-1.0wt%Zn	182	28.5
BZ_{13}	Cu-3wt%Si-1.5wt%Zn	198	26.3
BZ_{14}	Cu-3wt%Si-2wt%Zn	238	24.9
BZ_{15}	Cu-3wt%Si-3wt%Zn	254	24.4
BZ_{16}	Cu-3wt%Si-5wt%Zn	248	22.1
BZ_{17}	Cu-3wt%Si-0.1wt%Sn	129	31.0

Alloy designation	Alloy composition	Brinell hardness (MPa)	Impact strength (J)
BZ_{18}	Cu-3wt%Si-0.2wt%Sn	140	29.7
BZ_{19}	Cu-3wt%Si-0.3wt%Sn	151	27.2
BZ_{20}	Cu-3wt%Si-0.4wt%Sn	163	25.8
BZ_{21}	Cu-3wt%Si-0.5wt%Sn	176	23.6
BZ_{22}	Cu-3wt%Si-0.6wt%Sn	209	21.0
BZ_{23}	Cu-3wt%Si-0.7wt%Sn	230	19.9
BZ_{24}	Cu-3wt%Si-0.8wt%Sn	233	17.6
BZ_{25}	Cu-3wt%Si-1wt%Sn	243	15.4
BZ_{26}	Cu-3wt%Si-1.5wt%Sn	258	13.0
BZ_{27}	Cu-3wt%Si-2wt%Sn	264	12.4
BZ_{28}	Cu-3wt%Si-3wt%Sn	278	11.6
BZ_{29}	Cu-3wt%Si-5wt%Sn	273	10.2
BZ_{30}	Cu-3wt%Si-0.1wt%Mg	216	28.1
BZ_{31}	Cu-3wt%Si-0.2wt%Mg	238	26.7
BZ_{32}	Cu-3wt%Si-0.3wt%Mg	244	24.4
BZ_{33}	Cu-3wt%Si-0.4wt%Mg	258	21.3
BZ_{34}	Cu-3wt%Si-0.5wt%Mg	262	19.8
BZ_{35}	Cu -3wt%Si-0.6wt%Mg	277	16.7
BZ_{36}	Cu -3wt%Si-0.7wt%Mg	284	15.4
BZ_{37}	Cu -3wt%Si-0.8wt%Mg	318	13.2
BZ_{38}	Cu -3wt%Si-1wt%Mg	269	11.3
BZ_{39}	Cu -3wt%Si-1.5wt%Mg	250	9.8
BZ_{40}	Cu -3wt%Si-0.1wt%Mn	251	24.0
BZ_{41}	Cu -3wt%Si-0.2wt%Mn	257	21.4
BZ_{42}	Cu -3wt%Si-0.3wt%Mn	262	18.5
BZ_{43}	Cu -3wt%Si-0.4wt%Mn	268	16.9
BZ_{44}	Cu -3wt%Si-0.5wt%Mn	272	14.4
BZ_{45}	Cu -3wt%Si-0.6wt%Mn	285	13.1
BZ_{46}	Cu -3wt%Si-0.7wt%Mn	332	11.8
BZ_{47}	Cu -3wt%Si-0.8wt%Mn	348	10.5
BZ_{48}	Cu -3wt%Si-1wt%Mn	371	8.3
BZ_{49}	Cu -3wt%Si-1.5wt%Mn	368	6.7
BZ_{50}	Cu -3wt%Si-0.1wt%W	272	30.9
BZ_{51}	Cu -3wt%Si-0.2wt%W	284	28.7
BZ_{52}	Cu -3wt%Si-0.3wt%W	300	26.3
BZ_{53}	Cu -3wt%Si-0.4wt%W	314	24.9
BZ_{54}	Cu -3wt%Si-0.5wt%W	330	22.5
BZ_{55}	Cu -3wt%Si-0.6wt%W	348	20.2
BZ_{56}	Cu -3wt%Si-0.7wt%W	352	18.1
BZ_{57}	Cu -3wt%Si-0.8wt%W	358	16.6
BZ_{58}	Cu -3wt%Si-1wt%W	328	14.4
BZ_{59}	Cu -3wt%Si-1.5wt%W	303	12.1

Alloy designation	Alloy composition	Brinell hardness (MPa)	Impact strength (J)
BZ_{60}	Cu -3wt%Si-0.1wt%Ti	194	33.3
BZ_{61}	Cu -3wt%Si-0.2wt%Ti	209	31.7
BZ_{62}	Cu -3wt%Si-0.3wt%Ti	223	29.3
BZ_{63}	Cu -3wt%Si-0.4wt%Ti	238	26.2
BZ_{64}	Cu -3wt%Si-0.5wt%Ti	240	24.6
BZ_{65}	Cu -3wt%Si-0.6wt%Ti	246	22.8
BZ_{66}	Cu -3wt%Si-0.7wt%Ti	248	20.5
BZ_{67}	Cu -3wt%Si-0.8wt%Ti	252	18.6
BZ_{68}	Cu -3wt%Si-1wt%Ti	258	14.0
BZ_{69}	Cu -3wt%Si-1.5wt%Ti	267	11.7
BZ_{70}	Cu -3wt%Si-2wt%Ti	282	10.2
BZ_{71}	Cu -3wt%Si-3wt%Ti	273	9.4
BZ_{72}	Cu -3wt%Si-5wt%Ti	264	8.7
BZ_{73}	Cu -3wt%Si-0.1wt%Mo	133	25.8
BZ_{74}	Cu -3wt%Si-0.2wt%Mo	147	23.5
BZ_{75}	Cu -3wt%Si-0.3wt%Mo	149	21.9
BZ_{76}	Cu -3wt%Si-0.4wt%Mo	153	19.5
BZ_{77}	Cu -3wt%Si-0.5wt%Mo	158	16.3
BZ_{78}	Cu -3wt%Si-0.6wt%Mo	164	15.0
BZ_{79}	Cu -3wt%Si-0.7wt%Mo	172	13.4
BZ_{80}	Cu -3wt%Si-0.8wt%Mo	182	11.2
BZ_{81}	Cu -3wt%Si-1wt%Mo	187	9.9
BZ_{82}	Cu -3wt%Si-1.5wt%Mo	192	8.5
BZ_{83}	Cu -3wt%Si-2wt%Mo	191	7.8
BZ_{84}	Cu -3wt%Si-3wt%Mo	184	6.4
BZ_{85}	Cu -3wt%Si-5wt%Mo	173	5.2
BZ_{86}	Cu -3wt%Si-0.1wt%Al	186	39.0
BZ_{87}	Cu -3wt%Si-0.2wt%Al	190	36.1
BZ_{88}	Cu -3wt%Si-0.3wt%Al	197	34.8
BZ_{89}	Cu -3wt%Si-0.4wt%Al	201	32.2
BZ_{90}	Cu -3wt%Si-0.5wt%Al	204	30.5
BZ_{91}	Cu -3wt%Si-0.6wt%Al	209	29.0
BZ_{92}	Cu -3wt%Si-0.7wt%Al	218	27.8
BZ_{93}	Cu -3wt%Si-0.8wt%Al	224	25.6
BZ_{94}	Cu -3wt%Si-1wt%Al	228	24.0
BZ_{95}	Cu -3wt%Si-1.5wt%Al	248	21.0
BZ_{96}	Cu -3wt%Si-2wt%Al	262	18.6
BZ_{97}	Cu -3wt%Si-3wt%Al	278	14.2
BZ_{98}	Cu -3wt%Si-5wt%Al	275	11.8

Figure 4.26 shows the brinell hardness of silicon bronze doped with zinc, tin, magnesium, manganese, tungsten, titanium, molybdenum and aluminium. Analysis of Figure 4.26 shows that addition of these dopants to Cu-Si alloy system significantly improved the hardness of the alloy. From Figure 4.26, molybdenum show little effect on the hardness of silicon bronze compared with other dopants.

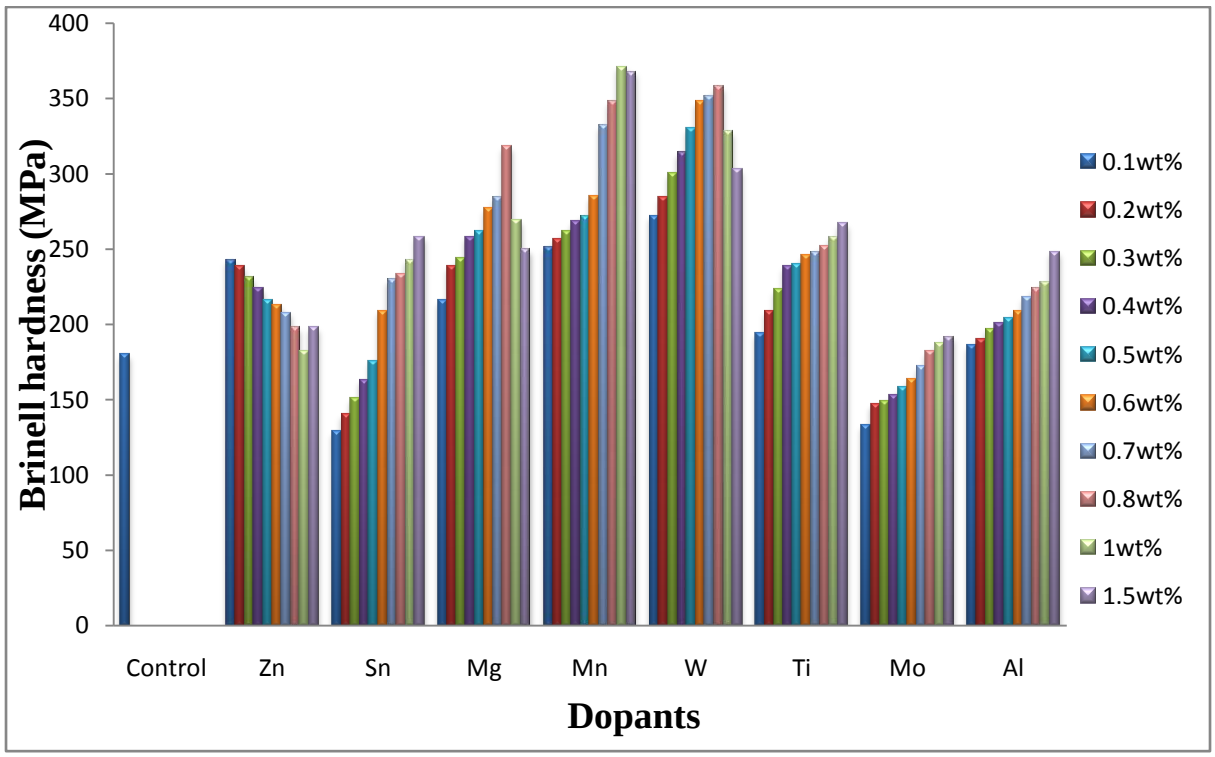

Figure 4.26: Effect of dopants on the hardness of silicon bronze (Cu-3wt%Si)

The effect of dopants concentrations on the hardness of silicon bronze is presented in Figures 4.27-4.34. Increase in hardness was noted as the concentration of Sn, Mg, Mn, W, Ti, Mo and Al increased. This could be attributed to the presence of refined and modified intermetallic phase in the

alloy structure. Decrease in hardness was observed as the concentrations of Sn, Mg, Mn, W, Ti, Mo and Al increased beyond 3, 0.8, 1, 0.8, 2, 1.5 and 3wt% respectively. Analysis of Figure 4.27 shows a decrease in hardness as the concentration of zinc is within the range of 0.1-1wt% and 3-5wt%. An increase in hardness was noted as the concentration of zinc is within the range of 1-3wt%. This was as a result of the presence of well distributed coherent α-β phase in the alloy structure.

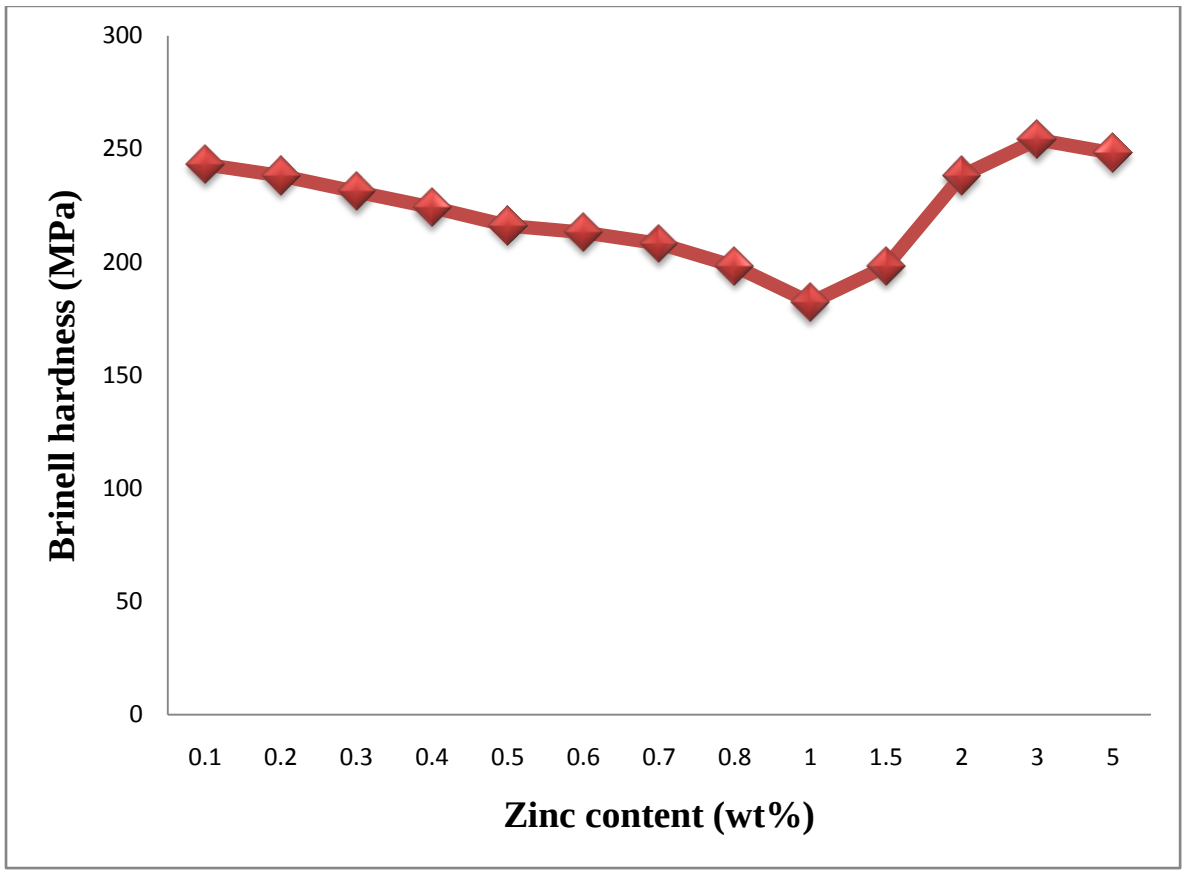

Figure 4.27: Effect of zinc content on the hardness of silicon bronze (Cu-3wt%Si)

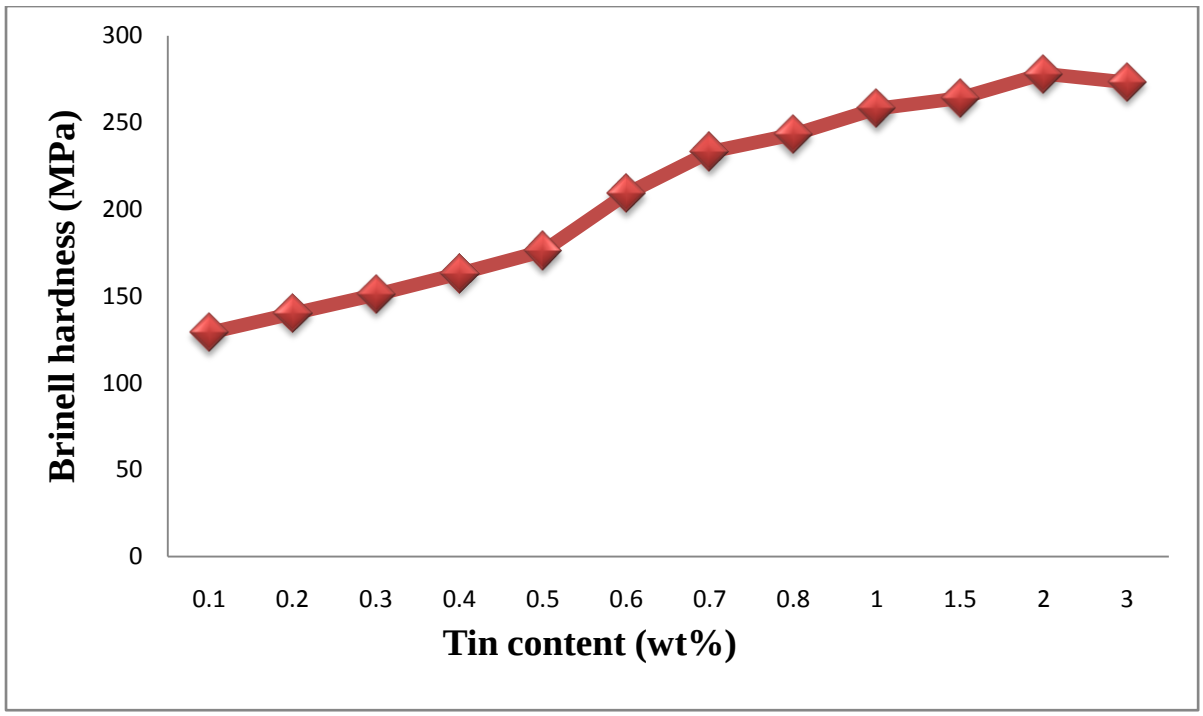

Figure 4.28: Effect of tin content on the hardness of silicon bronze (Cu-3wt%Si)

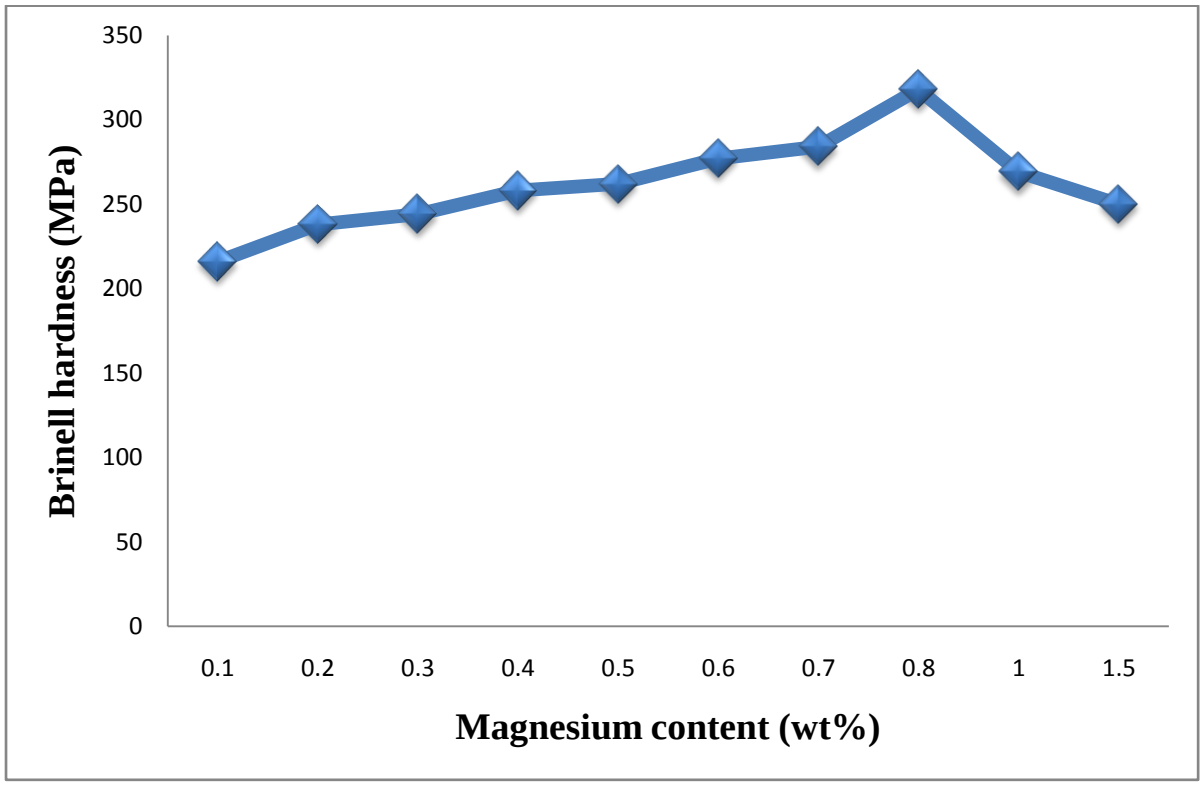

Figure 4.29: Effect of magnesium content on the hardness of silicon bronze (Cu-3wt%Si)

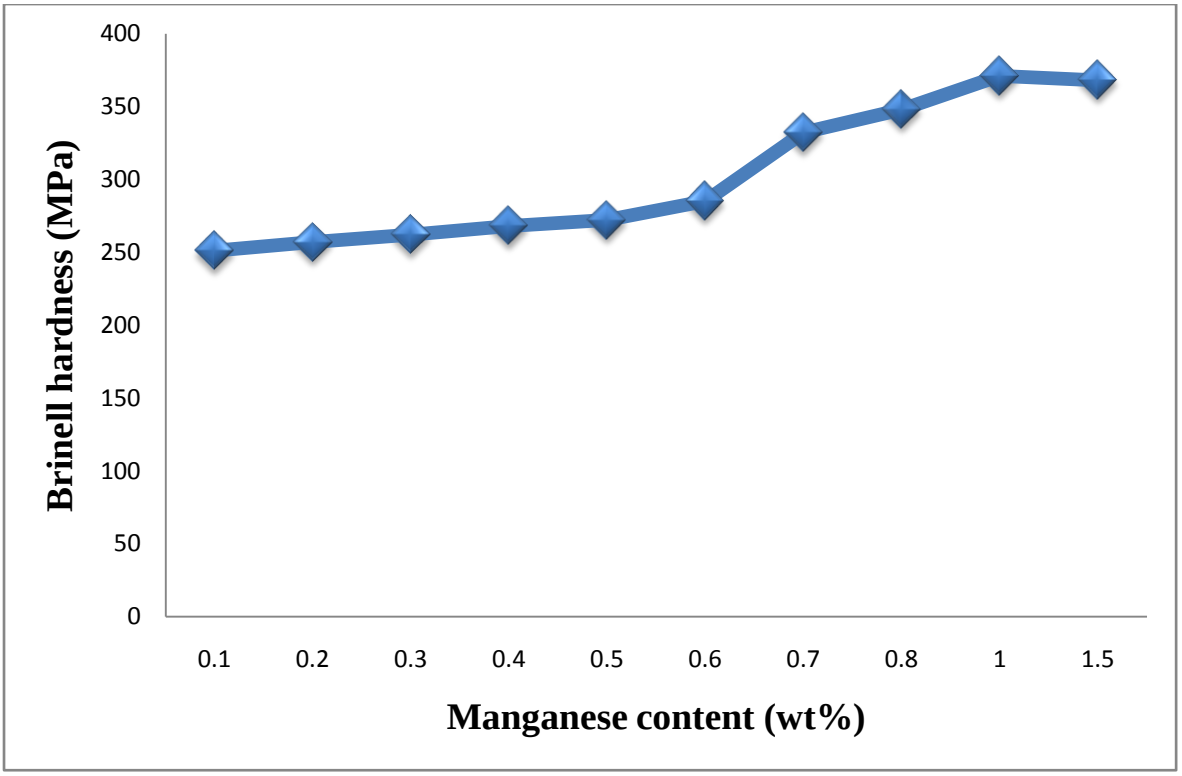

Figure 4.30: Effect of manganese content on the hardness of silicon bronze (Cu-3wt%Si)

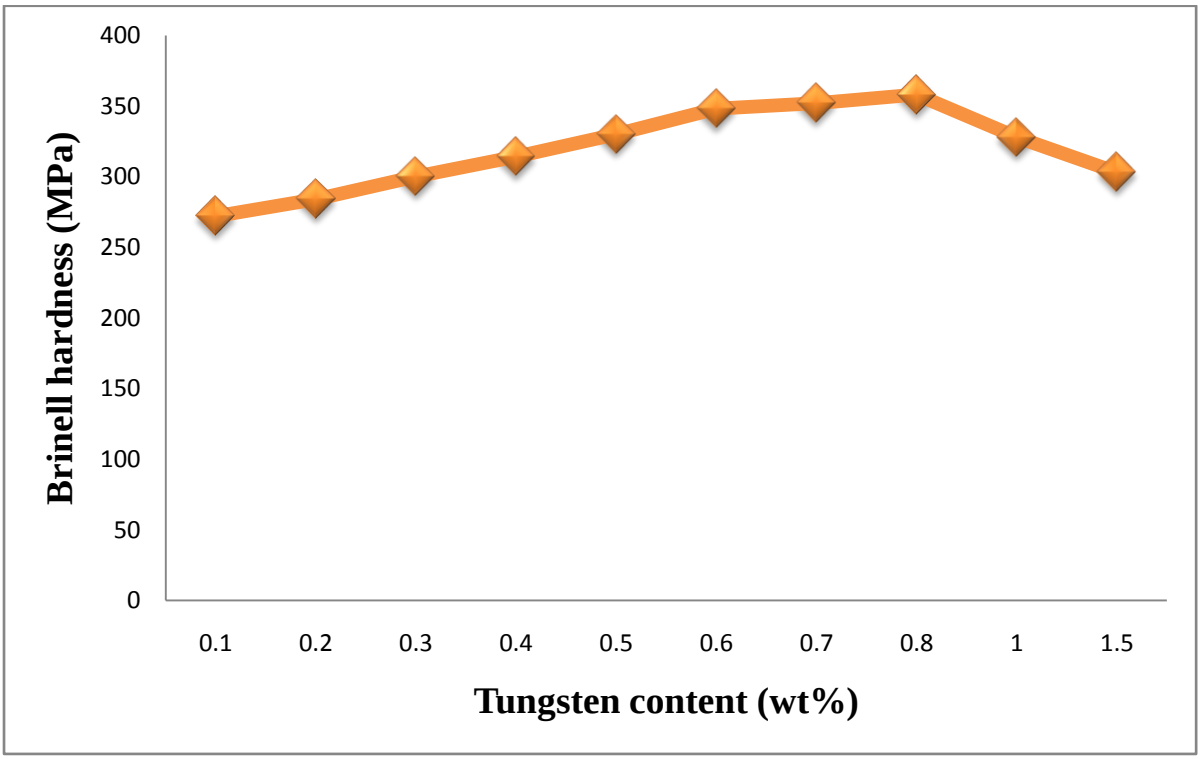

Figure 4.31: Effect of tungsten content on the hardness of silicon bronze (Cu-3wt%Si)

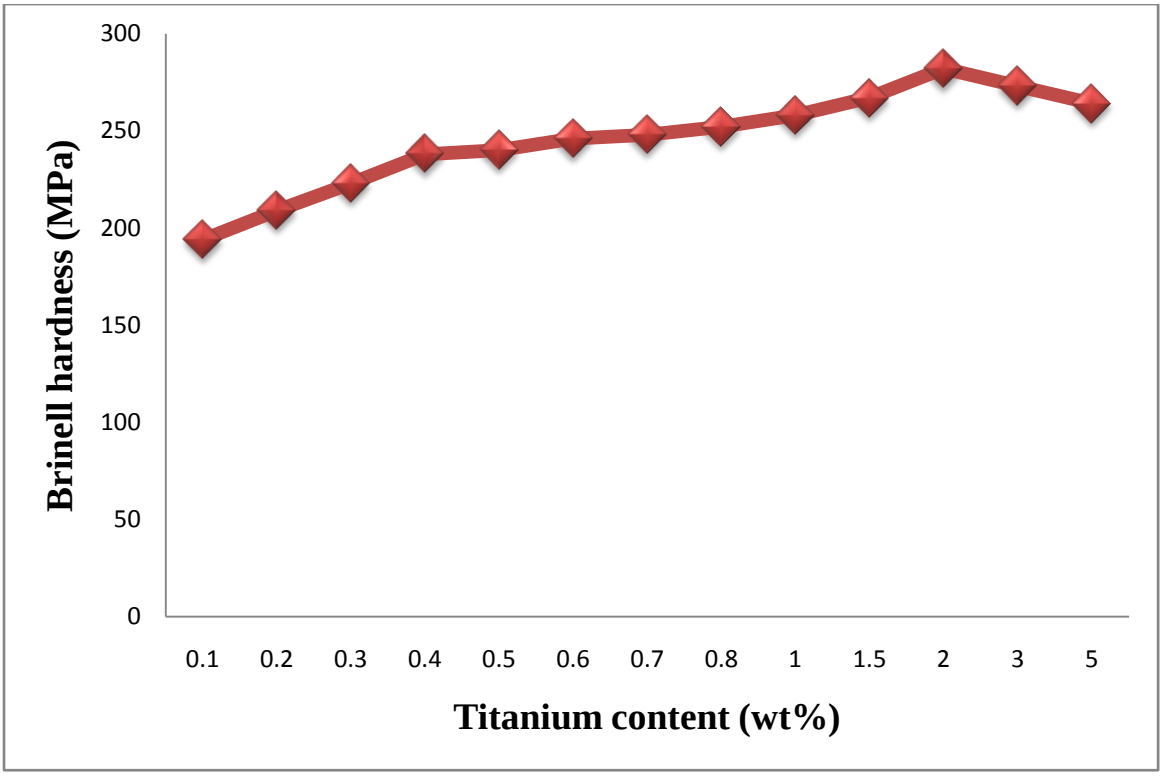

Figure 4.32: Effect of titanium content on the hardness of silicon bronze (Cu-3wt%Si)

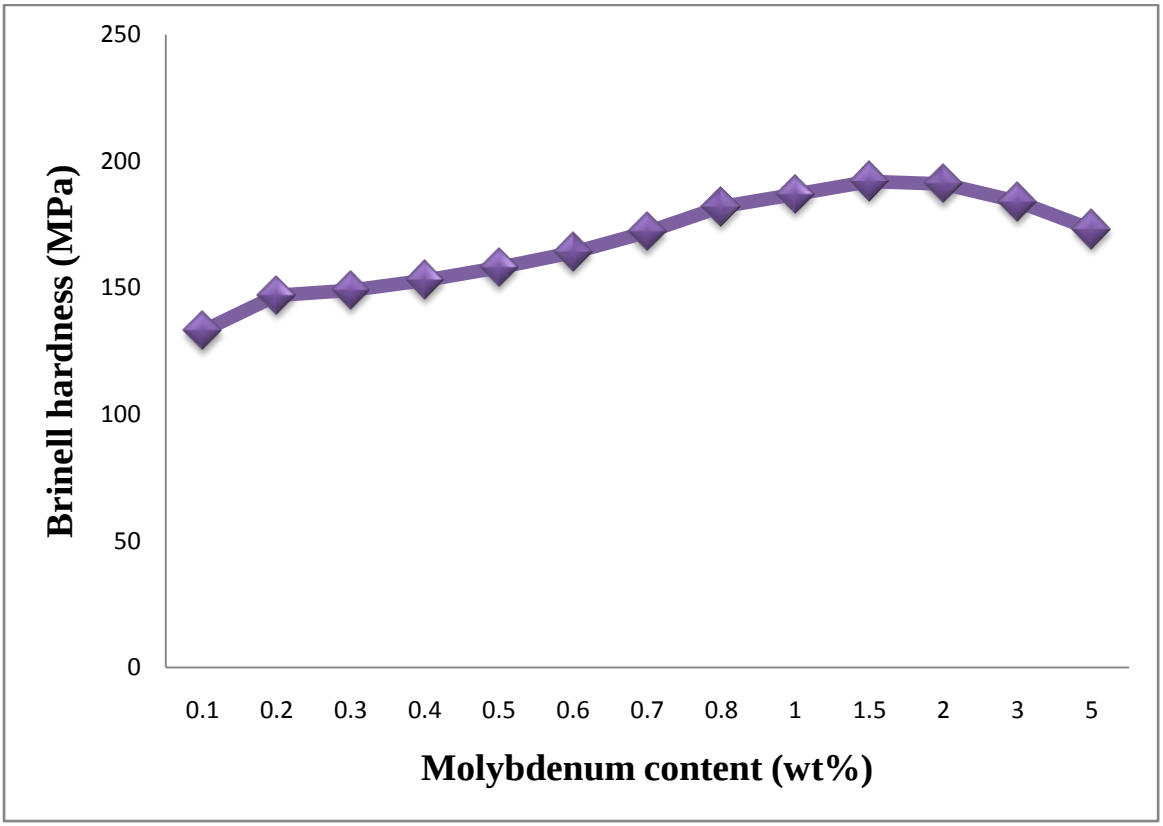

Figure 4.33: Effect of molybdenum content on the hardness of silicon bronze (Cu-3wt%Si)

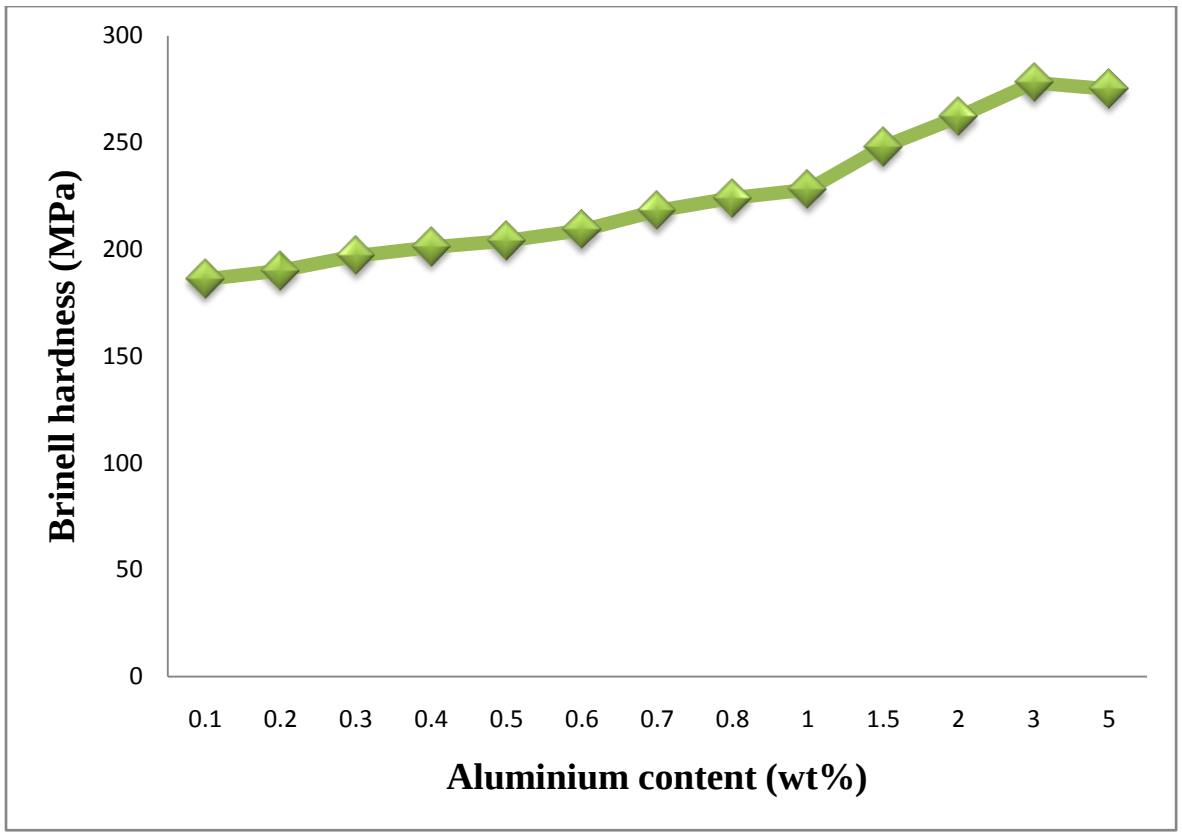

Figure 4.34: Effect of aluminium content on the hardness of silicon bronze (Cu-3wt%Si)

Analysis of the effect of dopants on the impact strength of silicon bronze is presented in Figure 4.44. A significant improvement in impact strength of the alloy was observed. Analysis of Figure 4.35 shows clearly that addition of the dopants increased the impact strength of silicon bronze. A systematic increase in impact strength was noted as the concentration of Sn, Mg, Mn, W, Ti, Mo and Al increased. Different trend was observed by zinc addition up to 1% by weight. Further increase in zinc concentration resulted to decrease in impact strength.

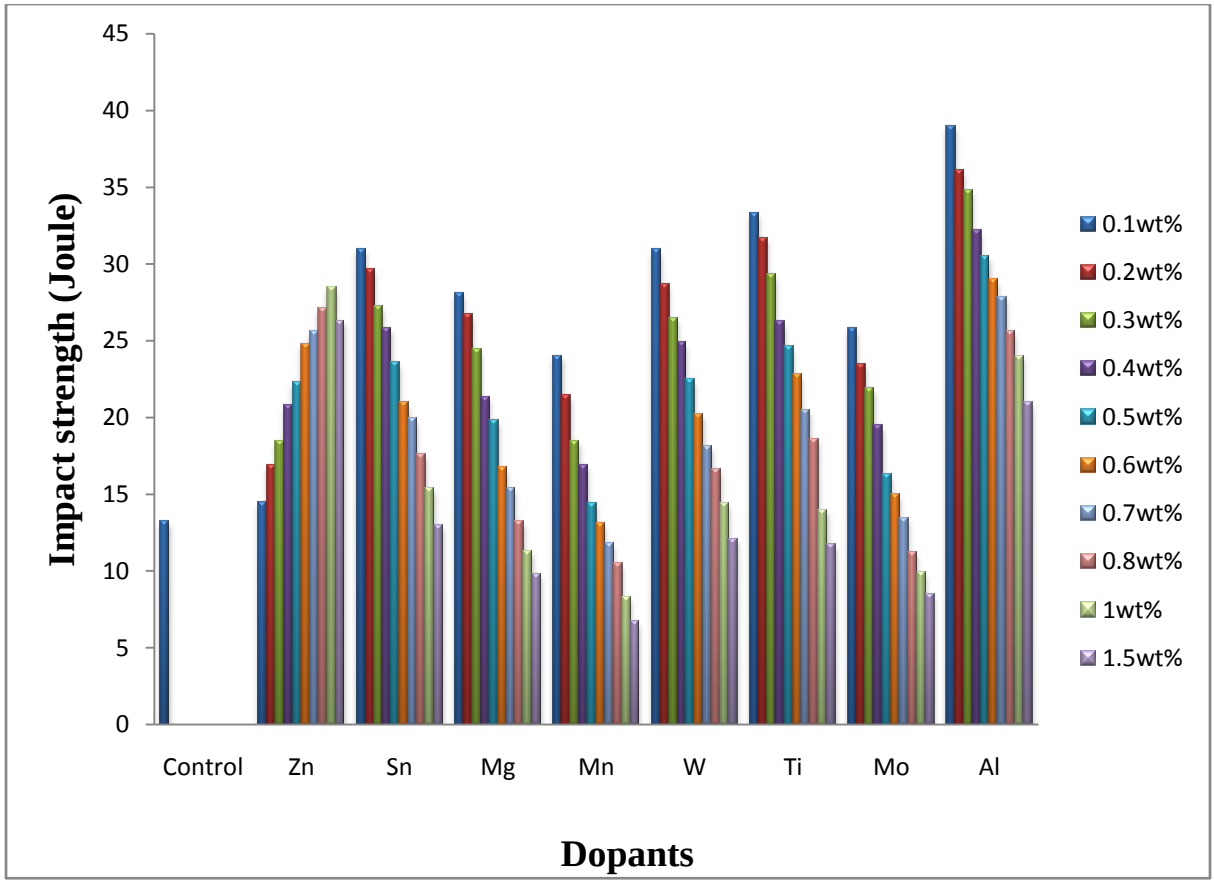

Figure 4.35: Effect of dopants on the impact strength of silicon bronze (Cu-3wt%Si)

Table 4.6 shows the effect of dopants on the density (ρ), electrical resistivity (ρ) and electrical conductivity (σ) of silicon bronze (Cu-3%wt.Si).

Table 4.6: Effect of dopants on the density (ρ), electrical resistivity (ρ) and electrical conductivity (σ) of silicon bronze (Cu-3%wt.Si).

Alloy designation	Alloy composition	ρ (g/cm^3)	ρ (x10^{-3}Ω-m)	σ(Sm^{-1})
BZ_4	Cu -3wt%Si-0.1wt%Zn	8.90	38.10	26.25
BZ_5	Cu -3wt%Si-0.2wt%Zn	9.00	38.18	26.19
BZ_6	Cu -3wt%Si-0.3wt%Zn	9.20	38.56	25.93
BZ_7	Cu -3wt%Si-0.4wt%Zn	9.50	39.20	25.51
BZ_8	Cu -3wt%Si-0.5wt%Zn	9.61	41.40	24.15
BZ_9	Cu -3wt%Si-0.6wt%Zn	9.62	42.0	23.81
BZ_{10}	Cu -3wt%Si-0.7wt%Zn	9.71	42.54	23.51
BZ_{11}	Cu -3wt%Si-0.8wt%Zn	9.75	43.3	23.09
BZ_{12}	Cu -3wt%Si-1wt%Zn	9.78	44.23	22.61

Alloy designation	Alloy composition	ρ (g/cm^3)	ρ (x10^{-3}Ω-m)	σ(Sm^{-1})
BZ_{13}	Cu -3wt%Si-1.5wt%Zn	9.8	45.16	22.14
BZ_{14}	Cu -3wt%Si-2wt%Zn	9.85	45.42	22.02
BZ_{15}	Cu -3wt%Si-3wt%Zn	9.88	45.70	21.88
BZ_{16}	Cu -3wt%Si-5wt%Zn	9.92	45.86	21.81
BZ_{17}	Cu -3wt%Si-0.1wt%Sn	8.41	44.19	22.63
BZ_{18}	Cu -3wt%Si-0.2wt%Sn	8.44	44.69	22.38
BZ_{19}	Cu -3wt%Si-0.3wt%Sn	8.55	45.20	22.12
BZ_{20}	Cu -3wt%Si-0.4wt%Sn	8.60	48.38	20.67
BZ_{21}	Cu -3wt%Si-0.5wt%Sn	8.62	49.40	20.24
BZ_{22}	Cu -3wt%Si-0.6wt%Sn	8.66	49.45	20.18
BZ_{23}	Cu -3wt%Si-0.7wt%Sn	8.68	49.58	20.17
BZ_{24}	Cu -3wt%Si-0.8wt%Sn	8.70	49.64	20.15
BZ_{25}	Cu -3wt%Si-1wt%Sn	8.84	49.68	20.13
BZ_{26}	Cu -3wt%Si-1.5wt%Sn	8.87	49.74	20.10
BZ_{27}	Cu -3wt%Si-2wt%Sn	9.20	49.80	20.08
BZ_{28}	Cu -3wt%Si-3wt%Sn	9.28	49.96	20.02
BZ_{29}	Cu -3wt%Si-5wt%Sn	9.35	50.30	19.88
BZ_{30}	Cu -3wt%Si-0.1wt%Mg	7.37	31.99	31.26
BZ_{31}	Cu -3wt%Si-0.2wt%Mg	7.41	32.82	30.47
BZ_{32}	Cu -3wt%Si-0.3wt%Mg	7.62	33.76	29.62
BZ_{33}	Cu -3wt%Si-0.4wt%Mg	7.80	34.33	29.13
BZ_{34}	Cu -3wt%Si-0.5wt%Mg	8.31	34.58	28.92
BZ_{35}	Cu -3wt%Si-0.6wt%Mg	8.53	34.74	28.79
BZ_{36}	Cu -3wt%Si-0.7wt%Mg	8.59	34.86	28.69
BZ_{37}	Cu -3wt%Si-0.8wt%Mg	8.64	35.03	28.55
BZ_{38}	Cu -3wt%Si-1wt%Mg	8.78	35.19	28.42
BZ_{39}	Cu -3wt%Si-1.5wt%Mg g	8.81	35.28	28.34
BZ_{40}	Cu -3wt%Si-0.1wt%Mn	8.64	44.69	22.38
BZ_{41}	Cu -3wt%Si-0.2wt%Mn	8.68	44.72	22.36
BZ_{42}	Cu -3wt%Si-0.3wt%Mn	8.70	44.80	22.32
BZ_{43}	Cu -3wt%Si-0.4wt%Mn	8.73	44.98	22.23
BZ_{44}	Cu -3wt%Si-0.5wt%Mn	8.78	45.80	21.83
BZ_{45}	Cu -3wt%Si-0.6wt%Mn	8.84	46.00	21.74
BZ_{46}	Cu -3wt%Si-0.7wt%Mn	8.90	46.59	21.46
BZ_{47}	Cu -3wt%Si-0.8wt%Mn	8.95	46.86	21.34
BZ_{48}	Cu -3wt%Si-1wt%Mn	9.02	47.64	21.00
BZ_{49}	Cu -3wt%Si-1.5wt%Mn	9.34	48.17	20.76
BZ_{50}	Cu -3wt%Si-0.1wt%W	8.95	28.15	35.52
BZ_{51}	Cu -3wt%Si-0.2wt%W	9.20	28.4	35.21
BZ_{52}	Cu -3wt%Si-0.3wt%W	9.25	29.50	33.90
BZ_{53}	Cu -3wt%Si-0.4wt%W	9.45	30.42	32.87
BZ_{54}	Cu -3wt%Si-0.5wt%W	9.52	31.86	31.39

Alloy designation	Alloy composition	ρ (g/cm^3)	ρ (x10^{-3}Ω-m)	σ(Sm^{-1})
BZ_{55}	Cu -3wt%Si-0.6wt%W	9.58	32.02	31.23
BZ_{56}	Cu -3wt%Si-0.7wt%W	9.59	32.10	31.15
BZ_{57}	Cu -3wt%Si-0.8wt%W	9.63	34.08	29.34
BZ_{58}	Cu -3wt%Si-1wt%W	9.65	35.19	28.42
BZ_{59}	Cu -3wt%Si-1.5wt%W	9.70	35.28	28.34
BZ_{60}	Cu -3wt%Si-0.1wt%Ti	8.45	35.98	27.79
BZ_{61}	Cu -3wt%Si-0.2wt%Ti	8.71	36.40	27.47
BZ_{62}	Cu -3wt%Si-0.3wt%Ti	8.90	36.42	27.46
BZ_{63}	Cu -3wt%Si-0.4wt%Ti	9.32	36.44	27.44
BZ_{64}	Cu -3wt%Si-0.5wt%Ti	9.35	36.56	27.35
BZ_{65}	Cu -3wt%Si-0.6wt%Ti	9.38	36.59	27.33
BZ_{66}	Cu -3wt%Si-0.7wt%Ti	9.40	36.70	27.25
BZ_{67}	Cu -3wt%Si-0.8wt%Ti	9.48	37.29	26.82
BZ_{68}	Cu -3wt%Si-1wt%Ti	9.59	37.32	26.80
BZ_{69}	Cu -3wt%Si-1.5wt%Ti	9.62	37.48	26.68
BZ_{70}	Cu -3wt%Si-2wt%Ti	9.68	37.60	26.60
BZ_{71}	Cu -3wt%Si-3wt%Ti	9.74	37.65	26.56
BZ_{72}	Cu -3wt%Si-5wt%Ti	9.78	37.71	26.52
BZ_{73}	Cu-3wt%Si-0.1wt%Mo	7.01	40.44	24.73
BZ_{74}	Cu-3wt%Si-0.2wt%Mo	7.05	41.86	23.89
B_{75}	Cu-3wt%Si-0.3wt%Mo	7.09	42.52	23.52
BZ_{76}	Cu-3wt%Si-0.4wt%Mo	7.21	42.74	23.40
BZ_{77}	Cu-3wt%Si-0.5wt%Mo	7.28	43.08	23.21
BZ_{78}	Cu-3wt%Si-0.6wt%Mo	7.30	43.56	22.96
BZ_{79}	Cu-3wt%Si-0.7wt%Mo	7.51	44.14	22.66
BZ_{80}	Cu-3wt%Si-0.8wt%Mo	7.58	44.38	22.53
BZ_{81}	Cu-3wt%Si-1wt%Mo	7.60	44.69	22.38
BZ_{82}	Cu-3wt%Si-1.5wt%Mo	7.81	45.18	22.13
BZ_{83}	Cu-3wt%Si-2wt%Mo	7.58	44.38	22.53
BZ_{84}	Cu-3wt%Si-3wt%Mo	7.60	44.69	22.38
BZ_{85}	Cu -3%wt.Si-5%wt.Mo	7.81	45.18	22.13
BZ_{86}	Cu-3wt%Si-0.1wt%Al	8.40	29.23	34.21
BZ_{87}	Cu-3wt%Si-0.2wt%Al	8.91	30.58	32.70
BZ_{88}	Cu-3wt%Si-0.3wt%Al	9.01	31.93	31.32
BZ_{89}	Cu-3wt%Si-0.4wt%Al	9.04	32.14	31.11
BZ_{90}	Cu-3wt%Si-0.5wt%Al	9.16	32.68	30.60
BZ_{91}	Cu-3wt%Si-0.6wt%Al	9.19	33.74	29.64
BZ_{92}	Cu-3wt%Si-0.7wt%Al	9.23	34.21	29.23
BZ_{93}	Cu-3wt%Si-0.8wt%Al	9.24	36.48	27.41
BZ_{94}	Cu-3wt%Si-1wt%Al	9.30	38.21	26.13
BZ_{95}	Cu-3wt%Si-1.5wt%Al	9.36	37.20	26.88
BZ_{96}	Cu-3wt%Si-2wt%Al	9.38	37.40	26.74
BZ_{97}	Cu-3wt%Si-3wt%Al	9.40	37.62	26.58
BZ_{98}	Cu-3wt%Si-5wt%Al	9.42	37.80	26.46

Figure 4.36 shows the effect of dopants on the density of silicon bronze. Figure 4.36 shows that addition of 0.1% by weight of magnesium and molybdenum decreased the density of silicon bronze. Addition of other dopants significantly increased the density of the alloy. The density was observed to increase with increase in dopants concentration.

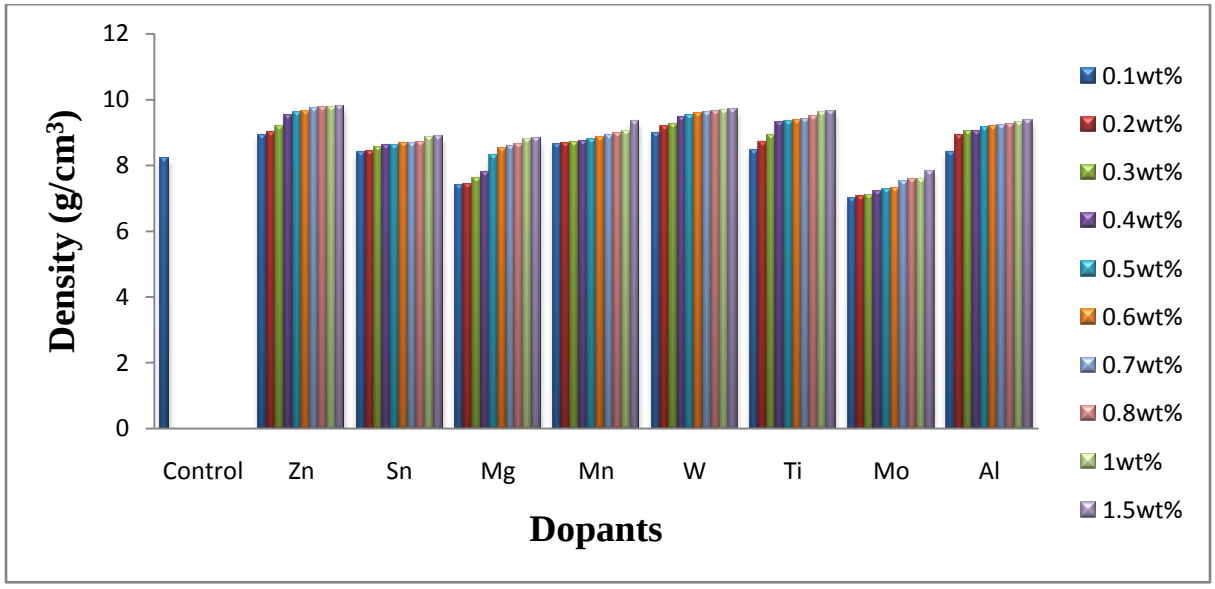

Figure 4.36: Effect of dopants on the density of silicon bronze (Cu-3wt%Si)

Figures 4.37 and 4.38 show the electrical resistivity and conductivity of silicon bronze doped with different concentration of alloying elements such as zinc, tin, magnesium, manganese, tungsten, titanium, molybdenum and aluminium metals. Increase in ρ and decrease in σ were observed as the concentration of the dopants increased. From electron theory, ρ for metal is a measure of the non-forwards scattering when the external electric field is accelerated (Nnuka, 1994). Addition of dopant to Cu-Si alloy system predominantly increased the impurity level which systematically increased the ρ and decrease the σ.

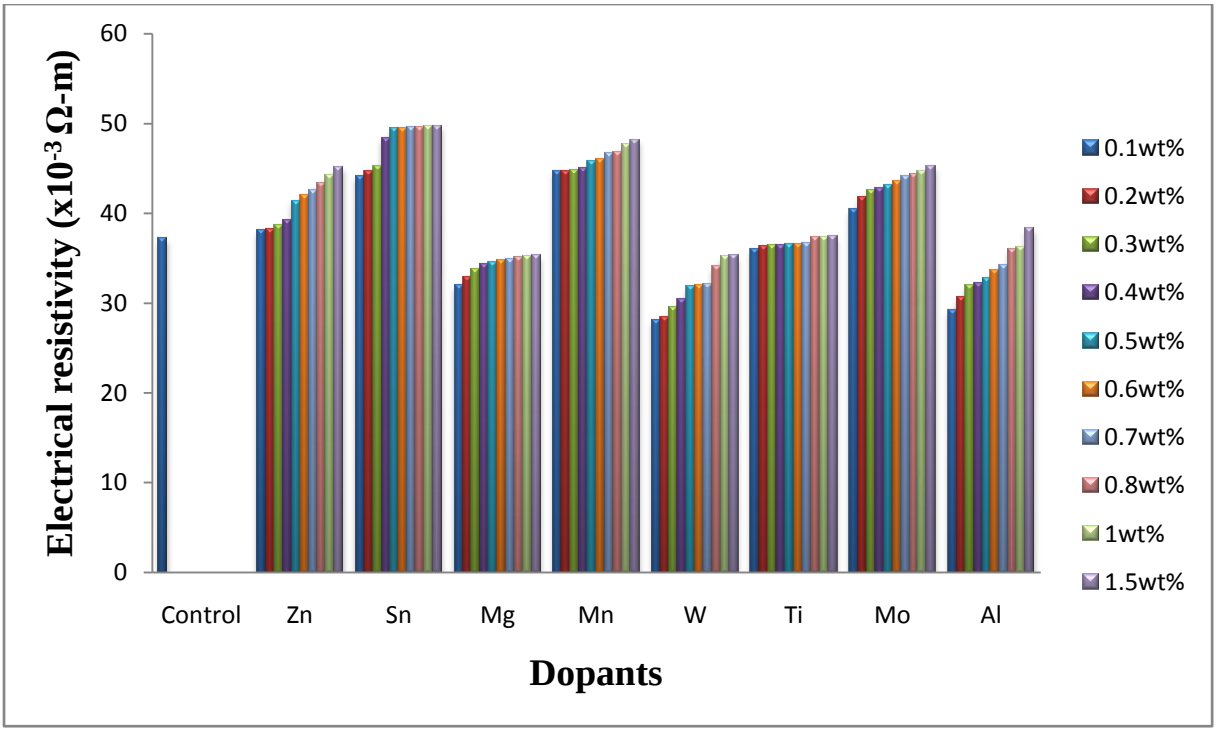

Figure 4.37: Effect of dopants on the electrical resistivity of silicon bronze (Cu-3wt%Si)

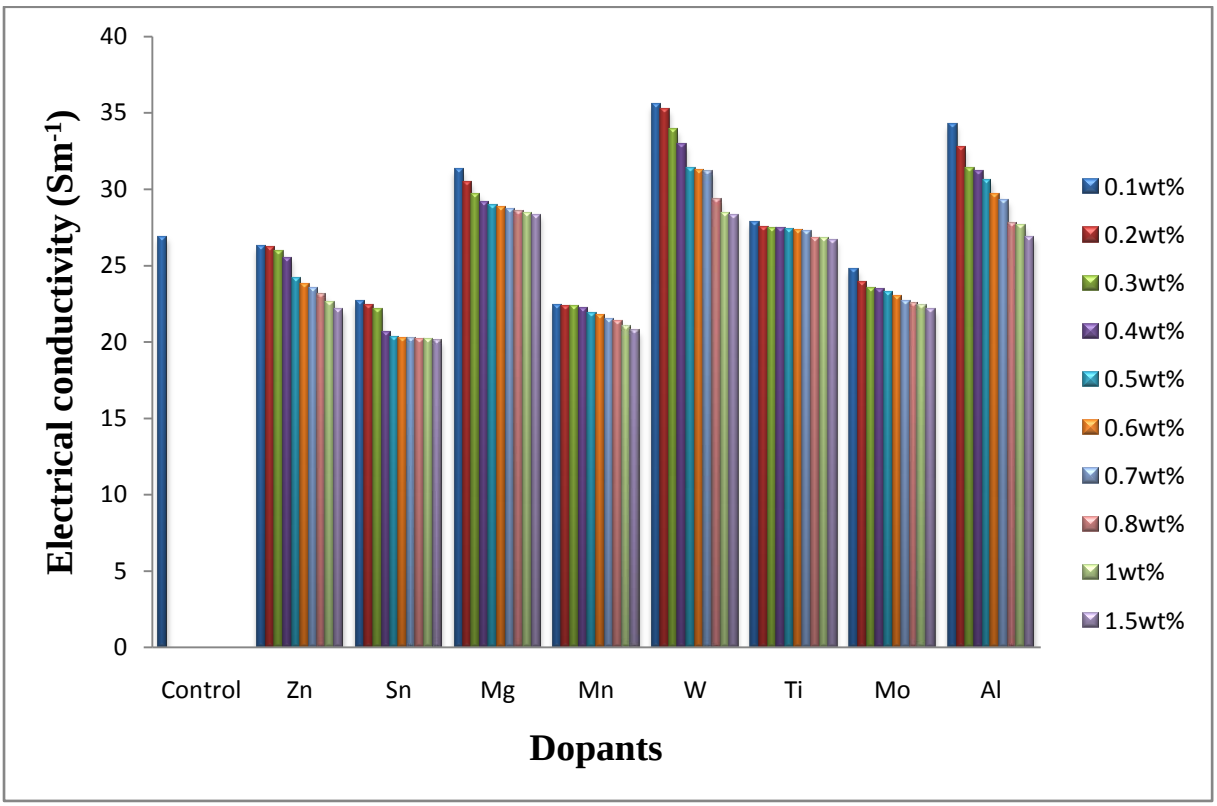

Figure 4.38: Effect of dopants on the electrical conductivity of silicon bronze (Cu-3wt%Si)

4.1.1 Effect of heat treatment on the mechanical properties of the best alloys compositions.

Table 4.7 indicates the effect of heat treatment on the percentage elongation and ultimate tensile strength of silicon bronzes

Table 4.7: Effect of heat treatment on the percentage elongation and ultimate tensile strength of silicon bronzes

Alloy composition	Condition	UTS (MPa)	%E
Cu-3wt%Si-3wt%Zn	non-heat treated	353	17.4
Cu-3wt%Si-3wt%Zn	heat treated	376	13.4
Cu-3wt%Si-3wt%Sn	non-heat treated	238	11.1
Cu-3wt%Si-3wt%Sn	heat treated	229	11.8
Cu-3wt%Si-0.8wt%Mg	non-heat treated	285	19.1
Cu-3wt%Si-0.8wt%Mg	heat treated	306	16.3
Cu-3wt%Si-1wt%Mn	non-heat treated	378	6.5
Cu-3wt%Si-1wt%Mn	heat treated	385	5.4
Cu-3wt%Si-0.8wt%W	non-heat treated	286	20.8
Cu-3wt%Si-0.8wt%W	heat treated	298	15.6
Cu-3wt%Si-2wt%Ti	non-heat treated	265	7.2
Cu-3wt%Si-2wt%Ti	heat treated	274	5.8
Cu-3wt%Si-1.5wt%Mo	non-heat treated	130	12.1
Cu-3wt%Si-1.5wt%Mo	heat treated	168	10.8
Cu-3wt%Si-3wt%Al	non-heat treated	314	5.1
Cu-3wt%Si-3wt%Al	heat treated	322	3.4

The percentage elongation of heat treated and non-heat treated silicon bronze is presented in Figure 4.39. Analysis of Figure 4.39 indicates that heat treatment significantly decreased the percentage elongation of silicon bronze doped with Zn, Mg, Mn, W, Ti, Mo and Al. This change is quantified by the existence of refined and coherent intermetallic compound in the alloy structure. The alloy doped with tin showed different behavior.

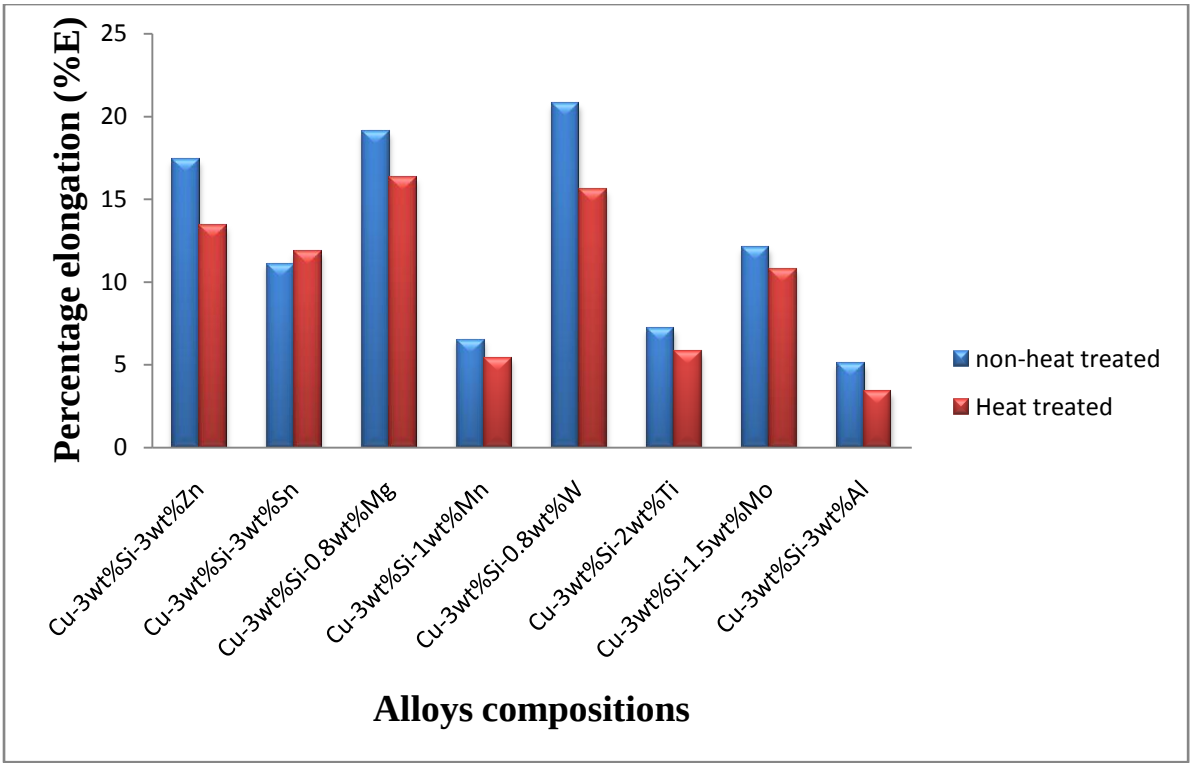

Figure 4.39: Effect of heat treatment on the percentage elongation of silicon bronzes.

Figure 4.40 shows the effect of heat treatment on the ultimate tensile strength of silicon bronzes. Analysis of Figure 4.40 shows increase in ultimate tensile strength of heat treated alloy doped with Zn, Mg, Mn, W, Ti, Mo and Al. This could be attributed to decrease in grain size and increase in distribution of the intermetallic compound in the copper matrix. Alloy doped with Sn showed different effect as a result of formation of non-coherent intermetallic compound in the alloy structure as evidenced in the microstructural analysis.

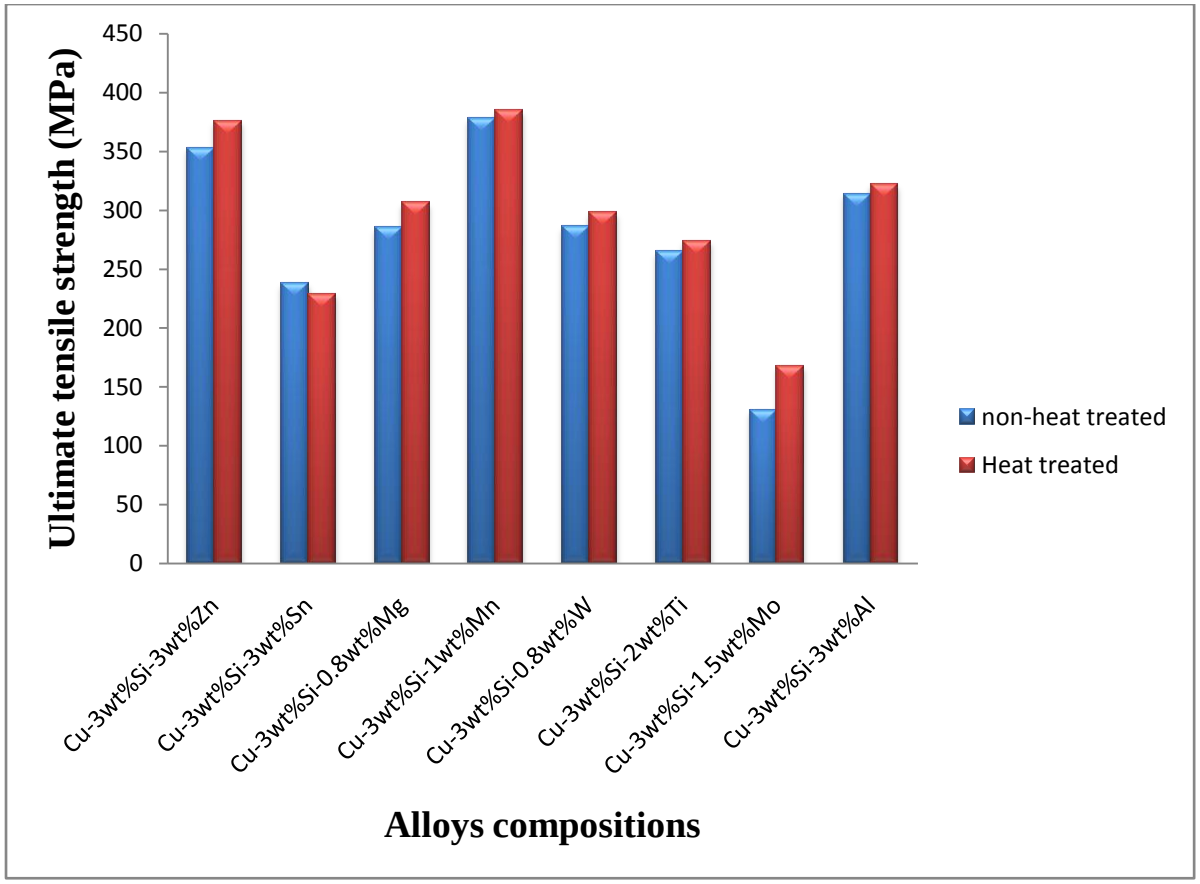

Figure 4.40: Effect of heat treatment on the ultimate tensile strength of silicon bronzes.

The effect of heat treatment on the hardness and impact strength of silicon bronzes is presented in Table 4.8. This table shows the comparison between the ultimate tensile strength of heat treated and non-heat treated silicon bronzes.

Table 4.8: Effect of heat treatment on the hardness and impact strength of silicon bronzes

Alloy composition	Condition	Brinell hardness (MPa)	Impact strength (J)
Cu-3wt%Si-3wt%Zn	non-heat treated	254	24.4
Cu-3wt%Si-3wt%Zn	heat treated	268	19.5
Cu-3wt%Si-3wt%Sn	non-heat treated	278	25.2
Cu-3wt%Si-3wt%Sn	heat treated	251	25.9
Cu-3wt%Si-0.8wt%Mg	non-heat treated	318	13.2
Cu-3wt%Si-0.8wt%Mg	heat treated	387	10.4
Cu-3wt%Si-1wt%Mn	non-heat treated	371	8.3
Cu-3wt%Si-1wt%Mn	heat treated	390	5.3
Cu-3wt%Si-0.8wt%W	non-heat treated	358	16.6
Cu-3wt%Si-0.8wt%W	heat treated	364	12.8
Cu-3wt%Si-2wt%Ti	non-heat treated	282	10.2
Cu-3wt%Si-2wt%Ti	heat treated	308	9.3
Cu-3wt%Si-1.5wt%Mo	non-heat treated	192	8.5
Cu-3wt%Si-1.5wt%Mo	heat treated	201	6.8
Cu-3wt%Si-3wt%Al	non-heat treated	278	14.2
Cu-3wt%Si-3wt%Al	heat treated	284	10.4

The hardness of silicon bronze solution heat treated at temperature of 900^{o}C for 30 minutes and cooled in air is presented in Figure 4.41. This figure shows that heat treatment significantly improved the hardness of silicon bronzes doped with Zn, Mg, Mn, W, Ti, Mo and Al. The observed increase in hardness could be attributed to the decrease in grain size and increase in distribution pattern of the intermetallic compound. Alloy doped with Sn showed decreased hardness when subjected to solution heat treatment.

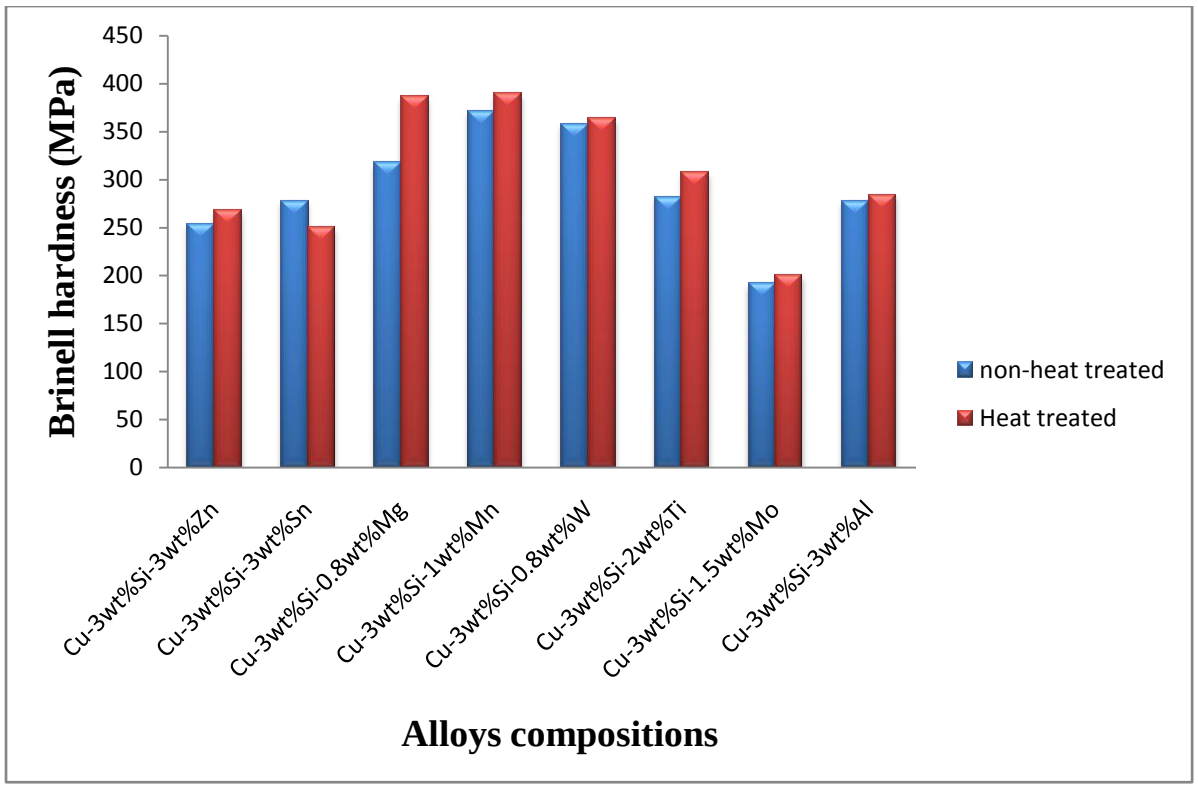

Figure 4.41: Effect of heat treatment on the hardness of silicon bronzes.

Figure 4.42 shows the effect of solution heat treatment on the impact strength of silicon bronze doped with Zn, Mg, Mn, W, Ti, Mo and Al. Figure 4.42 shows that the impact strength of silicon bronze doped with zinc, magnesium, manganese, titanium and aluminium decreased significantly when subjected to heat treatment. Silicon bronze doped with tin showed increase in impact strength when heat treated (Figure 4.42).

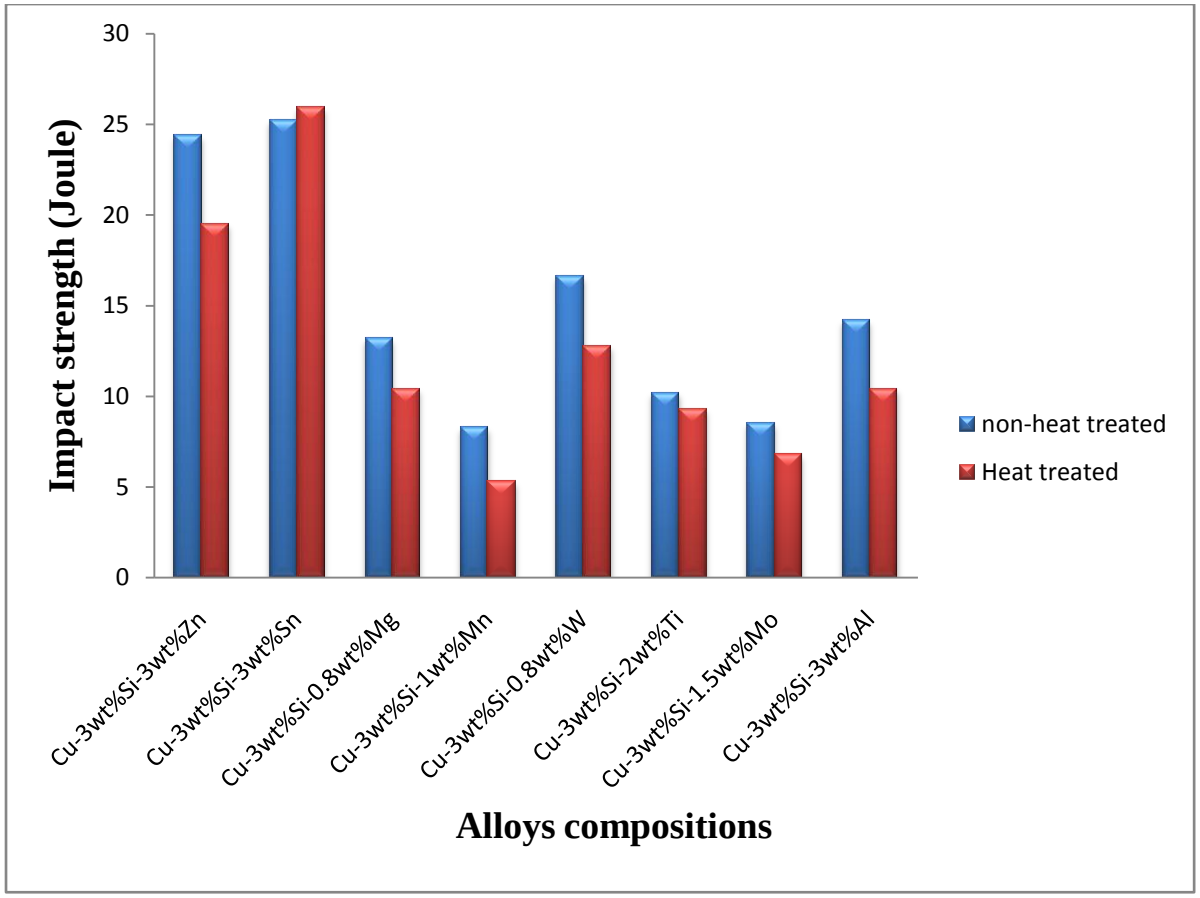

Figure 4.42: Effect of heat treatment on the impact strength of silicon bronzes.

4.1.2 Effect of heat treatment on the physical properties of the best alloys compositions

Table 4.9 indicates the effect of heat treatment on the density (ρ), electrical resistivity (ρ) and electrical conductivity (σ) of silicon bronzes. Table 4.9 shows the comparison between the density (ρ), electrical resistivity (ρ) and electrical conductivity (σ) of heat treated and non-heat treated silicon bronzes.

Table 4.9: Effect of heat treatment on the density (ρ), electrical resistivity (ρ) and electrical conductivity (σ) of silicon bronzes

Alloy composition	Condition	ρ (g/cm^3)	ρ (x10^{-3}Ω-m)	σ(Sm^{-1})
Cu-3wt%Si-3wt%Zn	non-heat treated	9.88	45.42	22.02
Cu-3wt%Si-3wt%Zn	heat treated	9.96	45.54	21.96
Cu-3wt%Si-3wt%Sn	non-heat treated	9.28	49.96	20.02
Cu-3wt%Si-3wt%Sn	heat treated	7.96	44.69	22.38
Cu-3wt%Si-0.8wt%Mg	non-heat treated	8.64	35.03	28.55
Cu-3wt%Si-0.8wt%Mg	heat treated	8.29	41.55	24.07
Cu-3wt%Si-1wt%Mn	non-heat treated	9.02	47.64	21.00
Cu-3wt%Si-1wt%Mn	heat treated	7.96	53.51	18.68
Cu-3wt%Si-0.8wt%W	non-heat treated	9.63	34.08	29.34
Cu-3wt%Si-0.8wt%W	heat treated	9.22	41.86	23.89
Cu-3wt%Si-2wt%Ti	non-heat treated	9.68	37.60	26.60
Cu-3wt%Si-2wt%Ti	heat treated	9.84	44.69	22.38
Cu-3wt%Si-1.5wt%Mo	non-heat treated	7.81	45.18	22.13
Cu-3wt%Si-1.5wt%Mo	heat treated	7.60	47.00	21.28
Cu-3wt%Si-3wt%Al	non-heat treated	9.40	37.62	26.58
Cu-3wt%Si-3wt%Al	heat treated	9.54	39.21	25.50

Figure 4.43 indicated that heat treatment has significant effect on the density of silicon bronzes. It was observed in Figure 4.43 that the density of heat treated silicon bronze doped with zinc, titanium and aluminium increased while the density of other samples doped with tin, magnesium, manganese, tungsten and molybdenum decreased when compared with the non-heat treated alloys.

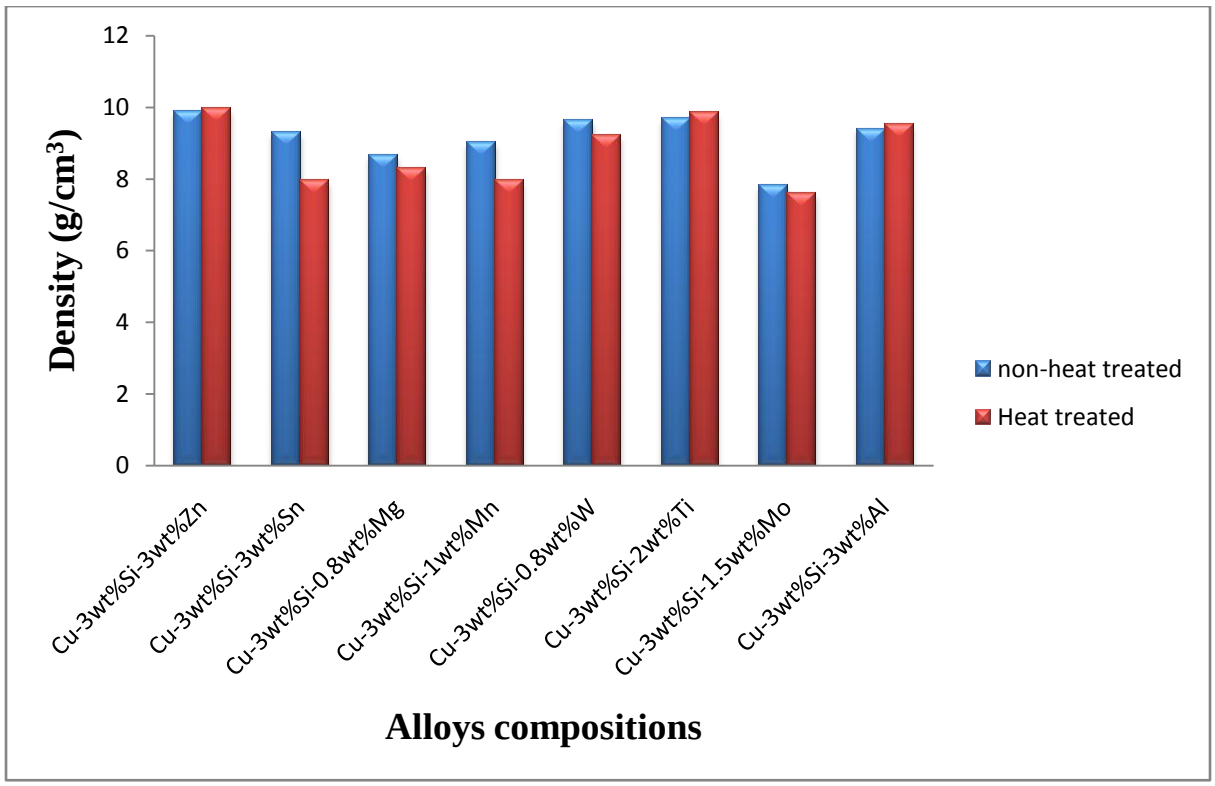

Figure 4.43: Effect of heat treatment on the impact strength of silicon bronzes.

Figures 4.44 and 4.45 depict the effect of heat treatment on the electrical resistivity and conductivity of the developed alloys. Figure 4.44 indicates that the electrical resistivity of heat treated silicon bronze doped with Zn, Mg, Mn, Mg, W, Mo and Al increased when compared with the non-heat treated alloy. This could be attributed to the presence of refined and well distributed intermetallic compounds in the alloy structure which generated local scattering point and led to electron scattering. This increased the electrical resistivity and decreased the electrical conductivity of the alloy. Alloy doped with Sn showed decreased electrical resistivity and increased electrical conductivity compared to

the non-heat treated alloy. This could be attributed to the presence of coarse intermetallic compound in the alloy structure (Plate 4.85).

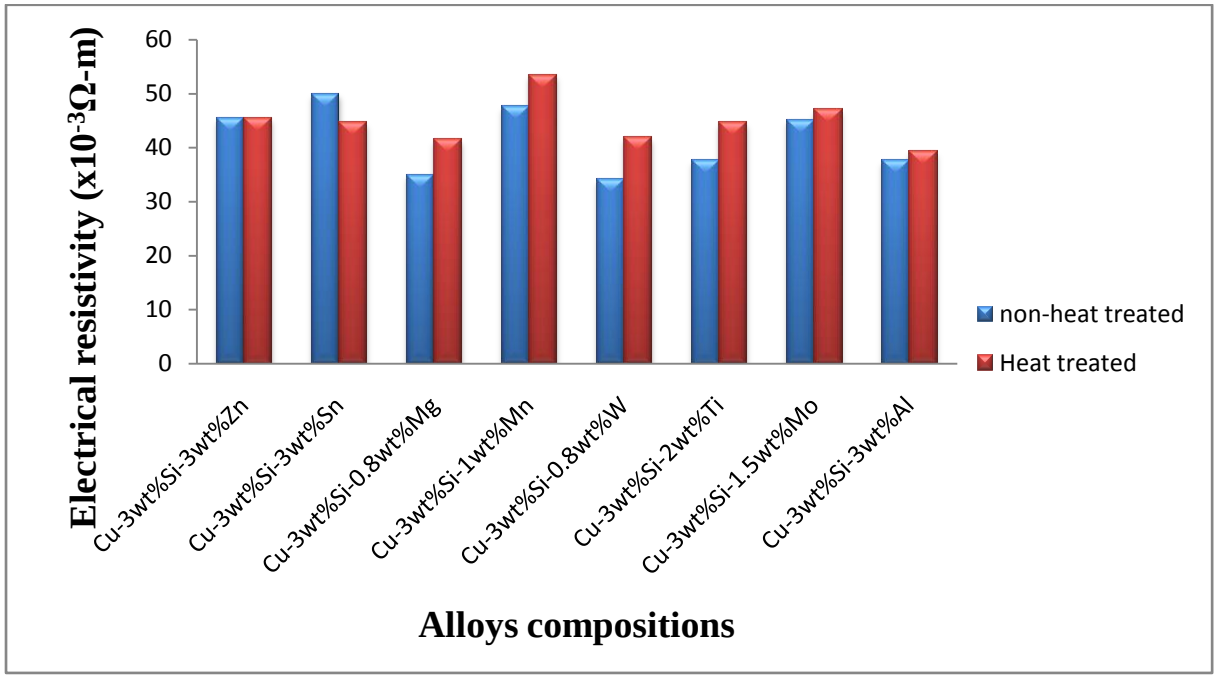

Figure 4.44: Effect of heat treatment on the electrical resistivity of silicon bronzes.

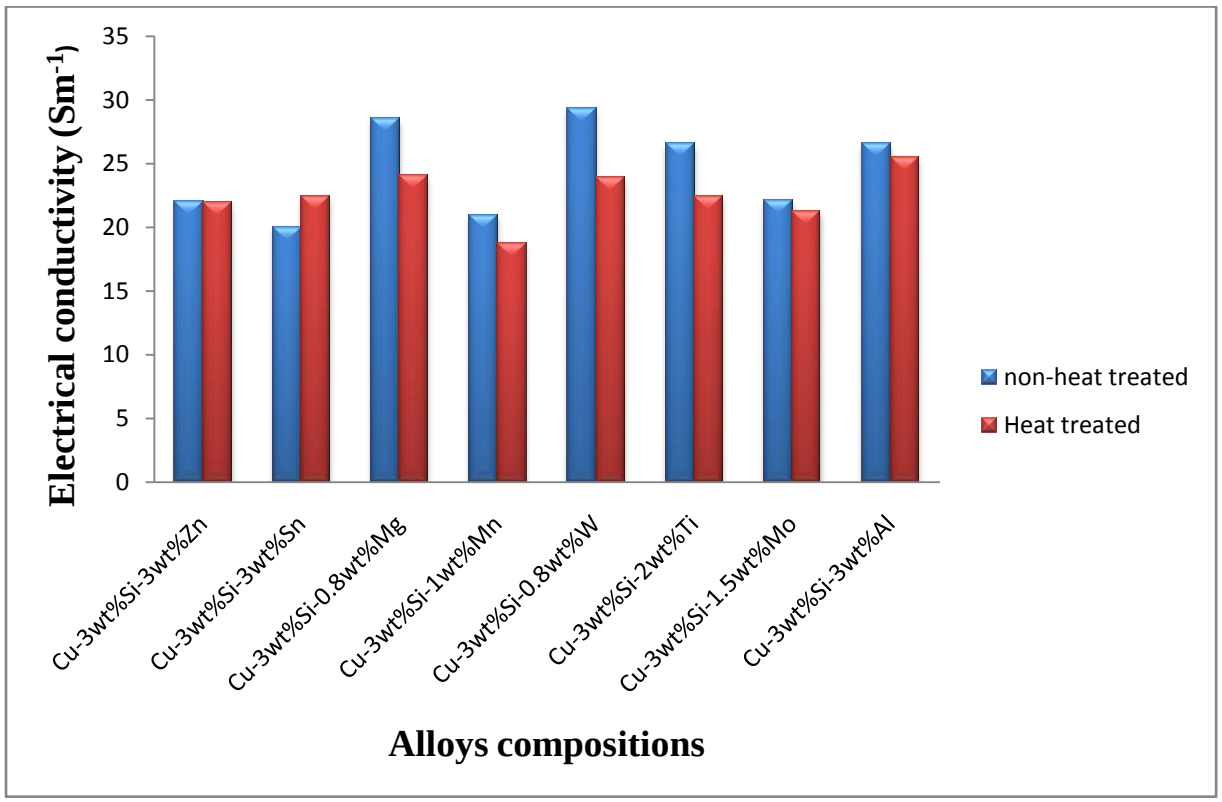

Figure 4.45: Effect of heat treatment on the electrical conductivity of silicon bronzes.

4.2 Correlation between mechanical and physical properties of silicon bronzes

The correlation between the mechanical (UTS and hardness) and physical (electrical resistivity and conductivity) properties of silicon bronze doped with different concentration of dopants is presented in Figures 4.46-4.57.

Analysis of Figures 4.46-4.57 shows clearly that ultimate tensile strength and hardness correlates with electrical resistivity while percentage elongation correlates with electrical conductivity. Mechanical and physical properties are highly sensitive to structural changes (Nnuka, 1994). From electron theory, ρ for metals is a measure of the non-forward scattering when the external electric field is accelerated (Miller et al., 2000; Nnuka, 1994). When 0.1wt% of dopant is added to Cu-Si alloy, the predominant effect on ρ is caused by the scattering of electrons on the irregularities of crystal lattice. Addition of dopant to silicon bronze caused grain refining effect which gave rise the increased ultimate tensile strength and hardness of the alloy with corresponding decrease in percentage elongation. Grain refinement caused scattering of electrons which resulted to increase and decrease in electrical resistivity and conductivity respectively (Joseph et al., 2014; Nnuka, 1994).

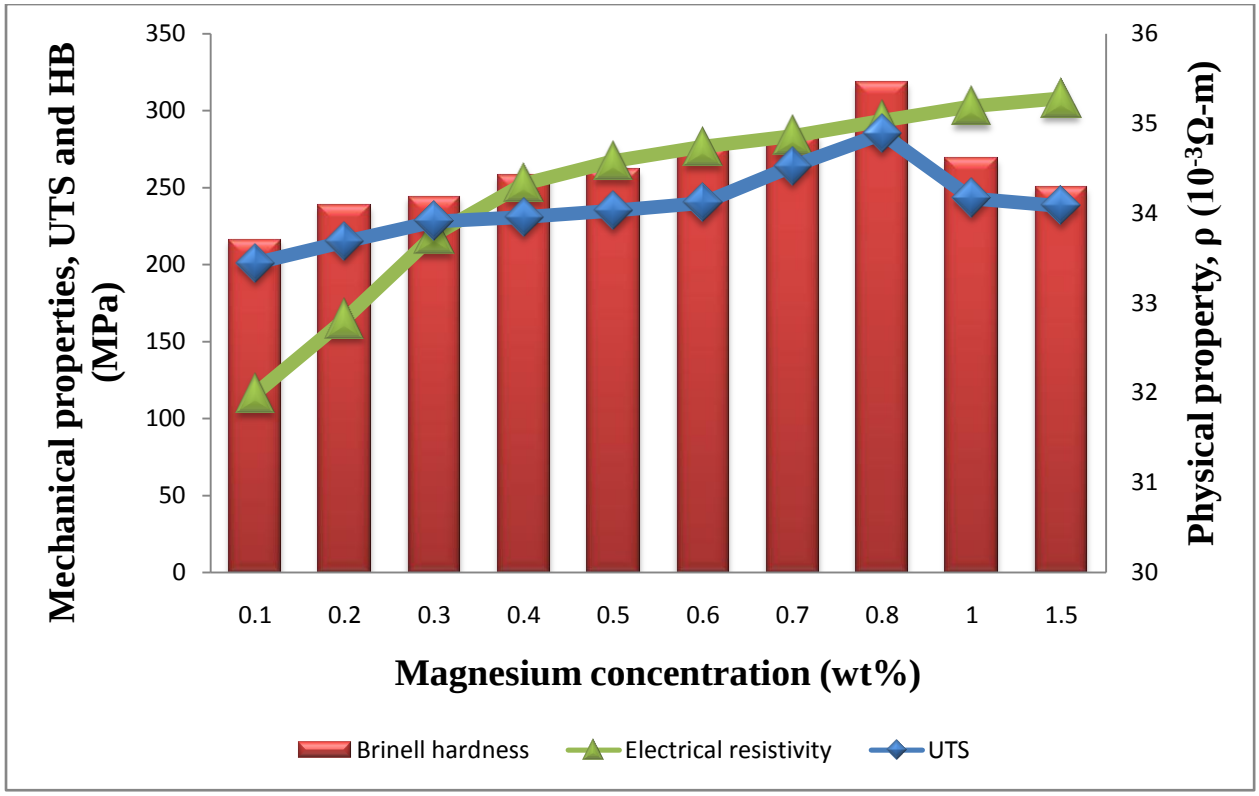

Figure 4.46: Effect of magnesium concentration on the ultimate tensile strength (UTS), Brinell hardness (HB) and electrical resistivity (ρ) of silicon bronze.

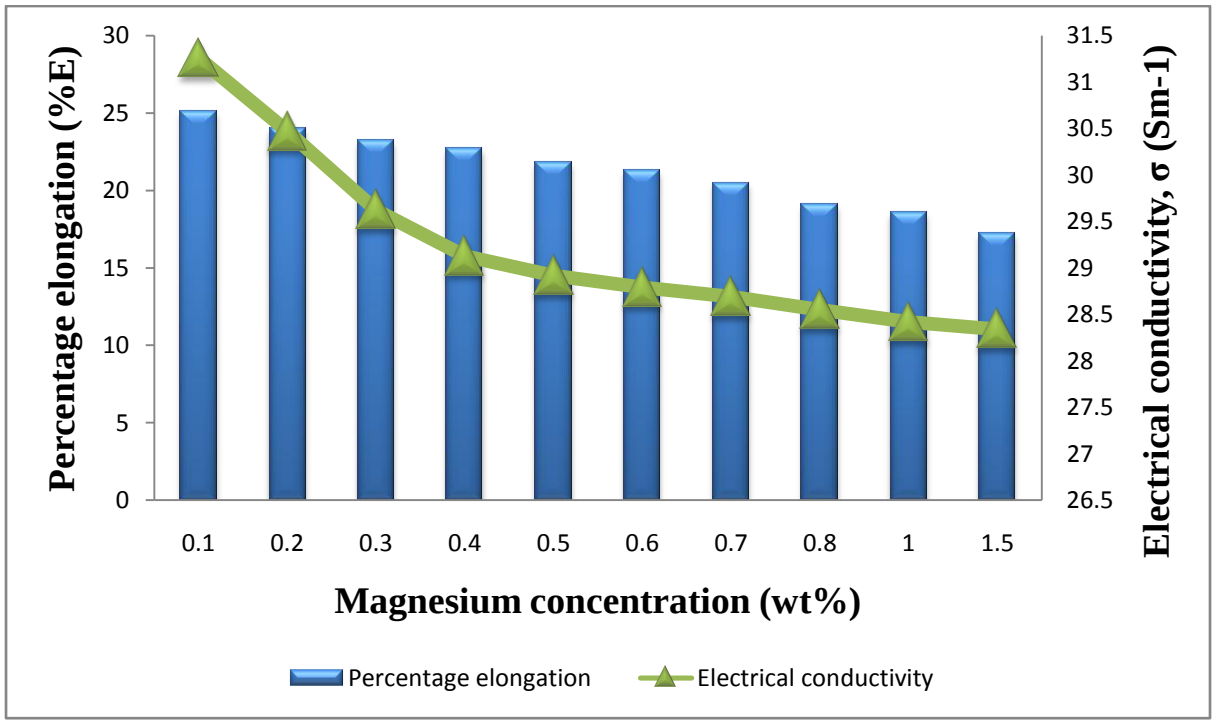

Figure 4.47: Effect of magnesium concentration on the percentage elongation and electrical conductivity (σ) of silicon bronze.

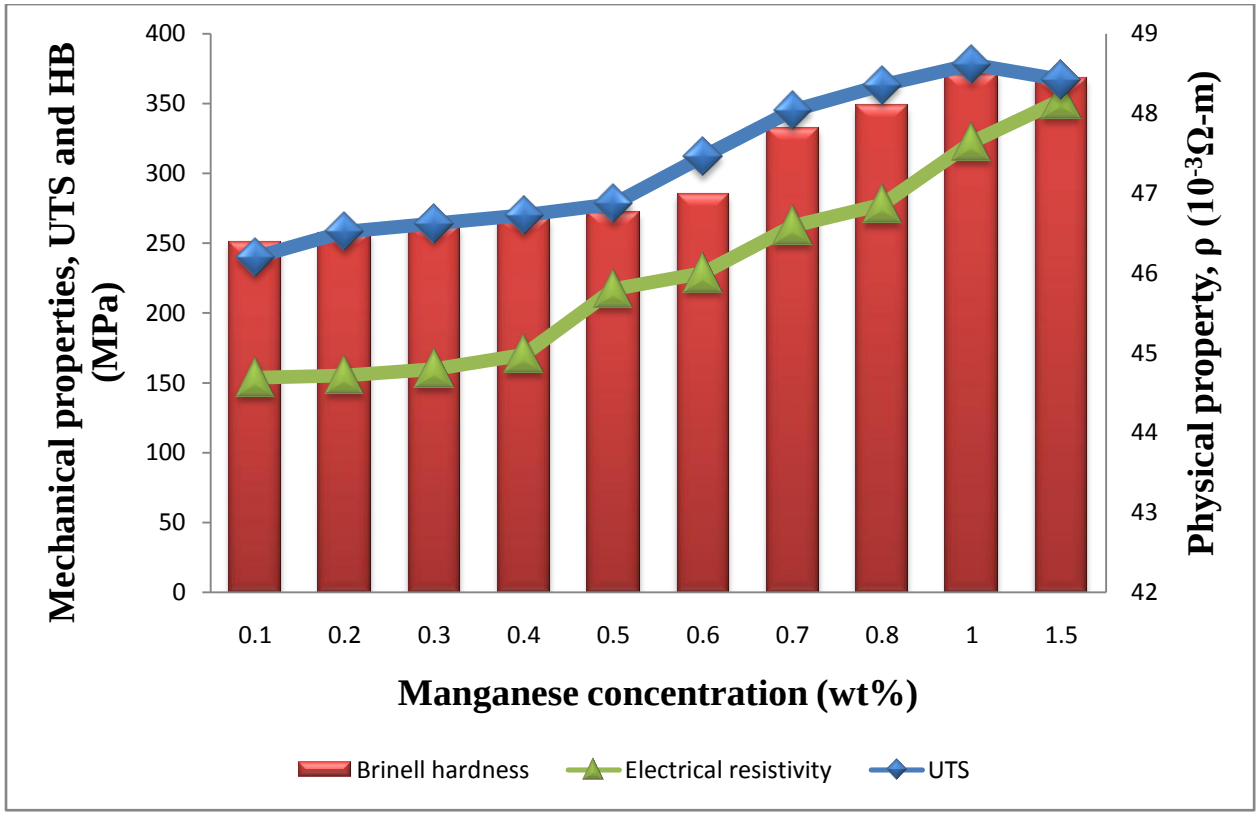

Figure 4.48: Effect of manganese concentration on the ultimate tensile strength (UTS), Brinell hardness (HB) and electrical resistivity (ρ) of silicon bronze.

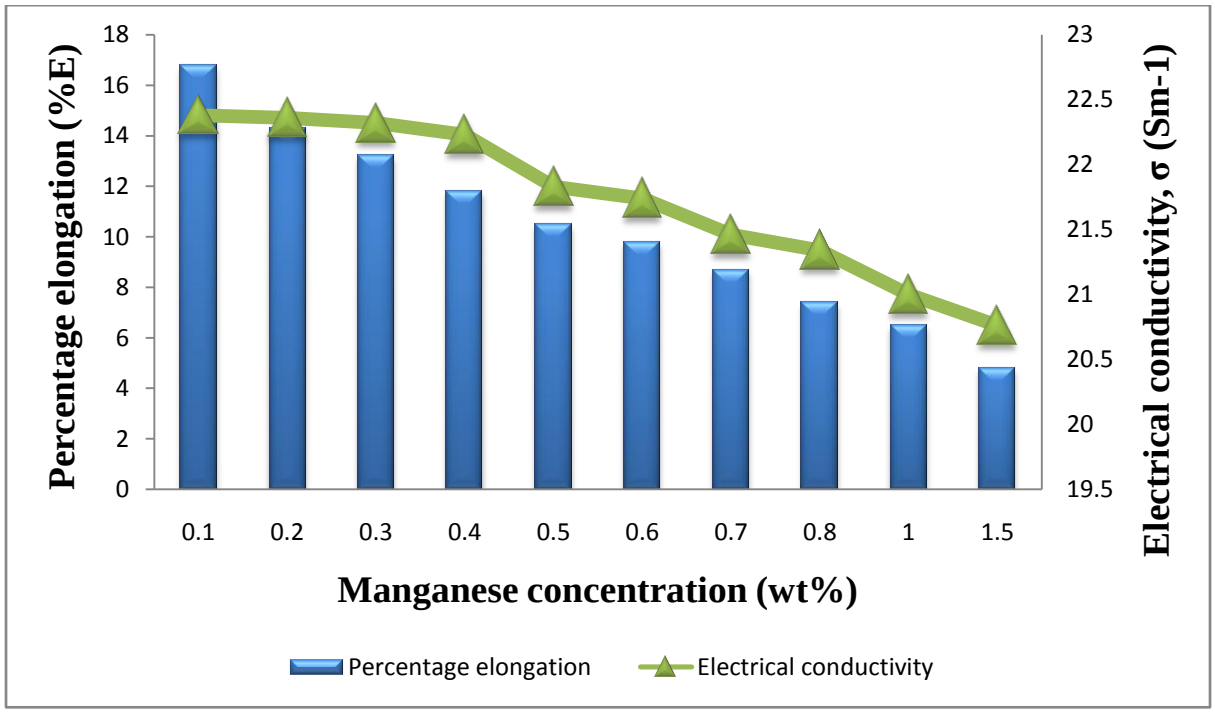

Figure 4.49: Effect of manganese concentration on the percentage elongation and electrical conductivity (σ) of silicon bronze.

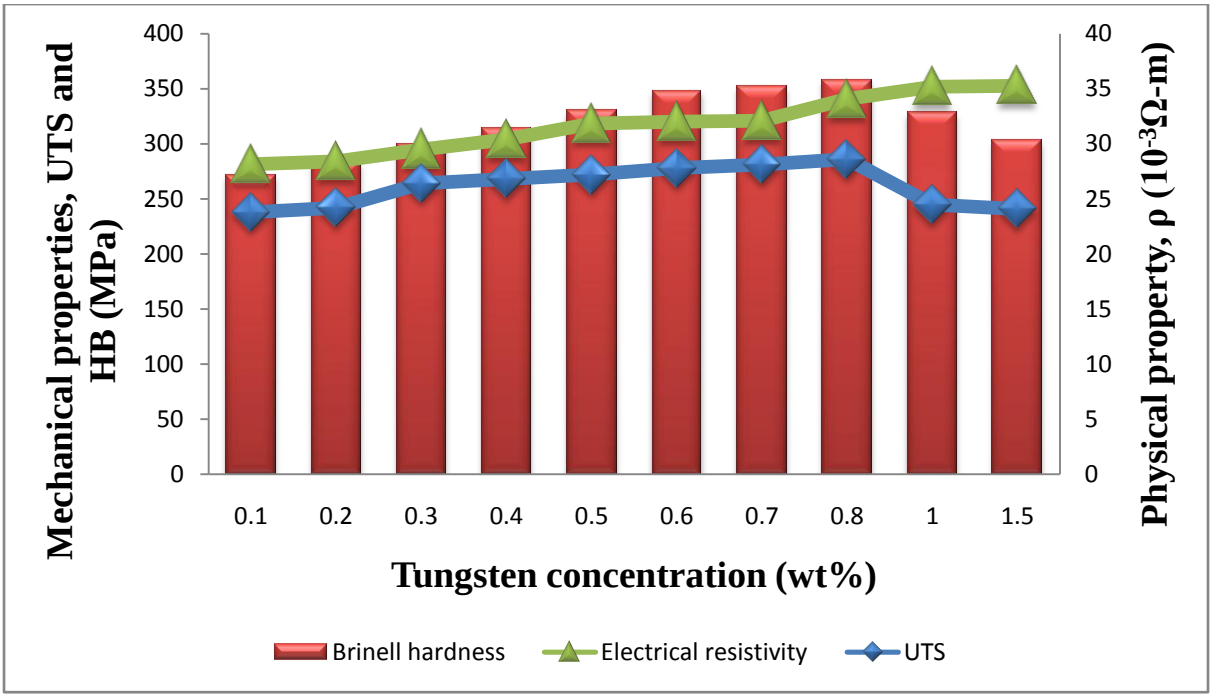

Figure 4.50: Effect of tungsten concentration on the ultimate tensile strength (UTS), Brinell hardness (HB) and electrical resistivity (ρ) of silicon bronze.

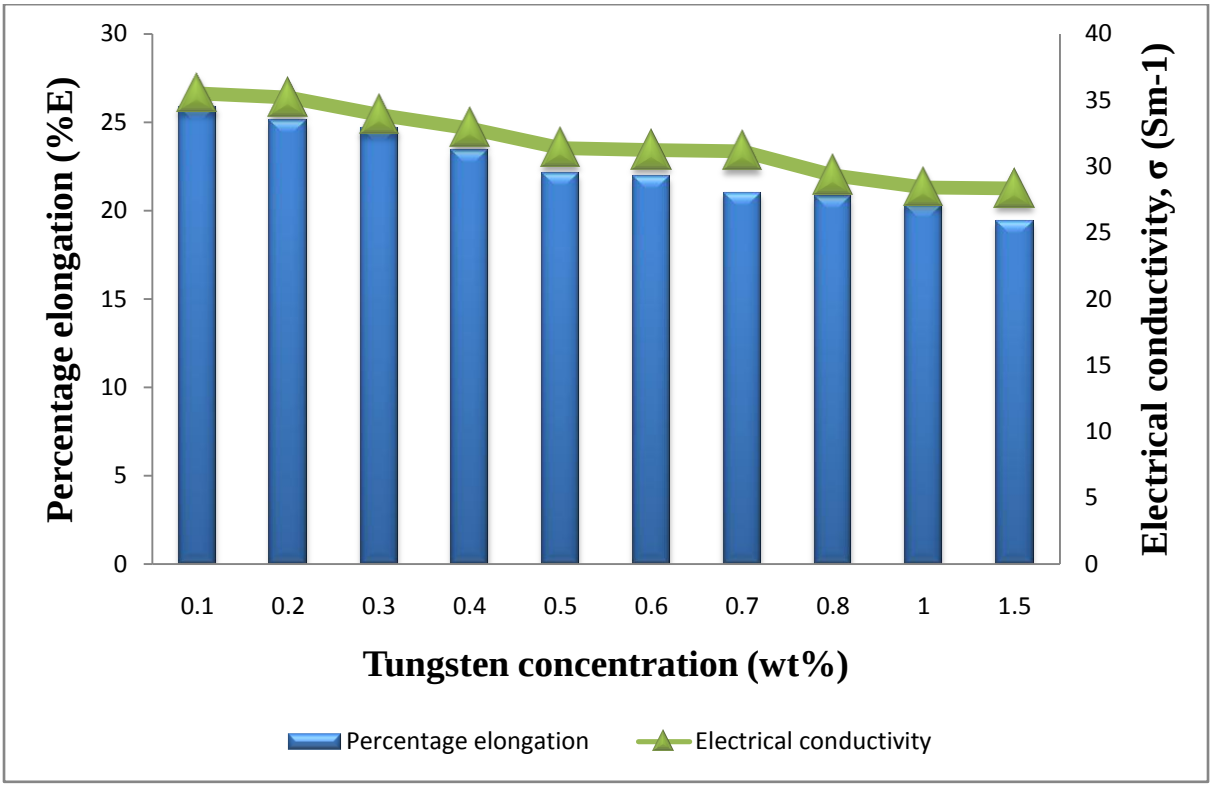

Figure 4.51: Effect of tungsten concentration on the percentage elongation and electrical conductivity (σ) of silicon bronze.

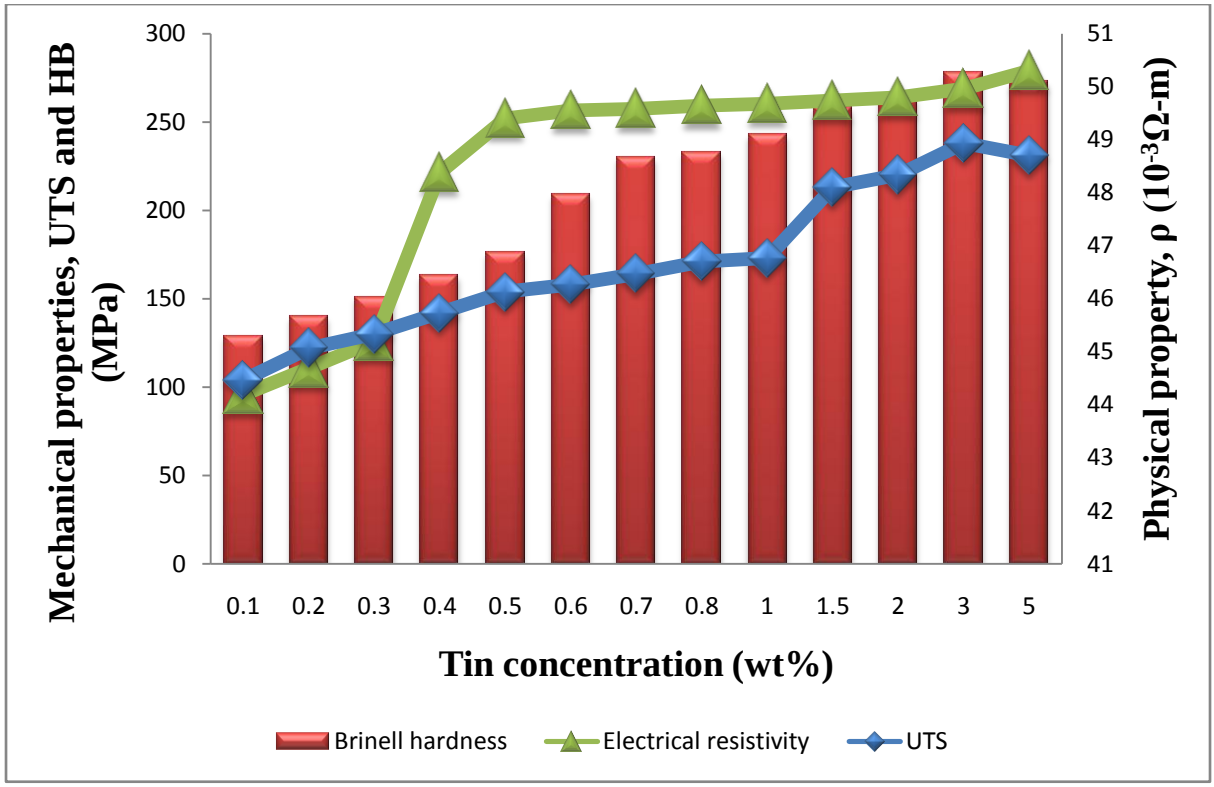

Figure 4.52: Effect of tin concentration on the ultimate tensile strength (UTS), Brinell hardness (HB) and electrical resistivity (ρ) of silicon bronze.

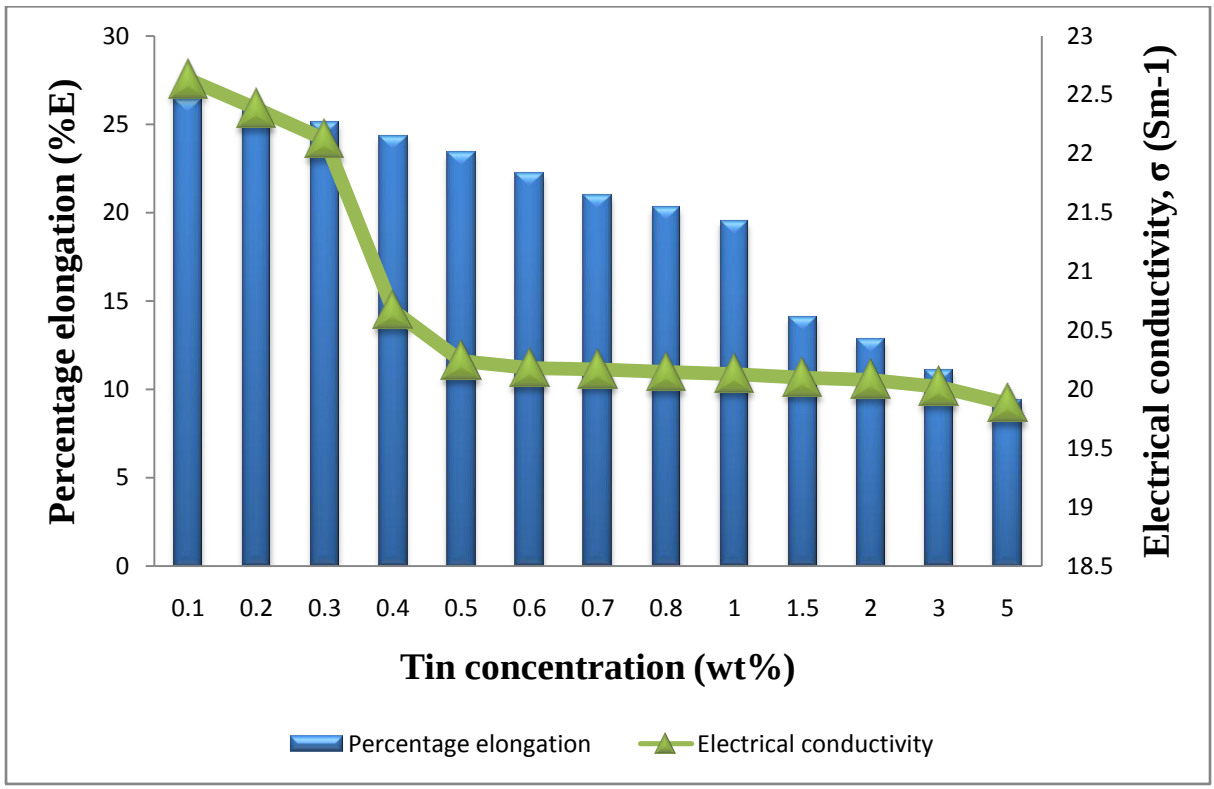

Figure 4.53: Effect of tin concentration on the percentage elongation and electrical conductivity (σ) of silicon bronze.

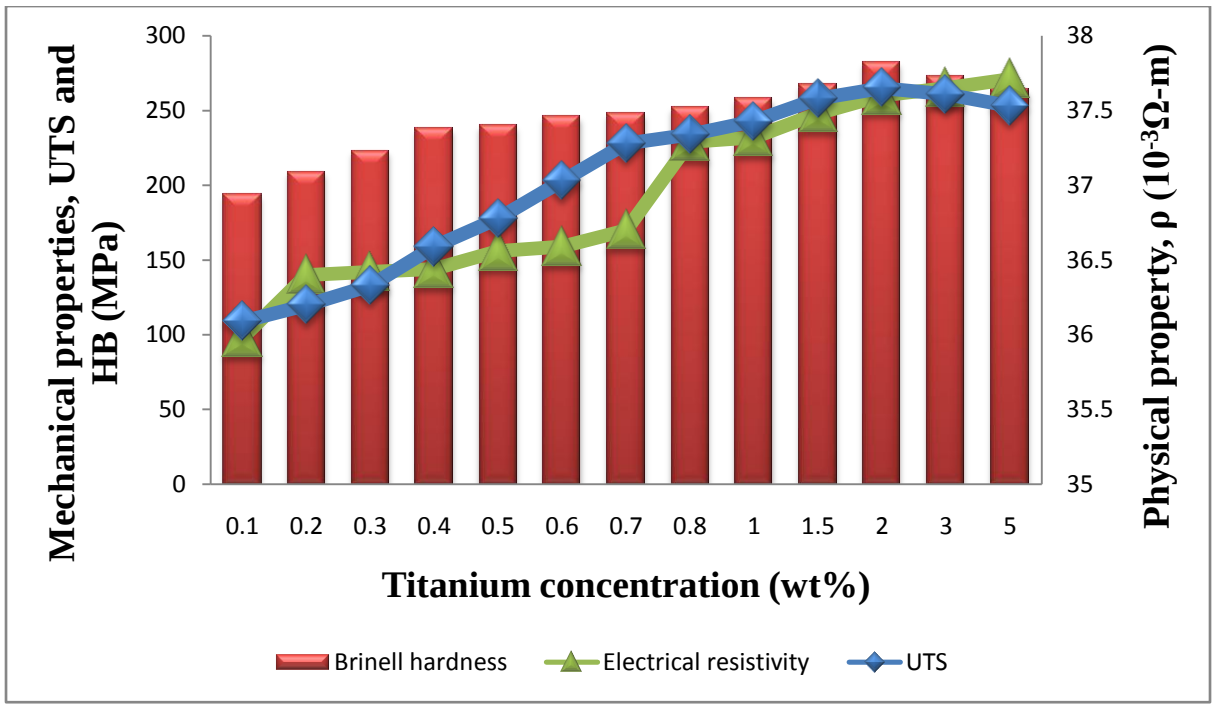

Figure 4.54: Effect of titanium concentration on the ultimate tensile strength (UTS), Brinell hardness (HB) and electrical resistivity (ρ) of silicon bronze.

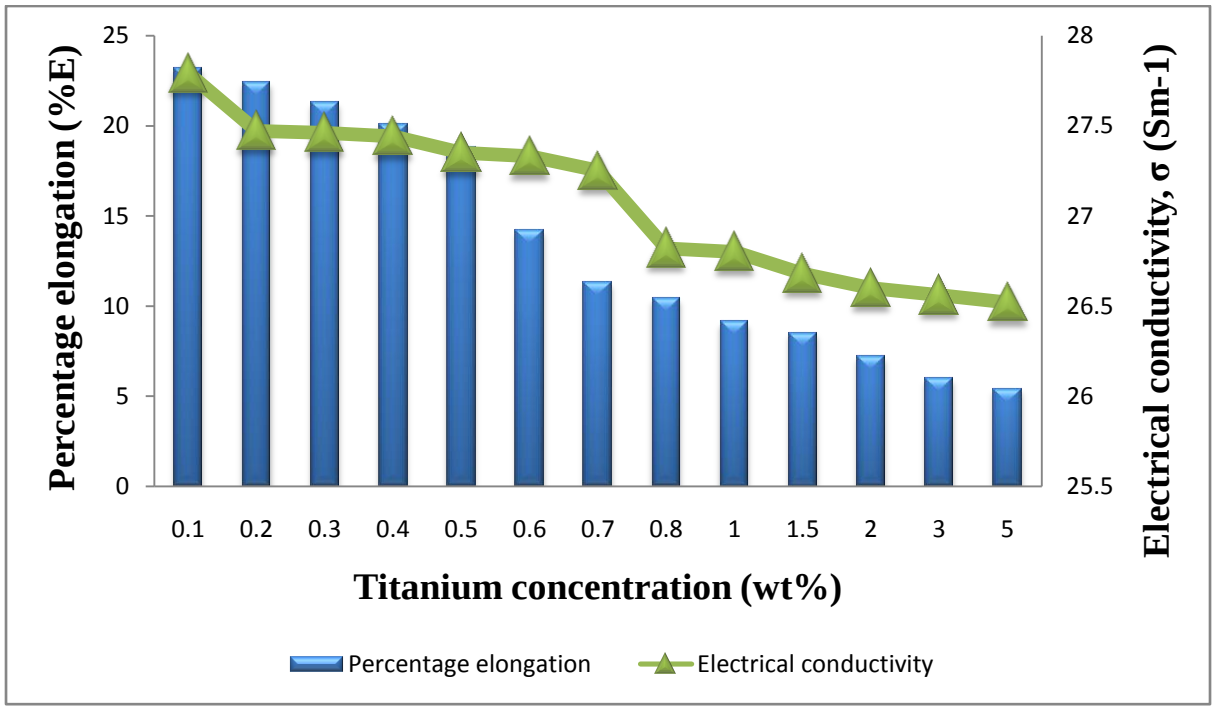

Figure 4.55: Effect of titanium concentration on the percentage elongation and electrical conductivity (σ) of silicon bronze.

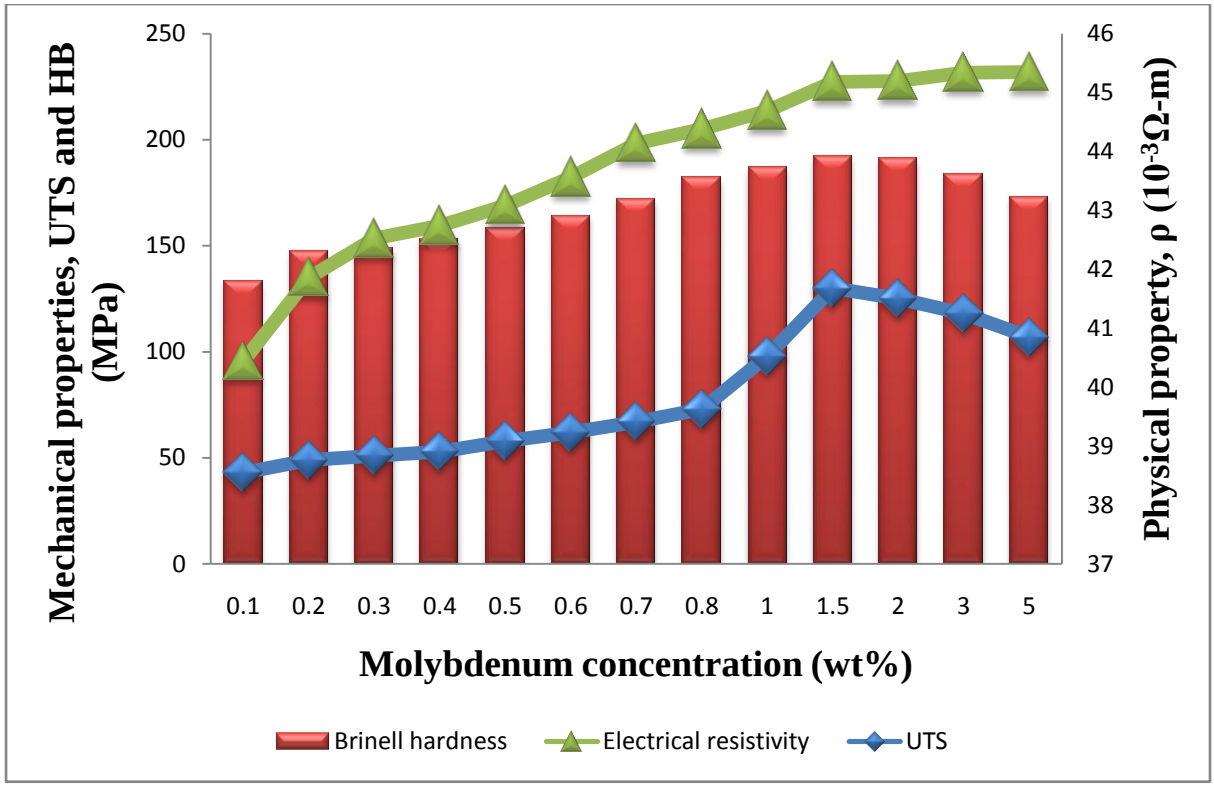

Figure 4.56: Effect of molybdenum concentration on the ultimate tensile strength (UTS), Brinell hardness (HB) and electrical resistivity (ρ) of silicon bronze.

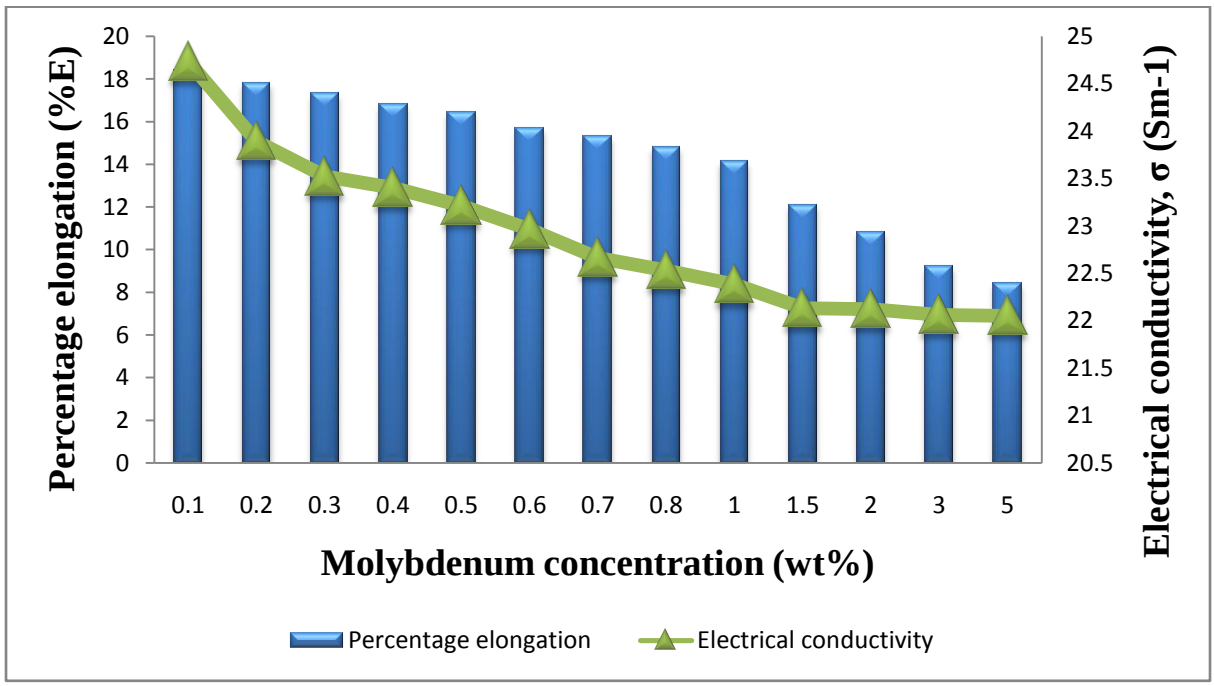

Figure 4.57: Effect of molybdenum concentration on the percentage elongation and electrical conductivity (σ) of silicon bronze.

4.3 Microstructural analysis of the studied alloys

4.3.1 Effect of silicon content on the surface morphology of silicon bronze

A detailed analysis of the surface morphology of silicon bronze of different silicon concentration is presented in Plates 4.1-4.3. The micrographs revealed the presence of primary silicon (Si) and an intermetallic phase (Cu_3Si). The micrograph of the alloy containing 5wt% silicon revealed more dendrite of primary silicon compared with the alloy containing 1 and 3%wt silicon. Analysis of Plates 4.1-4.3 shows that the size of primary silicon and the intermetallic phase increased with increase in silicon concentration and hence resulted to increased ultimate tensile strength and hardness with corresponding drastic decrease in percentage elongation and impact strength of the alloy. This was in agreement with the findings of Ketut *et al.* (2011a).

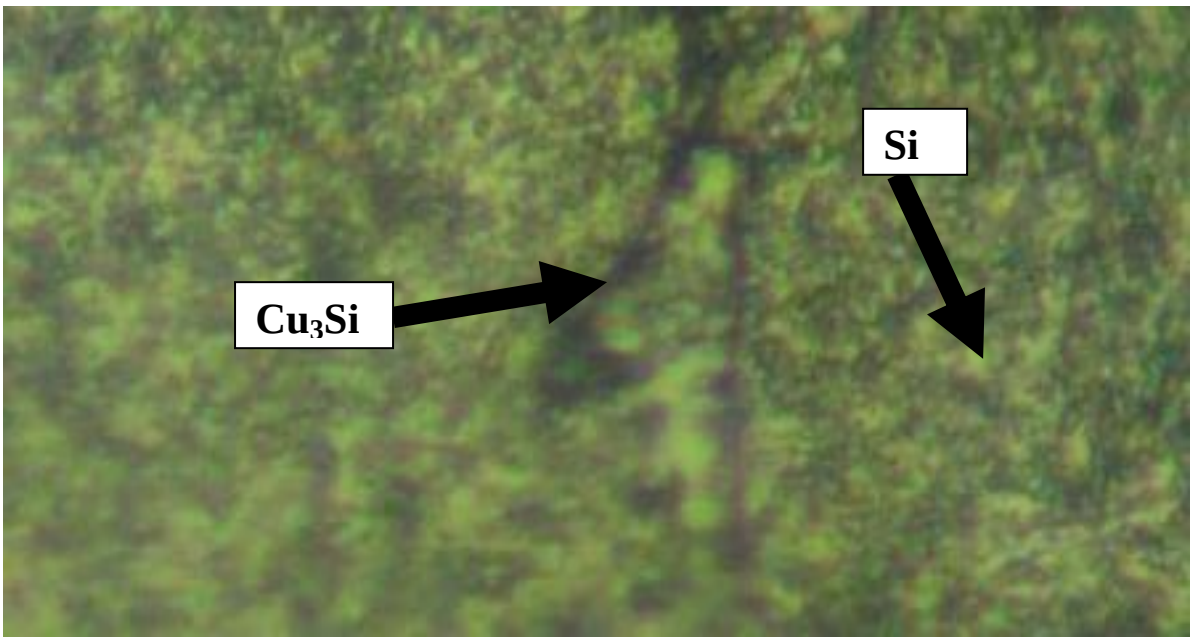

Plate 4.1: Micrograph of Cu-1wt%Si alloy

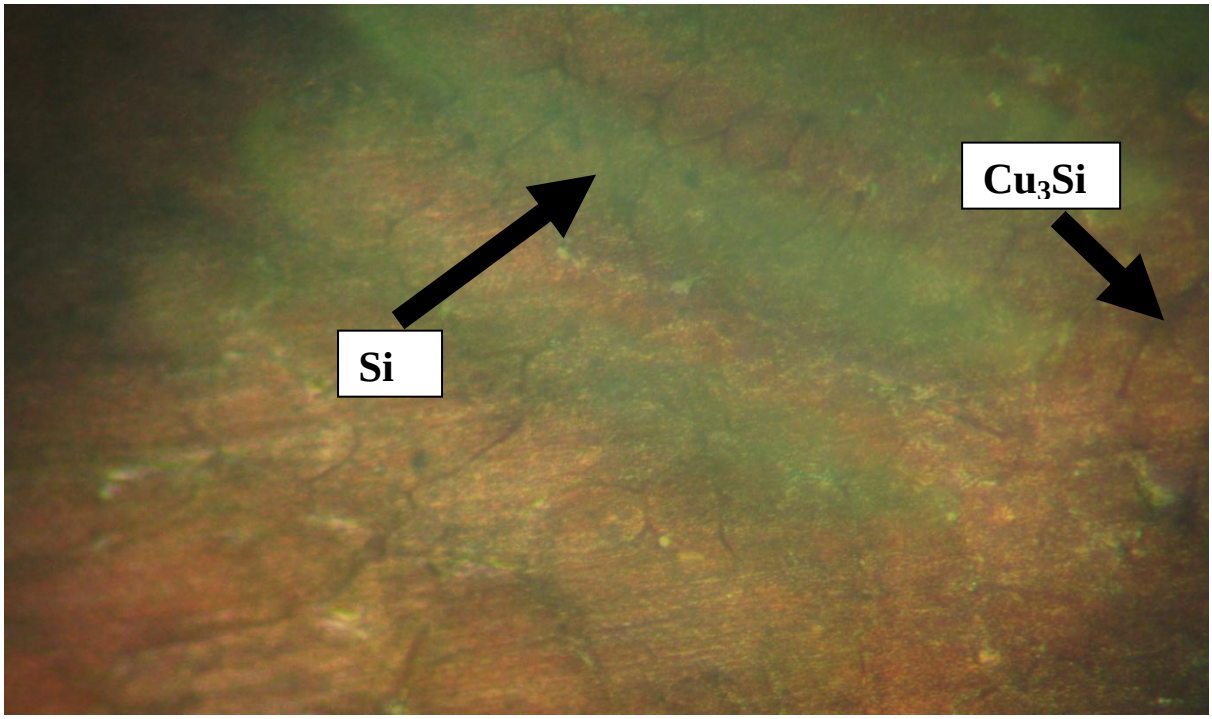

Plate 4.2: Micrograph of Cu-3wt%Si alloy

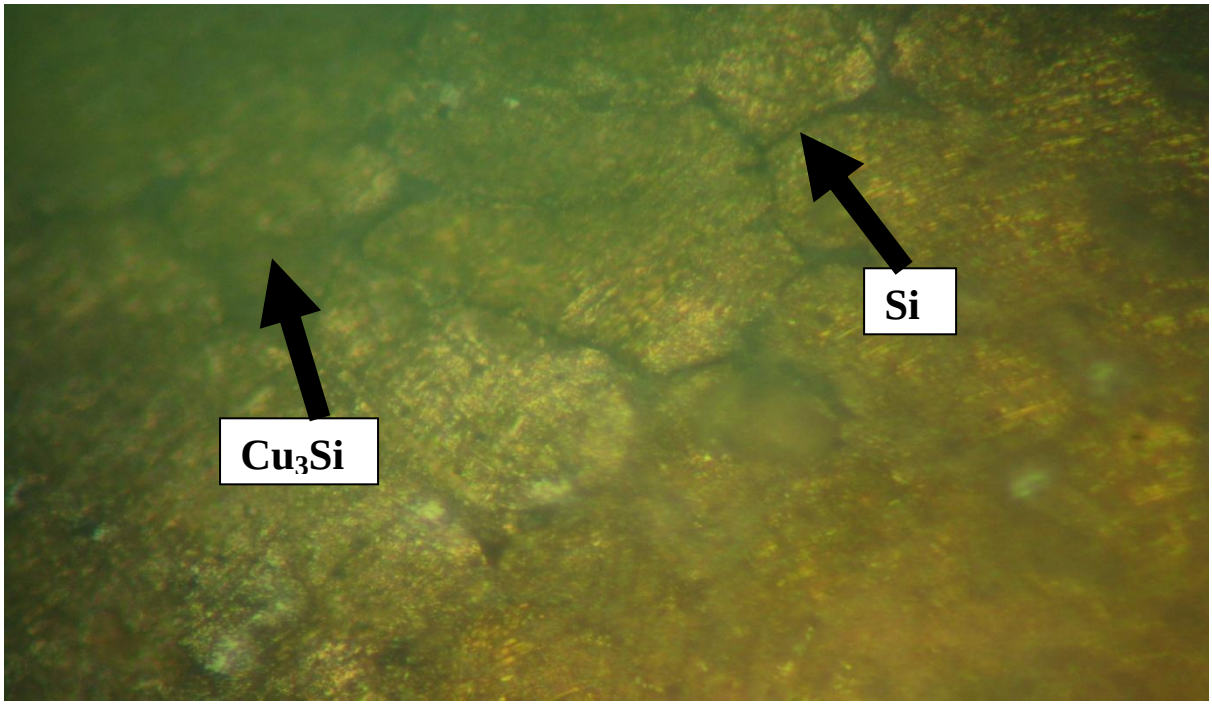

Plate 4.3: Micrograph of Cu-5wt%Si alloy

4.3.2 Effect of zinc content on the surface morphology of silicon bronze (Cu-3wt%Si)

The structural analysis of silicon bronze doped with zinc is presented in Plates 4.4-4.13. The micrographs revealed the presence of α-copper solid solution

containing silicon and zinc. It was evidenced in Plates 4.4-4.13 that addition of zinc slightly decreased the size of the dendritic primary silicon and hence resulted to an increased percentage elongation, ultimate tensile strength, hardness and impact strength of the alloy. Analysis of Plates 4.4-4.13 shows that the volume of the α-phase increased with increase in zinc concentration up to 1% by weight addition. At 1.5wt% zinc addition, the β-phase began to precipitate out of the α-phase and hence caused a systematic increase in hardness and ultimate tensile strength with corresponding decrease in percentage elongation and impact strength. Beyond 3wt% zinc addition, cored dendrite of β-phase was observed in the alloy structure which predominantly decreased the ultimate tensile strength and hardness of the alloy (Figure 4.18 and 4.27).

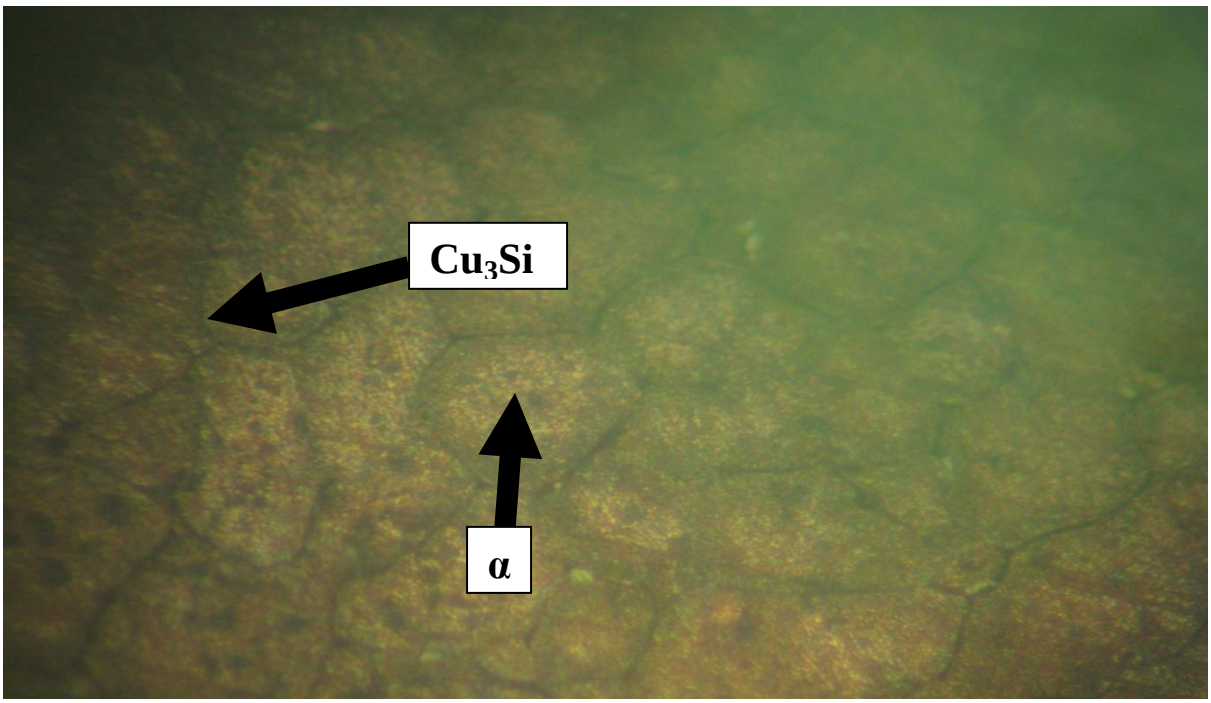

Plate 4.4: Micrograph of Cu-3wt%Si-0.1wt%Zn alloy

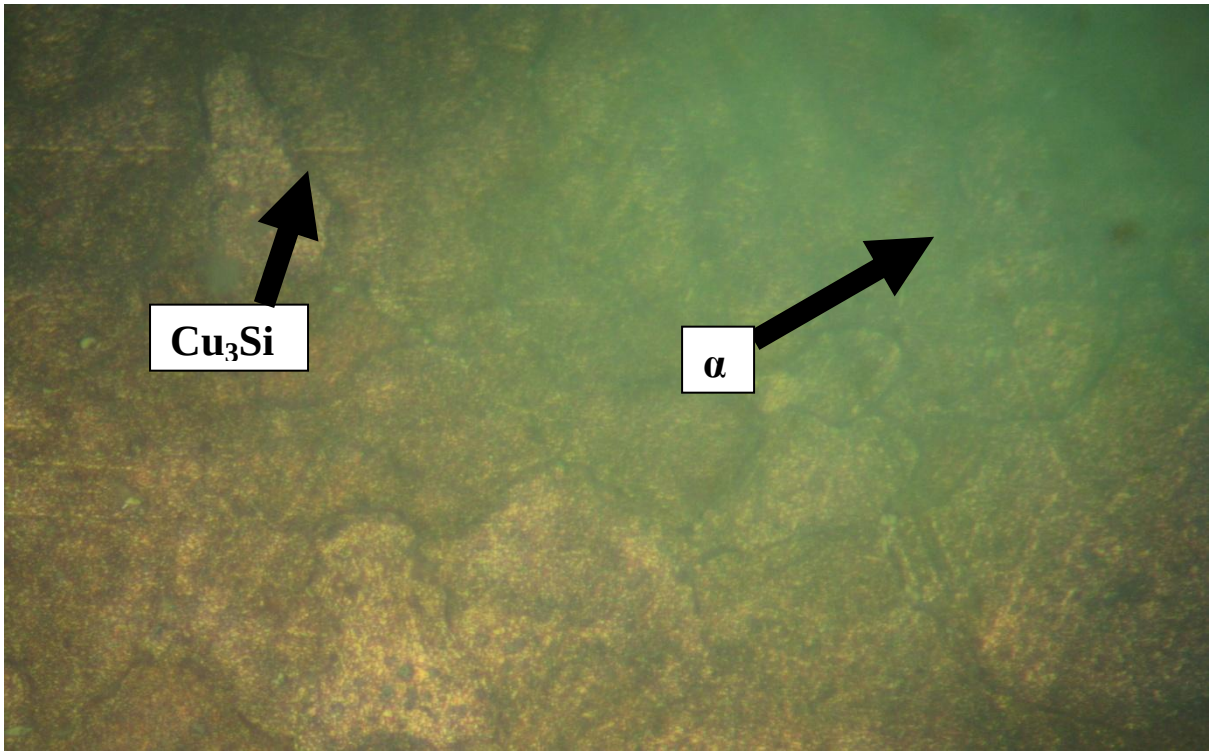

Plate 4.5: Micrograph of Cu-3wt%Si-0.3wt%Zn alloy

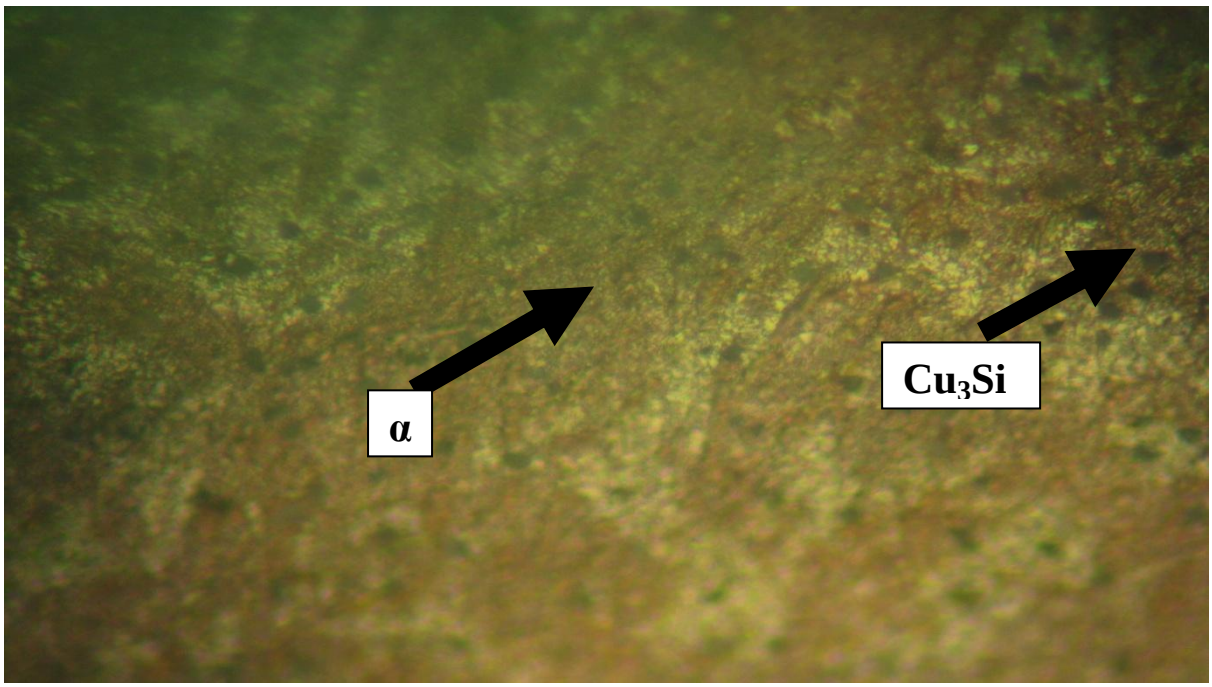

Plate 4.6: Micrograph of Cu-3wt%Si-0.5wt%Zn alloy

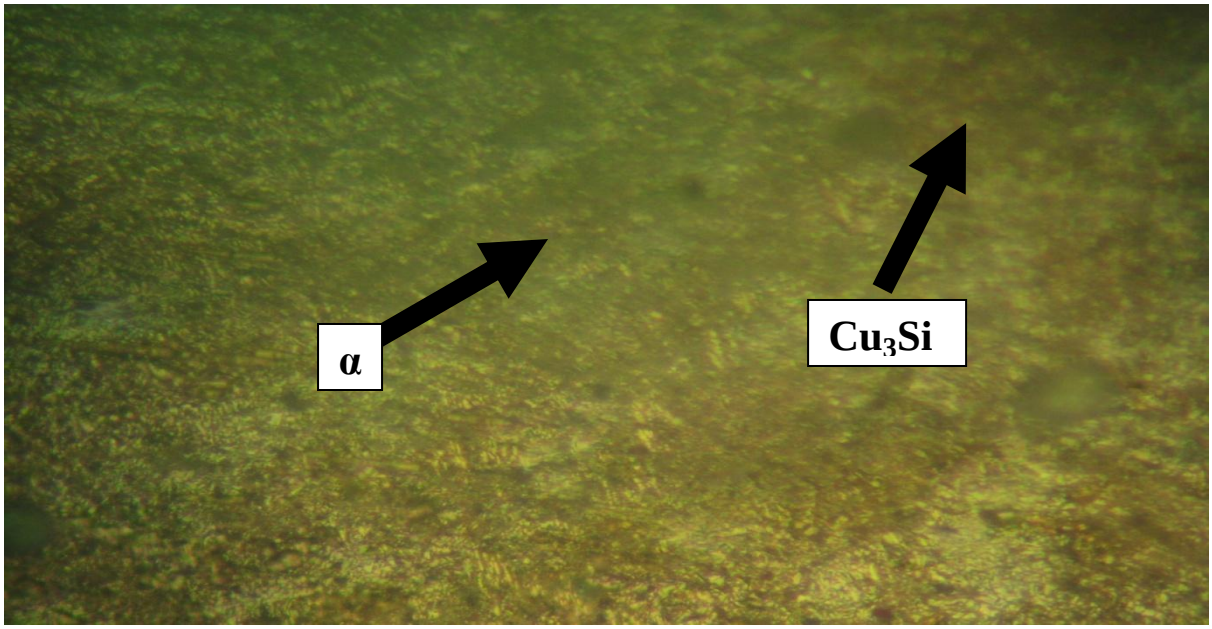

Plate 4.7: Micrograph of Cu-3wt%Si-0.7wt%Zn alloy

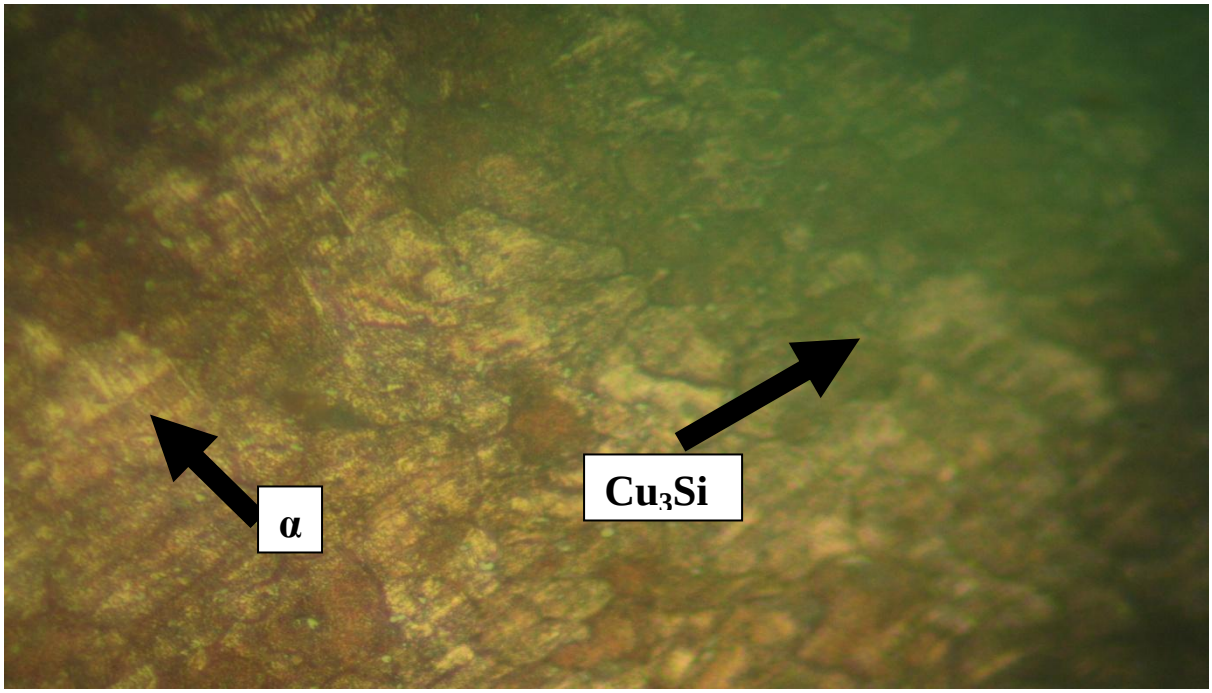

Plate 4.8: Micrograph of Cu-3wt%Si-0.8wt%Zn alloy

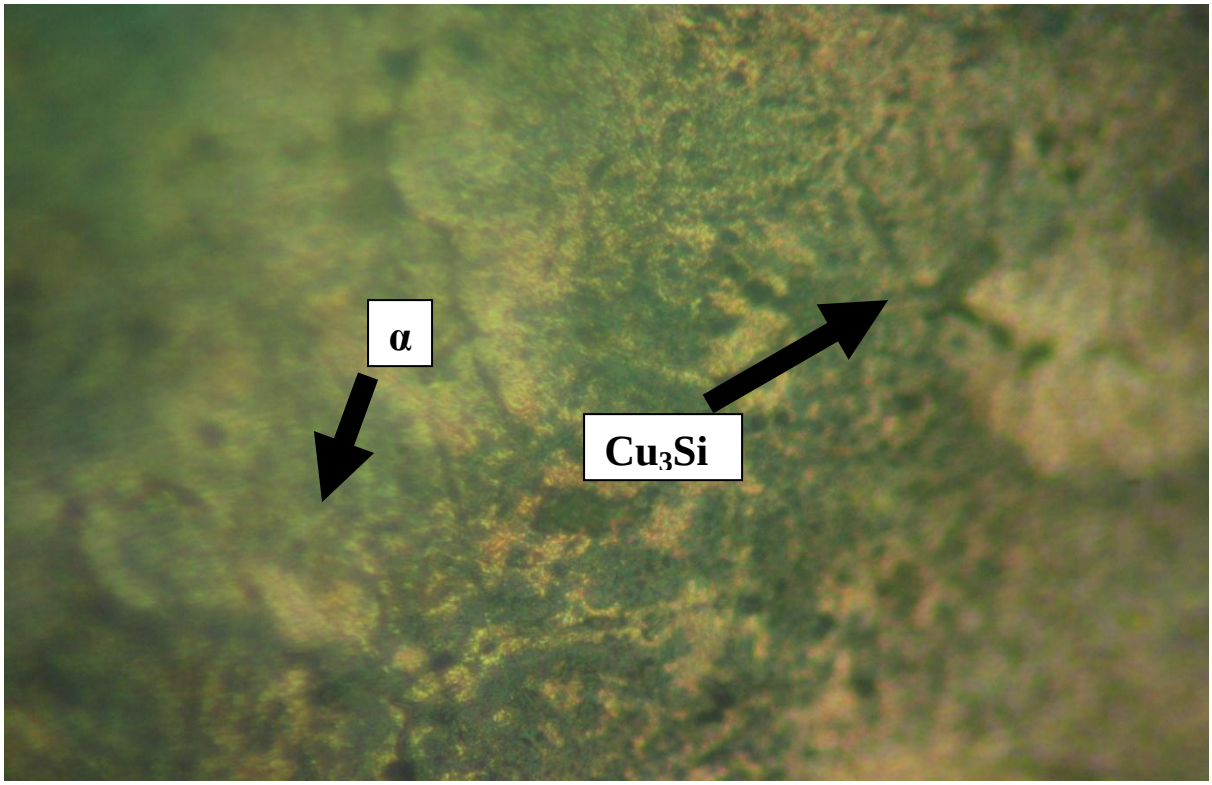

Plate 4.9: Micrograph of Cu-3wt%Si-1wt%Zn alloy

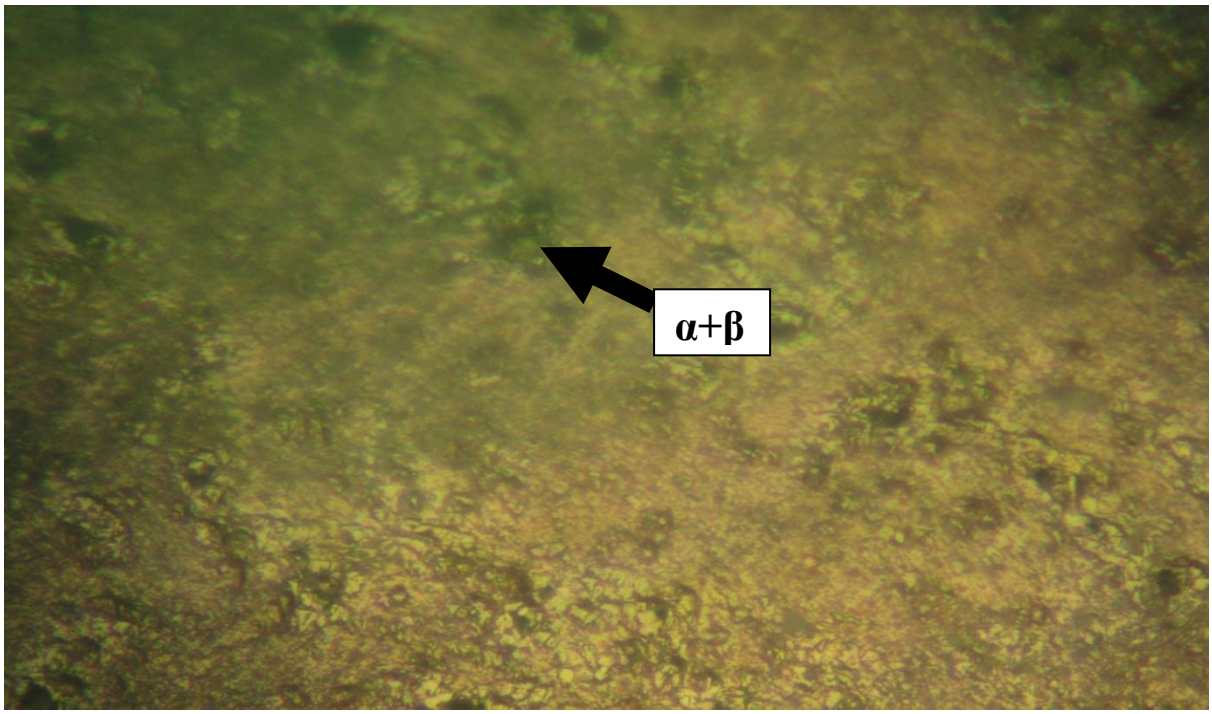

Plate 4.10: Micrograph of Cu-3wt%Si-1.5wt%Zn alloy

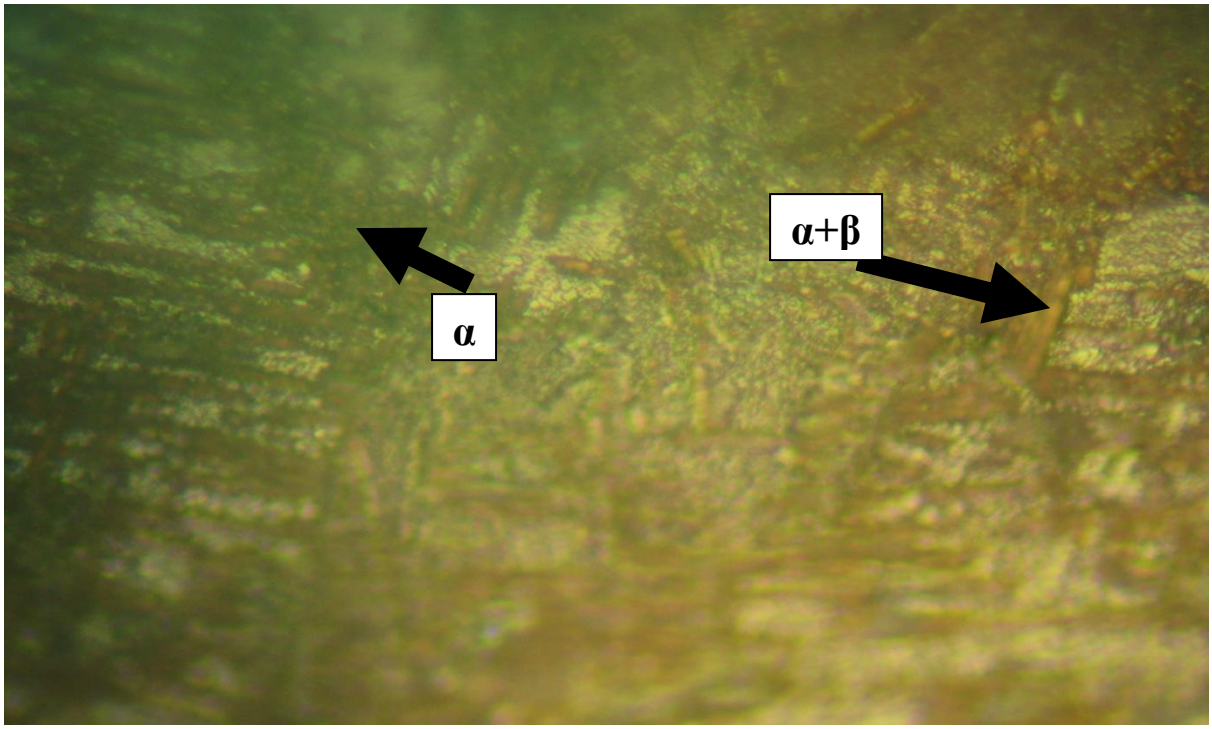

Plate 4.11: Micrograph of Cu-3wt%Si-2wt%Zn alloy

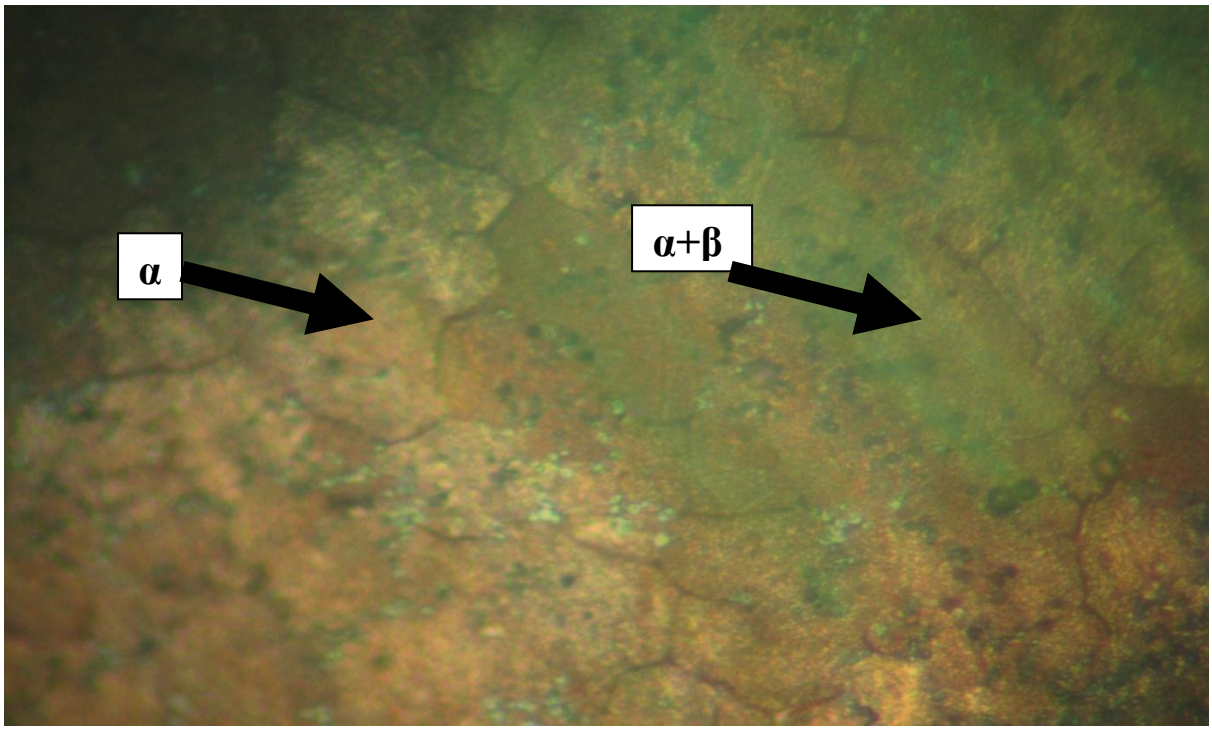

Plate 4.12: Micrograph of Cu-3wt%Si-3wt%Zn alloy

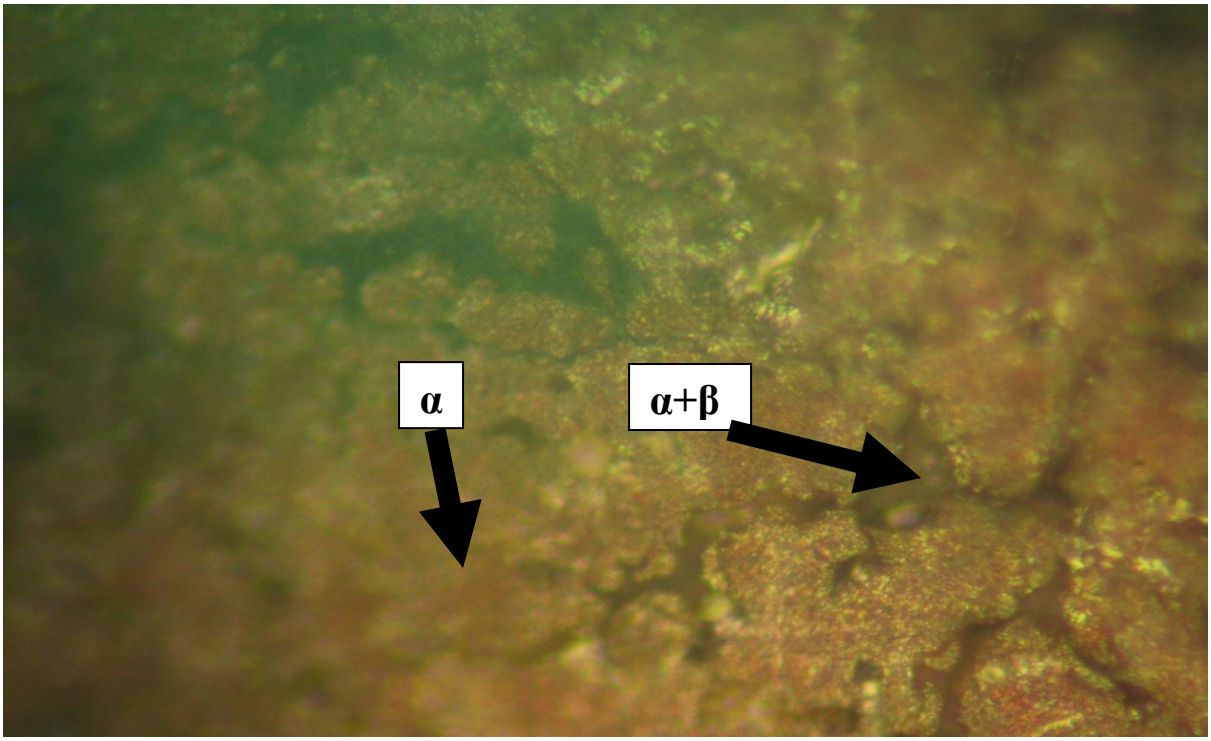

Plate 4.13: Micrograph of Cu-3wt%Si-5wt%Zn alloy

4.3.3. Effect of tin content on the surface morphology of silicon bronze (Cu-3wt%Si)

The structural analysis of silicon bronze doped with tin is presented in Plates 4.14-4.23. The micrographs indicated the presence of Cu_3Si and Cu_3Sn intermetallic compounds in the alloy structure. The morphology of the intermetallic compounds was refined and modified by the addition of tin, thereby resulting to an increase in percentage elongation, ultimate tensile strength, hardness and impact strength of the alloy (Figures 4.8, 4.17, 4.26 and 4.34). Analysis of Plates 4.14-4.23 revealed that the grain size decreased with increase in tin concentration up to 3wt% addition, thereby created more grain boundaries which ultimately increased the ultimate tensile strength and hardness with corresponding decrease in percentage elongation and impact strength

(Figures 4.10, 4.19, 4.28 and 4.36). Further increase in tin concentration beyond 3% by weight resulted to the formation of coarse intermetallic compound which decreased the ultimate tensile strength and hardness of the alloy (Figure 4.19 and 4.28).

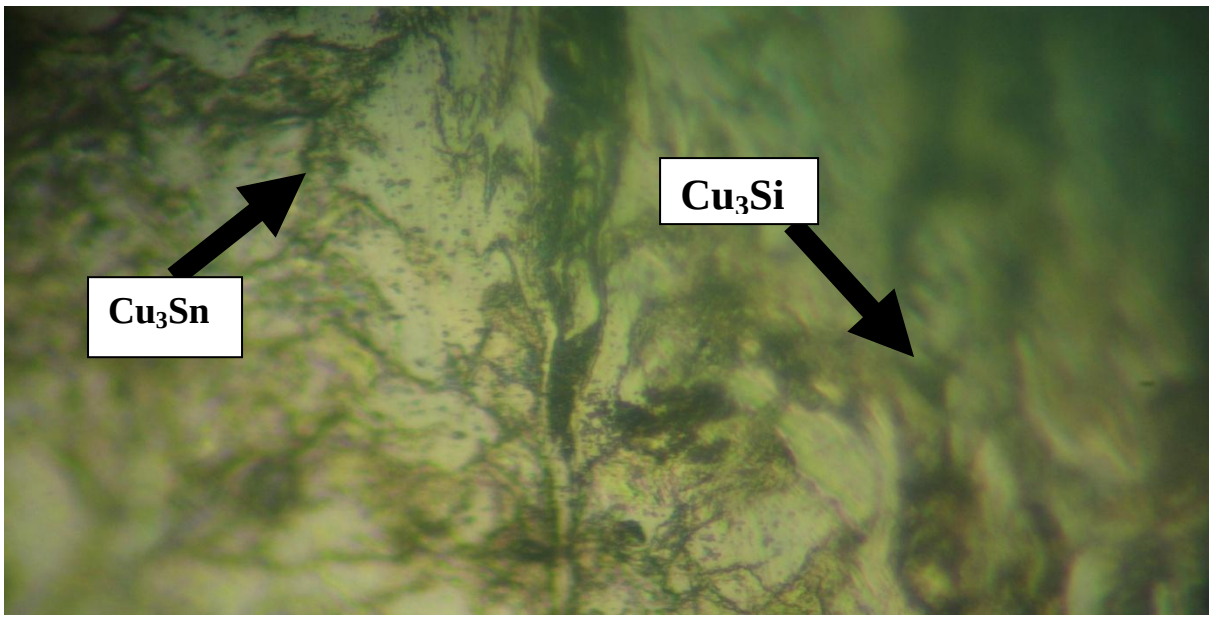

Plate 4.14: Micrograph of Cu-3wt%Si-0.1wt%Sn alloy

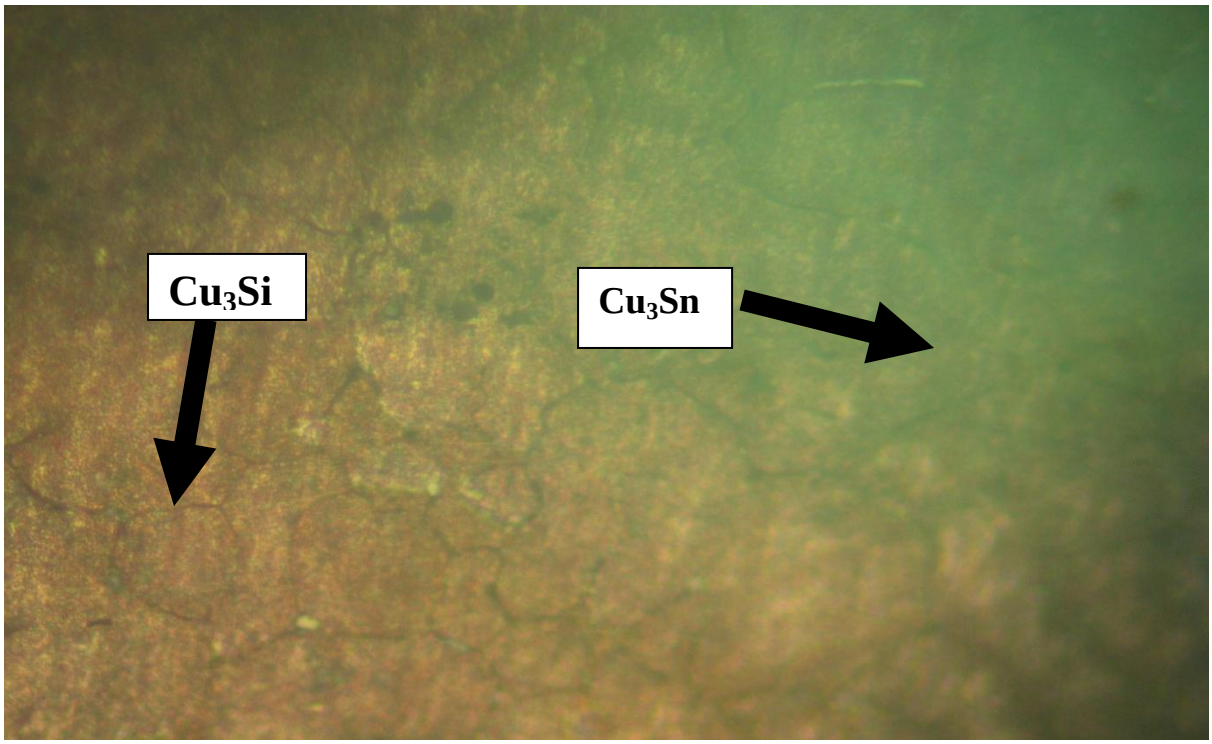

Plate 4.15: Micrograph of Cu-3wt%Si-0.3wt%Sn alloy

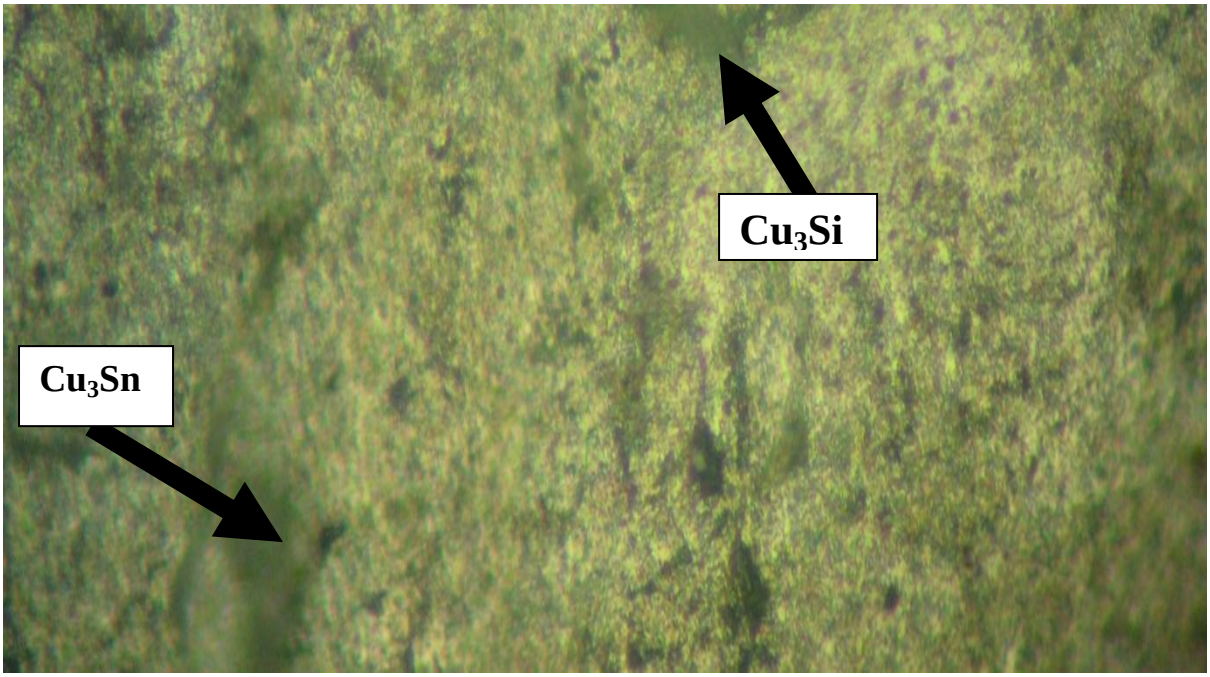

Plate 4.16: Micrograph of Cu-3wt%Si-0.5wt%Sn alloy

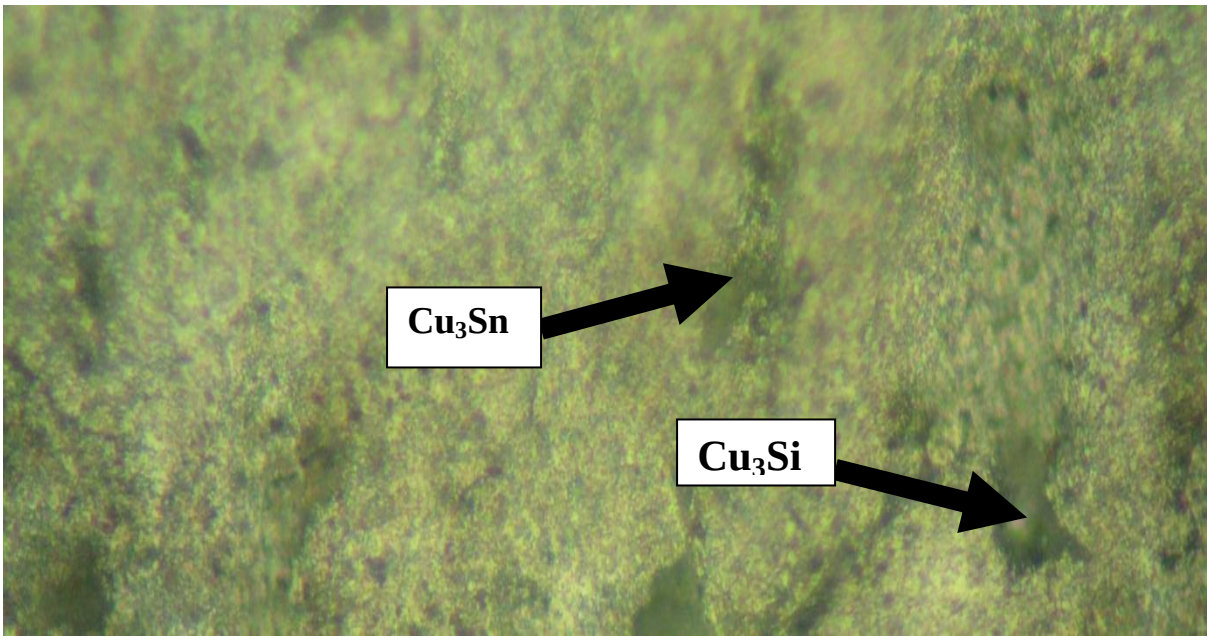

Plate 4.17: Micrograph of Cu-3wt%Si-0.7wt%Sn alloy

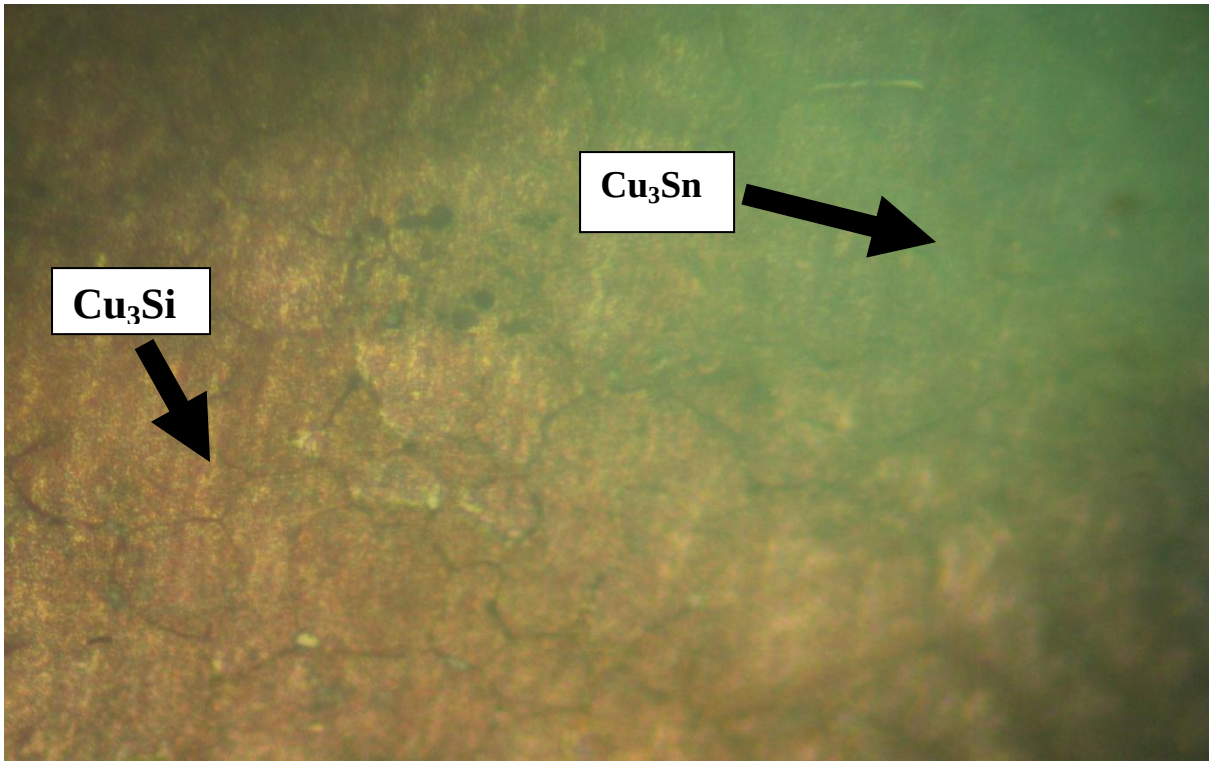

Plate 4.18: Micrograph of Cu-3wt%Si-0.8wt%Sn alloy

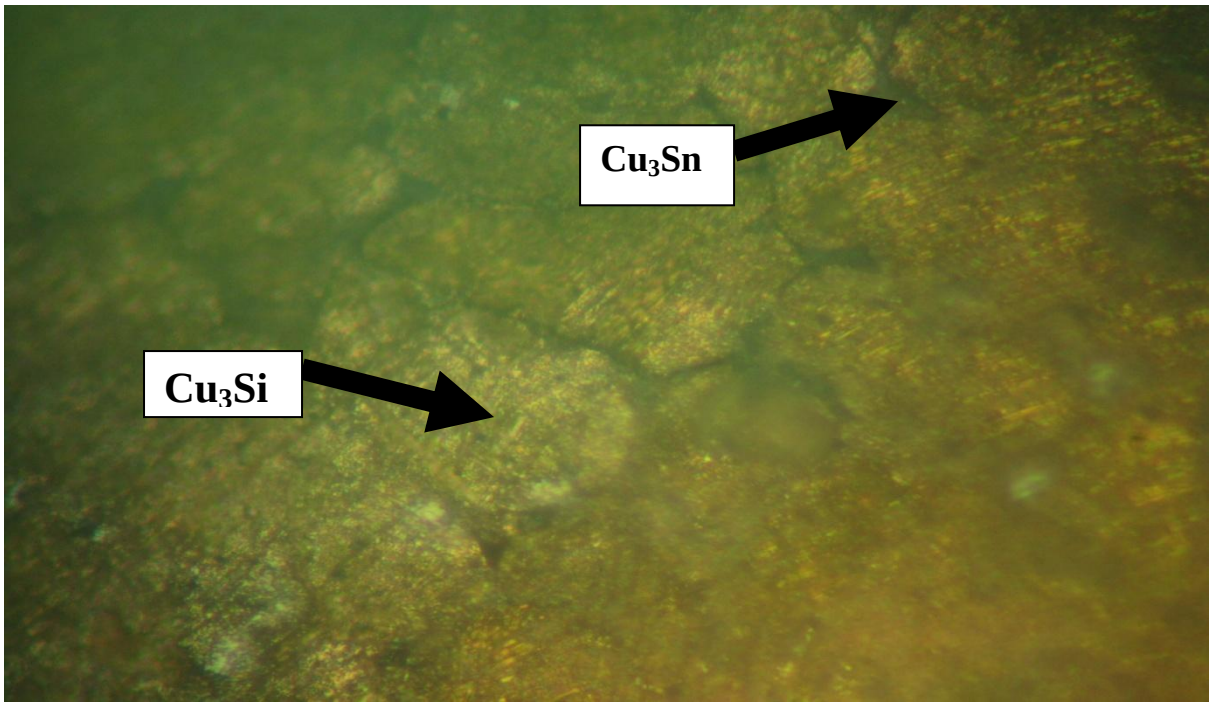

Plate 4.19: Micrograph of Cu-3wt%Si-1wt%Sn alloy

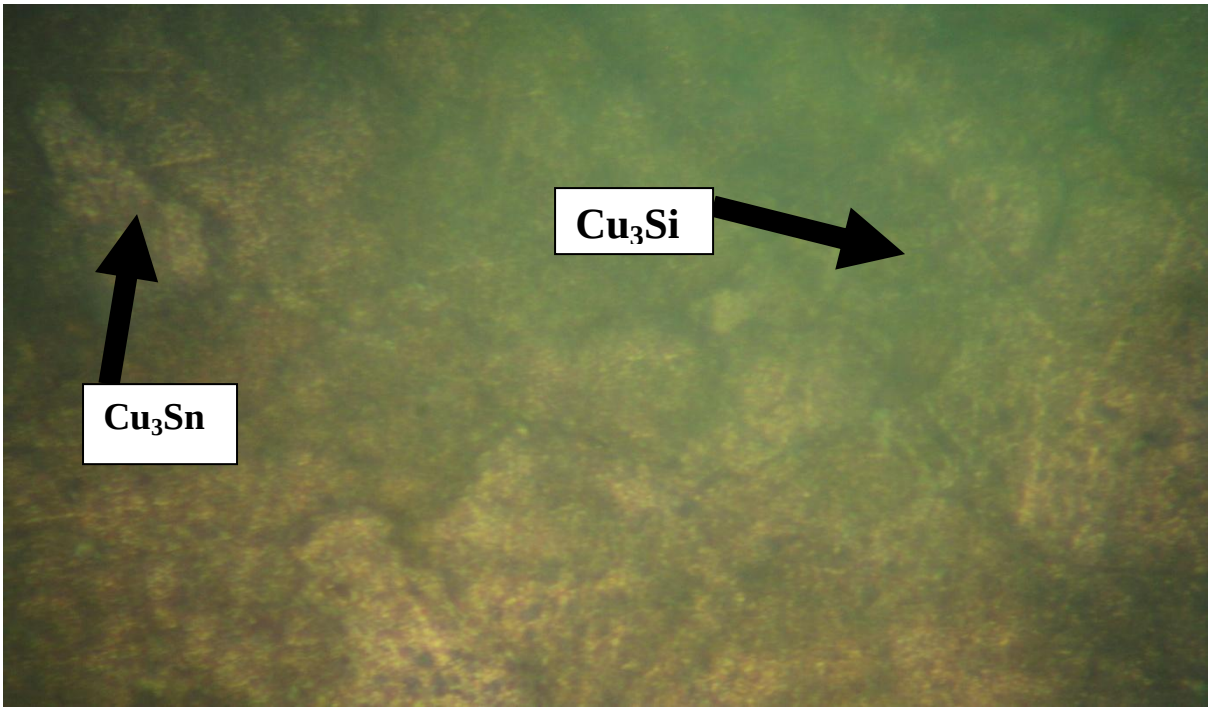

Plate 4.20: Micrograph of Cu-3wt%Si-1.5wt%Sn alloy

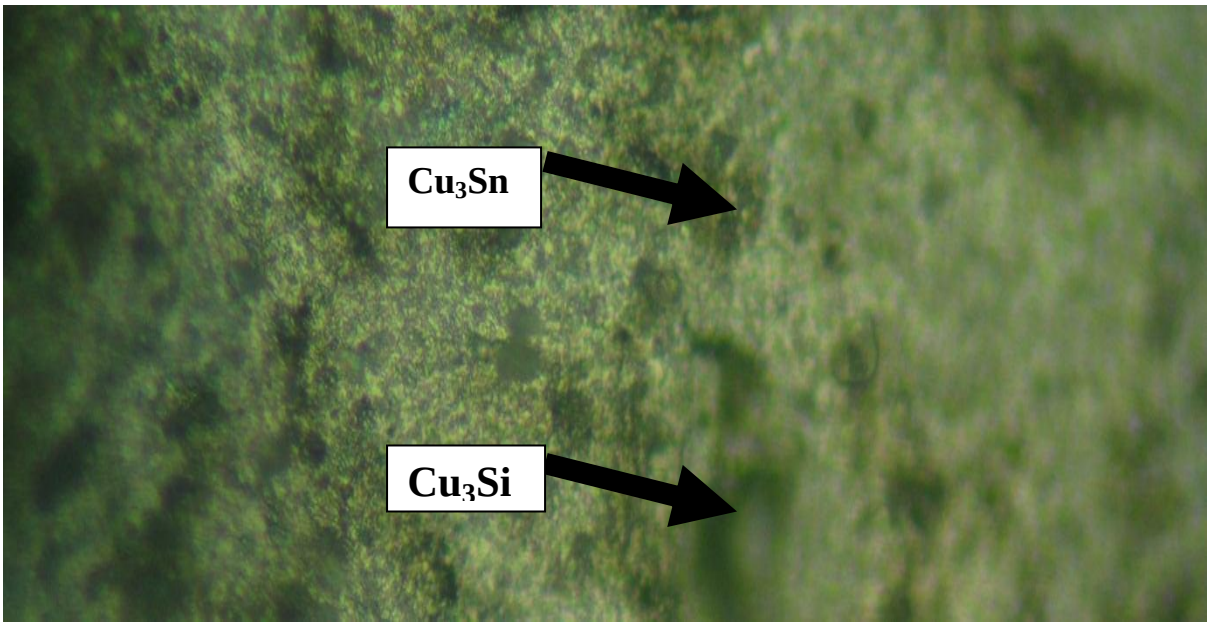

Plate 4.21: Micrograph of Cu-3wt%Si-2wt%Sn alloy

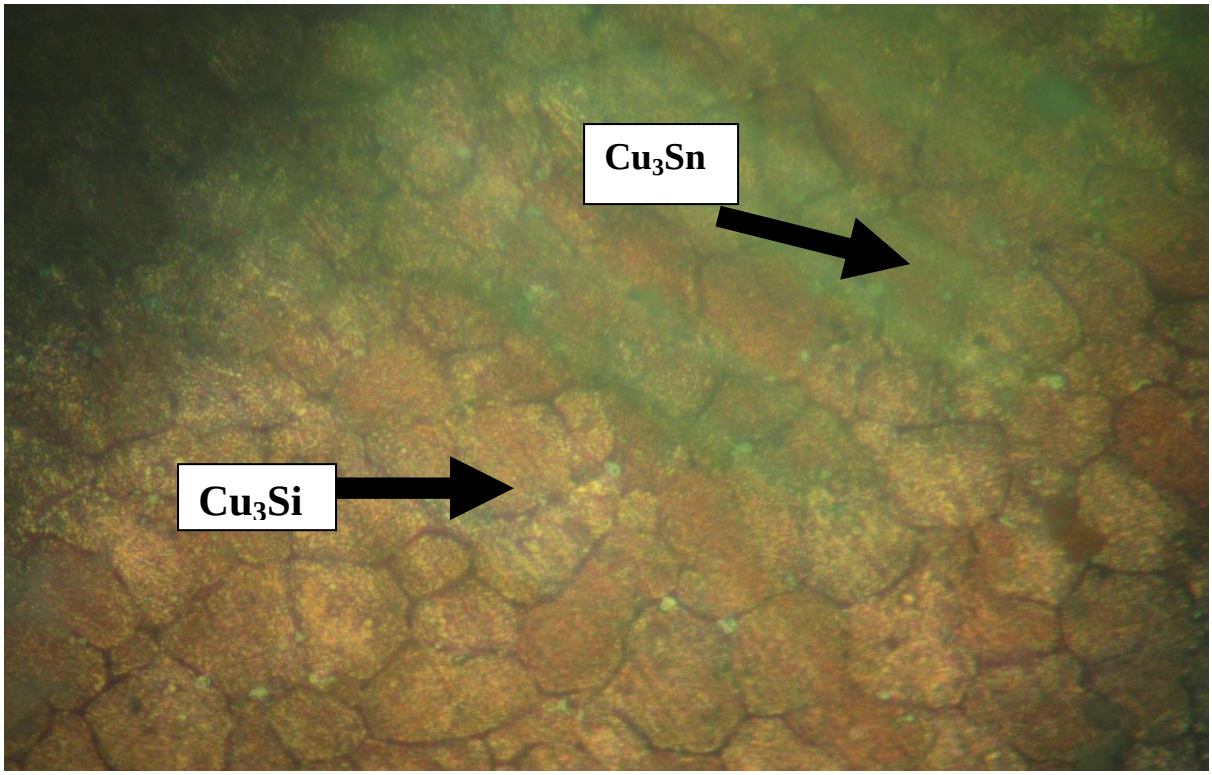

Plate 4.22: Micrograph of Cu-3wt%Si-3wt%Sn alloy

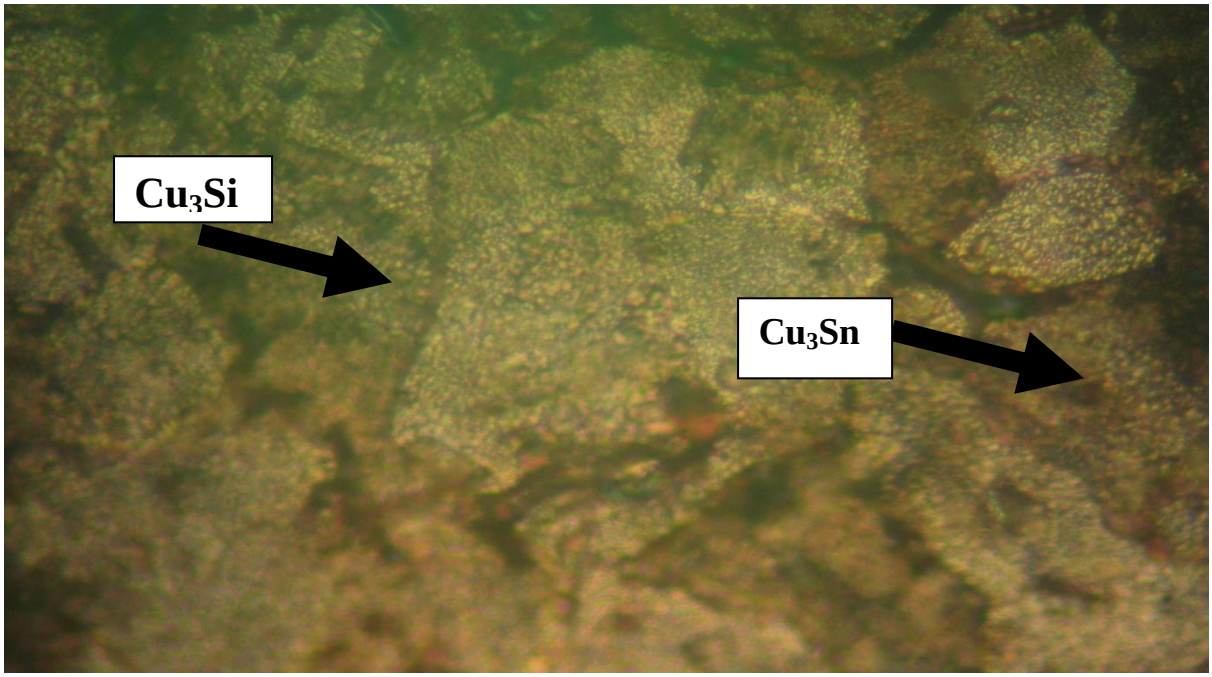

Plate 4.23: Micrograph of Cu-3wt%Si-5wt%Sn alloy

4.3.4. Effect of magnesium content on the surface morphology of silicon bronze (Cu-3wt%Si)

The surface morphology of silicon bronze doped with magnesium of different concentration is presented in Plates 4.24-4.33. The microstructures reveal the presence of copper silicide (Cu_3Si) and magnesium silicide (Mg_2Si) intermetallic phases. Analysis of Plates 4.24-4.33 shows that addition of magnesium refined and modified the dendritic primary silicon and intermetallic compound (Cu_3Si) respectively, thereby causing an increased percentage elongation, ultimate tensile strength, hardness and impact strength of the alloy (Figures 4.8, 4.17, 4.26 and 4.34). The micrographs also revealed that the intermetallic compound, Mg_2Si coarsened as the magnesium content increased beyond 0.8%wt (Plates 4.34-4.33). This resulted to decrease in ultimate tensile strength and hardness of the alloy (Figures 4.17 and 4.26).

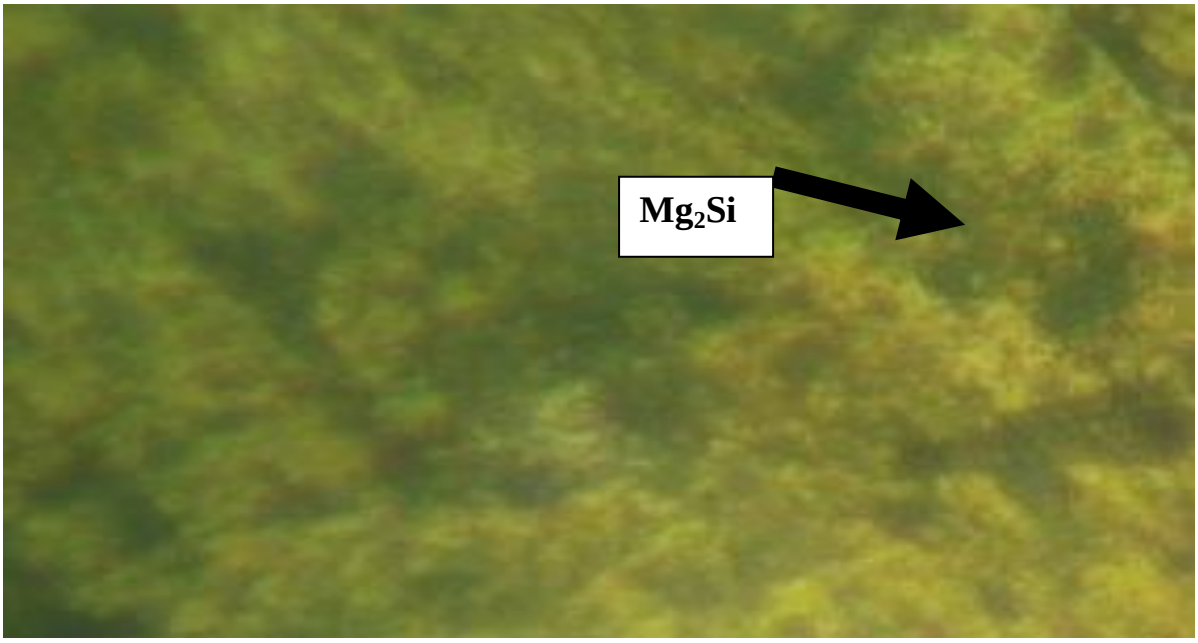

Plate 4.24: Micrograph of Cu-3wt%Si-0.1wt%Mg alloy

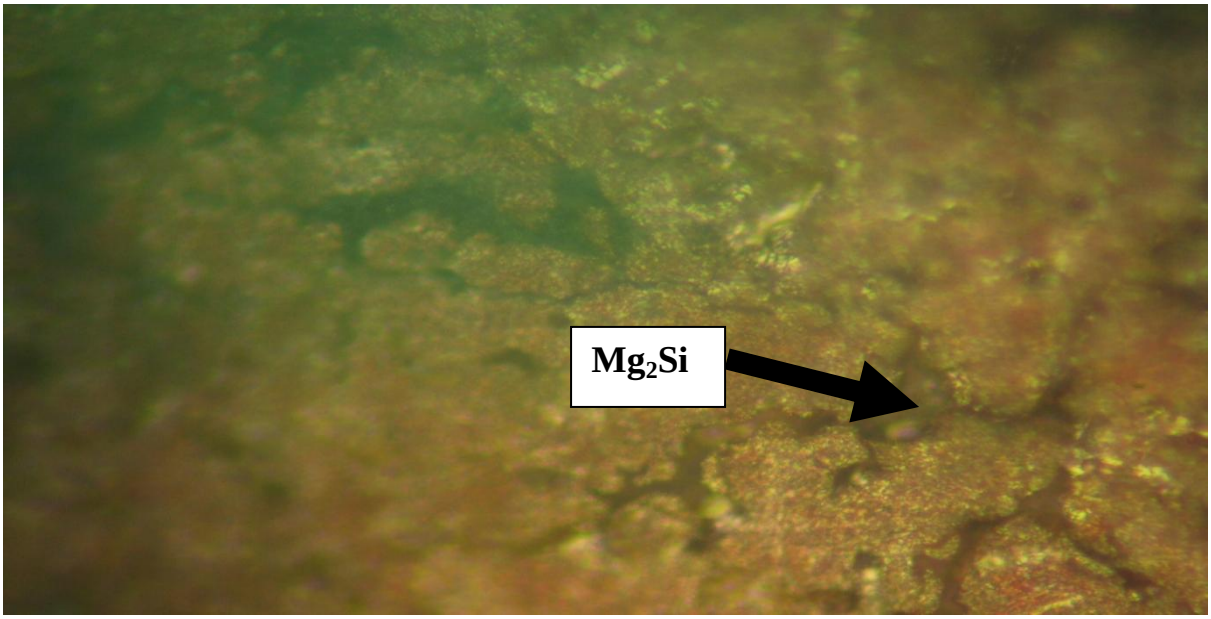

Plate 4.25: Micrograph of Cu-3wt%Si-0.2wt%Mg alloy

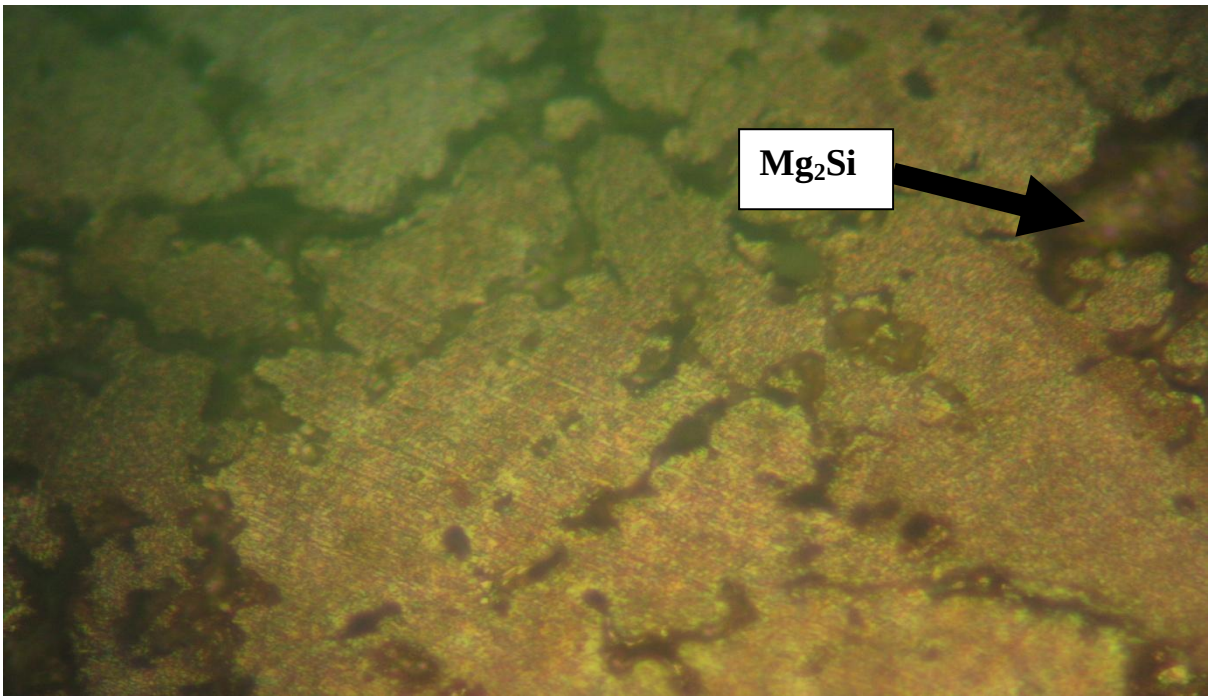

Plate 4.26: Micrograph of Cu-3wt%Si-0.3wt%Mg alloy

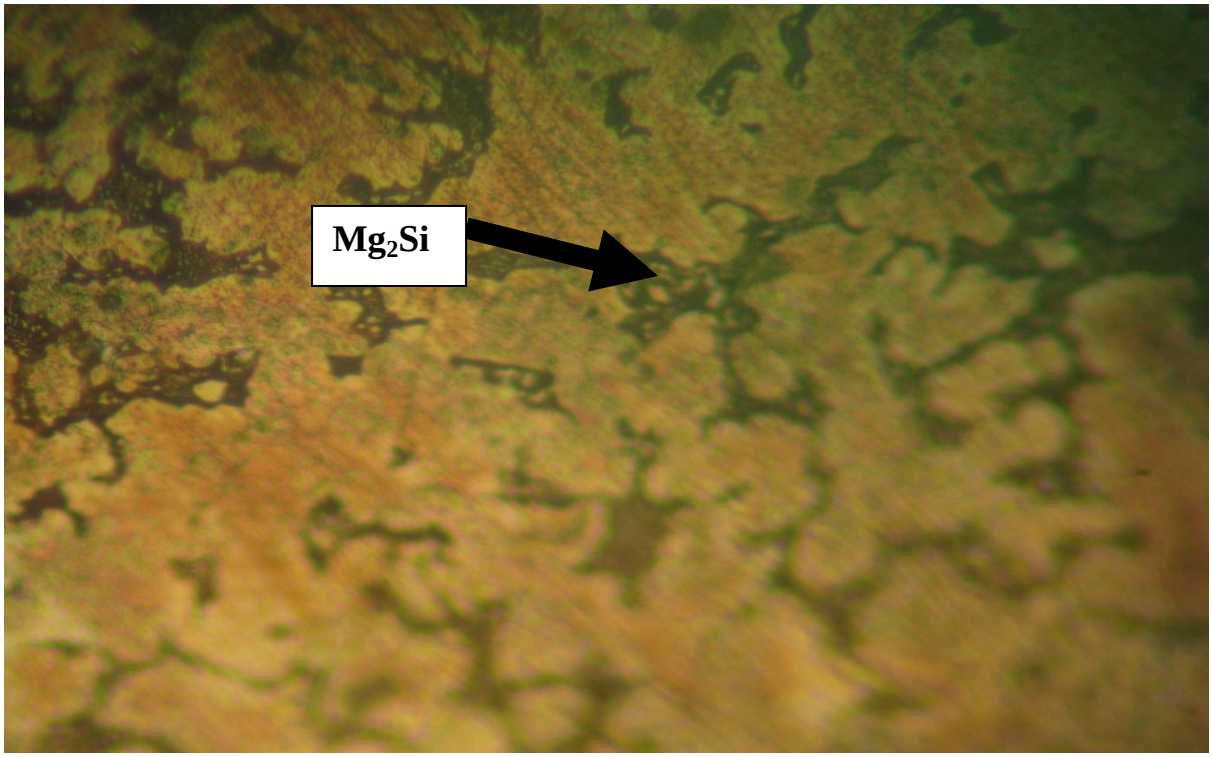

Plate 4.27: Micrograph of Cu-3wt%Si-0.4wt%Mg alloy

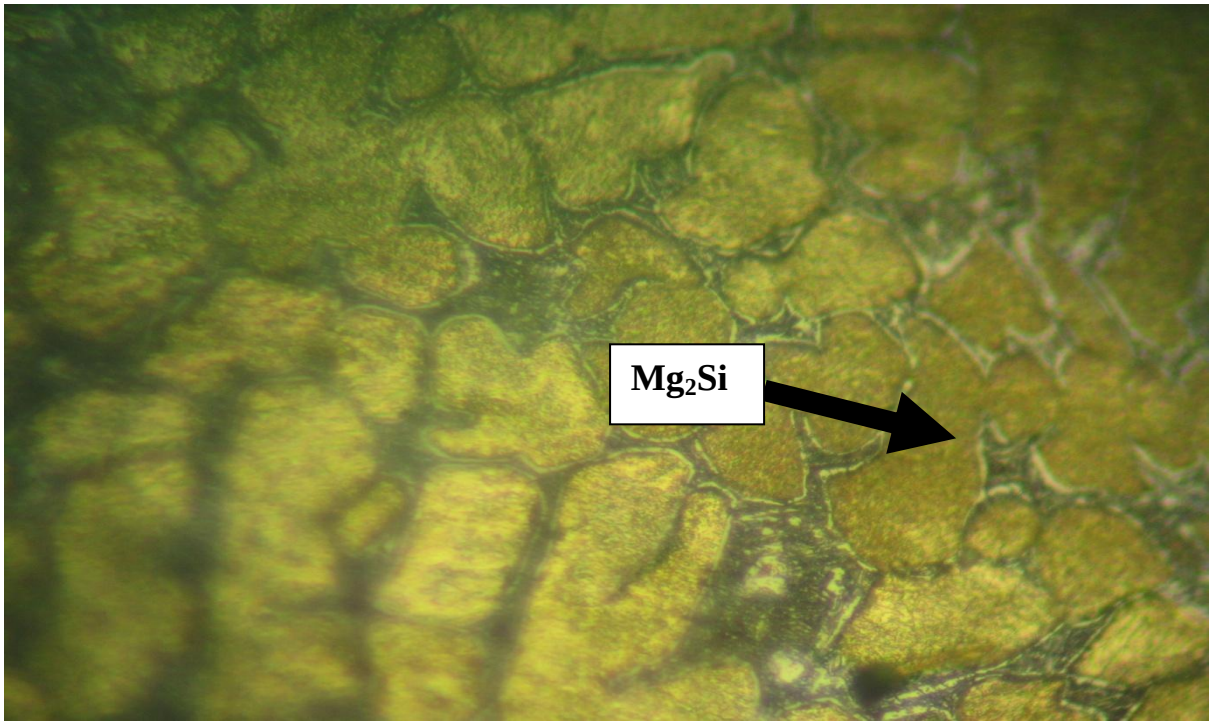

Plate 4.28: Micrograph of Cu-3wt%Si-0.5wt%Mg alloy

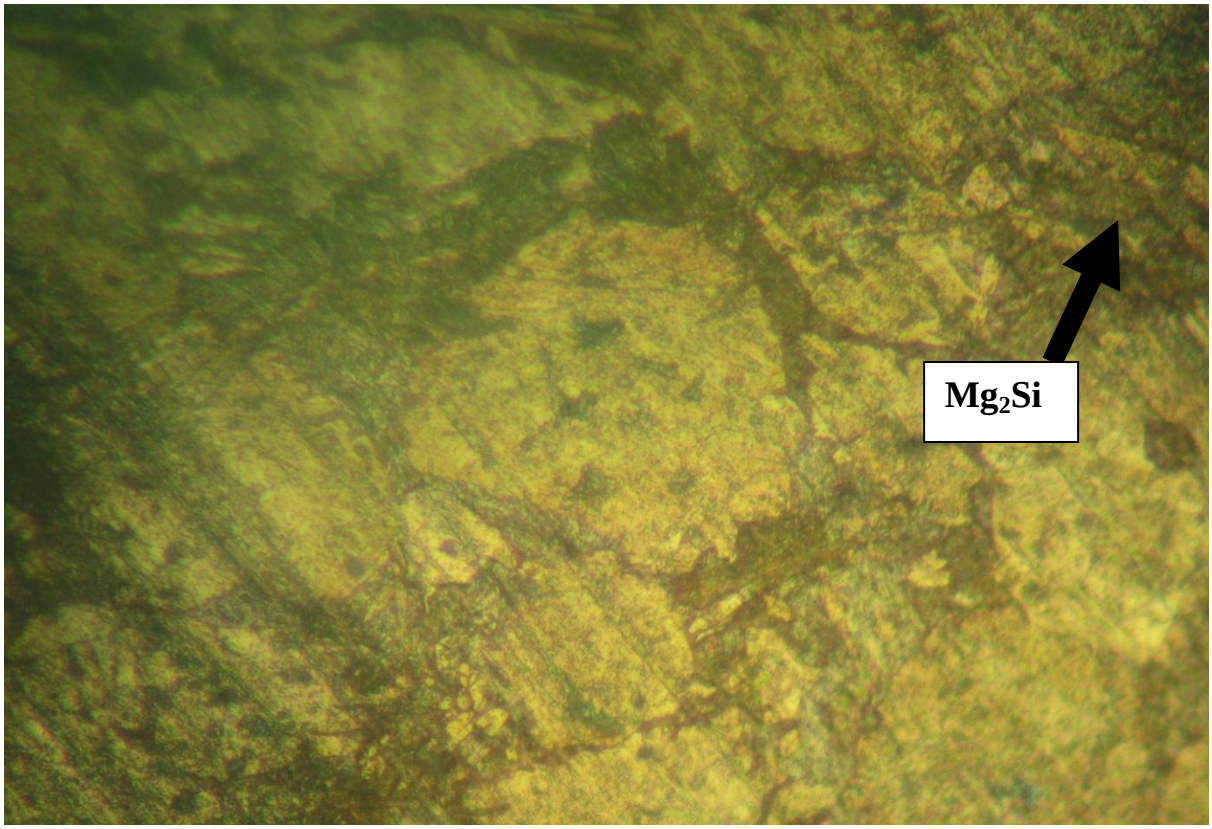

Plate 4.29: Micrograph of Cu-3wt%Si-0.6wt%Mg alloy

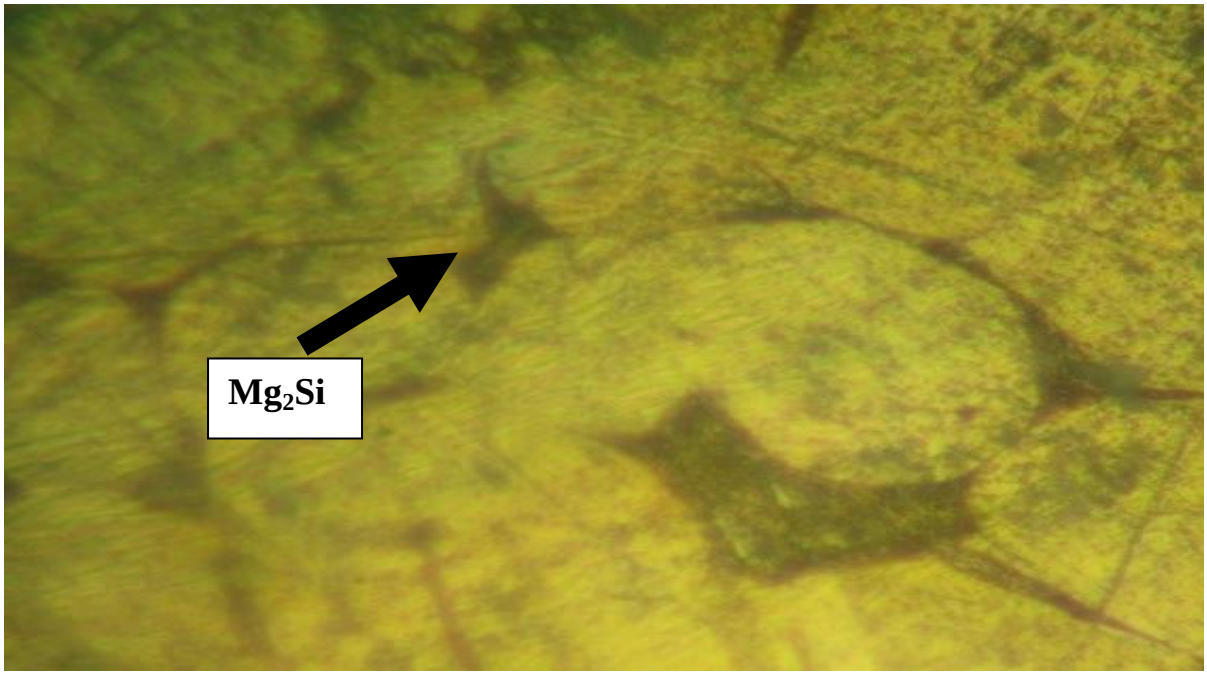

Plate 4.30: Micrograph of Cu-3wt%Si-0.7wt%Mg alloy

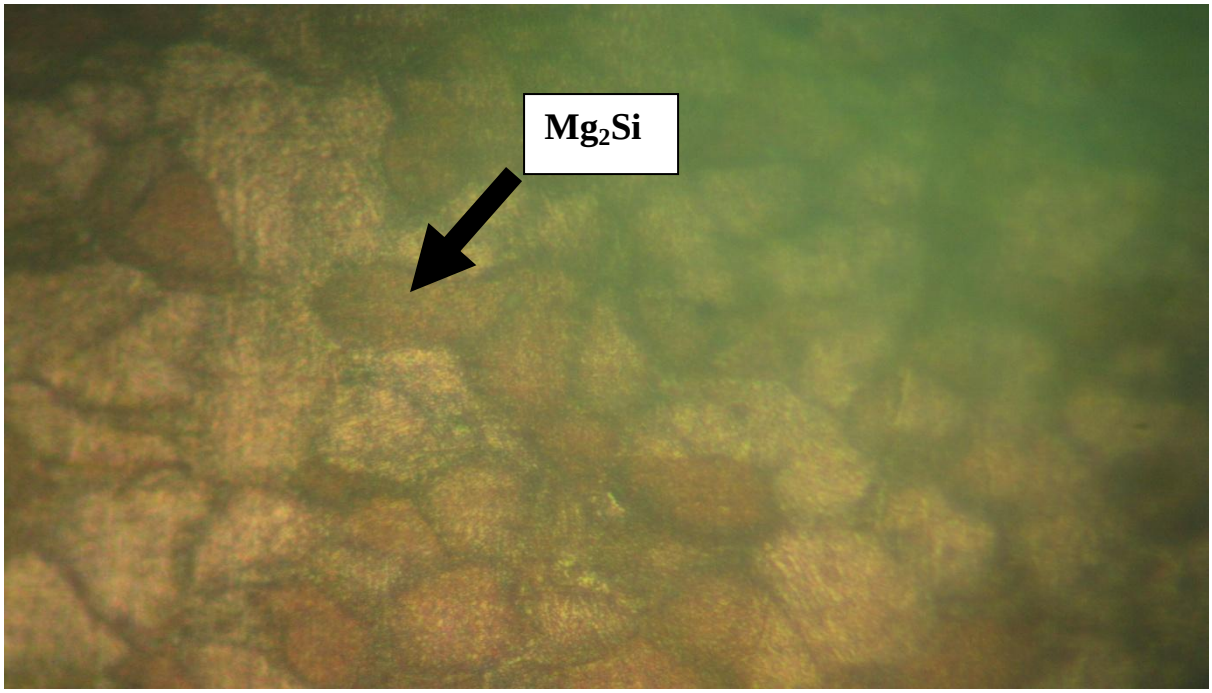

Plate 4.24: Micrograph of Cu-3wt%Si-0.8wt%Mg alloy

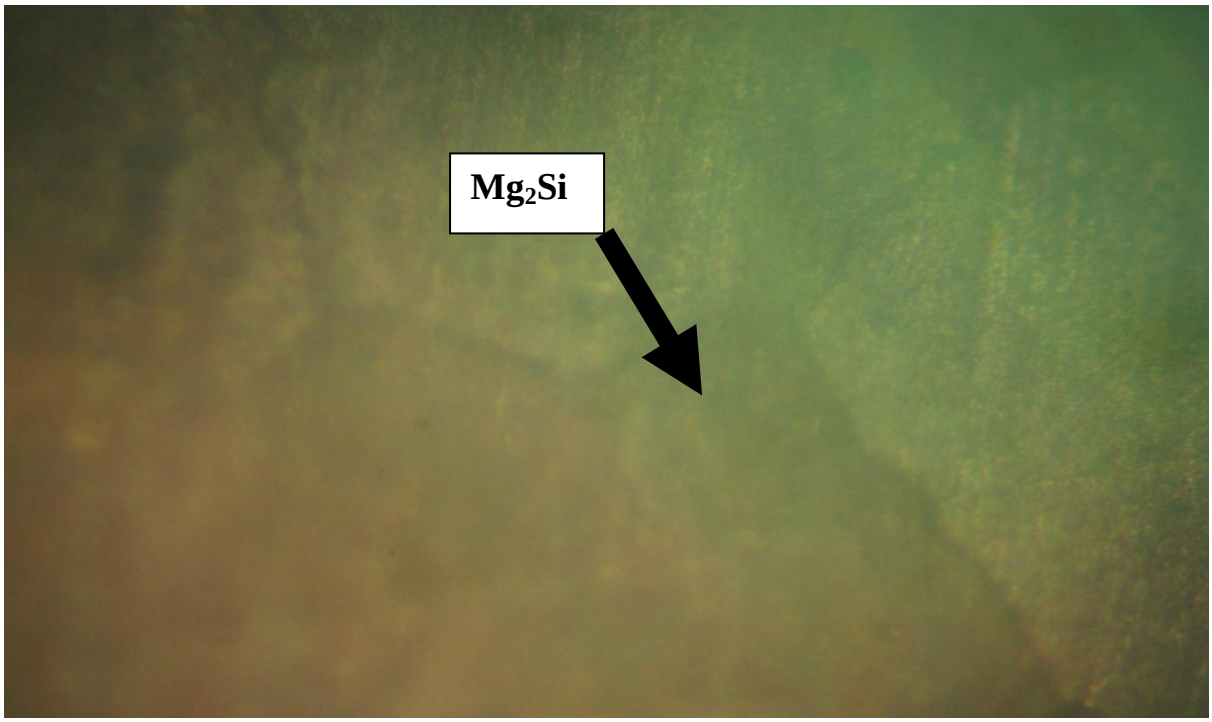

Plate 4.32: Micrograph of Cu-3wt%Si-1wt%Mg alloy

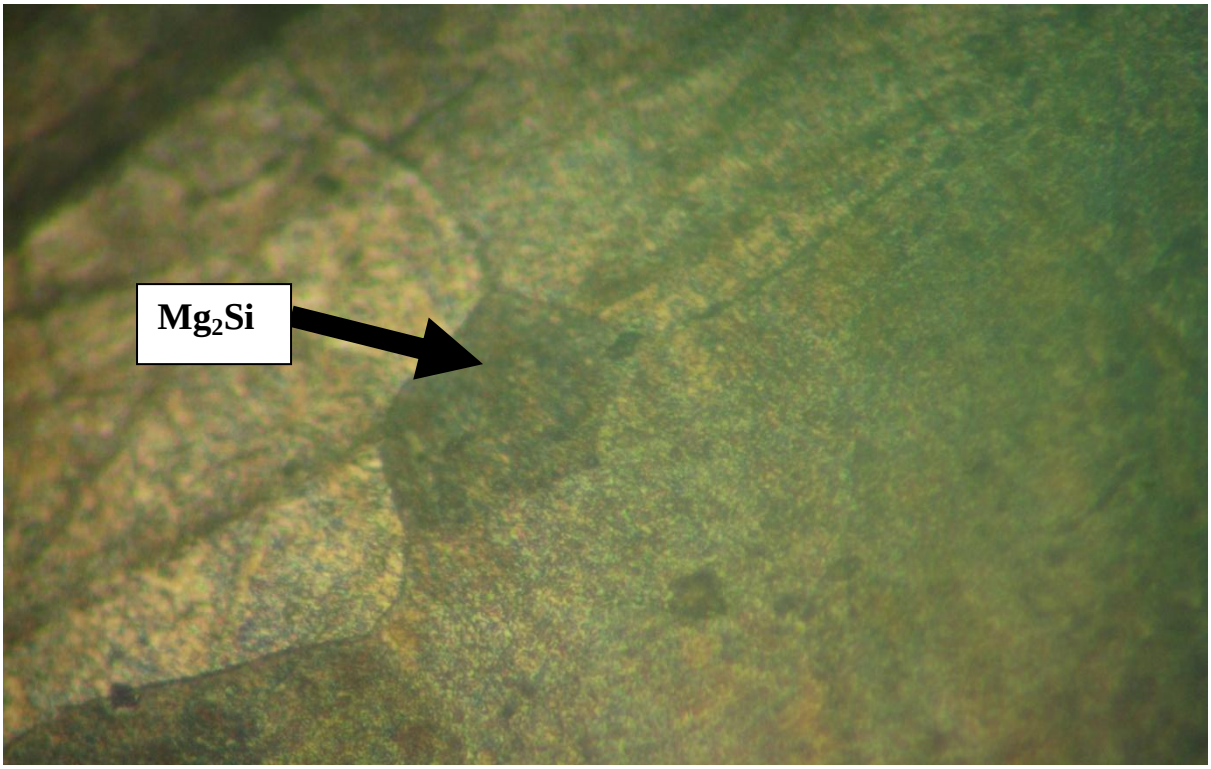

Plate 4.33: Micrograph of Cu-3wt%Si-1.5wt%Mg alloy

4.3.5. Effect of manganese content on the surface morphology of silicon bronze (Cu-3wt%Si)

The microstructural analysis of silicon bronze doped with manganese is presented in Plates 4.34-4.43. The micrographs revealed the presence of γ-phase (solid solubility of manganese in copper matrix) and manganese silicide (Mn_3Si) (Plates 4.34-4.43). The dendritic primary silicon was refined and modified by the addition of manganese, thereby caused an increased mechanical properties of the alloy (Figures 4.8, 4.17, 4.26 and 4.34). It was also revealed in Plates 4.34-4.43 that the volume of γ-phase and the intermetallic compound decreased and coarsened respectively as the manganese content exceeded 1wt%. This resulted to decrease in the ultimate tensile strength and hardness values of Cu-3wt%.Si-Mn alloy (Figures 4.17 and 4.26).

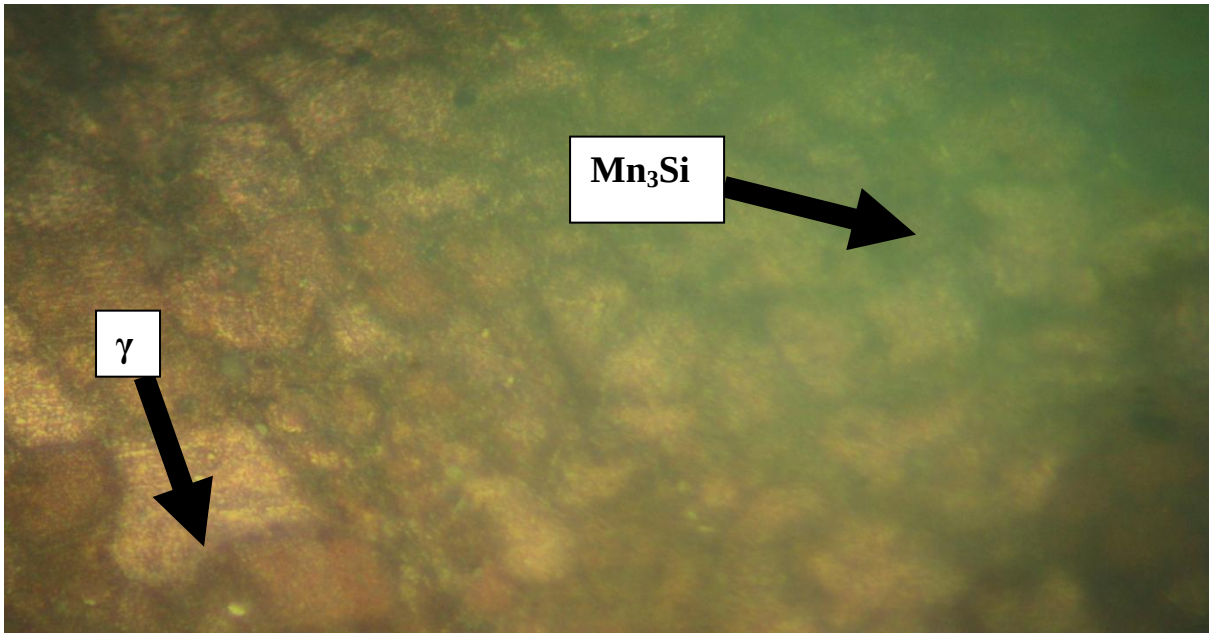

Plate 4.34: Micrograph of Cu-3wt%Si-0.1wt%Mn alloy

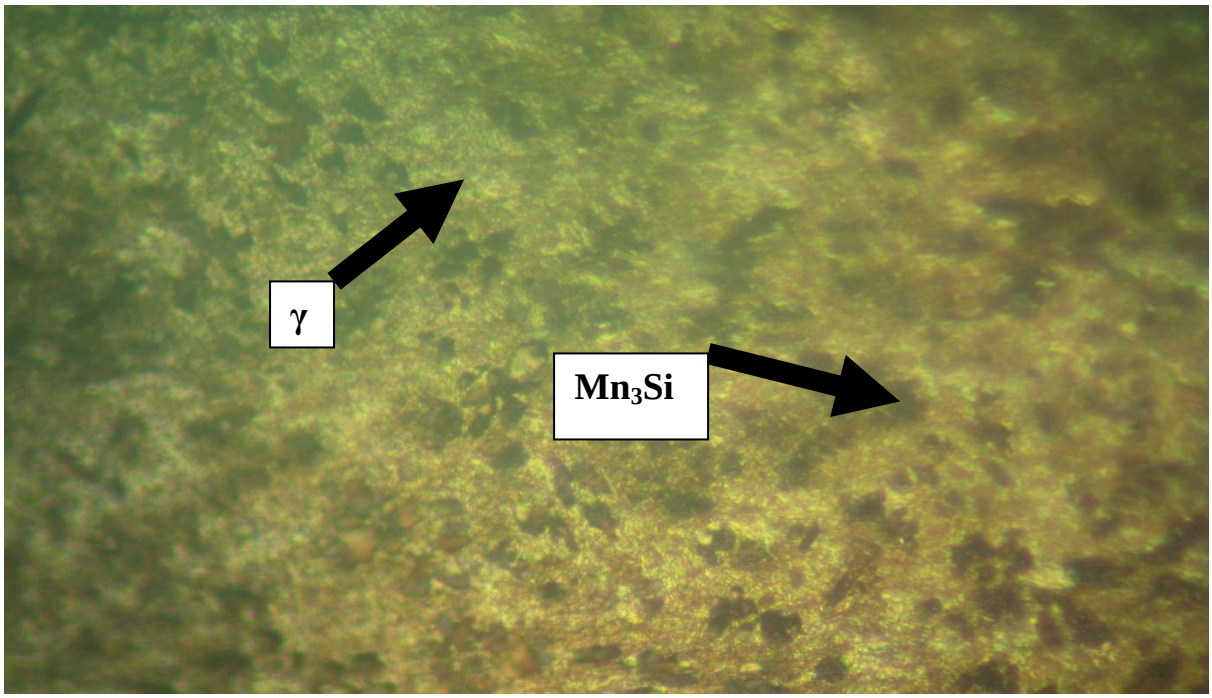

Plate 4.35: Micrograph of Cu-3wt%Si-0.2wt%Mn alloy

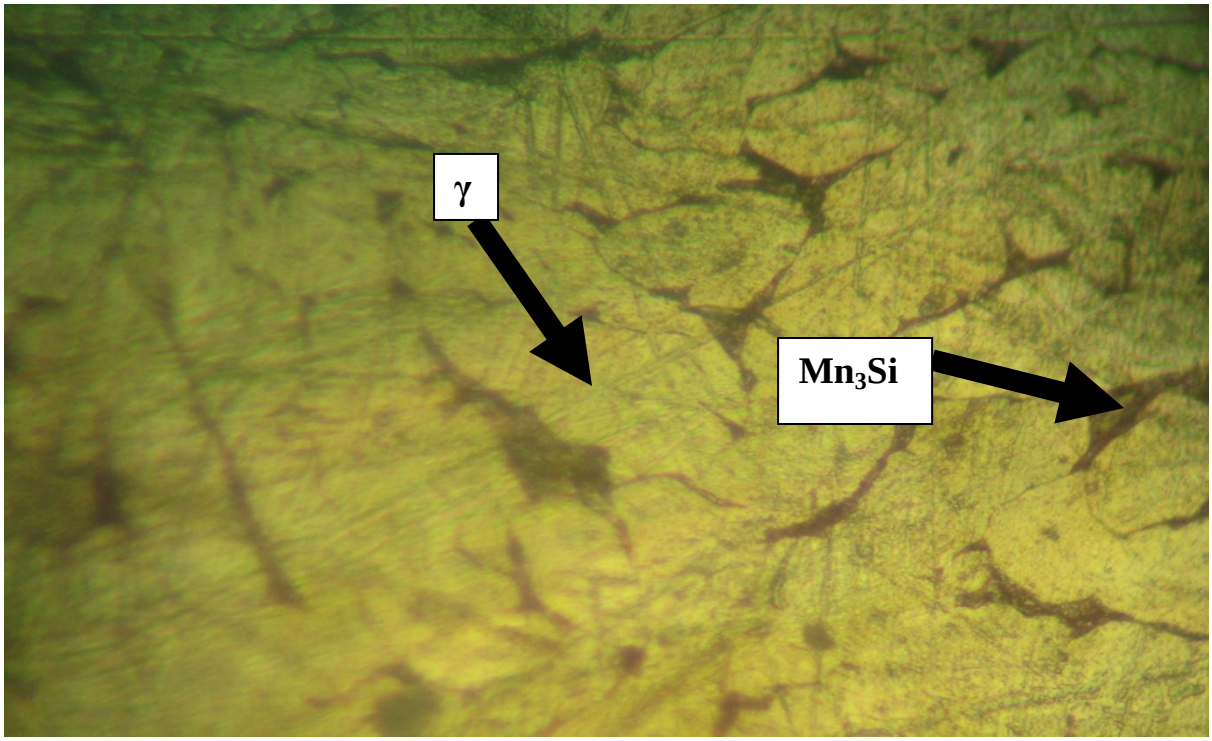

Plate 4.36: Micrograph of Cu-3wt%Si-0.3wt%Mn alloy

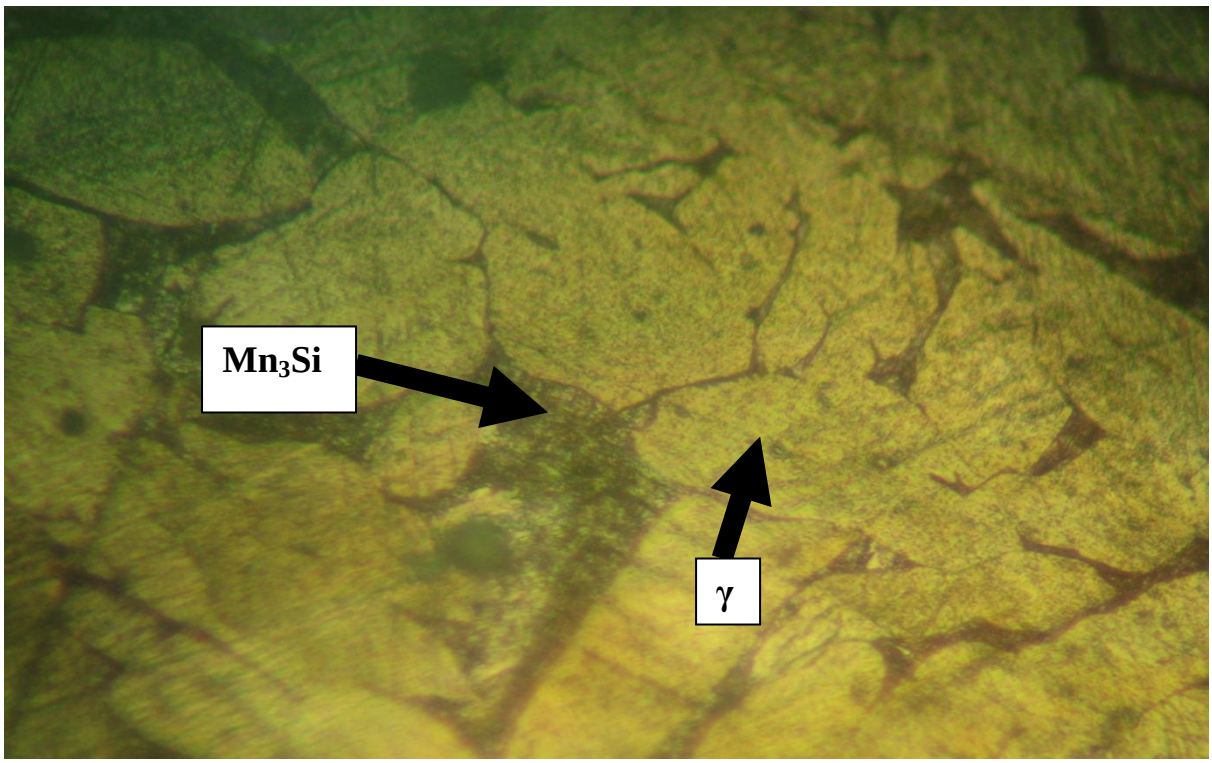

Plate 4.37: Micrograph of Cu-3wt%Si-0.4wt%Mn alloy

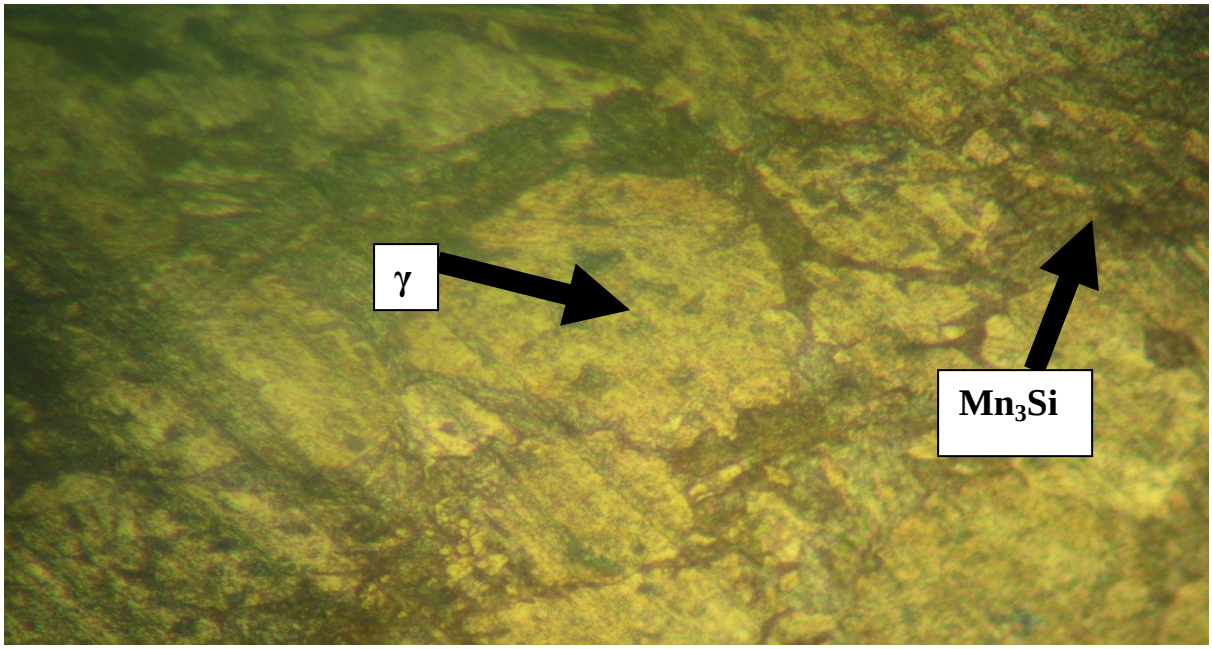

Plate 4.38: Micrograph of Cu-3wt%Si-0.5wt%Mn alloy

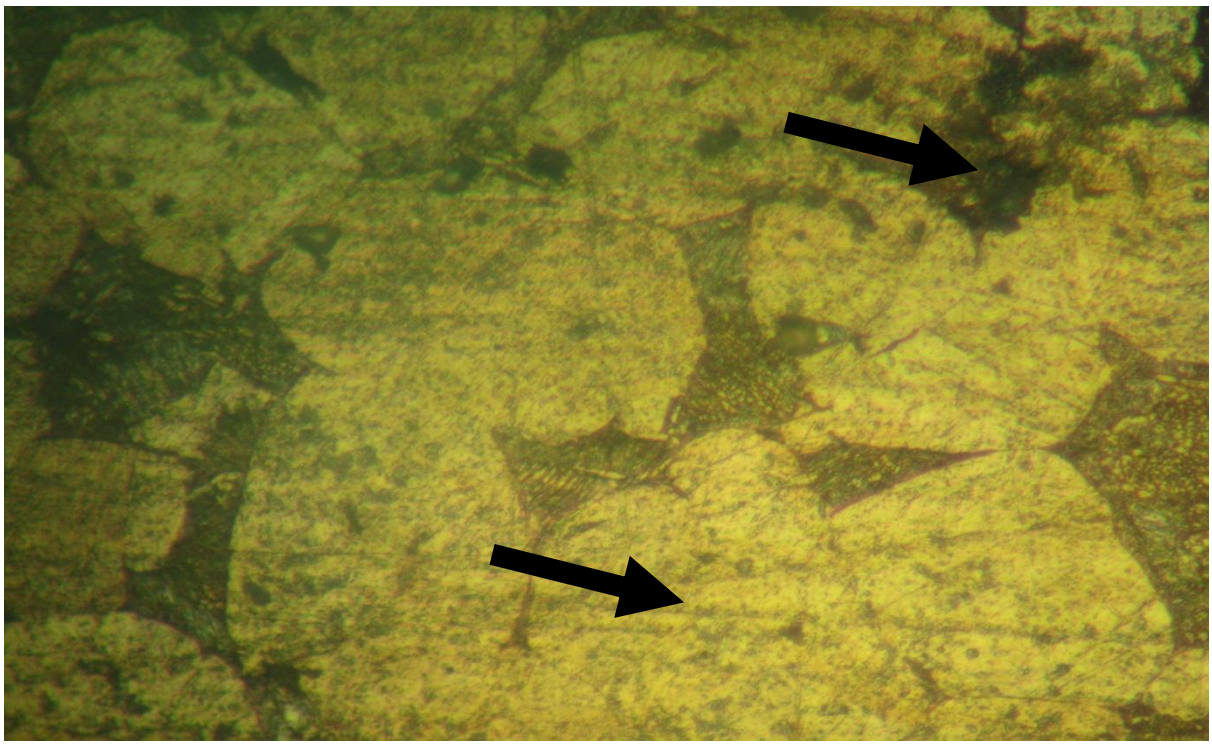

Plate 4.39: Micrograph of Cu-3wt%Si-0.6wt%Mn alloy

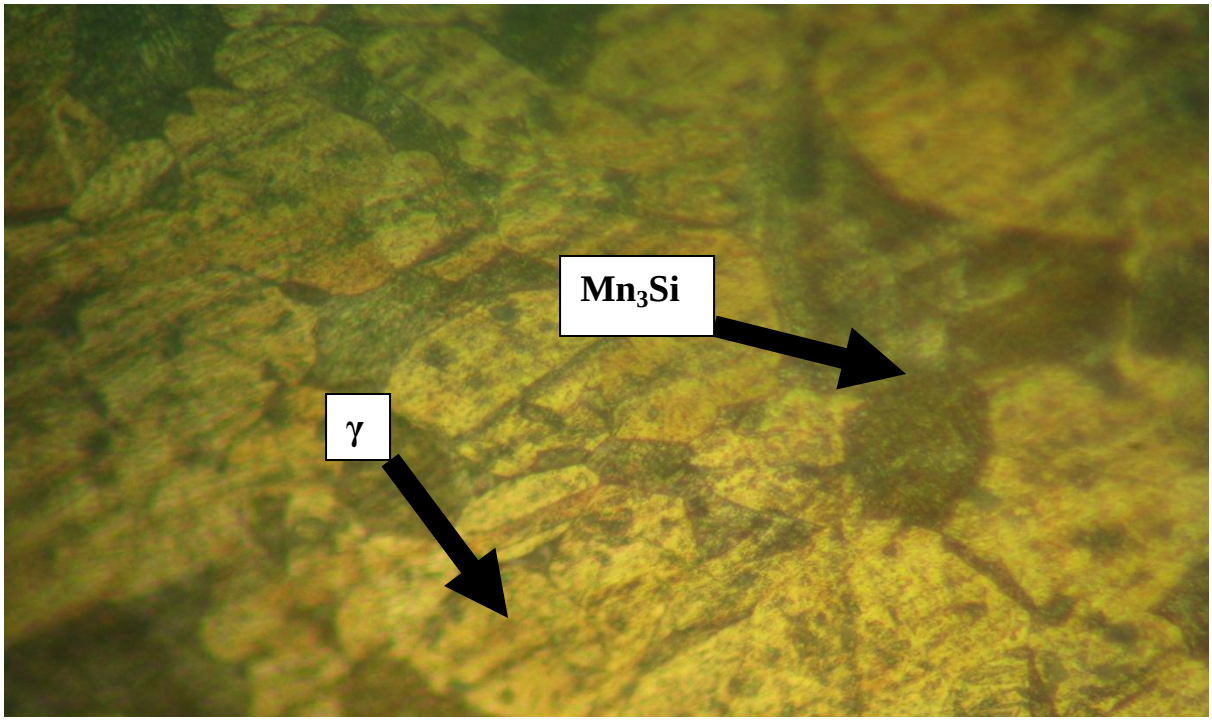

Plate 4.40: Micrograph of Cu-3wt%Si-0.7wt%Mn alloy

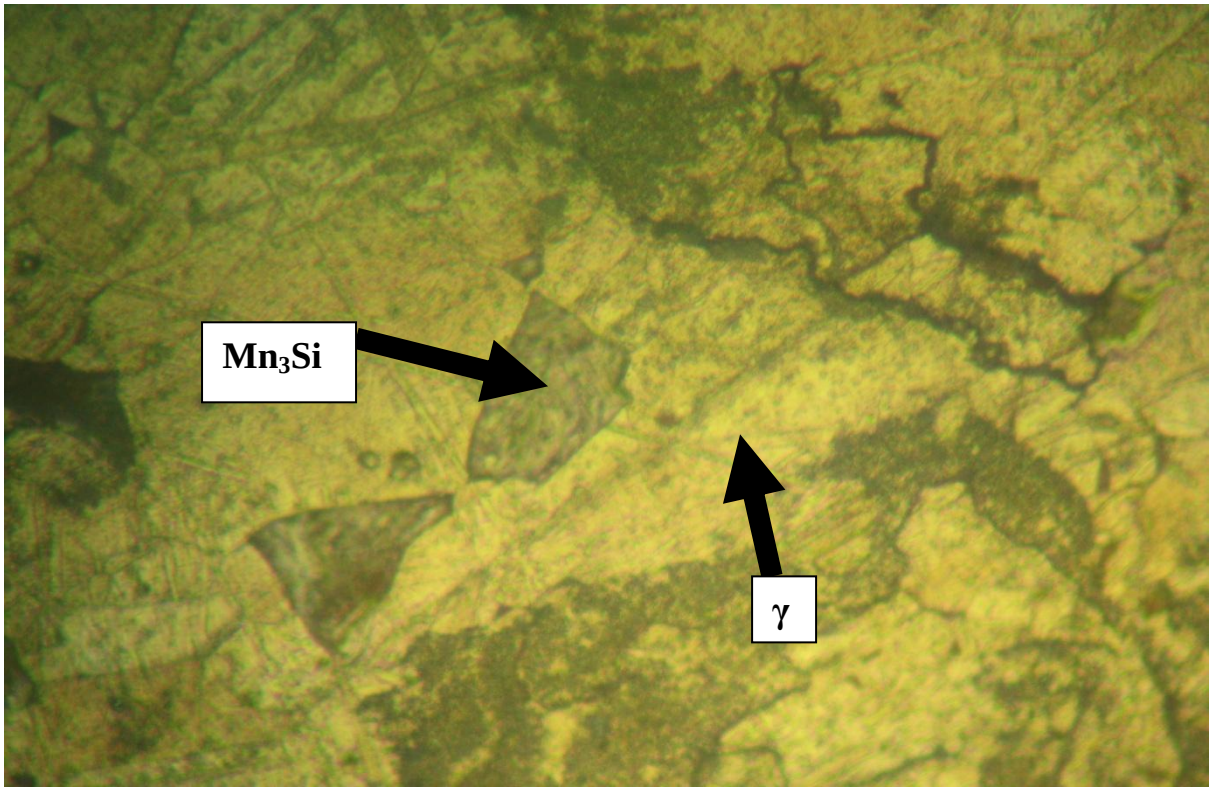

Plate 4.41: Micrograph of Cu-3wt%Si-0.8wt%Mn alloy

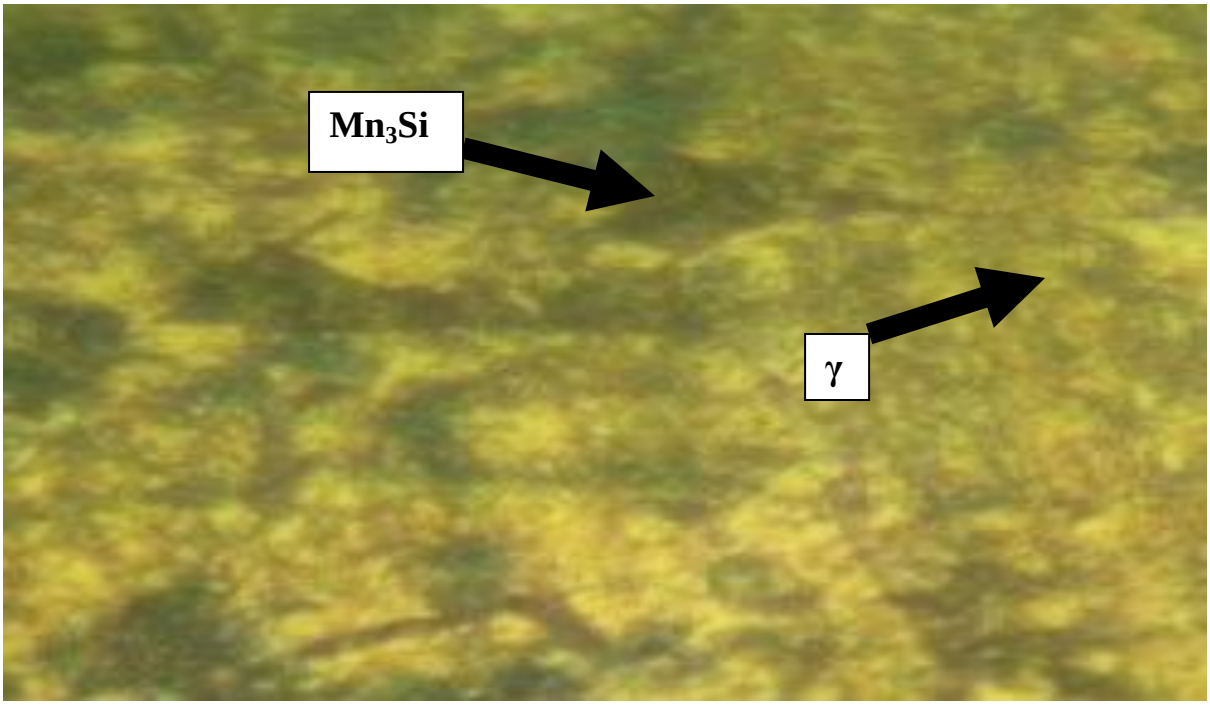

Plate 4.42: Micrograph of Cu-3wt%Si-1wt%Mn alloy

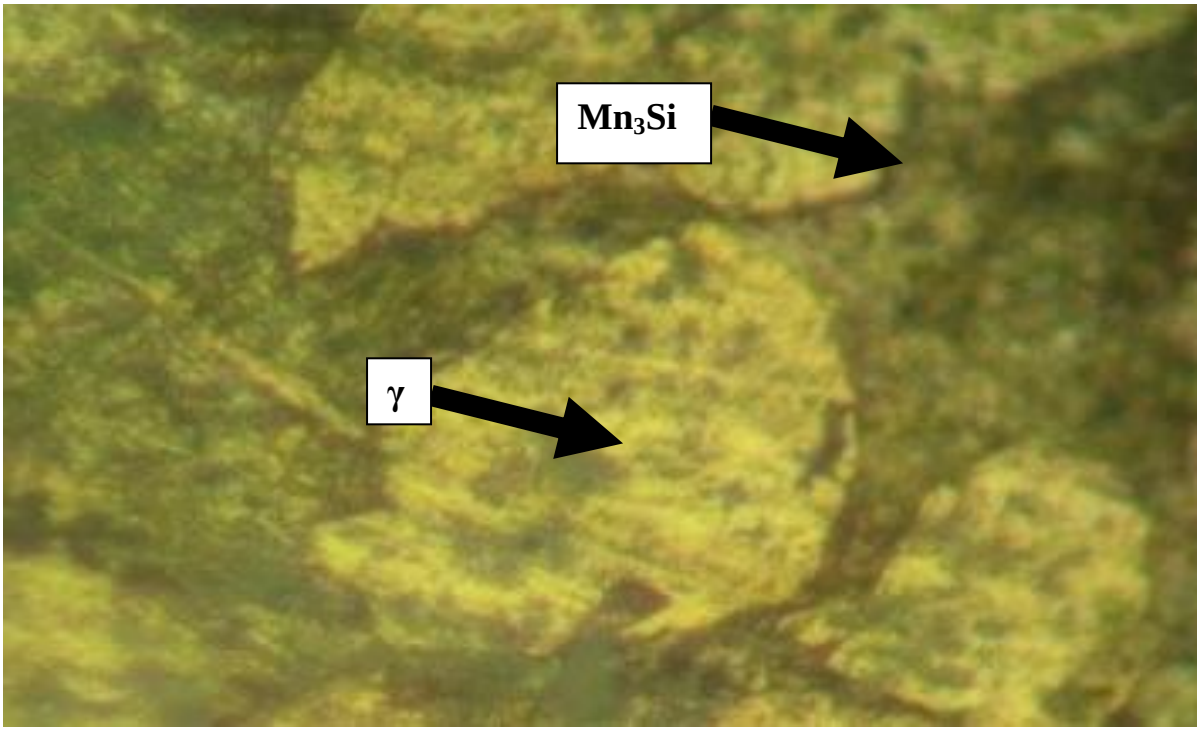

Plate 4.43: Micrograph of Cu-3wt%Si-1.5wt%Mn alloy

4.3.6. Effect of tungsten content on the surface morphology of silicon bronze (Cu-3wt%Si)

A detailed analysis of the surface morphology of silicon bronze doped with tungsten is presented in Plates 4.44-4.53. The micrographs revealed the

presence of Cu_3Si and WSi_2 intermetallic compounds in the copper matrix. Analysis of Plates 4.44-4.53 revealed that the addition of tungsten refined and modified the dendritic primary silicon, thereby increased the percentage elongation, ultimate tensile strength, hardness and impact strength of the alloy (Figures 4.8, 4.17, 4.26 and 4.34). The intermetallic compounds coarsened as the concentration of tungsten increased to 1wt% (Plates 4.49-4.53). This caused decrease in ultimate tensile strength and hardness of Cu-3wt%Si-W alloy (Figures 4.17 and 4.26).

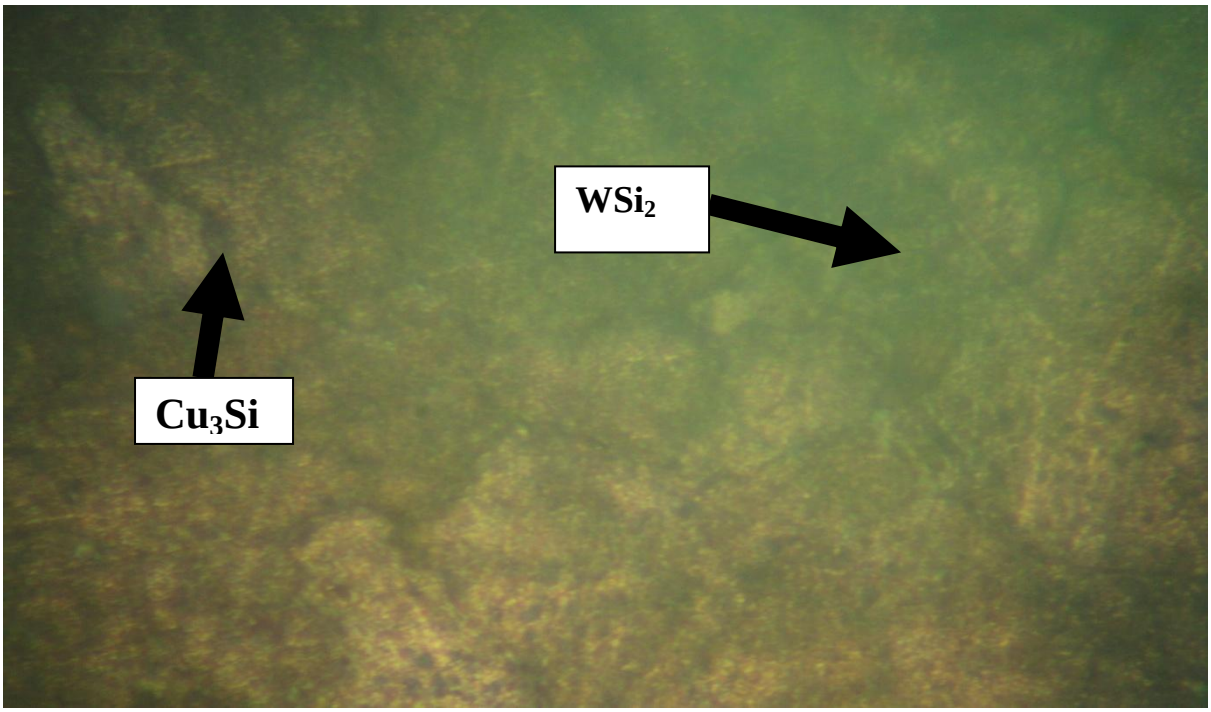

Plate 4.44: Micrograph of Cu-3wt%Si-0.1wt%W alloy

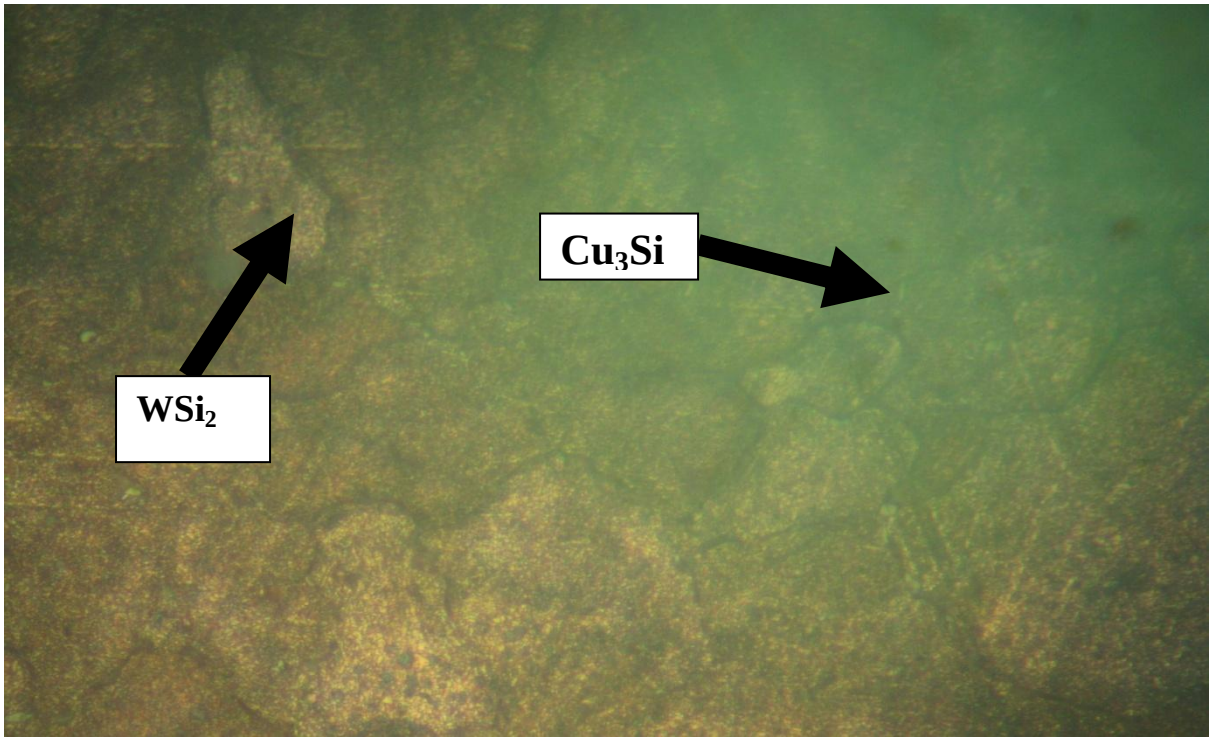

Plate 4.45 Micrograph of Cu-3wt%Si-0.2wt%W alloy

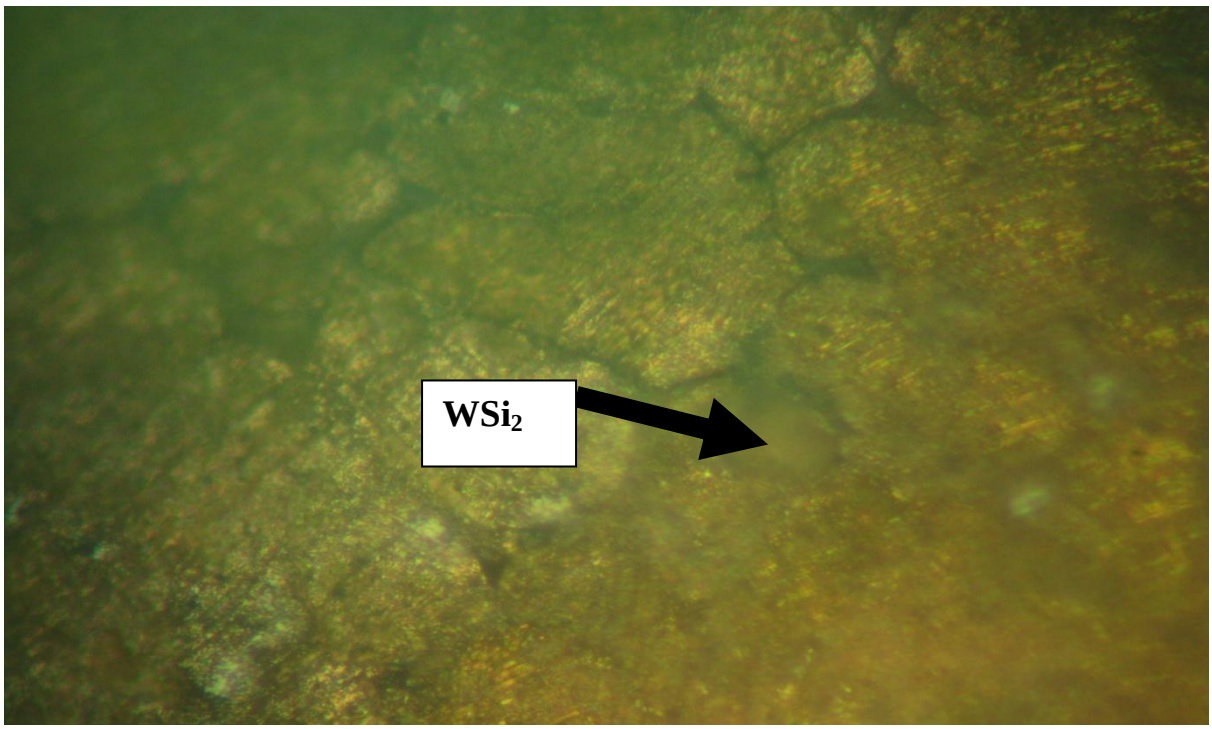

Plate 4.46: Micrograph of Cu-3wt%Si-0.3wt%W alloy

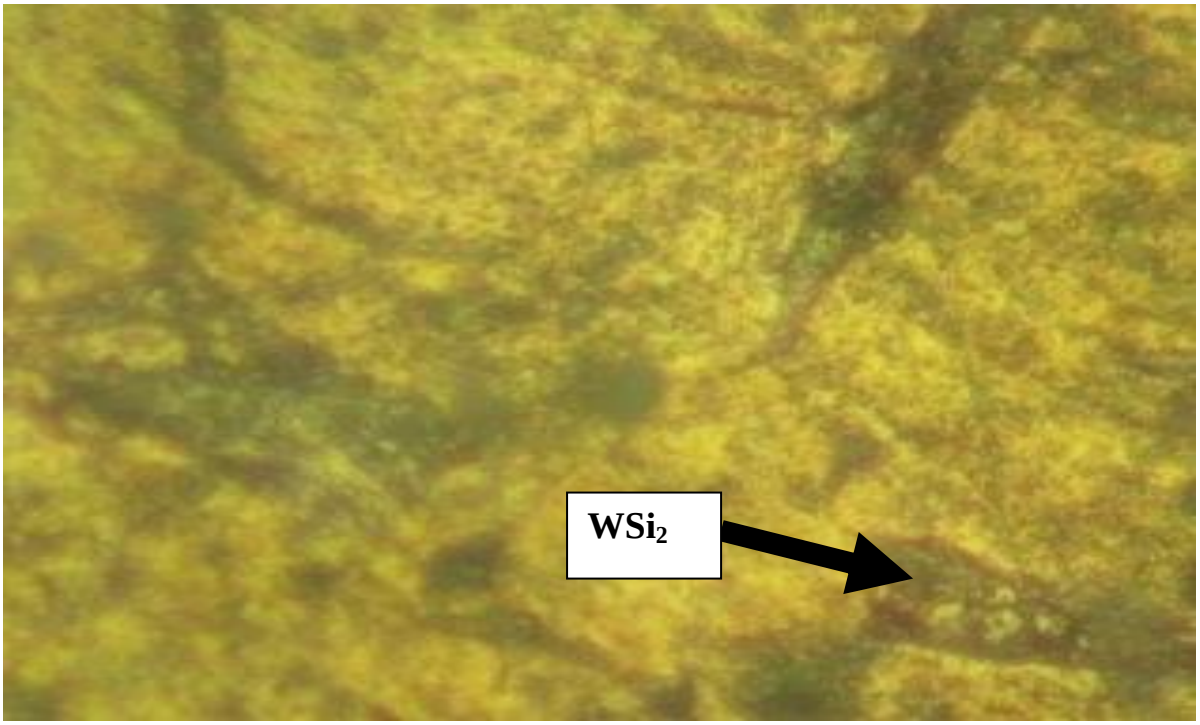

Plate 4.47: Micrograph of Cu-3wt%Si-0.4wt%W alloy

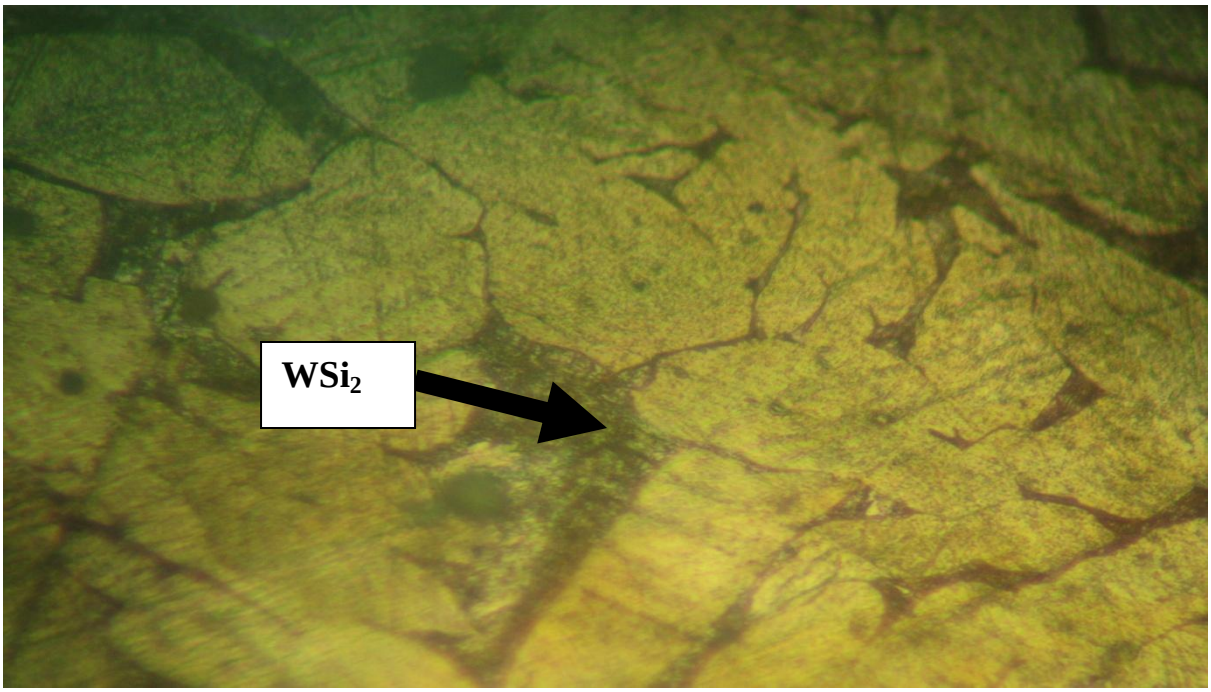

Plate 4.48 Micrograph of Cu-3wt%Si-0.5wt%W alloy

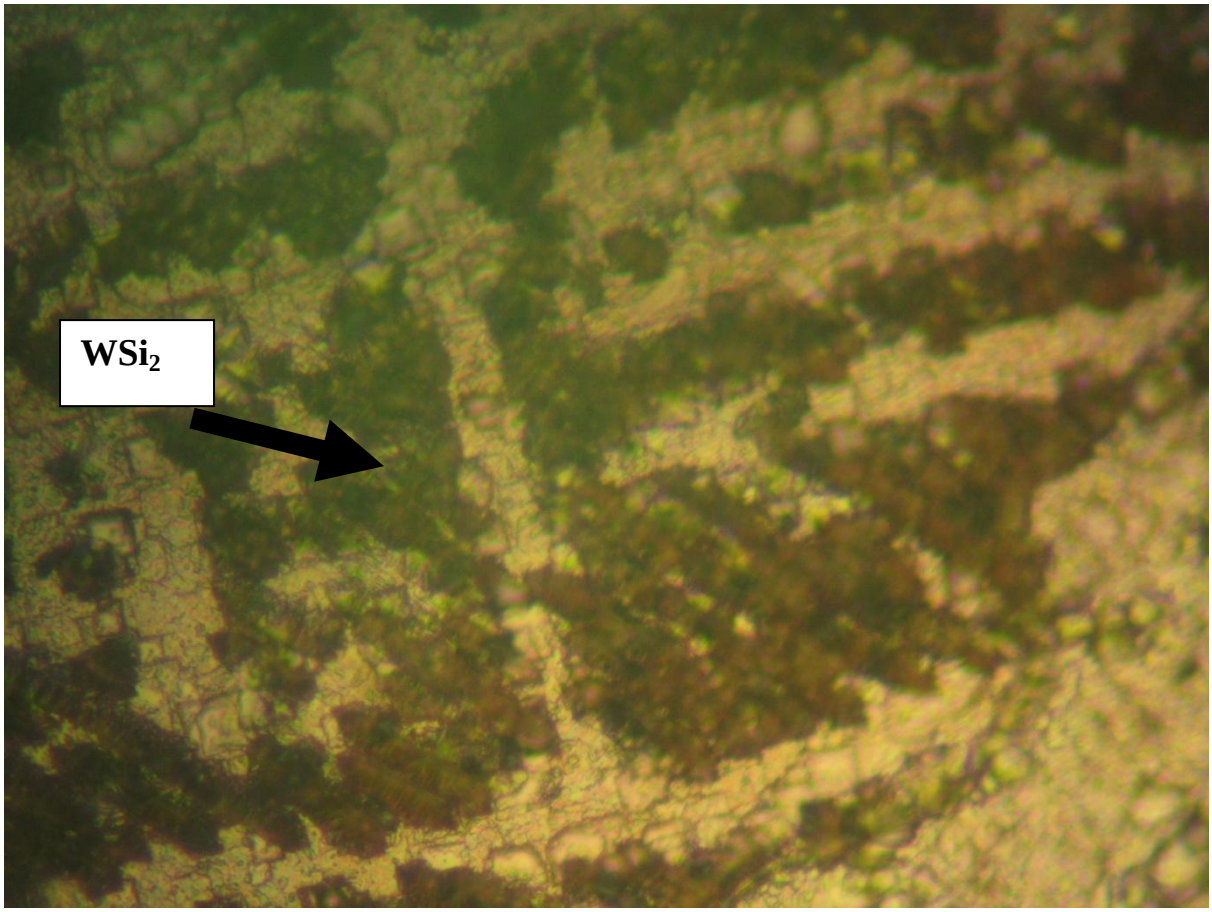

Plate 4.49: Micrograph of Cu-3wt%Si-0.6wt%W alloy

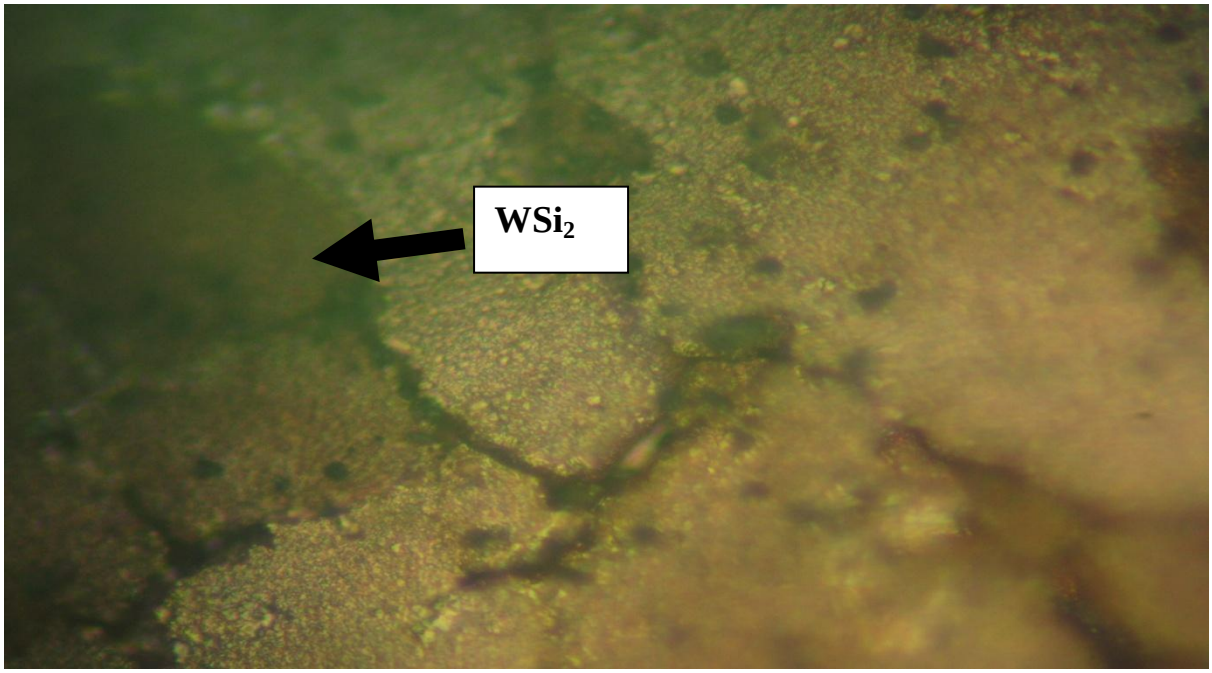

Plate 4.50: Micrograph of Cu-3wt%Si-0.7wt%W alloy

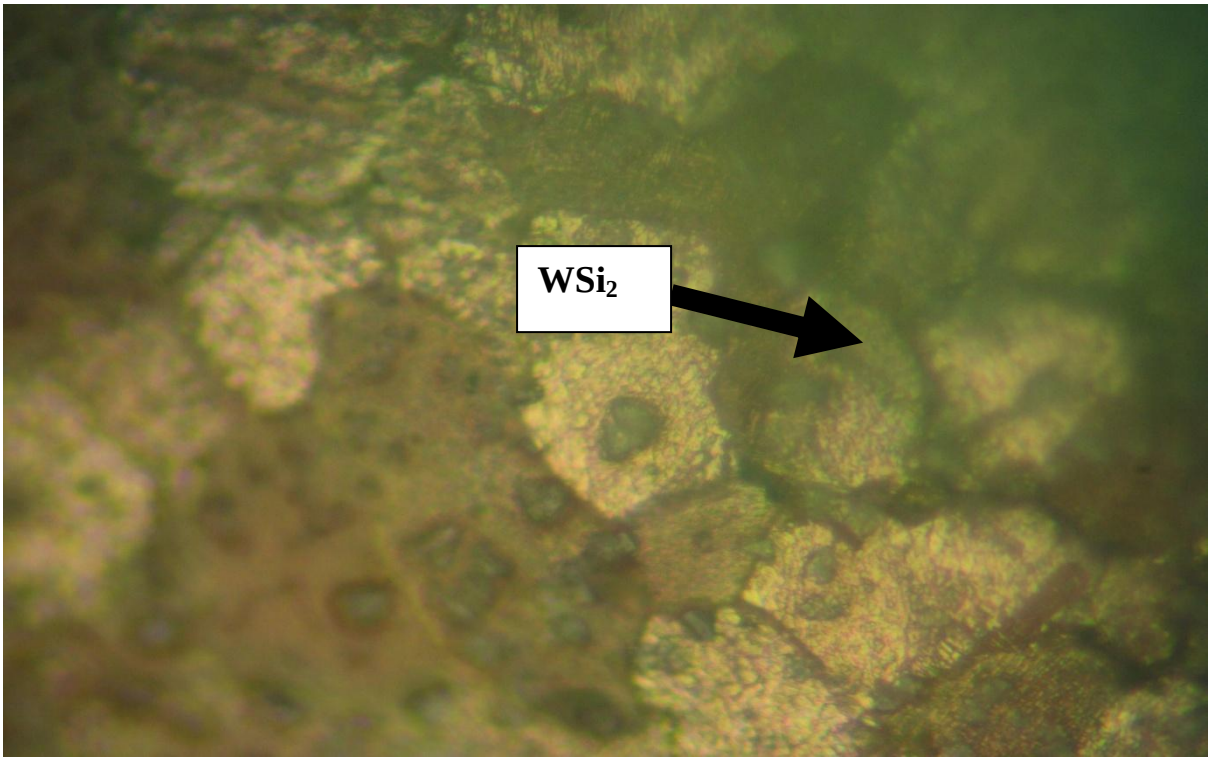

Plate 4.51: Micrograph of Cu-3wt%Si-0.8wt%W alloy

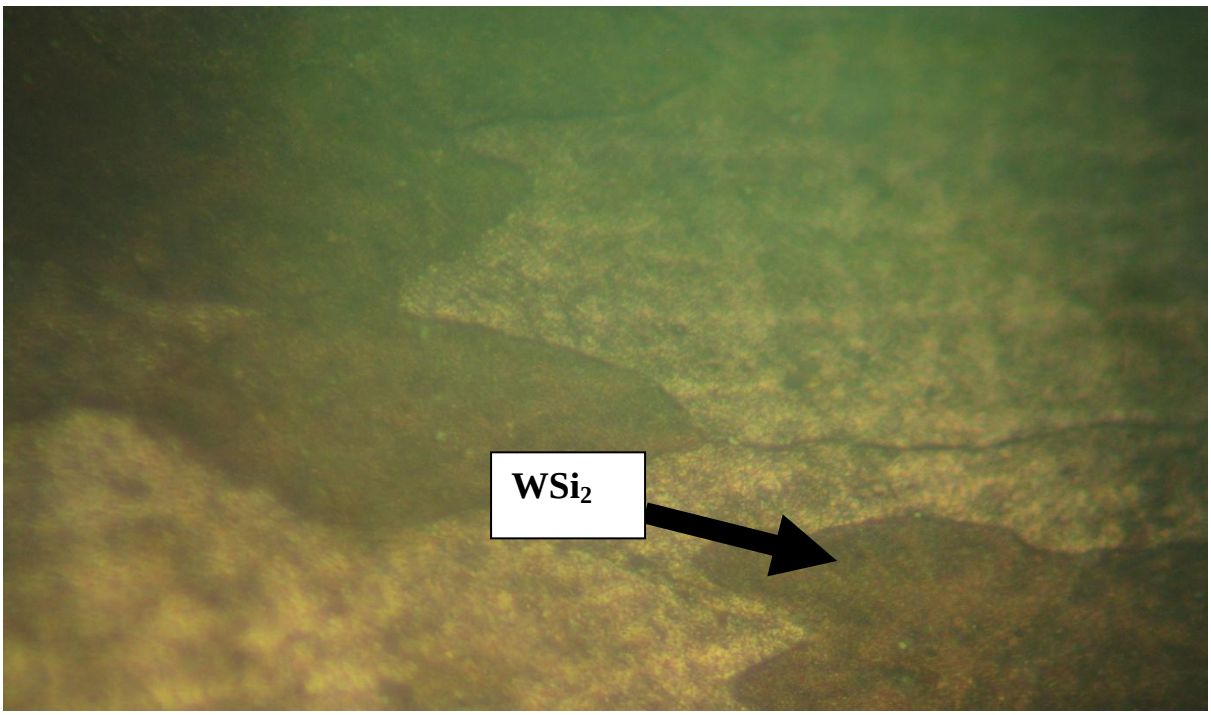

Plate 4.52: Micrograph of Cu-3wt%Si-1wt%W alloy

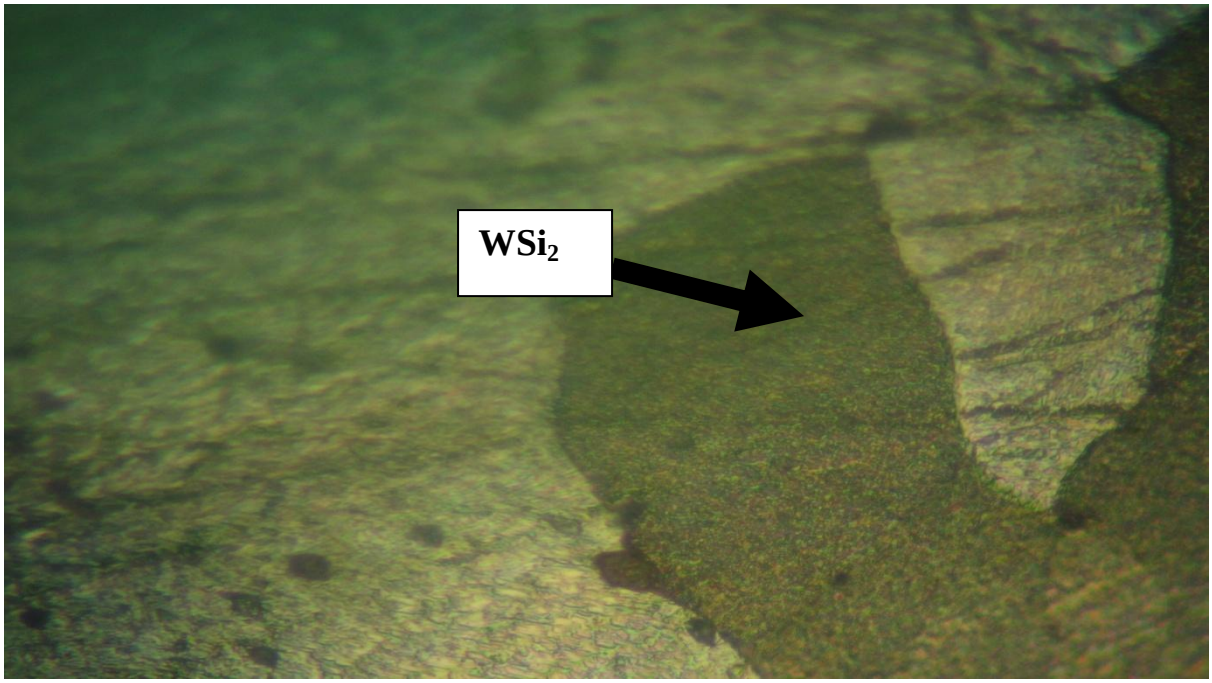

Plate 4.53: Micrograph of Cu-3wt%Si-1.5wt%W alloy

4.3.7. Effect of titanium content on the surface morphology of silicon bronze (Cu-3wt%Si)

Analysis of the surface morphology of silicon bronze doped with titanium is presented in Plates 4.54-4.63. The micrographs revealed the presence of Cu_4Ti and Ti_1Si intermetallic phases in the copper matrix. Analysis of Plates 4.54-4.63 indicates that the dendritic primary silicon and intermetallic compound (Cu_3Si) were refined and modified respectively by addition of titanium. This caused an increase in percentage elongation, ultimate tensile strength, hardness and impact strength of the studied alloy (Figures 4.8, 4.17, 4.26 and 4.36). Plates 4.54-4.63 revealed that the number of the intermetallic compounds, Cu_4Ti and Ti_1Si formed in the alloy structure increased as the concentration of titanium increased up to 2wt% (Plates 4.54-4.63). Further increase in titanium concentration resulted to the formation of coarsened intermetallic compound

which slightly decreased the ultimate tensile strength and hardness values of the alloy.

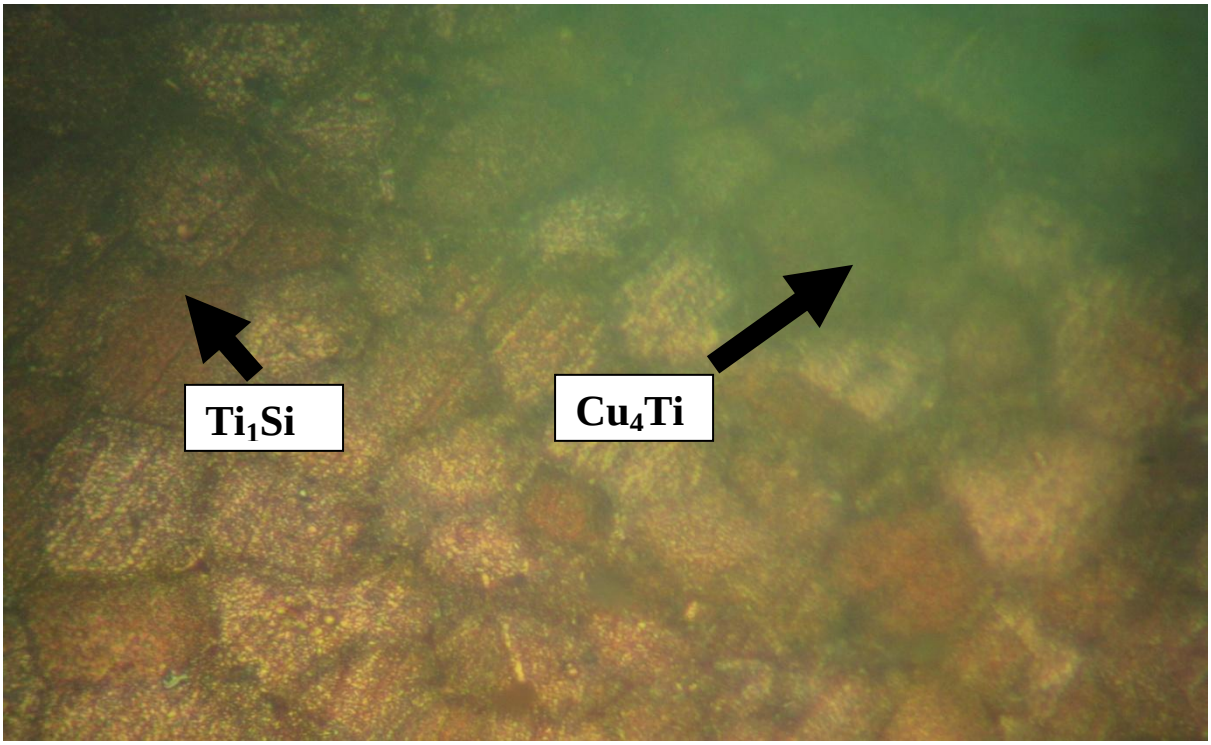

Plate 4.54: Micrograph of Cu-3wt%Si-0.1wt%Ti alloy

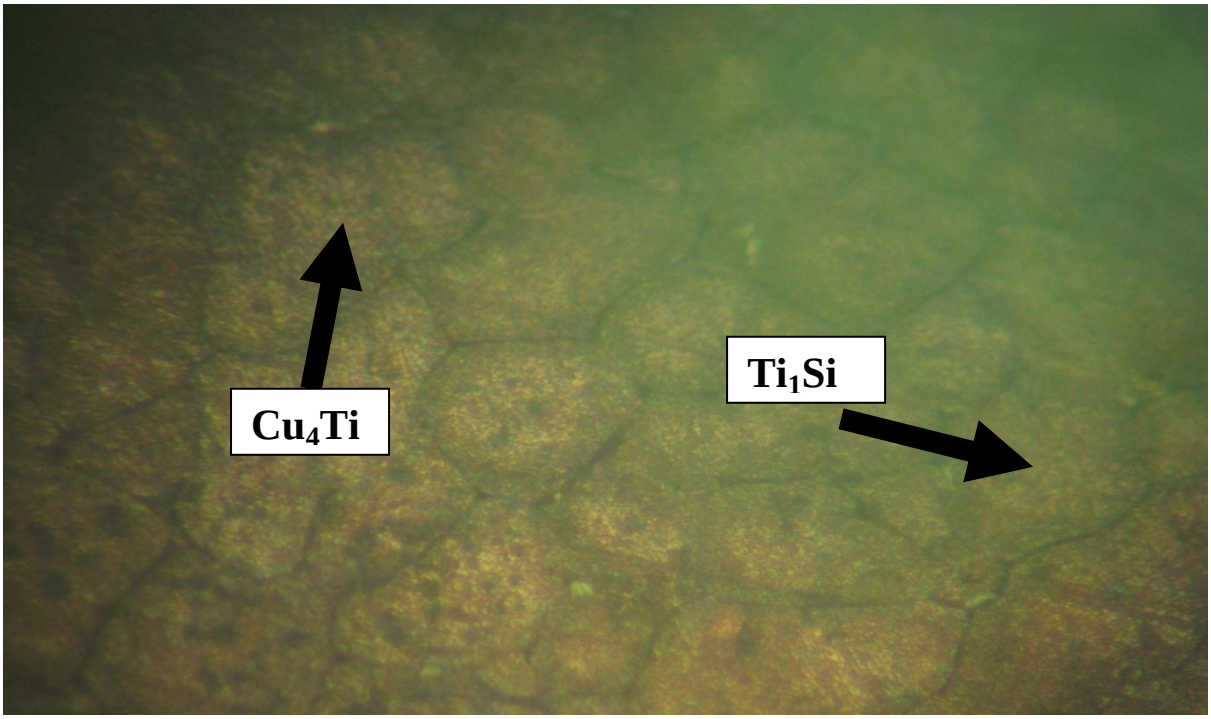

Plate 4.55: Micrograph of Cu-3wt%Si-0.3wt%Ti alloy

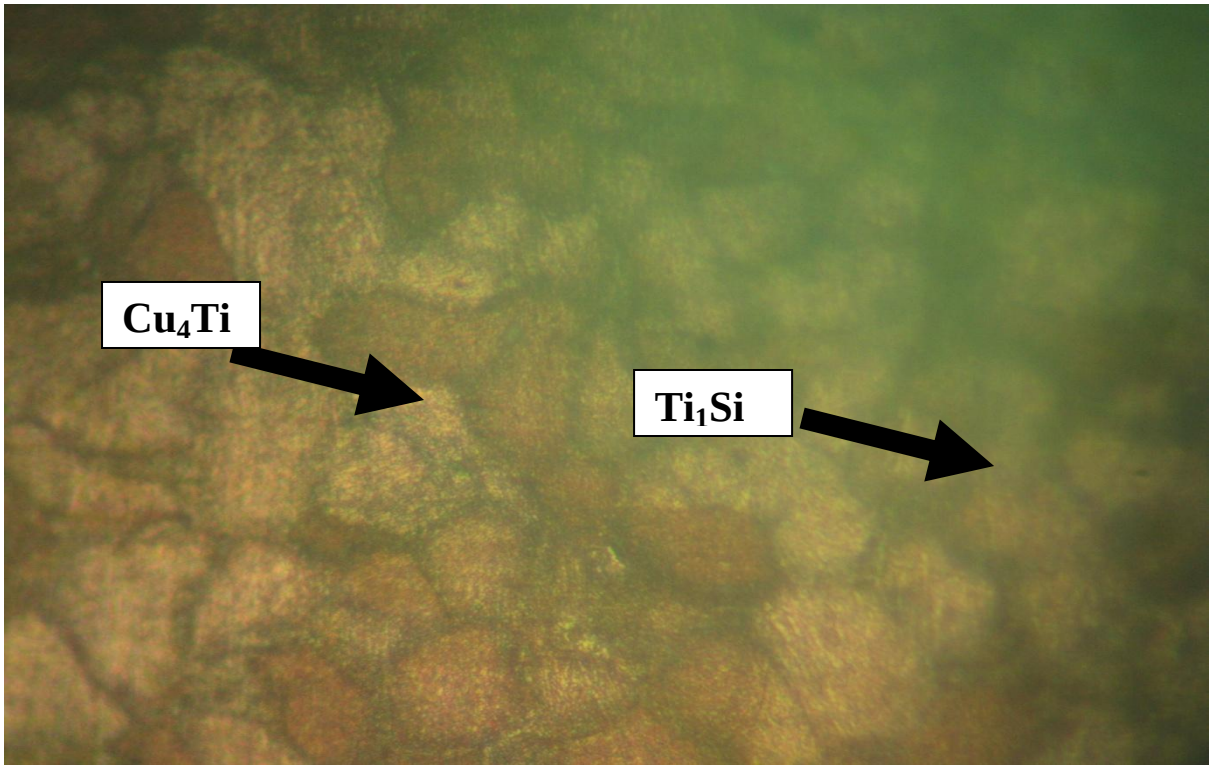

Plate 4.56: Micrograph of Cu-3wt%Si-0.5wt%Ti alloy

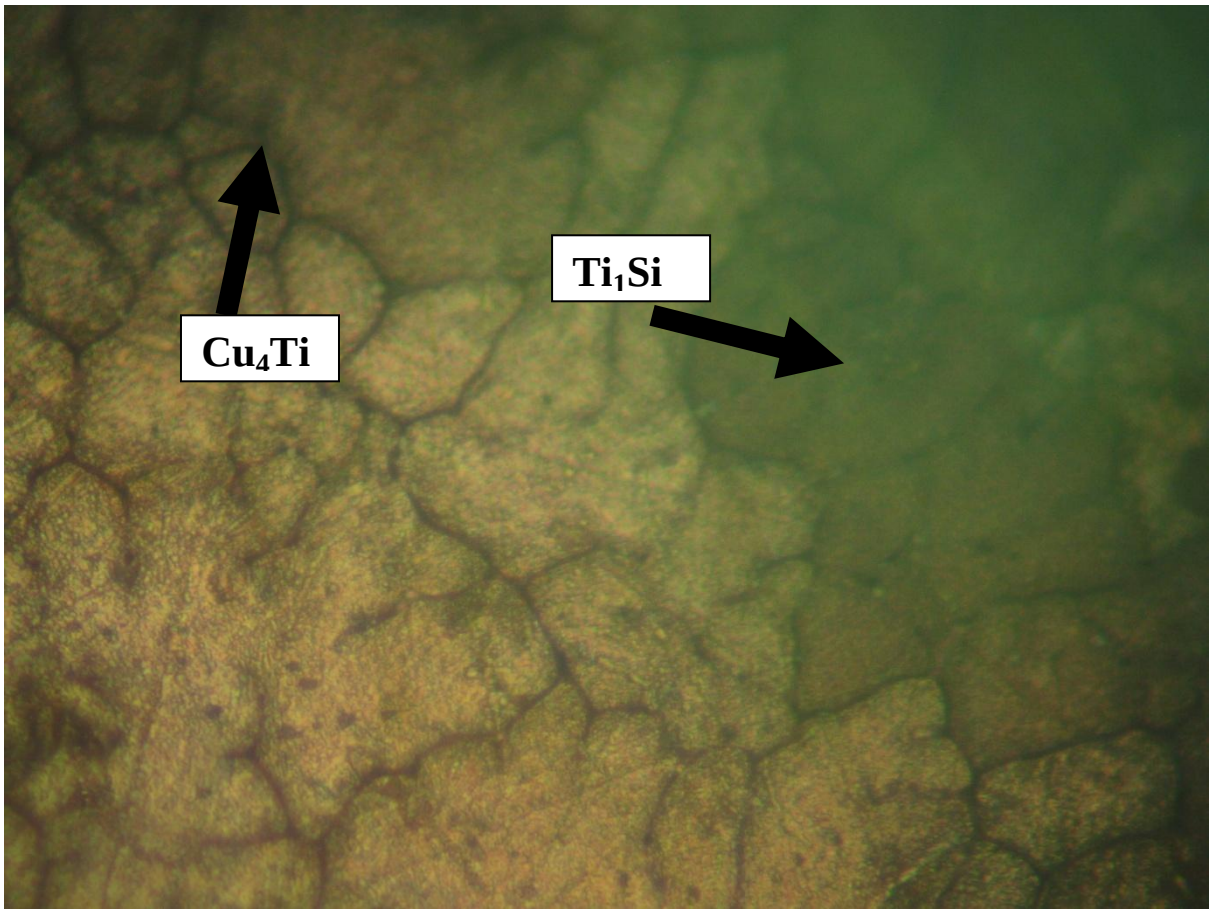

Plate 4.57: Micrograph of Cu-3wt%Si-0.7wt%Ti alloy

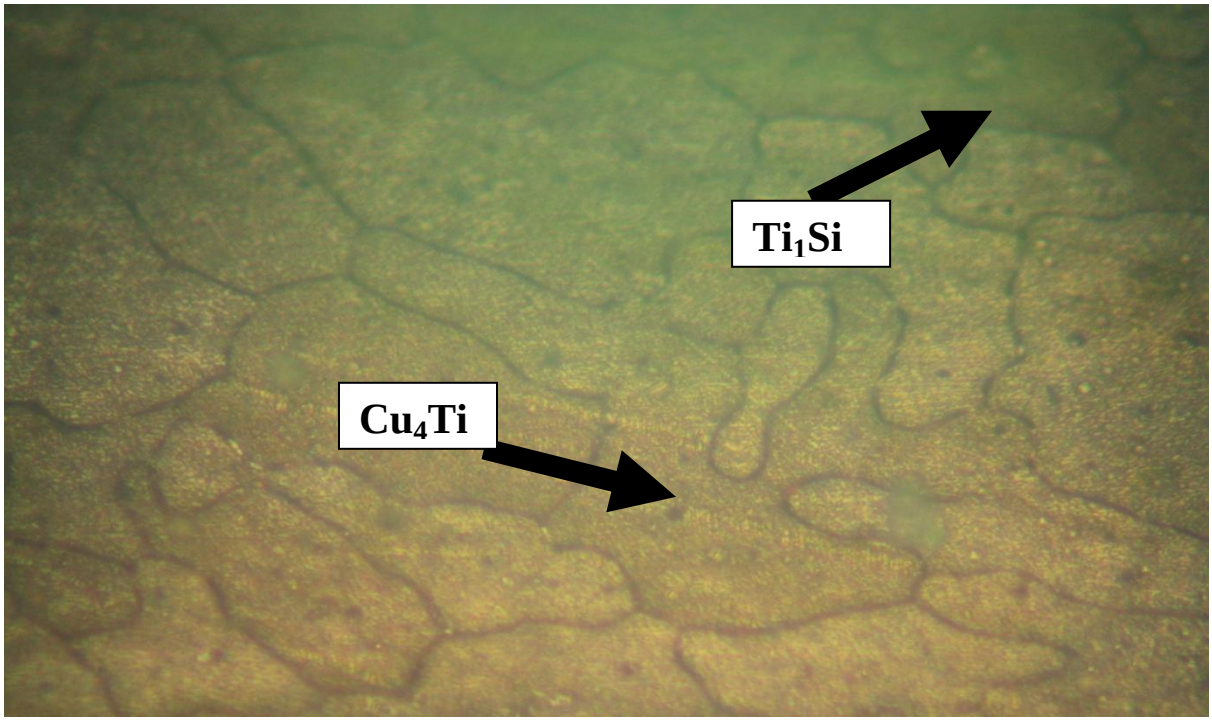

Plate 4.58: Micrograph of Cu-3wt%Si-0.8wt%Ti alloy

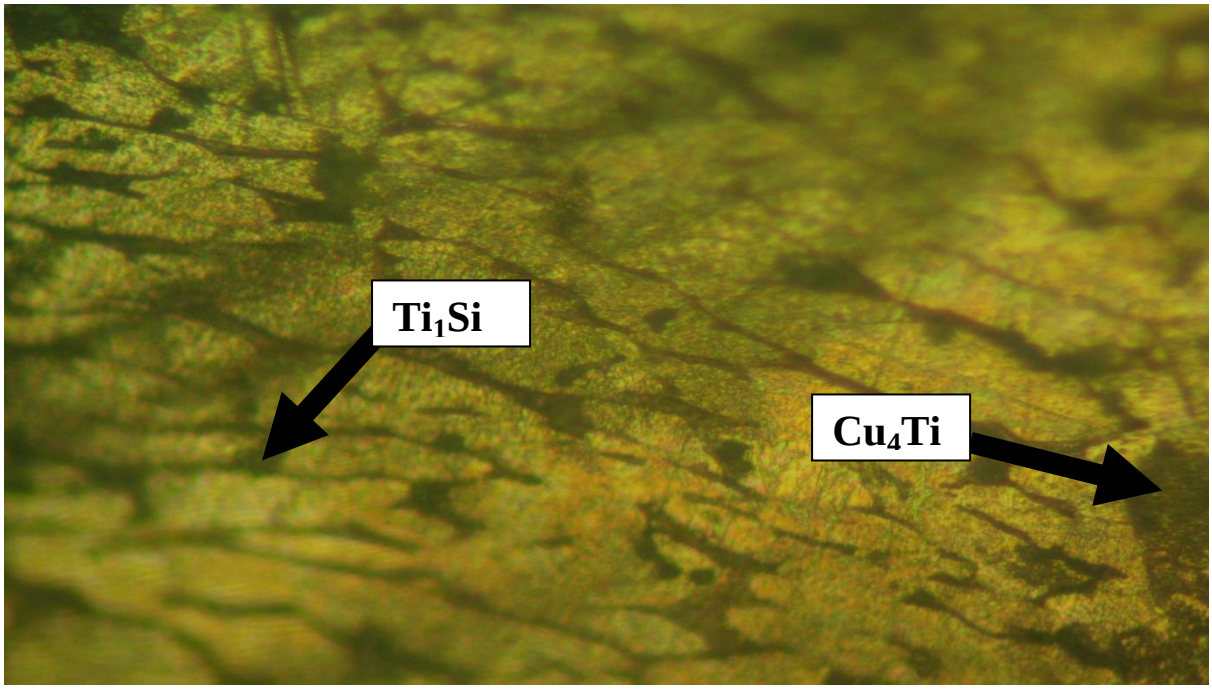

Plate 4.59: Micrograph of Cu-3wt%Si-1wt%Ti alloy

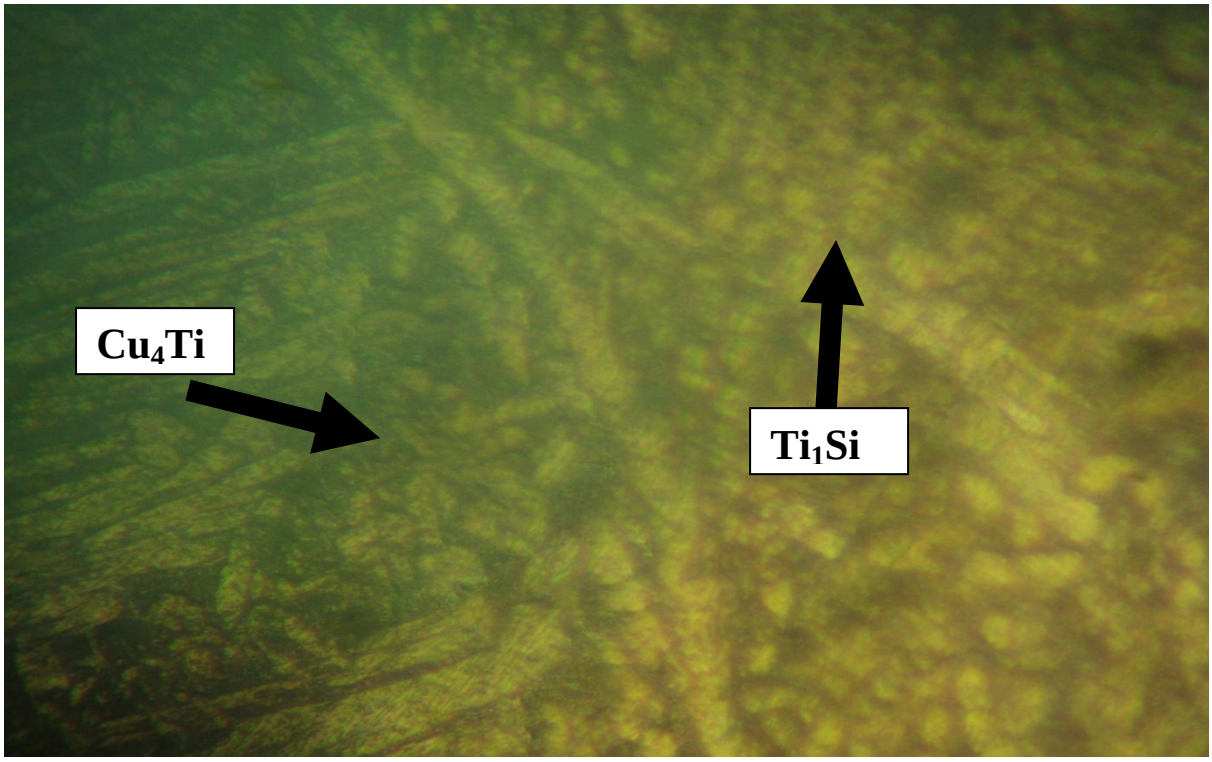

Plate 4.60 Micrograph of Cu-3wt%Si-1.5wt%Ti alloy

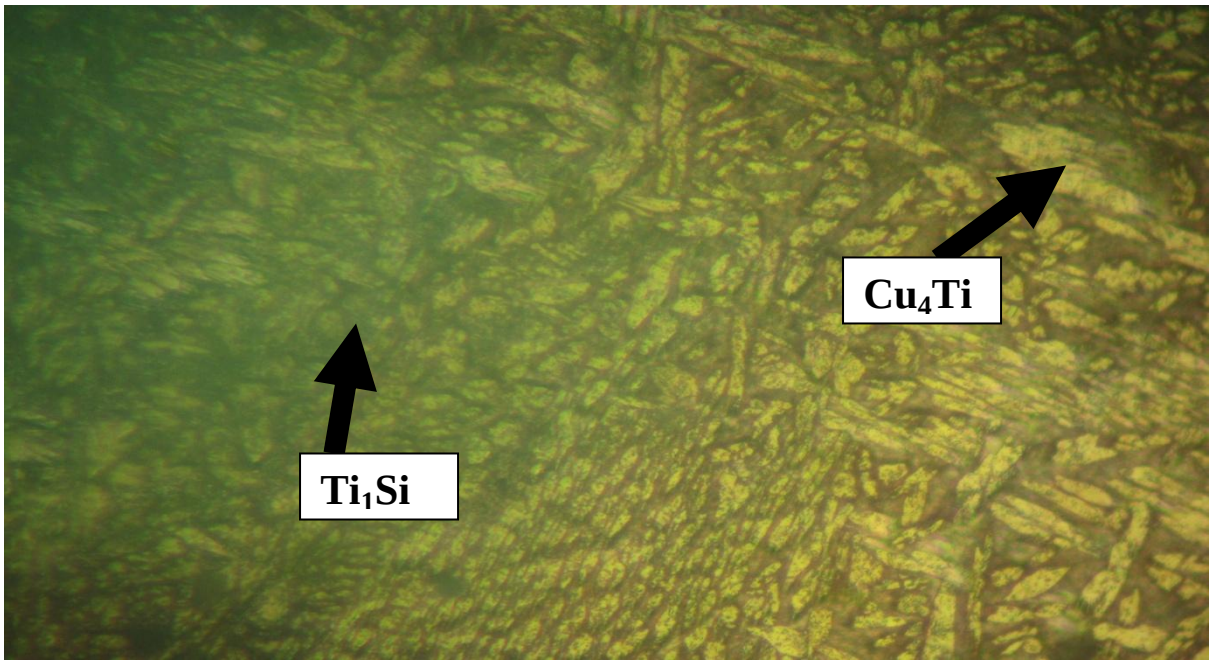

Plate 4.61: Micrograph of Cu-3wt%Si-2wt%Ti alloy

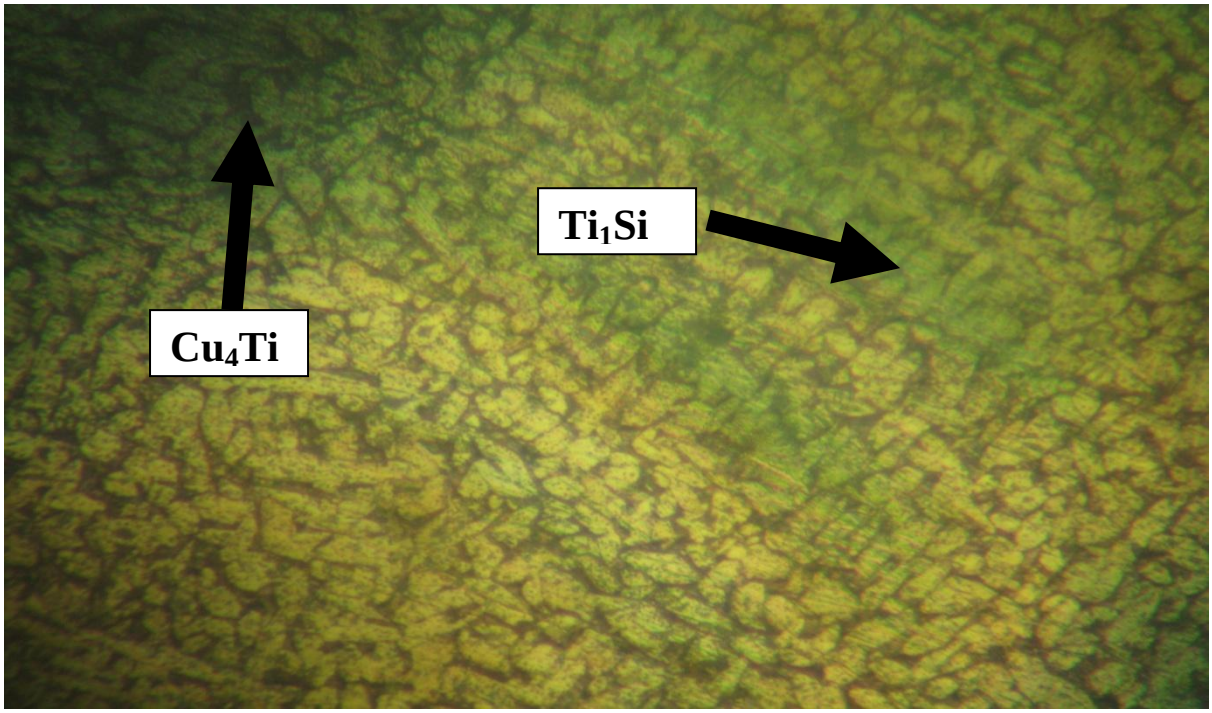

Plate 4.62: Micrograph of Cu-3wt%Si-3wt%Ti alloy

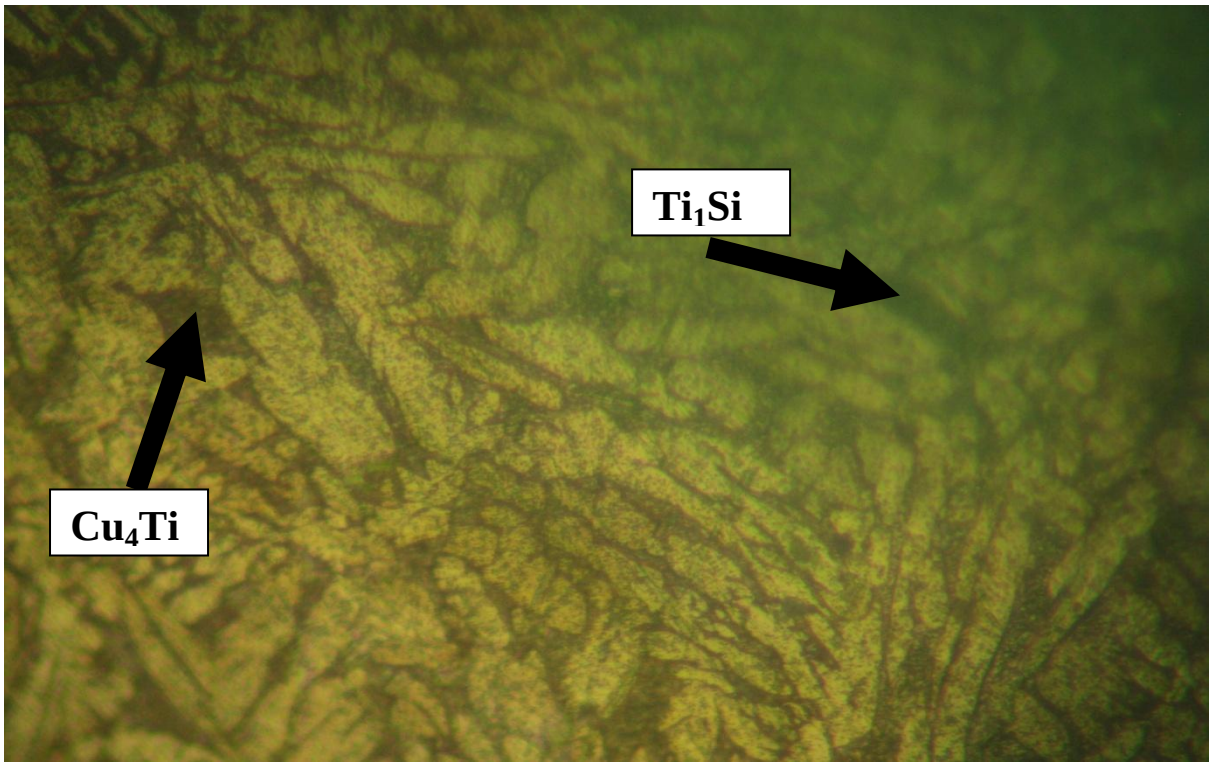

Plate 4.63: Micrograph of Cu-3wt%Si-5wt%Ti alloy

4.3.8. Effect of molybdenum content on the surface morphology of silicon bronze (Cu-3wt%Si)

The microstructure of silicon bronze doped with molybdenum is presented in Plates 4.64-4.73. The micrographs revealed the presence of $MoSi_2$ intermetallic phase (Plates 4.64-4.73). Analysis of Plates 4.64-4.73 shows that molybdenum addition decreased the size of the dendritic primary silicon; thereby increased the percentage elongation, ultimate tensile strength, hardness and impact strength of silicon bronze (Figures 4.8, 4.17, 4.26 and 4.34). Plates 4.64-4.73 also revealed the presence of modified intermetallic compound evenly distributed in the copper matrix. The intermetallic compound coarsened as the concentration of molybdenum increased to 2wt%, thereby causing a decrease in ultimate tensile strength and hardness of the alloy.

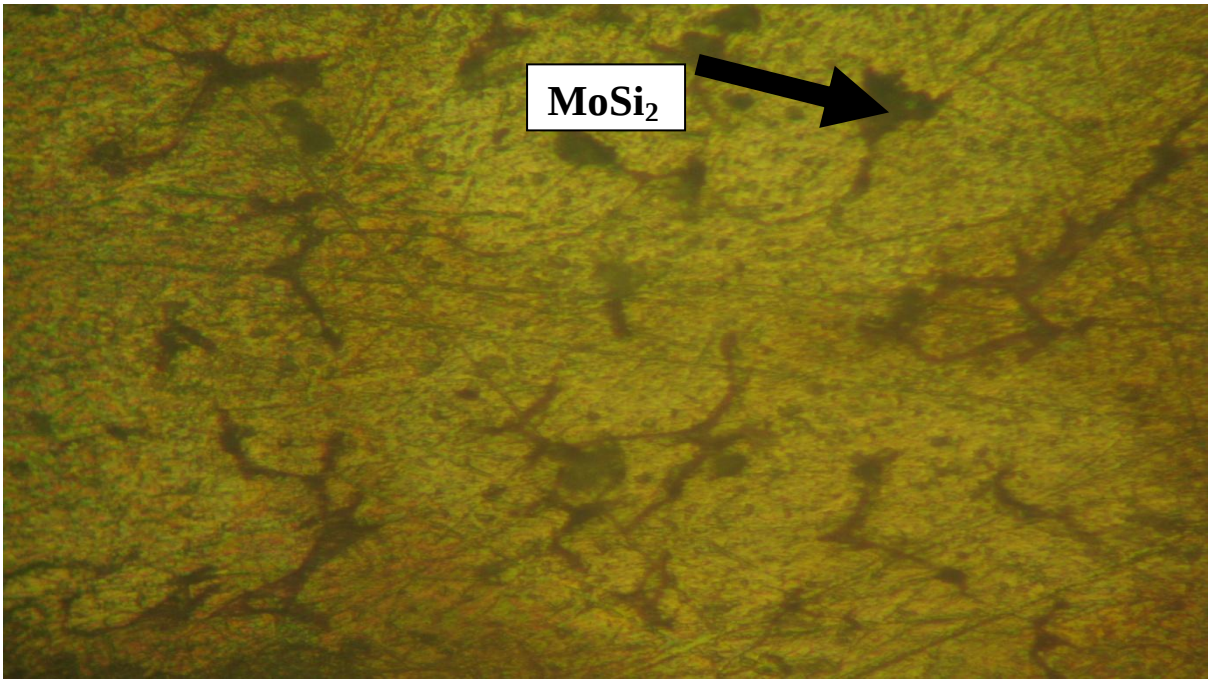

Plate 4.64: Micrograph of Cu-3wt%Si-0.1wt%Mo alloy

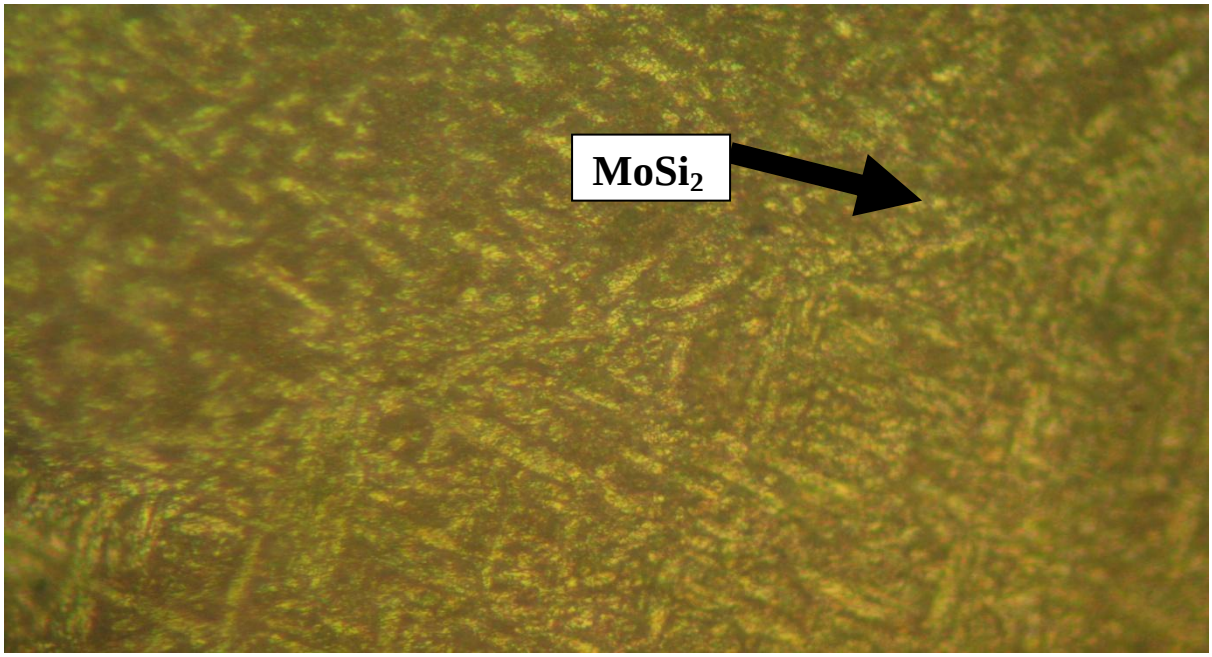

Plate 4.65: Micrograph of Cu-3wt%Si-0.3wt%Mo alloy

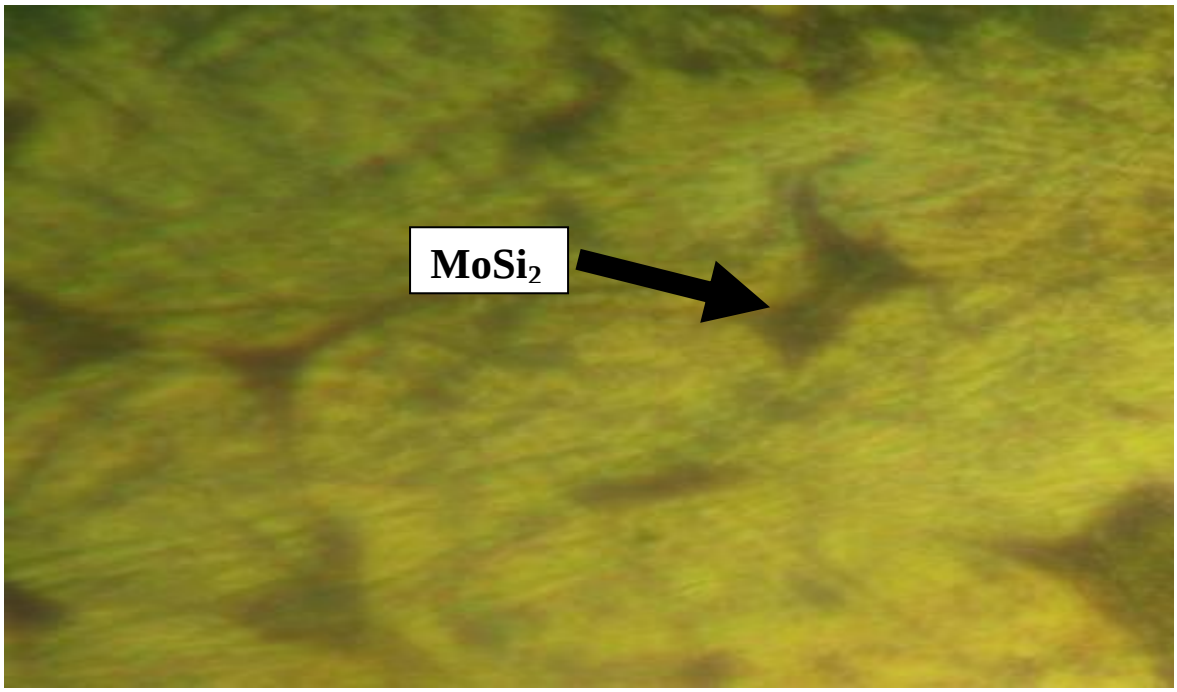

Plate 4.66: Micrograph of Cu-3wt%Si-0.5wt%Mo alloy

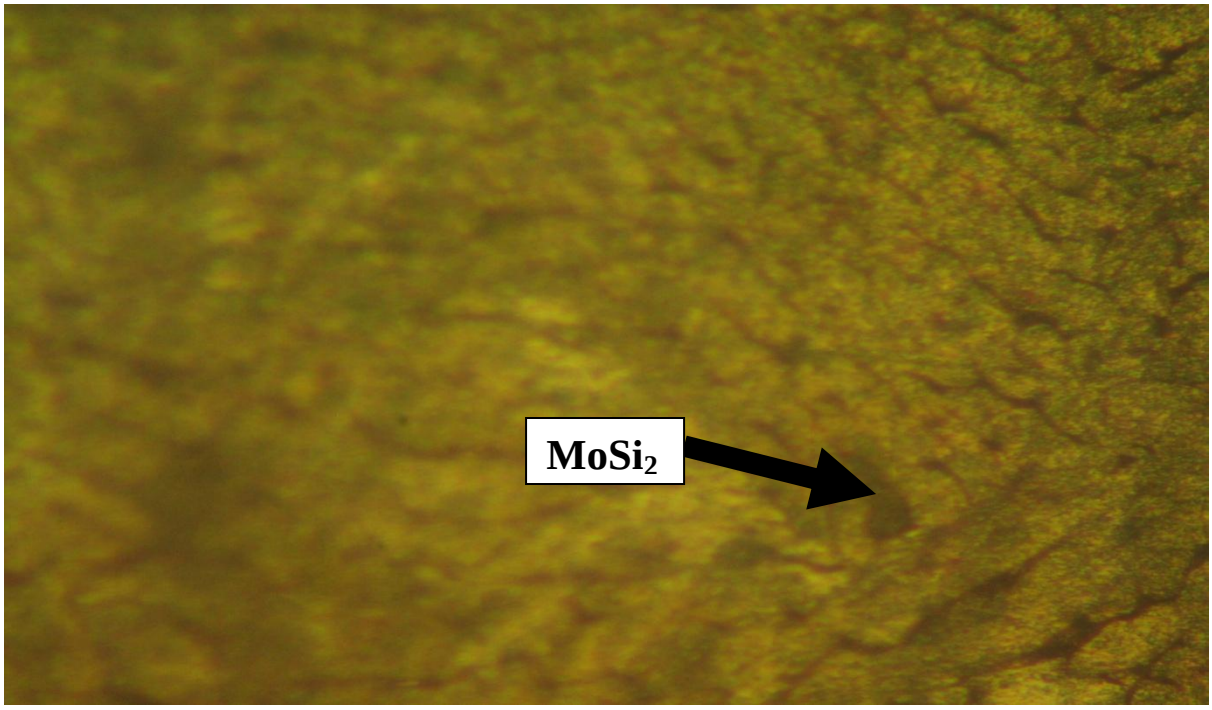

Plate 4.67: Micrograph of Cu-3wt%Si-0.7wt%Mo alloy

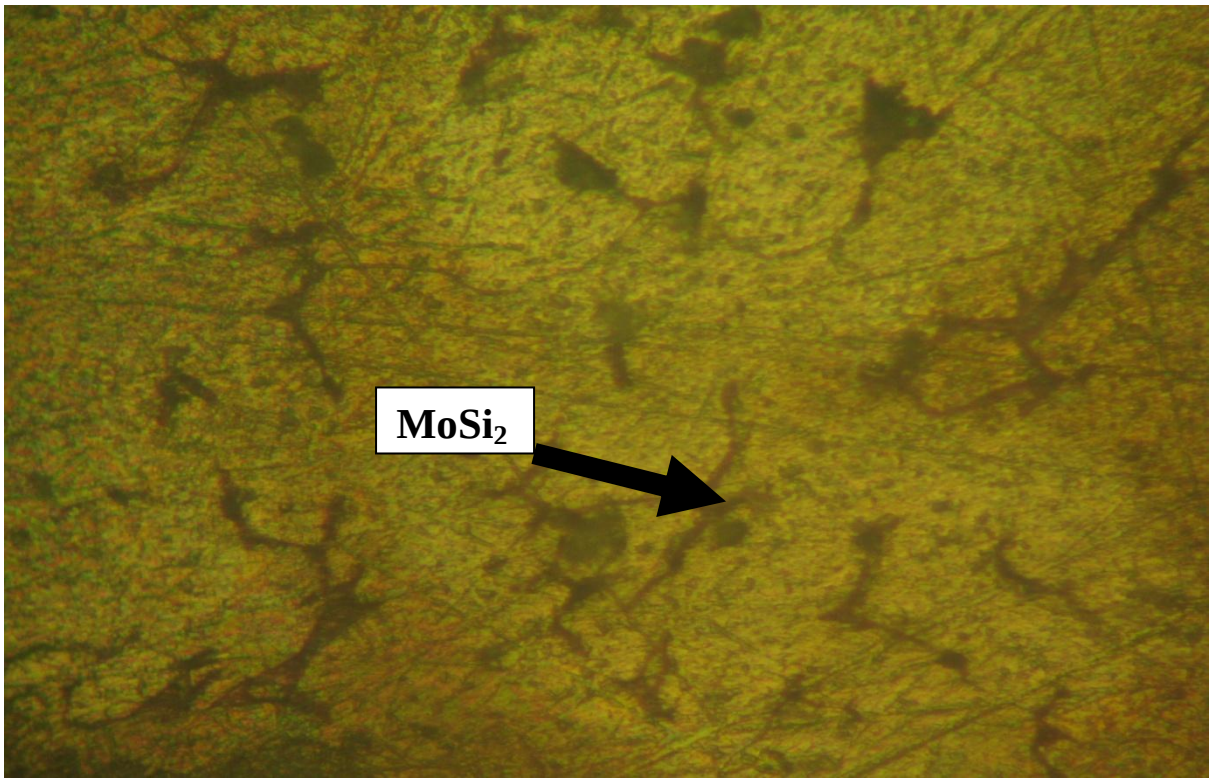

Plate 4.68: Micrograph of Cu-3wt%Si-0.8wt%Mo alloy

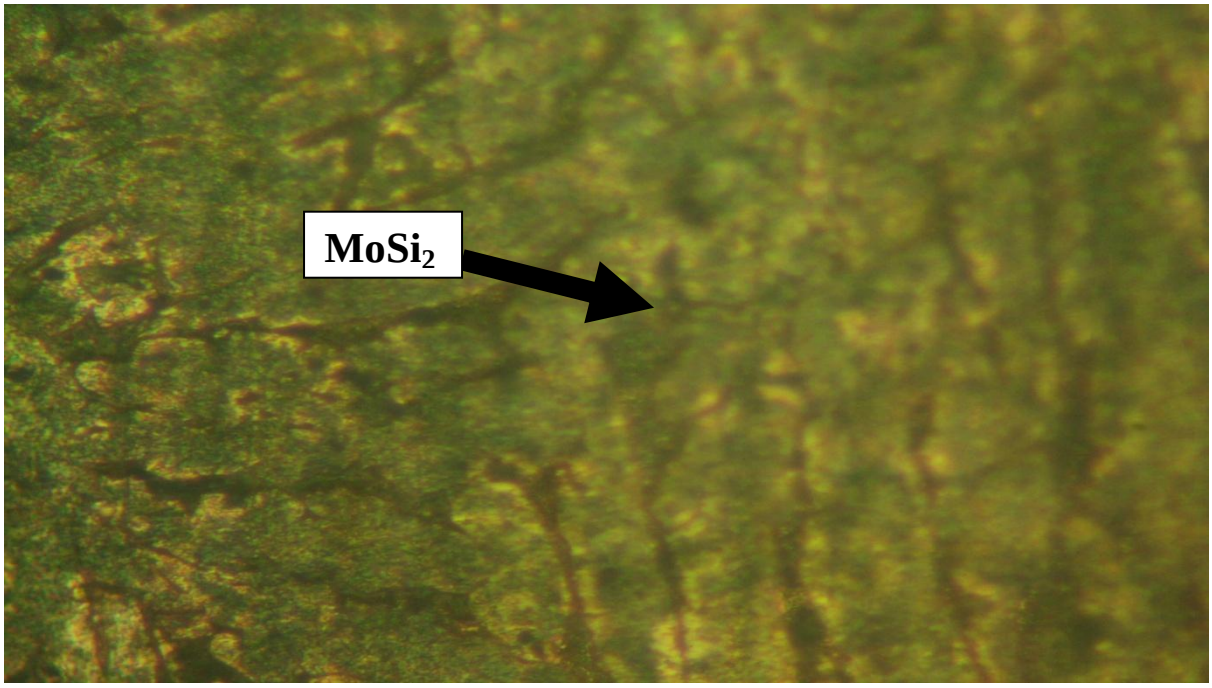

Plate 4.69: Micrograph of Cu-3wt%Si-1wt%Mo alloy

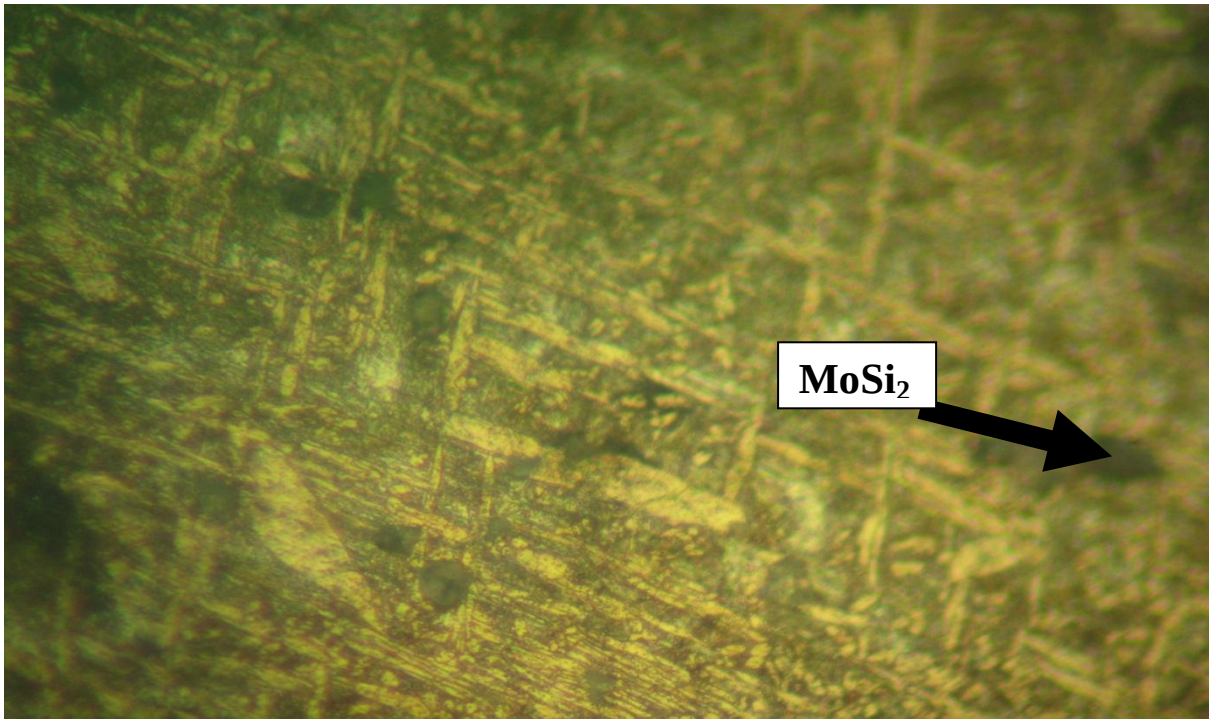

Plate 4.70: Micrograph of Cu-3wt%Si-1.5wt%Mo alloy

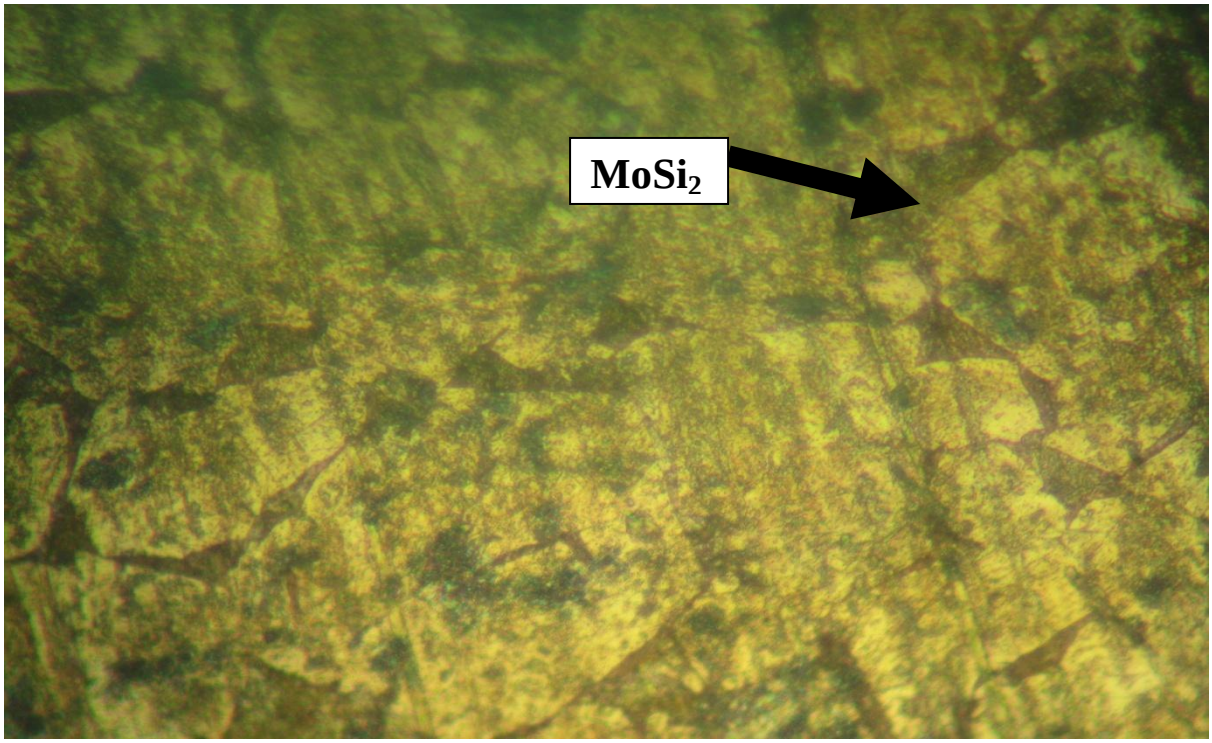

Plate 4.71: Micrograph of Cu-3wt%Si-2wt%Mo alloy

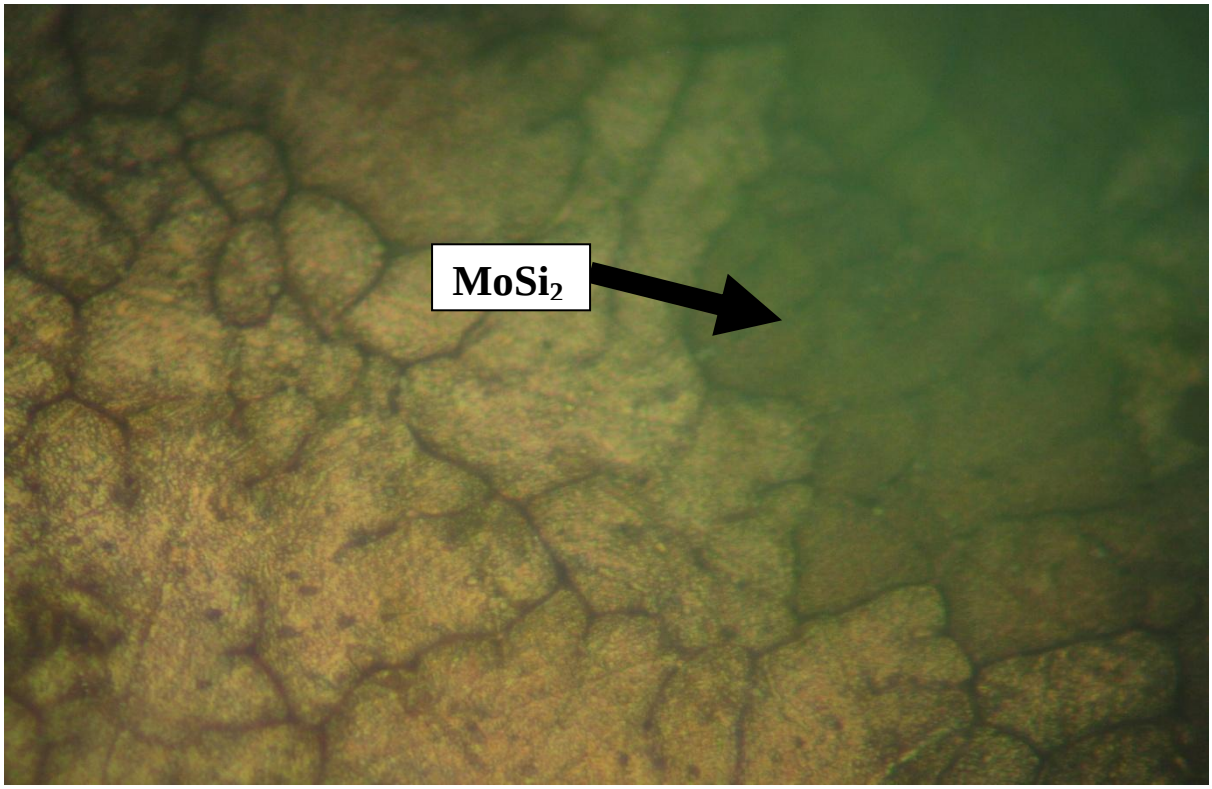

Plate 4.72: Micrograph of Cu-3wt%Si-3wt%Mo alloy

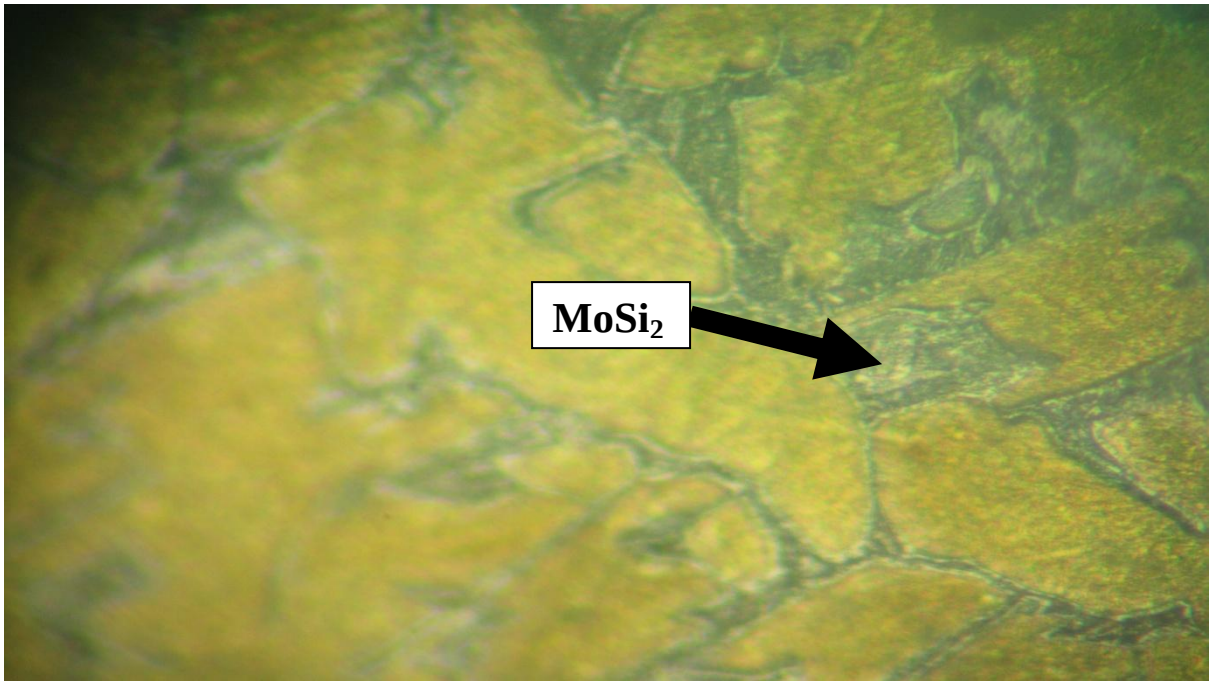

Plate 4.73: Micrograph of Cu-3wt%Si-5wt%Mo alloy

4.3.9. Effect of aluminium content on the surface morphology of silicon bronze (Cu-3wt%Si)

The microstructural analysis of silicon bronze doped with aluminium is presented in Plates 4.74-4.83. The micrographs revealed the presence α-phase (solid solubility of aluminium in copper matrix) and copper silicide (Cu_3Si) intermetallic compound. It was noted in Plates 4.74-4.83 that addition of aluminium decreased the size of the dendritic primary silicon in the copper matrix. This resulted to increase in mechanical properties of the alloy (Figures 4.8, 4.17, 4.26 and 4.34). At 5wt% aluminium addition, the ultimate tensile strength and hardness of the alloy decreased as a result of the presence of coarse intermetallic compound in the alloy structure.

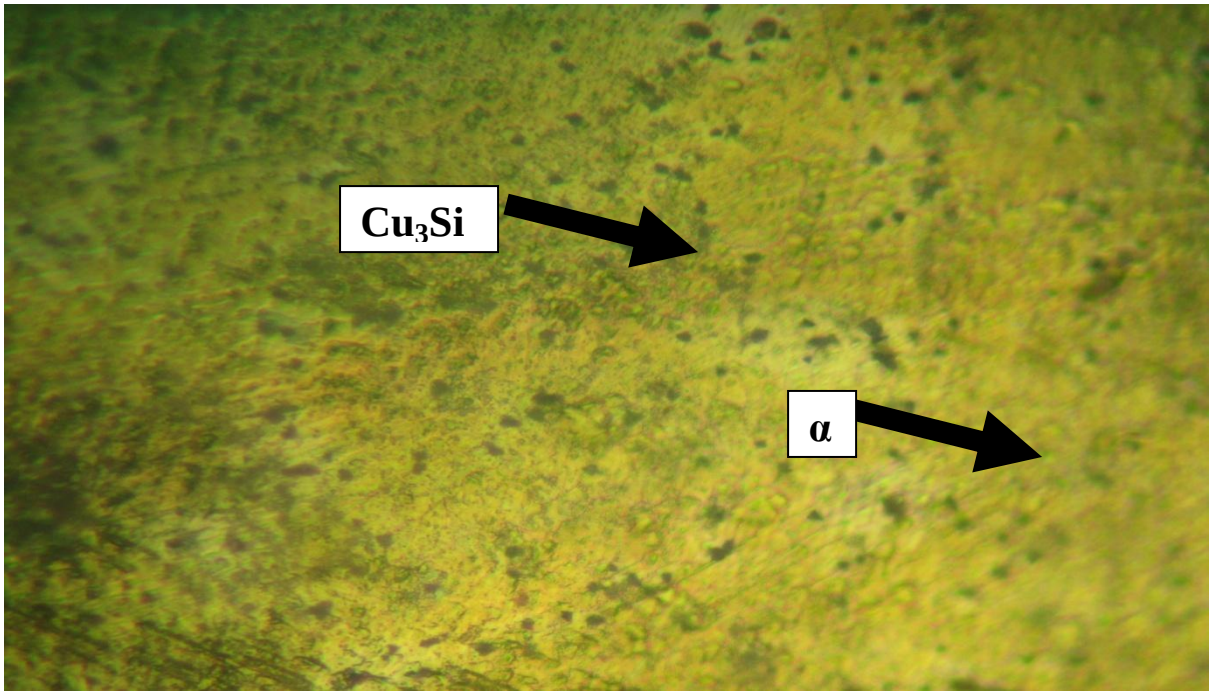

Plate 4.74: Micrograph of Cu-3wt%Si-0.1wt%Al alloy

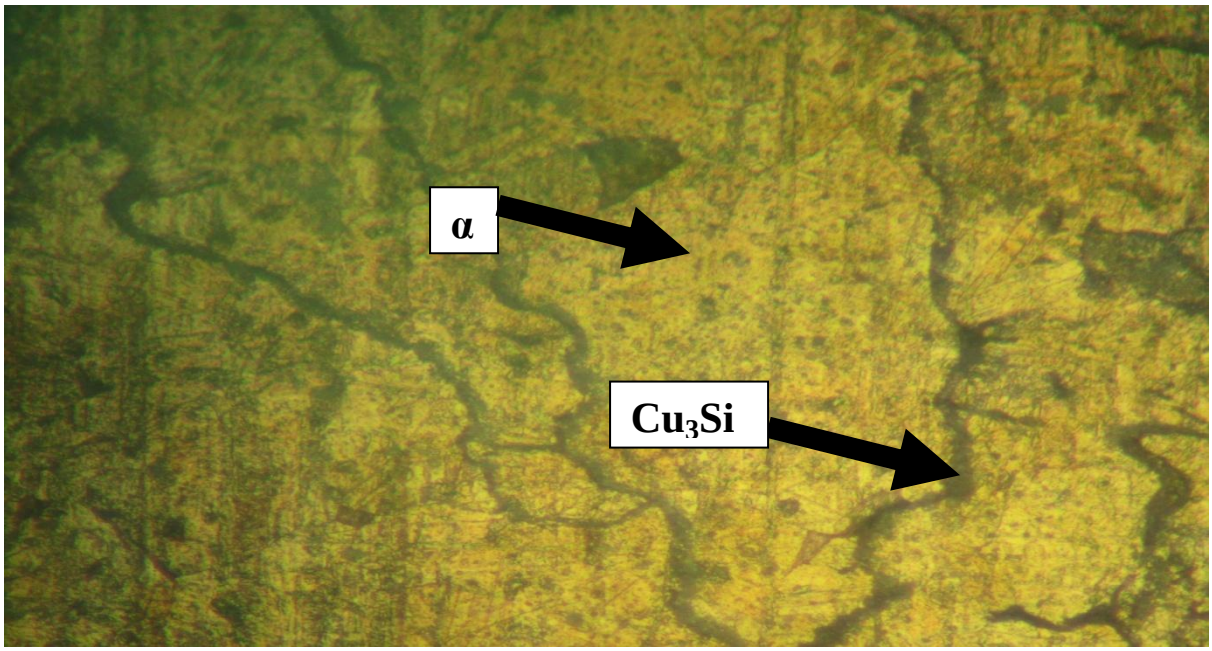

Plate 4.75: Micrograph of Cu-3wt%Si-0.3wt%Al alloy

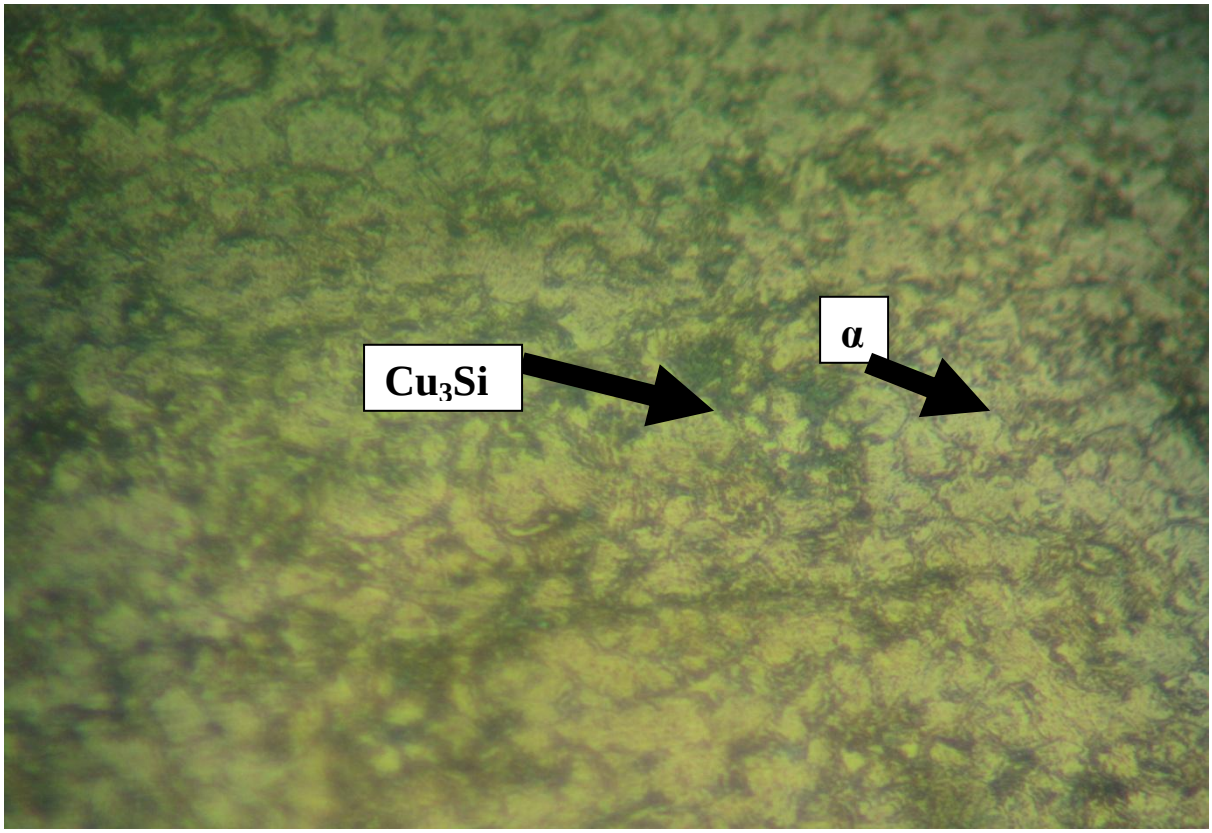

Plate 4.76: Micrograph of Cu-3wt%Si-0.5wt%Al alloy

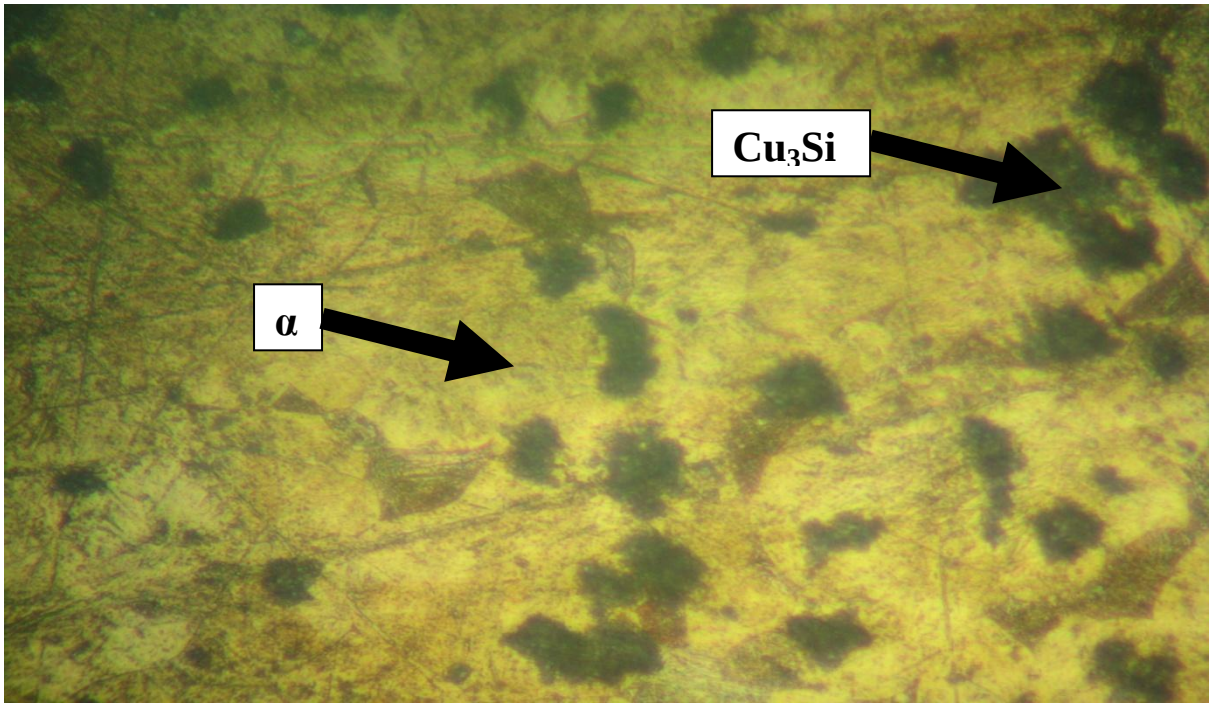

Plate 4.77: Micrograph of Cu-3wt%Si-0.7wt%Al alloy

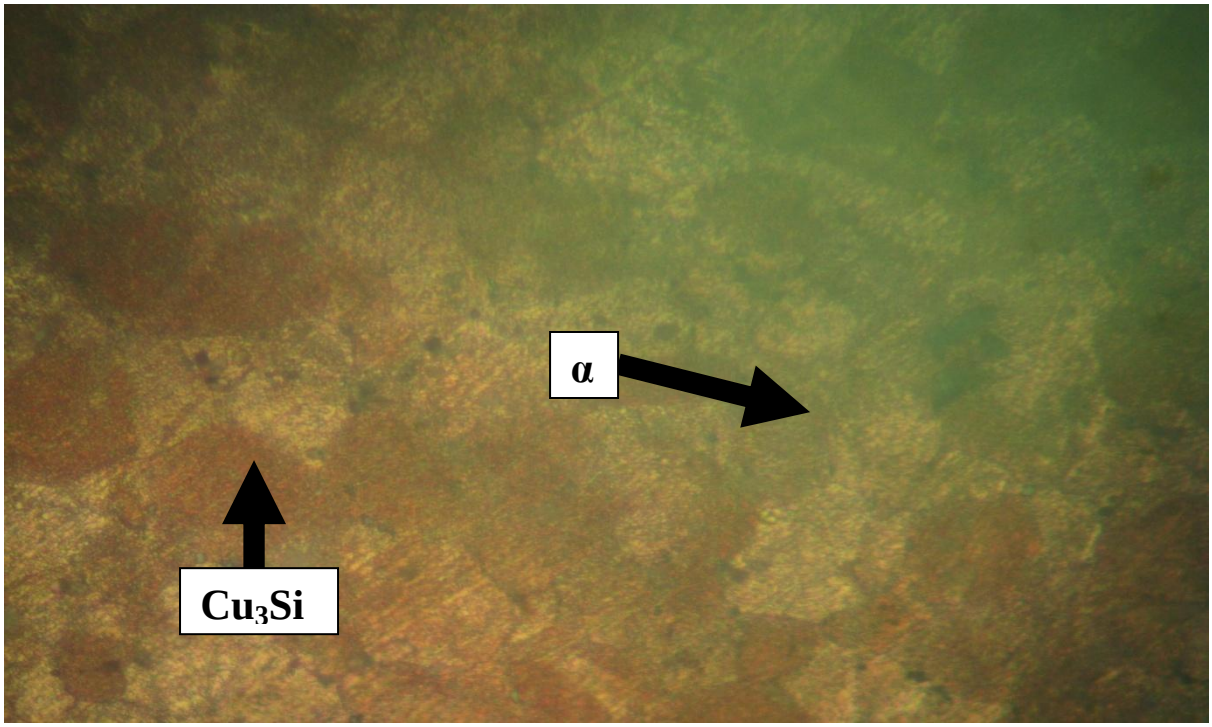

Plate 4.78: Micrograph of Cu-3wt%Si-0.8wt%Al alloy

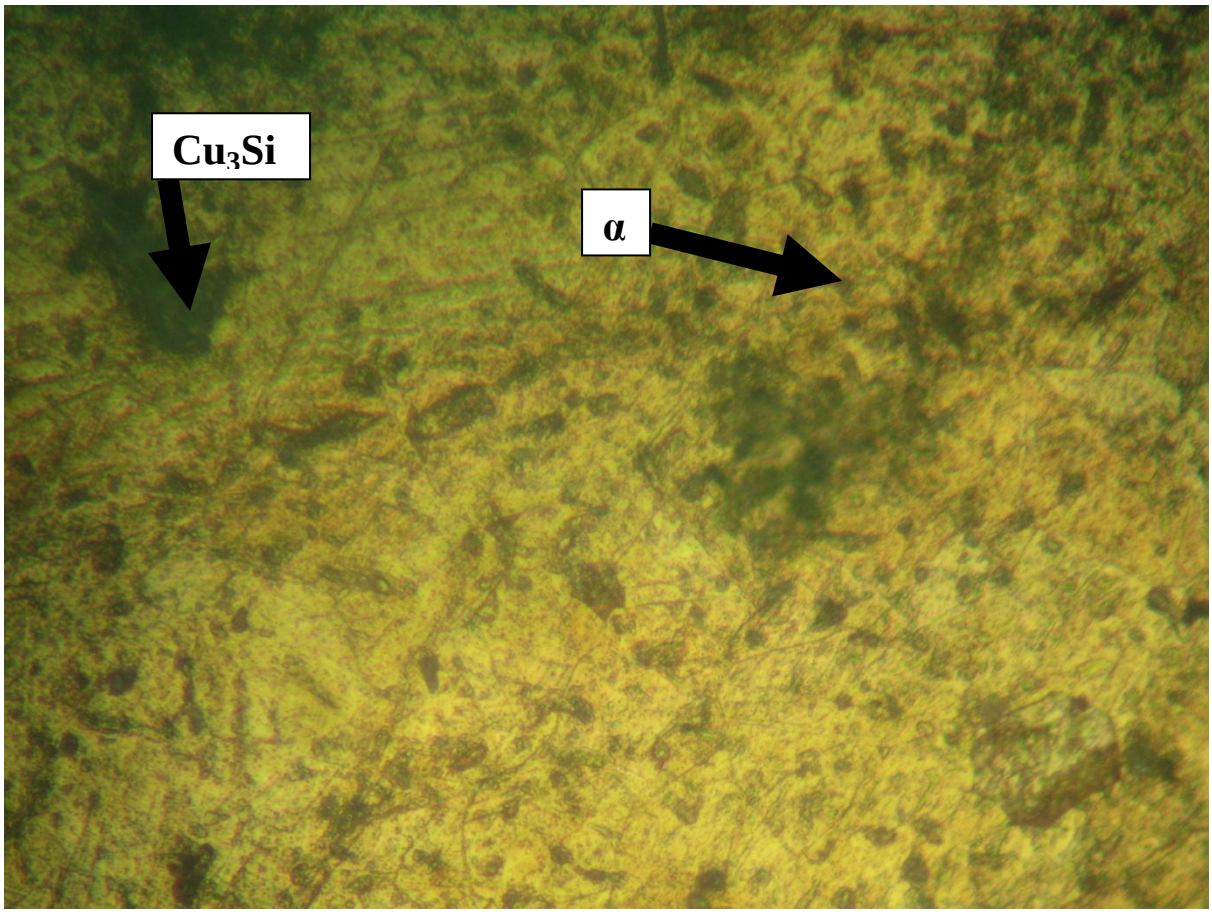

Plate 4.79: Micrograph of Cu-3wt%Si-1wt%Al alloy

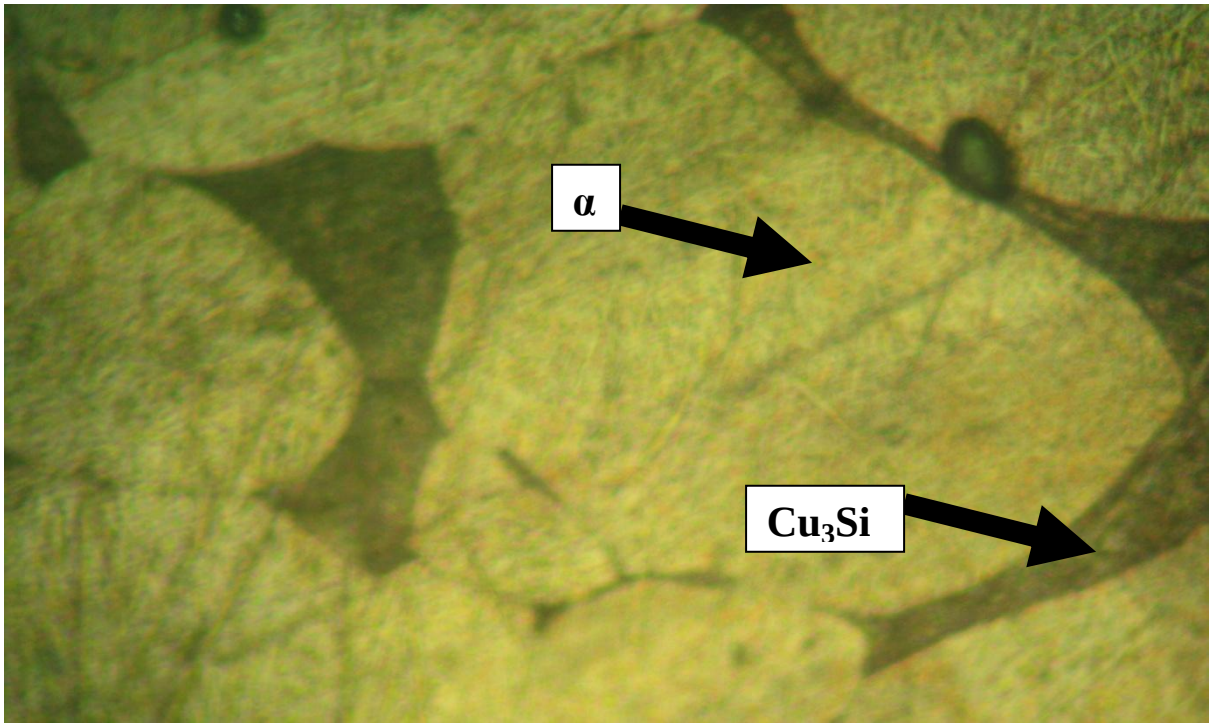

Plate 4.80: Micrograph of Cu-3wt%Si-1.5wt%Al alloy

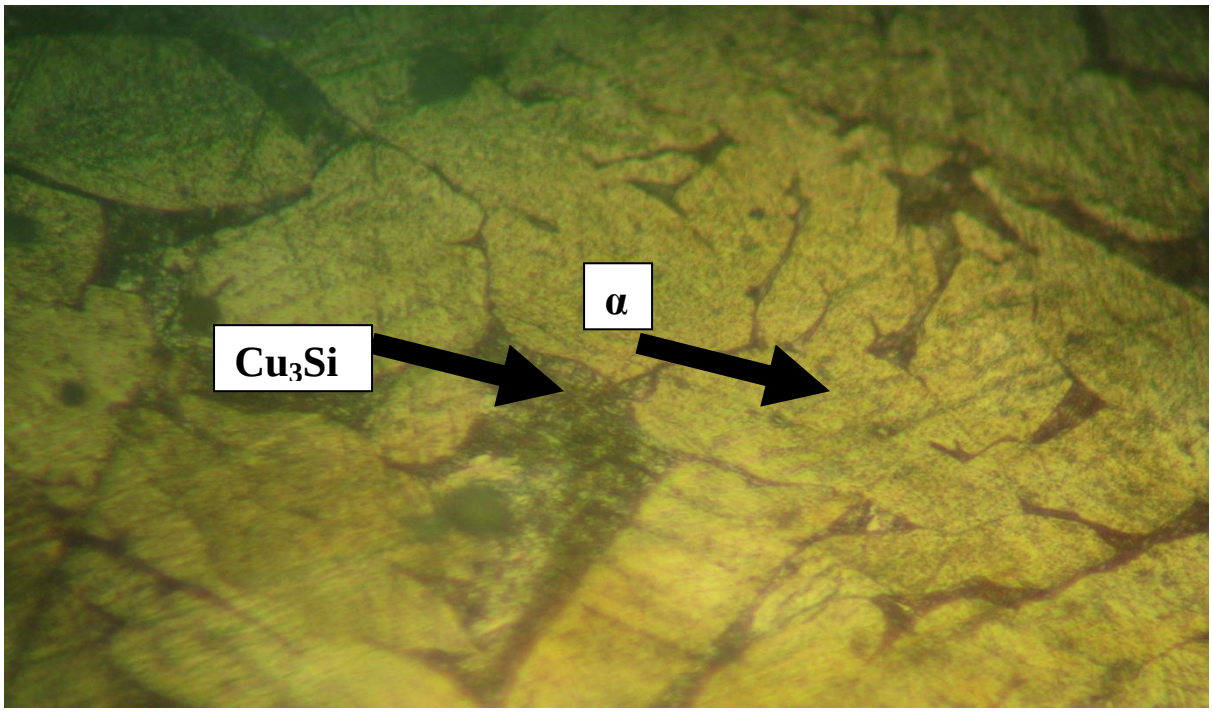

Plate 4.81: Micrograph of Cu-3wt%Si-2wt%Al alloy

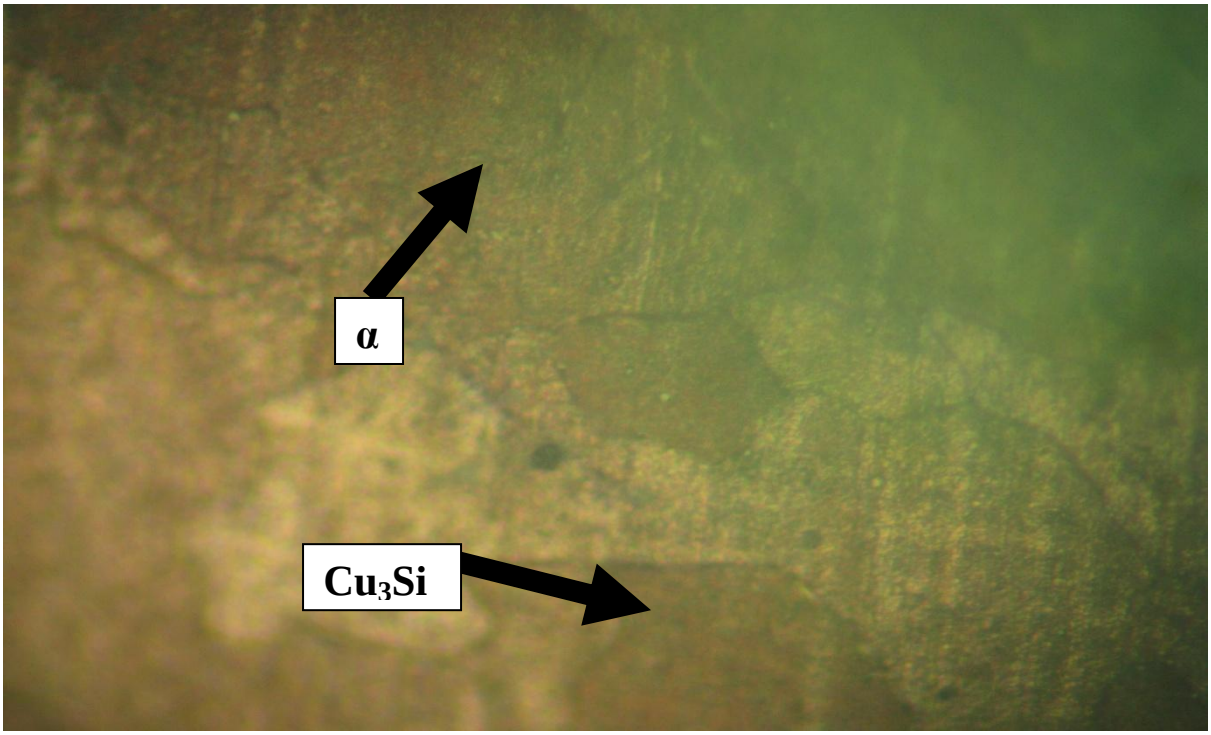

Plate 4.82: Micrograph of Cu-3wt%Si-3wt%Al alloy

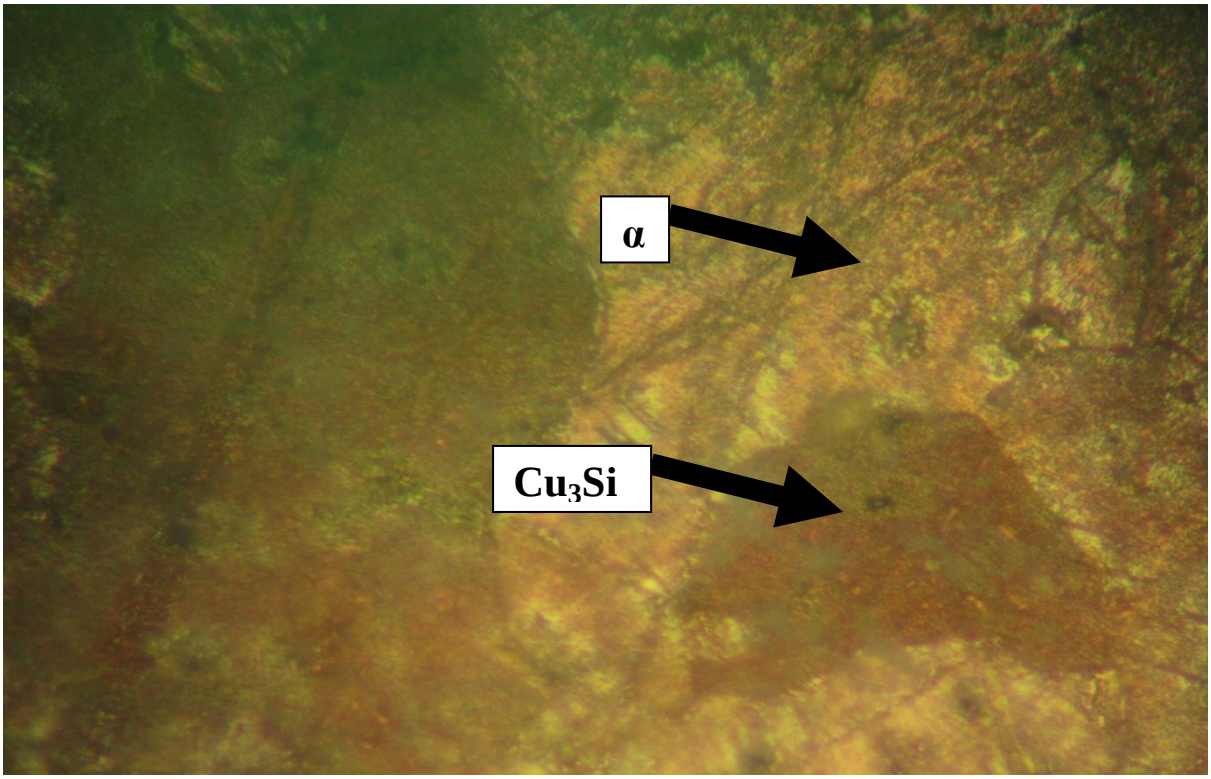

Plate 4.83: Micrograph of Cu-3wt%Si-5wt%Al alloy

4.3.10 Effect of heat treatment on the surface morphology of silicon bronzes

The analysis of the surface morphology of Cu-3wt%Si-3wt%Zn alloy subjected to solution heat treatment at temperature of 900^{o}C for 30 minutes and cooled in air is presented in Plate 4.84. The micrograph revealed the presence of fine α-β phase in the alloy structure which resulted to increase in ultimate tensile strength and hardness of the alloy with corresponding decrease in percentage elongation and impact strength compared to the non-heat treated alloy (Figures 4.39 and 4.42).

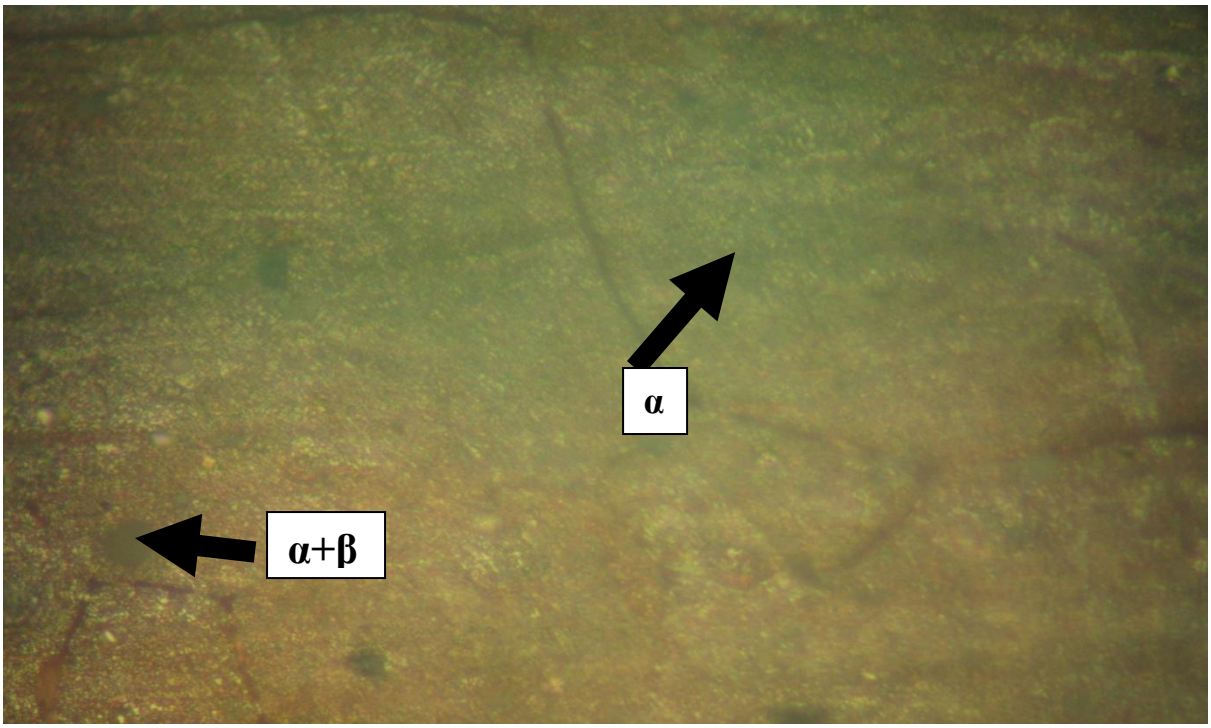

Plate 4.84: Micrograph of Cu-3wt%Si-3wt%Zn alloy solution heat treated at 900^{o}C for 30 minutes and cooled in air.

The result of the analysis of the surface morphology of Cu-3wt%Si-3wt%Sn alloy solution heat treated at 900^{o}C for 30 minutes and cooled in air is presented in Plate 4.85. The micrograph revealed the presence of plate like morphology of

large grains of intermetallic compound evenly distributed in the alloy structure (Plate 4.85). This caused decrease in ultimate tensile strength and hardness of the alloy compared to the non-heat treated sample (Figures 4.39-4.42).

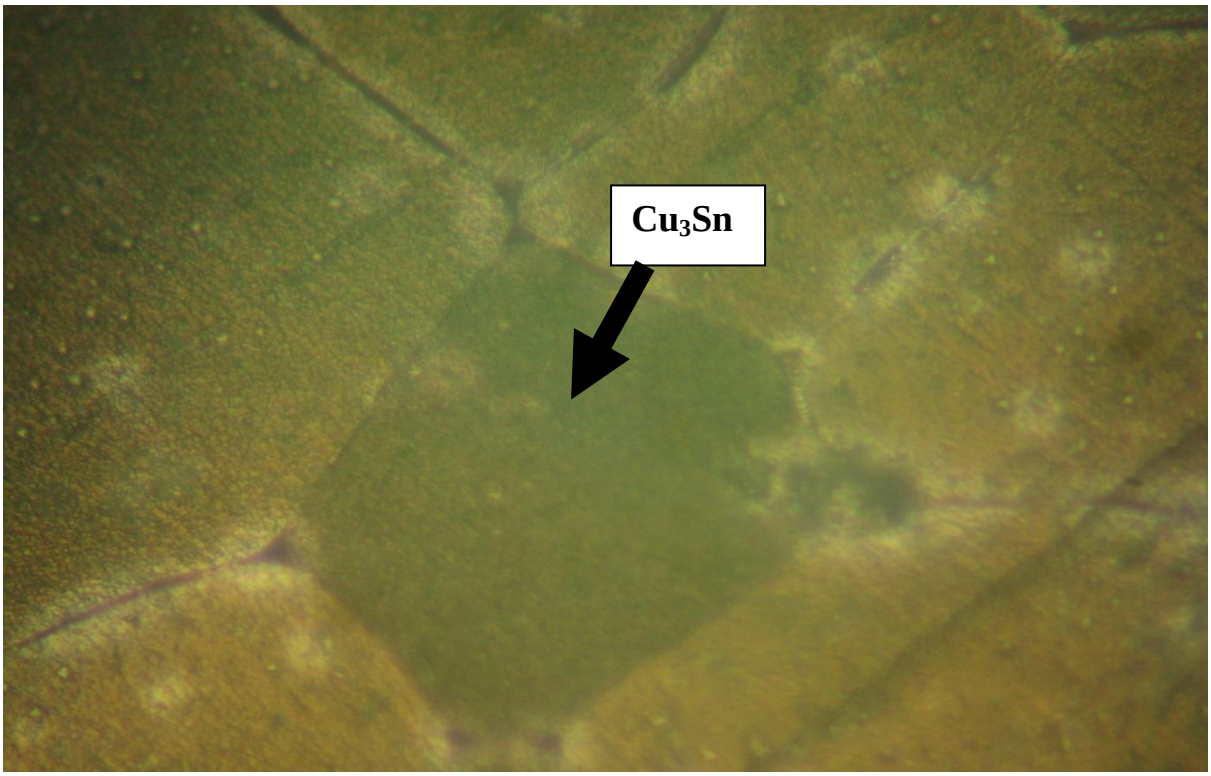

Plate 4.85: Micrograph of Cu-3wt%Si-1wt%Sn alloy solution heat treated at 900^{o}C for 30 minutes and cooled in air.

The surface morphology of heat treated Cu-3wt%Si-1wt%Mg is presented in Plate 4.86. The results of the analysis revealed the presence of fine and well distributed intermetallic compounds, Mg_2Si in the copper matrix. It was noted in Plate 4.86 that the magnesium silicide (Mg_2Si) was modified and evenly distributed in the copper matrix, thereby increased the ultimate tensile strength and hardness of the alloy with corresponding decrease in percentage elongation

and impact strength compared to the non-heat treated sample (Figures 4.39-4.42).

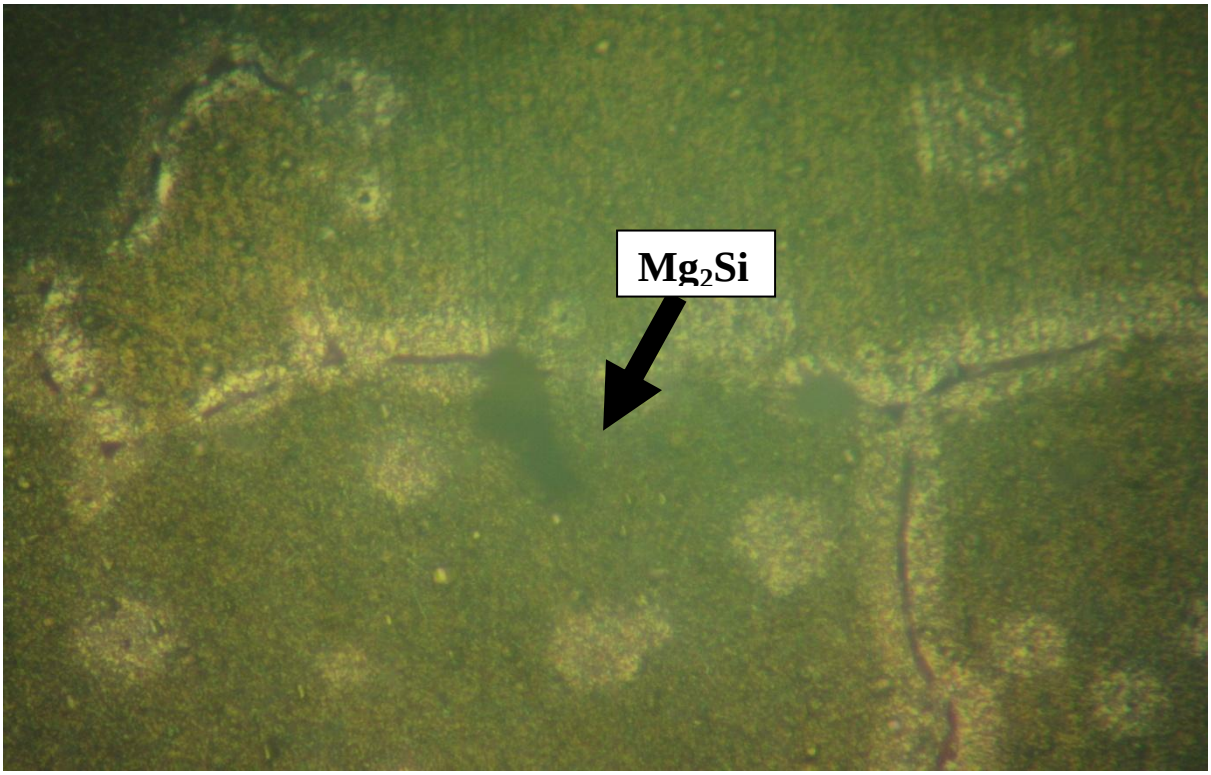

Plate 4.86: Micrograph of Cu-3wt%Si-0.8wt%Mg alloy solution heat treated at 900^{o}C for 30 minutes and cooled in air.

The surface morphology of heat treated silicon bronze doped with 1wt% manganese is presented in Plate 4.87. The micrograph revealed the presence of spherical intermetallic compound of manganese silicide (Mn_3Si) evenly distributed in the copper matrix (Plates 4.87). The coarsened intermetallic compound formed in the structure of the non-heat treated sample was refined and modified by the application of heat treatment. This resulted to increase in ultimate tensile strength and hardness of the alloy with corresponding decrease

in percentage elongation and impact strength compared to the non-heat treated sample (Figures 4.39-4.42).

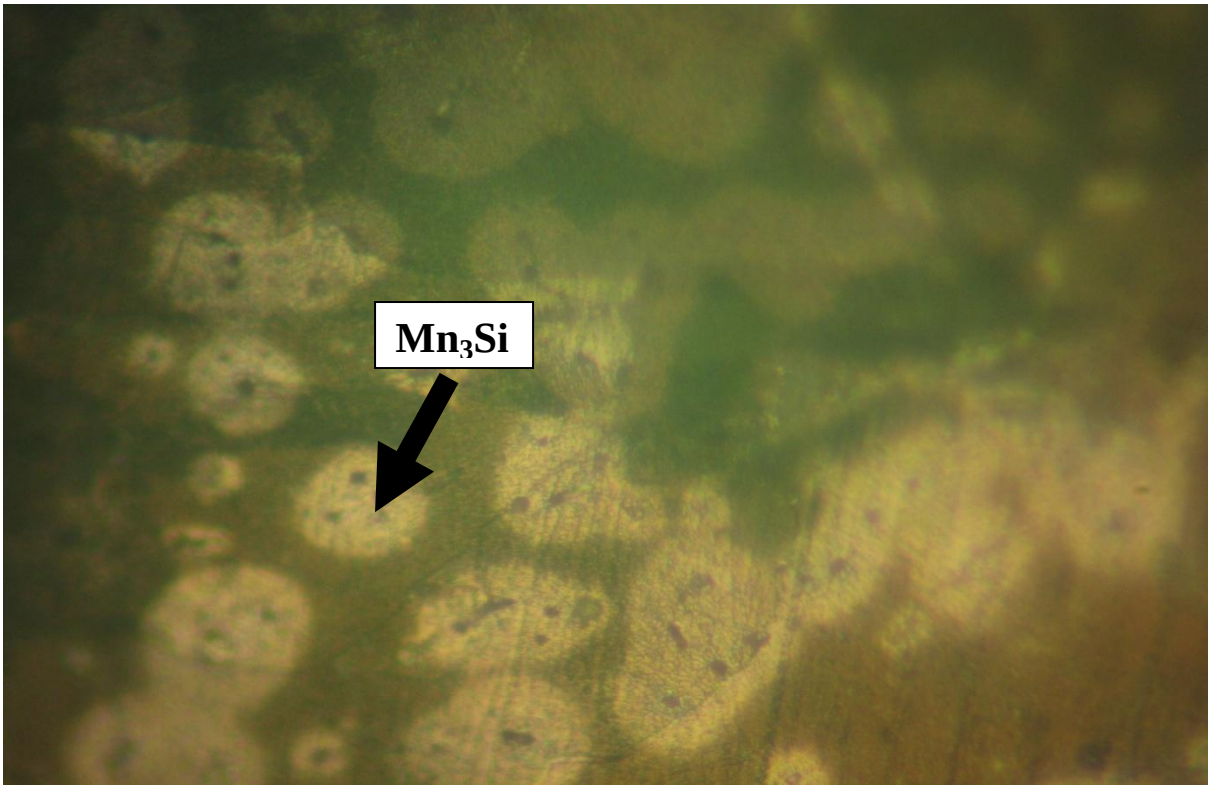

Plate 4.87: Micrograph of Cu-3wt%Si-1wt%Mn alloy solution heat treated at 900^{o}C for 30 minutes and cooled in air.

Plate 4.88 shows the optical microstructure of Cu-3wt%Si-0.8wt%W alloy subjected to solution heat treatment at temperature of 900^{o}C for 30 minutes and cooled in air. The micrograph revealed the presence of well distributed enlarged intermetallic compound (WSi_2) in the alloy structure. This resulted to increase in ultimate tensile strength and hardness of the alloy with corresponding decrease in percentage elongation and impact strength (Figures 4.39-4.42).

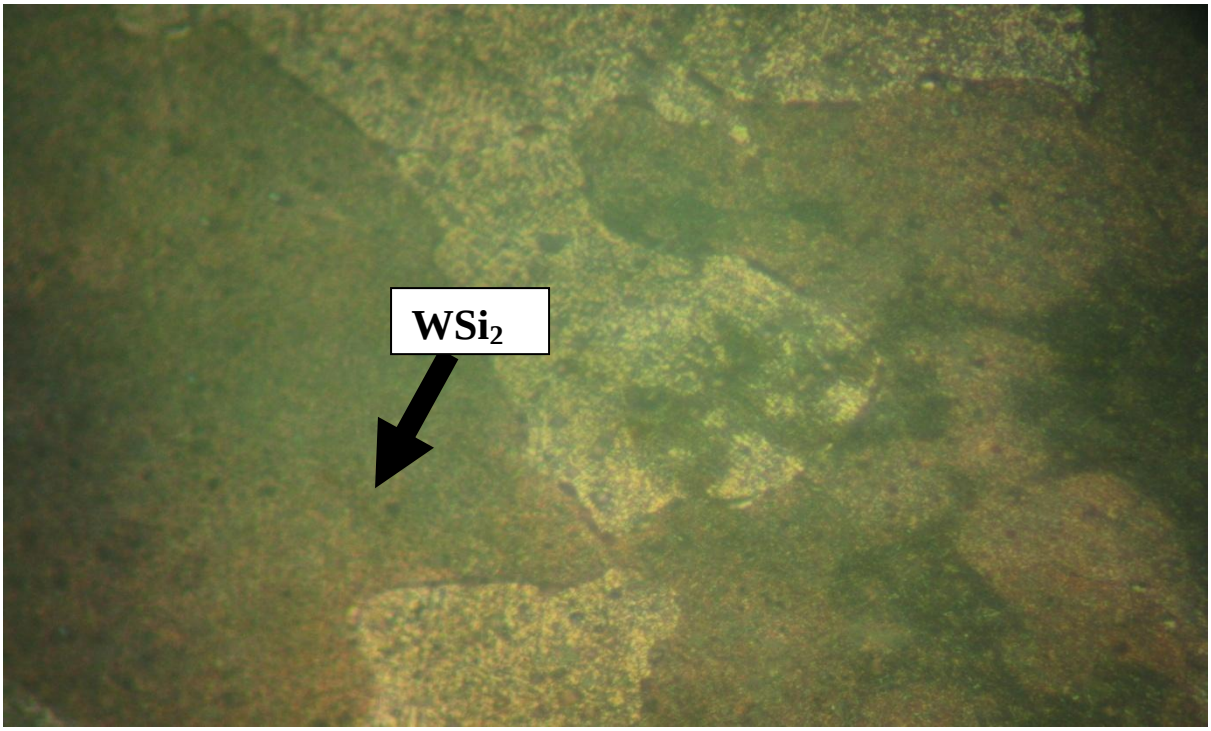

Plate 4.88: Micrograph of Cu-3wt%Si-0.8wt%W alloy solution heat treated at 900^{o}C for 30 minutes and cooled in air.

The surface morphology of Cu-3wt%Si-1wt%Ti subjected to solution heat treatment at temperature of 900^{o}C for 30 minutes and cooled in air is presented in Plate 4.89. The micrograph revealed the presence of fine Cu_4Ti precipitate, evenly distributed in the copper matrix. This resulted to increase in ultimate tensile strength and hardness with corresponding decrease in percentage elongation and impact strength of the alloy (Figure 4.39 and 4.42).

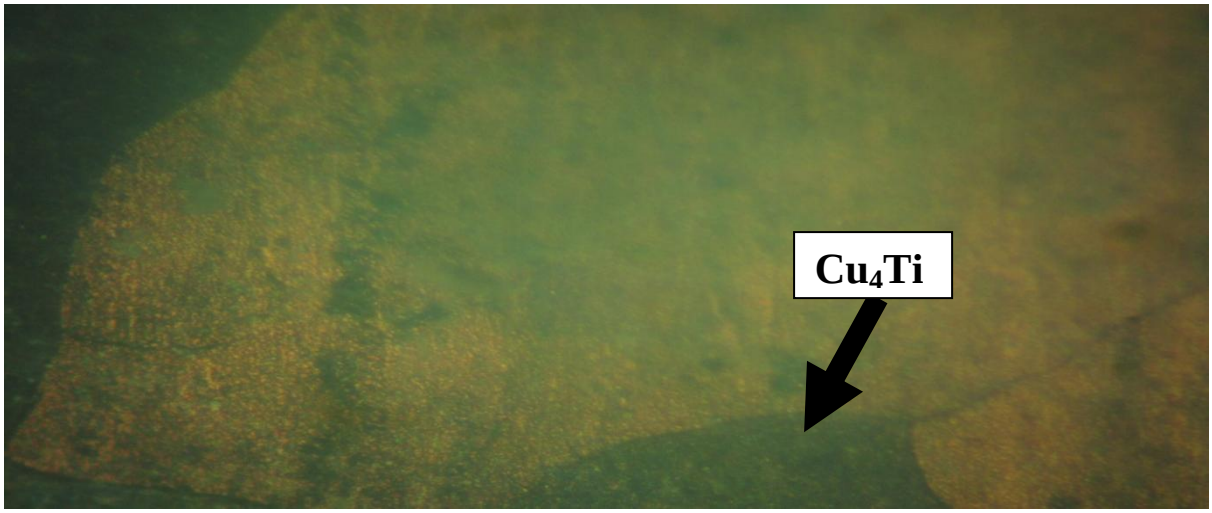

Plate 4.89: Micrograph of Cu-3wt%Si-2wt%Ti alloy solution heat treated at 900^{o}C for 30 minutes and cooled in air.

The microstructure of heat treated Cu-3wt%Si-1.5wt%Mo alloy is presented in Plate 4.90. The micrographs revealed presence of well distributed intermetallic compound, $MoSi_2$ in the copper matrix (Plate 4.90). This resulted to an increase in ultimate tensile strength and hardness values of the alloy compared to the un-heat treated sample (Figure 4.40 and 4.41).

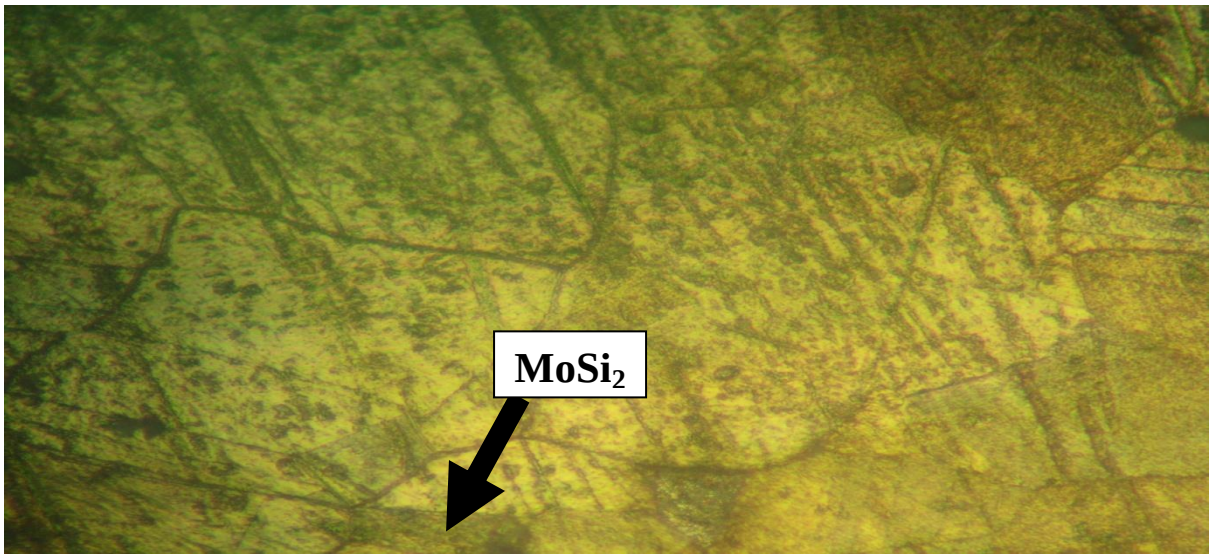

Plate 4.90: Micrograph of Cu-3wt%Si-1.5wt%Mo alloy solution heat treated at 900^{o}C for 30 minutes and cooled in air.

Plate 4.91 shows the surface morphology of Cu-3wt%Si-3wt%Al solution heat treatment at temperature of 900^{o}C for 30 minutes and cooled in air. The micrograph revealed the presence of fine grains evenly distributed in the copper matrix. This change in microstructure predominantly improved the ultimate tensile strength and hardness of the alloy compared to the un-heat treated alloy as evidenced in (Figures 4.40 and 4.41).

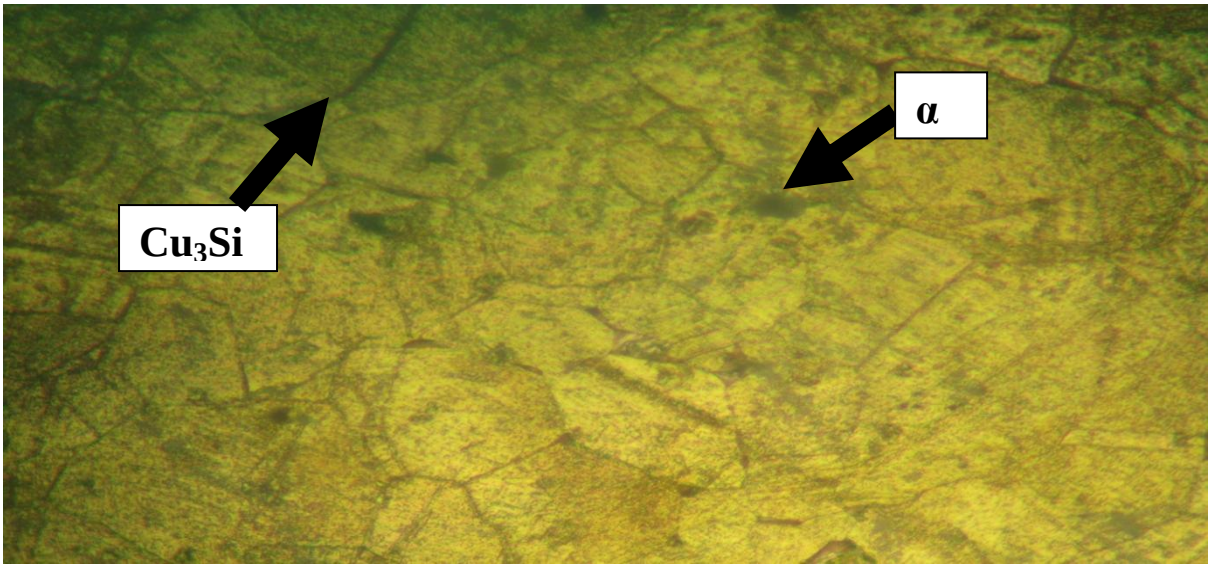

Plate 4.91: Micrograph of Cu-3wt%Si-3wt%Al alloy solution heat treated at 900^{o}C for 30 minutes and cooled in air.

4.4 Scanning electron microscopy and energy dispersive spectroscopy of the developed alloys

Scanning electron microscopy analysis of silicon bronze (Cu-3%wt.Si) is presented in Plate 4.92. The micrograph consisted of dendritic primary silicon and copper silicide (Cu_3Si). The energy dispersive spectroscopy analysis of the control specimen is presented in Figure 4.58. Figure 4.58 indicated the presence of eight major elements such as Cu, Si, Al, Fe, K, Ca, C and O etc.

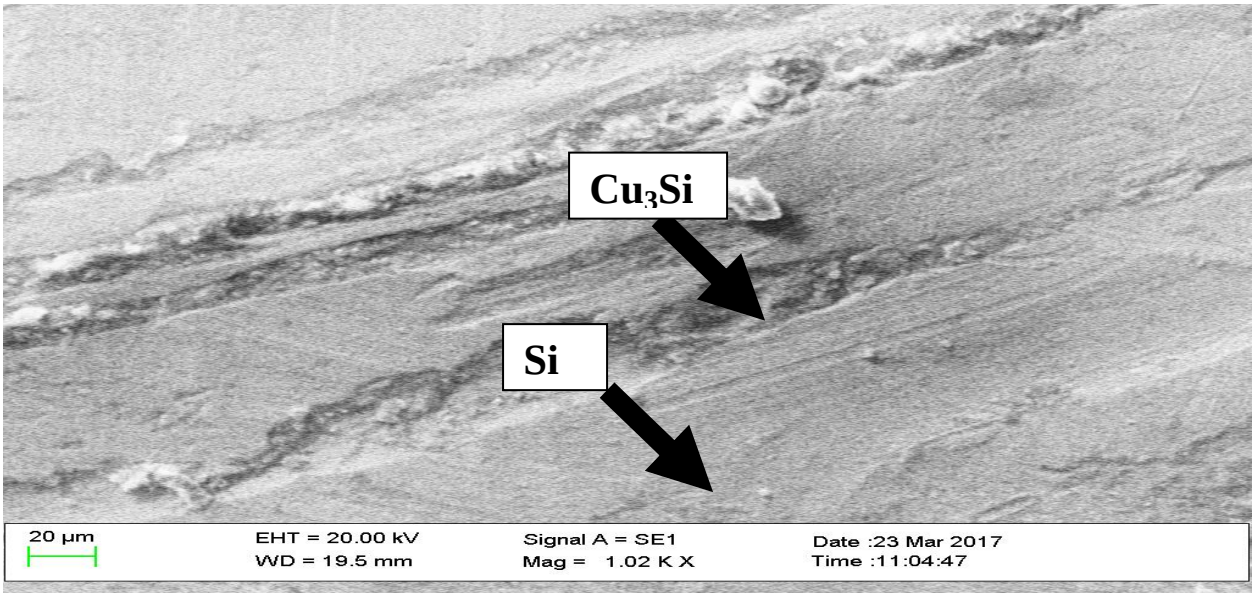

Plate 4.92: Scanning electron microscopy of Cu-3wt%Si alloy (Control)

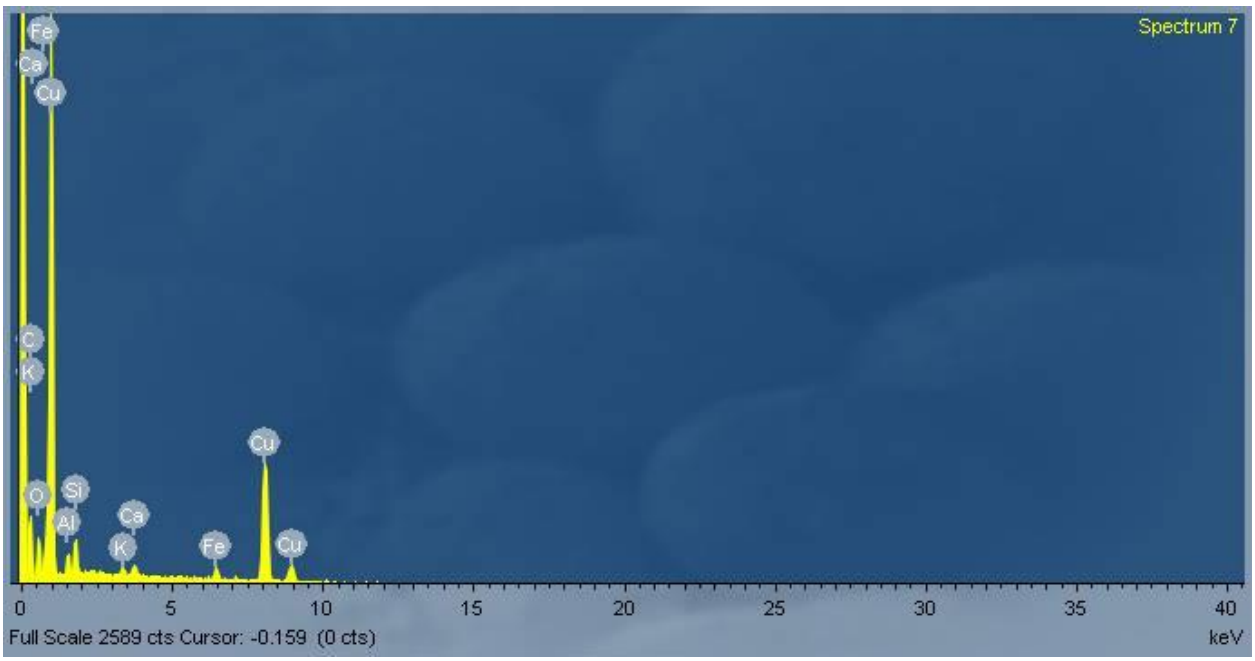

Figure 4.58: EDS spectrum of Cu-3wt%Si alloy (Control)

The scanning electron microscopy (SEM) and energy dispersive spectroscopy analyses of silicon bronze doped with zinc are presented in Plate 4.93 and Figure 4.59 respectively. The micrograph revealed the presence of α-phase (solid solution of zinc and silicon in copper matrix) and copper silicide (Cu_3Si) intermetallic phase (Plate 4.93). It was also indicated in Plate 4.93 that addition

of zinc decreased the size of the dendritic primary silicon and hence increased the ductility of the alloy. Plate 4.93 showed that addition of zinc modified the intermetallic compound formed in the alloy structure. These resulted to increased ductility, ultimate tensile strength and impact strength of the alloy (Figure 4.9, 4.18 and 4.35). The presence of Cu, Si, Zn, Al, Fe, C, Cl, Ca and O were revealed in Figure 4.59.

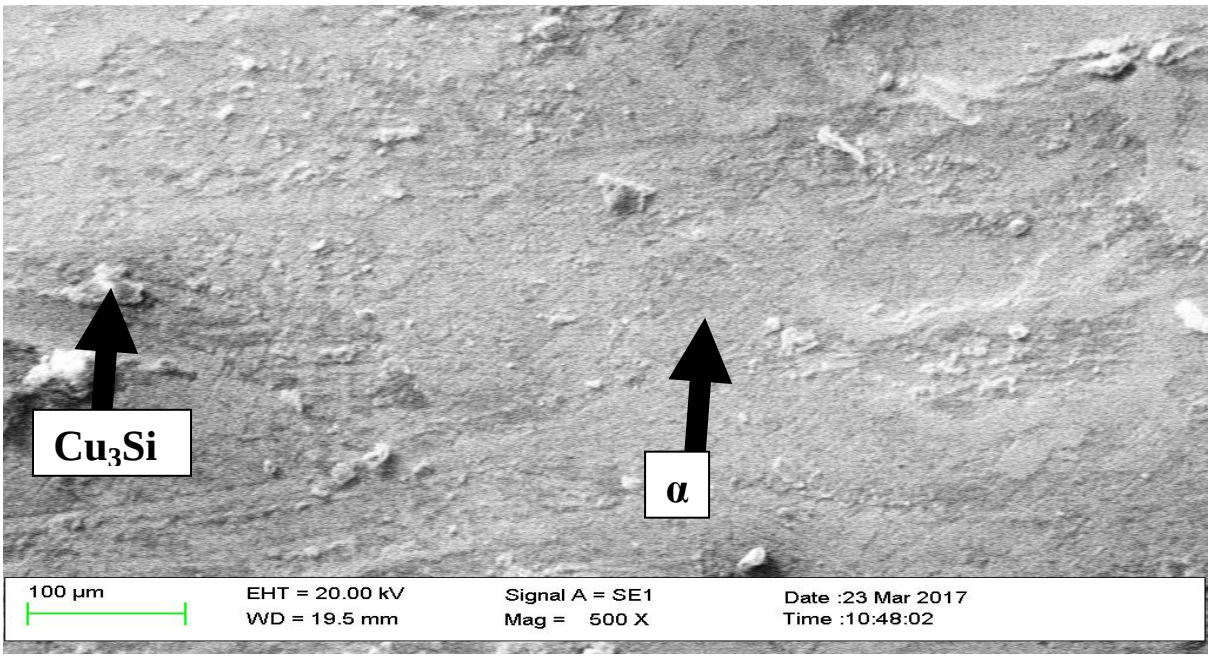

Plate 4.93: Scanning electron microscopy of Cu-3wt%Si-3wt%Zn alloy

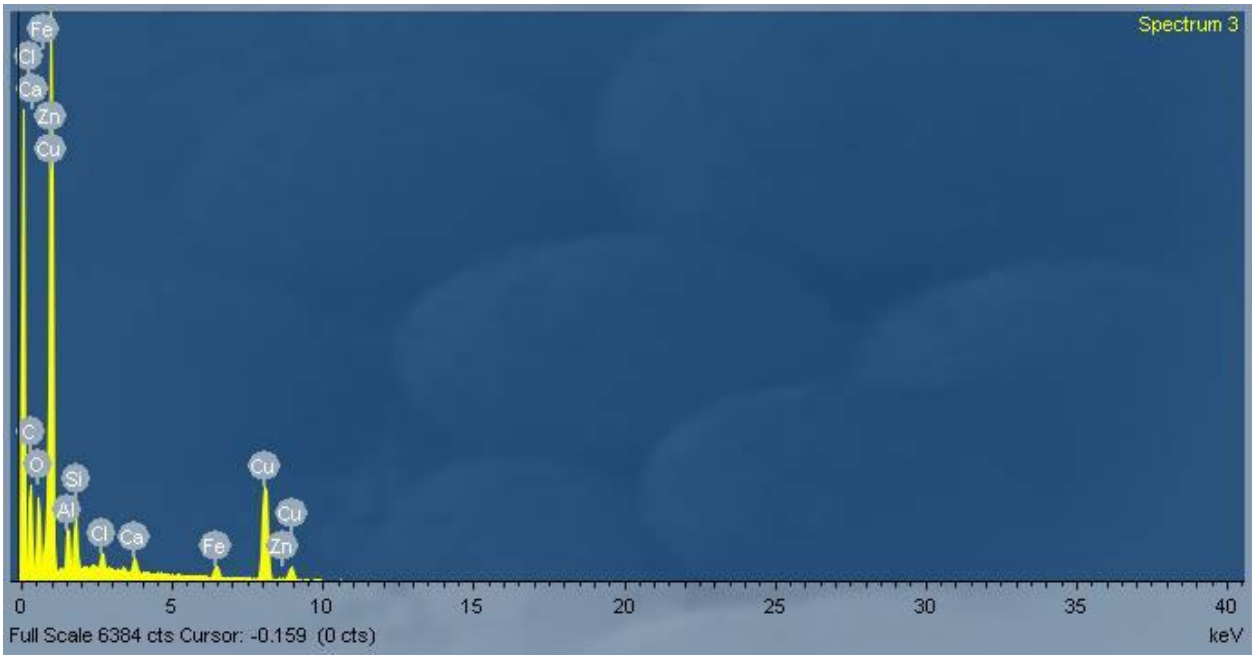

Figure 4.59: EDS spectrum of Cu-3wt%Si-3wt%Zn alloy

Plate 4.94 and Figure 4.60 show the scanning electron microscopy and energy dispersive spectroscopy analyses of silicon bronze doped with tin. The micrographs indicated the presence of Cu_3Si and Cu_3Sn intermetallic phases (Plates 4.94). It was evidenced in Plate 4.94 that the morphology of the phases was modified by addition of tin. Figure 4.60 indicated the presence of Cu, Si, Sn, Al, Fe, Cl, O and C etc.

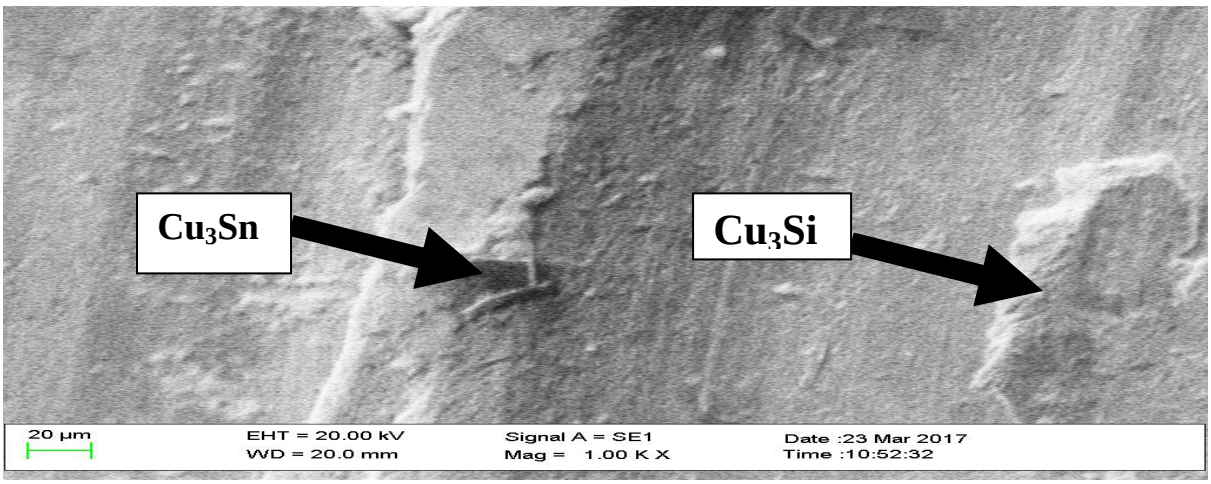

Plate 4.94: Scanning electron microscopy of Cu-3wt%Si-3wt%Sn alloy

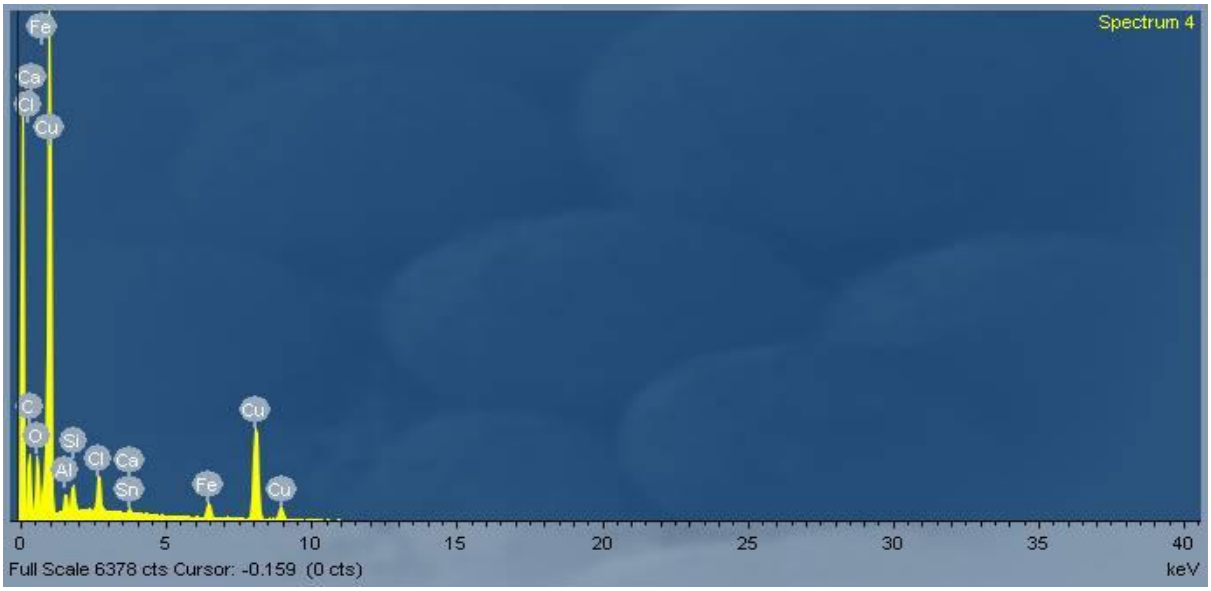

Figure 4.60: EDS spectrum of Cu-3wt%Si-3wt%Sn alloy

The scanning electron microscopy and energy dispersive spectroscopy analyses of silicon bronze doped with magnesium are presented in Plate 4.95 and Figure 4.61. The micrograph revealed the presence of copper silicide (Cu_3Si) and magnesium silicide (Mg_2Si) intermetallic phases in the alloy structure. Plate 4.95 showed that addition of magnesium refined and modified the dendritic primary silicon and intermetallic compound (Cu_3Si) respectively, thereby resulting to an increased percentage elongation, ultimate tensile strength, hardness and impact strength of silicon bronze (Figures 4.8, 4.18, 4.26 and 4.34). Analysis of Figure 4.61 indicated the presence of nine major elements such as Cu, Si, Mg, Al, Fe, Cl, C, O and Ca.

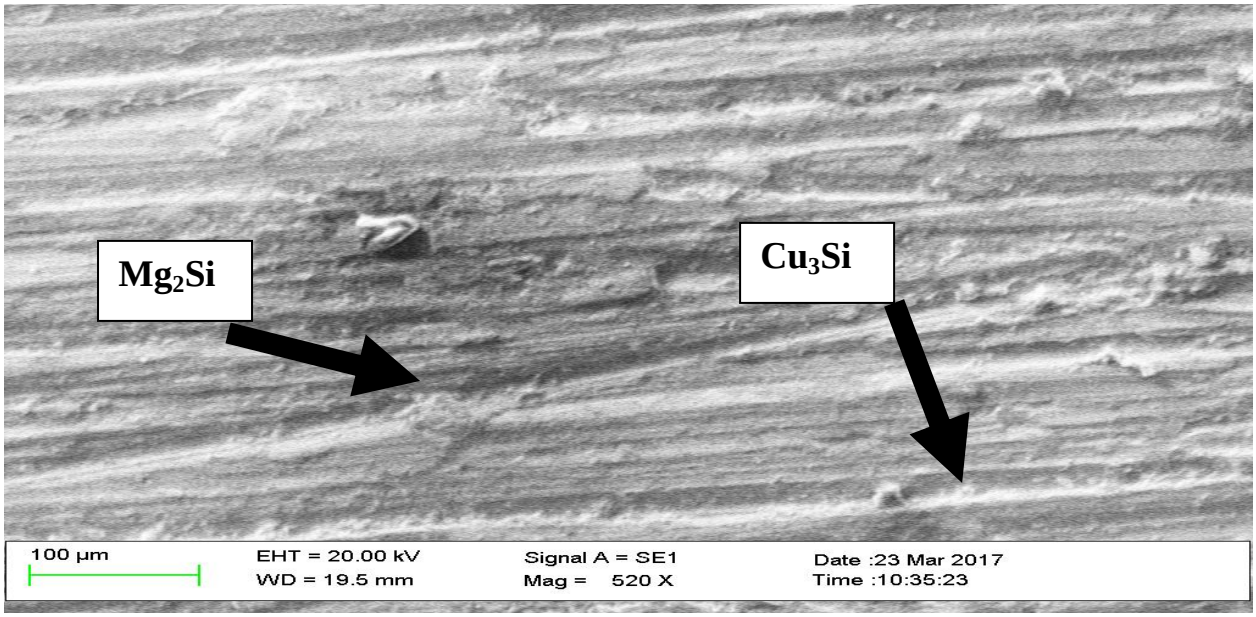

Plate 4.95: Scanning electron microscopy of Cu-3wt%Si-0.8wt%Mg alloy

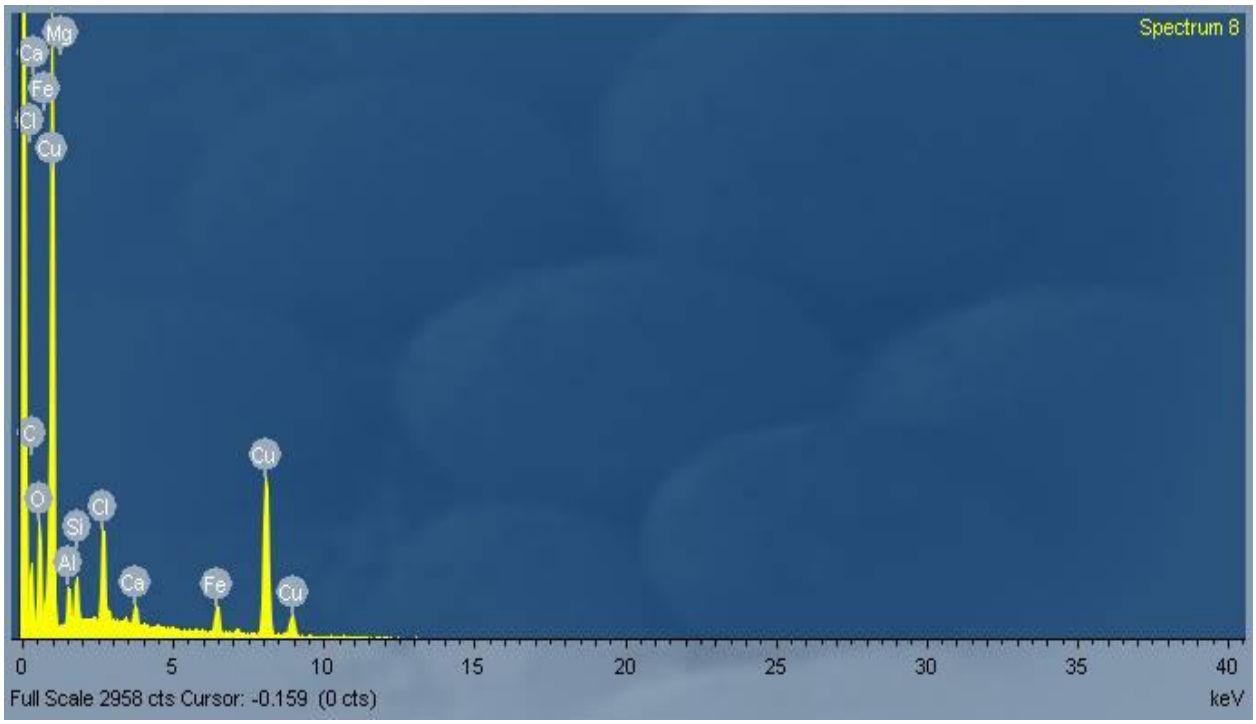

Figure 4.61: EDS spectrum of Cu-3wt%Si-0.8wt%Mg alloy

The scanning electron microscopy and energy dispersive spectroscopy analyses of silicon bronze doped with manganese are presented in Plate 4.96 and Figure 4.62 respectively. Plate 4.96 indicated the presence of three major intermetallic phases in the alloy structure. These phases include the γ-phase (solid solubility of manganese in copper matrix), manganese silicide (Mn_3Si) and Cu_3Si

precipitate. The dendritic primary silicon was refined and modified by the addition of manganese and hence increased the ultimate tensile strength and hardness of the studied alloy (Figures 4.17 and 4.26). The presence of Cu, Si, Mn, Al, Fe, O, Cl, Ca and C elements were indicated in Figure 4.62.

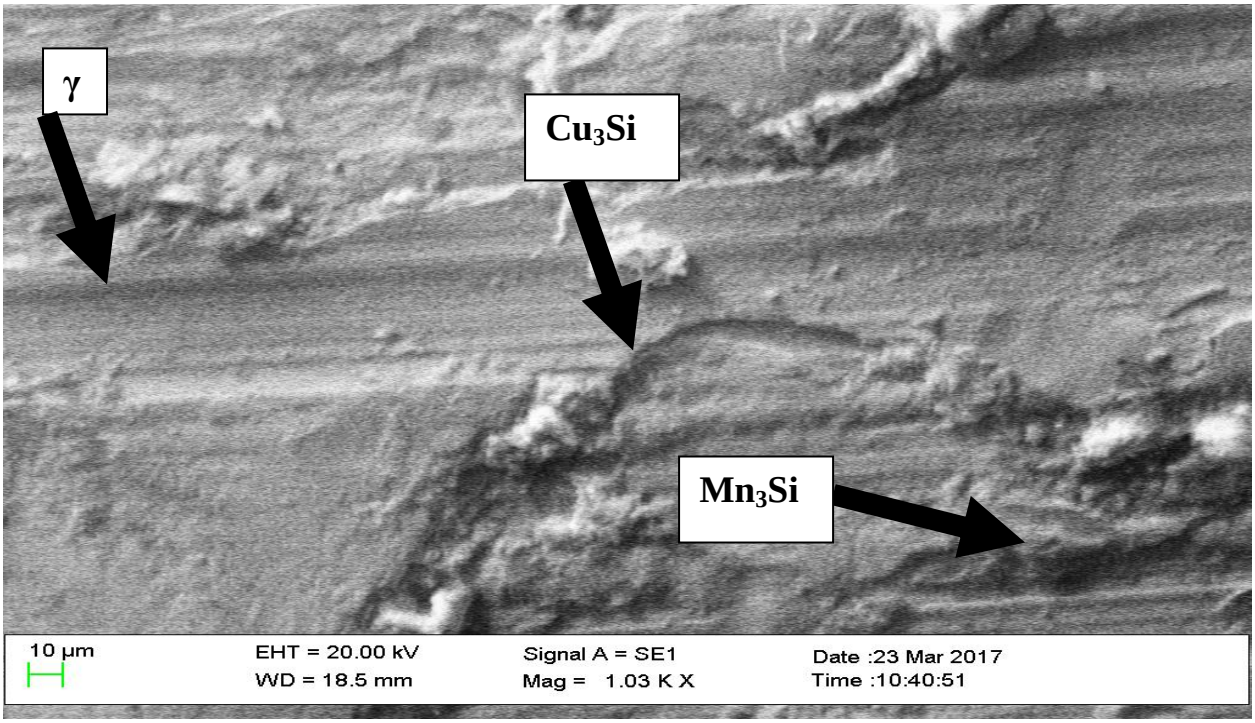

Plate 4.96: Scanning electron microscopy of Cu-3wt%Si-1wt%Mn alloy

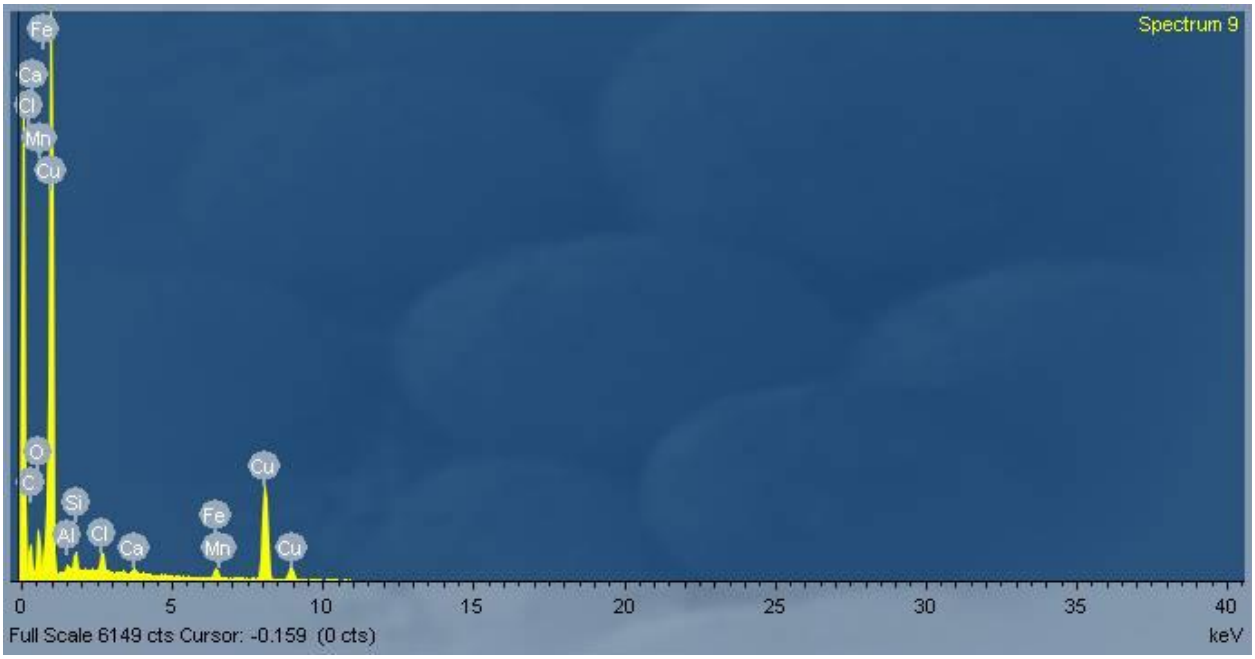

Figure 4.62: EDS spectrum of Cu-3wt%Si-1wt%Mn alloy

A detailed analysis of the scanning electron microscopy and energy dispersive spectroscopy analyses of Cu-3%wt.Si-1%wt.W alloy are presented in Plate 4.97 and Figure 4.63 respectively. The micrographs revealed the presence of Cu_3Si and WSi_2 intermetallic phases. Analysis of Plate 4.97 reveals the presence of evenly distributed WSi_2 precipitate in the copper matrix. It was evidence in Plate 4.97 that the Cu_3Si precipitate was scarcely distributed and surrounded by the WSi_2 precipitate in the copper matrix. Figure 4.63 revealed the presence of Cu, Si, W, Al, Fe, O, Cl and C elements etc.

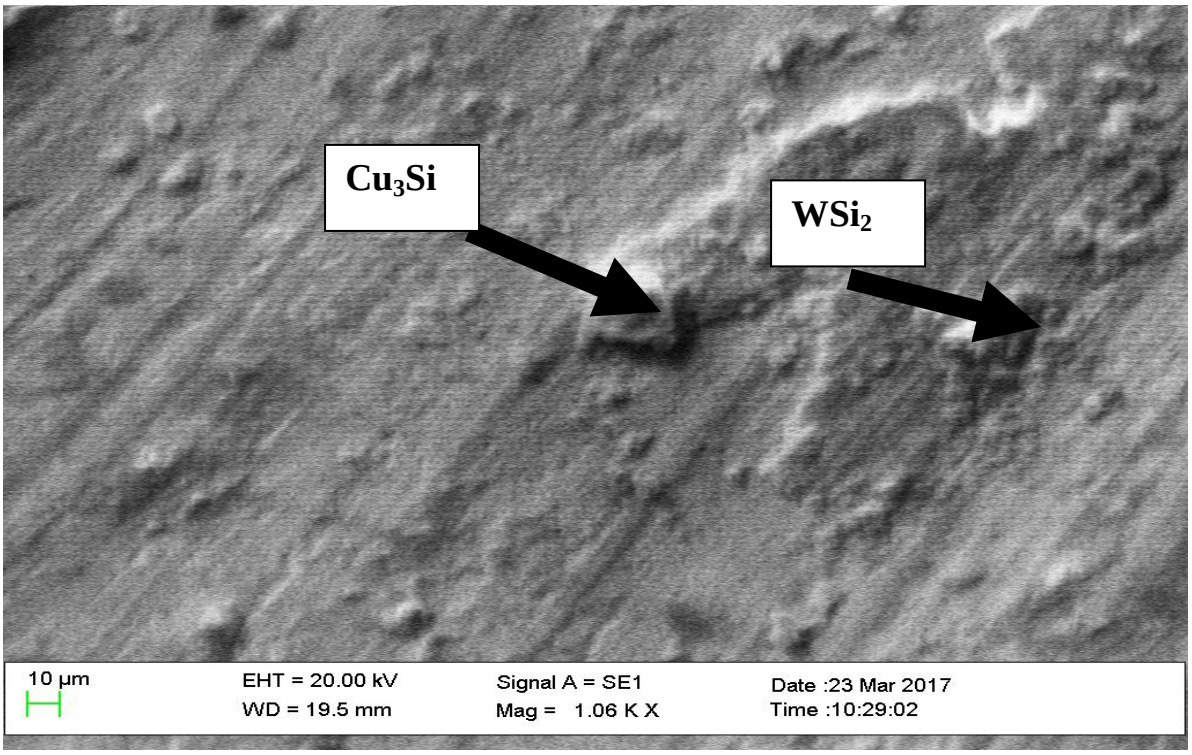

Plate 4.97: Scanning electron microscopy of Cu-3wt%Si-0.8wt%W alloy

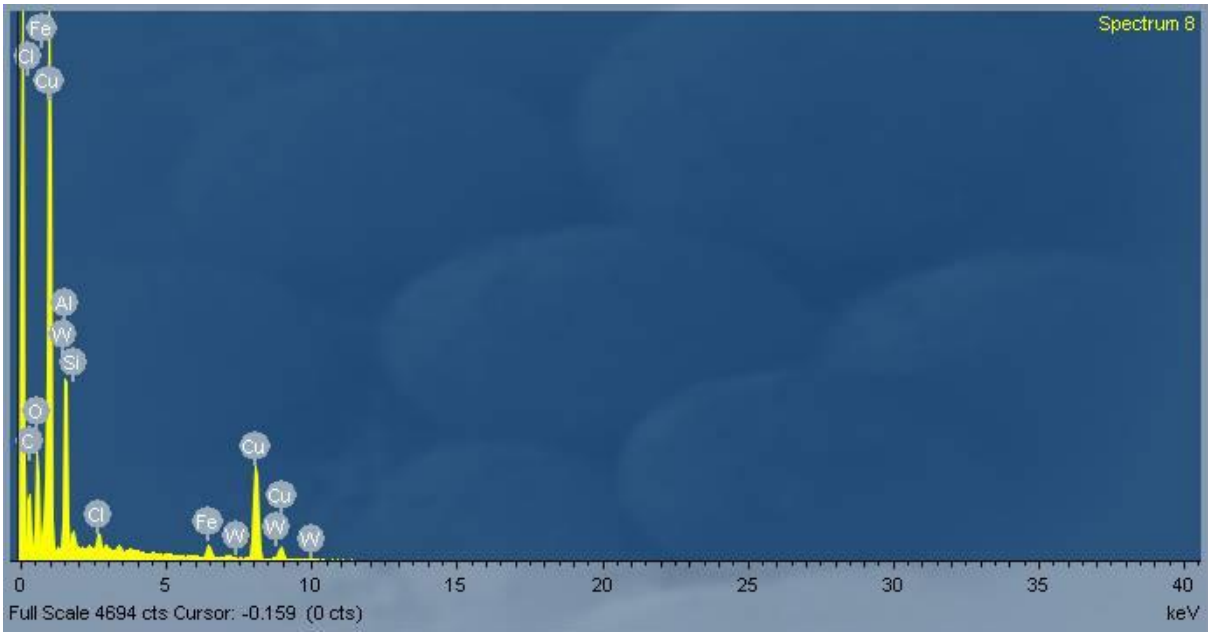

Figure 4.63: EDS spectrum of Cu-3wt%Si-0.8wt%W alloy

Plate 4.98 and Figure 4.8 depicts the scanning electron microscopy and energy dispersive spectroscopy analyses of silicon bronze doped with titanium. The micrograph revealed the presence of Cu_4Ti and Ti_1Si intermetallic phases in the alloy structure. The presence of Cu, Si, Ti, Al, Fe, Ca, Cl, C, K and O elements were indicated in Figure 4.64.

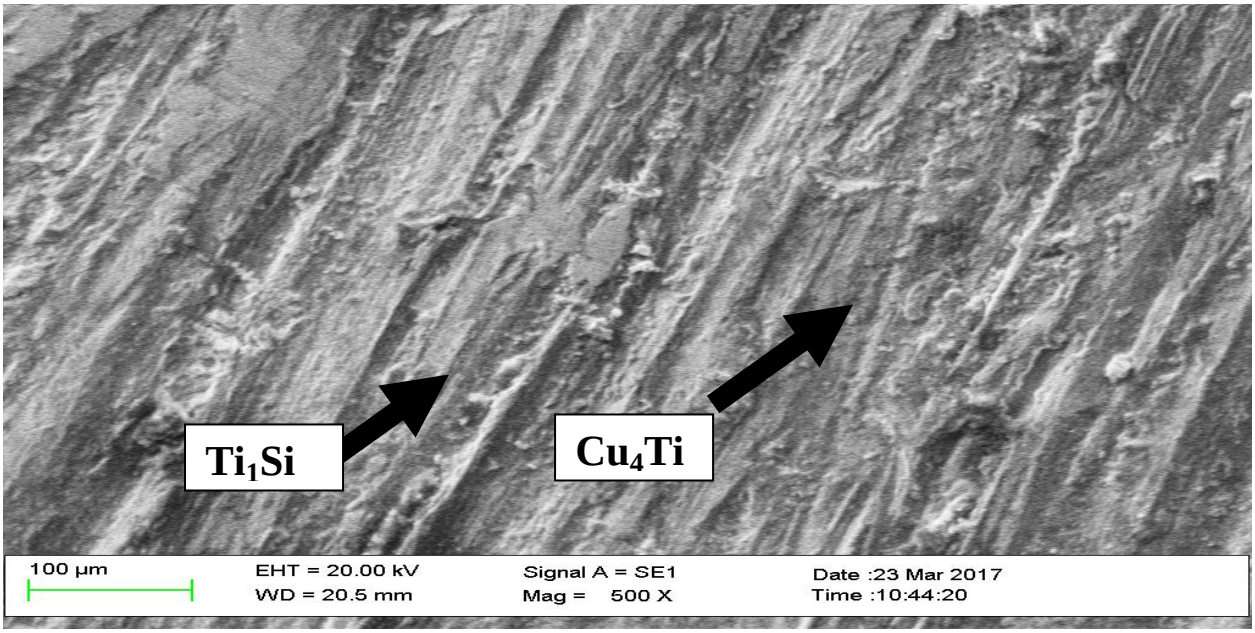

Plate 4.98: Scanning electron microscopy of Cu-3wt%Si-2wt%Ti alloy

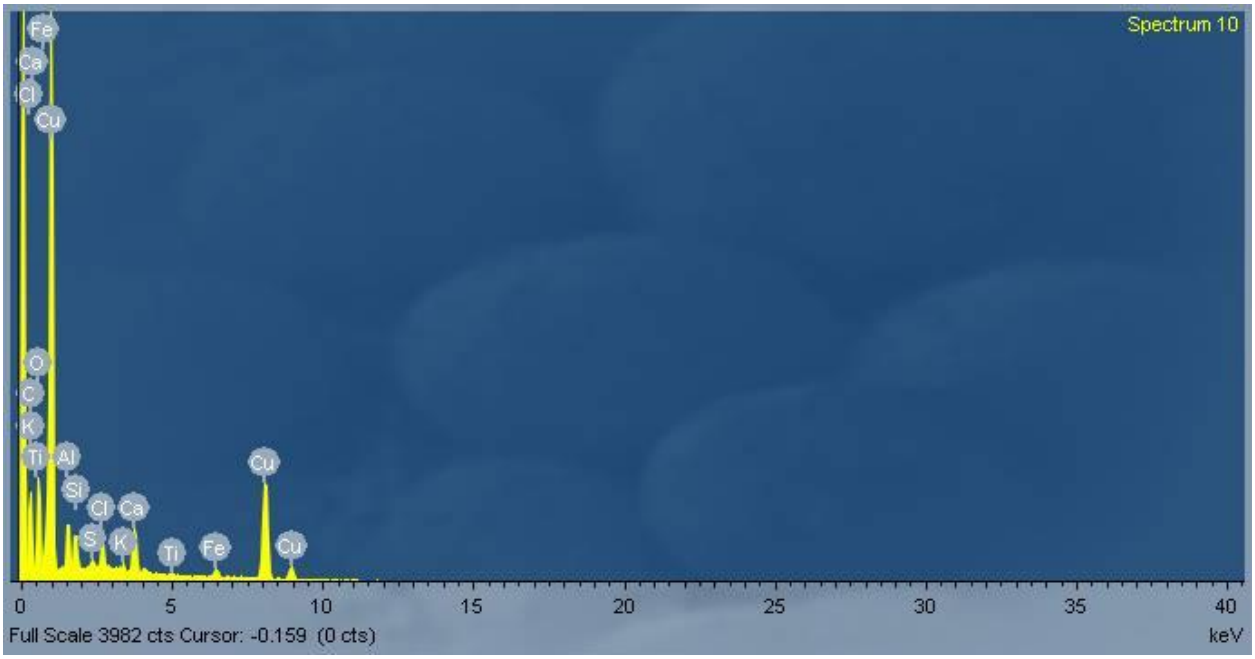

Figure 4.64: EDS spectrum of Cu-3wt%Si-2wt%Ti alloy

The scanning electron microscopy and energy dispersive spectroscopy analyses of silicon bronze doped with molybdenum are presented in Plate 4.99 and Figure 4.65 respectively. The micrograph revealed the presence of $MoSi_2$ intermetallic phase surrounded by the Cu_3Si intermetallic phase. Analysis of Plate 4.99 shows that addition of molybdenum decreased the size of the dendritic primary silicon and hence increased the ultimate tensile strength and hardness of the alloy (Figures 4.17 and 4.26). Figure 4.65 revealed the presence of Cu, Si, Mo, Al, Fe, Ca, Cl, C, Mg and O etc.

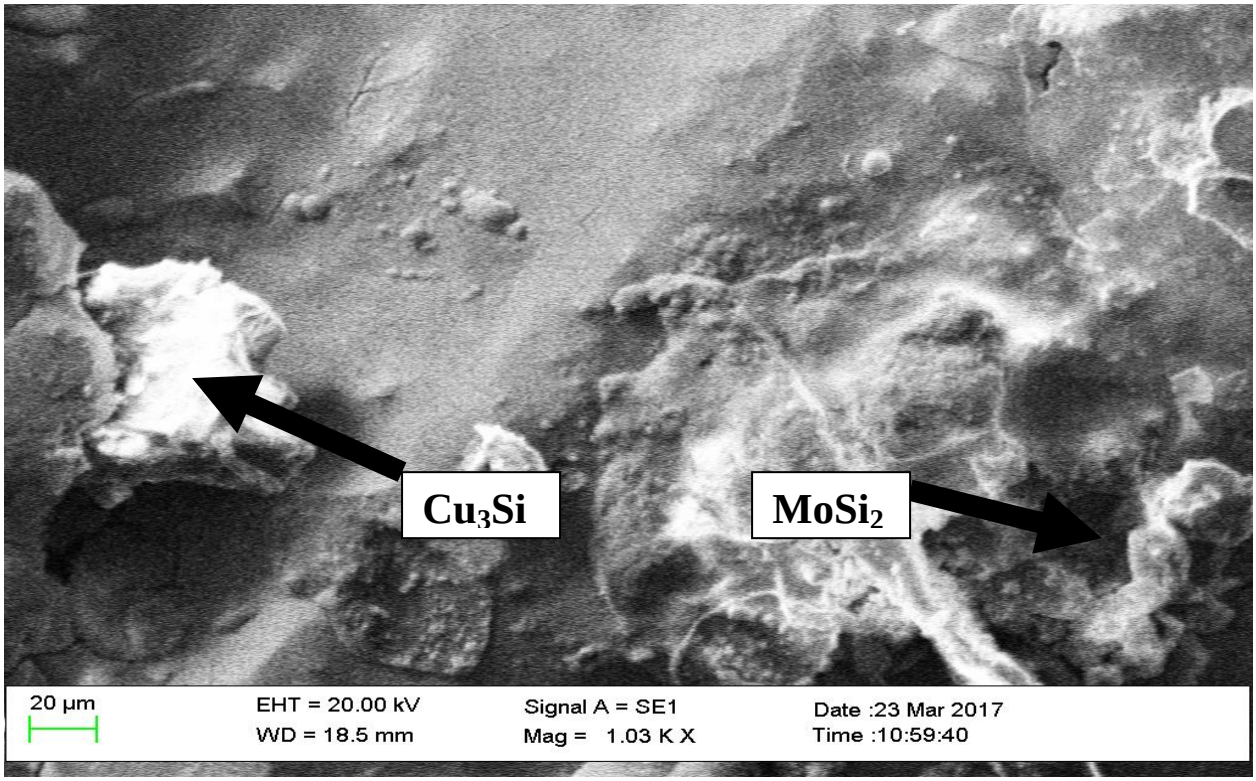

Plate 4.99: Scanning electron microscopy of Cu-3wt%Si-1.5wt%Mo alloy

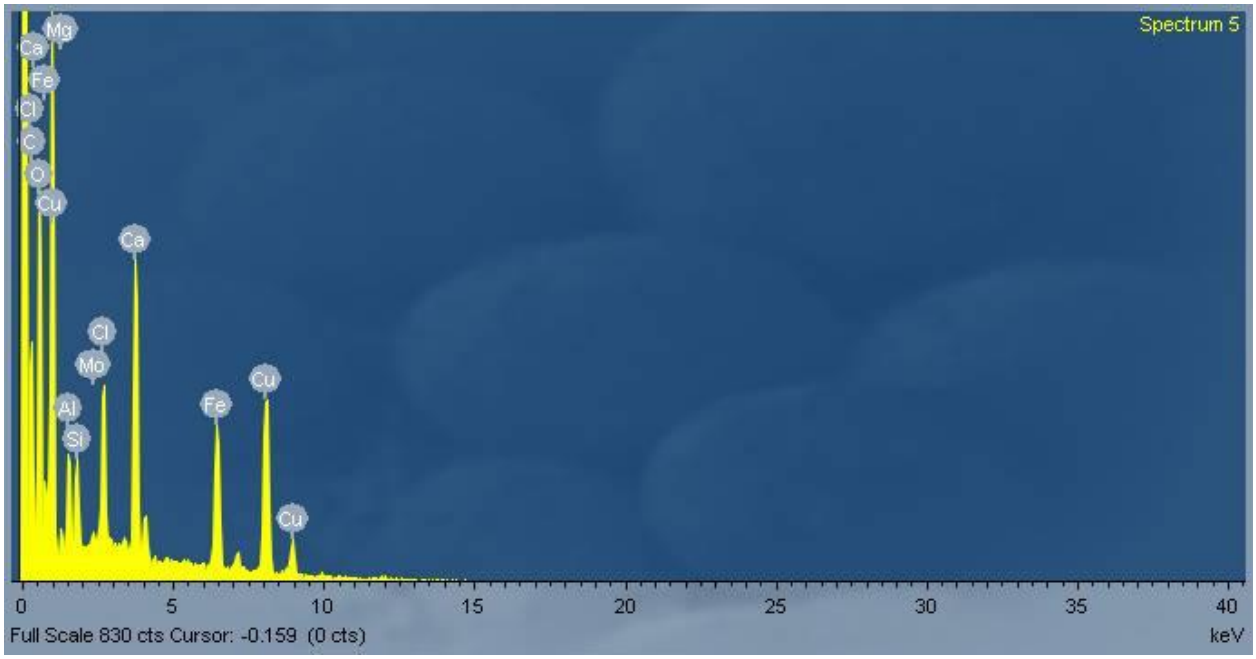

Figure 4.65: EDS spectrum of Cu-3wt%Si-1.5wt%Mo alloy

The scanning electron microscopy analysis of Cu-3wt%Si-Al alloy shown in Plate 4.100 revealed the presence α-phase (solid solubility of aluminium in copper matrix) and copper silicide (Cu_3Si) intermetallic phases. The α-phase

was surrounded by the Cu_3Si intermetallic phase. The energy dispersive spectroscopy analysis shown in Figure 4.66 indicated the presence of Cu, Si, Al, Fe, Ca, Cl, C and O etc.

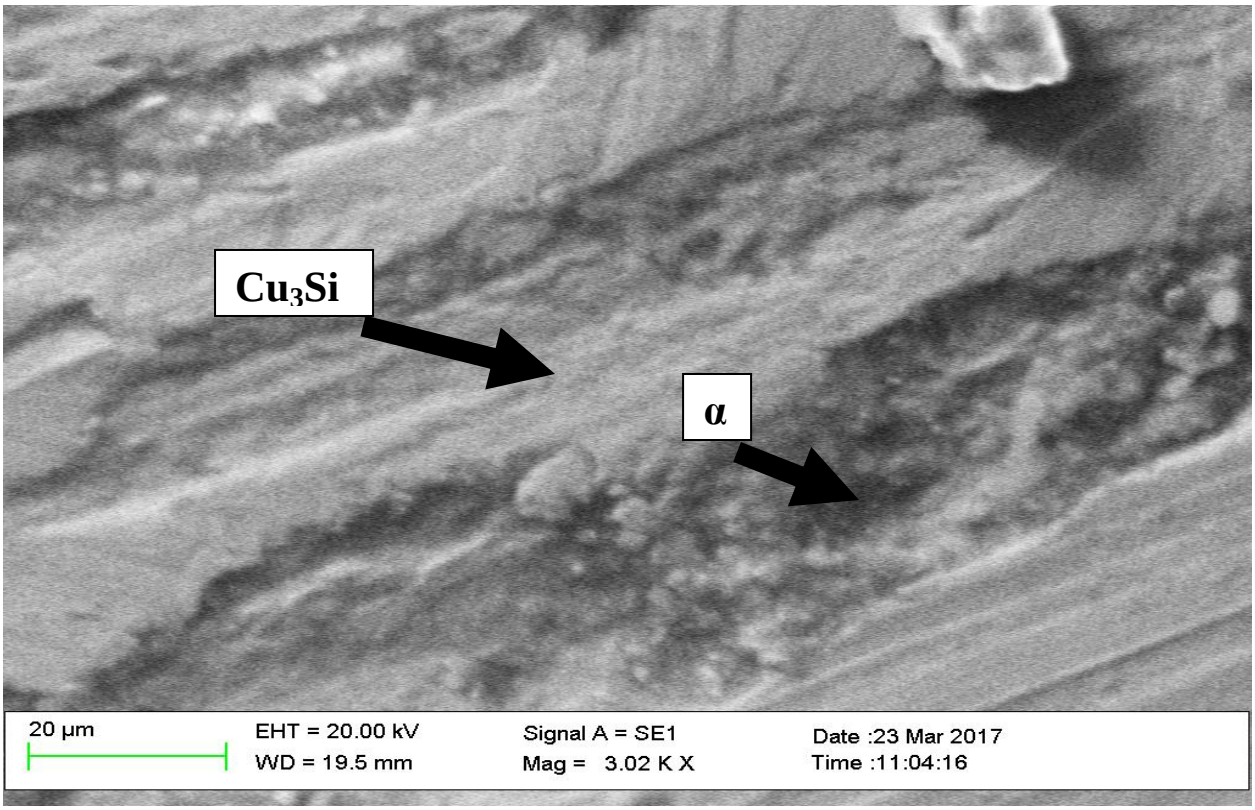

Plate 4.100: Scanning electron microscopy of Cu-3wt%Si-3wt%Al alloy

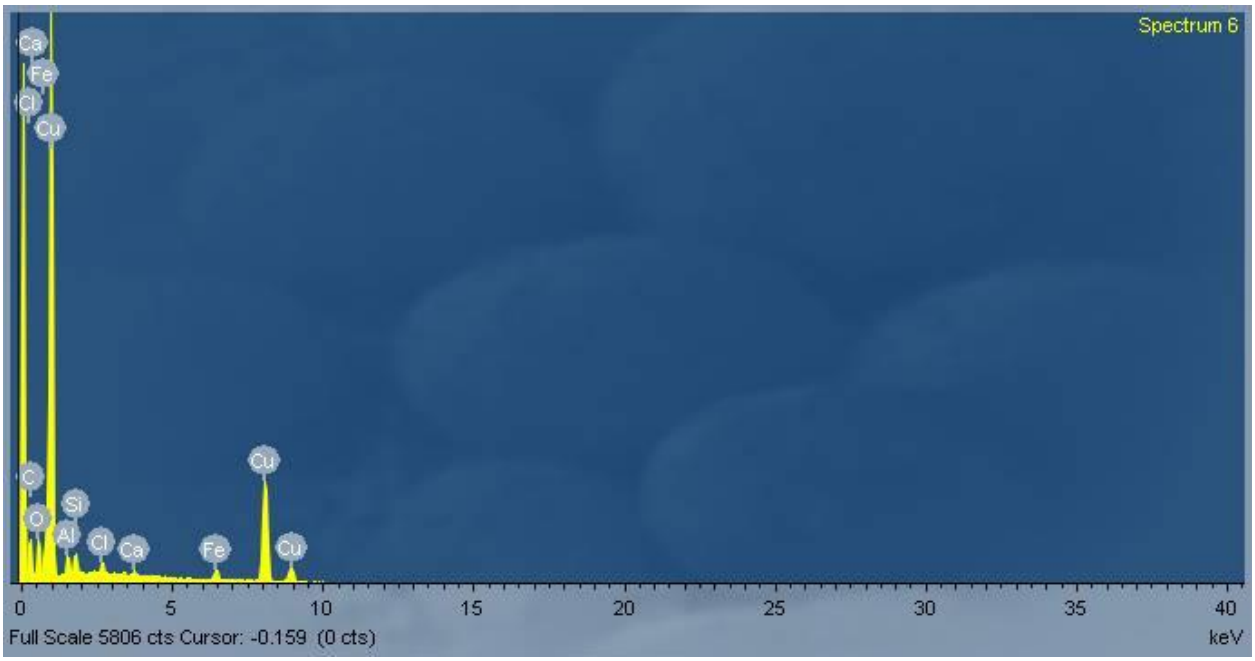

Figure 4.66: EDS spectrum of Cu-3wt%Si-3wt%Al alloy

4.5 Comparison of selected mechanical and physical properties of the developed silicon bronzes with those developed by other researchers

The comparison of the percentage elongation, ultimate tensile strength, hardness and electrical conductivity of the developed silicon bronzes with those developed by other researchers is presented in Table 4.10.

Table 4.10: Comparisons of selected mechanical and physical properties of the developed silicon bronzes with those developed by other researchers

Authors	Alloy/Condition	%E	UTS (MPa)	Hardness (MPa)	σ (%IACS)
Nnakwo K. C. (2017)	Cu-3wt%Si-3wt%Zn/ Solution heat-treated	13.4	376	268	37.9
	Cu-3wt%Si-3wt%Sn/ Cast	11.1	238	278	34.5
	Cu-3wt%Si-0.8wt%Mg/ Solution heat-treated	16.3	306	387	41.5
	Cu-3wt%Si-1wt%Mn/ Solution heat-treated	5.4	385	390	32.2
	Cu-3wt%Si-0.8wt%W/ Solution heat-treated	15.6	298	364	41.2
	Cu-3wt%Si-2wt%Ti/ Solution heat-treated	5.8	274	308	38.6
Li *et al.* (2009)	Cu-1.8wt%Si-8wt%Ni-0.6wt%Sn-0.15wt%Mg/ rolled & aged	2.8	1180	345	26.5
Huang *et al.* (2003)	Cu-0.7wt%Si-3.2wt%Ni-0.3wt%Zn/rolled & aged	-	-	250	31
	Cu-0.7wt%Si-3.2wt%Ni-0.3wt%Zn/cast & aged	-	-	240	24.5
Lei *et al.* (2013)	Cu-1.4wt%Si-6wt%Ni-0.1wt%Cr-0.15wt%Mg/ rolled & aged	3.5	1040	338	28.5

	Cu-1wt%Si-6wt%Ni-0.1 wt%Cr- 0.5wt%Al-0.15wt %Mg/ rolled & aged	3.1	1080	343	28.1
Puathawee *et al.* (2013)	Cu-0.5wt%Si-39.5wt%Zn/ Cast	-	-	123.4	-

4.6 Statistical analysis of comparisons of selected mechanical and physical properties of the developed silicon bronzes with those developed by other researchers

Tables 4.11-4.13 shows the statistical analysis of comparisons of hardness, percentage elongation and electrical resistivity of the developed silicon bronzes with those developed by other researchers. It was indicated that there was a statistically significant difference between groups as determined by one-way analysis of variance F(11,48)2.070, F(8,36)2.452 , F(10,44) 6.277, P =.000. The Turkey post hoc tests shown in Appendix 5 reveals that the percentage elongation and electrical conductivity of the silicon bronzes developed in this study were statistically significantly higher compared to the silicon bronzes developed by other researchers It was also noted from the post hoc tests that the hardness values of Cu-3wt%Si-0.8wt%Mg, Cu-3wt%Si-1wt%Mn, Cu-3wt%Si-0.8wt%W silicon bronzes developed in this study were statistically significantly higher compared to the silicon bronzes developed by Li *et al.* (2009), Huang *et al.* (2003), Puathawee *et al.* (2013) and Lei *et al.* (2013). The hardness values of Cu-3wt%Si-3wt%Zn, Cu-3wt%Si-3wt%Sn and Cu-3wt%Si-2wt%Ti silicon bronzes were statistically significantly higher compared to the silicon bronzes developed by Huang *et al.* (2003) and Puathawee *et al.* (2013), but statistically

significantly lower compared to the ones developed by Lei *et al.* (2013) and Li *et al.* (2009).

The significant higher hardness, ductility (%E) and electrical conductivity of the developed bronzes gave them an edge over those developed by other researchers in automobile, building and electrical industries where excellent hardness, excellent electrical conductivity and moderate ductility are of utmost demand. This makes the developed silicon bronzes more special than those developed by other researchers in automobile, building and electrical industries for production of electrical conduits, valve stems, tie rods, fasteners, nuts, bolts, screws, rivets, nails, and wire.

Table 4.11: Dependent variable: Hardness

	Sum of Squares	df	Mean Square	F	Sig.
Between Groups	319219.733	11	29019.976	2.070	.000
Within Groups	.000	48	.000		
Total	319219.733	59			

Table 4.12: Dependent variable: Percentage elongation

	Sum of Squares	df	Mean Square	F	Sig.
Between Groups	1227.711	8	153.464	2.452	.000
Within Groups	.000	36	.000		
Total	1227.711	44			

Table 4.13: Dependent variable: Electrical conductivity

	Sum of Squares	df	Mean Square	F	Sig.
Between Groups	1801.527	10	180.153	6.277	.000
Within Groups	.000	44	.000		
Total	1801.527	54			

4.7 Statistical analysis of results

The design layout and model analysis of various responses for individual factor are presented in Tables 4.14-4.36. The analysis of variance of various responses for each factor showed different model F-values with p-value of less than 0.05, which implies the models are significant.

Table 4.14: Design layout (Actual) for Mn addition

		Factor 7	Response 1	Response 2	Response 3	Response 4	Response 5	Response 6
Std	Run	A:Mn	%E	UTS	Hardness	Impact strength	Electrical resistivity	Electrical conductivity
		wt%	%	MPa	MPa	MPa	$10^{-3}\Omega m$	S/m
3	1	0.1	16.8	240	251	24	44.69	22.38
5	2	0.2	14.3	258	257	21.4	44.72	22.36
9	3	0.3	13.2	264	262	18.5	44.8	22.32
2	4	0.4	11.8	270	268	16.9	44.98	22.23
6	5	0.5	10.5	278	272	14.4	45.8	21.83
1	6	0.6	9.8	312	285	13.1	46	21.74
10	7	0.7	8.7	345	332	11.8	46.59	21.46
7	8	0.8	7.4	363	348	10.5	46.86	21.34
8	9	1	6.5	378	371	8.3	47.64	21
4	10	1.5	4.8	367	368	6.7	48.17	20.76

Table 4.15 shows model F-value of 652.24 with p-value of <0.0001 which is less than 0.05. This indicates that the model is significant. It was also indicated in Table 4.15 that manganese has statistical significant effect on the percentage elongation of the developed alloy with p-value less than 0.05.

Table 4.15: ANOVA for response surface quadratic model (Response 1: %E for Mn addition)

Analysis of variance table [Partial sum of squares - Type III]						
Source	Sum of Squares	df	Mean Square	F Value	p-value Prob > F	
Model	124.13	2	62.06	652.24	< 0.0001	significant
A-Mn	104.51	1	104.51	1098.29	< 0.0001	
A^2	12.10	1	12.10	127.16	< 0.0001	
Residual	0.67	7	0.095			
Cor Total	124.80	9				

Table 4.16 shows that the "Pred R-Squared" of 0.9753 is in reasonable agreement with the "Adj R-Squared" of 0.8425; i.e. the difference is less than 0.2. The "Adeq Precision" measures the signal to noise ratio. A ratio greater than 4 is desirable. Therefore, the ratio of 67.909 indicates an adequate signal. This model can be used to navigate the design space.

Table 4.16: Pred R-Squared of response 1, %E for Mn addition

Std. Dev.	0.31	R-Squared	0.9947
Mean	10.38	Adj R-Squared	0.9931
C.V. %	2.97	Pred R-Squared	0.9753
PRESS	3.08	Adeq Precision	67.909
-2 Log Likelihood	1.29	BIC	8.20
		AICc	11.29

Final equation in terms of coded factor:

$$\%E = 7.66-5.74\ (A) + 2.95\ (A^2) \quad (4.1)$$

Final equation in terms of actual factor:

$$\%E = +18.06979 - 17.82589\ (Mn) + 6.01891(Mn^2) \quad (4.2)$$

Table 4.17 indicates model F-value of 64.36 with p-value of <0.0001 which is less than 0.05. This indicates that the model is significant. It was also indicated in Table 4.17 that manganese has statistical significant effect on the hardness of the developed alloy with p-value less than 0.05.

Table 4.17: ANOVA for response surface cubic model (Response 3: Hardness for Mn addition)

Analysis of variance table [Partial sum of squares - Type III]						
Source	**Sum of Squares**	**df**	**Mean Square**	**F Value**	**p-value Prob > F**	
Model	20076.52	3	6692.17	64.36	< 0.0001	significant
A-Mn	7389.66	1	7389.66	71.07	0.0002	
A^2	1109.71	1	1109.71	10.67	0.0171	
A^3	2002.19	1	2002.19	19.26	0.0046	
Residual	623.88	6	103.98			
Cor Total	20700.40	9				

Table 4.18 shows "Pred R-Squared" value of 0.8490 which is in reasonable agreement with the "Adj R-Squared" of 0.9548; i.e. the difference is less than 0.2. The "Adeq Precision" measures the signal to noise ratio. A ratio greater

than 4 is desirable. Therefore, the ratio of 19.251 indicates an adequate signal. This model can be used to navigate the design space.

Table 4.18: Pred R-Squared of response 3, Hardness for Mn addition

Std. Dev.	10.20	R-Squared	0.9699
Mean	301.40	Adj R-Squared	0.9548
C.V. %	3.38	Pred R-Squared	0.8490
PRESS	3125.98	Adeq Precision	19.251
-2 Log Likelihood	69.71	BIC	78.92
		AICc	85.71

Final equation in terms of coded factor:

$$\text{Hardness} = +340.12 + 140.82\,(A) - 28.42\,(A^2) - 84.75\,(A^3) \quad (4.3)$$

Final equation in terms of actual factor:

$$\%E = +268.56805 - 180.43671(Mn) + 535.01039(Mn^2) - 247.08544\,(Mn^3) \quad (4.4)$$

Table 4.19 indicates model F-value of 164.88 with p-value of <0.0001 which is less than 0.05. This indicates that the model is significant. It was also indicated in Table 4.19 that manganese has statistical significant effect on the electrical conductivity of the developed alloy with p-value less than 0.05.

Table 4.19: ANOVA for Response surface cubic model (Response 6: Electrical conductivity for Mn addition)

Analysis of variance table [Partial sum of squares - Type III]

Source	Sum of Squares	df	Mean Square	F Value	p-value Prob > F	
Model	3.09	3	1.03	164.88	< 0.0001	significant
A-Mn	0.77	1	0.77	122.70	< 0.0001	
A^2	0.098	1	0.098	15.74	0.0074	
A^3	0.10	1	0.10	16.60	0.0065	
Residual	0.037	6	6.242E-003			

Cor Total	3.12	9

Table 4.20 shows "Pred R-Squared" value of 0.8179 which is in reasonable agreement with the "Adj R-Squared" of 0.9211; i.e. the difference is less than 0.2. The "Adeq Precision" measures the signal to noise ratio. A ratio greater than 4 is desirable. Therefore, the ratio of 25.735 indicates an adequate signal. This model can be used to navigate the design space.

Table 4.20: Pred R-Squared of response 6, electrical conductivity for Mn addition

Std. Dev.	0.17	R-Squared	0.9298
Mean	21.74	Adj R-Squared	0.9211
C.V. %	0.76	Pred R-Squared	0.8179
PRESS	0.57	Adeq Precision	25.735
-2 Log Likelihood	-9.82	BIC	-5.22
		AICc	-4.11

Final equation in terms of coded factor:

$$\text{Electrical conductivity} = +21.32 - 1.43(A) + 0.27(A^2) + 0.61(A^3) \quad (4.5)$$

Final equation in terms of actual factor:

$$\text{Electrical conductivity} = +22.40226 - 0.49110\,(Mn) - 3.71967(Mn^2) + 1.77725(Mn^3) \quad (4.6)$$

Table 4.21: Design layout (actual) for tungsten addition

Std	Run	Factor 8 A:W wt%	Response 1 %E %	Response 2 UTS MPa	Response 3 Hardness MPa	Response 4 Impact strength MPa	Response 5 Electrical resistivity $10^{-3}\Omega m$	Response 6 Electrical conductivity S/m
3	1	0.1	25.8	238	272	30.9	28.15	35.52
5	2	0.2	25.1	242	284	28.7	28.4	35.21
9	3	0.3	24.6	264	300	26.5	29.5	33.9
2	4	0.4	23.4	268	314	24.9	30.42	32.87
6	5	0.5	22.1	272	330	22.5	31.86	31.39
1	6	0.6	21.9	278	348	20.2	32.02	31.23
10	7	0.7	21	281	352	18.1	32.1	31.15
7	8	0.8	20.8	286	358	16.6	34.08	29.34
8	9	1	20.3	245	328	14.4	35.19	28.42
4	10	1.5	19.4	241	303	12.1	35.28	28.34

Table 4.22 indicates model F-value of 221.97 with p-value of <0.0001 which is less than 0.05. This indicates that the model is significant. It was also indicated in Table 4.22 that tungsten has statistical significant effect on the percentage elongation of the developed alloy with p-value less than 0.05.

Table 4.22: ANOVA for response surface quadratic model (Response 1: %E for W addition)

Analysis of variance table [Partial sum of squares - Type III]						
Source	Sum of Squares	df	Mean Square	F Value	p-value Prob > F	
Model	42.28	2	21.14	221.97	< 0.0001	significant
A-W	34.14	1	34.14	358.46	< 0.0001	
A^2	5.33	1	5.33	55.95	0.0001	
Residual	0.67	7	0.095			
Cor Total	42.94	9				

Table 4.23 indicated that the "Pred R-Squared" of 0.9531 is in reasonable agreement with the "Adj R-Squared" of 0.9800; i.e. the difference is less than 0.2.

Table 4.23: Pred R-Squared of response 1, %E for W addition

Std. Dev.	0.31	R-Squared	0.9845
Mean	22.44	Adj R-Squared	0.9800
C.V. %	1.38	Pred R-Squared	0.9531
PRESS	2.02	Adeq Precision	38.797
-2 Log Likelihood	1.30	BIC	8.21
		AICc	11.30

Final equation in terms of coded factor:

$$\%E = +20.78 - 3.28(A) + 1.96\ (A^2) \quad (4.7)$$

Final equation in terms of actual factor:

$$\%E = +27.08260 - 11.07455(W) + 3.99409\ (W^2) \quad (4.8)$$

Model F-value of 64.36 and p-value of <0.0001 where shown in Table 4.24. This indicates that the model is significant. It was also indicated in Table 4.24 that tungsten has statistical significant effect on the electrical conductivity of the developed alloy with p-value less than 0.05.

Table 4.24: ANOVA for response surface quadratic model (Response 6: Electrical conductivity for W addition)

Analysis of variance table [Partial sum of squares - Type III]

Source	Sum of Squares	df	Mean Square	F Value	p-value Prob > F	
Model	59.69	2	29.84	126.21	< 0.0001	significant
A-W	48.15	1	48.15	203.62	< 0.0001	
A^2	7.56	1	7.56	31.98	0.0008	
Residual	1.66	7	0.24			
Cor Total	61.34	9				

The "Pred R-Squared" of 0.8591 is in reasonable agreement with the "Adj R-Squared" of 0.9653; i.e. the difference is less than 0.2 (Table 4.25).

Table 4.25: Pred R-Squared of response 6, electrical conductivity for W addition

Std. Dev.	0.49	R-Squared	0.9730
Mean	31.74	Adj R-Squared	0.9653
C.V. %	1.53	Pred R-Squared	0.8591
PRESS	8.65	Adeq Precision	29.240
-2 Log Likelihood	10.39	BIC	17.30
		AICc	20.39

Final equation in terms of coded factor:

$$\text{Electrical conductivity} = +29.76 - 3.89(A) + 2.33(A^2) \quad (4.9)$$

Final equation in terms of actual factor:

$$\text{Electrical conductivity} = +37.25725 - 13.17585(W) + 4.75808(W^2) \quad (4.10)$$

Table 4.26: Design layout (Actual) for Mg addition

		Factor 1	Response 1	Response 2	Response 3	Response 4	Response 5	Response 6
Std	Run	A:Mg	%E	UTS	Hardness	Impact strength	Electrical resistivity	Electrical conductivity
		wt%	%	MPa	MPa	MPa	$10^{-3}\Omega m$	S/m
3	1	0.1	25.1	201	216	28.1	31.99	31.26
5	2	0.2	24	215	238	26.7	32.82	30.47
9	3	0.3	23.2	228	244	24.4	33.76	29.62
2	4	0.4	22.7	231	258	21.3	34.33	29.13
6	5	0.5	21.8	235	262	19.8	34.58	28.92
1	6	0.6	21.3	240	277	16.7	34.74	28.79
10	7	0.7	20.5	264	284	15.4	34.86	28.69
7	8	0.8	19.1	285	318	13.2	35.03	28.55
8	9	1	18.6	243	269	11.3	35.19	28.42
4	10	1.5	17.2	238	250	9.8	35.28	28.34

Table 4.27 indicates model F-value of 307.54 with p-value of <0.0001 which is less than 0.05. This indicates that the model is significant. It was also indicated in Table 4.27 that manganese had statistical significant effect on the percentage elongation of the developed alloy with p-value less than 0.05.

Table 4.27: ANOVA for response surface quadratic model (Response 1: %E Mg addition)

Analysis of variance table [Partial sum of squares - Type III]						
Source	Sum of Squares	df	Mean Square	F Value	p-value Prob > F	
Model	56.46	2	28.23	307.54	< 0.0001	significant
A-Mg	51.00	1	51.00	555.57	< 0.0001	
A^2	2.81	1	2.81	30.61	0.0009	
Residual	0.64	7	0.092			
Cor Total	57.11	9				

The "Pred R-Squared" of 0.9479 is in reasonable agreement with the "Adj R-Squared" of 0.9855; i.e. the difference is less than 0.2 (Table 4.28).

Table 4.28: Pred R-Squared of response 1, %E for Mg addition

Std. Dev.	0.30	R-Squared	0.9887
Mean	21.35	Adj R-Squared	0.9855
C.V. %	1.42	Pred R-Squared	0.9479
PRESS	2.97	Adeq Precision	48.299
-2 Log Likelihood	0.93	BIC	7.84
		AICc	10.93

Final equation in terms of coded factor:

$$\%E = +19.70 - 4.01(A) + 1.42(A^2) \quad (4.11)$$

Final equation in terms of actual factor:

$$\%E = +26.13885 - 10.36595(Mg) + 2.90052(Mg^2) \quad (4.12)$$

Table 4.29 indicates model F-value of 422.64 with p-value of <0.0001 which is less than 0.05. This indicates that the model is significant. It was also indicated in Table 4.29 that magnesium has statistical significant effect on the impact strength of the developed alloy with p-value less than 0.05.

Table 4.29: ANOVA for Response Surface Quadratic model (Response 4: impact strength for Mg addition)

Analysis of variance table [Partial sum of squares - Type III]						
Source	Sum of Squares	df	Mean Square	F Value	p-value Prob > F	
Model	368.87	2	184.43	422.64	< 0.0001	significant
A-Mg	302.89	1	302.89	694.09	< 0.0001	
A^2	42.27	1	42.27	96.86	< 0.0001	
Residual	3.05	7	0.44			
Cor Total	371.92	9				

The "Pred R-Squared" of 0.9491 is in reasonable agreement with the "Adj R-Squared" of 0.9894; i.e. the difference is less than 0.2. "Adeq Precision" measures the signal to noise ratio. A ratio greater than 4 is desirable. The ratio of 53.986 indicates an adequate signal. This model can be used to navigate the design space (Table 4.30).

Table 4.30: Pred R-Squared of response 4, impact strength for Mg addition

Std. Dev.	0.66	R-Squared	0.9918
Mean	18.67	Adj R-Squared	0.9894
C.V. %	3.54	Pred R-Squared	0.9491
PRESS	18.94	Adeq Precision	53.986
-2 Log Likelihood	16.52	BIC	23.43
		AICc	26.52

Final equation in terms of coded factor:

$$\text{Impact strength} = +13.85 - 9.77(A) + 5.51(A^2) \quad (4.13)$$

Final equation in terms of actual factor:

Impact strength = +32.20933 –31.95112(Mg) + 11.24926(Mg^2) (4.14)

Table 4.31: Design layout (Actual) for Ti addition

Std	Run	Factor 1 A:Ti wt%	Response 1 %E %	Response 2 UTS MPa	Response 3 Hardness MPa	Response 4 Impact Strength J	Response 5 Electrical resistivity $10^{-3}\Omega m$	Response 6 Electrical conductivity S/m
12	1	0.1	23.2	109	194	33.3	35.98	27.79
8	2	0.2	22.4	120	209	31.7	36.4	27.47
13	3	0.3	21.3	133	223	29.3	36.42	27.46
5	4	0.4	20.1	159	238	26.2	36.44	27.44
4	5	0.5	18.8	178	240	24.6	36.56	27.35
9	6	0.6	14.2	203	246	22.8	36.59	27.33
6	7	0.7	11.3	228	248	20.5	36.7	27.25
7	8	0.8	10.4	234	252	18.6	37.29	26.82
1	9	1	9.1	243	258	14	37.32	26.8
11	10	1.5	8.5	258	267	11.7	37.48	26.68
10	11	2	7.2	265	282	10.2	37.6	26.6
3	12	3	6	261	273	9.4	37.65	26.56
2	13	5	5.4	253	264	8.7	37.71	26.52

Table 4.32 indicates model F-value of 14.59 with p-value of <0.0028 which is less than 0.05. This indicates that the model is significant. It was also indicated in Table 4.32 that titanium has statistical significant effect on the percentage elongation of the developed alloy with p-value less than 0.05.

Table 4.32: ANOVA for response surface linear model (Response 1: %E for Ti addition)

Analysis of variance table [Partial sum of squares - Type III]						
Source	Sum of Squares	df	Mean Square	F Value	p-value Prob > F	
Model	299.96	1	299.96	14.59	0.0028	significant
A-Ti	299.96	1	299.96	14.59	0.0028	
Residual	226.23	11	20.57			
Cor Total	526.20	12				

Table 4.33 shows "Pred R-Squared" value of 0.8798 which is in reasonable agreement with the "Adj R-Squared" of 0.9245; i.e. the difference is less than 0.2. The "Adeq Precision" measures the signal to noise ratio. A ratio greater than 4 is desirable. Therefore, the ratio of 18.600 indicates an adequate signal. This model can be used to navigate the design space.

Table 4.33: Pred R-Squared of response 1, %E for Ti addition

Std. Dev.	0.12	R-Squared	0.9434
Mean	27.08	Adj R-Squared	0.9245
C.V. %	0.44	Pred R-Squared	0.8798
PRESS	0.27	Adeq Precision	18.600
-2 Log Likelihood	-23.44	BIC	-13.18
		AICc	-10.44

Final equation in terms of coded factor:

$$\%E = +8.98 - 8.78(A) \quad (4.15)$$

Final equation in terms of actual factor:

$$\%E = +18.12343 - -3.58413\ (Ti) \quad (4.16)$$

Table 4.34 indicates model F-value of 207.20 with p-value of <0.0001 which is less than 0.05. This indicates that the model is significant. It was also indicated in Table 4.34 that titanium has statistical significant effect on the ultimate tensile strength of the developed alloy with p-value less than 0.05.

Table 4.34: ANOVA for response surface sixth model (Response 2: UTS for Ti addition)

Analysis of variance table [Partial sum of squares - Type III]						
Source	**Sum of Squares**	**df**	**Mean Square**	**F Value**	**p-value Prob > F**	
Model	38915.26	6	6485.88	207.20	< 0.0001	significant
A-Ti	244.75	1	244.75	7.82	0.0313	
A^2	240.25	1	240.25	7.68	0.0324	
A^3	363.49	1	363.49	11.61	0.0144	
A^4	673.19	1	673.19	21.51	0.0035	
A^5	376.59	1	376.59	12.03	0.0133	
A^6	453.04	1	453.04	14.47	0.0089	
Residual	187.81	6	31.30			
Cor Total	39103.08	12				

Final equation in terms of coded factor:

$$UTS = +305.65 + +79.82\,(A) - 1095.46\,(A^2) - 3456.30\,(A^3) - 1593.87(A^4) + 3448.94\,(A^5) + 2564.22\,(A^6) \quad (4.17)$$

Final equation in terms of actual factor:

$$UTS = +109.64108 + -97.49655\,(Ti) + 930.86151\,(Ti^2) - 1175.16331\,(Ti^3) + 614.06442\,(Ti^4) - 142.33413\,(Ti^5) + 11.85655\,(Ti^6) \quad (4.18)$$

Table 4.35 indicates model F-value of 6477.82 with p-value of <0.0001 which is less than 0.05. This indicates that the model is significant. It was also indicated in Table 4.35 that molybdenum has statistical significant effect on the percentage elongation of the developed alloy with p-value less than 0.05.

Table 4.35: ANOVA for response surface cubic model (Response 1: %E for Mo addition)

Analysis of variance table [Partial sum of squares - Type III]						
Source	**Sum of Squares**	**df**	**Mean Square**	**F Value**	**p-value Prob > F**	
Model	129.71	3	43.24	6477.82	< 0.0001	significant
A-Mo	4.92	1	4.92	736.93	< 0.0001	
A^2	15.99	1	15.99	2395.22	< 0.0001	
A^3	0.29	1	0.29	43.75	< 0.0001	
Residual	0.060	9	6.675E-003			
Cor Total	129.77	12				

The "Pred R-Squared" of 0.9454 is in reasonable agreement with the "Adj R-Squared" of 0.9994; i.e. the difference is less than 0.2 (Table 4.36).

Table 4.36: Pred R-Squared of response 2, %E for Mo addition

Std. Dev.	0.082	R-Squared	0.9995
Mean	14.39	Adj R-Squared	0.9994
C.V. %	0.57	Pred R-Squared	0.9454
PRESS	7.09	Adeq Precision	221.430
-2 Log Likelihood	-33.01	BIC	-22.75
		AICc	-20.01

Final equation in terms of coded factor:

$$\%E = +9.76 - 3.94\,(A) + 3.66\,(A^2) - 1.08\,(A^3) \quad (4.19)$$

Final equation in terms of actual factor:

$$\%E = +19.04385 - 6.14944(Mo) + 1.17016(Mo^2) - 0.073158\,(Mo^3) \quad (4.20)$$

4.8 Univariate analysis of variance (Two-way anova)

The results of the study were analyzed using two-way analysis of variance (ANOVA) and the results are presented in Tables 4.37-4.39. The result of the two-way analysis of variance show that type of alloying element and composition have statistical significant effect on the mechanical and physical properties of the studied alloy with p-values less than 0.05 ($p<.05$).

Table 4.37: Tests of Between-Subjects Effects (Dependent Variable: %E

Source	Type III Sum of Squares	df	Mean Square	F	Sig.
Corrected Model	3894.800[a]	20	194.740	28.473	.000
Intercept	22782.756	1	22782.756	3331.118	.000
Element	1543.688	7	220.527	32.244	.000
Composition	1373.493	12	114.458	16.735	.000
Error	656.580	96	6.839		
Total	32694.740	117			
Corrected Total	4551.380	116			

a. R Squared = .856 (Adjusted R Squared = .826)

Table 4.38: Tests of Between-Subjects Effects (Dependent Variable: UTS

Source	Type III Sum of Squares	df	Mean Square	F	Sig.
Corrected Model	930320.545[a]	20	46516.027	56.549	.000
Intercept	4255180.010	1	4255180.010	5172.983	.000
Element	474859.565	7	67837.081	82.469	.000
Composition	234747.006	12	19562.251	23.782	.000
Error	78967.455	96	822.578		
Total	5057020.000	117			
Corrected Total	1009288.000	116			

a. R Squared = .922 (Adjusted R Squared = .905)

Table 4.39: Tests of Between-Subjects Effects (Dependent Variable: Brinell hardness

Source	Type III Sum of Squares	df	Mean Square	F	Sig.
Corrected Model	294231.193[a]	20	14711.560	33.398	.000
Intercept	6126964.353	1	6126964.353	13909.213	.000
Element	224022.220	7	32003.174	72.652	.000
Composition	72933.073	12	6077.756	13.798	.000
Error	42287.696	96	440.497		
Total	6712587.000	117			
Corrected Total	336518.889	116			

a. R Squared = .874 (Adjusted R Squared = .848)

CHAPTER FIVE

CONCLUSIONS AND RECOMMENDATIONS

5.1 Conclusion

The effect of dopants and heat treatment parameters on the structure, physical and mechanical properties of silicon bronze (Cu-3wt%Si) has been investigated. From the results of the analysis, the following conclusions were drawn:

1. The presence of dendritic primary silicon in Cu-Si alloy system contributed to the increased ultimate tensile strength and hardness with corresponding drastic decrease in percentage elongation and impact strength of the alloy as the concentration of silicon increased.

2. The increase in local scattering point created by increase in impurity level gave rise to the increased electrical resistivity of Cu-Si alloy system as the concentration of silicon increased.

3. The significant improvement in the percentage elongation, ultimate tensile strength, hardness and impact strength observed in the doped silicon bronze was attributed to the decrease in size, refinement and modification of the dendritic primary silicon in the alloy structure.

4. The increased hardness observed in Cu-3%wt.Si-Zn alloy at 1.5-3%wt zinc concentration was attributed to the precipitation of β phase in the alloy structure.

5. Application of solution heat treatment to silicon bronze doped with Zn, Mg, Mn, W, Ti, Mo and Al significantly decreased the grain size and increase the

distribution pattern of the intermetallic compound and hence increased the ultimate tensile strength and hardness of the alloy compared with the non-heat treated alloy.

6. Analysis of the mechanical and physical properties of silicon bronze doped with Zn, Sn, Mg, Mn, W, Ti, Mo and Al showed that ultimate tensile strength and hardness correlates with electrical resistivity while percentage elongation correlates with electrical conductivity.

7. Grain refinement of the alloys caused scattering of electrons which resulted to increased electrical resistivity and decreased electrical conductivity of the alloys.

5.2 Recommendations

1. Addition of magnesium, manganese and tungsten to silicon bronze should not be in excess of 0.8, 1 and 0.8%wt respectively as they caused precipitation of coarse intermetallic compound in the alloy structure.

2. Addition of zinc, tin, titanium, molybdenum and aluminium to silicon bronze in excess of 3, 3, 2, 1.5 and 3% by weight is not advisable as it decreased the mechanical properties of the alloy.

3. Further study should be carried out on the effect of ageing time and temperature on the structure and mechanical properties of silicon bronzes.

5.3 Contribution to knowledge

1. Silicon bronze with excellent ultimate tensile strength and hardness with good ductility, impact strength and electrical conductivity was developed.

2. Cu-3%wtSi-3%wtZn silicon bronze of higher hardness value than Cu-0.5%wtSi-39.5%wtZn alloy developed by Puathawee *et al.* (2003) has been developed simply by increasing the silicon content and decreasing the zinc content.

3. Silicon bronze of complete homogenized dendritic primary silicon was developed through alloying. This is less costly than the ageing process adopted by Bozica *et al.* (2008).

4. Silicon bronze of higher percentage elongation and electrical conductivity than those developed by Li *et al.* (2009), Huang *et al.* (2003), Puathawee *et al.* (2013) and Lei *et al.* (2013) was developed through alloying and subsequent solution heat treatment which is more cost effective than rolling and subsequent ageing heat treatment adopted by the researchers.

5. Cu-3wt%Si-0.8wt%Mg, Cu-3wt%Si-1wt%Mn, Cu-3wt%Si-0.8wt%W silicon bronzes of higher hardness value than those developed by Li *et al.* (2009), Huang *et al.* (2003), Puathawee *et al.* (2013) and Lei *et al.* (2013) was developed through more cost effective process.

6. The maximum concentration of the dopants required to produce silicon bronze of high mechanical properties was established.

7. The study established that electrical resistivity is not only dependent on the grain size, distribution of second phase and the volume fraction of matrix constituents in the alloy but also on the purity and amount of free copper atom in the alloy structure.

REFERENCES

Abdul, H. K. and Pravin, K. S. (2013). Influence of heat treatment on microstructure and mechanical properties of aluminium bronze. *International Journal of Metallurgical and Materials Science and Engineering (IJMMSE)*, *3*(1), 57-66.

Asanović, V. and Kemal, D. (2004). Mechanical behaviour and shape memory recovery of Cu-Zn-Al alloys. *Metalurgija-Journal of Metallurgy Association of Metallurgical Engineers of Serbia (AMES)*, *13*(1), 59-64.

Benchiheub, M., Belkahla, S., and Guénin, G. (2000). Study of the stabilization of a Cu-Zn-Al shape memory alloy under stress. *Revue de Métallurgie*, *97*(12), 1471-1479.

Bosacchi, B., and Franzosi, P. (1976). The electron-phonon enhancement factor on fermi surface of copper. *Physica Status Solidi (b)*, *77*(2), 457-464.

Božić, D., Dimčić, O., Dimčić, B., Cvijović, I., and Rajković, V. (2008). The combination of precipitation and dispersion hardening in powder metallurgy produced Cu–Ti–Si alloy. *Materials Characterization*, *59*(8), 1122-1126.

Celik H., Aldirmaz E., Sari U., and Aksoy I. (2009). Effect of cooling rate on stress-strain behaviour and microstructure of a Cu-Zn-Sn alloy. *Balkan Physics Letters °C Bog˘Azic¸I University Press*, *16*(1), 1-6.

Eggenschwiler, C. E. (2001). Effect of antimony on the mechanical properties of a bearing bronze (Cu 80: Sn 10: Pb 10). *Bureau of Standards Journal of Research, 8*(5), 625-634.

Garcia, P., Rivera, S., Palacios, M., and Belzunce, J. (2010). Comparative study of the parameters influencing the machinability of leaded brasses. *Engineering Failure Analyses, 17*(4), 771-776.

Górny, Z., Kluska, S. N., and Saja, K. (2013). The effect of toughening combined with microjet cooling during quenching (solution heat treatment) of calcium carbide-modified CuAl10Fe4Ni4 alloy on its mechanical properties. *Archives of Foundry Engineering, 13*(1), 29-32.

Haruhiko, A., Hisashi, I., Li, S., Yoshiharu, K., Akimichi, K., and Katsuyoshi, K. (2010). Microstructure and mechanical properties of high strength brass alloy with some elements. *Trans. Jpn. Soc. Mech. Eng. -Part A, 76*(771), 1501-1506.

Haruhiko, A., Imai, H., Li, S., Kondoh, K., Kousaka, Y., and Kojima, A. (2011). The effect of solid solutionizing Ti element on microstructure and mechanical properties of extruded Cu-40Zn-Ti ternary alloy. *Transactions of JWRI, 40*(1), 67-71.

Harun, Ç., Emine, A., and Đlhan, A. (2012). Effects of deformation on microstructure of Cu-Zn-Ni alloy. *Gazi University Journal of Science, 25*(2), 337-342.

Huang, F., Jusheng, M., Honglong, N., YuWen, C., and Zhiting, G. (2003). Precipitation in Cu–Ni–Si–Zn Alloy for Lead Frame. *Materials Letters*, *57*(13), 2135-2139.

Heidarzadeh, A., and Saeid, T. (2016). A comparative study of microstructure and mechanical properties between friction stir welded single and double phase brass alloys. *Materials Science and Engineering A*, *64*(9), 349-358.

Ilangovan, S., and Sellamuthu, R. (2013). Effects of tin on hardness, wear rate and coefficient of friction of cast Cu-Ni-Sn alloys. *Journal of Engineering Science and Technology, 8*(1), 34-43.

Istratov, A., Hieslmair, H., and Weber, E. (1999). Iron contamination in silicon technology. *Appl. Phys. A: Mater. Sci. Process*, *70*(5), 489-534.

Jinquan, L., Chunyan, D., Tao, X., Guirong, P., Jianhua, L., and Ruijun, Z. (2010). Effect of heat treatment on microstructure of Cu-Al alloys under 1GPa. *Journal of Materials Science and Engineering*, *4*(5), 58-60.

Joseph, A. O., Isiaka, O. O., and Wasiu, S. (2014). Effect of the degree of plastic deformation on the electrical resistance and thermal conductivity of Al-Mg-Si alloy. *Leonardo Electronic Journal of Practices and Technologies*, *1*(24), 37-50.

Jourdan C., Guenin G., Belkahla S., Gastaldi J. and Grange G. (1997) X-ray diffraction effects given by the austenitic phase during the training

process of shape-memory Cu-Zn-Al polycrystals. *Journal de Physique IV, 7(2)*, 489-494.

Kaplan, M., and Yildiz, A. K. (2003). The effects of production methods on the microstructures and mechanical properties of aluminium bronze. *Materials Letters, 57*(28), 4402-4411.

Kenneth, K. A., Ayoola, A. S., and Peter, A. O. (2013). Mechanical and corrosion behaviour of iron modified Cu-Zn-Al alloys. *Acta Metallurgica Slovaca*, *19*(4), 292-301.

Ketut, G. S. I., Soekrisno, R., Made, M. I., and Suyitno (2011a). Mechanical and damping properties of silicon bronze alloys for music applications. *International Journal of Engineering & Technology IJET-IJENS, 11*(06), 81-85.

Ketut, G. S. I., Soekrisno, R., Made, M. I., and Suyitno (2011b). The effect of annealing temperature on damping capacity of the bronze 20%Sn *A*lloy. *International Journal of Mechanical and Mechatronics Engineering IJMME-IJENS, 11*(04), 1-5.

Kexing, S., Yanjun, Z., Peifeng, Z., Yanmin, Z., and Ning, B. (2013). Cu-10Sn-4Ni-3Pb alloy prepared by crystallization under pressure: an experimental study. *Acta Metall. Sin. (Engl. Lett.), 26*(2), 199-205.

Kulczyk, M., Skiba, J., Przybysz, S., Pachla, W., Bazarnik, P., and Lewandowska, M. (2012). High strength silicon bronze (C65500)

obtained by hydrostatic extrusion. *Arc hives of Metallurgical and Materials*, *57*(3), 859-862.

Kumar, S., Narayanan, T. S. N., Manimaran, A., and Kumar, M. S. (2007). Effect of lead on the dezincification behaviour of leaded brass in neutral acid acidified 3.5% NaCl solution. *Materials Chemistry and Physics*, *106*(2), 134-141.

Kumoto, E. A., Alhadeff, R. O., and Martorano, M. A. (2002). Microsegregation and dendrite arm coarsening in tin bronze. *Materials Science and Technology*, *18*(9), 1001-1006.

Lei, Q., Li, Z., Dai, C., Wang, J., Chen, X., Xie, J. M., Yang, W. W., and Chen, D. L. (2013). Effect of aluminium on microstructure and property of Cu–Ni–Si alloys. *Materials Science and Engineering A*, *572*(46), 65-74.

Li, Z., Pan, Z. Y., Zhao, Y. Y., Xiao, Z., and Wang, M. P. (2009). Microstructure and properties of high-conductivity, super-high-strength Cu-8.0Ni-1.8Si-0.6Sn-0.15Mg alloy. *Journal of Materials Research Society*, *24*(6), 2123-2129.

Marcelo, A. M., and José, D. T. C. (2000). Effects of processing variables on the micro segregation of directionally cast samples. *Metallurgical and Materials Transactions A*, *31*(2), 3137-3148.

Martorano, M. A., and Capocchi, J. D. T (2000). Dendrite structure control in directionally solidified bronze castings. *International Journal of Cast Metals Res.*, *13*(1), 49-57.

Mattern, N., Seyrich, R., Wilde, L., Baehtz, C., Knapp, M., and Acker, J. (2007). Phase formation of rapidly quenched Cu–Si alloys. *Journal of Alloys and Compounds*, *429*(1-2), 211-215.

Miller, W., Zhuang, L., Botterma, J., and Wtterbrood, A. (2000). Recent development in aluminium alloys for the automobile industry. *Journal of Materials Science*, *273*(1-2), 204-215.

Mustafa, Y. (2009). Investigation of wear behaviors of C95200 and C95300 Cu-Al- Fe alloys. *Industrial Lubrication and Technology*, *61*(1), 40-46.

Naman, M. D. (2014). *Tribological investigation of aluminium bronze made by centrifugal casting process (Master's thesis)*. Retrieved from U. V. Patel College of Engineering Ganpat University Dissertations and Theses database. (ROLL NO. M12AMT02).

Nestorović, S., Ivanić, L., and Marković, D. (2003). Influence of time of annealing on anneal hardening effect of a cast CuZn alloy. *Journal of Mining and Metallurgy, 39*(3-4), 489-497.

Nnuka, E. E. (1994). Effect of dopants on the structure and properties of aluminium and some of its alloys. *Journal of Agriculture, Science and Technology, 4*(2), 145-153.

Obi, C. A., Nnuka, E. E., and Nnakwo, K. C. (2017). Effect of soaking time and quenching media on the structure and mechanical properties of aluminium bronze (Cu-10%wt.Al). *International Journal of Scientific Research in Science, Engineering and Technology, 3* (2), 311-317.

Ohkubo, Y., Matsumoto, K., and Nagai, K. (2005). Acceleration of Cu surface precipitation from bulk by adsorbed organic molecules. *Japanese Journal of Applied Physics, 44*(1), 3793-3797.

Ovat, F. A., Asuquo, L. O., and Abam, F. I. (2012). The influence of aluminium and manganese on some mechanical properties of brass. *Research Journal in Engineering and Applied Sciences, 1*(4), 214-218.

Peter, S., Jaromír, D., and Michal, K. (2014). Influence of heat treatment on the microstructure and mechanical properties of aluminium bronze. *Materials and Technology, 48*(4), 599-604.

Prabhash, J., and Praveen, K. N. (2013). Influence of heat treatment on microstructure and hardness of nickel aluminium bronze (Cu-10Al-5Ni-5Fe). *IOSR Journal of Mechanical and Civil Engineering (IOSR-JMCE), 4*(6), 16-21.

Praveen, K. N., and Prabhash, J. (2013). Effect of heat treatment on tensile and compression strength of nickel aluminium bronze (Cu-10%Al-5%Ni-5%Fe). *Archives of Applied Science Research, 5*(1), 224-230.

Puathawee, S., Rojananan, S., and Rojananan, S. (2013). Lead-free Cu-Si-Zn brass with tin addition. *Advanced Materials Research, 802(1),* 169-173.

Rajab, M. H., and Osama, I. A. (2014). Influence of Al and Ti additions on microstructure and mechanical properties of leaded brass alloys. *Indian Journal of Materials Science, 2*(4), 1-5.

Ronay, M., and Schad, R. G. (1990). New insight into silicide formation: the creation of silicon self-interstitials. *Phys. Rev. Lett., 64*(17), 20-42.

Sadayappan M., Cousineau D., Zavadil R., Sahoo M., and Michels H. (2002). Grain refinement of permanent mold cast copper base alloys. *AFS Transactions, 110(2),* 505-514.

Sade, M., Damiani, C., Gastien, R., Lovey, F. C., Malarría, J., and Yawny, A. (2007). Fatigue and martensitic transitions in Cu–Zn–Al and Cu–Al–Ni single crystals: mechanical behaviour, defects and diffusive phenomena. *Smart Materials and Structures, 16*(1), 1-26.

Sampath, V. (2006). Improvement of shape-memory characteristics and mechanical properties of copper–zinc–aluminum shape-memory alloy with low aluminium content by grain refinement. *Journal of Materials and Manufacturing Processes, 21*(8), 789-795.

Sarma S. V., Sivaprasad K., Sturm D., and Heilmaier M. (2008). The microstructure and mechanical properties of ultra fine grained Cu-Zn and Cu-Al alloys produced by cryorolling and annealing. *Material Science and Engineering A, 489*(1-2), 253-258.

Sekunowo O. I., Adeosun S. O., Lawal G. I., and Balogun S. A. (2013). Mechanical characterization of aluminium bronze-iron granules composite. *International Journal of Scientific and Technology Research, 2*(4), 179-185.

Shabestari S. G., and Moemeni H. (2004). Effect of copper and solidification conditions on the microstructure and mechanical properties of Al–Si–Mg alloy. *Journal of Materials Processing Technology, 153*(1), 193-198.

Shufeng, L., Hisashi, I., Haruhiko, A., and Katsuyoshi, K. (2011). Contribution of Ti addition to characteristics of extruded Cu40Zn brass alloy prepared by powder metallurgy. *Materials and Design*, *32*(1), 192-197.

Song, J. Y., Jin Y., and Lee, T. Y. (2004). Effects of reactive diffusion on stress evolution in Cu–Sn films. *Scripta Materialia, 51*(2), 167-170.

Uyime, D., Joseph, A. O., and Itopa, M. M. (2012). Mechanical properties and microstructures of locally produced aluminium-bronze alloy. *Journal of Minerals and Materials Characterization and Engineering*, *11*(1), 1020-1026.

Vilarinho, C., Davim, J. P., Soares, D., Castro, F., and Barbosa, J. (2005). Influence of the chemical composition on the machinability of brasses. *Journal of Materials Processing Technology, 170*(1), 441-447.

Warta, W. (2002). Defect and impurity diagnostics and process monitoring. *Solar Energy Materials and Solar Cells, 72*(1-4), 389-401.

William, D. N. J. (2010). *Metallurgy of copper based alloys*. Copper Development Association, Inc., pp. 1-3. Retrieved from https://www.copper.org/resources/properties/703_5/.

Youxiong, Y., Xuyue, Y., Chenze, L., Yangzhi, S., Xiangkai, Z., and Taku, S. (2014). Enhancement of strength and ductility of Cu–Sn–Zn alloy by iron addition. *Materials Science and Engineering A*, 612(1), 246–252.

Yuting, L., Liqiang, W., Xiaoyan, X., and Weijie, L. (2015). Effect of post heat treatment on the microstructure and microhardness of friction stir processed NiAl bronze (NAB) alloy. *Metals*, *5*(3), 1695-1703.

Zhang, W., Xia, W., Wen, L., Wu, Y. B., and Pan, G. (2003). Mechanical properties and tribological behavior of a cast heat resisting copper base alloy. *J.Cent. South Univ. TECHNO. (Journal CSUT), 9* (4), 235- 239.

APPENDICES

Appendix 1: Results modeling and analysis

Appendix 1.1: Response 1, %E for Mg addition

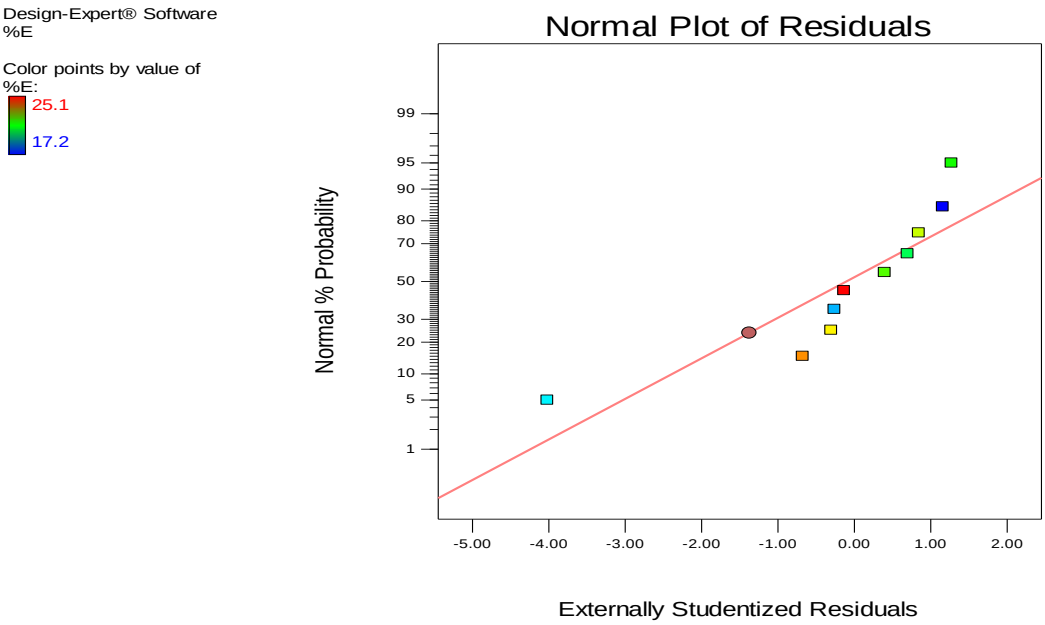

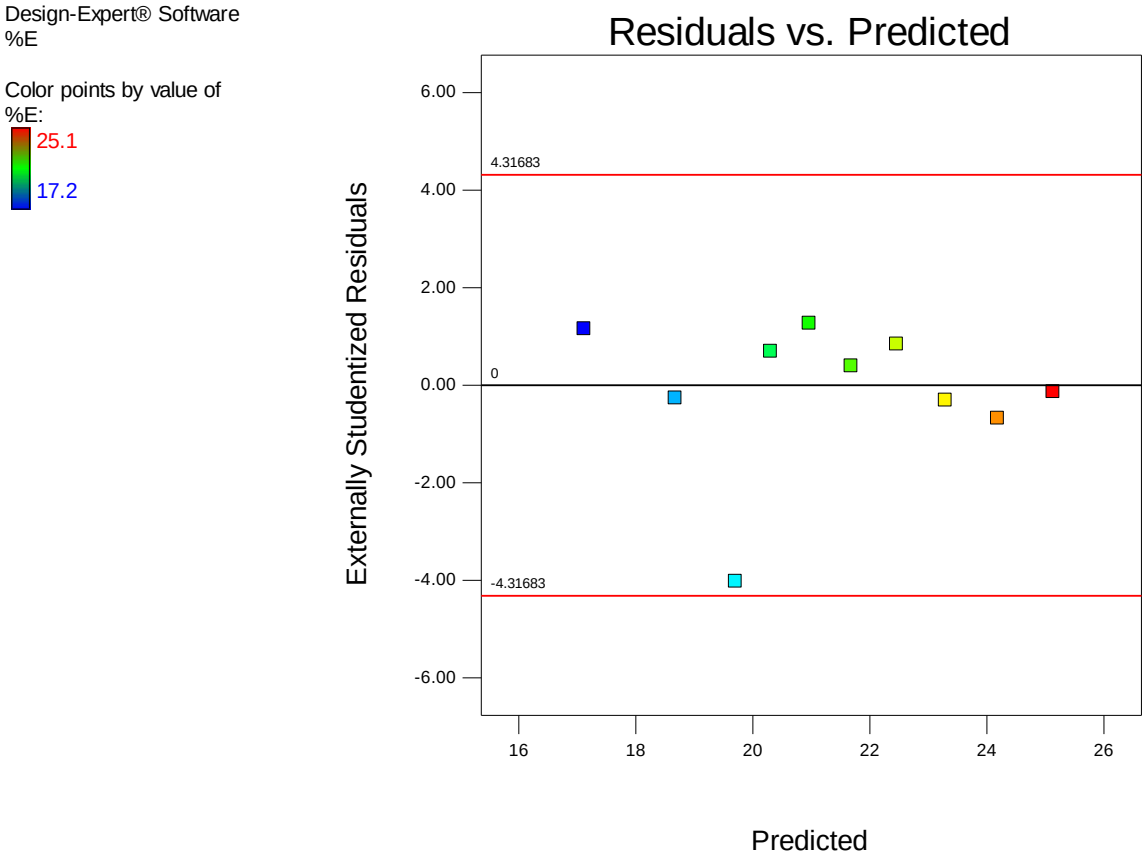

Design-Expert® Software
%E

Color points by value of
%E:
25.1
17.2

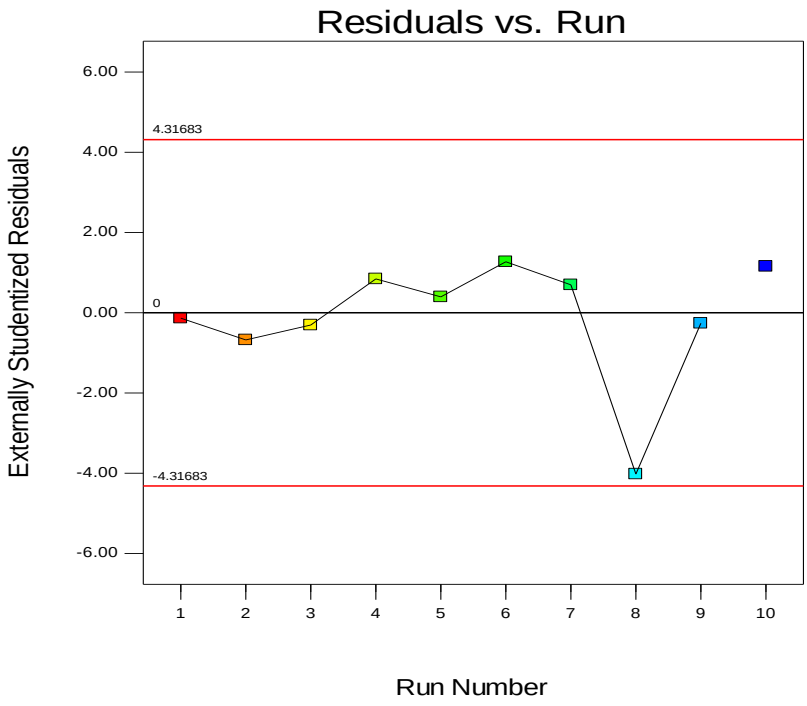

Design-Expert® Software
%E

Color points by value of
%E:
25.1
17.2

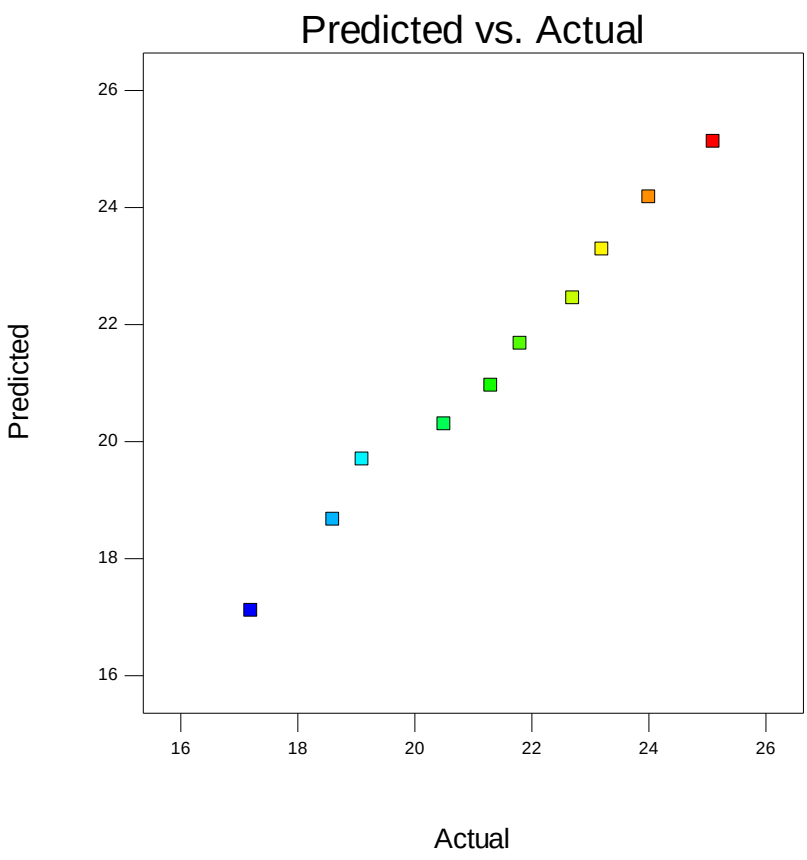

Design-Expert® Software
%E

Color points by value of
%E:
25.1
17.2

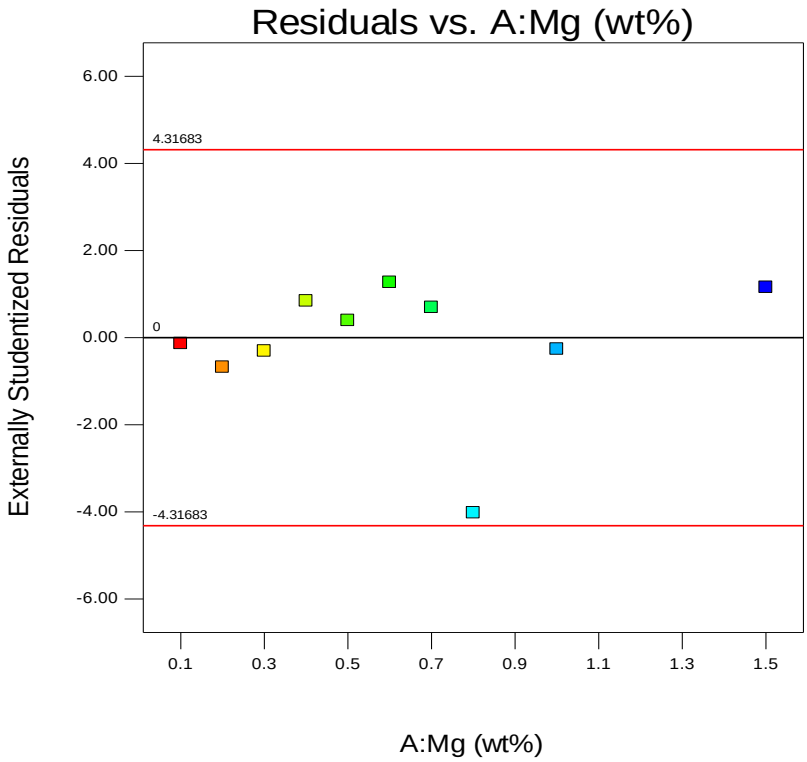

Design-Expert® Software
Factor Coding: Actual
%E (%)
Design Points
95% CI Bands

X1 = A: Mg

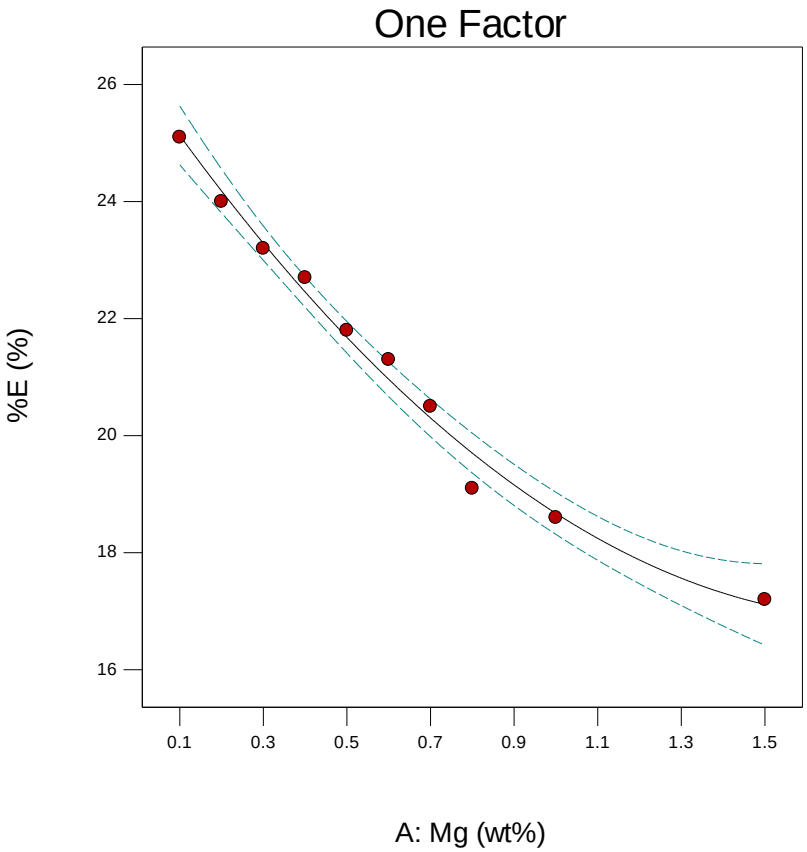

Appendix 1.2 Response 4, impact strength for Mg addition

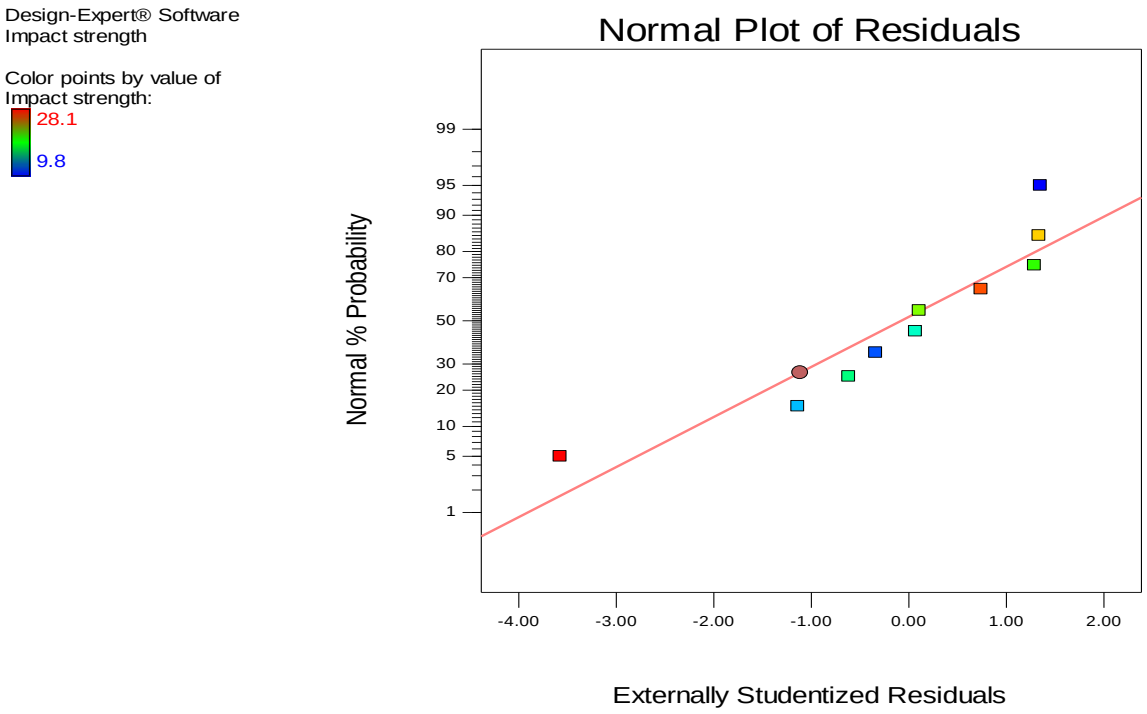

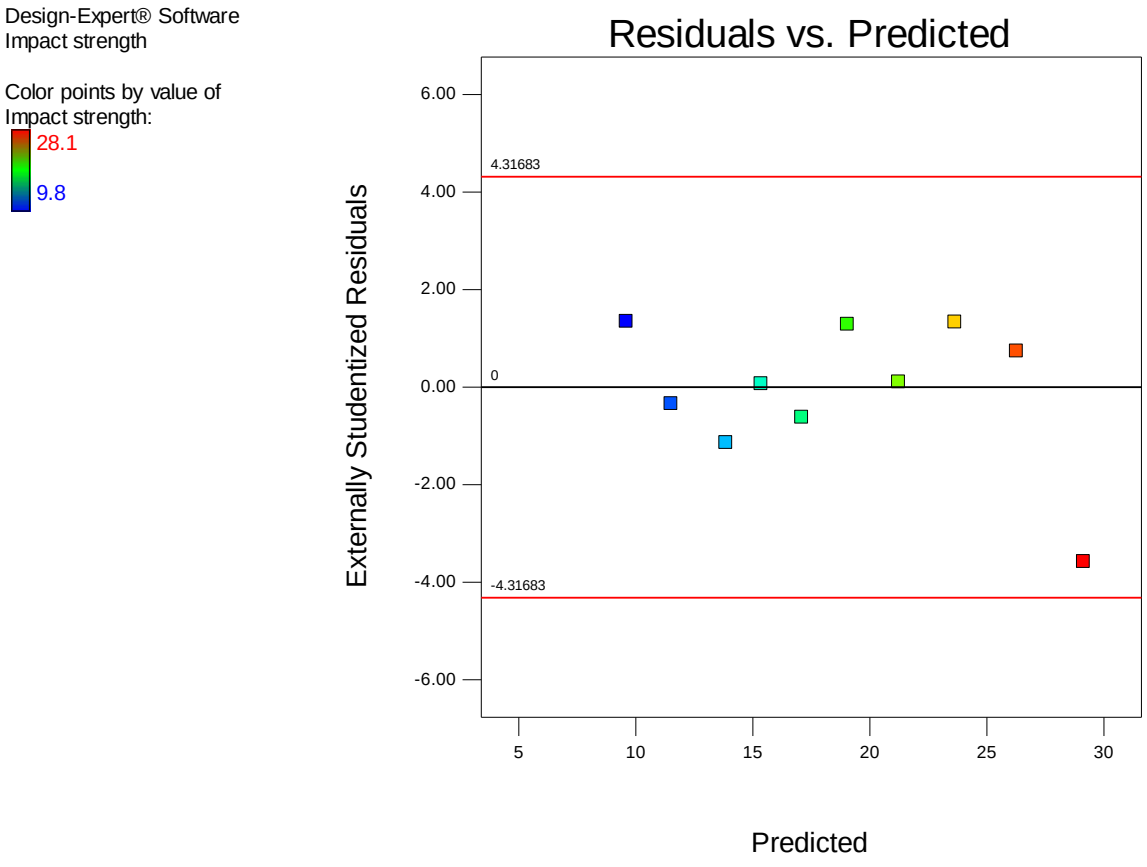

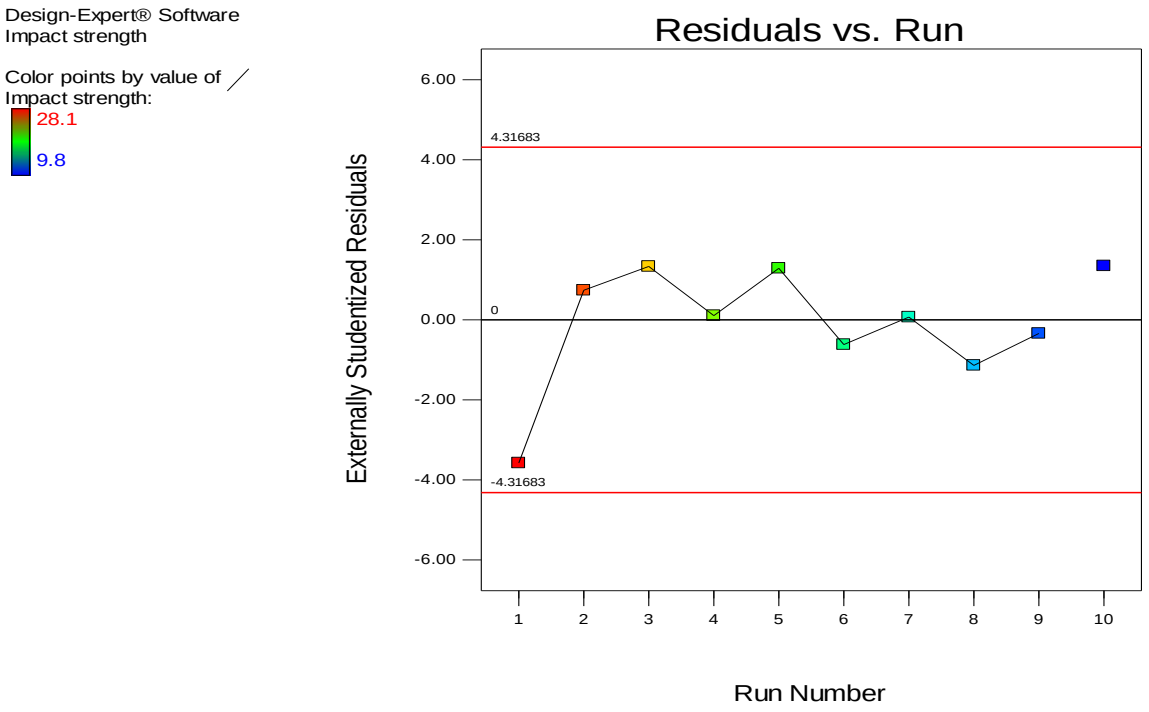
Design-Expert® Software
Impact strength
Color points by value of
Impact strength:
28.1
9.8
Residuals vs. Run
Externally Studentized Residuals
6.00
4.00
2.00
0.00
-2.00
-4.00
-6.00
4.31683
0
-4.31683
1
2
3
4
5
6
7
8
9
10
Run Number

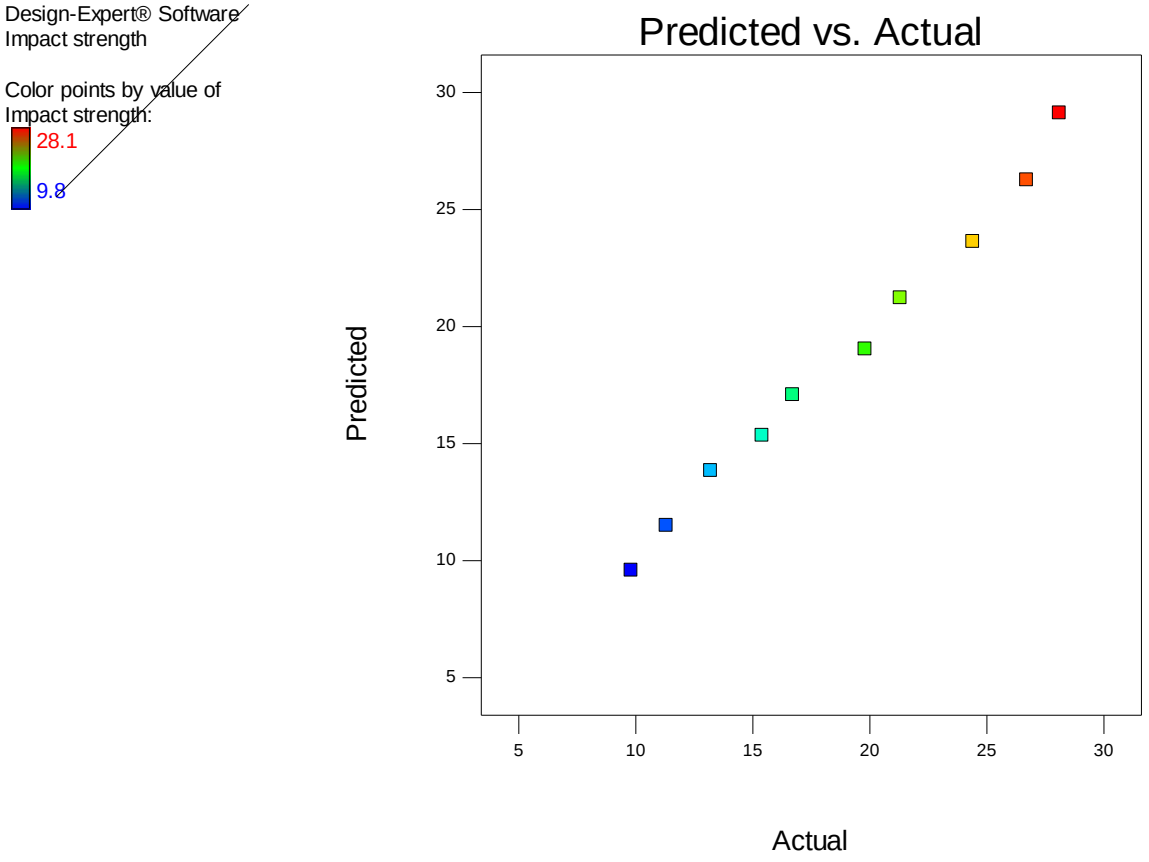
Design-Expert® Software
Impact strength
Color points by value of
Impact strength:
28.1
9.8
Predicted vs. Actual
Predicted
30
25
20
15
10
5
5
10
15
20
25
30
Actual

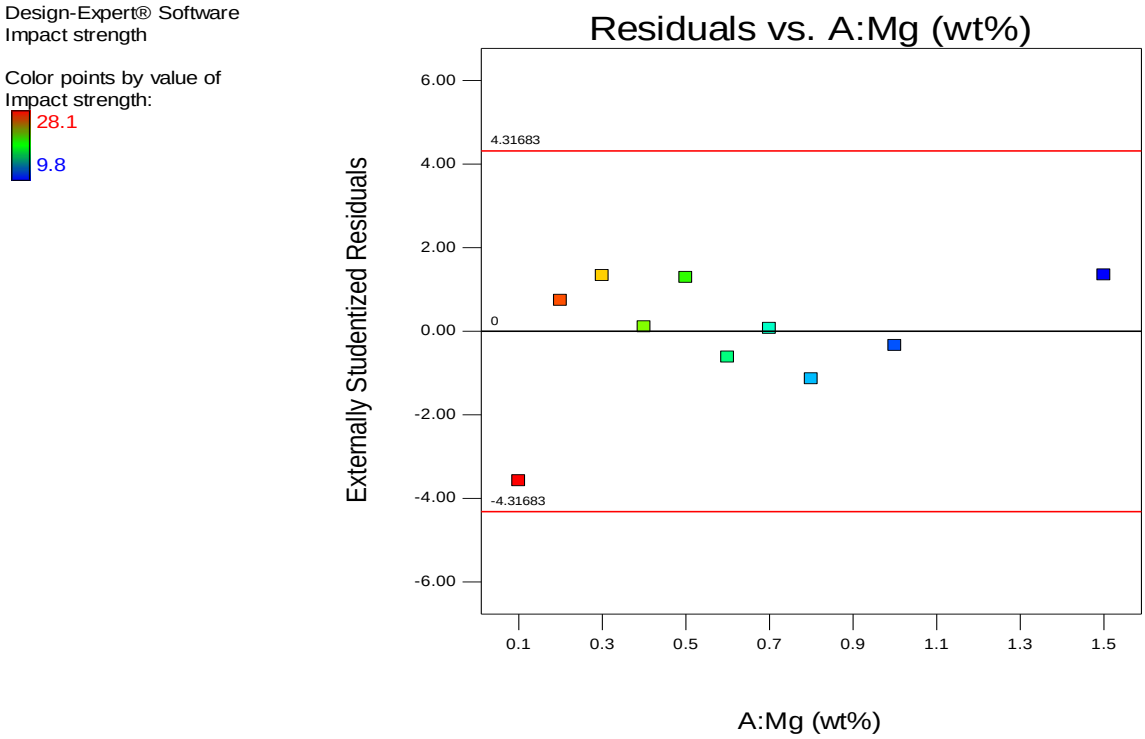
Design-Expert® Software
Impact strength
Color points by value of
Impact strength:
28.1
9.8
Residuals vs. A:Mg (wt%)
Externally Studentized Residuals
6.00
4.00
2.00
0.00
-2.00
-4.00
-6.00
4.31683
0
-4.31683
0.1
0.3
0.5
0.7
0.9
1.1
1.3
1.5
A:Mg (wt%)

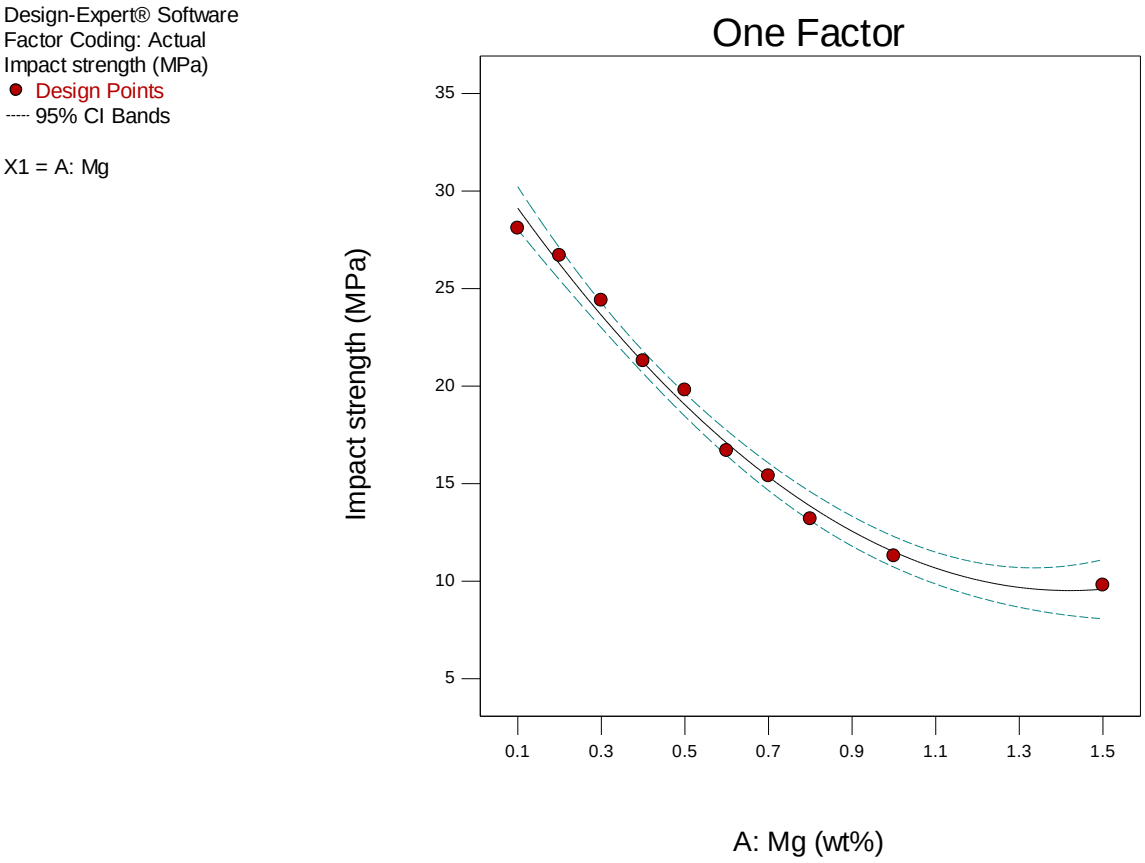
Design-Expert® Software
Factor Coding: Actual
Impact strength (MPa)
Design Points
95% CI Bands
X1 = A: Mg
One Factor
Impact strength (MPa)
35
30
25
20
15
10
5
0.1
0.3
0.5
0.7
0.9
1.1
1.3
1.5
A: Mg (wt%)

Appendix 1.3 Response 1, %E for Mn addition

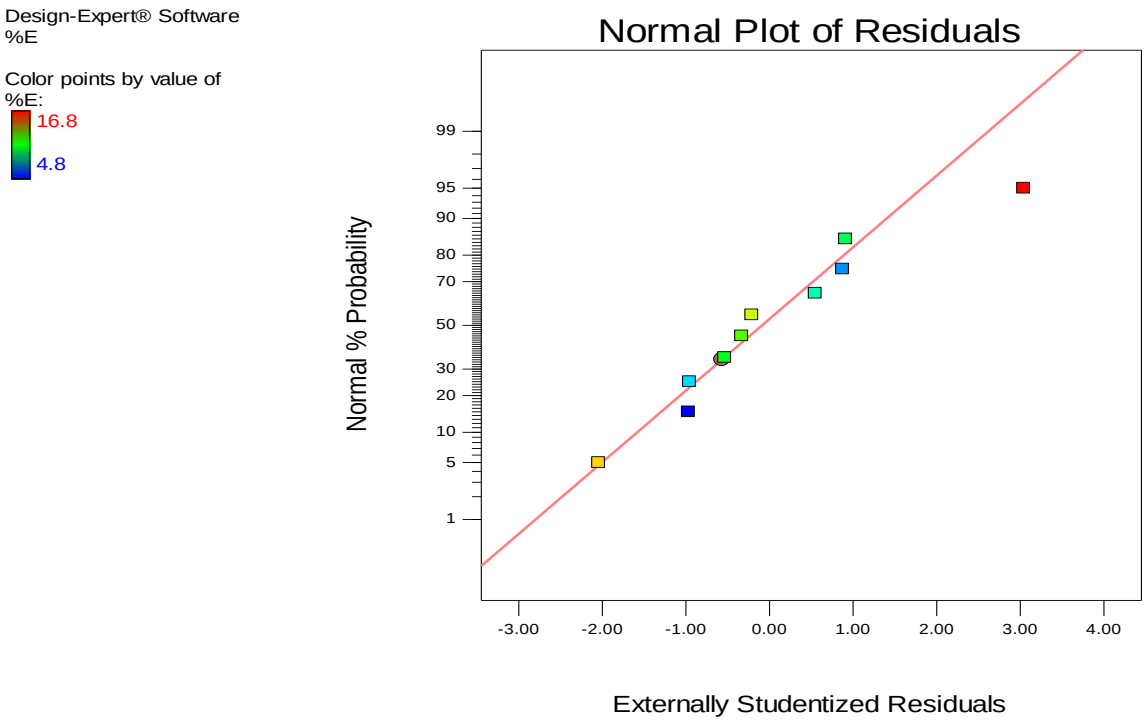

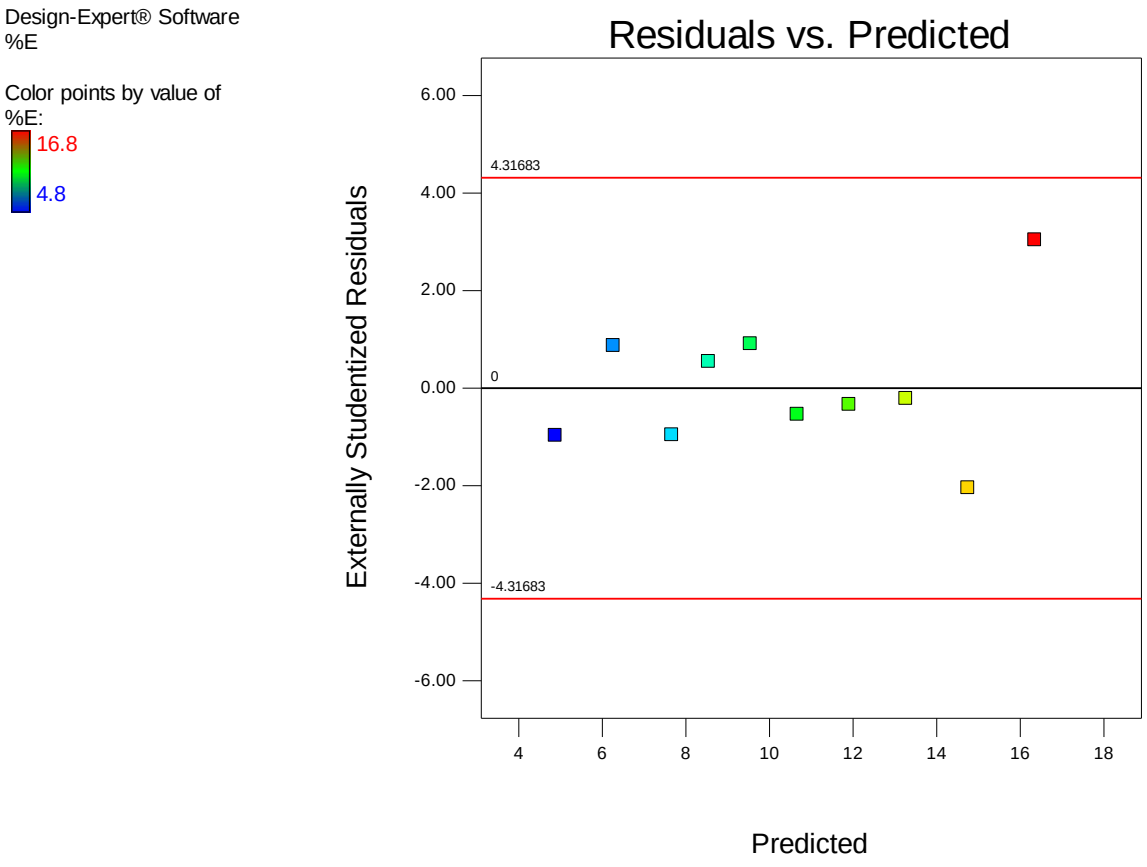

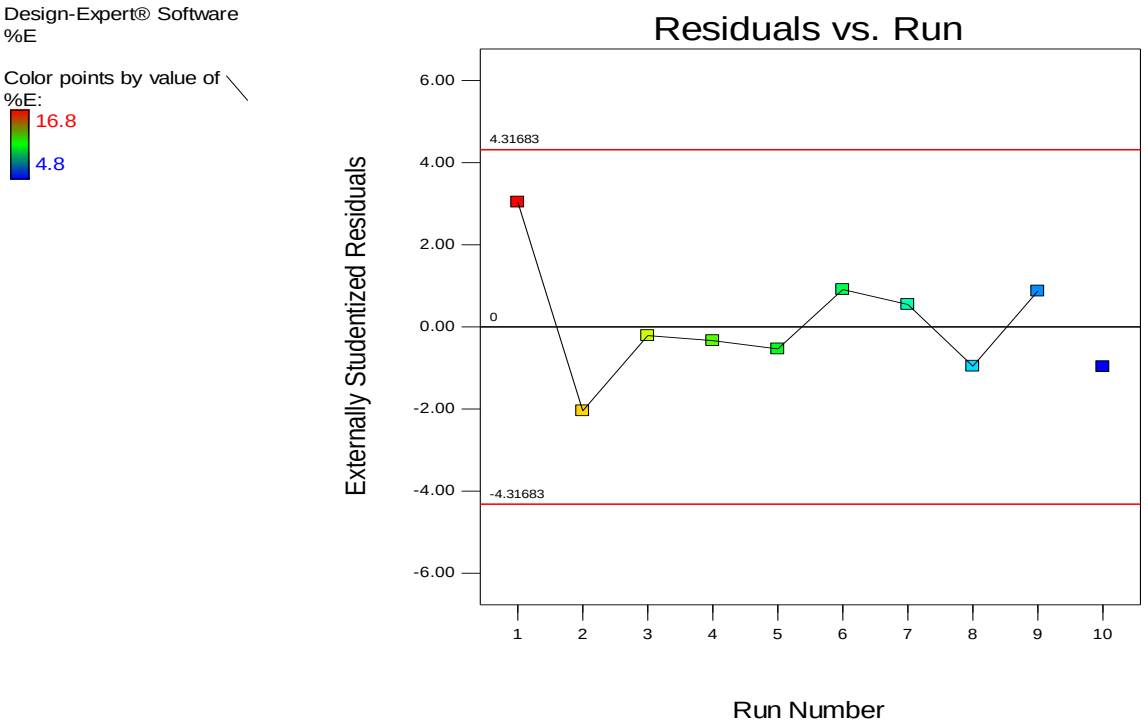
Design-Expert® Software
%E
Color points by value of
%E:
16.8
4.8
Residuals vs. Run
Externally Studentized Residuals
6.00
4.00
2.00
0.00
-2.00
-4.00
-6.00
4.31683
0
-4.31683
1
2
3
4
5
6
7
8
9
10
Run Number

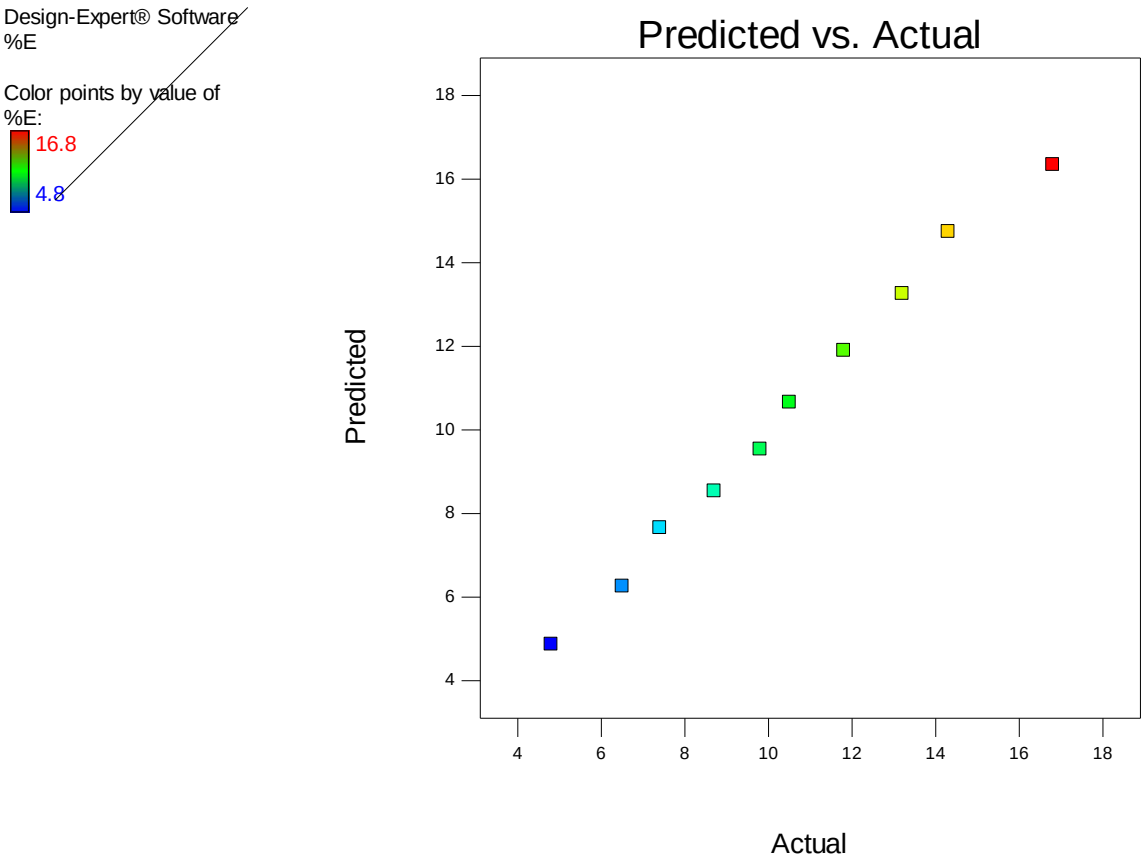
Design-Expert® Software
%E
Color points by value of
%E:
16.8
4.8
Predicted vs. Actual
Predicted
18
16
14
12
10
8
6
4
4
6
8
10
12
14
16
18
Actual

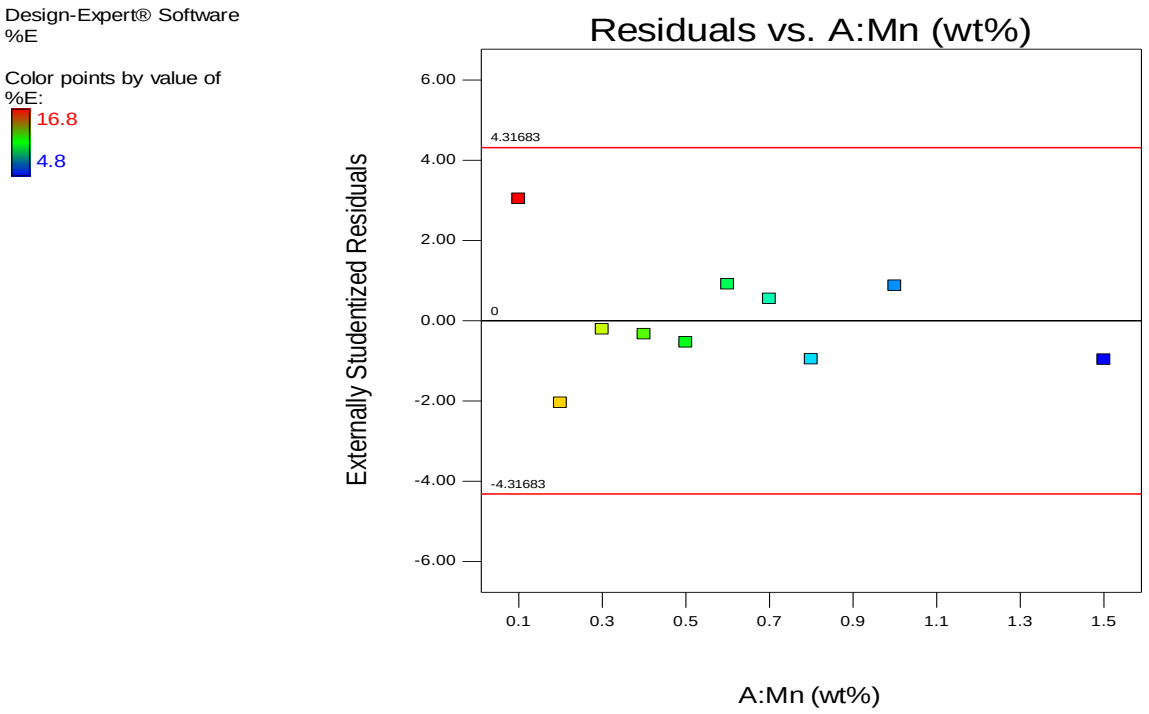
Design-Expert® Software
%E
Color points by value of
%E:
16.8
4.8
Residuals vs. A:Mn (wt%)
Externally Studentized Residuals
6.00
4.00
2.00
0.00
-2.00
-4.00
-6.00
4.31683
0
-4.31683
0.1
0.3
0.5
0.7
0.9
1.1
1.3
1.5
A:Mn (wt%)

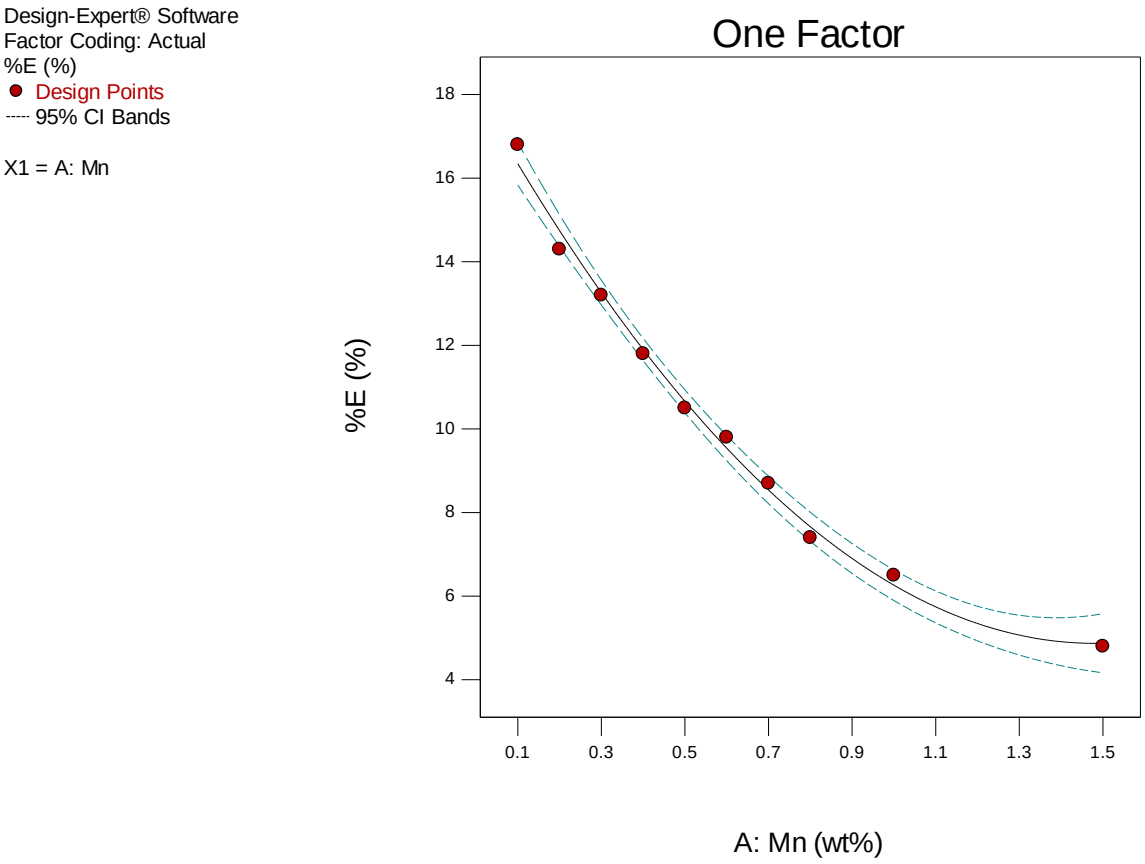
Design-Expert® Software
Factor Coding: Actual
%E (%)
Design Points
95% CI Bands
X1 = A: Mn
One Factor
%E (%)
18
16
14
12
10
8
6
4
0.1
0.3
0.5
0.7
0.9
1.1
1.3
1.5
A: Mn (wt%)

Factor	Coefficient Estimate	df	Standard Error	95% CI Low	95% CI High	VIF
Intercept	340.12	1	5.32	327.10	353.13	
A-Mn	140.82	1	16.70	99.95	181.70	8.59
A^2	-28.42	1	8.70	-49.70	-7.13	1.02
A^3	-84.75	1	19.31	-132.01	-37.49	8.65

Appendix 1.4: Response 3, hardness for Mn addition

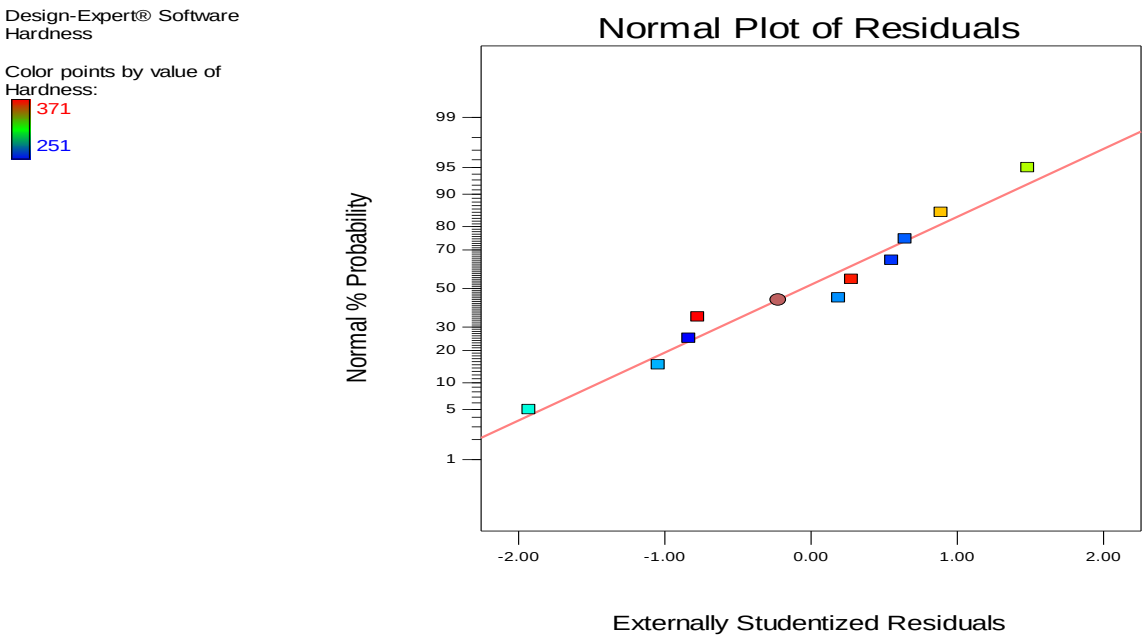

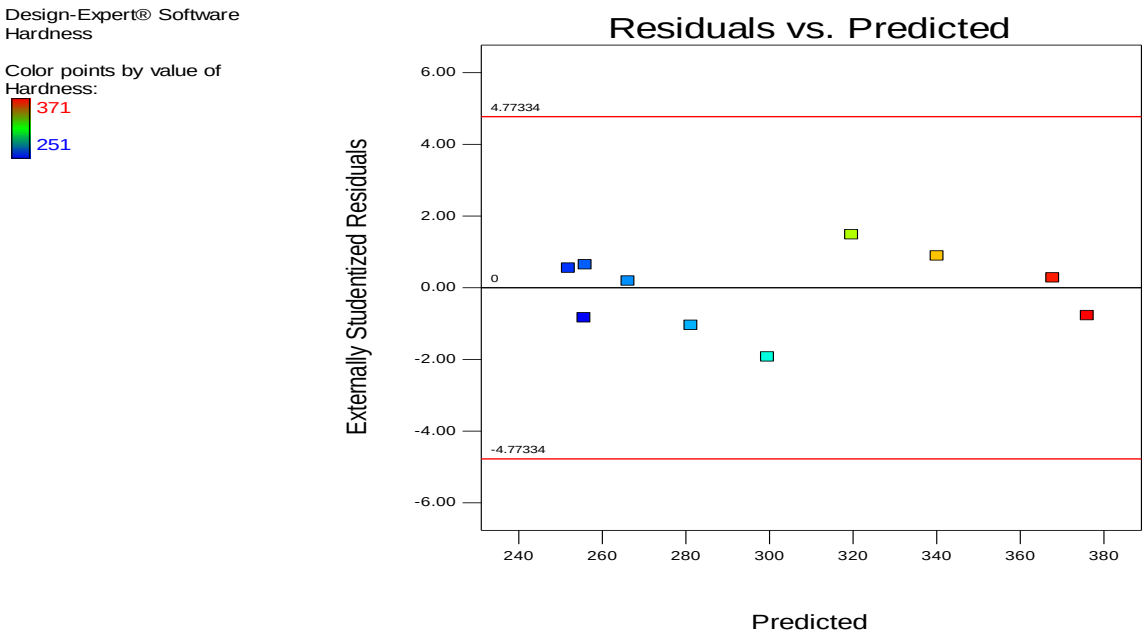

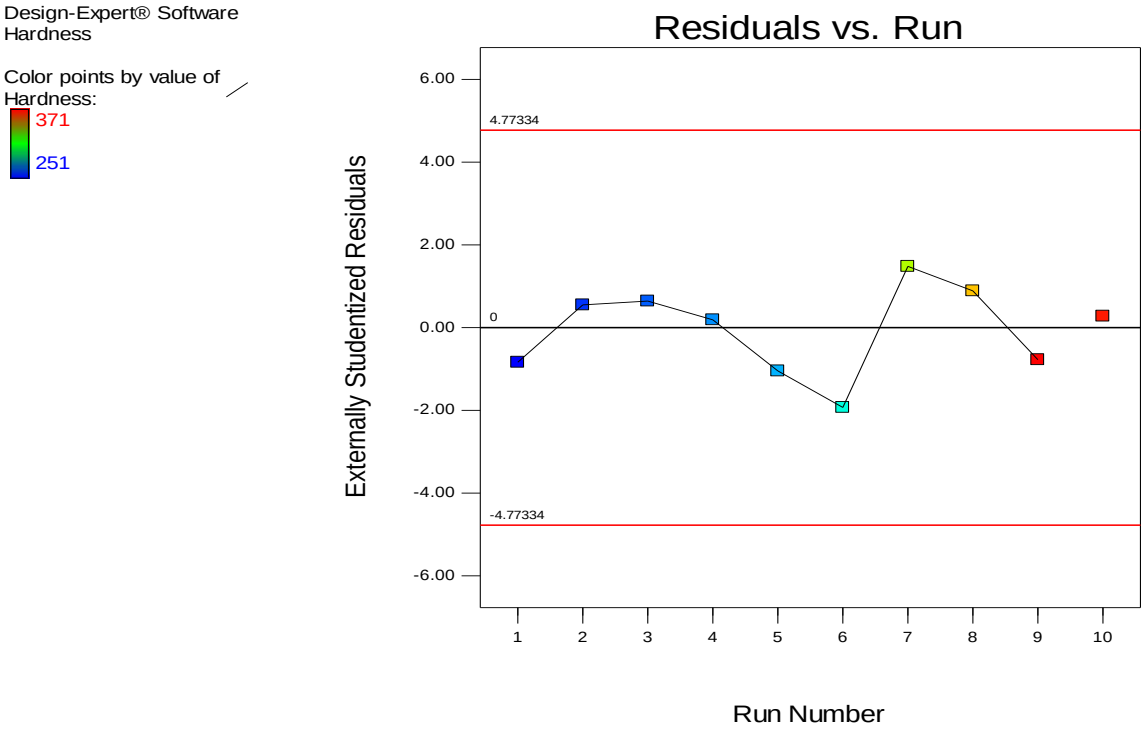
Design-Expert® Software
Hardness
Color points by value of
Hardness:
371
251
Residuals vs. Run
Externally Studentized Residuals
6.00
4.00
2.00
0.00
-2.00
-4.00
-6.00
4.77334
0
-4.77334
1
2
3
4
5
6
7
8
9
10
Run Number

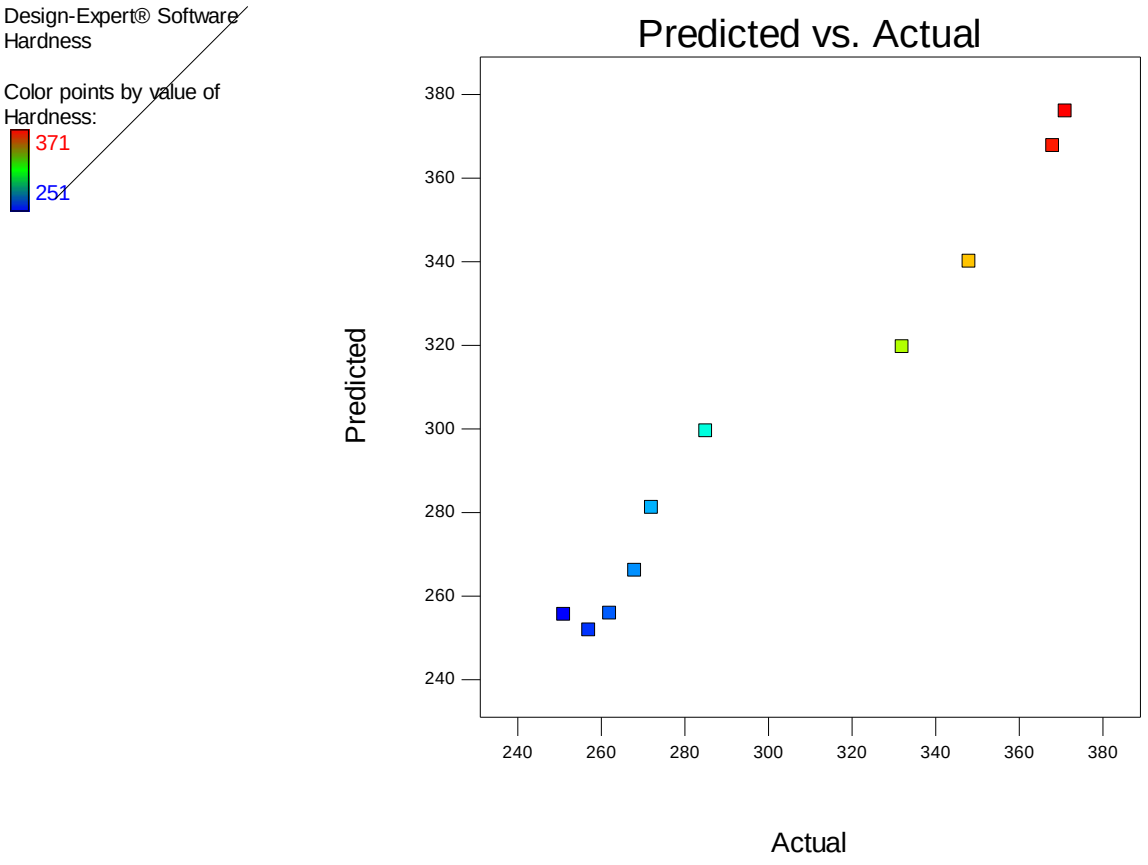
Design-Expert® Software
Hardness
Color points by value of
Hardness:
371
251
Predicted vs. Actual
Predicted
380
360
340
320
300
280
260
240
240
260
280
300
320
340
360
380
Actual

Design-Expert® Software
Hardness

Color points by value of
Hardness:
371
251

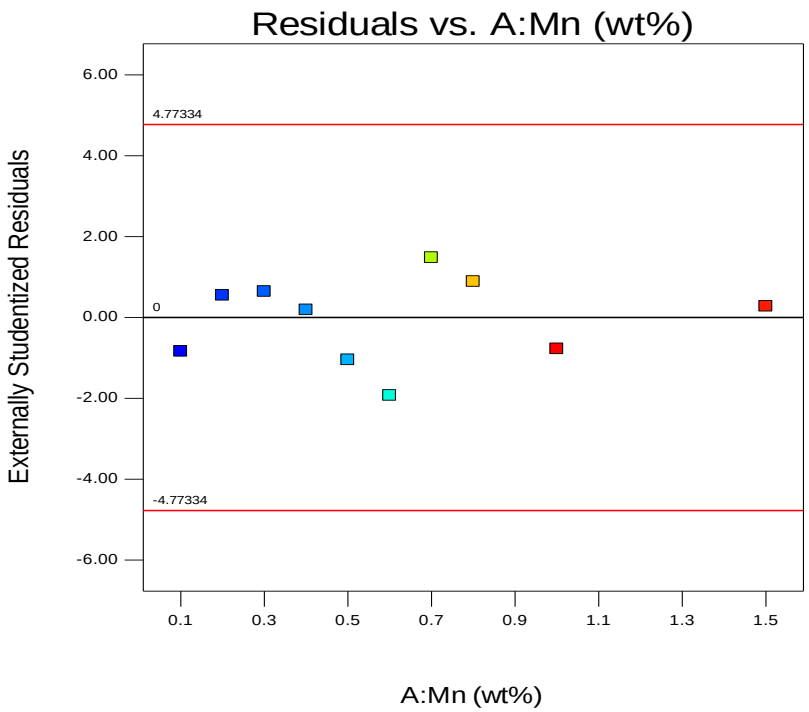

Design-Expert® Software
Factor Coding: Actual
Hardness (MPa)
Design Points
95% CI Bands

X1 = A: Mn

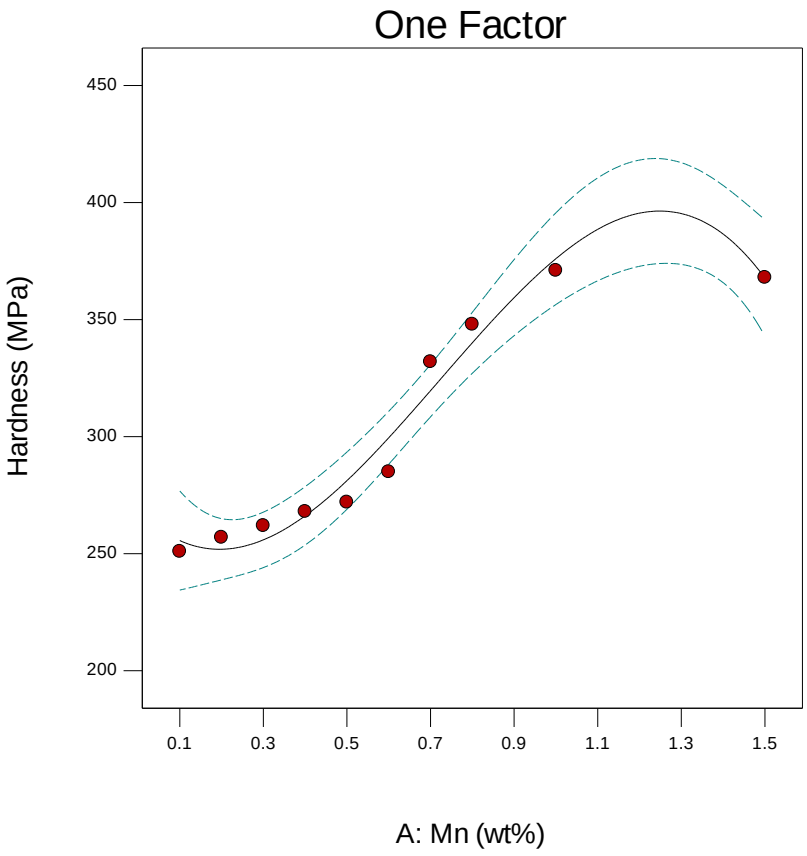

Appendix 1.5: Response 6, Electrical conductivity for n addition

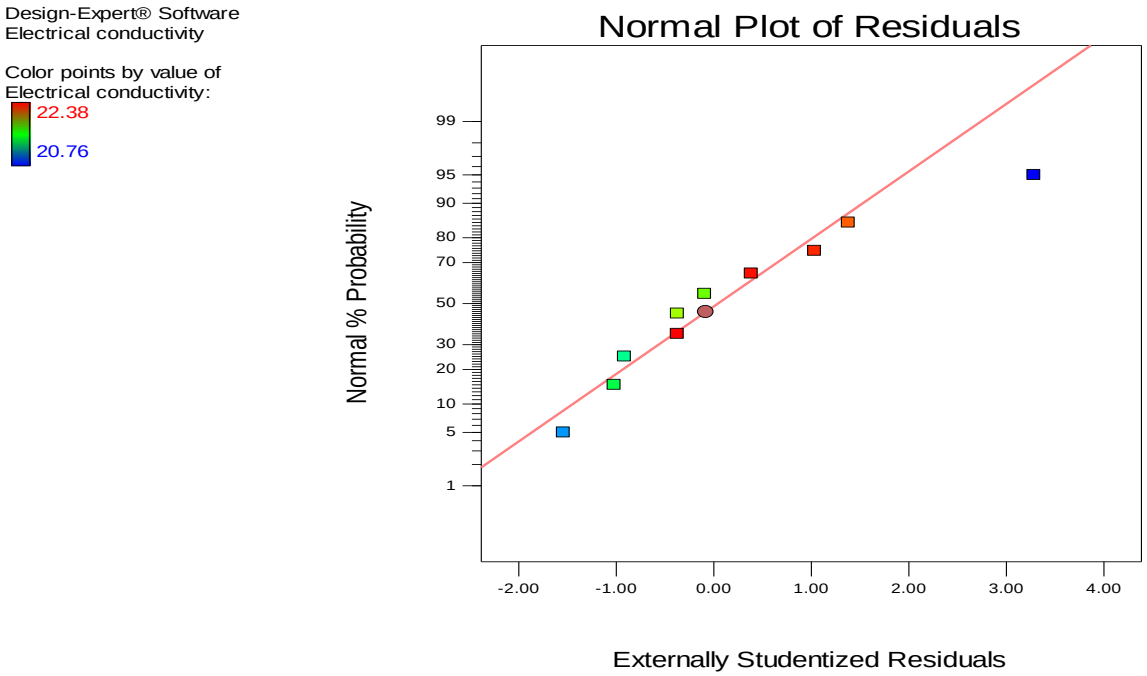

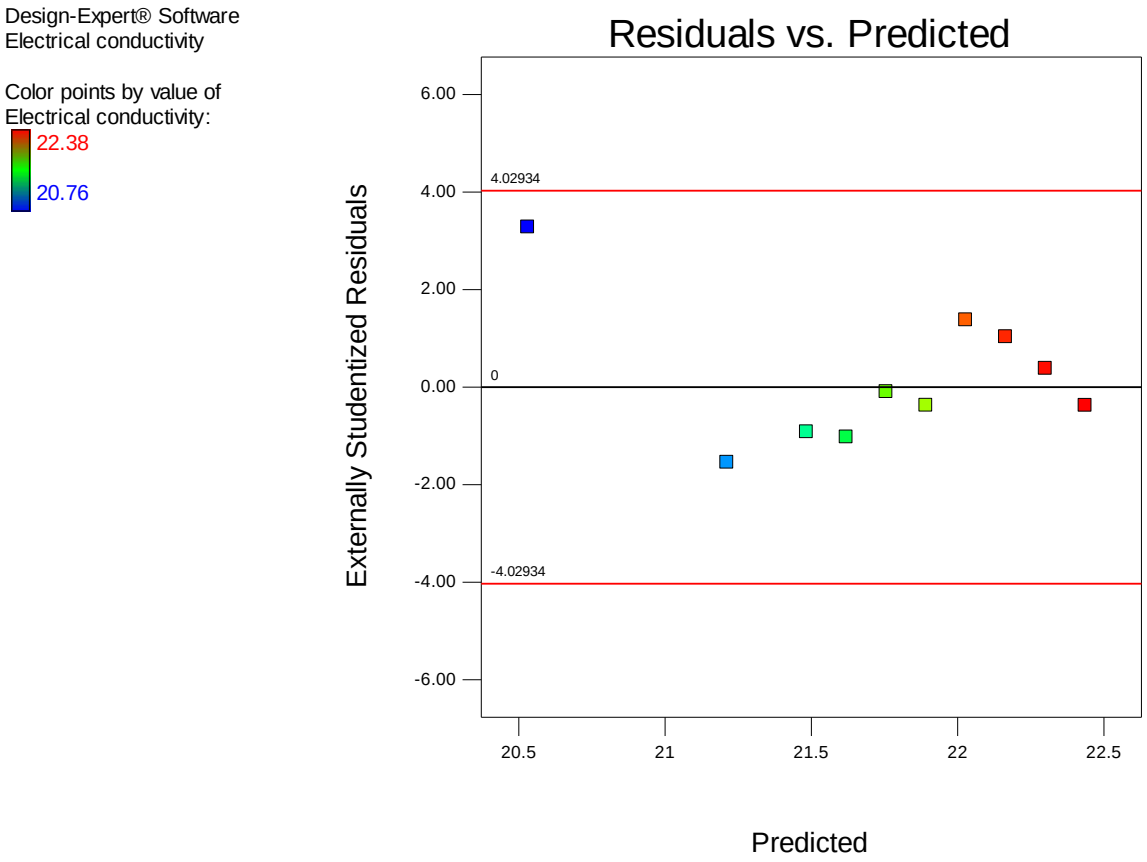

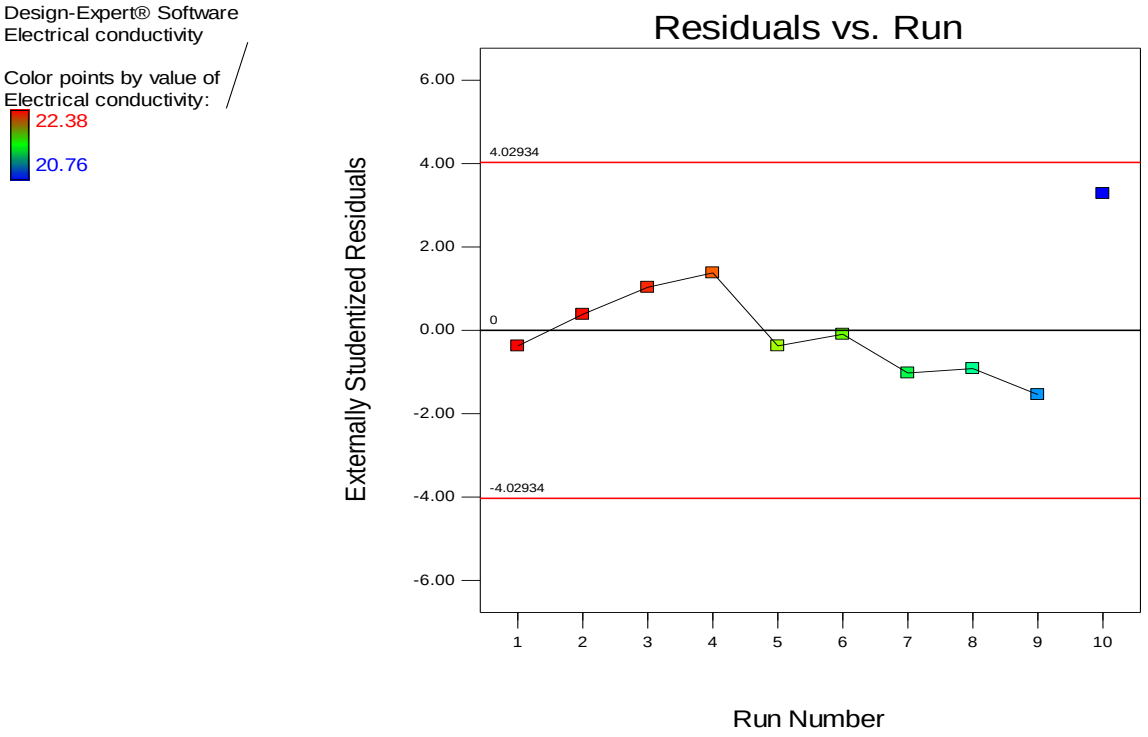
Design-Expert® Software
Electrical conductivity
Color points by value of
Electrical conductivity:
22.38
20.76
Residuals vs. Run
Externally Studentized Residuals
6.00
4.00
2.00
0.00
-2.00
-4.00
-6.00
4.02934
0
-4.02934
1
2
3
4
5
6
7
8
9
10
Run Number

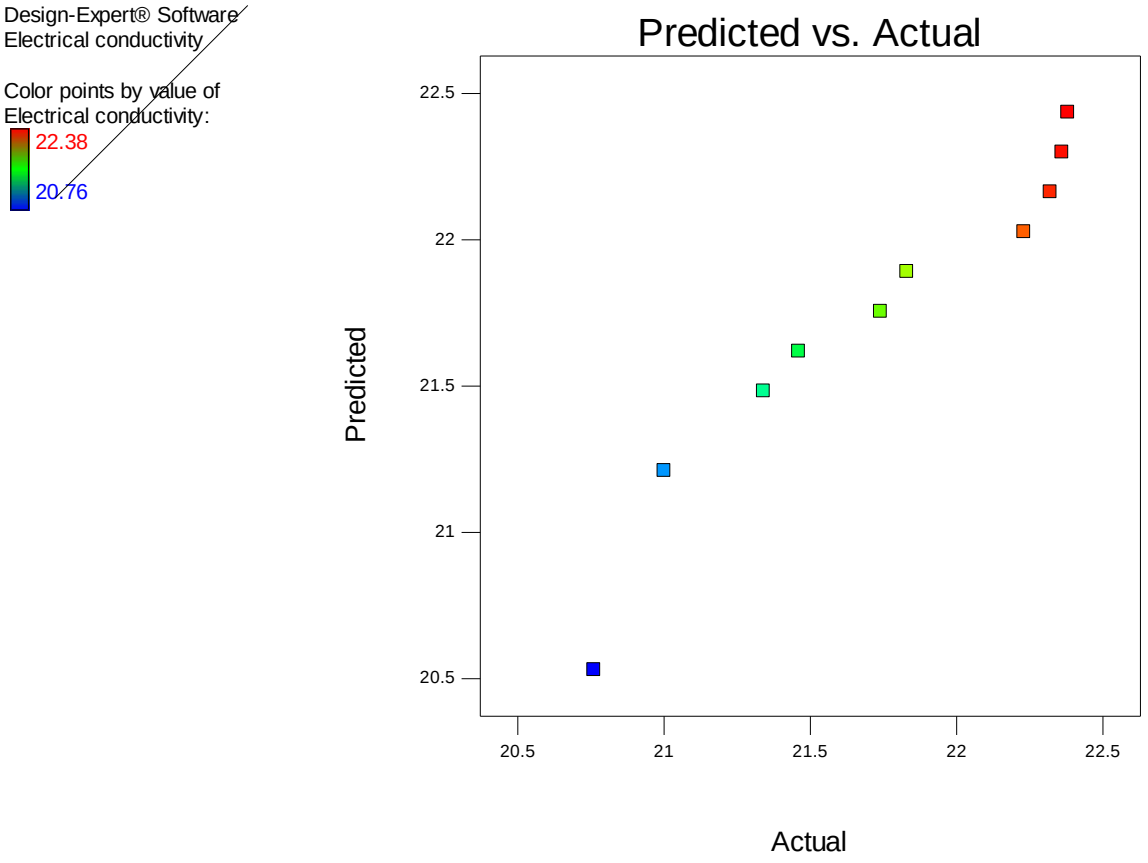
Design-Expert® Software
Electrical conductivity
Color points by value of
Electrical conductivity:
22.38
20.76
Predicted vs. Actual
Predicted
22.5
22
21.5
21
20.5
20.5
21
21.5
22
22.5
Actual

Design-Expert® Software
Electrical conductivity

Color points by value of
Electrical conductivity:
22.38
20.76

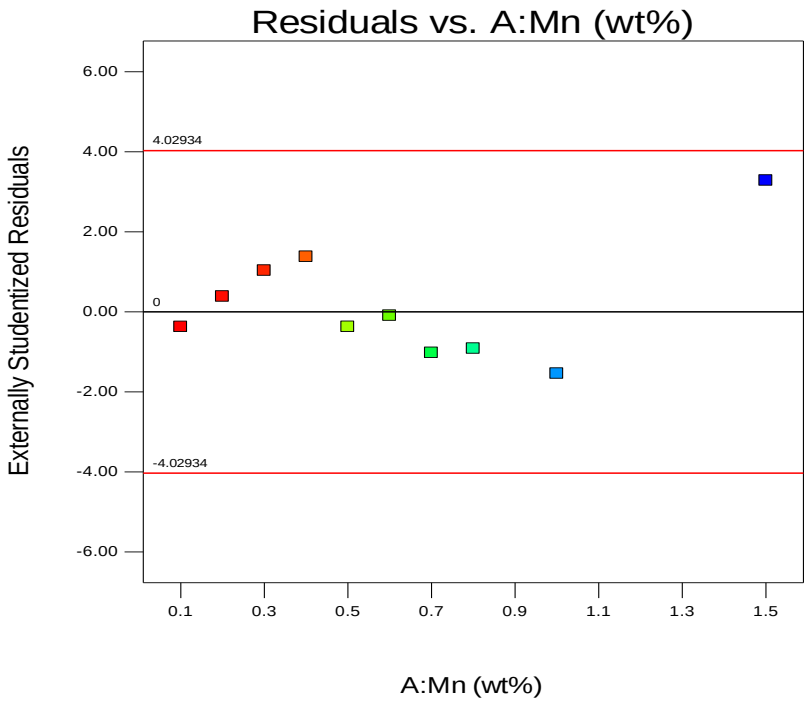

Design-Expert® Software
Factor Coding: Actual
Electrical conductivity (S/m)
Design Points
95% CI Bands

X1 = A: Mn

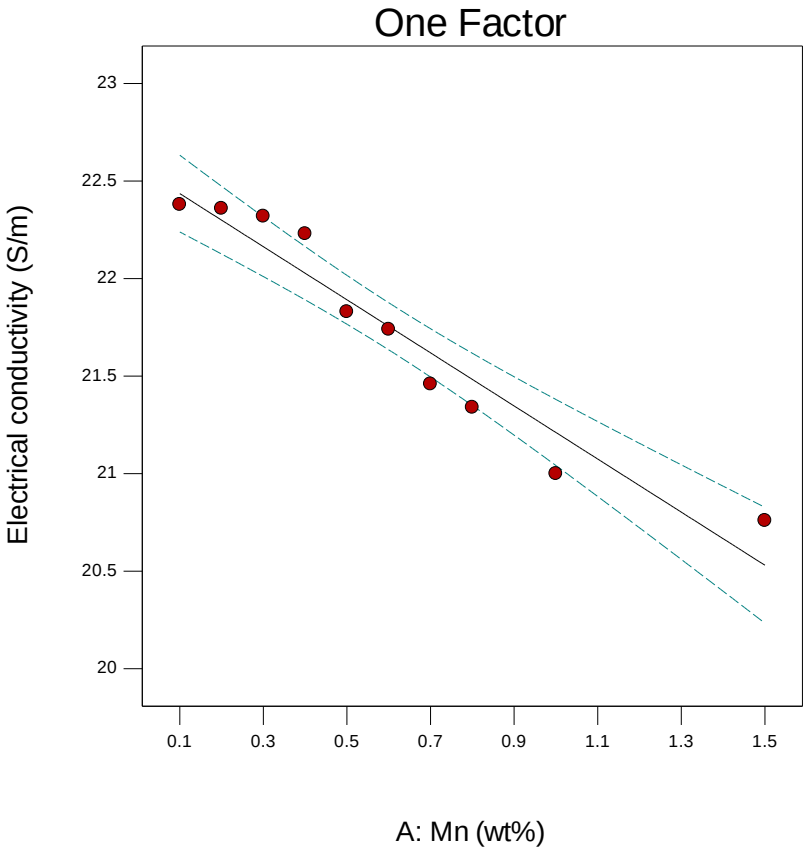

Appendix 1.6: Response 1, %E for tungsten addition

Model Summary Statistics

Source	Std. Dev.	R-Squared	Adjusted R-Squared	Predicted R-Squared	PRESS	
Linear	0.87	0.8604	0.8429	0.6119	16.67	
Quadratic	0.31	0.9845	0.9800	0.9531	2.02	Suggested
Cubic	0.33	0.9846	0.9769	-0.2527	53.80	
Quartic	0.25	0.9930	0.9873	-2.9866	171.20	
Fifth	0.25	0.9940	0.9864	-18.9245	855.64	
Sixth	0.28	0.9944	0.9831			

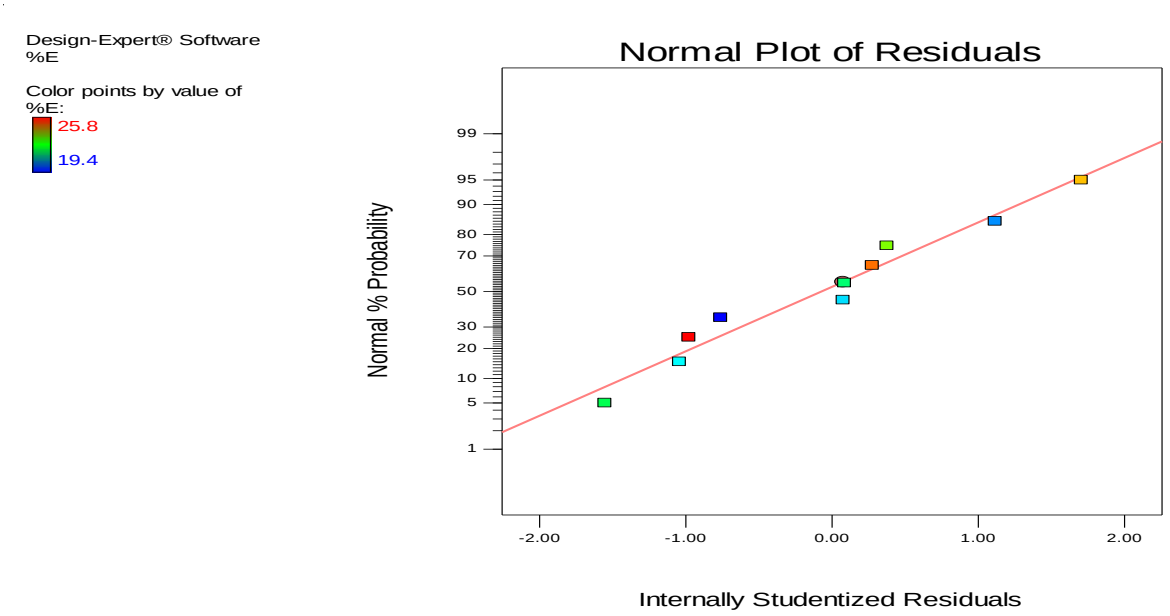

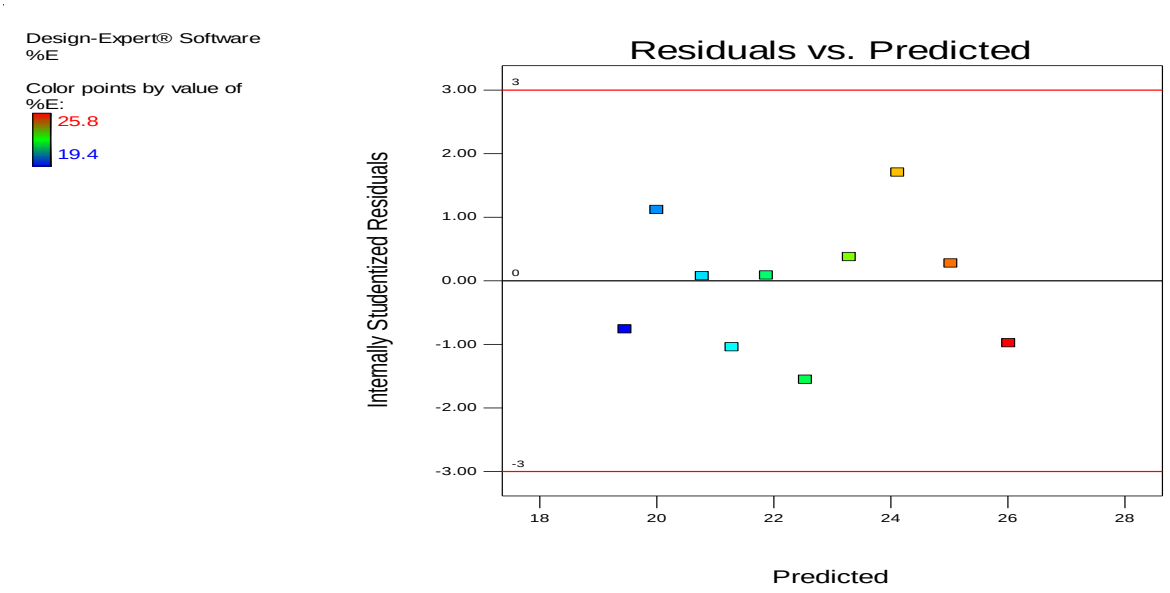

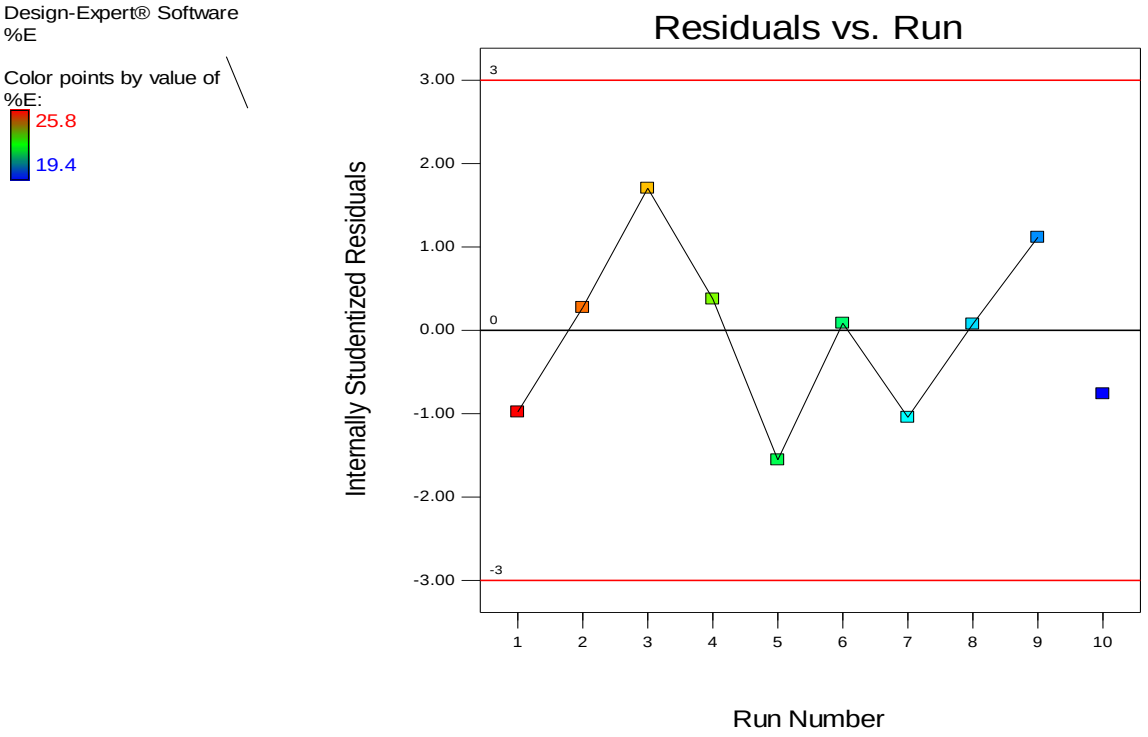
Design-Expert® Software
%E
Color points by value of
%E:
25.8
19.4
Residuals vs. Run
Internally Studentized Residuals
3.00
2.00
1.00
0.00
-1.00
-2.00
-3.00
3
0
-3
1
2
3
4
5
6
7
8
9
10
Run Number

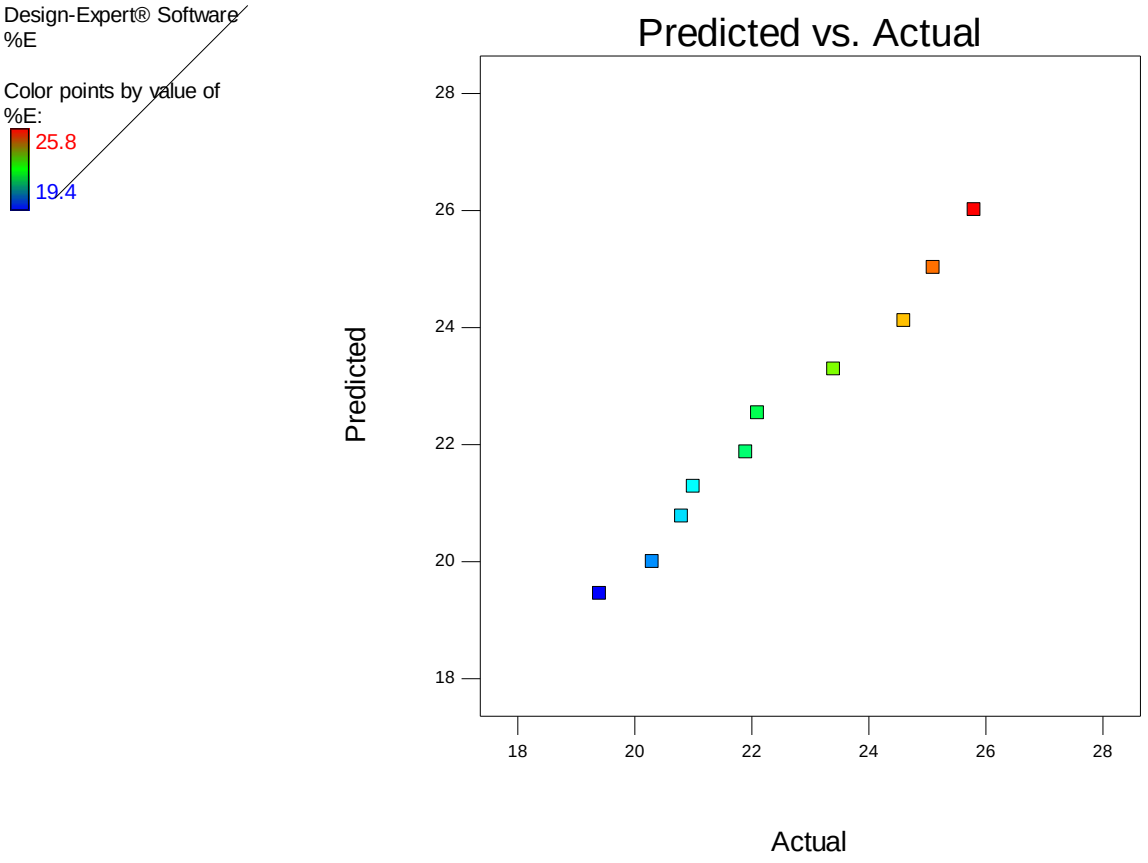
Design-Expert® Software
%E
Color points by value of
%E:
25.8
19.4
Predicted vs. Actual
Predicted
28
26
24
22
20
18
18
20
22
24
26
28
Actual

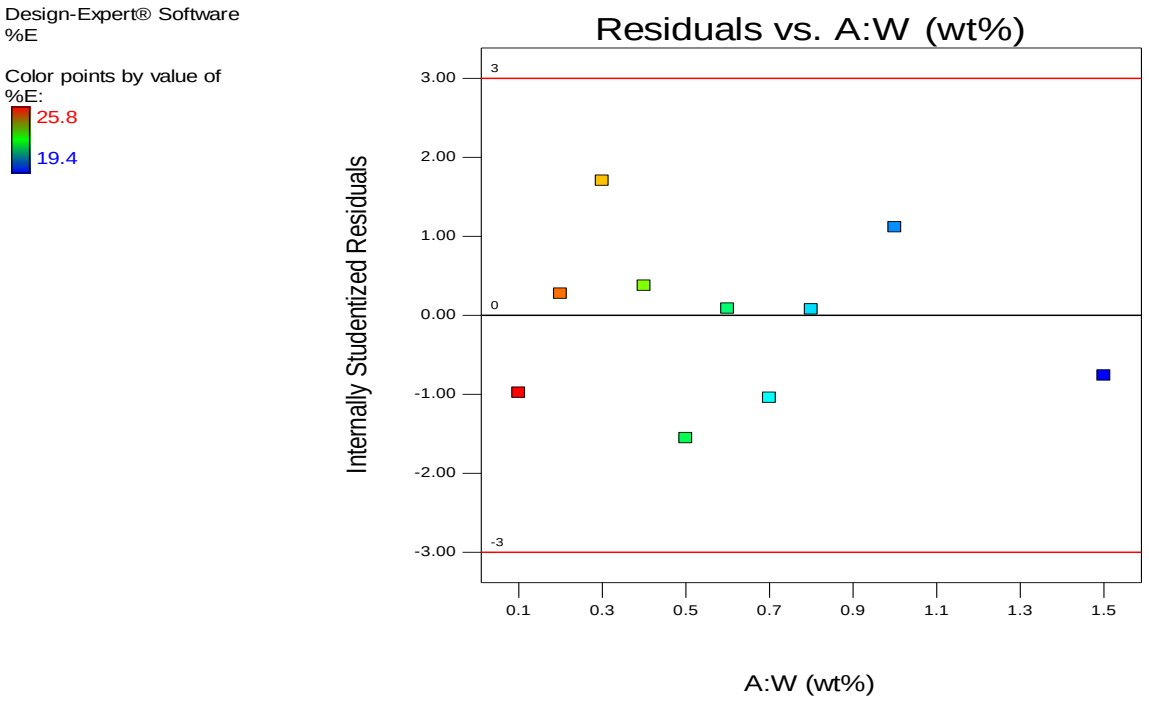
Design-Expert® Software
%E
Color points by value of
%E:
25.8
19.4
Residuals vs. A:W (wt%)
Internally Studentized Residuals
3.00
2.00
1.00
0.00
-1.00
-2.00
-3.00
3
0
-3
0.1
0.3
0.5
0.7
0.9
1.1
1.3
1.5
A:W (wt%)

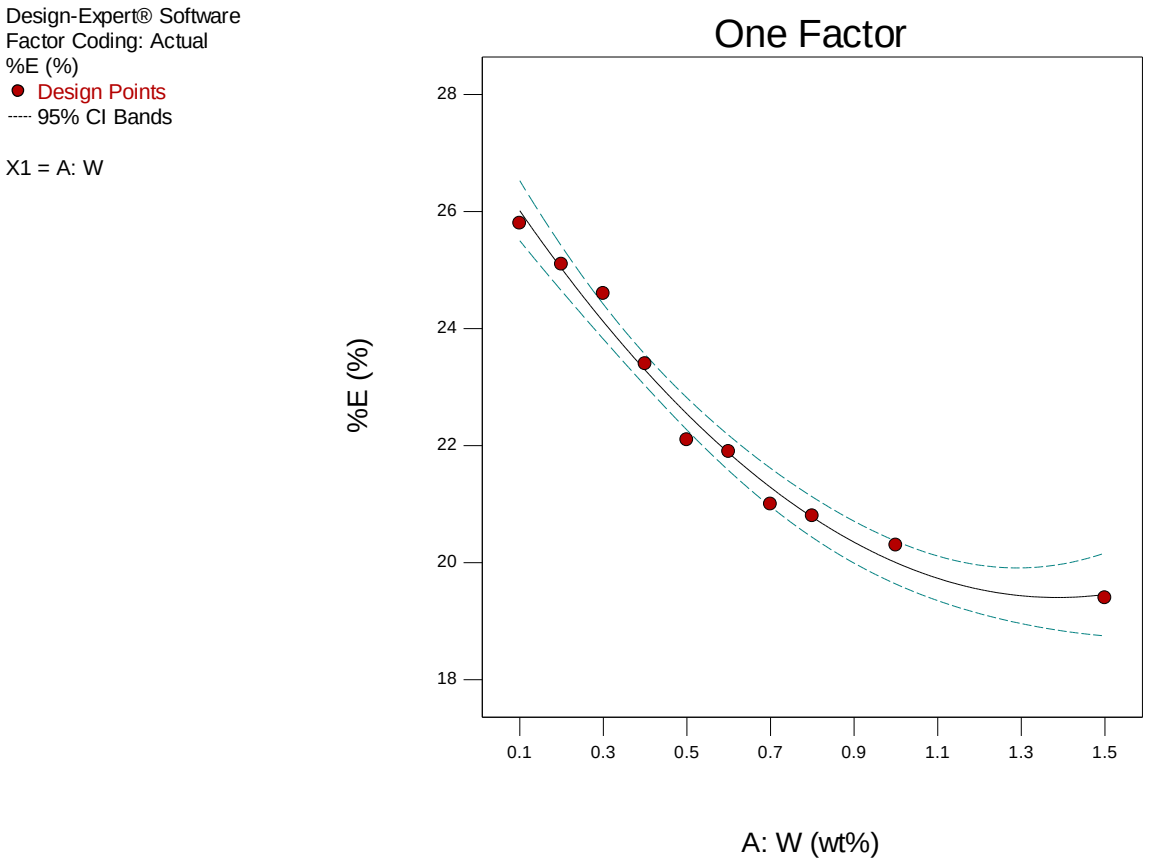
Design-Expert® Software
Factor Coding: Actual
%E (%)
Design Points
95% CI Bands
X1 = A: W
One Factor
%E (%)
28
26
24
22
20
18
0.1
0.3
0.5
0.7
0.9
1.1
1.3
1.5
A: W (wt%)

Appendix 1.7: Response 6, Electrical conductivity for tungsten addition

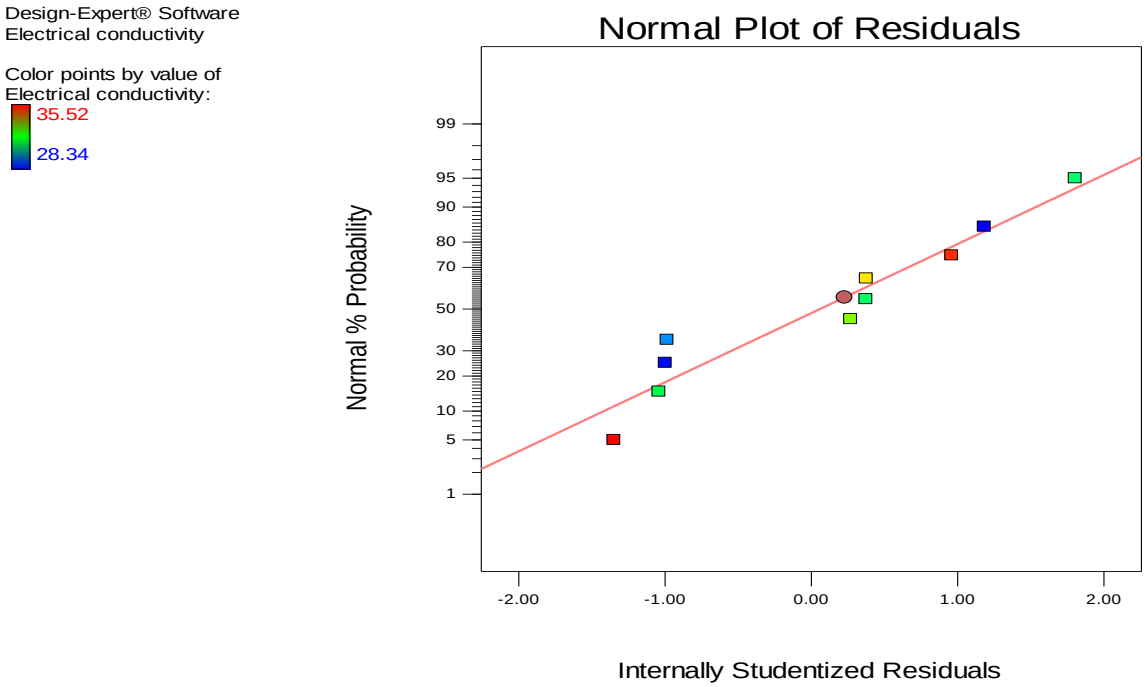

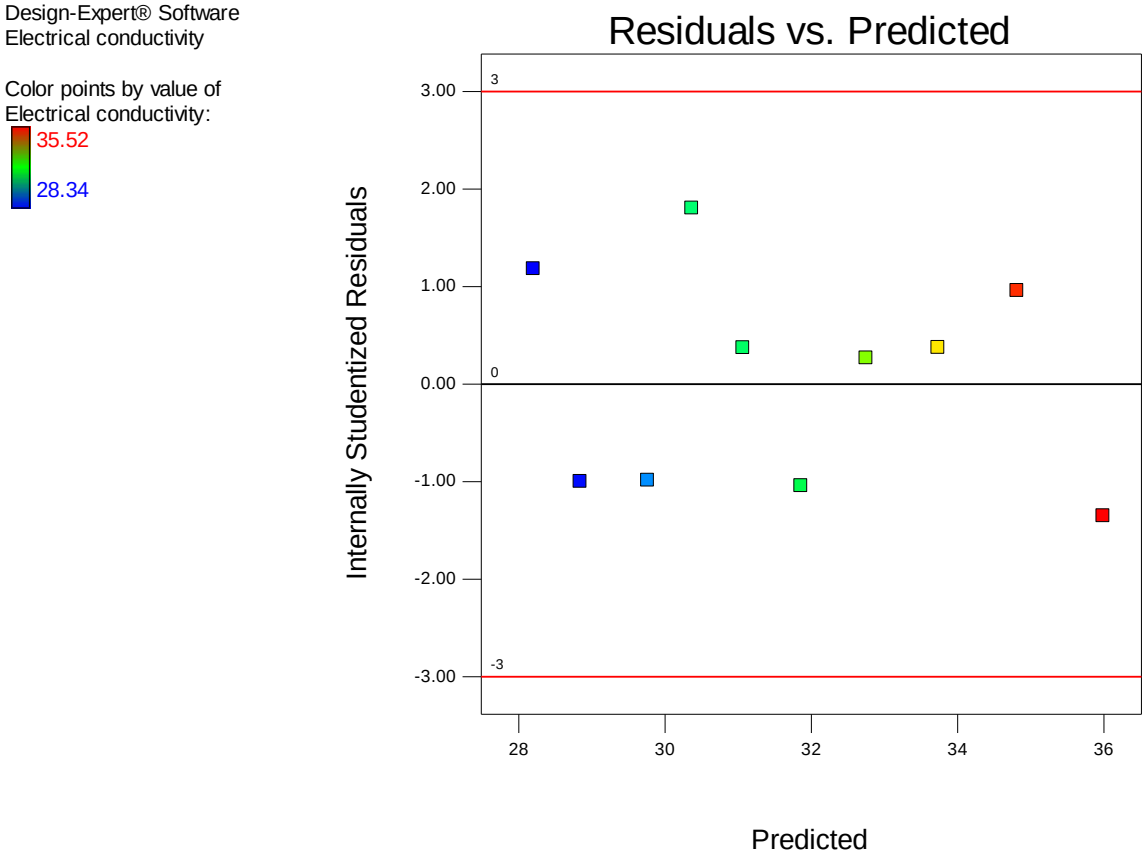

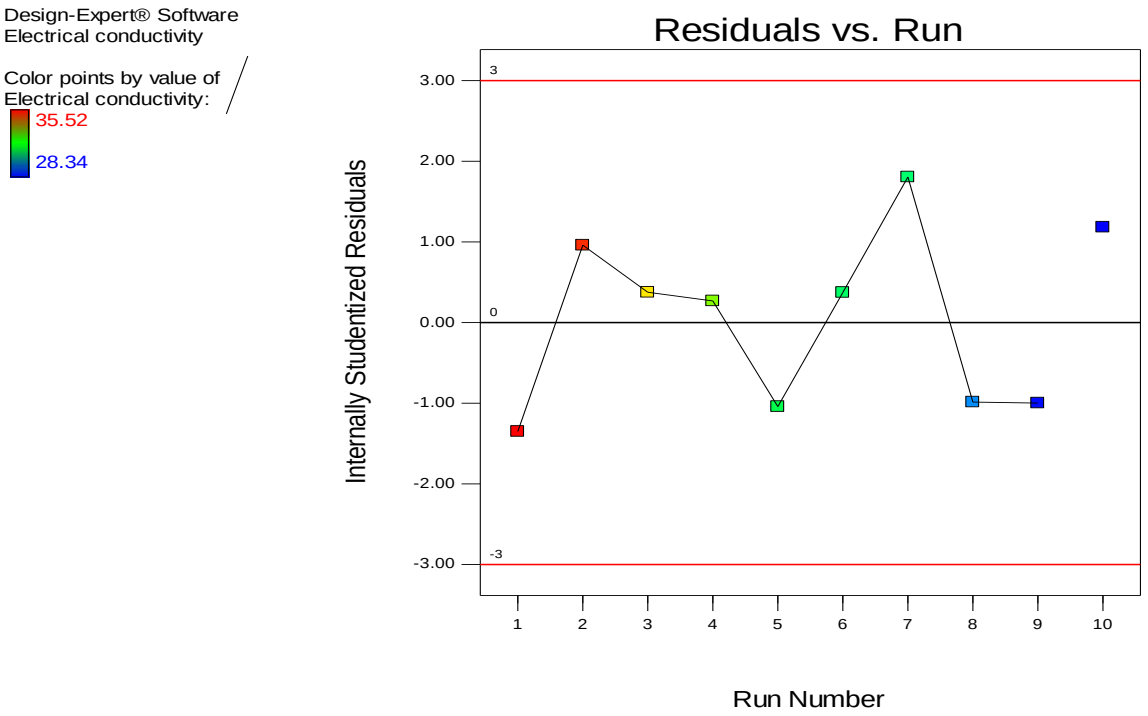
Design-Expert® Software
Electrical conductivity
Color points by value of
Electrical conductivity:
35.52
28.34
Residuals vs. Run
Internally Studentized Residuals
3.00
2.00
1.00
0.00
-1.00
-2.00
-3.00
3
0
-3
1
2
3
4
5
6
7
8
9
10
Run Number

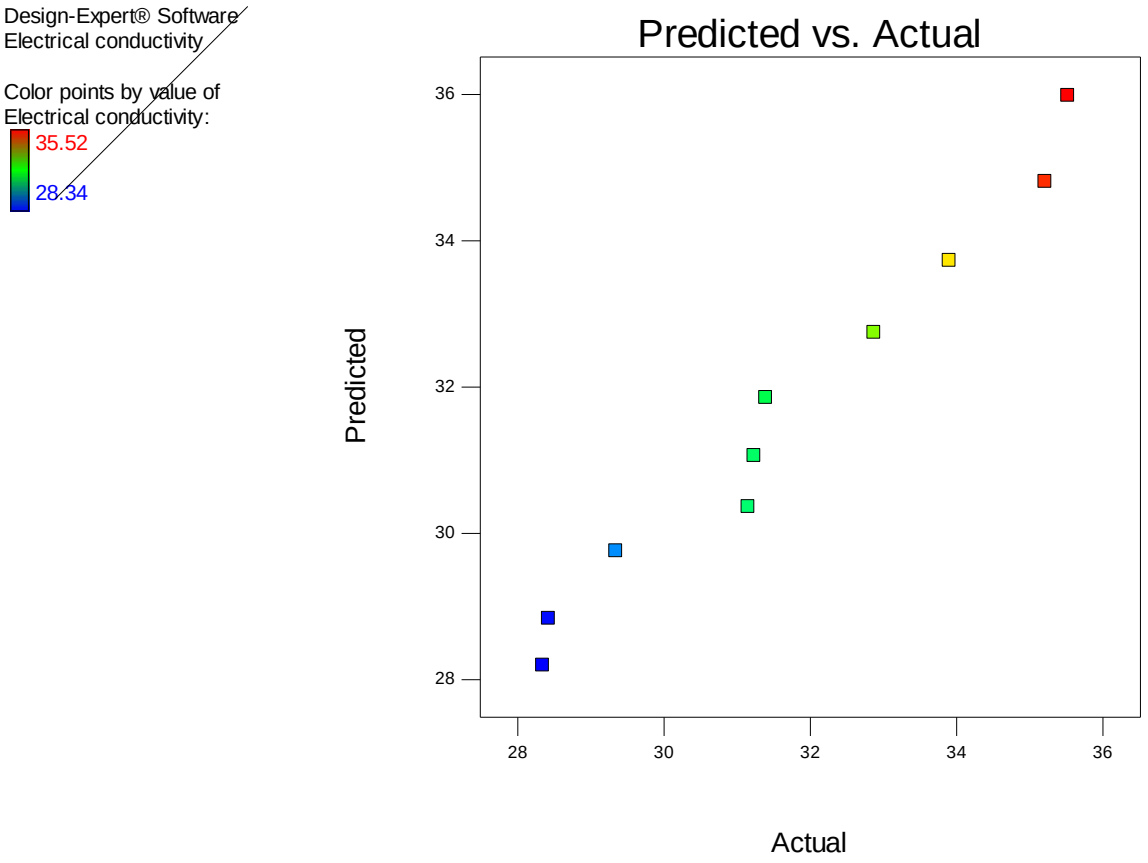
Design-Expert® Software
Electrical conductivity
Color points by value of
Electrical conductivity:
35.52
28.34
Predicted vs. Actual
Predicted
36
34
32
30
28
28
30
32
34
36
Actual

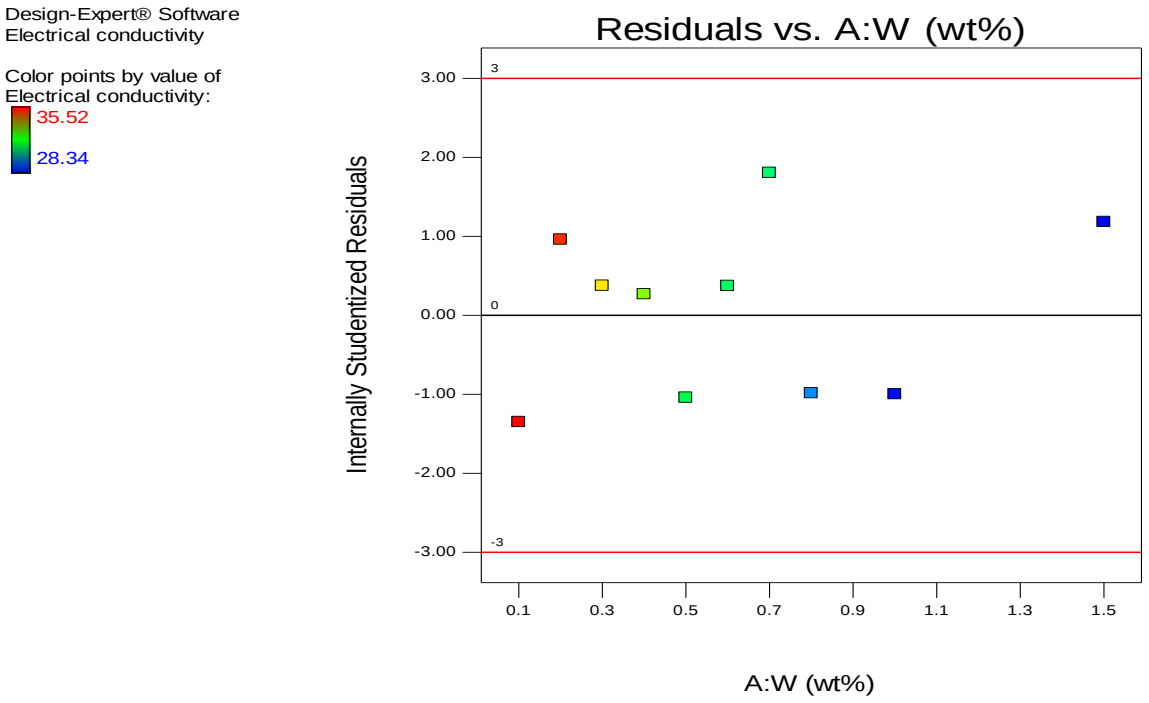
Design-Expert® Software
Electrical conductivity
Color points by value of
Electrical conductivity:
35.52
28.34
Residuals vs. A:W (wt%)
Internally Studentized Residuals
3.00
2.00
1.00
0.00
-1.00
-2.00
-3.00
3
0
-3
0.1
0.3
0.5
0.7
0.9
1.1
1.3
1.5
A:W (wt%)

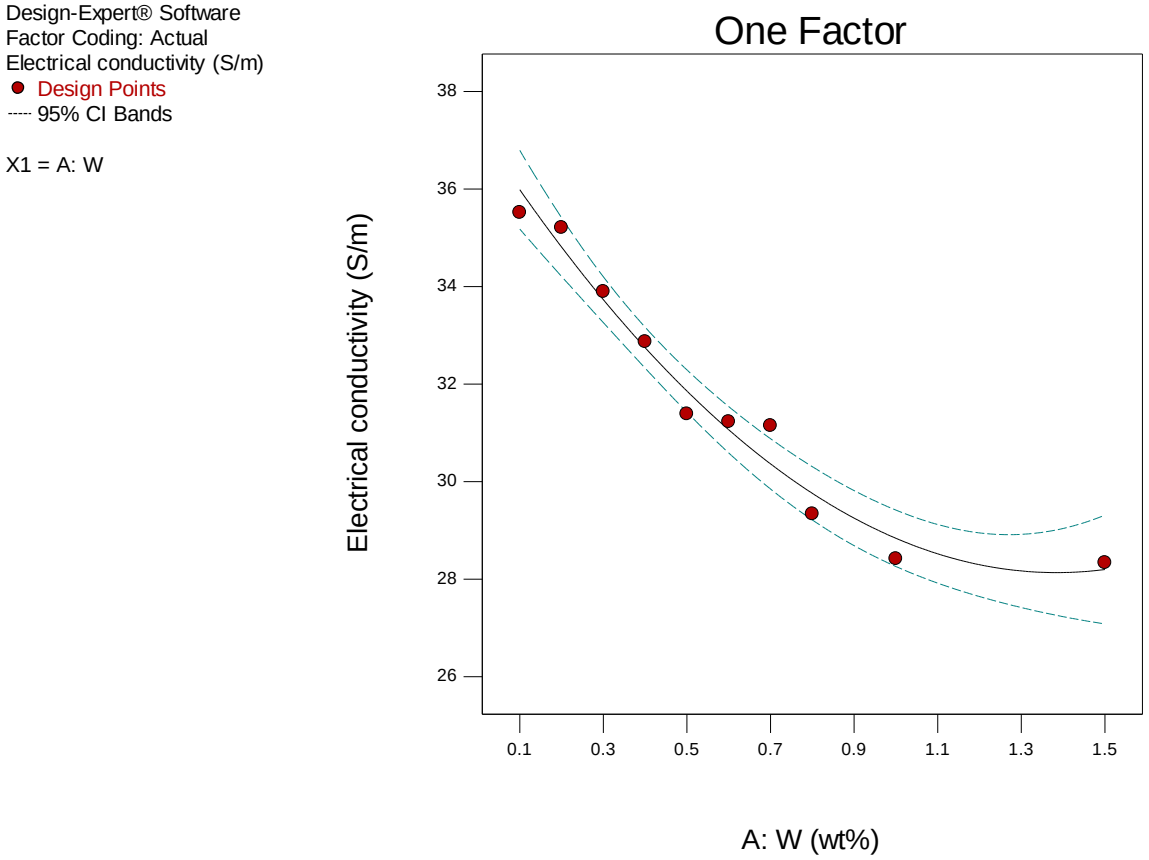
Design-Expert® Software
Factor Coding: Actual
Electrical conductivity (S/m)
Design Points
95% CI Bands
X1 = A: W
One Factor
Electrical conductivity (S/m)
38
36
34
32
30
28
26
0.1
0.3
0.5
0.7
0.9
1.1
1.3
1.5
A: W (wt%)

Appendix 1.8: Response 6, Electrical conductivity for titanium addition

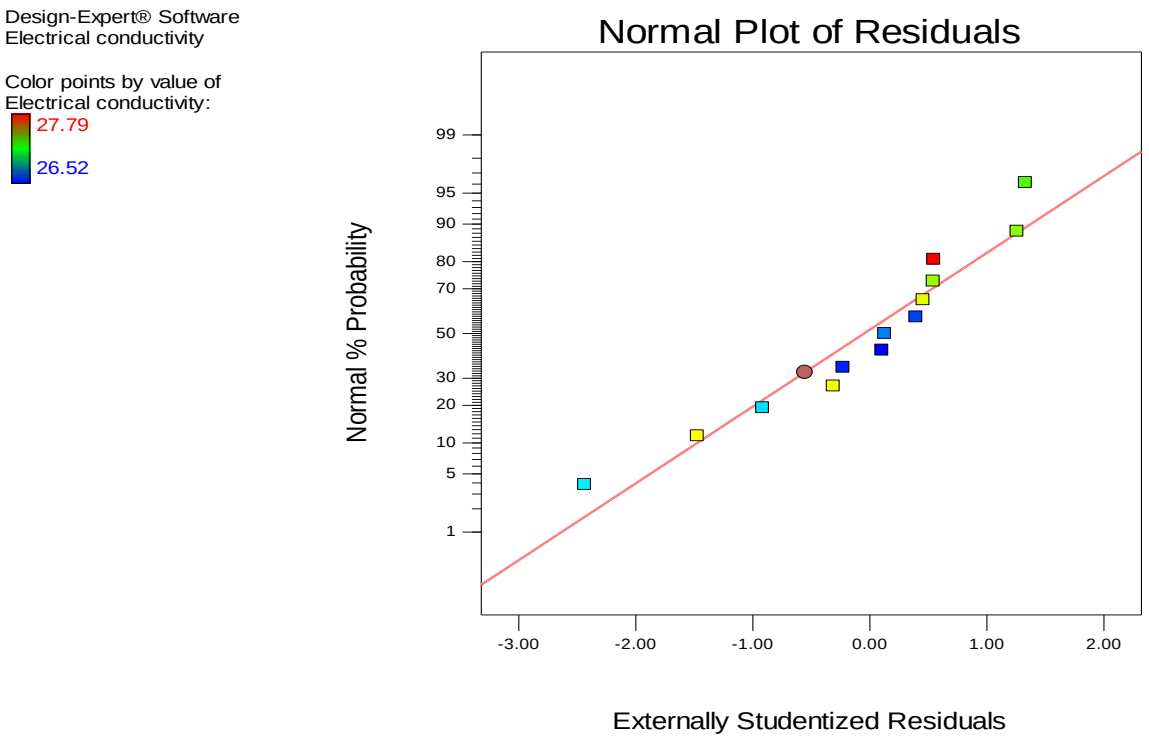

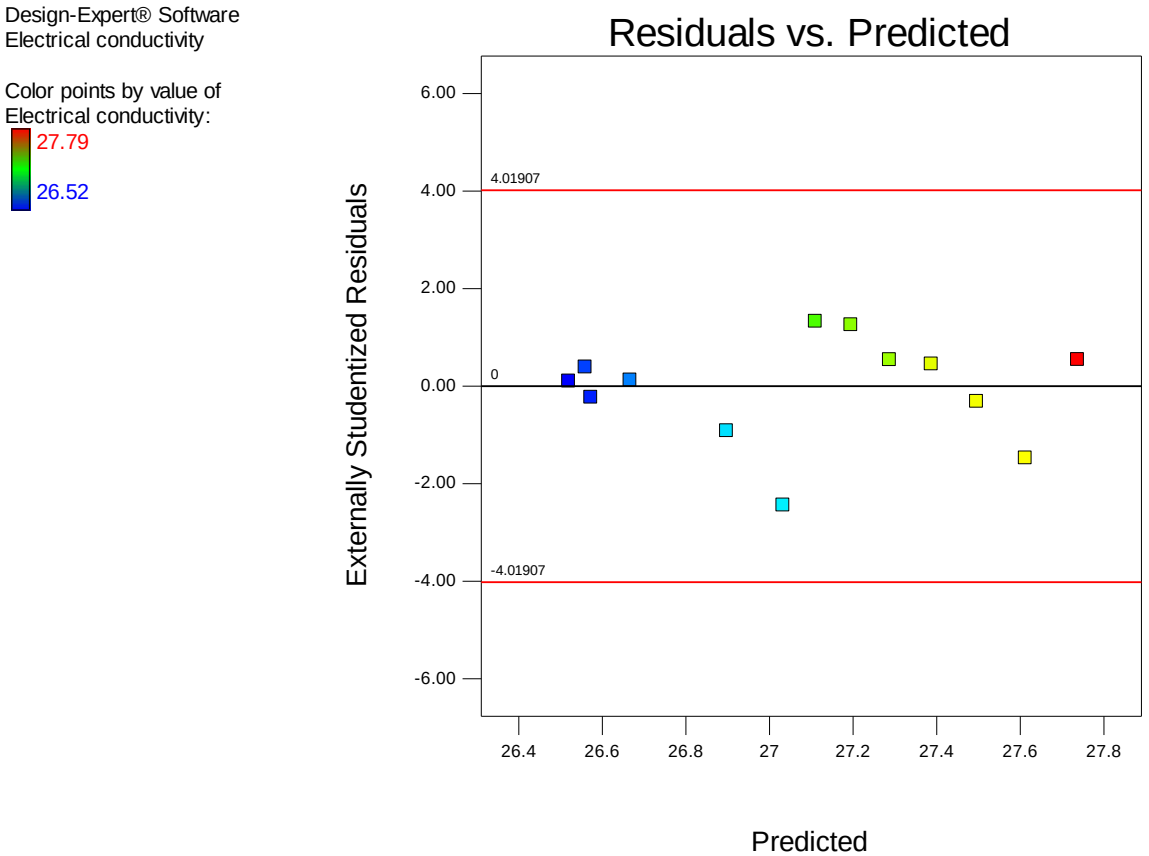

Design-Expert® Software
Electrical conductivity

Color points by value of
Electrical conductivity:
27.79
26.52

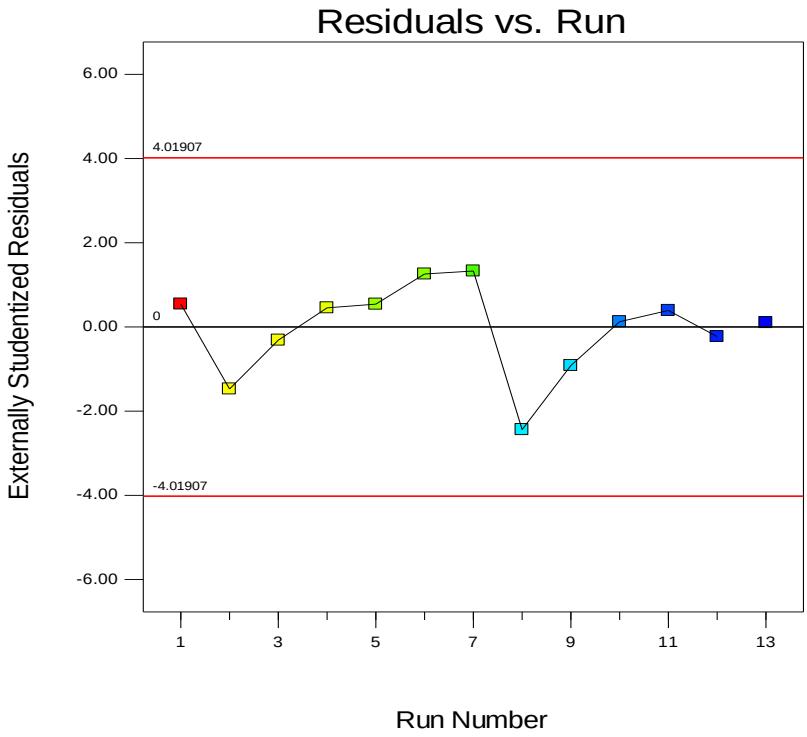

Design-Expert® Software
Electrical conductivity

Color points by value of
Electrical conductivity:
27.79
26.52

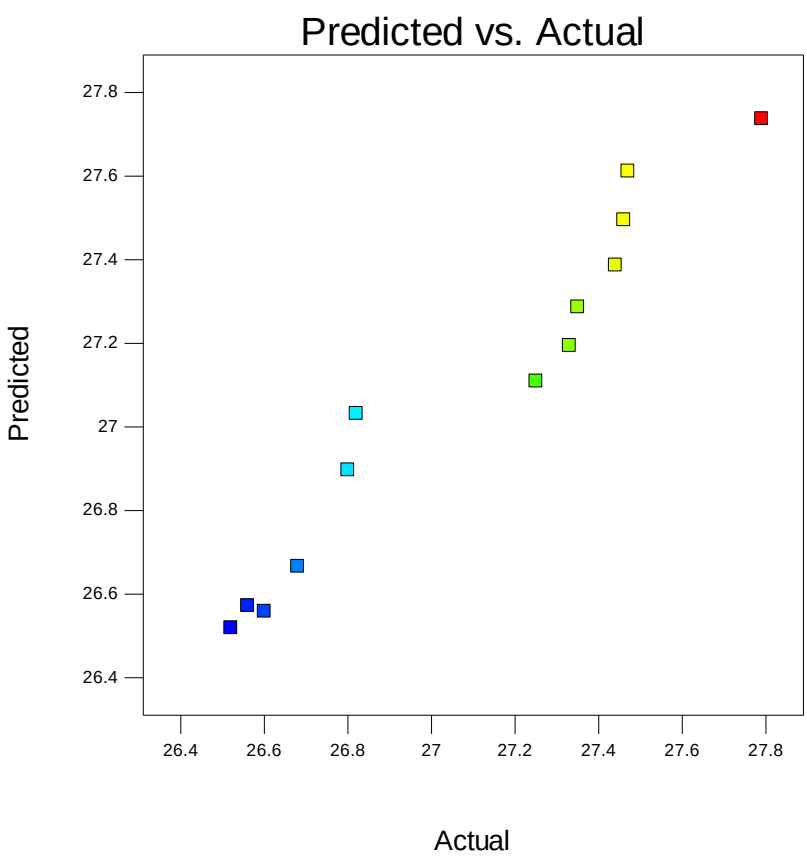

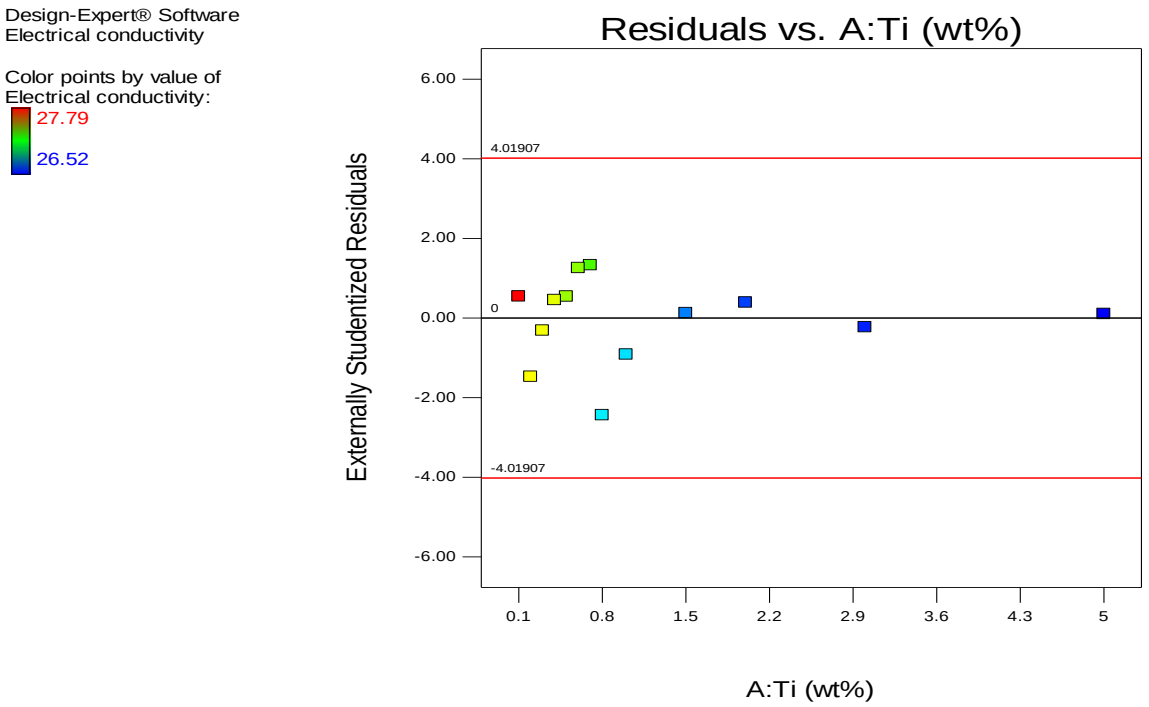
Design-Expert® Software
Electrical conductivity
Color points by value of
Electrical conductivity:
27.79
26.52
Residuals vs. A:Ti (wt%)
Externally Studentized Residuals
6.00
4.00
2.00
0.00
-2.00
-4.00
-6.00
4.01907
0
-4.01907
0.1
0.8
1.5
2.2
2.9
3.6
4.3
5
A:Ti (wt%)

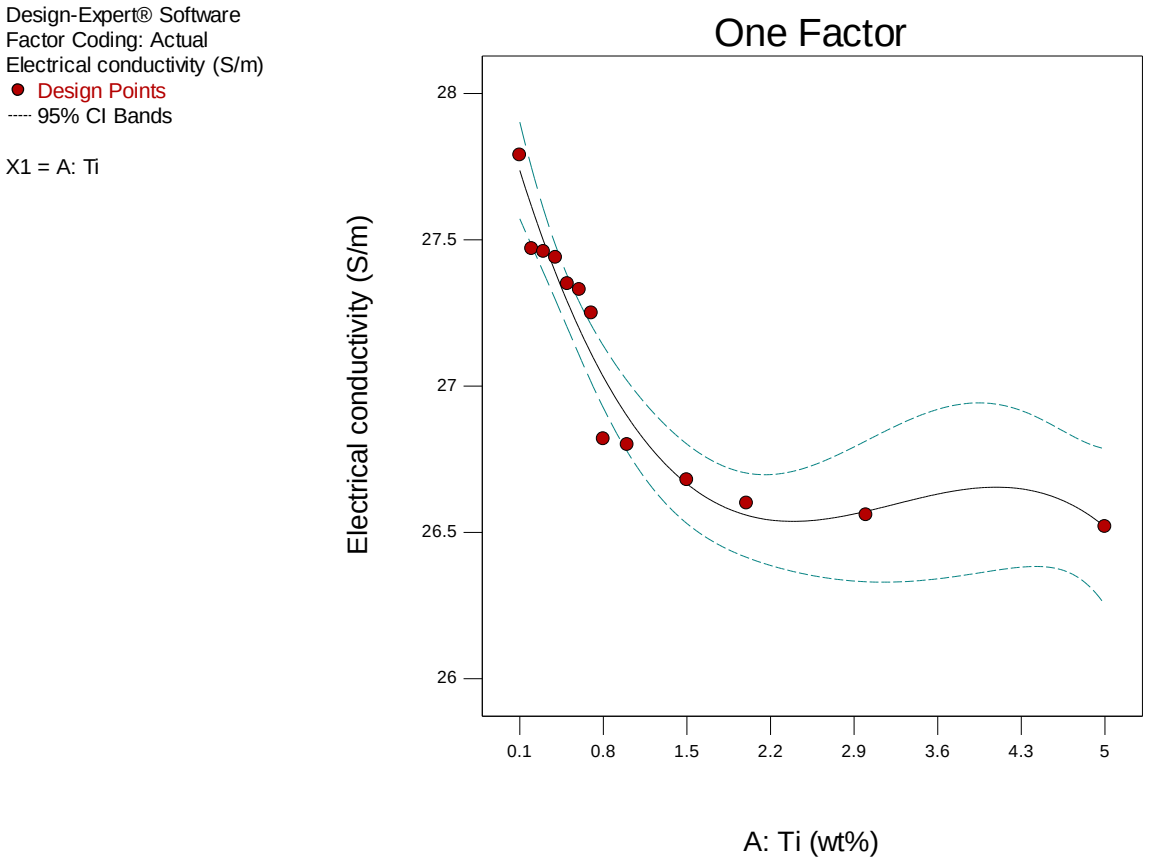
Design-Expert® Software
Factor Coding: Actual
Electrical conductivity (S/m)
Design Points
95% CI Bands
X1 = A: Ti
One Factor
Electrical conductivity (S/m)
28
27.5
27
26.5
26
0.1
0.8
1.5
2.2
2.9
3.6
4.3
5
A: Ti (wt%)

Appendix 1.9: Response 1, %E for molybdenum addition

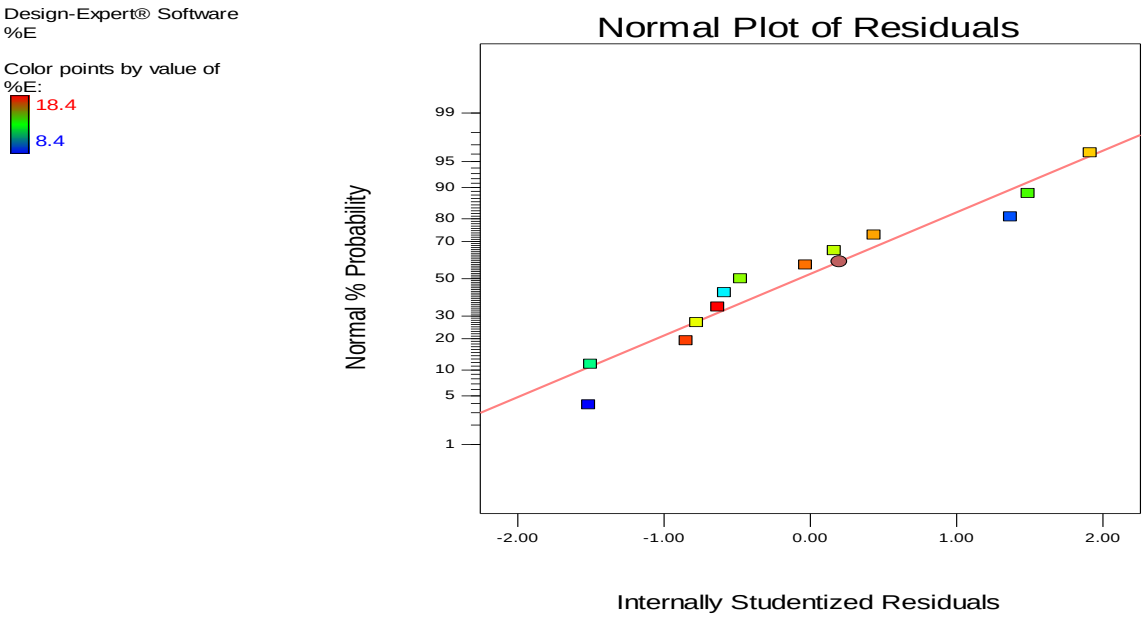

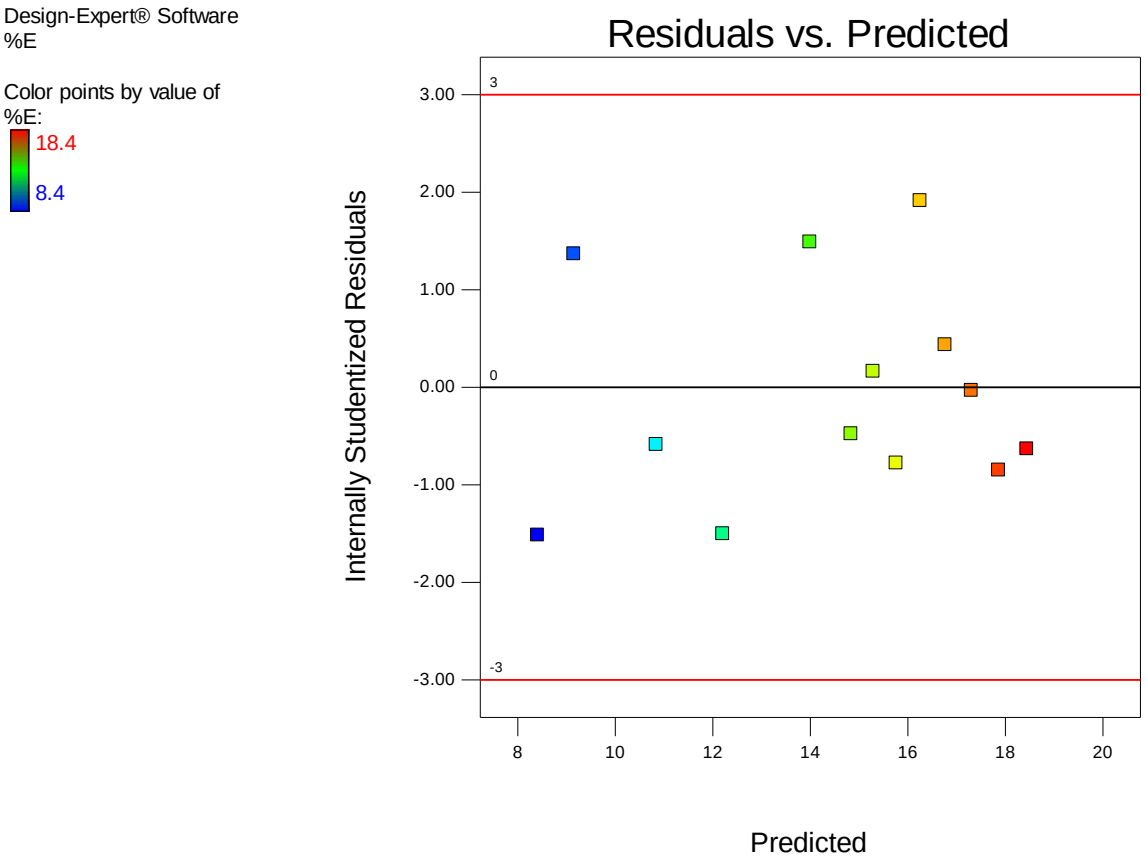

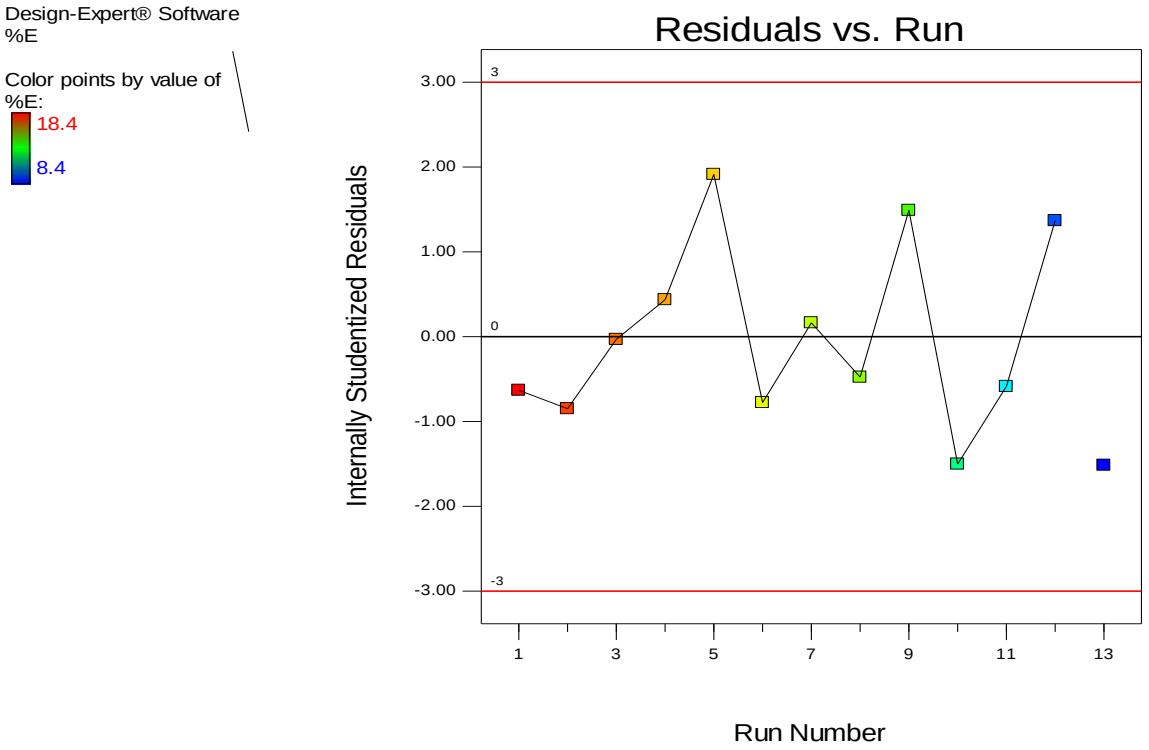
Design-Expert® Software
%E
Color points by value of
%E:
18.4
8.4
Residuals vs. Run
Internally Studentized Residuals
3.00
2.00
1.00
0.00
-1.00
-2.00
-3.00
3
0
-3
1
3
5
7
9
11
13
Run Number

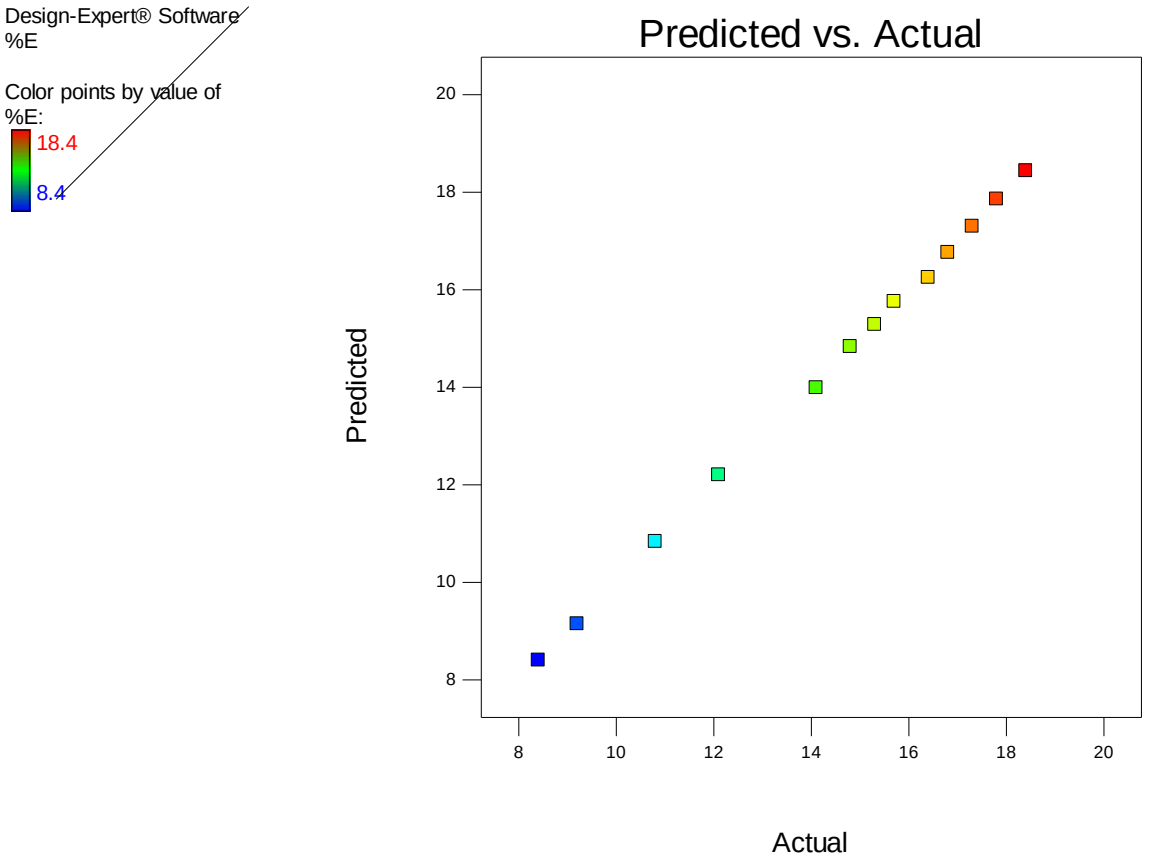
Design-Expert® Software
%E
Color points by value of
%E:
18.4
8.4
Predicted vs. Actual
Predicted
20
18
16
14
12
10
8
8
10
12
14
16
18
20
Actual

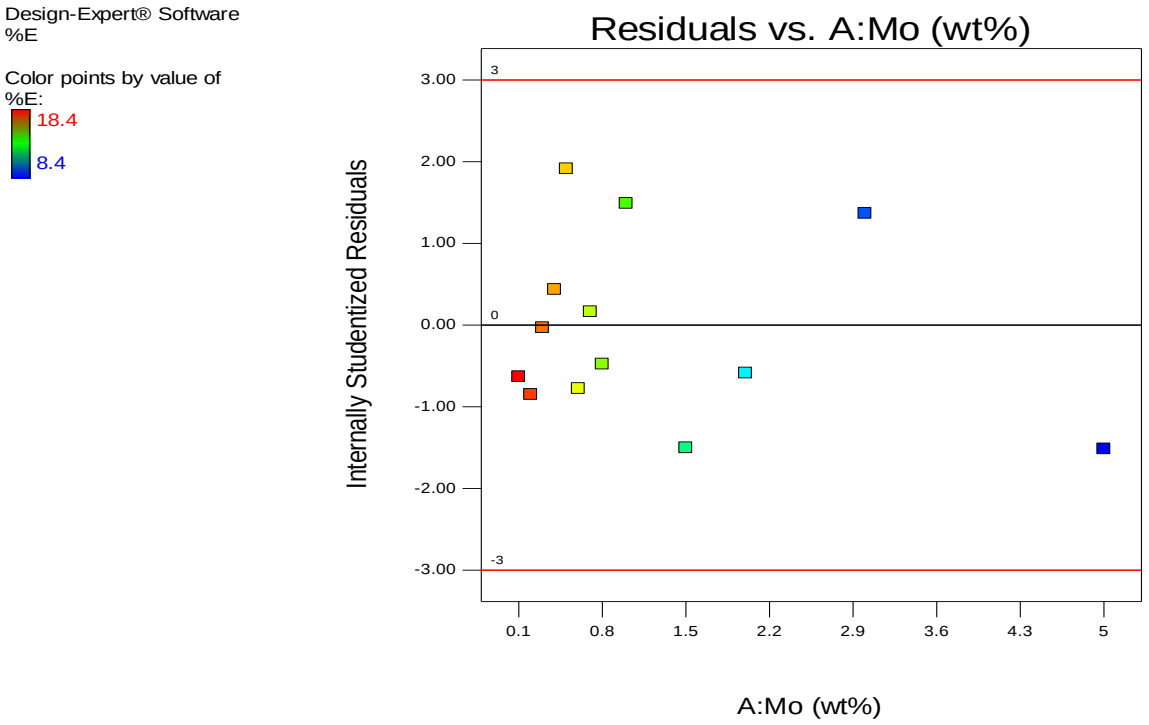
Design-Expert® Software
%E
Color points by value of
%E:
18.4
8.4
Residuals vs. A:Mo (wt%)
Internally Studentized Residuals
3.00
2.00
1.00
0.00
-1.00
-2.00
-3.00
3
0
-3
0.1
0.8
1.5
2.2
2.9
3.6
4.3
5
A:Mo (wt%)

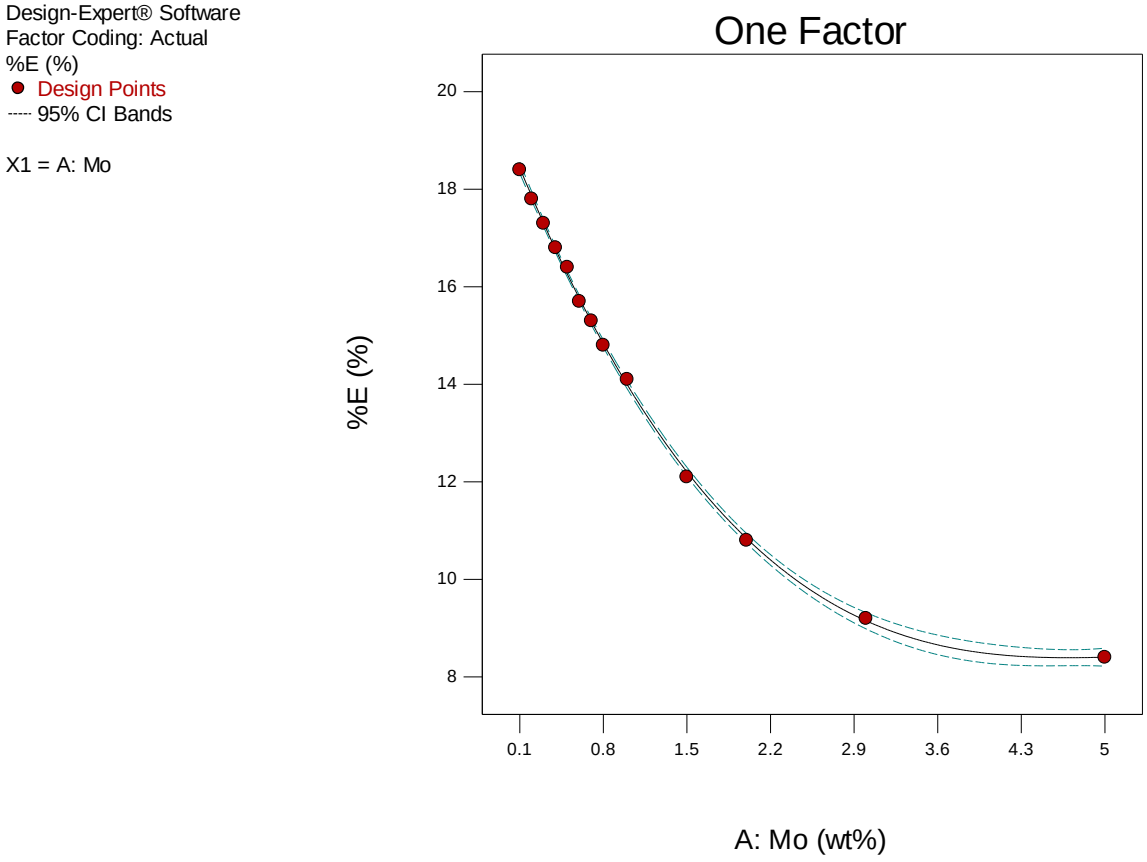
Design-Expert® Software
Factor Coding: Actual
%E (%)
Design Points
95% CI Bands
X1 = A: Mo
One Factor
%E (%)
20
18
16
14
12
10
8
0.1
0.8
1.5
2.2
2.9
3.6
4.3
5
A: Mo (wt%)

Appendix 2: Summary of solution of optimization

Appendix 2.1: Titanium addition

Number	Ti	%E	UTS	Hardness	Impact Strength	Electrical resistivity	Electrical conductivity	Desirability	
1	0.612	15.932	203.706	246.632	22.058	36.792	27.185	0.567	Selected
2	2.985	7.424	264.998	273.980	9.895	37.640	26.571	0.183	

Appendix 2.2: Molybdenum addition

Number	Mo	%E	UTS	Hardness	Electrical resistivity	Electrical conductivity	Desirability	
1	0.800	14.836	75.652	176.099	44.337	22.543	0.504	Selected
2	5.000	8.406	107.878	173.157	45.350	22.050	0.004	

Appendix 2.3: Magnesium addition

Number	Mg	%E	UTS	Hardness	Electrical conductivity	Desirability	
1	0.385	22.581	233.836	258.704	29.553	0.517	Selected
2	1.436	17.235	241.958	256.578	28.362	0.050	

Appendix 2.4: Manganese addition

Number	Mn	%E	UTS	Hardness	Electrical conductivity	Desirability	
1	0.693	8.606	332.988	318.253	21.547	0.555	Selected
2	1.497	4.873	375.452	368.500	20.764	0.043	

Appendix 2.5: Tungsten addition

Number	W	%E	UTS	Hardness	Electrical conductivity	Desirability	
1	0.404	23.258	270.391	319.173	32.708	0.642	Selected

Appendix 3: Graphical reprsentation of optimization results

Design-Expert® Software
Factor Coding: Actual
%E (%)
Design Points
95% CI Bands

X1 = A: Mg

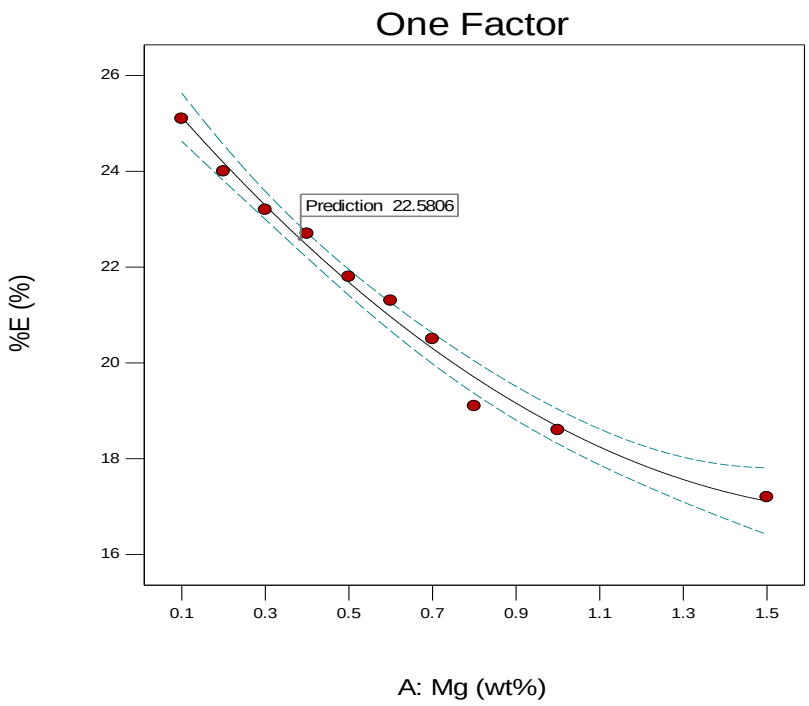

Design-Expert® Software
Factor Coding: Actual
UTS (MPa)
Design Points
95% CI Bands

X1 = A: Mg

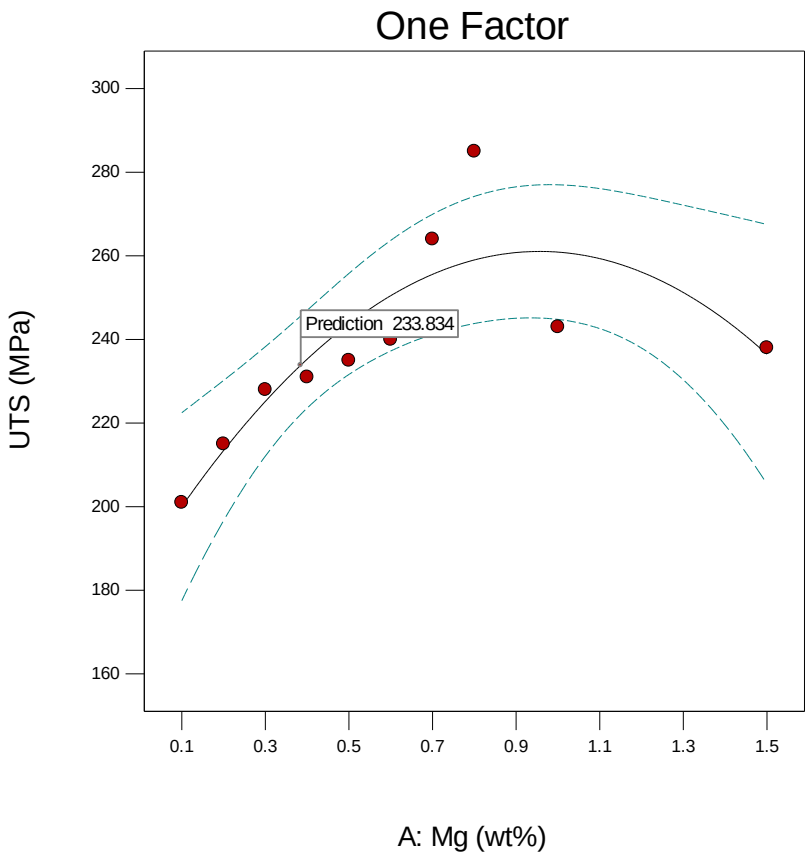

Design-Expert® Software
Factor Coding: Actual
Hardness (MPa)
Design Points
95% CI Bands

X1 = A: Mg

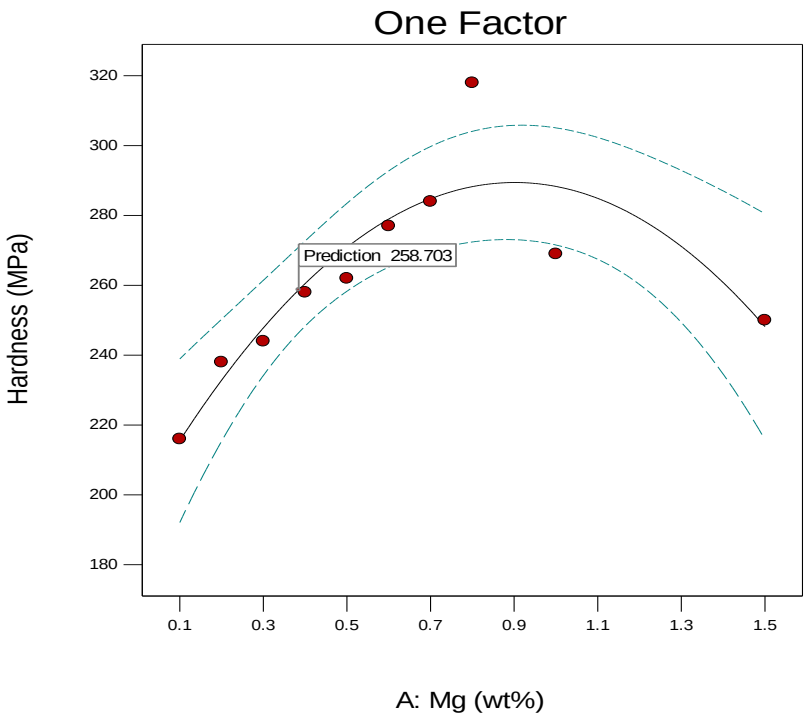

Design-Expert® Software
Factor Coding: Actual
Electrical conductivity (S/m)
Design Points
95% CI Bands

X1 = A: Mg

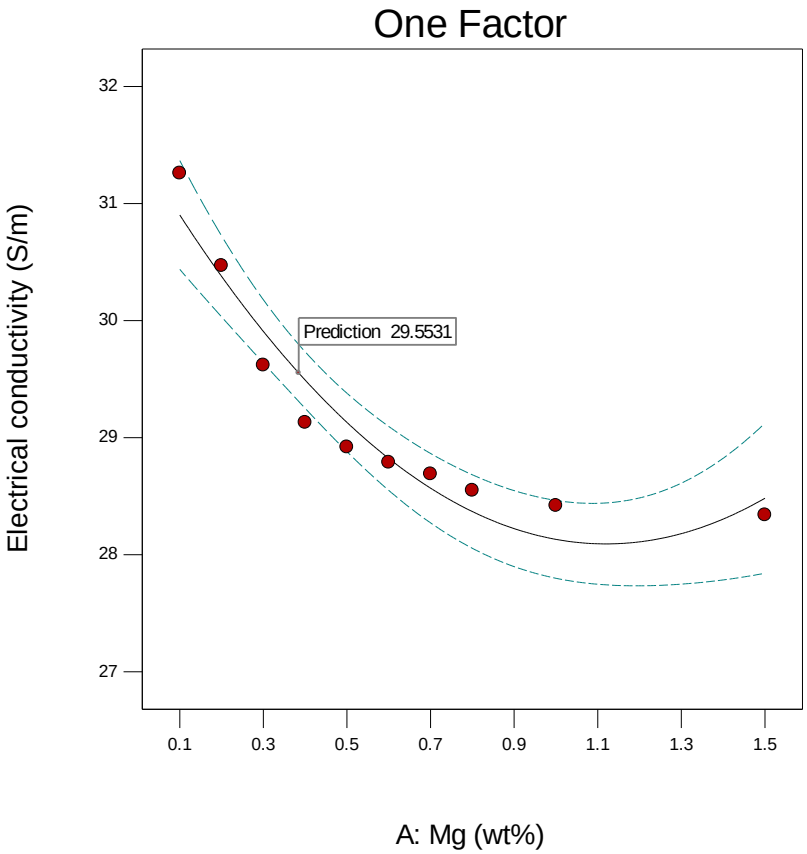

Design-Expert® Software
Factor Coding: Actual
Desirability
Design Points

X1 = A: Mg

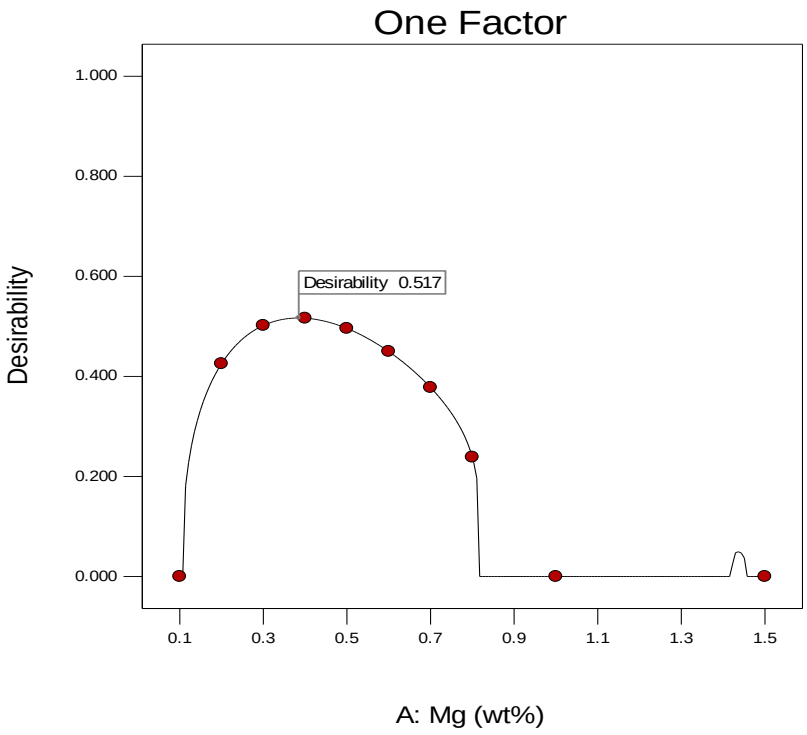

Design-Expert® Software
Factor Coding: Actual
%E (%)
Design Points
95% CI Bands

X1 = A: W

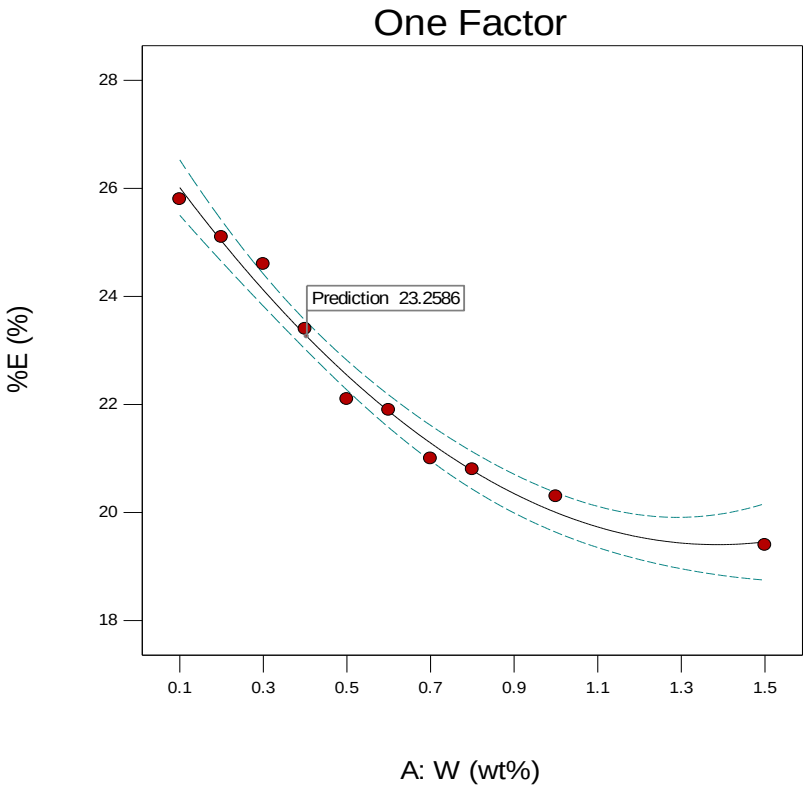

Design-Expert® Software
Factor Coding: Actual
UTS (MPa)
Design Points
95% CI Bands

X1 = A: W

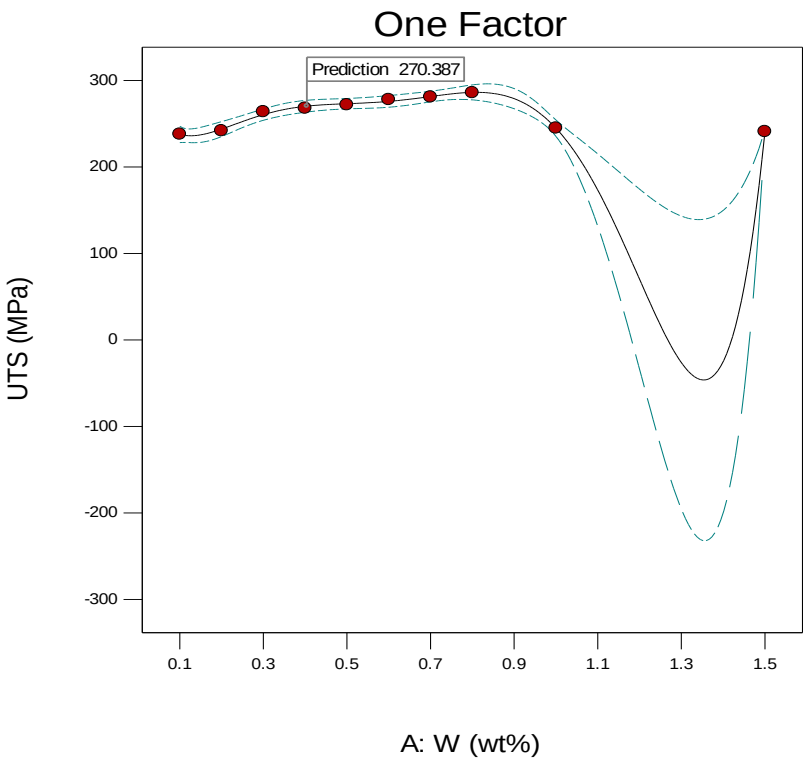

Design-Expert® Software
Factor Coding: Actual
Hardness (MPa)
Design Points
95% CI Bands

X1 = A: W

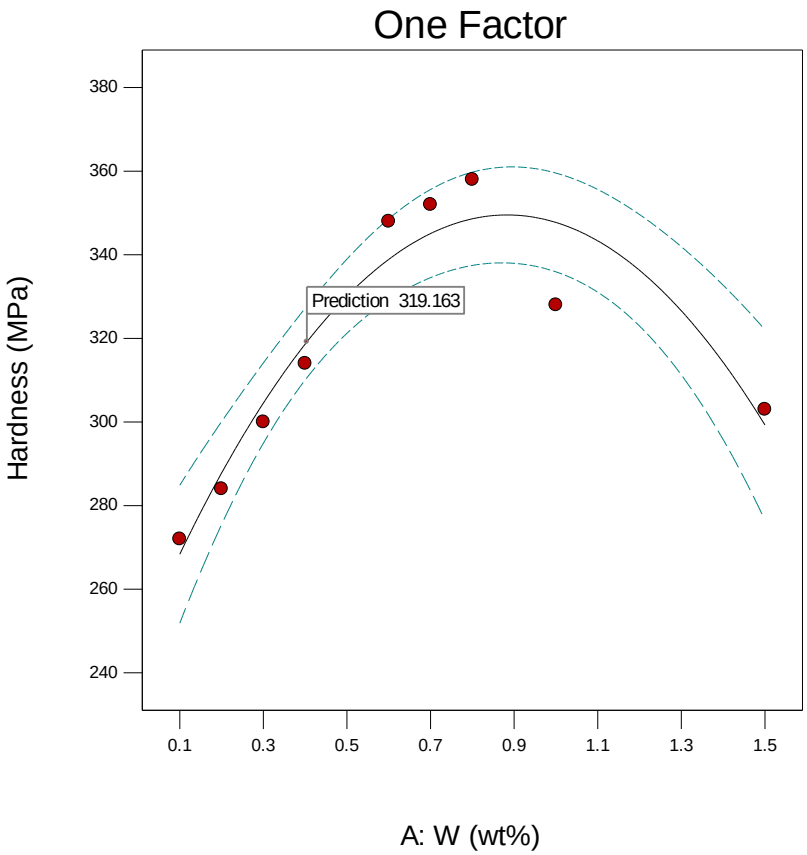

Design-Expert® Software
Factor Coding: Actual
Electrical conductivity (S/m)
Design Points
95% CI Bands

X1 = A: W

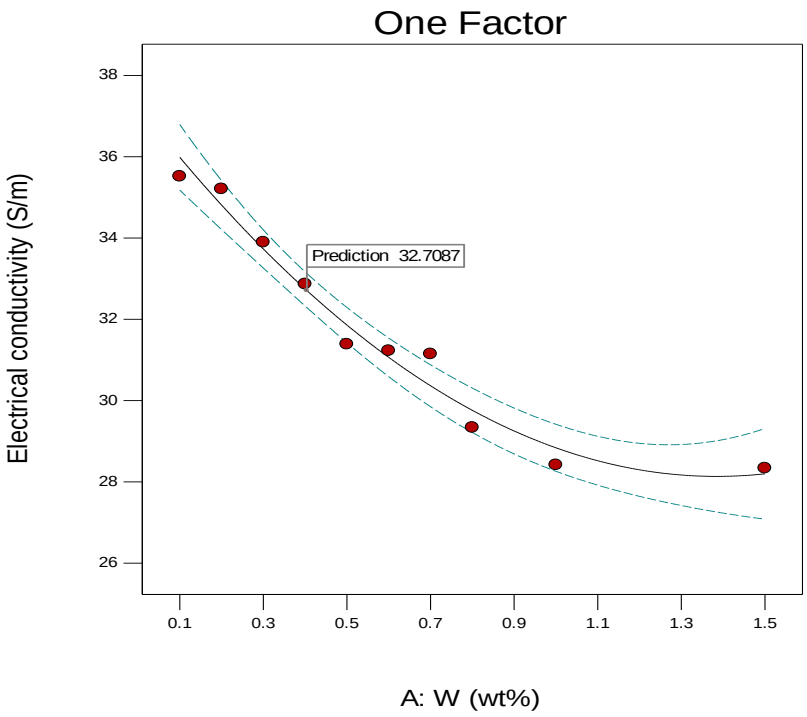

Design-Expert® Software
Factor Coding: Actual
Desirability
Design Points

X1 = A: W

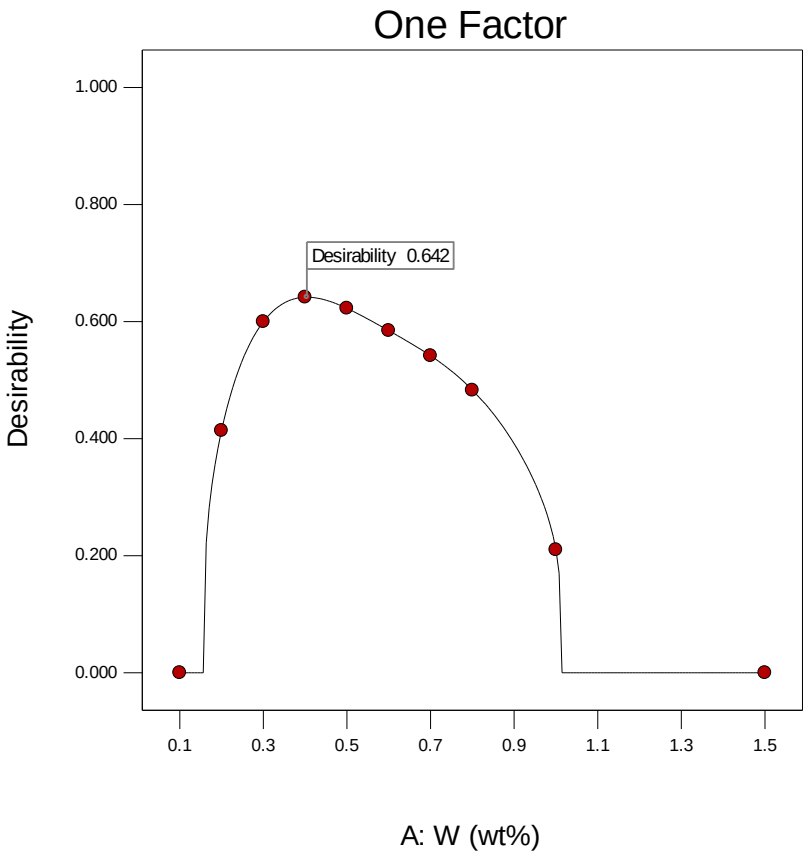

Appendix 4: Univariate Analysis of Variance

Between-Subjects Factors

		Value Label	N
Dopants	.00	Zn	13
	.01	Control	13
	1.00	Sn	13
	2.00	Mg	13
	3.00	Mn	13
	4.00	W	13
	5.00	Ti	13
	6.00	Mo	13
	7.00	Al	13
Composition	.20	Control	13
	2.00	0.1wt%	17
	3.00	0.2wt%	8
	4.00	0.3wt%	8
	5.00	0.4wt%	8
	6.00	0.5wt%	8
	7.00	0.6wt%	8
	8.00	0.7wt%	8
	9.00	0.8wt%	8
	10.00	1wt%	8
	11.00	1.5wt%	8
	12.00	2wt%	5
	13.00	3wt%	5
	14.00	5wt%	5

Appendix 4.1 Post Hoc Tests

Dopants

Multiple Comparisons

Dependent Variable: %E

Tukey HSD

(I) Dopant	(J) Dopant	Mean Difference (I-J)	Std. Error	Sig.	95% Confidence Interval	
					Lower Bound	Upper Bound
Zn	Control	3.3462*	1.02577	.039	.0906	6.6017
	Sn	-6.9077*	1.02577	.000	-10.1632	-3.6522
	Mg	-9.4692*	1.02577	.000	-12.7247	-6.2137
	Mn	.8846	1.02577	.994	-2.3709	4.1401
	W	-10.4692*	1.02577	.000	-13.7247	-7.2137
	Ti	-.9385	1.02577	.992	-4.1940	2.3170
	Mo	-1.6462	1.02577	.800	-4.9017	1.6094
	Al	.3308	1.02577	1.000	-2.9247	3.5863
Control	Zn	-3.3462*	1.02577	.039	-6.6017	-.0906
	Sn	-10.2538*	1.02577	.000	-13.5094	-6.9983
	Mg	-12.8154*	1.02577	.000	-16.0709	-9.5599
	Mn	-2.4615	1.02577	.296	-5.7170	.7940
	W	-13.8154*	1.02577	.000	-17.0709	-10.5599
	Ti	-4.2846*	1.02577	.002	-7.5401	-1.0291
	Mo	-4.9923*	1.02577	.000	-8.2478	-1.7368
	Al	-3.0154	1.02577	.092	-6.2709	.2401
Sn	Zn	6.9077*	1.02577	.000	3.6522	10.1632
	Control	10.2538*	1.02577	.000	6.9983	13.5094
	Mg	-2.5615	1.02577	.247	-5.8170	.6940
	Mn	7.7923*	1.02577	.000	4.5368	11.0478
	W	-3.5615*	1.02577	.021	-6.8170	-.3060
	Ti	5.9692*	1.02577	.000	2.7137	9.2247
	Mo	5.2615*	1.02577	.000	2.0060	8.5170
	Al	7.2385*	1.02577	.000	3.9830	10.4940
Mg	Zn	9.4692*	1.02577	.000	6.2137	12.7247
	Control	12.8154*	1.02577	.000	9.5599	16.0709
	Sn	2.5615	1.02577	.247	-.6940	5.8170
	Mn	10.3538*	1.02577	.000	7.0983	13.6094
	W	-1.0000	1.02577	.987	-4.2555	2.2555
	Ti	8.5308*	1.02577	.000	5.2753	11.7863
	Mo	7.8231*	1.02577	.000	4.5676	11.0786
	Al	9.8000*	1.02577	.000	6.5445	13.0555
Mn	Zn	-.8846	1.02577	.994	-4.1401	2.3709

	Control	2.4615	1.02577	.296	-.7940	5.7170
	Sn	-7.7923*	1.02577	.000	-11.0478	-4.5368
	Mg	-10.3538*	1.02577	.000	-13.6094	-7.0983
	W	-11.3538*	1.02577	.000	-14.6094	-8.0983
	Ti	-1.8231	1.02577	.697	-5.0786	1.4324
	Mo	-2.5308	1.02577	.261	-5.7863	.7247
	Al	-.5538	1.02577	1.000	-3.8094	2.7017
	Zn	10.4692*	1.02577	.000	7.2137	13.7247
W	Control	13.8154*	1.02577	.000	10.5599	17.0709
	Sn	3.5615*	1.02577	.021	.3060	6.8170
	Mg	1.0000	1.02577	.987	-2.2555	4.2555
	Mn	11.3538*	1.02577	.000	8.0983	14.6094
	Ti	9.5308*	1.02577	.000	6.2753	12.7863
	Mo	8.8231*	1.02577	.000	5.5676	12.0786
	Al	10.8000*	1.02577	.000	7.5445	14.0555
	Zn	.9385	1.02577	.992	-2.3170	4.1940
	Control	4.2846*	1.02577	.002	1.0291	7.5401
	Sn	-5.9692*	1.02577	.000	-9.2247	-2.7137
	Mg	-8.5308*	1.02577	.000	-11.7863	-5.2753
Ti	Mn	1.8231	1.02577	.697	-1.4324	5.0786
	W	-9.5308*	1.02577	.000	-12.7863	-6.2753
	Mo	-.7077	1.02577	.999	-3.9632	2.5478
	Al	1.2692	1.02577	.946	-1.9863	4.5247
	Zn	1.6462	1.02577	.800	-1.6094	4.9017
	Control	4.9923*	1.02577	.000	1.7368	8.2478
	Sn	-5.2615*	1.02577	.000	-8.5170	-2.0060
	Mg	-7.8231*	1.02577	.000	-11.0786	-4.5676
Mo	Mn	2.5308	1.02577	.261	-.7247	5.7863
	W	-8.8231*	1.02577	.000	-12.0786	-5.5676
	Ti	.7077	1.02577	.999	-2.5478	3.9632
	Al	1.9769	1.02577	.597	-1.2786	5.2324
	Zn	-.3308	1.02577	1.000	-3.5863	2.9247
	Control	3.0154	1.02577	.092	-.2401	6.2709
	Sn	-7.2385*	1.02577	.000	-10.4940	-3.9830
	Mg	-9.8000*	1.02577	.000	-13.0555	-6.5445
Al	Mn	.5538	1.02577	1.000	-2.7017	3.8094
	W	-10.8000*	1.02577	.000	-14.0555	-7.5445
	Ti	-1.2692	1.02577	.946	-4.5247	1.9863
	Mo	-1.9769	1.02577	.597	-5.2324	1.2786

Based on observed means.

The error term is Mean Square(Error) = 6.839.

*. The mean difference is significant at the .05 level.

Composition

Multiple Comparisons

Dependent Variable: %E

Tukey HSD

(I) Composition	(J) Composition	Mean Difference (I-J)	Std. Error	Sig.	95% Confidence Interval	
					Lower Bound	Upper Bound
Control	0.1wt%	-12.3706*	.96355	.000	-15.6865	-9.0547
	0.2wt%	-10.7875*	1.17517	.000	-14.8317	-6.7433
	0.3wt%	-10.1000*	1.17517	.000	-14.1442	-6.0558
	0.4wt%	-8.8375*	1.17517	.000	-12.8817	-4.7933
	0.5wt%	-8.0500*	1.17517	.000	-12.0942	-4.0058
	0.6wt%	-6.9500*	1.17517	.000	-10.9942	-2.9058
	0.7wt%	-6.1250*	1.17517	.000	-10.1692	-2.0808
	0.8wt%	-5.5000*	1.17517	.001	-9.5442	-1.4558
	1wt%	-4.9375*	1.17517	.004	-8.9817	-.8933
	1.5wt%	-3.0625	1.17517	.351	-7.1067	.9817
	2wt%	-.8200	1.37622	1.000	-5.5560	3.9160
	3wt%	.8400	1.37622	1.000	-3.8960	5.5760
	5wt%	2.0400	1.37622	.968	-2.6960	6.7760
0.1wt%	Control	12.3706*	.96355	.000	9.0547	15.6865
	0.2wt%	1.5831	1.12127	.978	-2.2756	5.4417
	0.3wt%	2.2706	1.12127	.748	-1.5881	6.1292
	0.4wt%	3.5331	1.12127	.109	-.3256	7.3917
	0.5wt%	4.3206*	1.12127	.014	.4619	8.1792
	0.6wt%	5.4206*	1.12127	.000	1.5619	9.2792
	0.7wt%	6.2456*	1.12127	.000	2.3869	10.1042
	0.8wt%	6.8706*	1.12127	.000	3.0119	10.7292
	1wt%	7.4331*	1.12127	.000	3.5744	11.2917
	1.5wt%	9.3081*	1.12127	.000	5.4494	13.1667
	2wt%	11.5506*	1.33048	.000	6.9719	16.1292
	3wt%	13.2106*	1.33048	.000	8.6319	17.7892
	5wt%	14.4106*	1.33048	.000	9.8319	18.9892
0.2wt%	Control	10.7875*	1.17517	.000	6.7433	14.8317
	0.1wt%	-1.5831	1.12127	.978	-5.4417	2.2756
	0.3wt%	.6875	1.30761	1.000	-3.8124	5.1874
	0.4wt%	1.9500	1.30761	.966	-2.5499	6.4499
	0.5wt%	2.7375	1.30761	.704	-1.7624	7.2374
	0.6wt%	3.8375	1.30761	.182	-.6624	8.3374

	0.7wt%	4.6625*	1.30761	.035	.1626	9.1624
	0.8wt%	5.2875*	1.30761	.008	.7876	9.7874
	1wt%	5.8500*	1.30761	.002	1.3501	10.3499
	1.5wt%	7.7250*	1.30761	.000	3.2251	12.2249
	2wt%	9.9675*	1.49090	.000	4.8368	15.0982
	3wt%	11.6275*	1.49090	.000	6.4968	16.7582
	5wt%	12.8275*	1.49090	.000	7.6968	17.9582
	Control	10.1000*	1.17517	.000	6.0558	14.1442
	0.1wt%	-2.2706	1.12127	.748	-6.1292	1.5881
	0.2wt%	-.6875	1.30761	1.000	-5.1874	3.8124
	0.4wt%	1.2625	1.30761	.999	-3.2374	5.7624
	0.5wt%	2.0500	1.30761	.950	-2.4499	6.5499
	0.6wt%	3.1500	1.30761	.482	-1.3499	7.6499
0.3wt%	0.7wt%	3.9750	1.30761	.143	-.5249	8.4749
	0.8wt%	4.6000*	1.30761	.040	.1001	9.0999
	1wt%	5.1625*	1.30761	.010	.6626	9.6624
	1.5wt%	7.0375*	1.30761	.000	2.5376	11.5374
	2wt%	9.2800*	1.49090	.000	4.1493	14.4107
	3wt%	10.9400*	1.49090	.000	5.8093	16.0707
	5wt%	12.1400*	1.49090	.000	7.0093	17.2707
	Control	8.8375*	1.17517	.000	4.7933	12.8817
	0.1wt%	-3.5331	1.12127	.109	-7.3917	.3256
	0.2wt%	-1.9500	1.30761	.966	-6.4499	2.5499
	0.3wt%	-1.2625	1.30761	.999	-5.7624	3.2374
	0.5wt%	.7875	1.30761	1.000	-3.7124	5.2874
	0.6wt%	1.8875	1.30761	.974	-2.6124	6.3874
0.4wt%	0.7wt%	2.7125	1.30761	.716	-1.7874	7.2124
	0.8wt%	3.3375	1.30761	.385	-1.1624	7.8374
	1wt%	3.9000	1.30761	.163	-.5999	8.3999
	1.5wt%	5.7750*	1.30761	.002	1.2751	10.2749
	2wt%	8.0175*	1.49090	.000	2.8868	13.1482
	3wt%	9.6775*	1.49090	.000	4.5468	14.8082
	5wt%	10.8775*	1.49090	.000	5.7468	16.0082
	Control	8.0500*	1.17517	.000	4.0058	12.0942
	0.1wt%	-4.3206*	1.12127	.014	-8.1792	-.4619
	0.2wt%	-2.7375	1.30761	.704	-7.2374	1.7624
	0.3wt%	-2.0500	1.30761	.950	-6.5499	2.4499
	0.6wt%	-.7875	1.30761	1.000	-5.2874	3.7124
0.5wt%	0.7wt%	1.1000	1.30761	1.000	-3.3999	5.5999
	0.8wt%	1.9250	1.30761	.969	-2.5749	6.4249
	1wt%	2.5500	1.30761	.793	-1.9499	7.0499
	1.5wt%	3.1125	1.30761	.502	-1.3874	7.6124
	2wt%	4.9875*	1.30761	.016	.4876	9.4874

	3wt%	7.2300*	1.49090	.000	2.0993	12.3607
	5wt%	8.8900*	1.49090	.000	3.7593	14.0207
	Control	10.0900*	1.49090	.000	4.9593	15.2207
	0.1wt%	6.9500*	1.17517	.000	2.9058	10.9942
	0.2wt%	-5.4206*	1.12127	.000	-9.2792	-1.5619
	0.3wt%	-3.8375	1.30761	.182	-8.3374	.6624
	0.5wt%	-3.1500	1.30761	.482	-7.6499	1.3499
	0.7wt%	-1.8875	1.30761	.974	-6.3874	2.6124
	0.8wt%	-1.1000	1.30761	1.000	-5.5999	3.3999
0.6wt%	1wt%	.8250	1.30761	1.000	-3.6749	5.3249
	1.5wt%	1.4500	1.30761	.998	-3.0499	5.9499
	2wt%	2.0125	1.30761	.957	-2.4874	6.5124
	3wt%	3.8875	1.30761	.167	-.6124	8.3874
	5wt%	6.1300*	1.49090	.006	.9993	11.2607
	Control	7.7900*	1.49090	.000	2.6593	12.9207
	0.1wt%	8.9900*	1.49090	.000	3.8593	14.1207
	0.2wt%	6.1250*	1.17517	.000	2.0808	10.1692
	0.3wt%	-6.2456*	1.12127	.000	-10.1042	-2.3869
	0.5wt%	-4.6625*	1.30761	.035	-9.1624	-.1626
	0.6wt%	-3.9750	1.30761	.143	-8.4749	.5249
	0.8wt%	-2.7125	1.30761	.716	-7.2124	1.7874
	1wt%	-1.9250	1.30761	.969	-6.4249	2.5749
0.7wt%	1.5wt%	-.8250	1.30761	1.000	-5.3249	3.6749
	2wt%	.6250	1.30761	1.000	-3.8749	5.1249
	3wt%	1.1875	1.30761	1.000	-3.3124	5.6874
	5wt%	3.0625	1.30761	.529	-1.4374	7.5624
	0.1wt%	5.3050*	1.49090	.036	.1743	10.4357
	0.2wt%	6.9650*	1.49090	.001	1.8343	12.0957
	1wt%	8.1650*	1.49090	.000	3.0343	13.2957
	Control	5.5000*	1.17517	.001	1.4558	9.5442
	0.1wt%	-6.8706*	1.12127	.000	-10.7292	-3.0119
	0.2wt%	-5.2875*	1.30761	.008	-9.7874	-.7876
	0.3wt%	-4.6000*	1.30761	.040	-9.0999	-.1001
	0.4wt%	-3.3375	1.30761	.385	-7.8374	1.1624
	0.5wt%	-2.5500	1.30761	.793	-7.0499	1.9499
0.8wt%	0.6wt%	-1.4500	1.30761	.998	-5.9499	3.0499
	0.7wt%	-.6250	1.30761	1.000	-5.1249	3.8749
	1wt%	.5625	1.30761	1.000	-3.9374	5.0624
	1.5wt%	2.4375	1.30761	.840	-2.0624	6.9374
	2wt%	4.6800	1.49090	.112	-.4507	9.8107
	3wt%	6.3400*	1.49090	.004	1.2093	11.4707
	5wt%	7.5400*	1.49090	.000	2.4093	12.6707
1wt%	Control	4.9375*	1.17517	.004	.8933	8.9817

	0.1wt%	-7.4331*	1.12127	.000	-11.2917	-3.5744
	0.2wt%	-5.8500*	1.30761	.002	-10.3499	-1.3501
	0.3wt%	-5.1625*	1.30761	.010	-9.6624	-.6626
	0.4wt%	-3.9000	1.30761	.163	-8.3999	.5999
	0.5wt%	-3.1125	1.30761	.502	-7.6124	1.3874
	0.6wt%	-2.0125	1.30761	.957	-6.5124	2.4874
	0.7wt%	-1.1875	1.30761	1.000	-5.6874	3.3124
	0.8wt%	-.5625	1.30761	1.000	-5.0624	3.9374
	1.5wt%	1.8750	1.30761	.975	-2.6249	6.3749
	2wt%	4.1175	1.49090	.262	-1.0132	9.2482
	3wt%	5.7775*	1.49090	.013	.6468	10.9082
	5wt%	6.9775*	1.49090	.001	1.8468	12.1082
	Control	3.0625	1.17517	.351	-.9817	7.1067
	0.1wt%	-9.3081*	1.12127	.000	-13.1667	-5.4494
	0.2wt%	-7.7250*	1.30761	.000	-12.2249	-3.2251
	0.3wt%	-7.0375*	1.30761	.000	-11.5374	-2.5376
	0.4wt%	-5.7750*	1.30761	.002	-10.2749	-1.2751
	0.5wt%	-4.9875*	1.30761	.016	-9.4874	-.4876
1.5wt%	0.6wt%	-3.8875	1.30761	.167	-8.3874	.6124
	0.7wt%	-3.0625	1.30761	.529	-7.5624	1.4374
	0.8wt%	-2.4375	1.30761	.840	-6.9374	2.0624
	1wt%	-1.8750	1.30761	.975	-6.3749	2.6249
	2wt%	2.2425	1.49090	.964	-2.8882	7.3732
	3wt%	3.9025	1.49090	.344	-1.2282	9.0332
	5wt%	5.1025	1.49090	.053	-.0282	10.2332
	Control	.8200	1.37622	1.000	-3.9160	5.5560
	0.1wt%	-11.5506*	1.33048	.000	-16.1292	-6.9719
	0.2wt%	-9.9675*	1.49090	.000	-15.0982	-4.8368
	0.3wt%	-9.2800*	1.49090	.000	-14.4107	-4.1493
	0.4wt%	-8.0175*	1.49090	.000	-13.1482	-2.8868
	0.5wt%	-7.2300*	1.49090	.000	-12.3607	-2.0993
2wt%	0.6wt%	-6.1300*	1.49090	.006	-11.2607	-.9993
	0.7wt%	-5.3050*	1.49090	.036	-10.4357	-.1743
	0.8wt%	-4.6800	1.49090	.112	-9.8107	.4507
	1wt%	-4.1175	1.49090	.262	-9.2482	1.0132
	1.5wt%	-2.2425	1.49090	.964	-7.3732	2.8882
	3wt%	1.6600	1.65401	.999	-4.0320	7.3520
	5wt%	2.8600	1.65401	.900	-2.8320	8.5520
	Control	-.8400	1.37622	1.000	-5.5760	3.8960
	0.1wt%	-13.2106*	1.33048	.000	-17.7892	-8.6319
3wt%	0.2wt%	-11.6275*	1.49090	.000	-16.7582	-6.4968
	0.3wt%	-10.9400*	1.49090	.000	-16.0707	-5.8093
	0.4wt%	-9.6775*	1.49090	.000	-14.8082	-4.5468

	0.5wt%	-8.8900*	1.49090	.000	-14.0207	-3.7593
	0.6wt%	-7.7900*	1.49090	.000	-12.9207	-2.6593
	0.7wt%	-6.9650*	1.49090	.001	-12.0957	-1.8343
	0.8wt%	-6.3400*	1.49090	.004	-11.4707	-1.2093
	1wt%	-5.7775*	1.49090	.013	-10.9082	-.6468
	1.5wt%	-3.9025	1.49090	.344	-9.0332	1.2282
	2wt%	-1.6600	1.65401	.999	-7.3520	4.0320
	5wt%	1.2000	1.65401	1.000	-4.4920	6.8920
	Control	-2.0400	1.37622	.968	-6.7760	2.6960
	0.1wt%	-14.4106*	1.33048	.000	-18.9892	-9.8319
	0.2wt%	-12.8275*	1.49090	.000	-17.9582	-7.6968
	0.3wt%	-12.1400*	1.49090	.000	-17.2707	-7.0093
	0.4wt%	-10.8775*	1.49090	.000	-16.0082	-5.7468
	0.5wt%	-10.0900*	1.49090	.000	-15.2207	-4.9593
5wt%	0.6wt%	-8.9900*	1.49090	.000	-14.1207	-3.8593
	0.7wt%	-8.1650*	1.49090	.000	-13.2957	-3.0343
	0.8wt%	-7.5400*	1.49090	.000	-12.6707	-2.4093
	1wt%	-6.9775*	1.49090	.001	-12.1082	-1.8468
	1.5wt%	-5.1025	1.49090	.053	-10.2332	.0282
	2wt%	-2.8600	1.65401	.900	-8.5520	2.8320
	3wt%	-1.2000	1.65401	1.000	-6.8920	4.4920

Based on observed means.

The error term is Mean Square (Error) = 6.839.

*. The mean difference is significant at the .05 level.

Post Hoc Tests

Dopants

Multiple Comparisons

Dependent Variable: UTS

Tukey HSD

(I) Dopant	(J) Dopant	Mean Difference (I-J)	Std. Error	Sig.	95% Confidence Interval	
					Lower Bound	Upper Bound
	Control	168.1538*	11.24946	.000	132.4513	203.8564
	Sn	31.3846	11.24946	.132	-4.3179	67.0872
Zn	Mg	-27.3077	11.24946	.281	-63.0102	8.3948
	Mn	-89.7692*	11.24946	.000	-125.4718	-54.0667
	W	-53.9231*	11.24946	.000	-89.6256	-18.2205

	Ti	-1.2308	11.24946	1.000	-36.9333	34.4718
	Mo	121.9231*	11.24946	.000	86.2205	157.6256
	Al	-3.8462	11.24946	1.000	-39.5487	31.8564
	Zn	-168.1538*	11.24946	.000	-203.8564	-132.4513
	Sn	-136.7692*	11.24946	.000	-172.4718	-101.0667
	Mg	-195.4615*	11.24946	.000	-231.1641	-159.7590
	Mn	-257.9231*	11.24946	.000	-293.6256	-222.2205
Control	W	-222.0769*	11.24946	.000	-257.7795	-186.3744
	Ti	-169.3846*	11.24946	.000	-205.0872	-133.6821
	Mo	-46.2308*	11.24946	.003	-81.9333	-10.5282
	Al	-172.0000*	11.24946	.000	-207.7025	-136.2975
	Zn	-31.3846	11.24946	.132	-67.0872	4.3179
	Control	136.7692*	11.24946	.000	101.0667	172.4718
	Mg	-58.6923*	11.24946	.000	-94.3948	-22.9898
	Mn	-121.1538*	11.24946	.000	-156.8564	-85.4513
Sn	W	-85.3077*	11.24946	.000	-121.0102	-49.6052
	Ti	-32.6154	11.24946	.102	-68.3179	3.0872
	Mo	90.5385*	11.24946	.000	54.8359	126.2410
	Al	-35.2308	11.24946	.056	-70.9333	.4718
	Zn	27.3077	11.24946	.281	-8.3948	63.0102
	Control	195.4615*	11.24946	.000	159.7590	231.1641
	Sn	58.6923*	11.24946	.000	22.9898	94.3948
	Mn	-62.4615*	11.24946	.000	-98.1641	-26.7590
Mg	W	-26.6154	11.24946	.315	-62.3179	9.0872
	Ti	26.0769	11.24946	.342	-9.6256	61.7795
	Mo	149.2308*	11.24946	.000	113.5282	184.9333
	Al	23.4615	11.24946	.489	-12.2410	59.1641
	Zn	89.7692*	11.24946	.000	54.0667	125.4718
	Control	257.9231*	11.24946	.000	222.2205	293.6256
	Sn	121.1538*	11.24946	.000	85.4513	156.8564
	Mg	62.4615*	11.24946	.000	26.7590	98.1641
Mn	W	35.8462*	11.24946	.048	.1436	71.5487
	Ti	88.5385*	11.24946	.000	52.8359	124.2410
	Mo	211.6923*	11.24946	.000	175.9898	247.3948
	Al	85.9231*	11.24946	.000	50.2205	121.6256
	Zn	53.9231*	11.24946	.000	18.2205	89.6256
	Control	222.0769*	11.24946	.000	186.3744	257.7795
	Sn	85.3077*	11.24946	.000	49.6052	121.0102
	Mg	26.6154	11.24946	.315	-9.0872	62.3179
W	Mn	-35.8462*	11.24946	.048	-71.5487	-.1436
	Ti	52.6923*	11.24946	.000	16.9898	88.3948
	Mo	175.8462*	11.24946	.000	140.1436	211.5487
	Al	50.0769*	11.24946	.001	14.3744	85.7795

Ti	Zn	1.2308	11.24946	1.000	-34.4718	36.9333
	Control	169.3846*	11.24946	.000	133.6821	205.0872
	Sn	32.6154	11.24946	.102	-3.0872	68.3179
	Mg	-26.0769	11.24946	.342	-61.7795	9.6256
	Mn	-88.5385*	11.24946	.000	-124.2410	-52.8359
	W	-52.6923*	11.24946	.000	-88.3948	-16.9898
	Mo	123.1538*	11.24946	.000	87.4513	158.8564
	Al	-2.6154	11.24946	1.000	-38.3179	33.0872
Mo	Zn	-121.9231*	11.24946	.000	-157.6256	-86.2205
	Control	46.2308*	11.24946	.003	10.5282	81.9333
	Sn	-90.5385*	11.24946	.000	-126.2410	-54.8359
	Mg	-149.2308*	11.24946	.000	-184.9333	-113.5282
	Mn	-211.6923*	11.24946	.000	-247.3948	-175.9898
	W	-175.8462*	11.24946	.000	-211.5487	-140.1436
	Ti	-123.1538*	11.24946	.000	-158.8564	-87.4513
	Al	-125.7692*	11.24946	.000	-161.4718	-90.0667
Al	Zn	3.8462	11.24946	1.000	-31.8564	39.5487
	Control	172.0000*	11.24946	.000	136.2975	207.7025
	Sn	35.2308	11.24946	.056	-.4718	70.9333
	Mg	-23.4615	11.24946	.489	-59.1641	12.2410
	Mn	-85.9231*	11.24946	.000	-121.6256	-50.2205
	W	-50.0769*	11.24946	.001	-85.7795	-14.3744
	Ti	2.6154	11.24946	1.000	-33.0872	38.3179
	Mo	125.7692*	11.24946	.000	90.0667	161.4718

Based on observed means.

The error term is Mean Square(Error) = 822.578.

*. The mean difference is significant at the .05 level.

Composition

Multiple Comparisons

Dependent Variable: UTS
Tukey HSD

(I) Composition	(J) Composition	Mean Difference (I-J)	Std. Error	Sig.	95% Confidence Interval	
					Lower Bound	Upper Bound
Control	0.1wt%	-151.8235*	10.56703	.000	-188.1882	-115.4588
	0.2wt%	-117.7500*	12.88788	.000	-162.1015	-73.3985
	0.3wt%	-129.1250*	12.88788	.000	-173.4765	-84.7735
	0.4wt%	-138.1250*	12.88788	.000	-182.4765	-93.7735
	0.5wt%	-150.0000*	12.88788	.000	-194.3515	-105.6485
	0.6wt%	-165.2500*	12.88788	.000	-209.6015	-120.8985
	0.7wt%	-182.2500*	12.88788	.000	-226.6015	-137.8985
	0.8wt%	-193.2500*	12.88788	.000	-237.6015	-148.8985
	1wt%	-197.5000*	12.88788	.000	-241.8515	-153.1485
	1.5wt%	-221.5000*	12.88788	.000	-265.8515	-177.1485
	2wt%	-211.4000*	15.09274	.000	-263.3392	-159.4608
	3wt%	-222.8000*	15.09274	.000	-274.7392	-170.8608
	5wt%	-214.8000*	15.09274	.000	-266.7392	-162.8608
0.1wt%	Control	151.8235*	10.56703	.000	115.4588	188.1882
	0.2wt%	34.0735	12.29671	.257	-8.2436	76.3906
	0.3wt%	22.6985	12.29671	.849	-19.6186	65.0156
	0.4wt%	13.6985	12.29671	.998	-28.6186	56.0156
	0.5wt%	1.8235	12.29671	1.000	-40.4936	44.1406
	0.6wt%	-13.4265	12.29671	.998	-55.7436	28.8906
	0.7wt%	-30.4265	12.29671	.436	-72.7436	11.8906
	0.8wt%	-41.4265	12.29671	.061	-83.7436	.8906
	1wt%	-45.6765*	12.29671	.022	-87.9936	-3.3594
	1.5wt%	-69.6765*	12.29671	.000	-111.9936	-27.3594
	2wt%	-59.5765*	14.59118	.007	-109.7896	-9.3633
	3wt%	-70.9765*	14.59118	.000	-121.1896	-20.7633
	5wt%	-62.9765*	14.59118	.003	-113.1896	-12.7633
0.2wt%	Control	117.7500*	12.88788	.000	73.3985	162.1015
	0.1wt%	-34.0735	12.29671	.257	-76.3906	8.2436
	0.3wt%	-11.3750	14.34031	1.000	-60.7248	37.9748
	0.4wt%	-20.3750	14.34031	.977	-69.7248	28.9748
	0.5wt%	-32.2500	14.34031	.596	-81.5998	17.0998
	0.6wt%	-47.5000	14.34031	.071	-96.8498	1.8498

	0.7wt%	-64.5000*	14.34031	.002	-113.8498	-15.1502
	0.8wt%	-75.5000*	14.34031	.000	-124.8498	-26.1502
	1wt%	-79.7500*	14.34031	.000	-129.0998	-30.4002
	1.5wt%	-103.7500*	14.34031	.000	-153.0998	-54.4002
	2wt%	-93.6500*	16.35047	.000	-149.9174	-37.3826
	3wt%	-105.0500*	16.35047	.000	-161.3174	-48.7826
	5wt%	-97.0500*	16.35047	.000	-153.3174	-40.7826
	Control	129.1250*	12.88788	.000	84.7735	173.4765
	0.1wt%	-22.6985	12.29671	.849	-65.0156	19.6186
	0.2wt%	11.3750	14.34031	1.000	-37.9748	60.7248
	0.4wt%	-9.0000	14.34031	1.000	-58.3498	40.3498
	0.5wt%	-20.8750	14.34031	.972	-70.2248	28.4748
	0.6wt%	-36.1250	14.34031	.406	-85.4748	13.2248
0.3wt%	0.7wt%	-53.1250*	14.34031	.023	-102.4748	-3.7752
	0.8wt%	-64.1250*	14.34031	.002	-113.4748	-14.7752
	1wt%	-68.3750*	14.34031	.001	-117.7248	-19.0252
	1.5wt%	-92.3750*	14.34031	.000	-141.7248	-43.0252
	2wt%	-82.2750*	16.35047	.000	-138.5424	-26.0076
	3wt%	-93.6750*	16.35047	.000	-149.9424	-37.4076
	5wt%	-85.6750*	16.35047	.000	-141.9424	-29.4076
	Control	138.1250*	12.88788	.000	93.7735	182.4765
	0.1wt%	-13.6985	12.29671	.998	-56.0156	28.6186
	0.2wt%	20.3750	14.34031	.977	-28.9748	69.7248
	0.3wt%	9.0000	14.34031	1.000	-40.3498	58.3498
	0.5wt%	-11.8750	14.34031	1.000	-61.2248	37.4748
	0.6wt%	-27.1250	14.34031	.826	-76.4748	22.2248
0.4wt%	0.7wt%	-44.1250	14.34031	.131	-93.4748	5.2248
	0.8wt%	-55.1250*	14.34031	.015	-104.4748	-5.7752
	1wt%	-59.3750*	14.34031	.005	-108.7248	-10.0252
	1.5wt%	-83.3750*	14.34031	.000	-132.7248	-34.0252
	2wt%	-73.2750*	16.35047	.002	-129.5424	-17.0076
	3wt%	-84.6750*	16.35047	.000	-140.9424	-28.4076
	5wt%	-76.6750*	16.35047	.001	-132.9424	-20.4076
	Control	150.0000*	12.88788	.000	105.6485	194.3515
	0.1wt%	-1.8235	12.29671	1.000	-44.1406	40.4936
	0.2wt%	32.2500	14.34031	.596	-17.0998	81.5998
	0.3wt%	20.8750	14.34031	.972	-28.4748	70.2248
	0.6wt%	11.8750	14.34031	1.000	-37.4748	61.2248
0.5wt%	0.7wt%	-15.2500	14.34031	.998	-64.5998	34.0998
	0.8wt%	-32.2500	14.34031	.596	-81.5998	17.0998
	1wt%	-43.2500	14.34031	.151	-92.5998	6.0998
	1.5wt%	-47.5000	14.34031	.071	-96.8498	1.8498
	2wt%	-71.5000*	14.34031	.000	-120.8498	-22.1502

	3wt%	-61.4000*	16.35047	.020	-117.6674	-5.1326
	5wt%	-72.8000*	16.35047	.002	-129.0674	-16.5326
	Control	-64.8000*	16.35047	.010	-121.0674	-8.5326
	0.1wt%	165.2500*	12.88788	.000	120.8985	209.6015
	0.2wt%	13.4265	12.29671	.998	-28.8906	55.7436
	0.3wt%	47.5000	14.34031	.071	-1.8498	96.8498
	0.5wt%	36.1250	14.34031	.406	-13.2248	85.4748
	0.7wt%	27.1250	14.34031	.826	-22.2248	76.4748
	0.8wt%	15.2500	14.34031	.998	-34.0998	64.5998
0.6wt%	1wt%	-17.0000	14.34031	.995	-66.3498	32.3498
	1.5wt%	-28.0000	14.34031	.792	-77.3498	21.3498
	2wt%	-32.2500	14.34031	.596	-81.5998	17.0998
	3wt%	-56.2500*	14.34031	.011	-105.5998	-6.9002
	5wt%	-46.1500	16.35047	.231	-102.4174	10.1174
	Control	-57.5500*	16.35047	.040	-113.8174	-1.2826
	0.1wt%	-49.5500	16.35047	.146	-105.8174	6.7174
	0.2wt%	182.2500*	12.88788	.000	137.8985	226.6015
	0.3wt%	30.4265	12.29671	.436	-11.8906	72.7436
	0.5wt%	64.5000*	14.34031	.002	15.1502	113.8498
	0.6wt%	53.1250*	14.34031	.023	3.7752	102.4748
	0.8wt%	44.1250	14.34031	.131	-5.2248	93.4748
	1wt%	32.2500	14.34031	.596	-17.0998	81.5998
0.7wt%	1.5wt%	17.0000	14.34031	.995	-32.3498	66.3498
	2wt%	-11.0000	14.34031	1.000	-60.3498	38.3498
	3wt%	-15.2500	14.34031	.998	-64.5998	34.0998
	5wt%	-39.2500	14.34031	.275	-88.5998	10.0998
	0.1wt%	-29.1500	16.35047	.878	-85.4174	27.1174
	0.2wt%	-40.5500	16.35047	.433	-96.8174	15.7174
	1wt%	-32.5500	16.35047	.769	-88.8174	23.7174
	Control	193.2500*	12.88788	.000	148.8985	237.6015
	0.1wt%	41.4265	12.29671	.061	-.8906	83.7436
	0.2wt%	75.5000*	14.34031	.000	26.1502	124.8498
	0.3wt%	64.1250*	14.34031	.002	14.7752	113.4748
	0.4wt%	55.1250*	14.34031	.015	5.7752	104.4748
	0.5wt%	43.2500	14.34031	.151	-6.0998	92.5998
0.8wt%	0.6wt%	28.0000	14.34031	.792	-21.3498	77.3498
	0.7wt%	11.0000	14.34031	1.000	-38.3498	60.3498
	1wt%	-4.2500	14.34031	1.000	-53.5998	45.0998
	1.5wt%	-28.2500	14.34031	.782	-77.5998	21.0998
	2wt%	-18.1500	16.35047	.998	-74.4174	38.1174
	3wt%	-29.5500	16.35047	.867	-85.8174	26.7174
	5wt%	-21.5500	16.35047	.988	-77.8174	34.7174
1wt%	Control	197.5000*	12.88788	.000	153.1485	241.8515

	0.1wt%	45.6765*	12.29671	.022	3.3594	87.9936
	0.2wt%	79.7500*	14.34031	.000	30.4002	129.0998
	0.3wt%	68.3750*	14.34031	.001	19.0252	117.7248
	0.4wt%	59.3750*	14.34031	.005	10.0252	108.7248
	0.5wt%	47.5000	14.34031	.071	-1.8498	96.8498
	0.6wt%	32.2500	14.34031	.596	-17.0998	81.5998
	0.7wt%	15.2500	14.34031	.998	-34.0998	64.5998
	0.8wt%	4.2500	14.34031	1.000	-45.0998	53.5998
	1.5wt%	-24.0000	14.34031	.920	-73.3498	25.3498
	2wt%	-13.9000	16.35047	1.000	-70.1674	42.3674
	3wt%	-25.3000	16.35047	.955	-81.5674	30.9674
	5wt%	-17.3000	16.35047	.999	-73.5674	38.9674
	Control	221.5000*	12.88788	.000	177.1485	265.8515
	0.1wt%	69.6765*	12.29671	.000	27.3594	111.9936
	0.2wt%	103.7500*	14.34031	.000	54.4002	153.0998
	0.3wt%	92.3750*	14.34031	.000	43.0252	141.7248
	0.4wt%	83.3750*	14.34031	.000	34.0252	132.7248
	0.5wt%	71.5000*	14.34031	.000	22.1502	120.8498
1.5wt%	0.6wt%	56.2500*	14.34031	.011	6.9002	105.5998
	0.7wt%	39.2500	14.34031	.275	-10.0998	88.5998
	0.8wt%	28.2500	14.34031	.782	-21.0998	77.5998
	1wt%	24.0000	14.34031	.920	-25.3498	73.3498
	2wt%	10.1000	16.35047	1.000	-46.1674	66.3674
	3wt%	-1.3000	16.35047	1.000	-57.5674	54.9674
	5wt%	6.7000	16.35047	1.000	-49.5674	62.9674
	Control	211.4000*	15.09274	.000	159.4608	263.3392
	0.1wt%	59.5765*	14.59118	.007	9.3633	109.7896
	0.2wt%	93.6500*	16.35047	.000	37.3826	149.9174
	0.3wt%	82.2750*	16.35047	.000	26.0076	138.5424
	0.4wt%	73.2750*	16.35047	.002	17.0076	129.5424
	0.5wt%	61.4000*	16.35047	.020	5.1326	117.6674
2wt%	0.6wt%	46.1500	16.35047	.231	-10.1174	102.4174
	0.7wt%	29.1500	16.35047	.878	-27.1174	85.4174
	0.8wt%	18.1500	16.35047	.998	-38.1174	74.4174
	1wt%	13.9000	16.35047	1.000	-42.3674	70.1674
	1.5wt%	-10.1000	16.35047	1.000	-66.3674	46.1674
	3wt%	-11.4000	18.13921	1.000	-73.8231	51.0231
	5wt%	-3.4000	18.13921	1.000	-65.8231	59.0231
	Control	222.8000*	15.09274	.000	170.8608	274.7392
	0.1wt%	70.9765*	14.59118	.000	20.7633	121.1896
3wt%	0.2wt%	105.0500*	16.35047	.000	48.7826	161.3174
	0.3wt%	93.6750*	16.35047	.000	37.4076	149.9424
	0.4wt%	84.6750*	16.35047	.000	28.4076	140.9424

	0.5wt%	72.8000*	16.35047	.002	16.5326	129.0674
	0.6wt%	57.5500*	16.35047	.040	1.2826	113.8174
	0.7wt%	40.5500	16.35047	.433	-15.7174	96.8174
	0.8wt%	29.5500	16.35047	.867	-26.7174	85.8174
	1wt%	25.3000	16.35047	.955	-30.9674	81.5674
	1.5wt%	1.3000	16.35047	1.000	-54.9674	57.5674
	2wt%	11.4000	18.13921	1.000	-51.0231	73.8231
	5wt%	8.0000	18.13921	1.000	-54.4231	70.4231
	Control	214.8000*	15.09274	.000	162.8608	266.7392
	0.1wt%	62.9765*	14.59118	.003	12.7633	113.1896
	0.2wt%	97.0500*	16.35047	.000	40.7826	153.3174
	0.3wt%	85.6750*	16.35047	.000	29.4076	141.9424
	0.4wt%	76.6750*	16.35047	.001	20.4076	132.9424
	0.5wt%	64.8000*	16.35047	.010	8.5326	121.0674
5wt%	0.6wt%	49.5500	16.35047	.146	-6.7174	105.8174
	0.7wt%	32.5500	16.35047	.769	-23.7174	88.8174
	0.8wt%	21.5500	16.35047	.988	-34.7174	77.8174
	1wt%	17.3000	16.35047	.999	-38.9674	73.5674
	1.5wt%	-6.7000	16.35047	1.000	-62.9674	49.5674
	2wt%	3.4000	18.13921	1.000	-59.0231	65.8231
	3wt%	-8.0000	18.13921	1.000	-70.4231	54.4231

Based on observed means.

The error term is Mean Square (Error) = 822.578.

*. The mean difference is significant at the .05 level.

Post Hoc Tests

Element

Multiple Comparisons

Dependent Variable: Brinell hardness

Tukey HSD

(I) Dopant	(J) Dopant	Mean Difference (I-J)	Std. Error	Sig.	95% Confidence Interval	
					Lower Bound	Upper Bound
	Control	42.3846*	8.23218	.000	16.2581	68.5112
	Sn	11.0769	8.23218	.915	-15.0496	37.2035
Zn	Mg	-28.6923*	8.23218	.020	-54.8189	-2.5658
	Mn	-67.3846*	8.23218	.000	-93.5112	-41.2581
	W	-85.6923*	8.23218	.000	-111.8189	-59.5658

Control	Ti	-23.3077	8.23218	.120	-49.4342	2.8189
	Mo	54.3077*	8.23218	.000	28.1811	80.4342
	Al	-2.2308	8.23218	1.000	-28.3573	23.8958
	Zn	-42.3846*	8.23218	.000	-68.5112	-16.2581
	Sn	-31.3077*	8.23218	.007	-57.4342	-5.1811
	Mg	-71.0769*	8.23218	.000	-97.2035	-44.9504
	Mn	-109.7692*	8.23218	.000	-135.8958	-83.6427
	W	-128.0769*	8.23218	.000	-154.2035	-101.9504
Sn	Ti	-65.6923*	8.23218	.000	-91.8189	-39.5658
	Mo	11.9231	8.23218	.876	-14.2035	38.0496
	Al	-44.6154*	8.23218	.000	-70.7419	-18.4888
	Zn	-11.0769	8.23218	.915	-37.2035	15.0496
	Control	31.3077*	8.23218	.007	5.1811	57.4342
	Mg	-39.7692*	8.23218	.000	-65.8958	-13.6427
	Mn	-78.4615*	8.23218	.000	-104.5881	-52.3350
	W	-96.7692*	8.23218	.000	-122.8958	-70.6427
Mg	Ti	-34.3846*	8.23218	.002	-60.5112	-8.2581
	Mo	43.2308*	8.23218	.000	17.1042	69.3573
	Al	-13.3077	8.23218	.793	-39.4342	12.8189
	Zn	28.6923*	8.23218	.020	2.5658	54.8189
	Control	71.0769*	8.23218	.000	44.9504	97.2035
	Sn	39.7692*	8.23218	.000	13.6427	65.8958
	Mn	-38.6923*	8.23218	.000	-64.8189	-12.5658
	W	-57.0000*	8.23218	.000	-83.1266	-30.8734
Mn	Ti	5.3846	8.23218	.999	-20.7419	31.5112
	Mo	83.0000*	8.23218	.000	56.8734	109.1266
	Al	26.4615*	8.23218	.045	.3350	52.5881
	Zn	67.3846*	8.23218	.000	41.2581	93.5112
	Control	109.7692*	8.23218	.000	83.6427	135.8958
	Sn	78.4615*	8.23218	.000	52.3350	104.5881
	Mg	38.6923*	8.23218	.000	12.5658	64.8189
	W	-18.3077	8.23218	.399	-44.4342	7.8189
W	Ti	44.0769*	8.23218	.000	17.9504	70.2035
	Mo	121.6923*	8.23218	.000	95.5658	147.8189
	Al	65.1538*	8.23218	.000	39.0273	91.2804
	Zn	85.6923*	8.23218	.000	59.5658	111.8189
	Control	128.0769*	8.23218	.000	101.9504	154.2035
	Sn	96.7692*	8.23218	.000	70.6427	122.8958
	Mg	57.0000*	8.23218	.000	30.8734	83.1266
	Mn	18.3077	8.23218	.399	-7.8189	44.4342
	Ti	62.3846*	8.23218	.000	36.2581	88.5112
	Mo	140.0000*	8.23218	.000	113.8734	166.1266
	Al	83.4615*	8.23218	.000	57.3350	109.5881

Ti	Zn	23.3077	8.23218	.120	-2.8189	49.4342
	Control	65.6923*	8.23218	.000	39.5658	91.8189
	Sn	34.3846*	8.23218	.002	8.2581	60.5112
	Mg	-5.3846	8.23218	.999	-31.5112	20.7419
	Mn	-44.0769*	8.23218	.000	-70.2035	-17.9504
	W	-62.3846*	8.23218	.000	-88.5112	-36.2581
	Mo	77.6154*	8.23218	.000	51.4888	103.7419
	Al	21.0769	8.23218	.217	-5.0496	47.2035
Mo	Zn	-54.3077*	8.23218	.000	-80.4342	-28.1811
	Control	-11.9231	8.23218	.876	-38.0496	14.2035
	Sn	-43.2308*	8.23218	.000	-69.3573	-17.1042
	Mg	-83.0000*	8.23218	.000	-109.1266	-56.8734
	Mn	-121.6923*	8.23218	.000	-147.8189	-95.5658
	W	-140.0000*	8.23218	.000	-166.1266	-113.8734
	Ti	-77.6154*	8.23218	.000	-103.7419	-51.4888
	Al	-56.5385*	8.23218	.000	-82.6650	-30.4119
Al	Zn	2.2308	8.23218	1.000	-23.8958	28.3573
	Control	44.6154*	8.23218	.000	18.4888	70.7419
	Sn	13.3077	8.23218	.793	-12.8189	39.4342
	Mg	-26.4615*	8.23218	.045	-52.5881	-.3350
	Mn	-65.1538*	8.23218	.000	-91.2804	-39.0273
	W	-83.4615*	8.23218	.000	-109.5881	-57.3350
	Ti	-21.0769	8.23218	.217	-47.2035	5.0496
	Mo	56.5385*	8.23218	.000	30.4119	82.6650

Based on observed means.

The error term is Mean Square(Error) = 440.497.

*. The mean difference is significant at the .05 level.

Composition

Multiple Comparisons

Dependent Variable: Brinell hardness

Tukey HSD

(I) Composition	(J) Composition	Mean Difference (I-J)	Std. Error	Sig.	95% Confidence Interval	
					Lower Bound	Upper Bound
Control	0.1wt%	-45.9412*	7.73278	.000	-72.5523	-19.3301
	0.2wt%	-32.8750*	9.43114	.044	-65.3307	-.4193
	0.3wt%	-39.6250*	9.43114	.004	-72.0807	-7.1693
	0.4wt%	-47.3750*	9.43114	.000	-79.8307	-14.9193
	0.5wt%	-52.2500*	9.43114	.000	-84.7057	-19.7943
	0.6wt%	-63.8750*	9.43114	.000	-96.3307	-31.4193
	0.7wt%	-75.5000*	9.43114	.000	-107.9557	-43.0443
	0.8wt%	-84.1250*	9.43114	.000	-116.5807	-51.6693
	1wt%	-78.2500*	9.43114	.000	-110.7057	-45.7943
	1.5wt%	-80.5000*	9.43114	.000	-112.9557	-48.0443
	2wt%	-67.4000*	11.04462	.000	-105.4083	-29.3917
	3wt%	-73.4000*	11.04462	.000	-111.4083	-35.3917
	5wt%	-66.6000*	11.04462	.000	-104.6083	-28.5917
0.1wt%	Control	45.9412*	7.73278	.000	19.3301	72.5523
	0.2wt%	13.0662	8.99854	.973	-17.9008	44.0332
	0.3wt%	6.3162	8.99854	1.000	-24.6508	37.2832
	0.4wt%	-1.4338	8.99854	1.000	-32.4008	29.5332
	0.5wt%	-6.3088	8.99854	1.000	-37.2758	24.6582
	0.6wt%	-17.9338	8.99854	.768	-48.9008	13.0332
	0.7wt%	-29.5588	8.99854	.077	-60.5258	1.4082
	0.8wt%	-38.1838*	8.99854	.004	-69.1508	-7.2168
	1wt%	-32.3088*	8.99854	.032	-63.2758	-1.3418
	1.5wt%	-34.5588*	8.99854	.015	-65.5258	-3.5918
	2wt%	-21.4588	10.67759	.758	-58.2040	15.2863
	3wt%	-27.4588	10.67759	.372	-64.2040	9.2863
	5wt%	-20.6588	10.67759	.802	-57.4040	16.0863
0.2wt%	Control	32.8750*	9.43114	.044	.4193	65.3307
	0.1wt%	-13.0662	8.99854	.973	-44.0332	17.9008
	0.3wt%	-6.7500	10.49401	1.000	-42.8634	29.3634
	0.4wt%	-14.5000	10.49401	.982	-50.6134	21.6134
	0.5wt%	-19.3750	10.49401	.849	-55.4884	16.7384
	0.6wt%	-31.0000	10.49401	.174	-67.1134	5.1134
	0.7wt%	-42.6250*	10.49401	.007	-78.7384	-6.5116
	0.8wt%	-51.2500*	10.49401	.000	-87.3634	-15.1366

	1wt%	-45.3750*	10.49401	.003	-81.4884	-9.2616
	1.5wt%	-47.6250*	10.49401	.001	-83.7384	-11.5116
	2wt%	-34.5250	11.96501	.202	-75.7006	6.6506
	3wt%	-40.5250	11.96501	.058	-81.7006	.6506
	5wt%	-33.7250	11.96501	.233	-74.9006	7.4506
	Control	39.6250*	9.43114	.004	7.1693	72.0807
	0.1wt%	-6.3162	8.99854	1.000	-37.2832	24.6508
	0.2wt%	6.7500	10.49401	1.000	-29.3634	42.8634
	0.4wt%	-7.7500	10.49401	1.000	-43.8634	28.3634
	0.5wt%	-12.6250	10.49401	.995	-48.7384	23.4884
	0.6wt%	-24.2500	10.49401	.551	-60.3634	11.8634
0.3wt%	0.7wt%	-35.8750	10.49401	.053	-71.9884	.2384
	0.8wt%	-44.5000*	10.49401	.004	-80.6134	-8.3866
	1wt%	-38.6250*	10.49401	.025	-74.7384	-2.5116
	1.5wt%	-40.8750*	10.49401	.012	-76.9884	-4.7616
	2wt%	-27.7750	11.96501	.544	-68.9506	13.4006
	3wt%	-33.7750	11.96501	.231	-74.9506	7.4006
	5wt%	-26.9750	11.96501	.592	-68.1506	14.2006
	Control	47.3750*	9.43114	.000	14.9193	79.8307
	0.1wt%	1.4338	8.99854	1.000	-29.5332	32.4008
	0.2wt%	14.5000	10.49401	.982	-21.6134	50.6134
	0.3wt%	7.7500	10.49401	1.000	-28.3634	43.8634
	0.5wt%	-4.8750	10.49401	1.000	-40.9884	31.2384
	0.6wt%	-16.5000	10.49401	.949	-52.6134	19.6134
0.4wt%	0.7wt%	-28.1250	10.49401	.307	-64.2384	7.9884
	0.8wt%	-36.7500*	10.49401	.042	-72.8634	-.6366
	1wt%	-30.8750	10.49401	.179	-66.9884	5.2384
	1.5wt%	-33.1250	10.49401	.107	-69.2384	2.9884
	2wt%	-20.0250	11.96501	.920	-61.2006	21.1506
	3wt%	-26.0250	11.96501	.648	-67.2006	15.1506
	5wt%	-19.2250	11.96501	.940	-60.4006	21.9506
	Control	52.2500*	9.43114	.000	19.7943	84.7057
	0.1wt%	6.3088	8.99854	1.000	-24.6582	37.2758
	0.2wt%	19.3750	10.49401	.849	-16.7384	55.4884
	0.3wt%	12.6250	10.49401	.995	-23.4884	48.7384
	0.6wt%	4.8750	10.49401	1.000	-31.2384	40.9884
0.5wt%	0.7wt%	-11.6250	10.49401	.998	-47.7384	24.4884
	0.8wt%	-23.2500	10.49401	.619	-59.3634	12.8634
	1wt%	-31.8750	10.49401	.143	-67.9884	4.2384
	1.5wt%	-26.0000	10.49401	.434	-62.1134	10.1134
	2wt%	-28.2500	10.49401	.300	-64.3634	7.8634
	3wt%	-15.1500	11.96501	.992	-56.3256	26.0256
	5wt%	-21.1500	11.96501	.885	-62.3256	20.0256

	Control	-14.3500	11.96501	.995	-55.5256	26.8256
	0.1wt%	63.8750*	9.43114	.000	31.4193	96.3307
	0.2wt%	17.9338	8.99854	.768	-13.0332	48.9008
	0.3wt%	31.0000	10.49401	.174	-5.1134	67.1134
	0.5wt%	24.2500	10.49401	.551	-11.8634	60.3634
	0.7wt%	16.5000	10.49401	.949	-19.6134	52.6134
	0.8wt%	11.6250	10.49401	.998	-24.4884	47.7384
0.6wt%	1wt%	-11.6250	10.49401	.998	-47.7384	24.4884
	1.5wt%	-20.2500	10.49401	.805	-56.3634	15.8634
	2wt%	-14.3750	10.49401	.983	-50.4884	21.7384
	3wt%	-16.6250	10.49401	.946	-52.7384	19.4884
	5wt%	-3.5250	11.96501	1.000	-44.7006	37.6506
	Control	-9.5250	11.96501	1.000	-50.7006	31.6506
	0.1wt%	-2.7250	11.96501	1.000	-43.9006	38.4506
	0.2wt%	75.5000*	9.43114	.000	43.0443	107.9557
	0.3wt%	29.5588	8.99854	.077	-1.4082	60.5258
	0.5wt%	42.6250*	10.49401	.007	6.5116	78.7384
	0.6wt%	35.8750	10.49401	.053	-.2384	71.9884
	0.8wt%	28.1250	10.49401	.307	-7.9884	64.2384
	1wt%	23.2500	10.49401	.619	-12.8634	59.3634
0.7wt%	1.5wt%	11.6250	10.49401	.998	-24.4884	47.7384
	2wt%	-8.6250	10.49401	1.000	-44.7384	27.4884
	3wt%	-2.7500	10.49401	1.000	-38.8634	33.3634
	5wt%	-5.0000	10.49401	1.000	-41.1134	31.1134
	0.1wt%	8.1000	11.96501	1.000	-33.0756	49.2756
	0.2wt%	2.1000	11.96501	1.000	-39.0756	43.2756
	1wt%	8.9000	11.96501	1.000	-32.2756	50.0756
	Control	84.1250*	9.43114	.000	51.6693	116.5807
	0.1wt%	38.1838*	8.99854	.004	7.2168	69.1508
	0.2wt%	51.2500*	10.49401	.000	15.1366	87.3634
	0.3wt%	44.5000*	10.49401	.004	8.3866	80.6134
	0.4wt%	36.7500*	10.49401	.042	.6366	72.8634
	0.5wt%	31.8750	10.49401	.143	-4.2384	67.9884
0.8wt%	0.6wt%	20.2500	10.49401	.805	-15.8634	56.3634
	0.7wt%	8.6250	10.49401	1.000	-27.4884	44.7384
	1wt%	5.8750	10.49401	1.000	-30.2384	41.9884
	1.5wt%	3.6250	10.49401	1.000	-32.4884	39.7384
	2wt%	16.7250	11.96501	.980	-24.4506	57.9006
	3wt%	10.7250	11.96501	1.000	-30.4506	51.9006
	5wt%	17.5250	11.96501	.971	-23.6506	58.7006
	Control	78.2500*	9.43114	.000	45.7943	110.7057
1wt%	0.1wt%	32.3088*	8.99854	.032	1.3418	63.2758
	0.2wt%	45.3750*	10.49401	.003	9.2616	81.4884

	0.3wt%	38.6250*	10.49401	.025	2.5116	74.7384
	0.4wt%	30.8750	10.49401	.179	-5.2384	66.9884
	0.5wt%	26.0000	10.49401	.434	-10.1134	62.1134
	0.6wt%	14.3750	10.49401	.983	-21.7384	50.4884
	0.7wt%	2.7500	10.49401	1.000	-33.3634	38.8634
	0.8wt%	-5.8750	10.49401	1.000	-41.9884	30.2384
	1.5wt%	-2.2500	10.49401	1.000	-38.3634	33.8634
	2wt%	10.8500	11.96501	1.000	-30.3256	52.0256
	3wt%	4.8500	11.96501	1.000	-36.3256	46.0256
	5wt%	11.6500	11.96501	.999	-29.5256	52.8256
	Control	80.5000*	9.43114	.000	48.0443	112.9557
	0.1wt%	34.5588*	8.99854	.015	3.5918	65.5258
	0.2wt%	47.6250*	10.49401	.001	11.5116	83.7384
	0.3wt%	40.8750*	10.49401	.012	4.7616	76.9884
	0.4wt%	33.1250	10.49401	.107	-2.9884	69.2384
	0.5wt%	28.2500	10.49401	.300	-7.8634	64.3634
1.5wt%	0.6wt%	16.6250	10.49401	.946	-19.4884	52.7384
	0.7wt%	5.0000	10.49401	1.000	-31.1134	41.1134
	0.8wt%	-3.6250	10.49401	1.000	-39.7384	32.4884
	1wt%	2.2500	10.49401	1.000	-33.8634	38.3634
	2wt%	13.1000	11.96501	.998	-28.0756	54.2756
	3wt%	7.1000	11.96501	1.000	-34.0756	48.2756
	5wt%	13.9000	11.96501	.996	-27.2756	55.0756
	Control	67.4000*	11.04462	.000	29.3917	105.4083
	0.1wt%	21.4588	10.67759	.758	-15.2863	58.2040
	0.2wt%	34.5250	11.96501	.202	-6.6506	75.7006
	0.3wt%	27.7750	11.96501	.544	-13.4006	68.9506
	0.4wt%	20.0250	11.96501	.920	-21.1506	61.2006
	0.5wt%	15.1500	11.96501	.992	-26.0256	56.3256
2wt%	0.6wt%	3.5250	11.96501	1.000	-37.6506	44.7006
	0.7wt%	-8.1000	11.96501	1.000	-49.2756	33.0756
	0.8wt%	-16.7250	11.96501	.980	-57.9006	24.4506
	1wt%	-10.8500	11.96501	1.000	-52.0256	30.3256
	1.5wt%	-13.1000	11.96501	.998	-54.2756	28.0756
	3wt%	-6.0000	13.27399	1.000	-51.6802	39.6802
	5wt%	.8000	13.27399	1.000	-44.8802	46.4802
	Control	73.4000*	11.04462	.000	35.3917	111.4083
	0.1wt%	27.4588	10.67759	.372	-9.2863	64.2040
	0.2wt%	40.5250	11.96501	.058	-.6506	81.7006
3wt%	0.3wt%	33.7750	11.96501	.231	-7.4006	74.9506
	0.4wt%	26.0250	11.96501	.648	-15.1506	67.2006
	0.5wt%	21.1500	11.96501	.885	-20.0256	62.3256
	0.6wt%	9.5250	11.96501	1.000	-31.6506	50.7006

	0.7wt%	-2.1000	11.96501	1.000	-43.2756	39.0756
	0.8wt%	-10.7250	11.96501	1.000	-51.9006	30.4506
	1wt%	-4.8500	11.96501	1.000	-46.0256	36.3256
	1.5wt%	-7.1000	11.96501	1.000	-48.2756	34.0756
	2wt%	6.0000	13.27399	1.000	-39.6802	51.6802
	5wt%	6.8000	13.27399	1.000	-38.8802	52.4802
	Control	66.6000*	11.04462	.000	28.5917	104.6083
	0.1wt%	20.6588	10.67759	.802	-16.0863	57.4040
	0.2wt%	33.7250	11.96501	.233	-7.4506	74.9006
	0.3wt%	26.9750	11.96501	.592	-14.2006	68.1506
	0.4wt%	19.2250	11.96501	.940	-21.9506	60.4006
	0.5wt%	14.3500	11.96501	.995	-26.8256	55.5256
5wt%	0.6wt%	2.7250	11.96501	1.000	-38.4506	43.9006
	0.7wt%	-8.9000	11.96501	1.000	-50.0756	32.2756
	0.8wt%	-17.5250	11.96501	.971	-58.7006	23.6506
	1wt%	-11.6500	11.96501	.999	-52.8256	29.5256
	1.5wt%	-13.9000	11.96501	.996	-55.0756	27.2756
	2wt%	-.8000	13.27399	1.000	-46.4802	44.8802
	3wt%	-6.8000	13.27399	1.000	-52.4802	38.8802

Based on observed means.

The error term is Mean Square (Error) = 440.497.

*. The mean difference is significant at the .05 level.

Appendix 5: Multiple Comparisons of selected mechanical properties of the developed silicon bronzes and those developed by other researchers

Dependent Variable: Hardness

Tukey HSD

(I) Alloys	(J) Alloys	Mean Difference (I-J)	Std. Error	Sig.	95% Confidence Interval	
					Lower Bound	Upper Bound
Cu-3wt%Si-3wt%Zn/S.H	Cu-3wt%Si-3wt%Sn/ cast	-10.00000*	.00000	.000	-10.0000	-10.0000
	Cu-3wt%Si-0.8wt%Mg/S.H	-119.00000*	.00000	.000	-119.0000	-119.0000
	Cu-3wt%Si-1wt%Mn/S.H	-122.00000*	.00000	.000	-122.0000	-122.0000
	Cu-3wt%Si-0.8wt%W/S.H	-96.00000*	.00000	.000	-96.0000	-96.0000
	Cu-3wt%Si-2wt%Ti/S.H	-40.00000*	.00000	.000	-40.0000	-40.0000
	Cu-1.8wt%Si-8wt%Ni-0.6wt%Sn-0.15wt%Mg/rolled & aged	-77.00000*	.00000	.000	-77.0000	-77.0000

	Cu-0.7wt%Si-3.2wt%Ni-0.3wt%Zn/rolled & aged	18.00000*	.00000	.000	18.0000	18.0000
	Cu-0.7wt%Si-3.2wt%Ni-0.3wt%Zn/cast & aged	28.00000*	.00000	.000	28.0000	28.0000
	Cu-1.4wt%Si-6wt%Ni-0.1wt%Cr-0.15wt%Mg/rolled & aged	-70.00000*	.00000	.000	-70.0000	-70.0000
	Cu-1wt%Si-6wt%Ni-0.1wt%Cr-0.5wt%Al-0.15wt%Mg/ rolled & aged	-75.00000*	.00000	.000	-75.0000	-75.0000
	Cu-0.5wt%Si-39.5wt%Zn/Cast	144.60000*	.00000	.000	144.6000	144.6000
	Cu-3wt%Si-3wt%Zn/S.H	10.00000*	.00000	.000	10.0000	10.0000
	Cu-3wt%Si-0.8wt%Mg/S.H	-109.00000*	.00000	.000	-109.0000	-109.0000
	Cu-3wt%Si-1wt%Mn/S.H	-112.00000*	.00000	.000	-112.0000	-112.0000
	Cu-3wt%Si-0.8wt%W/S.H	-86.00000*	.00000	.000	-86.0000	-86.0000
	Cu-3wt%Si-2wt%Ti/S.H	-30.00000*	.00000	.000	-30.0000	-30.0000
	Cu-1.8wt%Si-8wt%Ni-0.6wt%Sn-0.15wt%Mg/rolled & aged	-67.00000*	.00000	.000	-67.0000	-67.0000
Cu-3wt%Si-3wt%Sn/ cast	Cu-0.7wt%Si-3.2wt%Ni-0.3wt%Zn/rolled & aged	28.00000*	.00000	.000	28.0000	28.0000
	Cu-0.7wt%Si-3.2wt%Ni-0.3wt%Zn/cast & aged	38.00000*	.00000	.000	38.0000	38.0000
	Cu-1.4wt%Si-6wt%Ni-0.1wt%Cr-0.15wt%Mg/rolled & aged	-60.00000*	.00000	.000	-60.0000	-60.0000
	Cu-1wt%Si-6wt%Ni-0.1wt%Cr-0.5wt%Al-0.15wt%Mg/ rolled & aged	-65.00000*	.00000	.000	-65.0000	-65.0000
	Cu-0.5wt%Si-39.5wt%Zn/Cast	154.60000*	.00000	.000	154.6000	154.6000
	Cu-3wt%Si-3wt%Zn/S.H	119.00000*	.00000	.000	119.0000	119.0000
	Cu-3wt%Si-3wt%Sn/ cast	109.00000*	.00000	.000	109.0000	109.0000
	Cu-3wt%Si-1wt%Mn/S.H	-3.00000*	.00000	.000	-3.0000	-3.0000
	Cu-3wt%Si-0.8wt%W/S.H	23.00000*	.00000	.000	23.0000	23.0000
Cu-3wt%Si-0.8wt%Mg/S.H	Cu-3wt%Si-2wt%Ti/S.H	79.00000*	.00000	.000	79.0000	79.0000
	Cu-1.8wt%Si-8wt%Ni-0.6wt%Sn-0.15wt%Mg/rolled & aged	42.00000*	.00000	.000	42.0000	42.0000
	Cu-0.7wt%Si-3.2wt%Ni-0.3wt%Zn/rolled & aged	137.00000*	.00000	.000	137.0000	137.0000

	Cu-0.7wt%Si-3.2wt%Ni-0.3wt%Zn/cast & aged	147.00000*	.00000	.000	147.0000	147.0000
	Cu-1.4wt%Si-6wt%Ni-0.1wt%Cr-0.15wt%Mg/rolled & aged	49.00000*	.00000	.000	49.0000	49.0000
	Cu-1wt%Si-6wt%Ni-0.1wt%Cr-0.5wt%Al-0.15wt%Mg/ rolled & aged	44.00000*	.00000	.000	44.0000	44.0000
	Cu-0.5wt%Si-39.5wt%Zn/Cast	263.60000*	.00000	.000	263.6000	263.6000
	Cu-3wt%Si-3wt%Zn/S.H	122.00000*	.00000	.000	122.0000	122.0000
	Cu-3wt%Si-3wt%Sn/ cast	112.00000*	.00000	.000	112.0000	112.0000
	Cu-3wt%Si-0.8wt%Mg/S.H	3.00000*	.00000	.000	3.0000	3.0000
	Cu-3wt%Si-0.8wt%W/S.H	26.00000*	.00000	.000	26.0000	26.0000
	Cu-3wt%Si-2wt%Ti/S.H	82.00000*	.00000	.000	82.0000	82.0000
	Cu-1.8wt%Si-8wt%Ni-0.6wt%Sn-0.15wt%Mg/rolled & aged	45.00000*	.00000	.000	45.0000	45.0000
Cu-3wt%Si-1wt%Mn/S.H	Cu-0.7wt%Si-3.2wt%Ni-0.3wt%Zn/rolled & aged	140.00000*	.00000	.000	140.0000	140.0000
	Cu-0.7wt%Si-3.2wt%Ni-0.3wt%Zn/cast & aged	150.00000*	.00000	.000	150.0000	150.0000
	Cu-1.4wt%Si-6wt%Ni-0.1wt%Cr-0.15wt%Mg/rolled & aged	52.00000*	.00000	.000	52.0000	52.0000
	Cu-1wt%Si-6wt%Ni-0.1wt%Cr-0.5wt%Al-0.15wt%Mg/ rolled & aged	47.00000*	.00000	.000	47.0000	47.0000
	Cu-0.5wt%Si-39.5wt%Zn/Cast	266.60000*	.00000	.000	266.6000	266.6000
	Cu-3wt%Si-3wt%Zn/S.H	96.00000*	.00000	.000	96.0000	96.0000
	Cu-3wt%Si-3wt%Sn/ cast	86.00000*	.00000	.000	86.0000	86.0000
	Cu-3wt%Si-0.8wt%Mg/S.H	-23.00000*	.00000	.000	-23.0000	-23.0000
	Cu-3wt%Si-1wt%Mn/S.H	-26.00000*	.00000	.000	-26.0000	-26.0000
	Cu-3wt%Si-2wt%Ti/S.H	56.00000*	.00000	.000	56.0000	56.0000
Cu-3wt%Si-0.8wt%W/S.H	Cu-1.8wt%Si-8wt%Ni-0.6wt%Sn-0.15wt%Mg/rolled & aged	19.00000*	.00000	.000	19.0000	19.0000
	Cu-0.7wt%Si-3.2wt%Ni-0.3wt%Zn/rolled & aged	114.00000*	.00000	.000	114.0000	114.0000
	Cu-0.7wt%Si-3.2wt%Ni-0.3wt%Zn/cast & aged	124.00000*	.00000	.000	124.0000	124.0000

	Cu-1.4wt%Si-6wt%Ni-0.1wt%Cr-0.15wt%Mg/rolled & aged	26.00000*	.00000	.000	26.0000	26.0000
	Cu-1wt%Si-6wt%Ni-0.1wt%Cr-0.5wt%Al-0.15wt%Mg/ rolled & aged	21.00000*	.00000	.000	21.0000	21.0000
	Cu-0.5wt%Si-39.5wt%Zn/Cast	240.60000*	.00000	.000	240.6000	240.6000
	Cu-3wt%Si-3wt%Zn/S.H	40.00000*	.00000	.000	40.0000	40.0000
	Cu-3wt%Si-3wt%Sn/ cast	30.00000*	.00000	.000	30.0000	30.0000
	Cu-3wt%Si-0.8wt%Mg/S.H	-79.00000*	.00000	.000	-79.0000	-79.0000
	Cu-3wt%Si-1wt%Mn/S.H	-82.00000*	.00000	.000	-82.0000	-82.0000
	Cu-3wt%Si-0.8wt%W/S.H	-56.00000*	.00000	.000	-56.0000	-56.0000
	Cu-1.8wt%Si-8wt%Ni-0.6wt%Sn-0.15wt%Mg/rolled & aged	-37.00000*	.00000	.000	-37.0000	-37.0000
Cu-3wt%Si-2wt%Ti/S.H	Cu-0.7wt%Si-3.2wt%Ni-0.3wt%Zn/rolled & aged	58.00000*	.00000	.000	58.0000	58.0000
	Cu-0.7wt%Si-3.2wt%Ni-0.3wt%Zn/cast & aged	68.00000*	.00000	.000	68.0000	68.0000
	Cu-1.4wt%Si-6wt%Ni-0.1wt%Cr-0.15wt%Mg/rolled & aged	-30.00000*	.00000	.000	-30.0000	-30.0000
	Cu-1wt%Si-6wt%Ni-0.1wt%Cr-0.5wt%Al-0.15wt%Mg/ rolled & aged	-35.00000*	.00000	.000	-35.0000	-35.0000
	Cu-0.5wt%Si-39.5wt%Zn/Cast	184.60000*	.00000	.000	184.6000	184.6000
	Cu-3wt%Si-3wt%Zn/S.H	77.00000*	.00000	.000	77.0000	77.0000
	Cu-3wt%Si-3wt%Sn/ cast	67.00000*	.00000	.000	67.0000	67.0000
	Cu-3wt%Si-0.8wt%Mg/S.H	-42.00000*	.00000	.000	-42.0000	-42.0000
	Cu-3wt%Si-1wt%Mn/S.H	-45.00000*	.00000	.000	-45.0000	-45.0000
	Cu-3wt%Si-0.8wt%W/S.H	-19.00000*	.00000	.000	-19.0000	-19.0000
Cu-1.8wt%Si-8wt%Ni-0.6wt%Sn-0.15wt%Mg/rolled & aged	Cu-3wt%Si-2wt%Ti/S.H	37.00000*	.00000	.000	37.0000	37.0000
	Cu-0.7wt%Si-3.2wt%Ni-0.3wt%Zn/rolled & aged	95.00000*	.00000	.000	95.0000	95.0000
	Cu-0.7wt%Si-3.2wt%Ni-0.3wt%Zn/cast & aged	105.00000*	.00000	.000	105.0000	105.0000
	Cu-1.4wt%Si-6wt%Ni-0.1wt%Cr-0.15wt%Mg/rolled & aged	7.00000*	.00000	.000	7.0000	7.0000

	Cu-1wt%Si-6wt%Ni-0.1wt%Cr-0.5wt%Al-0.15wt%Mg/ rolled & aged	2.00000*	.00000	.000	2.0000	2.0000
	Cu-0.5wt%Si-39.5wt%Zn/Cast	221.60000*	.00000	.000	221.6000	221.6000
Cu-0.7wt%Si-3.2wt%Ni-0.3wt%Zn/rolled & aged	Cu-3wt%Si-3wt%Zn/S.H	-18.00000*	.00000	.000	-18.0000	-18.0000
	Cu-3wt%Si-3wt%Sn/ cast	-28.00000*	.00000	.000	-28.0000	-28.0000
	Cu-3wt%Si-0.8wt%Mg/S.H	-137.00000*	.00000	.000	-137.0000	-137.0000
	Cu-3wt%Si-1wt%Mn/S.H	-140.00000*	.00000	.000	-140.0000	-140.0000
	Cu-3wt%Si-0.8wt%W/S.H	-114.00000*	.00000	.000	-114.0000	-114.0000
	Cu-3wt%Si-2wt%Ti/S.H	-58.00000*	.00000	.000	-58.0000	-58.0000
	Cu-1.8wt%Si-8wt%Ni-0.6wt%Sn-0.15wt%Mg/rolled & aged	-95.00000*	.00000	.000	-95.0000	-95.0000
	Cu-0.7wt%Si-3.2wt%Ni-0.3wt%Zn/cast & aged	10.00000*	.00000	.000	10.0000	10.0000
	Cu-1.4wt%Si-6wt%Ni-0.1wt%Cr-0.15wt%Mg/rolled & aged	-88.00000*	.00000	.000	-88.0000	-88.0000
	Cu-1wt%Si-6wt%Ni-0.1wt%Cr-0.5wt%Al-0.15wt%Mg/ rolled & aged	-93.00000*	.00000	.000	-93.0000	-93.0000
	Cu-0.5wt%Si-39.5wt%Zn/Cast	126.60000*	.00000	.000	126.6000	126.6000
Cu-0.7wt%Si-3.2wt%Ni-0.3wt%Zn/cast & aged	Cu-3wt%Si-3wt%Zn/S.H	-28.00000*	.00000	.000	-28.0000	-28.0000
	Cu-3wt%Si-3wt%Sn/ cast	-38.00000*	.00000	.000	-38.0000	-38.0000
	Cu-3wt%Si-0.8wt%Mg/S.H	-147.00000*	.00000	.000	-147.0000	-147.0000
	Cu-3wt%Si-1wt%Mn/S.H	-150.00000*	.00000	.000	-150.0000	-150.0000
	Cu-3wt%Si-0.8wt%W/S.H	-124.00000*	.00000	.000	-124.0000	-124.0000
	Cu-3wt%Si-2wt%Ti/S.H	-68.00000*	.00000	.000	-68.0000	-68.0000
	Cu-1.8wt%Si-8wt%Ni-0.6wt%Sn-0.15wt%Mg/rolled & aged	-105.00000*	.00000	.000	-105.0000	-105.0000
	Cu-0.7wt%Si-3.2wt%Ni-0.3wt%Zn/rolled & aged	-10.00000*	.00000	.000	-10.0000	-10.0000
	Cu-1.4wt%Si-6wt%Ni-0.1wt%Cr-0.15wt%Mg/rolled & aged	-98.00000*	.00000	.000	-98.0000	-98.0000
	Cu-1wt%Si-6wt%Ni-0.1wt%Cr-0.5wt%Al-0.15wt%Mg/ rolled & aged	-103.00000*	.00000	.000	-103.0000	-103.0000
	Cu-0.5wt%Si-39.5wt%Zn/Cast	116.60000*	.00000	.000	116.6000	116.6000

Cu-1.4wt%Si-6wt%Ni-0.1wt%Cr-0.15wt%Mg/rolled & aged	Cu-3wt%Si-3wt%Zn/S.H	70.00000*	.00000	.000	70.0000	70.0000
	Cu-3wt%Si-3wt%Sn/ cast	60.00000*	.00000	.000	60.0000	60.0000
	Cu-3wt%Si-0.8wt%Mg/S.H	-49.00000*	.00000	.000	-49.0000	-49.0000
	Cu-3wt%Si-1wt%Mn/S.H	-52.00000*	.00000	.000	-52.0000	-52.0000
	Cu-3wt%Si-0.8wt%W/S.H	-26.00000*	.00000	.000	-26.0000	-26.0000
	Cu-3wt%Si-2wt%Ti/S.H	30.00000*	.00000	.000	30.0000	30.0000
	Cu-1.8wt%Si-8wt%Ni-0.6wt%Sn-0.15wt%Mg/rolled & aged	-7.00000*	.00000	.000	-7.0000	-7.0000
	Cu-0.7wt%Si-3.2wt%Ni-0.3wt%Zn/rolled & aged	88.00000*	.00000	.000	88.0000	88.0000
	Cu-0.7wt%Si-3.2wt%Ni-0.3wt%Zn/cast & aged	98.00000*	.00000	.000	98.0000	98.0000
	Cu-1wt%Si-6wt%Ni-0.1wt%Cr-0.5wt%Al-0.15wt%Mg/ rolled & aged	-5.00000*	.00000	.000	-5.0000	-5.0000
	Cu-0.5wt%Si-39.5wt%Zn/Cast	214.60000*	.00000	.000	214.6000	214.6000
Cu-1wt%Si-6wt%Ni-0.1wt%Cr-0.5wt%Al-0.15wt%Mg/ rolled & aged	Cu-3wt%Si-3wt%Zn/S.H	75.00000*	.00000	.000	75.0000	75.0000
	Cu-3wt%Si-3wt%Sn/ cast	65.00000*	.00000	.000	65.0000	65.0000
	Cu-3wt%Si-0.8wt%Mg/S.H	-44.00000*	.00000	.000	-44.0000	-44.0000
	Cu-3wt%Si-1wt%Mn/S.H	-47.00000*	.00000	.000	-47.0000	-47.0000
	Cu-3wt%Si-0.8wt%W/S.H	-21.00000*	.00000	.000	-21.0000	-21.0000
	Cu-3wt%Si-2wt%Ti/S.H	35.00000*	.00000	.000	35.0000	35.0000
	Cu-1.8wt%Si-8wt%Ni-0.6wt%Sn-0.15wt%Mg/rolled & aged	-2.00000*	.00000	.000	-2.0000	-2.0000
	Cu-0.7wt%Si-3.2wt%Ni-0.3wt%Zn/rolled & aged	93.00000*	.00000	.000	93.0000	93.0000
	Cu-0.7wt%Si-3.2wt%Ni-0.3wt%Zn/cast & aged	103.00000*	.00000	.000	103.0000	103.0000
	Cu-1.4wt%Si-6wt%Ni-0.1wt%Cr-0.15wt%Mg/rolled & aged	5.00000*	.00000	.000	5.0000	5.0000
	Cu-0.5wt%Si-39.5wt%Zn/Cast	219.60000*	.00000	.000	219.6000	219.6000
Cu-0.5wt%Si-39.5wt%Zn/Cast	Cu-3wt%Si-3wt%Zn/S.H	-144.60000*	.00000	.000	-144.6000	-144.6000
	Cu-3wt%Si-3wt%Sn/ cast	-154.60000*	.00000	.000	-154.6000	-154.6000
	Cu-3wt%Si-0.8wt%Mg/S.H	-263.60000*	.00000	.000	-263.6000	-263.6000
	Cu-3wt%Si-1wt%Mn/S.H	-266.60000*	.00000	.000	-266.6000	-266.6000
	Cu-3wt%Si-0.8wt%W/S.H	-240.60000*	.00000	.000	-240.6000	-240.6000

	Cu-3wt%Si-2wt%Ti/S.H	-184.60000*	.00000	.000	-184.6000	-184.6000
	Cu-1.8wt%Si-8wt%Ni-0.6wt%Sn-0.15wt%Mg/rolled & aged	-221.60000*	.00000	.000	-221.6000	-221.6000
	Cu-0.7wt%Si-3.2wt%Ni-0.3wt%Zn/rolled & aged	-126.60000*	.00000	.000	-126.6000	-126.6000
	Cu-0.7wt%Si-3.2wt%Ni-0.3wt%Zn/cast & aged	-116.60000*	.00000	.000	-116.6000	-116.6000
	Cu-1.4wt%Si-6wt%Ni-0.1wt%Cr-0.15wt%Mg/rolled & aged	-214.60000*	.00000	.000	-214.6000	-214.6000
	Cu-1wt%Si-6wt%Ni-0.1wt%Cr-0.5wt%Al-0.15wt%Mg/ rolled & aged	-219.60000*	.00000	.000	-219.6000	-219.6000

*. The mean difference is significant at the 0.05 level.

Multiple Comparisons

Dependent Variable: Percentage elongation

Tukey HSD

(I) Alloys	(J) Alloys	Mean Difference (I-J)	Std. Error	Sig.	95% Confidence Interval	
					Lower Bound	Upper Bound
Cu-3wt%Si-3wt%Zn/S.H	Cu-3wt%Si-3wt%Sn/ cast	2.30000*	.00000	.000	2.3000	2.3000
	Cu-3wt%Si-0.8wt%Mg/S.H	-2.90000*	.00000	.000	-2.9000	-2.9000
	Cu-3wt%Si-1wt%Mn/S.H	8.00000*	.00000	.000	8.0000	8.0000
	Cu-3wt%Si-0.8wt%W/S.H	-2.20000*	.00000	.000	-2.2000	-2.2000
	Cu-3wt%Si-2wt%Ti/S.H	7.60000*	.00000	.000	7.6000	7.6000
	Cu-1.8wt%Si-8wt%Ni-0.6wt%Sn-0.15wt%Mg/rolled & aged	10.60000*	.00000	.000	10.6000	10.6000
	Cu-1.4wt%Si-6wt%Ni-0.1wt%Cr-0.15wt%Mg/rolled & aged	9.90000*	.00000	.000	9.9000	9.9000
	Cu-1wt%Si-6wt%Ni-0.1wt%Cr-0.5wt%Al-0.15wt%Mg/ rolled & aged	10.30000*	.00000	.000	10.3000	10.3000
Cu-3wt%Si-3wt%Sn/ cast	Cu-3wt%Si-3wt%Zn/S.H	-2.30000*	.00000	.000	-2.3000	-2.3000
	Cu-3wt%Si-0.8wt%Mg/S.H	-5.20000*	.00000	.000	-5.2000	-5.2000
	Cu-3wt%Si-1wt%Mn/S.H	5.70000*	.00000	.000	5.7000	5.7000
	Cu-3wt%Si-0.8wt%W/S.H	-4.50000*	.00000	.000	-4.5000	-4.5000
	Cu-3wt%Si-2wt%Ti/S.H	5.30000*	.00000	.000	5.3000	5.3000

	Cu-1.8wt%Si-8wt%Ni-0.6wt%Sn-0.15wt%Mg/rolled & aged	8.30000*	.00000	.000	8.3000	8.3000
	Cu-1.4wt%Si-6wt%Ni-0.1wt%Cr-0.15wt%Mg/rolled & aged	7.60000*	.00000	.000	7.6000	7.6000
	Cu-1wt%Si-6wt%Ni-0.1wt%Cr-0.5wt%Al-0.15wt%Mg/ rolled & aged	8.00000*	.00000	.000	8.0000	8.0000
	Cu-3wt%Si-3wt%Zn/S.H	2.90000*	.00000	.000	2.9000	2.9000
	Cu-3wt%Si-3wt%Sn/ cast	5.20000*	.00000	.000	5.2000	5.2000
	Cu-3wt%Si-1wt%Mn/S.H	10.90000*	.00000	.000	10.9000	10.9000
	Cu-3wt%Si-0.8wt%W/S.H	.70000*	.00000	.000	.7000	.7000
Cu-3wt%Si-0.8wt%Mg/S.H	Cu-3wt%Si-2wt%Ti/S.H	10.50000*	.00000	.000	10.5000	10.5000
	Cu-1.8wt%Si-8wt%Ni-0.6wt%Sn-0.15wt%Mg/rolled & aged	13.50000*	.00000	.000	13.5000	13.5000
	Cu-1.4wt%Si-6wt%Ni-0.1wt%Cr-0.15wt%Mg/rolled & aged	12.80000*	.00000	.000	12.8000	12.8000
	Cu-1wt%Si-6wt%Ni-0.1wt%Cr-0.5wt%Al-0.15wt%Mg/ rolled & aged	13.20000*	.00000	.000	13.2000	13.2000
	Cu-3wt%Si-3wt%Zn/S.H	-8.00000*	.00000	.000	-8.0000	-8.0000
	Cu-3wt%Si-3wt%Sn/ cast	-5.70000*	.00000	.000	-5.7000	-5.7000
	Cu-3wt%Si-0.8wt%Mg/S.H	-10.90000*	.00000	.000	-10.9000	-10.9000
	Cu-3wt%Si-0.8wt%W/S.H	-10.20000*	.00000	.000	-10.2000	-10.2000
	Cu-3wt%Si-2wt%Ti/S.H	-.40000*	.00000	.000	-.4000	-.4000
Cu-3wt%Si-1wt%Mn/S.H	Cu-1.8wt%Si-8wt%Ni-0.6wt%Sn-0.15wt%Mg/rolled & aged	2.60000*	.00000	.000	2.6000	2.6000
	Cu-1.4wt%Si-6wt%Ni-0.1wt%Cr-0.15wt%Mg/rolled & aged	1.90000*	.00000	.000	1.9000	1.9000
	Cu-1wt%Si-6wt%Ni-0.1wt%Cr-0.5wt%Al-0.15wt%Mg/ rolled & aged	2.30000*	.00000	.000	2.3000	2.3000
	Cu-3wt%Si-3wt%Zn/S.H	2.20000*	.00000	.000	2.2000	2.2000
	Cu-3wt%Si-3wt%Sn/ cast	4.50000*	.00000	.000	4.5000	4.5000
	Cu-3wt%Si-0.8wt%Mg/S.H	-.70000*	.00000	.000	-.7000	-.7000
	Cu-3wt%Si-1wt%Mn/S.H	10.20000*	.00000	.000	10.2000	10.2000
Cu-3wt%Si-0.8wt%W/S.H	Cu-3wt%Si-2wt%Ti/S.H	9.80000*	.00000	.000	9.8000	9.8000
	Cu-1.8wt%Si-8wt%Ni-0.6wt%Sn-0.15wt%Mg/rolled & aged	12.80000*	.00000	.000	12.8000	12.8000
	Cu-1.4wt%Si-6wt%Ni-0.1wt%Cr-0.15wt%Mg/rolled & aged	12.10000*	.00000	.000	12.1000	12.1000
	Cu-1wt%Si-6wt%Ni-0.1wt%Cr-0.5wt%Al-0.15wt%Mg/ rolled & aged	12.50000*	.00000	.000	12.5000	12.5000
Cu-3wt%Si-2wt%Ti/S.H	Cu-3wt%Si-3wt%Zn/S.H	-7.60000*	.00000	.000	-7.6000	-7.6000

	Cu-3wt%Si-3wt%Sn/ cast	-5.30000*	.00000	.000	-5.3000	-5.3000
	Cu-3wt%Si-0.8wt%Mg/S.H	-10.50000*	.00000	.000	-10.5000	-10.5000
	Cu-3wt%Si-1wt%Mn/S.H	.40000*	.00000	.000	.4000	.4000
	Cu-3wt%Si-0.8wt%W/S.H	-9.80000*	.00000	.000	-9.8000	-9.8000
	Cu-1.8wt%Si-8wt%Ni-0.6wt%Sn-0.15wt%Mg/rolled & aged	3.00000*	.00000	.000	3.0000	3.0000
	Cu-1.4wt%Si-6wt%Ni-0.1wt%Cr-0.15wt%Mg/rolled & aged	2.30000*	.00000	.000	2.3000	2.3000
	Cu-1wt%Si-6wt%Ni-0.1wt%Cr-0.5wt%Al-0.15wt%Mg/ rolled & aged	2.70000*	.00000	.000	2.7000	2.7000
	Cu-3wt%Si-3wt%Zn/S.H	-10.60000*	.00000	.000	-10.6000	-10.6000
	Cu-3wt%Si-3wt%Sn/ cast	-8.30000*	.00000	.000	-8.3000	-8.3000
Cu-1.8wt%Si-8wt%Ni-0.6wt%Sn-0.15wt%Mg/rolled & aged	Cu-3wt%Si-0.8wt%Mg/S.H	-13.50000*	.00000	.000	-13.5000	-13.5000
	Cu-3wt%Si-1wt%Mn/S.H	-2.60000*	.00000	.000	-2.6000	-2.6000
	Cu-3wt%Si-0.8wt%W/S.H	-12.80000*	.00000	.000	-12.8000	-12.8000
	Cu-3wt%Si-2wt%Ti/S.H	-3.00000*	.00000	.000	-3.0000	-3.0000
	Cu-1.4wt%Si-6wt%Ni-0.1wt%Cr-0.15wt%Mg/rolled & aged	-.70000*	.00000	.000	-.7000	-.7000
	Cu-1wt%Si-6wt%Ni-0.1wt%Cr-0.5wt%Al-0.15wt%Mg/ rolled & aged	-.30000*	.00000	.000	-.3000	-.3000
	Cu-3wt%Si-3wt%Zn/S.H	-9.90000*	.00000	.000	-9.9000	-9.9000
	Cu-3wt%Si-3wt%Sn/ cast	-7.60000*	.00000	.000	-7.6000	-7.6000
Cu-1.4wt%Si-6wt%Ni-0.1wt%Cr-0.15wt%Mg/rolled & aged	Cu-3wt%Si-0.8wt%Mg/S.H	-12.80000*	.00000	.000	-12.8000	-12.8000
	Cu-3wt%Si-1wt%Mn/S.H	-1.90000*	.00000	.000	-1.9000	-1.9000
	Cu-3wt%Si-0.8wt%W/S.H	-12.10000*	.00000	.000	-12.1000	-12.1000
	Cu-3wt%Si-2wt%Ti/S.H	-2.30000*	.00000	.000	-2.3000	-2.3000
	Cu-1.8wt%Si-8wt%Ni-0.6wt%Sn-0.15wt%Mg/rolled & aged	.70000*	.00000	.000	.7000	.7000
	Cu-1wt%Si-6wt%Ni-0.1wt%Cr-0.5wt%Al-0.15wt%Mg/ rolled & aged	.40000*	.00000	.000	.4000	.4000
	Cu-3wt%Si-3wt%Zn/S.H	-10.30000*	.00000	.000	-10.3000	-10.3000
	Cu-3wt%Si-3wt%Sn/ cast	-8.00000*	.00000	.000	-8.0000	-8.0000
Cu-1wt%Si-6wt%Ni-0.1wt%Cr-0.5wt%Al-0.15wt%Mg/ rolled & aged	Cu-3wt%Si-0.8wt%Mg/S.H	-13.20000*	.00000	.000	-13.2000	-13.2000
	Cu-3wt%Si-1wt%Mn/S.H	-2.30000*	.00000	.000	-2.3000	-2.3000
	Cu-3wt%Si-0.8wt%W/S.H	-12.50000*	.00000	.000	-12.5000	-12.5000
	Cu-3wt%Si-2wt%Ti/S.H	-2.70000*	.00000	.000	-2.7000	-2.7000
	Cu-1.8wt%Si-8wt%Ni-0.6wt%Sn-0.15wt%Mg/rolled & aged	.30000*	.00000	.000	.3000	.3000

	Cu-1.4wt%Si-6wt%Ni-0.1wt%Cr-0.15wt%Mg/rolled & aged	-.40000*	.00000	.000	-.4000	-.4000

*. The mean difference is significant at the 0.05 level.

Multiple Comparisons

Dependent Variable: Electrical conductivity

Tukey HSD

(I) Alloys	(J) Alloys	Mean Difference (I-J)	Std. Error	Sig.	95% Confidence Interval	
					Lower Bound	Upper Bound
Cu-3wt%Si-3wt%Zn/S.H	Cu-3wt%Si-3wt%Sn/ cast	3.40000*	.00000	.000	3.4000	3.4000
	Cu-3wt%Si-0.8wt%Mg/S.H	-3.60000*	.00000	.000	-3.6000	-3.6000
	Cu-3wt%Si-1wt%Mn/S.H	5.70000*	.00000	.000	5.7000	5.7000
	Cu-3wt%Si-0.8wt%W/S.H	-3.30000*	.00000	.000	-3.3000	-3.3000
	Cu-3wt%Si-2wt%Ti/S.H	-.70000*	.00000	.000	-.7000	-.7000
	Cu-1.8wt%Si-8wt%Ni-0.6wt%Sn-0.15wt%Mg/rolled & aged	11.40000*	.00000	.000	11.4000	11.4000
	Cu-0.7wt%Si-3.2wt%Ni-0.3wt%Zn/rolled & aged	6.90000*	.00000	.000	6.9000	6.9000
	Cu-0.7wt%Si-3.2wt%Ni-0.3wt%Zn/cast & aged	13.40000*	.00000	.000	13.4000	13.4000
	Cu-1.4wt%Si-6wt%Ni-0.1wt%Cr-0.15wt%Mg/rolled & aged	9.40000*	.00000	.000	9.4000	9.4000
	Cu-1wt%Si-6wt%Ni-0.1wt%Cr-0.5wt%Al-0.15wt%Mg/ rolled & aged	9.80000*	.00000	.000	9.8000	9.8000
Cu-3wt%Si-3wt%Sn/ cast	Cu-3wt%Si-3wt%Zn/S.H	-3.40000*	.00000	.000	-3.4000	-3.4000
	Cu-3wt%Si-0.8wt%Mg/S.H	-7.00000*	.00000	.000	-7.0000	-7.0000
	Cu-3wt%Si-1wt%Mn/S.H	2.30000*	.00000	.000	2.3000	2.3000
	Cu-3wt%Si-0.8wt%W/S.H	-6.70000*	.00000	.000	-6.7000	-6.7000
	Cu-3wt%Si-2wt%Ti/S.H	-4.10000*	.00000	.000	-4.1000	-4.1000
	Cu-1.8wt%Si-8wt%Ni-0.6wt%Sn-0.15wt%Mg/rolled & aged	8.00000*	.00000	.000	8.0000	8.0000
	Cu-0.7wt%Si-3.2wt%Ni-0.3wt%Zn/rolled & aged	3.50000*	.00000	.000	3.5000	3.5000
	Cu-0.7wt%Si-3.2wt%Ni-0.3wt%Zn/cast & aged	10.00000*	.00000	.000	10.0000	10.0000
	Cu-1.4wt%Si-6wt%Ni-0.1wt%Cr-0.15wt%Mg/rolled & aged	6.00000*	.00000	.000	6.0000	6.0000

	Cu-1wt%Si-6wt%Ni-0.1wt%Cr-0.5wt%Al-0.15wt%Mg/ rolled & aged	6.40000*	.00000	.000	6.4000	6.4000
Cu-3wt%Si-0.8wt%Mg/S.H	Cu-3wt%Si-3wt%Zn/S.H	3.60000*	.00000	.000	3.6000	3.6000
	Cu-3wt%Si-3wt%Sn/ cast	7.00000*	.00000	.000	7.0000	7.0000
	Cu-3wt%Si-1wt%Mn/S.H	9.30000*	.00000	.000	9.3000	9.3000
	Cu-3wt%Si-0.8wt%W/S.H	.30000*	.00000	.000	.3000	.3000
	Cu-3wt%Si-2wt%Ti/S.H	2.90000*	.00000	.000	2.9000	2.9000
	Cu-1.8wt%Si-8wt%Ni-0.6wt%Sn-0.15wt%Mg/rolled & aged	15.00000*	.00000	.000	15.0000	15.0000
	Cu-0.7wt%Si-3.2wt%Ni-0.3wt%Zn/rolled & aged	10.50000*	.00000	.000	10.5000	10.5000
	Cu-0.7wt%Si-3.2wt%Ni-0.3wt%Zn/cast & aged	17.00000*	.00000	.000	17.0000	17.0000
	Cu-1.4wt%Si-6wt%Ni-0.1wt%Cr-0.15wt%Mg/rolled & aged	13.00000*	.00000	.000	13.0000	13.0000
	Cu-1wt%Si-6wt%Ni-0.1wt%Cr-0.5wt%Al-0.15wt%Mg/ rolled & aged	13.40000*	.00000	.000	13.4000	13.4000
Cu-3wt%Si-1wt%Mn/S.H	Cu-3wt%Si-3wt%Zn/S.H	-5.70000*	.00000	.000	-5.7000	-5.7000
	Cu-3wt%Si-3wt%Sn/ cast	-2.30000*	.00000	.000	-2.3000	-2.3000
	Cu-3wt%Si-0.8wt%Mg/S.H	-9.30000*	.00000	.000	-9.3000	-9.3000
	Cu-3wt%Si-0.8wt%W/S.H	-9.00000*	.00000	.000	-9.0000	-9.0000
	Cu-3wt%Si-2wt%Ti/S.H	-6.40000*	.00000	.000	-6.4000	-6.4000
	Cu-1.8wt%Si-8wt%Ni-0.6wt%Sn-0.15wt%Mg/rolled & aged	5.70000*	.00000	.000	5.7000	5.7000
	Cu-0.7wt%Si-3.2wt%Ni-0.3wt%Zn/rolled & aged	1.20000*	.00000	.000	1.2000	1.2000
	Cu-0.7wt%Si-3.2wt%Ni-0.3wt%Zn/cast & aged	7.70000*	.00000	.000	7.7000	7.7000
	Cu-1.4wt%Si-6wt%Ni-0.1wt%Cr-0.15wt%Mg/rolled & aged	3.70000*	.00000	.000	3.7000	3.7000
	Cu-1wt%Si-6wt%Ni-0.1wt%Cr-0.5wt%Al-0.15wt%Mg/ rolled & aged	4.10000*	.00000	.000	4.1000	4.1000
Cu-3wt%Si-0.8wt%W/S.H	Cu-3wt%Si-3wt%Zn/S.H	3.30000*	.00000	.000	3.3000	3.3000
	Cu-3wt%Si-3wt%Sn/ cast	6.70000*	.00000	.000	6.7000	6.7000
	Cu-3wt%Si-0.8wt%Mg/S.H	-.30000*	.00000	.000	-.3000	-.3000
	Cu-3wt%Si-1wt%Mn/S.H	9.00000*	.00000	.000	9.0000	9.0000
	Cu-3wt%Si-2wt%Ti/S.H	2.60000*	.00000	.000	2.6000	2.6000
	Cu-1.8wt%Si-8wt%Ni-0.6wt%Sn-0.15wt%Mg/rolled & aged	14.70000*	.00000	.000	14.7000	14.7000
	Cu-0.7wt%Si-3.2wt%Ni-0.3wt%Zn/rolled & aged	10.20000*	.00000	.000	10.2000	10.2000

	Cu-0.7wt%Si-3.2wt%Ni-0.3wt%Zn/cast & aged	16.70000*	.00000	.000	16.7000	16.7000
	Cu-1.4wt%Si-6wt%Ni-0.1wt%Cr-0.15wt%Mg/rolled & aged	12.70000*	.00000	.000	12.7000	12.7000
	Cu-1wt%Si-6wt%Ni-0.1wt%Cr-0.5wt%Al-0.15wt%Mg/ rolled & aged	13.10000*	.00000	.000	13.1000	13.1000
Cu-3wt%Si-2wt%Ti/S.H	Cu-3wt%Si-3wt%Zn/S.H	.70000*	.00000	.000	.7000	.7000
	Cu-3wt%Si-3wt%Sn/ cast	4.10000*	.00000	.000	4.1000	4.1000
	Cu-3wt%Si-0.8wt%Mg/S.H	-2.90000*	.00000	.000	-2.9000	-2.9000
	Cu-3wt%Si-1wt%Mn/S.H	6.40000*	.00000	.000	6.4000	6.4000
	Cu-3wt%Si-0.8wt%W/S.H	-2.60000*	.00000	.000	-2.6000	-2.6000
	Cu-1.8wt%Si-8wt%Ni-0.6wt%Sn-0.15wt%Mg/rolled & aged	12.10000*	.00000	.000	12.1000	12.1000
	Cu-0.7wt%Si-3.2wt%Ni-0.3wt%Zn/rolled & aged	7.60000*	.00000	.000	7.6000	7.6000
	Cu-0.7wt%Si-3.2wt%Ni-0.3wt%Zn/cast & aged	14.10000*	.00000	.000	14.1000	14.1000
	Cu-1.4wt%Si-6wt%Ni-0.1wt%Cr-0.15wt%Mg/rolled & aged	10.10000*	.00000	.000	10.1000	10.1000
	Cu-1wt%Si-6wt%Ni-0.1wt%Cr-0.5wt%Al-0.15wt%Mg/ rolled & aged	10.50000*	.00000	.000	10.5000	10.5000
Cu-1.8wt%Si-8wt%Ni-0.6wt%Sn-0.15wt%Mg/rolled & aged	Cu-3wt%Si-3wt%Zn/S.H	-11.40000*	.00000	.000	-11.4000	-11.4000
	Cu-3wt%Si-3wt%Sn/ cast	-8.00000*	.00000	.000	-8.0000	-8.0000
	Cu-3wt%Si-0.8wt%Mg/S.H	-15.00000*	.00000	.000	-15.0000	-15.0000
	Cu-3wt%Si-1wt%Mn/S.H	-5.70000*	.00000	.000	-5.7000	-5.7000
	Cu-3wt%Si-0.8wt%W/S.H	-14.70000*	.00000	.000	-14.7000	-14.7000
	Cu-3wt%Si-2wt%Ti/S.H	-12.10000*	.00000	.000	-12.1000	-12.1000
	Cu-0.7wt%Si-3.2wt%Ni-0.3wt%Zn/rolled & aged	-4.50000*	.00000	.000	-4.5000	-4.5000
	Cu-0.7wt%Si-3.2wt%Ni-0.3wt%Zn/cast & aged	2.00000*	.00000	.000	2.0000	2.0000
	Cu-1.4wt%Si-6wt%Ni-0.1wt%Cr-0.15wt%Mg/rolled & aged	-2.00000*	.00000	.000	-2.0000	-2.0000
	Cu-1wt%Si-6wt%Ni-0.1wt%Cr-0.5wt%Al-0.15wt%Mg/ rolled & aged	-1.60000*	.00000	.000	-1.6000	-1.6000
Cu-0.7wt%Si-3.2wt%Ni-0.3wt%Zn/rolled & aged	Cu-3wt%Si-3wt%Zn/S.H	-6.90000*	.00000	.000	-6.9000	-6.9000
	Cu-3wt%Si-3wt%Sn/ cast	-3.50000*	.00000	.000	-3.5000	-3.5000
	Cu-3wt%Si-0.8wt%Mg/S.H	-10.50000*	.00000	.000	-10.5000	-10.5000
	Cu-3wt%Si-1wt%Mn/S.H	-1.20000*	.00000	.000	-1.2000	-1.2000
	Cu-3wt%Si-0.8wt%W/S.H	-10.20000*	.00000	.000	-10.2000	-10.2000

	Cu-3wt%Si-2wt%Ti/S.H	-7.60000*	.00000	.000	-7.6000	-7.6000
	Cu-1.8wt%Si-8wt%Ni-0.6wt%Sn-0.15wt%Mg/rolled & aged	4.50000*	.00000	.000	4.5000	4.5000
	Cu-0.7wt%Si-3.2wt%Ni-0.3wt%Zn/cast & aged	6.50000*	.00000	.000	6.5000	6.5000
	Cu-1.4wt%Si-6wt%Ni-0.1wt%Cr-0.15wt%Mg/rolled & aged	2.50000*	.00000	.000	2.5000	2.5000
	Cu-1wt%Si-6wt%Ni-0.1wt%Cr-0.5wt%Al-0.15wt%Mg/ rolled & aged	2.90000*	.00000	.000	2.9000	2.9000
Cu-0.7wt%Si-3.2wt%Ni-0.3wt%Zn/cast & aged	Cu-3wt%Si-3wt%Zn/S.H	-13.40000*	.00000	.000	-13.4000	-13.4000
	Cu-3wt%Si-3wt%Sn/ cast	-10.00000*	.00000	.000	-10.0000	-10.0000
	Cu-3wt%Si-0.8wt%Mg/S.H	-17.00000*	.00000	.000	-17.0000	-17.0000
	Cu-3wt%Si-1wt%Mn/S.H	-7.70000*	.00000	.000	-7.7000	-7.7000
	Cu-3wt%Si-0.8wt%W/S.H	-16.70000*	.00000	.000	-16.7000	-16.7000
	Cu-3wt%Si-2wt%Ti/S.H	-14.10000*	.00000	.000	-14.1000	-14.1000
	Cu-1.8wt%Si-8wt%Ni-0.6wt%Sn-0.15wt%Mg/rolled & aged	-2.00000*	.00000	.000	-2.0000	-2.0000
	Cu-0.7wt%Si-3.2wt%Ni-0.3wt%Zn/rolled & aged	-6.50000*	.00000	.000	-6.5000	-6.5000
	Cu-1.4wt%Si-6wt%Ni-0.1wt%Cr-0.15wt%Mg/rolled & aged	-4.00000*	.00000	.000	-4.0000	-4.0000
	Cu-1wt%Si-6wt%Ni-0.1wt%Cr-0.5wt%Al-0.15wt%Mg/ rolled & aged	-3.60000*	.00000	.000	-3.6000	-3.6000
Cu-1.4wt%Si-6wt%Ni-0.1wt%Cr-0.15wt%Mg/rolled & aged	Cu-3wt%Si-3wt%Zn/S.H	-9.40000*	.00000	.000	-9.4000	-9.4000
	Cu-3wt%Si-3wt%Sn/ cast	-6.00000*	.00000	.000	-6.0000	-6.0000
	Cu-3wt%Si-0.8wt%Mg/S.H	-13.00000*	.00000	.000	-13.0000	-13.0000
	Cu-3wt%Si-1wt%Mn/S.H	-3.70000*	.00000	.000	-3.7000	-3.7000
	Cu-3wt%Si-0.8wt%W/S.H	-12.70000*	.00000	.000	-12.7000	-12.7000
	Cu-3wt%Si-2wt%Ti/S.H	-10.10000*	.00000	.000	-10.1000	-10.1000
	Cu-1.8wt%Si-8wt%Ni-0.6wt%Sn-0.15wt%Mg/rolled & aged	2.00000*	.00000	.000	2.0000	2.0000
	Cu-0.7wt%Si-3.2wt%Ni-0.3wt%Zn/rolled & aged	-2.50000*	.00000	.000	-2.5000	-2.5000
	Cu-0.7wt%Si-3.2wt%Ni-0.3wt%Zn/cast & aged	4.00000*	.00000	.000	4.0000	4.0000
	Cu-1wt%Si-6wt%Ni-0.1wt%Cr-0.5wt%Al-0.15wt%Mg/ rolled & aged	.40000*	.00000	.000	.4000	.4000
Cu-1wt%Si-6wt%Ni-0.1wt%Cr-0.5wt%Al-	Cu-3wt%Si-3wt%Zn/S.H	-9.80000*	.00000	.000	-9.8000	-9.8000
	Cu-3wt%Si-3wt%Sn/ cast	-6.40000*	.00000	.000	-6.4000	-6.4000
	Cu-3wt%Si-0.8wt%Mg/S.H	-13.40000*	.00000	.000	-13.4000	-13.4000

0.15wt%Mg/ rolled & aged	Cu-3wt%Si-1wt%Mn/S.H	-4.10000*	.00000	.000	-4.1000	-4.1000
	Cu-3wt%Si-0.8wt%W/S.H	-13.10000*	.00000	.000	-13.1000	-13.1000
	Cu-3wt%Si-2wt%Ti/S.H	-10.50000*	.00000	.000	-10.5000	-10.5000
	Cu-1.8wt%Si-8wt%Ni-0.6wt%Sn-0.15wt%Mg/rolled & aged	1.60000*	.00000	.000	1.6000	1.6000
	Cu-0.7wt%Si-3.2wt%Ni-0.3wt%Zn/rolled & aged	-2.90000*	.00000	.000	-2.9000	-2.9000
	Cu-0.7wt%Si-3.2wt%Ni-0.3wt%Zn/cast & aged	3.60000*	.00000	.000	3.6000	3.6000
	Cu-1.4wt%Si-6wt%Ni-0.1wt%Cr-0.15wt%Mg/rolled & aged	-.40000*	.00000	.000	-.4000	-.4000

*. The mean difference is significant at the 0.05 level.